This document is:

Pons, S., ed. *Proceedings of the 5th International Conference on Cold Fusion*. 1995, IMRA Europe, Sophia Antipolis Cedex, France: Monte-Carlo, Monaco. 640.

The printed book is in one volume, but this version has been split into two parts to facilitate downloading.

This is Part 2, page 201 to page 640, is here:

http://lenr-canr.org/acrobat/PonsSproceedinga.pdf

Part 1, cover page to page 200, is here:

http://lenr-canr.org/acrobat/PonsSproceeding.pdf

Fifth International Conference on Cold Fusion
9-13 April, 1995 - Monte Carlo, Monaco
ICCF5 ©1995

Cold Fusion and anomalous effects in deuteron conductors during non-stationary high-temperature electrolysis

Samgin A.L., Finodeyev O.*, Tsvetkov S.A.,
Andreev V.S., Khokhlov V.A., Filatov E.S.,
Murygin I.V., Gorelov V.P., Vakarin S.V.
Institute of High-Temperature Electrochemistry,
Russian Academy of Sciences
S.Kovalevskaya 20
620219 Ekaterinburg, RUSSIA
*ENECO
391-B Chipeta Way
Salt Lake City, Utah 84108, USA

Abstract

The studies were conducted with the perovskite-type solid electrolytes based on the strontium and barium cerates under hydrogen and deuterium atmosphere. Anomalous effects were found manifesting themselves in the overbackground neutron bursts, excess heat release, phase composition and crystal lattice parameter changes. At 200-750° C the regions of the temperature were identified which accompained by significant heat evolution that was greater in the deuteron conductors than in the proton conductors.

1. Intoduction

It is known /1,2/ that the hydrogen and deuterium absorption and transfer induced electrochemically in the solid oxide electrolytes is affended with the "excess" heat evolution. In specific cases excess heat power has been ranged up to several tens of percent. Meanwhile the poor reproducibility of these experiments was observed. As a result there is no escape from the correct conclusion concerning the causes of anomalous heat liberation. The calculation of the power balance has been pointed to the possibility of the processes associated with overstoichiometrical hydrogen and deuterium concentration in the crystal lattice resulting in the cold fusion or other anomalous phenomena.

In order to obtain the valid data about the reasons of the phenomena observed we carried out the complex investigation of solid electrolytes involving the careful measurements of heat and radiation, the correct determination of above temperature regions, the thorough research of the structure and phase transformations.

In this paper the results of calorimetric and radiometric experiments with samples of $Sr(Ba)CeO_3$-type proton (deuterium) conductors doped by Dy- and Nd-oxides during high temperature non-stationary electrolysis under D_2 or H_2 atmosphere is presented.

2. Methods

Samples was produced as a tablet 10 mm of diameter and 1-2 mm in thickness with Pd- or Pt-electrodes applied. The design of electrochemical cell used is showed in Fig. 1. As calorimeter the metall cylinder was used. Two hole was bored through its walls for fixing the termocouples. The inner plane heater was placed under sample studied for calibrating calorimeter and providing the temperature gradient through the tablet. The fixed temperature was supported with the outer calorimeter heater. The electrochemical cell was connected with the gas system. It was housed in two-ring neutron detector /3/. Multiple measurements of the neutron background during 1-2 day period showed that the maximum background counts did not exeed 8 pulses for the inner detector ring and 9 pulses for outer detector ring per 16,77 s.

Before the measurements the cell was evacuated with the vacuum pump, then it was heated up to initial working temperature the heat losses being compensated. After this operation the gas was admitted into cell. The heating regime provided a means for the establishment of initial constant temperature. Then the calorimeter calibration was carried out at the several fixed power loads (50, 100, 150 and 200 mW) on the inner heater. The calibrating curve is approximated by equation $W=f(dT)$ where W and dT are the heat power of the inner heater and the after temperature of the calorimeter. In all cases the same order of the principle steps in the experimental procedure was used.

I. After achievment of constant temperature over the cell the invariable electrical potential was applied to the electrodes for producing the electrolytic process. Within a few hours heat quasiequilibrium have been established.

II. Then the electrolysis was continued with the periodic sign-variable /reversible/ electrical potential supplied.

III. When fixed thermal steady-state condition the sample was sharply heated up to the cycling temperature Tcycl, the reverse electrolysis being contineed.

IV. Further thermal cycling was conducted by means of the inner and outer heaters in the range of temperature from 200 ° C to Tcycl. For the same sample all above experimental stages has been repeated a few times. Troughout the whole experiment the calorimeter temperature and that of sample surface was being steadely recorded as well as the time distribution of the neutron counte rate with digitization time of detection of 4 microseconds. By means of crate CAMAC all the data is stored in PC memory for subsequent processing.The heat power was determined with the calibrating curves found for both stationary conditions and non-steady-state ones. The typical examples of dT-t and W-dT dependences are presentad in Fig.2 and 3.

A wariety of ceramic samples with the Pt- and Pd- electrodes was examined under different gas atmosphere. It was recently shown / 4/ that the perovskite-type

oxide electrolytes with about the same chemical composition as the ones stadied by us has been transformated to the proton conductors under the influence of H_2-gas or H_2O-vapour medium. Therefore in the subsequent discussion we shall use the terms "protonconducting" and "deuteronconducting" ceramic samples with respect to the ones researched under H_2 or D_2 gas atmosphere.

Besides the additional investigations of heat releasing processes during the electrolysis under hydrogen and deuterium atmosphere were carried out using the scanning Calvet-microcalorimeter with the constant heating rate in the temperature range from 200 to 750°C.

3.Results and Discussion

Deuteronconducting electrolyte (No.1).

Many-day experiment was being conducted in above consequence. Under heating and cooling dopped $SrCeO_3$-sample the unknown phase transition was found at the 445°C. All fortscoming operations involving current reversing and heat cycling was conducted with special attention to the temperature changes and neutron flashes close to the phase transition point. The runs were broken when the current density at constant electrical potential sharpy diminished. This fact was evidence of scaling electrodes off the oxide tablet.

Anomalous heat effects and overbackground neutron bursts were found in this experiment. They were observed with supplied constant electrical potential about 10V. The heat power released exceeded one expended for producing electrolytic process by 10-1000% depending on way of electrical current loading. Within 18 hours the six events emitting neutrons as the individual bursts out the experimental errors were observed.

Deuteronconducting electrolyte (No.2).

In this run with unlike sample of deuteronconducting ceramics we were deciding the problem to obtain additional information on the heat evolution under non-steady-state heating or cooling regime as well as to fix temperature in situ. Only distinction from the run No.1 was the dynamical dT-t curves was recording for every heat power given up to the stationary temperature. Besides, inner surface of two-ring neutron detector was controlled thermostatically.

The results of these examinations were used to calculate excess heat liberated during electrolysis. To do this the value of heat power released (W_{libr}) compared with one expended (W_{exp}). When electrolyzing without thermocycling

$W_{exp}=W_{outer\ heater}+W_{electr}$, while when electrolyzing with thermocycling

$W_{exp}=W_{outer\ heater}+W_{electr}+W_{inner\ heater}$. Then the relative excess heat effect is

$$\frac{W_{libr}-W_{exp}}{W_{electr}} \times 100\%.$$

In our calculations the initial stationary temperature was taken as the reference one. The heat power of outer heater was constant throughout every experiment. It was expended for the compensating thermal losses. The heat power put in reverse electrolysis was evaluated by maximum electrical current observed. Its real magnitude could be not correctly found without using special integrating recorder. This naturally decreased the real excess heat effect. The results obtained is listed in Tabl. 1-4.

Table 1. The electrolysis with time-constant electrical potential.

t, min	$W_{outer\ heater}$, W	W_{electr} (max), W	W_{exp}, W	W_{libr}, W	$\frac{W_{libr}-W_{exp}}{W_{electr}}$, %
5	14.686	0.1276	14.813	14.838	20
10	14.686	0.1150	14.801	14.823	19
20	14.686	0.1042	14.790	14.806	15
30	14.686	1.0360	14.789	14.799	10
360	14.686	0.0790	14.765	14.788	29

Table 2. The electrolysis with reverse electrical load (U=10 V)

t, min	$W_{outer\ heater}$, W	W_{electr} (max), W	W_{exp}, W	W_{libr}, W	$\frac{W_{libr}-W_{exp}}{W_{electr}}$, %
60	14.686	0.016	14.702	14.734	200
360	14.686	0.015	14.071	14.732	206
24 hours	14.686	0.014	14.700	14.763	450

Table 3. The electrolysis with reverse electrical load (U=41 V)

t, min	$W_{outer\ heater}$, W	W_{electr} (max), W	W_{exp}, W	W_{libr}, W	$\frac{W_{libr}-W_{exp}}{W_{electr}}$, %
30	14.686	0.238	14.924	15.103	75
75	14.686	0.238	14.924	15.026	43

Table 4. The electrolysis with reversing electrical load and thermocycling

t, min	$W_{outer\ heater}$ W	$W_{inner\ heater}$ W	W_{electr} (max), W	W_{exp}, W	W_{libr} W	$\frac{W_{libr}-W_{exp}}{W_{electr}}$, %
N1 5	14.686	23.994	2.11	40.800	43.300	118
N1 10	14.686	23.994	1.057	39.737	40.400	62.7
N2 5	14.686	24.108	1.283	40.071	41.100	80.2
N2 10	14.686	24.222	0.585	39.490	39.600	18.8

Total errors in finding heat power are ± 10,5mW for electrolyzing regime without thermocycling and ± 154 mW for one with thermocycling. The overbackground neutron bursts of duration of 100 microseconds were observed in ten hours from beginning the electro lysis. The eight exceeding events (Count number is greater than 10) were registated within time interval 16.7 s during 32 hours. A half of them was found for direct electrolisis, while the others were measured for reverse electrolisis.

Protonconducting electrolyte

According to the above procedure the experiments were carred out with the same ceramic probe under H_2-atmosphere. The thermal treatment and evacuation were brought about to remove residual D_2-gas from the sample.

After control calibrating calorimetr and establishing heat steady-state condition the experiment was continued. The calculation showed the heat power released was lower than one for deuteroncondùcting sample. The excess heat effect was not found in the case of the electrolysis with direct electrical supply while one was fixed under reverse electrolyzing and thermocycling. The last fell down for a short time the natural neutron background was not exceeded.

Microcalorimetric investigation

The studies showed three temperature regions with the anomalous thermal effects for the both deuteron and proton conductors in the temperature range from 200 to 750 ° C (See fig.4). The heat evolution for deuteron conductor is greater than proton one. One can suppose the phase transition (I) are occured. The cathastrofic change of the heat liberation can be associated to some processes at phase transitions in the systems of ceramics - isotopic hydrogen. To elucidate these phenomena the additional investigations ough to conduct.

The X-ray diffraction studies.

The X-ray examination with deuteron conducting solid electrolytes fixed change of the phase composition and crystal lattice parameters after electrolysis. In particular, for the samples with the significant excess heat release two separate phase was found including $SrCeO_3$-type phase and CeO_2-type one. As a rule for the samples under thermocycling the crack formation was clearly observed.

References

1. A.Samgin, A.Baraboshkin, I.Murigin, S.Tsvetkov, V.Andreev, S.Vakarin "The influence of conductivity on neutron generation process in proton conducting solid electrolytes". *Proc Fourth International Conference on Cold Fusion*, Hawaii, December 6-9, 1993, **3**, p.5-1, EPRI, Palo Alto, USA (1994).

2. T.Mizuno, M.Enio, T.Akimoto, K.Azumi "Anomalous Heat Evolution from SrCeO3-type Proton Conductors during Absorption/Desorption of Deuterium in Alternate Electric Field". *Proc. Fourth International Conference on Cold Fusion*, Hawaii, December 6-9, 1993, **2**, p.14-1, EPRI, Palo Alto, USA (1994).

3. A.Samgin, V.Andreev. S.Tsvetkov, A.Cherepanov "Electrolysis of solid deuteron conducting electrolytes in deuterium atmosphere: microsecond structure analysis of neutron pulses by means of two-ring detector". Cold Fusion source book (Minsk Cold Fusion conference proceedings, May 21-26, 1994), USA (1994).

4. N.V.Arestova, V.P.Gorelov "Electroconductivity and ionic transport in the $BaCeNdO_3$-type perovskite", *Electrochemistry*, **30**, 988 (1994) (In Russian).

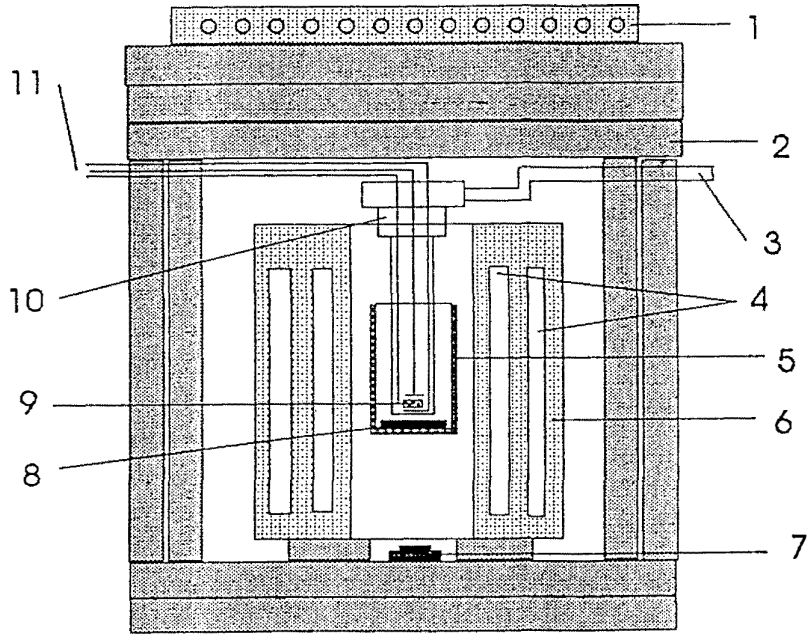

fig. 1.

1 - Block of detectors SI-19N.
2 - Neutron protective wall (3% boron).
3 - Vacuum-pumping system tube.
4 - Two rings of detectors SNMO-5.
5 - Heat shield.
6 - Moderator.
7 - Ventilator.
8 - The heater.
9 - The sample.
10 - The working cell.
11 - Two current conductors and thermocouple.

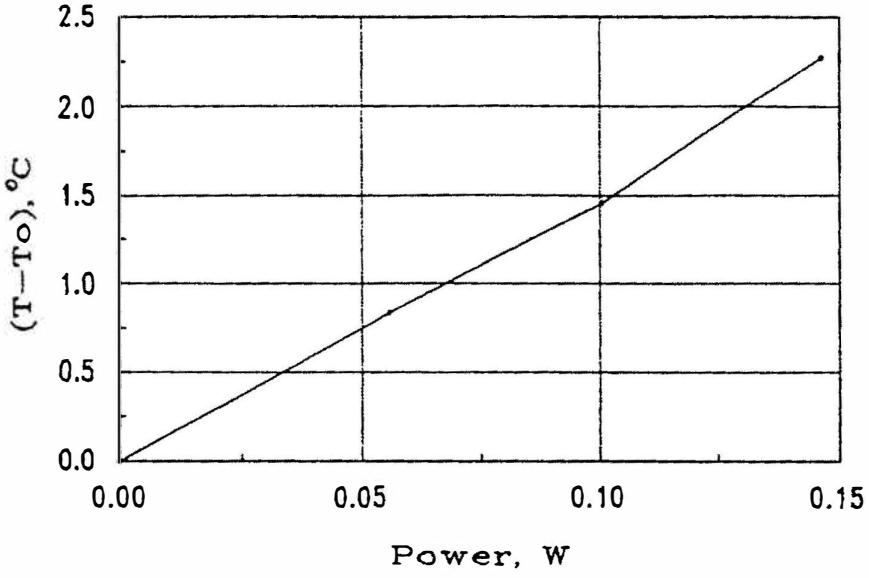
2.5
2.0
1.5
1.0
0.5
0.0
(T−To), °C
0.00
0.05
0.10
0.15
Power, W

Fig.3

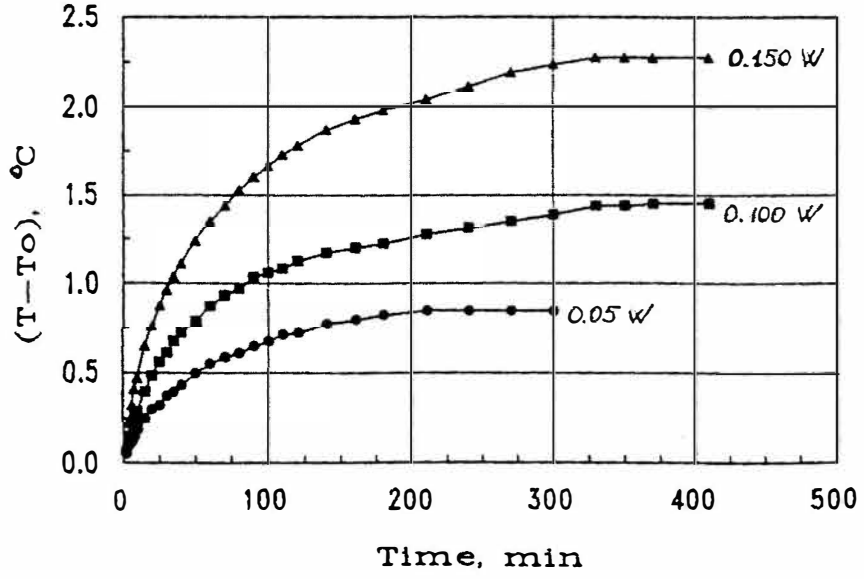
2.5
2.0
1.5
1.0
0.5
0.0
(T−To), °C
0.150 W
0.100 W
0.05 W
0
100
200
300
400
500
Time, min

Fig.2

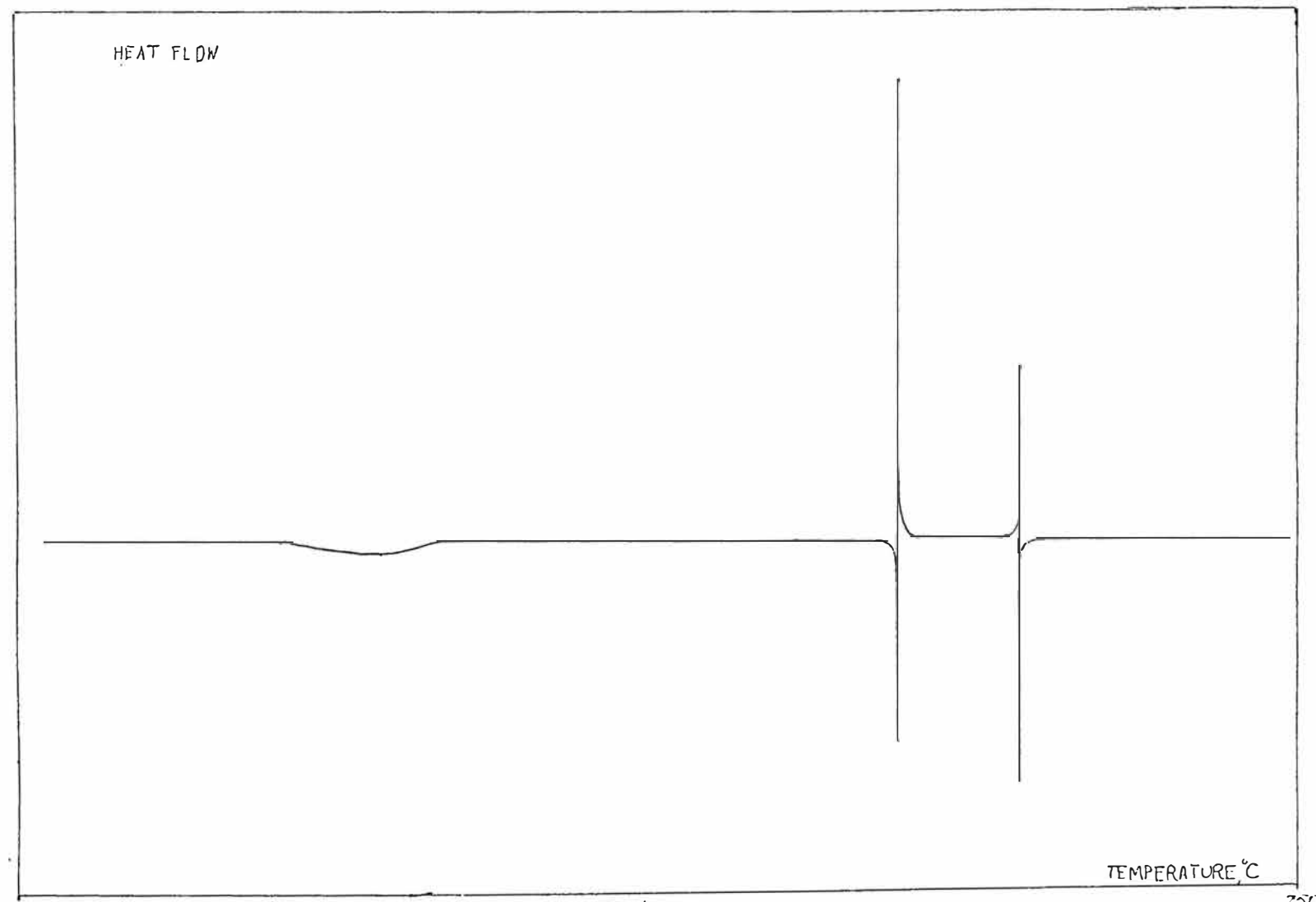

Fig. 4

Fifth International Conference on Cold Fusion
9-13 April, 1995 - Monte Carlo, Monaco
ICCF5 ©1995

Radioactivity of the Cathode Samples after Glow Discharge.

SAVVATIMOVA I.B, KARABUT A.B.
Scientific Industrial Association "Lutch"
142100 Podolsk, Moscow Region, 24 Zhelesnodorozhnaya St. Russian Federation
Phone:(7-095) 137-9258; Fax:(7-095) 137-93-84;
E-mail: postmaster@npoluch.msk.su

We registered the residual radioactivity of the cathode foils (Pd, Ag, Nb and other materials) after irradiation at the glow discharge. The samples were irradiated by proton, deuteron and argon, xenon ions with low energy. We consider that main activity is beta emission from samples after experiments /1/. Samples were placed in the contact with X-ray films. Semiquantitative radiographic method with measurement of the degree of blackening x-ray films by micro photometer was used. We made the estimate of beta activity of the samples . The x-ray film was calibrated with use of a tritium beta source with activity of $4.1 \cdot 10^9 \beta.s^{-1}$(Ti implanted). The characteristic curve from this film was gotten in vacuum chamber. The high energy radiation was compared with ^{90}Sr radiation ($E\beta$ ~546 keV). Within ~10^3 s after discharge termination the second x-ray film exposure corresponds to equivalent dose of $(1.5\text{-}4.5) \cdot 10^{10}$ β/cm^2 from ^{90}Sr. Activity of the isotope(s) with high radiation energy is estimated as corresponding to ^{90}Sr activity of ~$(2\text{-}5) \cdot 10^4$ $\beta/(cm^2 \cdot s)$.

Earlier we said that there were at least two isotopes with different energy: first < 20 keV and second (0.1...0.5) MeV /2/. Now we would like to note that activity was not observed for ion irradiated zones some times, when high ion's density was at the experiments with compound cathode samples (put together of the 2-7 foils from different materials). In this case high energy activity isotope was observed only in the second layer of the X-ray film.

Activity of the irradiated surface in comparison with non irradiated surface was less to 2-10 times (Fig.1,2). Encrease of the radioactive isotopes energy were registered after experiment only during 2-4 hours (Fig. 3).

When we took other cathodes (Ag, Nb, Ti... instead of Pd), its activity was less Pd to 10-100 times under equal conditions of the experiments. Activity Ag,Nb, Ti was less 10^2-$10^4 cm^{-2}s^{-1}$.

Activity of the Pd films under Ag, Nb and others was more to 10^5 -10^6 $cm^{-2}s^{-1}$ (Fig.2).

We observed increase of the sample radioactivity during the first several hours after experiment and its decreasing later. It means, that radioactive chains of the nuclear decay was regestrated.

We did not observe activity of the Ag cathode after deuterium ions and watched the Pd cathodes activity after Ar, Xe ions under other equal conditions of the experiment. Thus we registered the irradiation in the resuit of the blackening films that was not the result of the formation tritium or chemical interaction H, D, T with X-ray films.

We have to note the following main results:

- increase of the sample radioactivity during the first several hours after experiment and its decreasing later;
- presence of the radioactive nucleus with different energy from units to hundreds keV on the cathode ;
- radioactivity of the samples after Ar, Xe irradiation presence.

As the result we can suppose that we observed radioactive chains of the nuclear decay. It means that we have more universal phenomenon than reactions in the system Pd-D (passing nuclear process during and after irradiated low energy ions).

References:

1. I.Savvatimova, Ya.Kucherov and A. Karabut, "Cathode Material Change after Deuterium Glow Discharge Experiments," Transactions of Fusion Technology, v.26:1994, pp. 389-394, Fourth Int. Conf. on Cold Fusion, Dec. 6-9,1993, Hawaii.

2. A.Karabut, Ya.Kucherov, I.Savvatimova "Nuclear product ratio for glow discharge in deuterium". Physics Letters A, 170, 1992, 265-272 .

3. A.Karabut, Ya.Kucherov, I.Savvatimova "Possible Nuclear Reactions mechanisms at Glow Discharge in Deuterium," Proc.of the Third the Int. Conf, on Cold Fusion, Nagoya, Japan October 21-25,1992, pp. 165-168.

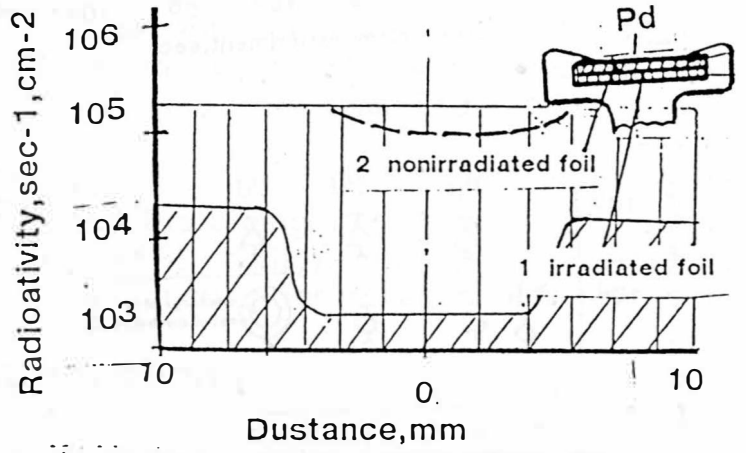

Fig. 1 Activity of the foils of the complite cathode after experiment in the deuterium (Pd+Pd)

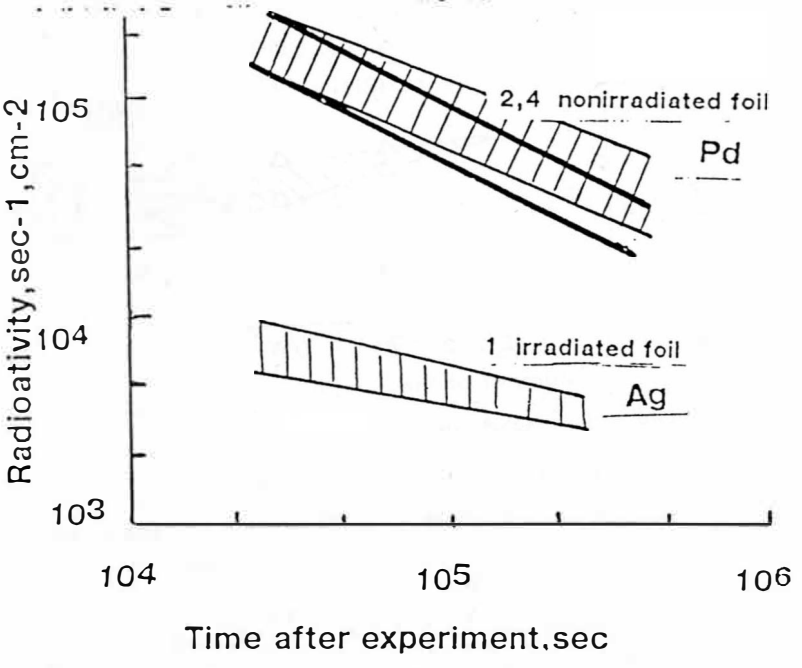

Fig. 2 Activity of the foils of the complite cathode after experiment in the deuterium (Ag+Pd+Ag+Pd)

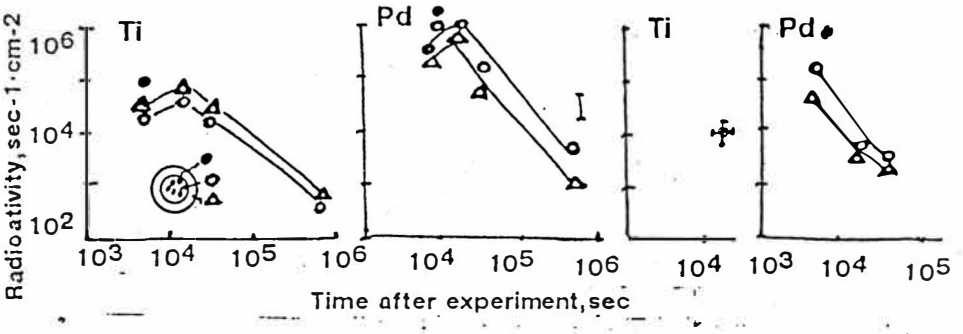

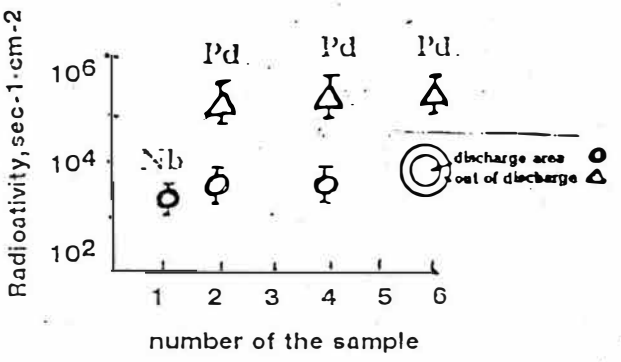

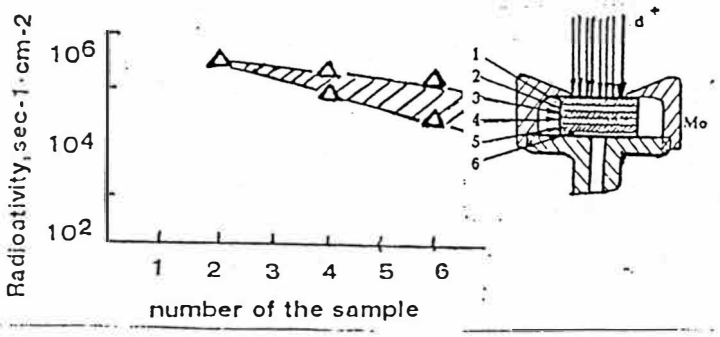

Fig3 Activity of the foils of the complite cathode after experiment in the deuterium (Ti+Pd+Ti+Pd)

1-Ti; 2-Pd; 3-Ti; 4-Pd. ● specks o center of the sample △ under screen area

(Nb-Pd-Nb-Pd-Nb-Pd)

1 - irradiated foil, 2,3,4,5,6 - nonirradiated foil

1,3,5 - Nb; 2,4,6 - Pd

O - discharge area, △ - out of discharge

b - $2.3 \cdot 10^4$ second after experiment,

c - $4.5 \cdot 10^4$ second after experiment,

Fifth International Conference on Cold Fusion
9-13 April, 1995 - Monte Carlo, Monaco
ICCF5 ©1995

Nuclear Reaction Products Registration on the Cathode after Glow Discharge

IRINA SAVVATIMOVA, ALEKSANDR KARABUT

Scientific Industrial Association "Luch"
24 Zhelesnodorozhnaya St., 142100 Podolsk, Moscow Region.
Russian Federation

Abstract

We watched the changing of some impurity elements on tft7; Pd cathode (99,9 % purity) after proton, proton-deuteron and deuteron ion's irradiation under the equal glow discharge conditions.

1. Introduction

Early we observed excess heat. weak neutron generation, 41-1e. x-rays, weak gamma radiation. α - particle emission and other charged particles• emission /1-3/. Impurity increasing at the Pd cathode (99,99 % purity) after the deuterium glow discharge we noted early from units to hundreds times /1/. As published in /2,3/ that probable mechanism may be "fusion" and "fusion--fission" reactions as follow:

$$_{46}Pd \quad ---> \quad (_{36}Kr_{10}+Ne);\ (_{35}Br+_{11}Na)\ (_{34}Se+_{12}Mg);$$

$$(_{32}Ge +_{14}Si);\ (_{30}Zn +_{16}S);\ (_{28}Ni+_{18}Ar); \qquad (1)$$

$$_{46}Pd + {}_{1}d \text{ ---> } (^{95\text{-}97}mo+^{11}B);\ (^{90}Zr+^{14}N). \qquad (2)$$

$$_{46}Pd + 2{}_{2}d \text{ ---> } (^{87}Sr+^{22}Ne);\ (^{73}Ge+^{36}S). \qquad (3)$$

$$_{46}Pd +\cdot\ 3{}_{2}d \text{ ---> } (^{95,97}Mo+^{19}F),\ (^{98\text{-}104}Ru+^{10}B). \qquad (4)$$

2. Method

We used of the spark mass spectrometry method (SMS) in the Testing Analytical Center GIREDMET. The sensitivity threshold of this method is 10^{-7} at % for masses 1-10 and $>5.10^{-6}$ at % for masses >100. Standard deviation was 0.15-0.20. was 20 mm^2 and a analyzed depth was 10-20 micron. The second method was ions mass spectrometry (SIMS), and third method was x-ray microprobe analyzes, resolution 0.01%, analyzed area was 1 square micron, a depth 1 micron.

3. Results

New in confirmation above-state we reaffirm a host of new elements by SMS and the tendency to changing of the natural isotopic abundance for some elements and Pd.

We detected the 107 and 109 masses' contents on the surface (layer ~ 10 microns), on the next layer (10 microns too) and on the lower sample (non-irradiated) by spark mass-spectrometry. We can see these data in Table 1.

Transmutation products concentrate near surface. There were places with only Ag maximum (Fig. 1). For example, we found by microprobe analysis), that Ag reached to 12-15%, Mo to 5-7%. Concentration of such elements as As, Br, Rb, Sr, Y, Cd approach to 0,1-0.2 % (Fig. 2). Authors have never used such elements as As, Br, Rb, Sr, Cd, in this discharge chamber. These spectrums were observed as for points which might be localized melting places, so for points without visible new formation (whiskers growth or micro explosion). Similar results with Ag on the Pd had Duch et al. /4/. As can see spectrum Pd have Ag, As, Br, Rb, Sr, Y, Cd after deuterium glow discharge.Nb and Al was found after hydrogen glow discharge, after Xe and Ar was found S and Al.

We found that 107 and 109 masses' contents increased near surface (by SMS) up to 250 times for the most density current of deuteron ions. On the second layer this increasing was only to 10 times (on the depth 10-20 micron). For the most density of the proton ions changing of the 107 and 109 masses' contents was not observed. Contents of the 107 and 109 masses for less current density increased to 130 - 135 times for deuteron. 45-50 times for proton and to 15-19 times for proton-deuterium irradiation. The increasing of these masses on the second layer (10-20 micron from surface) and the less current ions density was ~ 5; 4.5, and 3 times for D; H and H-D environments, accordingly.

When we had maximum increasing of the 107 and 109 masses, we observed the growth for other masses too: increasing 10 and 11 masses (B) to 4 - 20 times, 12 and 13 (C?) the to 10 and more times, 90 and 91 to 4-17, 79 and 81 masses (Br) to 6-20 times.

We observed the tendency to natural isotopic ratio changing for some elements in the Pd cathode (Table 2) from results SMS. We received the higher isotopic ratio changing for Ca with Ni simultaneously.

We did not observe the great changing for the natural ratio isotopes Pd (by SIMS) and presence the 111.112 masses, which could explain formation of the masses 107 and 109 as the result of the PdH and PdD experience at the cathode (Fig.3).

The increasing of the masses 110 from 10 to 65 % and small decreasing 104. 105 masses under was observed. It should be noted that we observed Cd (by microprobe analysis) in the Fig. 1

There is change of the natural isotopic abundance for 109 and 107 masses by SIMS. We have got only mass 109 for four samples under different conditions at the glow discharge and in three different places for each one. We can explain this fact only by the formation 109 mass and change of the Ag isotopic ratio. It means that main change took place at near surface layer to a depth of about 1 micron (Fig. 2). Spectrum on the Fig. 4 (by x-ray microprobe analysis) received from one sample.

4. Discussion

Formation of the new elements observed both at deuterium glow discharge and at hydrogen glow discharge. This fact correlated with gamma-radiation which observed during and after glow discharge.

Spectrums with transmutation elements were observed as for points which might be localized melting places (Fig. 5), so for points without visible new formation (whiskers growth or micro explosion).

As the result the total sum quantity of the main nuclide impurities was more 10^{17} atoms in the irradiated zone. Considering that energy of the suggested nuclear reaction fission and (fusion-fission) is 3-10 MeV /2/, registered quantity of the impurity corresponded to output heat ~ 10^4-10^5 J /3/, In this case total dose of the gamma-emission was 10^7-10^8 per experiment. It means that the result of the most nuclear reactions was with stable nuclide formation /2/.

Conclusion

The authors came to the conclusion made after deuterium and hydrogen bombardment of Pd cathode in a glow discharge:

1. Formation of the new elements observed both at deuterium glow discharge and at hydrogen glow discharge.

2. Greater changes in the element composition have been observed after more intense deuterium ion bombardment. Transmutation effect is higher for deuterium in comparison with hydrogen to 10-100 and more times.

3. There is tendency to changing natural isotopic abundance. The authors observed maximum effects for changing isotopic ratio near surface in the lay a depth 1 micron and more (for example, Ca and Ni).

   It is difficult to explain detected increase 109 /107 mass's to 5 and more times as a result of the interaction with H or D.

This result confirms The presence of Cd On the cathode surface after experiment (by x-ray microprobe, analysis) and the growth 110 mass may be the result or the nuclear reactions.

4. Increase of individual elements in the Pd cathodes up to 10000 times depends upon the experiment conditions. In some cases this data may be the result of new structure formation such as whi.-3kers or similar micro explosive structure. But sometimes we don't watch this phenomena and watch the surface without visible structure formation.

Change of the isotope ratio for individual elements up to 2-4 times for the following elements: B, C, Zr, Ni in the lay a depth about 10 micron and Ag (5), 110 masses for a depth about 1 micron.

The quantity of the each isotope may be different in different analyses zones.

Weak radioactivity of the sample and large impurity concentration may be a result of "cold" nuclear products.

The results of the element and isotopic change in cathode material reaffirmed to the earlier suggestion [3] that the transmutation reason and the formation of elements and tendency to the changing if the isotopic ratio for some elements in the glow discharge experiments is fission and fusion-fission nuclear reactions in the cathode materials.

The authors are grateful to Prof. A.A. Babad-Zahryapin for help from outset and Prof. B. Ya. Guzovsky and P. Hagelstein for helpful discussions and critical remarks.

Referencqs:

1. I. Savvatimova, Ya. Kucherov and A. Karabut. "Cathode Material Change after Deuterium Glow Discharge Experiments," Transactions of Fusion Technology, v.26:1994, pp. 389-'394. Fourth Int. Conf. on Cold Fusion. Dec. 6-9.1991 Hawaii.

2. A. Karabut, Ya. Kucherov. I. Savvatimova "Possible Nuclear Reactions mechanisms at Glow Discharge in Deuterium." Proceeding of the Third Int. Conference on Cold Fusion, Frontiers of Cold Fusion. H. Ikegami (Ed). Nagoya, Japan October 21-25.1992. pp. 165- 168.

3. A. Karabut, Va. Kucherov, I. Savvatimova "Nuclear product ratio for discharge in deuterium". Physics Letters A, 170, 1992. 265-272 .

4. I. Dash. G. Noble and D. Diman Surface morphology and micro composition of Palladium Cathodes after Electrolysis in Acidified light and heavy Water: Correlation with excess Heat.

Transaction of Fusion Technology (December 1994); Forth International Conference on Cold Fusion, December 6-9,1993: v.26, number 4T(1994):ISSN:0748-1896, pp. 299-306.

Table 1

Change of Isotopic Composition of Pd Cathode after Deuterium Glow Discharge Experiments
(by secondary ion mass-spectrometry, 10^{-1} ppm)

Mass				10	11	12	13	23	58	60	61	62	78	80	79	81	90	91	107	109
Cur	Gas	Element		B	B	C	C	Na+2	Ni	Ni	Ni	Ni	Se	Se	Br	Br	Zr	Zr	Ag+2	Ag+2
mA		# exp.\before ex		2.6	2.5	12x1	13x1	200	45	46	<0.6	<32	<3	<4.6	<1.2	<1.3	1.7	<3	<20	<20
25	H2	1670	lay 1	0.7	0.28	4x1	5x1	110	97	120	76	1.3x	<2.4	5.2	<1.2	<2	5.5	5.x	<20	8.0
			lay 2	1.6	2.0	2x1	2x1	5.6	44	50	<40	42	3.1	4.3	<0.8	<1	5.5	5.5	32	33
25	H2 D2	1668	lay 1	<2.4	0.7	4x1	17x1	75	73	77	<16x1	<22	12	11	<1	<1.5	11	11	15x	31x
			lay 2	<2.1	0.7	1.0x	1.5x	21	51	45	<67	<22	5.7	6.4	<1.5	<1.5	11	<6	67	56
			under	<2.7	<0.4	2x1	1.5x	12	10	<6.5	<40	<14	6.2	7.9	<1.5	<1	<1	5	<21	55
25	D2	1671	lay 1	25	22	5x1	11x1	9x1	19x	18x	56x	63x	4.4	5.4	17	21	31	31	27x1	26x0
			lay 2	<1.5	1.1	750	11x1	4.6	31	28	<50	<25	3.2	5.x	<1.2	<0.6	0.9	<5	13x	19x
25	H2	1667	lay 1	<1.3	0.45	2x1	4x1	13	18	10	<37	<12	2.9	4.5	<0.9	<2.5	5.5	<3	<20	<20
			lay 2	<2	<0.4	4x1	5x1	<1.2	9.3	6.2	<28	<15	4.9	5.6	<0.7	<0.7	<0.6	<5	<21	<20
			under	<1.9	<0.3	2.0	9x1	11	21	9	<69	<10	13	12	<3.4	<0.8	<0.42	<1.5	<21	<20
25	D2	1666	lay 1	21	19	1x0x	20x1	23x1	28x1	31x1	45x	54x	11	11	<2	<1.6	25	16	5x1x	52x0
			lay 2	<2	<2.5	6x1x	6x1x	21	69	61	<52	35	9	10	<1.2	<6	8.5	5	210	210
			under	<2.8	<1.3	610	7x0	21	26	17	<35	<35	12	14	<1.6	<1	<1	<2.4	<11	<11

Analyses after experiment	upper - irradiated sample under - nonirradiated sample
1 lay (0-10 micron) 2 lay (10 -20 micron) below upper 100 micron	

* Data are the bringing isotipic content to 100% content

Table 2

NATURAL ISOTOPES RATIO CHANGING OF THE Pd CATHODE AFTER GLOW DISCHARGE
(spark mass-spectrometry)

Isotope ratio after experiment				11 / 10	13 / 12	61 / 60	62 / 60	44 / 40	90 / 91
Current mA	Gas	Sample number	Element Lay	B	C	Ni	Ni	Ca	Zr
25	H_2	1670	lay 1 lay 2	1.2 1.8	1.12 1.25	1.3	1.7	1.36 1.59	
25	H_2 – D_2	1668	lay 1 lay 2 under		3.35 1.6 0.69			2.23 1.1 1.1	
25	D_2	1671	lay 1 lay 2		2.2 1.46	2.9	3.6	1.7 0.7	
35	H_2	1667	lay 1 lay 2 under		1.7 1.12 3.3			2.5 0.83 0.58	
35	D_2	1666	lay 1 lay 2 under		1 1 1	1.7	1.6	0.93 1.93 2.87	1.5 1.7

* Data are the bringing isotopic content to 100% content.

lay 1 0	10 micron near irradiated surface
lay 2 10	20 micron from irradiated surface
Under second sample	100 micron from irradiated surface

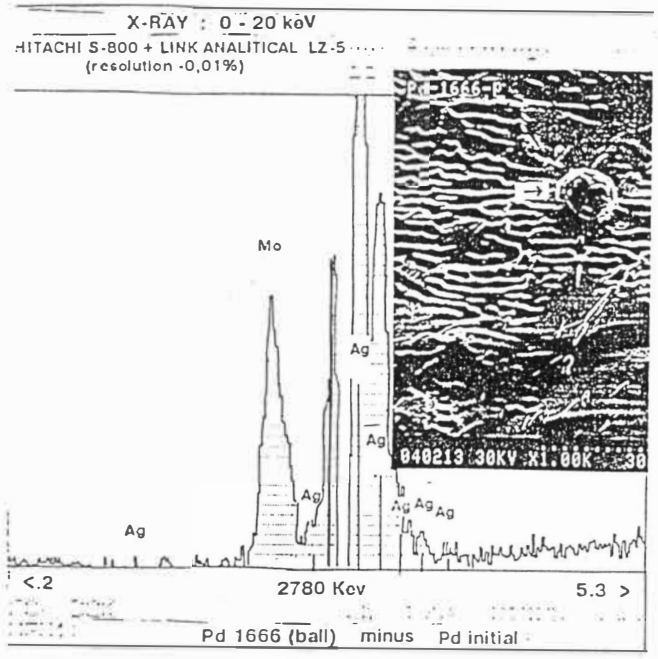

Fig 1

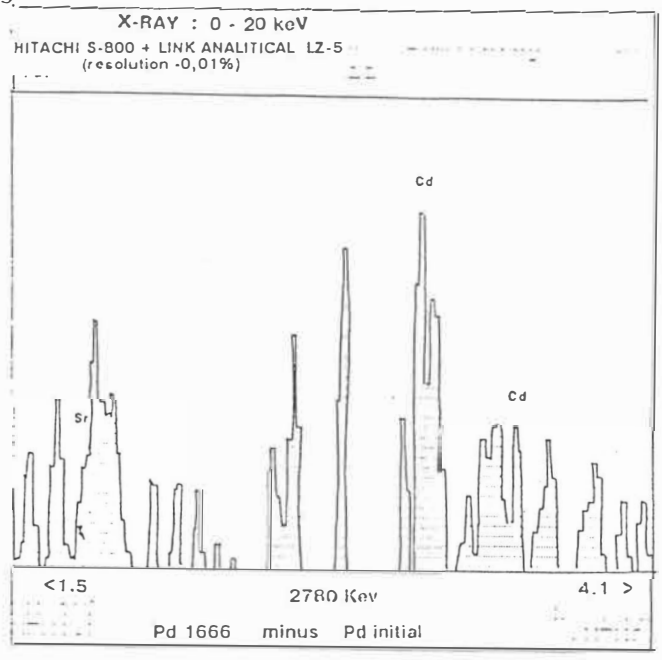

Fig.2 Spectrum from Pd cathode surface after deuterim experiment (X-ray microprobe analysis)- minus of the Pd initial spectrum - maximum As, Br, Rb, Y, Nb, Sr and Cd

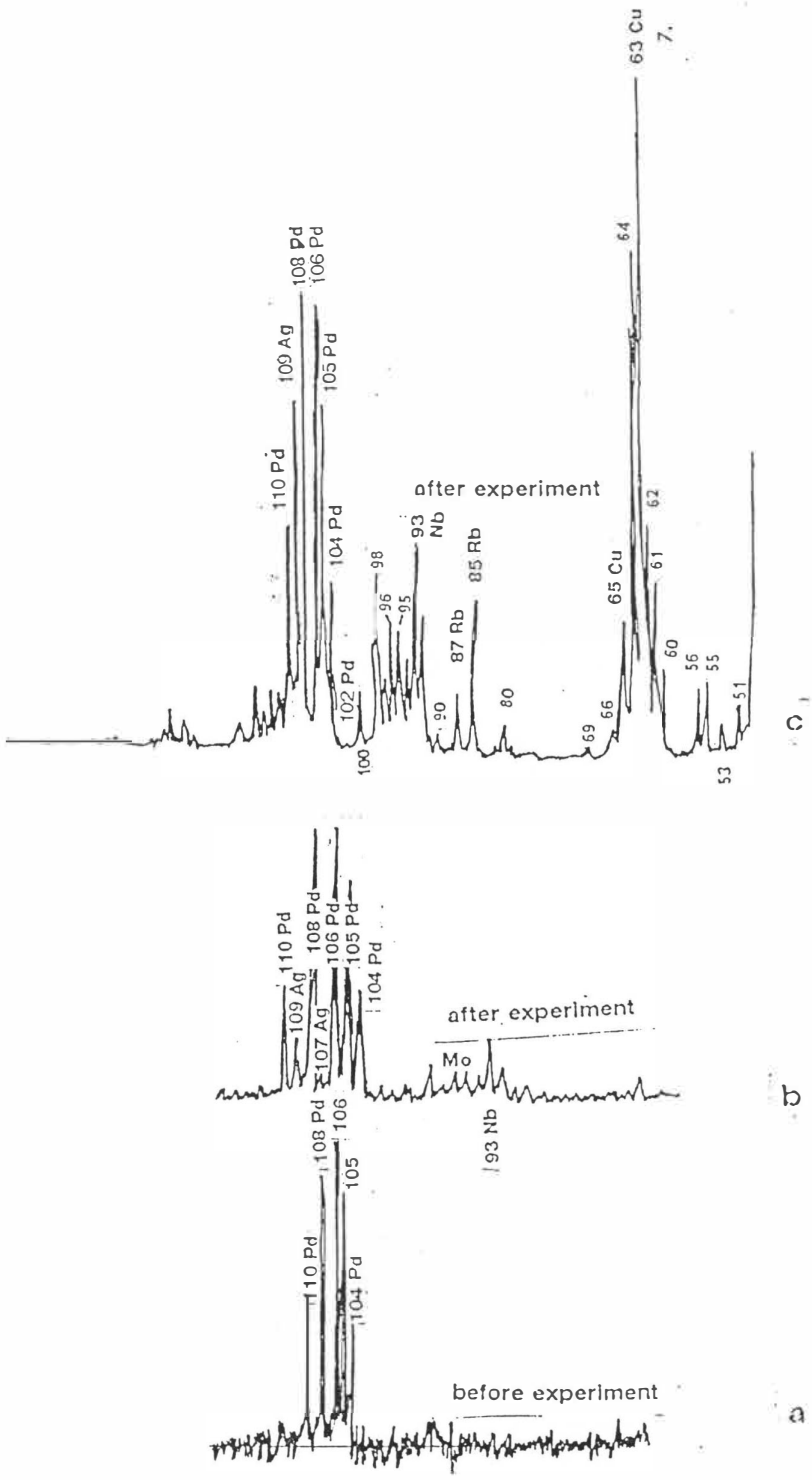

Fig. 3 Spectrum from Pd cathode surface before (a) and after different experiment condition (b, c) by SIMS

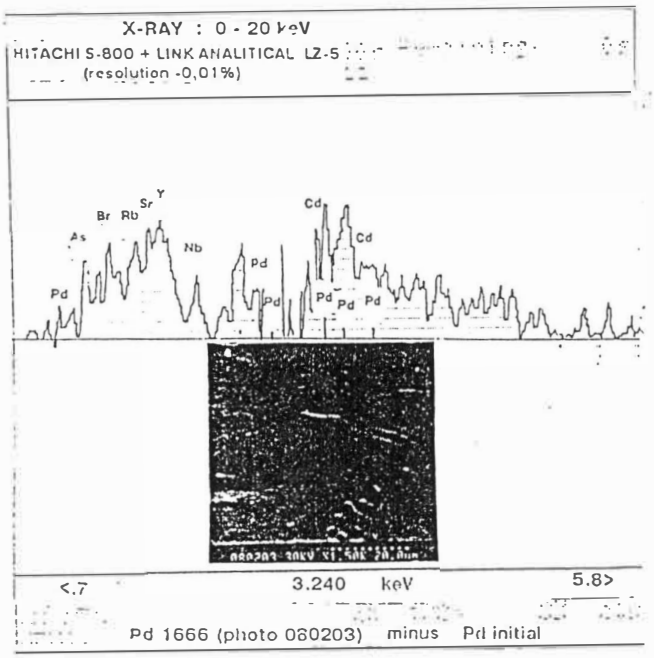

Fig.2 Spectrum from Pd cathode surface after deuterim experiment (X-ray microprobe analysis)- minus of the Pd initial spectrum - maximum As, Br, Rb, Y, Nb and Sr

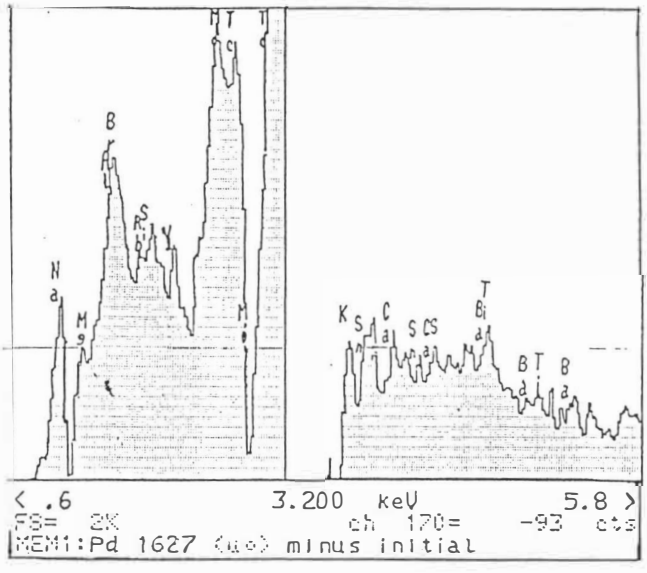

Na,Mg,Al,Br,Rb,Si,Y,Mo,Tc,K,Ca,S,Ti,Ba

Fig.4 Spectrum from Pd cathode surface minus spectrum initial Pd before experiment (X-ray microprobe analysis) after deuterim experiment for Fig.3

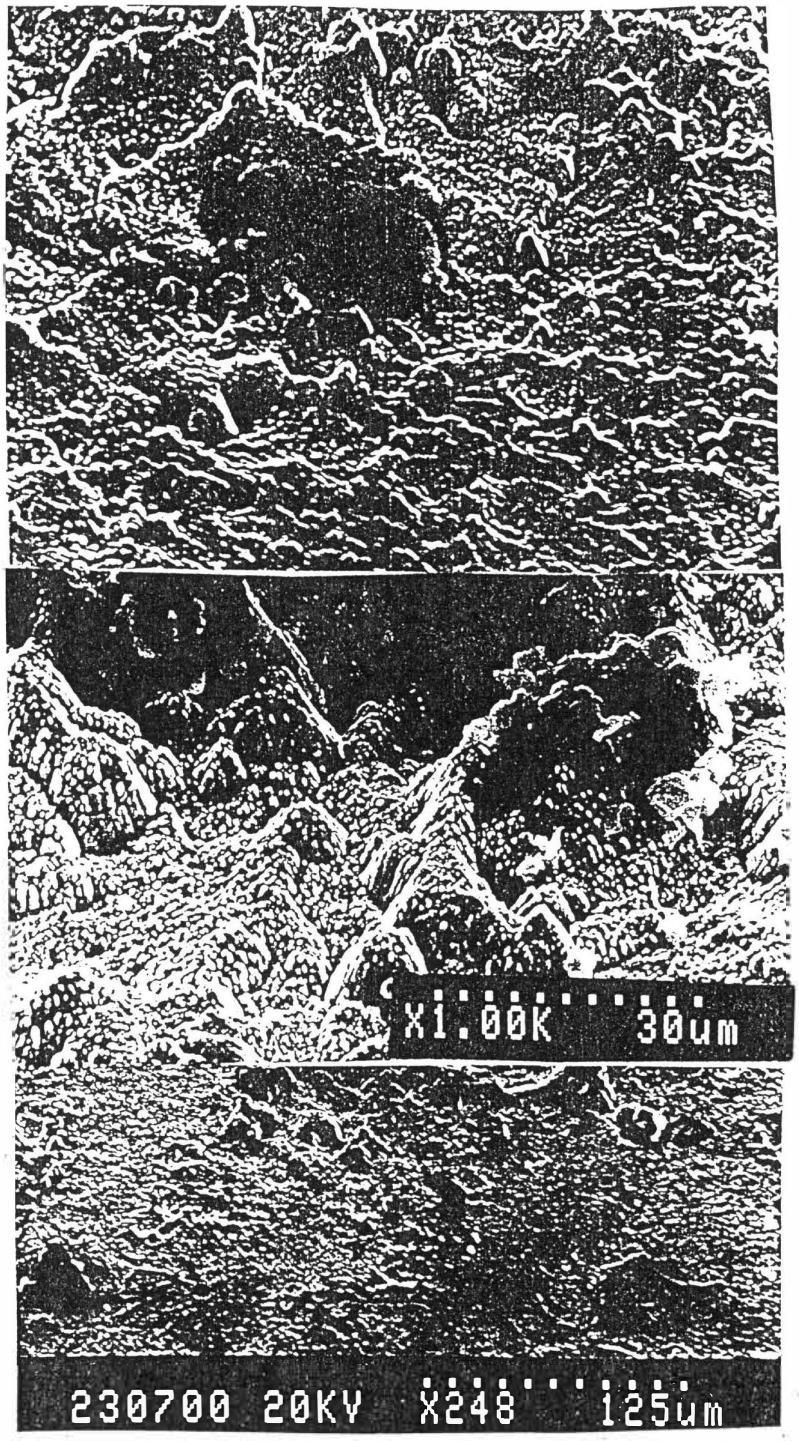

Fig.5 Sptructure of the Pd cathode surface after duiterium glow discharge

Fifth International Conference on Cold Fusion
9-13 April, 1995 - Monte Carlo, Monaco
ICCF5 ©1995

Excess Heat Measurements in Glow Discharge Using Flow "Calorimeter-2"

A.B. Karabut, Ya.R. Kucherov, I.B. Savvatimova

Scientific Industrial Association "Luch"
24 Zheleznodorozhnaya St.,
142100 Podolsk, Moscow Region,
Russian Federation

ABSTRACT

Experimental facts and results of heat and electric power measurements (including nuclear products) are presented.

1. INTRODUCTION

Excess heat was registered using a continuous flow calorimeter. These measurements confirmed our previous results [1] obtained with a dynamic calorimeter. The main limitations of the dynamic calorimeter were; non-stationary conditions of the experiment, and low precision of heat power measurements. A continuous flow calorimeter measured excess heat in the glow discharge system with better precision.

2. EXPERIMENTAL METHOD

Experimental device "Calorimeter-2" consists of vacuum chamber having a volume of 1200 cm^3, a gas pumping system, a water cooling system, a power supply and a measuring system. The vacuum chamber consists of a quartz tube having a diameter of 56 mm and a length of 500 mm (Fig. 1). Two flanges of the cathode and anode assembly were mounted on the top and bottom of the tube. Another quartz coaxial tube is put on the vacuum tube with a gap of 0,5-0,7 mm. Thise gap is water cooled chamber jaket. The cathode and anode assemblies have water conveyances to the cooled surfaces of the cathode and anode. The design of cathode assembly permits placement of samples made of different materials on the cooled cathode surface.

The gas system provided a residual pressure of less than 10^{-5} Torr. After evacuation, the chamber was filled with gases such as D_2, H_2, Ar and Xe at low pressure. The pressure in the chambere was controlled by diaphragm micromanometer.

The cathode, anode and quartz discharge chamber of the discharge device were cooled separately. The water cooled system consisted of three separate channels, which included two differential termoresistors. Two termoresistors were placed in the cooling water inlets and outlets of the anode, chatode and chamber respectively. The termoresistors were pairs of silicicon KTS 394 transistors. The water flow rate was measured by the volume control in each channel.

The time dependences of current I(t) and voltages U(t) were registered by a shunt, voltages divider and digital oscilloscope S9-27. The discharge power P_{el} was calculated using the equation.

$$P_{el} = \int U(t)\, I(t)\, dt$$

The system for excess power heat measurement was calibrated as follows. The electric heater was placed at the inlet of each cooling channel

on the anode, cathode and chamber outlets. The electric heater was powered by a requalated power supply. Uniform water flow rate g_{wi} was used in calibration (index "i" means respectively cathode, anode or chamber). The calibration results are presented in Fig. 2.

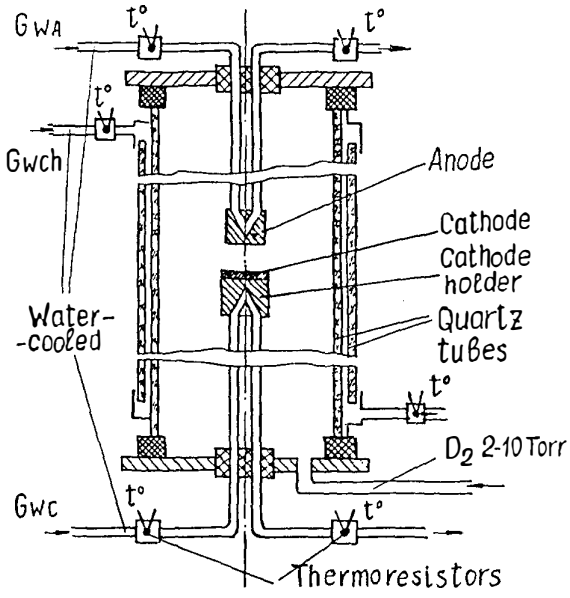

Fig. 1. Experimental glow discharge device "Calorimeter-2".

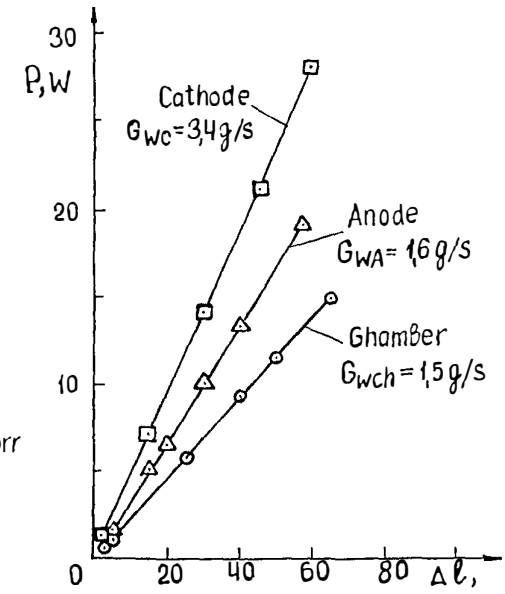

Fig. 2. Calibrated curves of heat power measurement system.

The cooling water temperature rise ΔT_i was calculated as

$$\Delta T_i = P_{el} / (g_{wi} \cdot Cw)$$

The heat balance was calculated at given time moment as

$$P_{EH} = (P_{HC} + P_{HA} + P_{HCh}) - P_{el}$$

$$P_{Hi} = C_w \cdot g_{wi} \Delta T_i$$

The heat efficiency η was determined by a reference experiment with a silver cathode which was presumed to be inert on the basis of previous experiments with glow discharge in deuterium and hydrogen as

$$\eta = (P_{HC} + P_{HA} + P_{HCh}) / P_{el}$$

The cummulative measuring error was no more than 3 % .

3. EXPERIMENTAL RESULTS

The D/Pd loading ratio was determined by the measurement of D_2 pressure drop in chambere (Fig. 3). The loading ratio presented here is the average through the cathode thickness. The loading ratio is probably much higher in thin near-surface layer.

Aproximately 30 experiments were conducted for the system D/Pd to determine excess heat. The duration of a separate experiment was from 10 min to 1 hour. Excess heat power was registed in most experiments. The

typical time dependence of the excess power is shown in Fig. 4. The excess heat power increases as the current density increase (Fig.5). At the same time, the efficiency of the process (ouput to imput ratio) goes down with current density. In some of the experiments the efficiency was 170-190%.

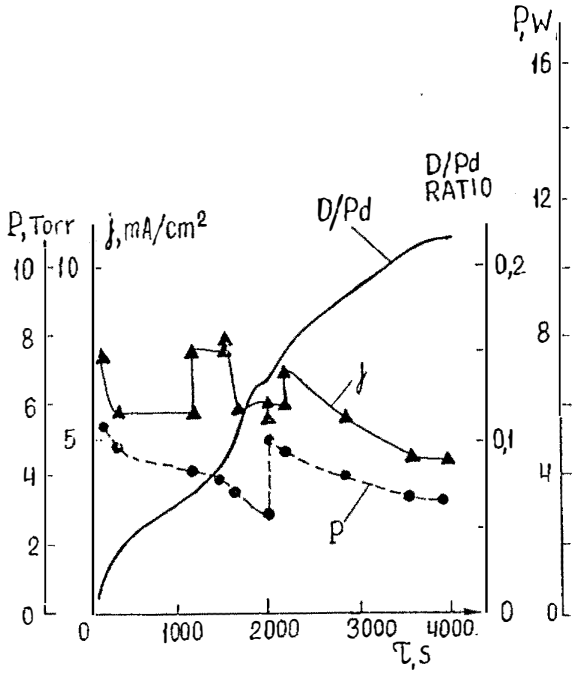

Fig. 3. Time dependence of D/Pd loading ratio, current density and D_2 pressure.

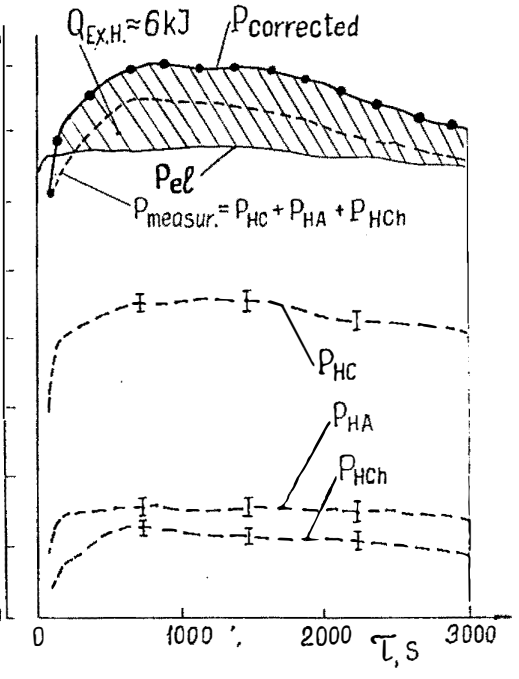

Fig. 4. Typical time dependence of heat power in "Calorimeter2".

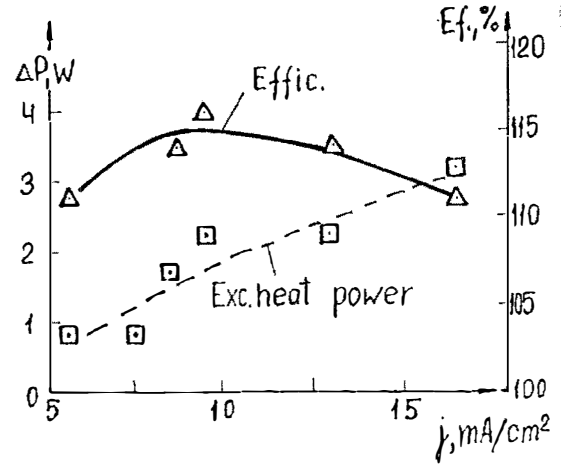

Fig. 5. Dependence of excess heat power and efficiency on current density.

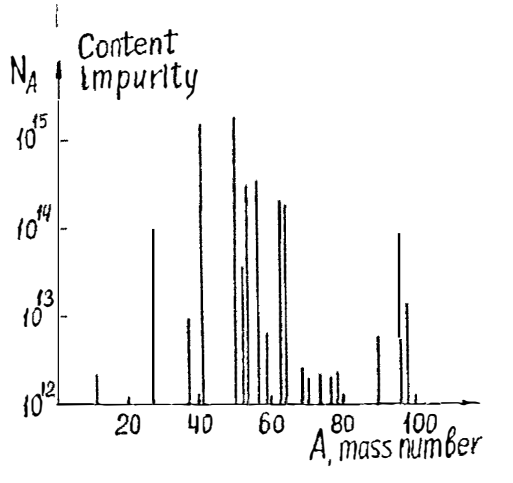

Fig. 6. Impurity in Pd-cathode after glow discharge.

Note that the low power input region with a higher efficiency described in our previous work [2] was not included in this work, because of unsufficient accuracy of a flow calorimeter in this region.

4.DISCUSSION

The analyses of the impurities, appeared in pure palladium foil after glow discharge treatment[2], give a satisfactory correlation between the quantity of impurities (Fig. 6) and the registered excess heat, estimated on the basis of mass defect from isotopic shift [4]. Gamma- and beta- radiation was found to be very weak and is not the basis for explaining excess heat.

5. CONCLUSIONS

Summarize some of the experimental facts [1-4]:

1. Excess heat (~10 kJ per hour).
2. Gamma-radiation after glow discharge with intensity (10^3-10^4) s^{-1} and energy 0.1-3 MeV.
3. Beta-radiation from cathode samples after glow discharge with intensity (10^4-10^6) cm^{-2} s^{-1} and energy 0.01-2.0 MeV.
4. Fast electrons-beamed radiation with intensity (10^8-10^{11}) cm^{-2} in 10^{-8} s bursts and energy 0.01-2.0 MeV.
5. Weak neutron signals with intensity (10-10^4) s^{-1} and energy 2-18 MeV.
6. Heavy charged particles registration (He,Li,B,C and other) with energy more than 10 Mev.
7. Increase of impurities concentration in Pd-cathode up to 10^{18}-10^{19} cm^{-3}.
8. Change of the natural isotope ratio for some elements (B,C,Ni and other).

These results provid good ground for developing glow discharge device "Calorimeter -2" as a heat producing reactor.

List of Symbols

C_w - water specific heat capacity, J/(kg·°C); g_{wi} -water flow rate, kg/s; P_{EH} -excess heat power in watts; P_{el}-discharge power, watts; P_{HC}, P_{HA}, P_{HCh} -heat power of cathode, anode and chamber respectively, watts; ΔT - water temperature rise,°C; I -discharge current, A; U -voltages,volts; η -heat efficiency.

REFERENCES

1. A.B. Karabut, Ya.R. Kucherov, I.B. Savvatimova, "Nuclear reaction on the cathde in gas discharge", *Pisma v GTF (Sov. Tech. Phys. Lett.)*, v. 16, release 12, 1990, p 53-57.

2. A.B. Karabut, Ya.R. Kucherov, I.B. Savvatimova, "Nuclear product ratio for glow discharge in deuterium", *Physics Letters A*, 170, p.265,1992.

3. I.B. Savvatimova, A.B. Karabut, Ya.R. Kucherov, "Cathode material change after deuterium glow discharge experiments", *Proc. of the Fourth International Conf. on Cold Fusion*, December 6-9, 1993, Hawaii, USA, p.

4. A.B. Karabut, Ya.R. Kucherov, I.B. Savvatimova, "Possible nuclear reactions mechanisms at glow discharge in deuterium", Frontiers of cold fusion , *Proc, of the Third International Conf. on Cold Fusion*, October 21-25, 1992, Nagoya, Japan, p. 165.

Fifth International Conference on Cold Fusion
9-13 April, 1995 - Monte Carlo, Monaco
ICCF5 ©1995

INFLUENCE OF PERFECTION OF SODIUM TUNGSTEN BRONZE SINGLE CRYSTALS ON NEUTRON EMISSION

S.V.Vakarin, A.L.Samgin, V.S.Andreev and S.A.Tsvetkov
Institute of High-Temperature Electrochemistry,
Russian Academy of Sciences
S.Kovalevskaya 20
620219 Ekaterinburg, RUSSIA

Abstract

Correlation between crystal structure perfection and neutron emission has been found. Positive result on neutron generation has been established only for crystals with "specific" X-ray diffraction pattern. This allows to treat X-ray data as a selection criterion. The crystals has proven to be rather perfect. Damage of perfection of the surface layer results in absence of the effect .

1. Introduction

Tentative selection of single crystals as catode material[1] seems to be the most optimal way to reproduce positive results on cold fusion. Up to now no experiments have been performed to find fitness criterion of crystals.

Thanks to X-ray analysis of a crystal structure before and after cold fusion experiments such criterion has been found for sodium tungsten bronzes.

2. Results and discussion

X-ray measurements were done on a diffractometer DRON-3 at U= 20 kV, I = 10mA and Cu k_α radiation.

X-ray diffraction patterns of the crystals without the surface admixtures (e.g. polytungstates, tungsten etc.) were chosen for analysis. However, it does not mean that there were no admixtures inside single crystals. Since the {100} plane was exposed to X-rays, the patterns show four maxima corresponding to the (100), (200), (300) and (400) reflections of different orders.

Intensities of the above diffraction maxima are seen to be high (Fig.1) for the crystals with a positive result (i.e., neutron counters registered signals on the level not less than 4σ). Alternatively, for crystals without a positive result peak intensities of the third and forth order (sometimes even of the second one) are essentially lower ($I/I_0 < 50$) (Fig.2). Similar X-ray patterns are observed for crystals which loose their ability to generate neutrons during experiments (Fig.3).

Such variation in the intensity of the diffraction peaks may, seemingly, be attributed to the second extinction. In this case with X-ray penetration intensity weakens in different mosaic blocks, resulting in damage of strict phase relations by dislocations, point defects and subgrain boundaries.

Increasing number of microblocks as well as structural imperfections occurring during tranformation from a "fitting" to "unfitting" crystal is supported by the X-ray topograms. Surface topograms for "fitting" and "unfitting" crystals are shown, respectively, in Figs. 4 and 5. It is also found that a transformation from "fitting" to "unfitting" crystal is accompanied by change for the worse in the surface layer perfection, the reflection being smeared (Fig.6).

This allows to conclude that one condition to attempt a positive result is a structure perfection of the working plane of sodium tungsten bronze. Damage of perfection of the surface layers results in absence of the effect.

Probably, neutron emission can take place during the change from perfect to mosaic crystal, which, to a certain extent, supports the "accelerated" model of cold fusion[2].

Tentative evaluation of the crystal quality allows to give some recommendations concerning crystal growth. For instance, it is of no sense to keep on growing crystal from a "unfitting" seed since it will not be perfect enough (Fig.7) as shown by our experiments.

To obtain a crystal with positive effect we recommend to grow it under optimal conditions from the first moment of nucleation. Attempts undertaken to prepare the working plane by polishing and etching have failed (Fig.8).

Acknowledgments

The research was supported by Russian Fundamental Research Fund.

References

1. K.Kaliev, A. Baraboshkin, A. Samgin et al., "Reproducible Nuclear Reactions during Interection of Deuterium with Oxide Tungsten Bronze," *Physics Letters A.*,**172**, 199 (1993).

2. V.Tsarev, "Cold Fusion," *Uspekhi Fizicheskih Nauk*, **160**, 1 (1990).

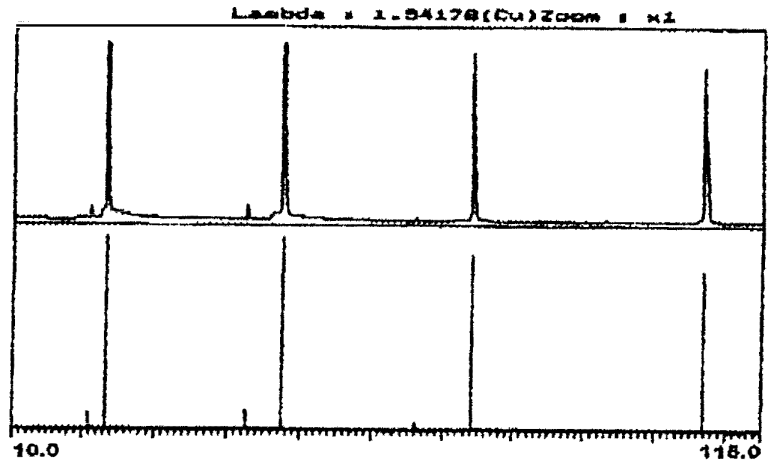

Fi g.1. Typical X-ray diffraction pattern for the {100} plane of a cubic sodium tungsten bronze single crystal before experiment. Positive result on neutron emissio experiment at the level of 4σ.

Fig.2. Typical X-ray diffraction pattern for the {100} plane of a cubic sodium tungsten bronze single crystal before experiment. No positive result.

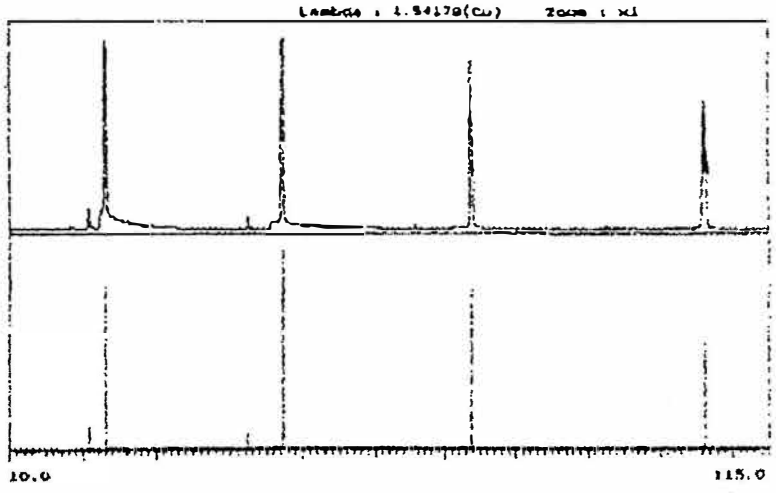

a)

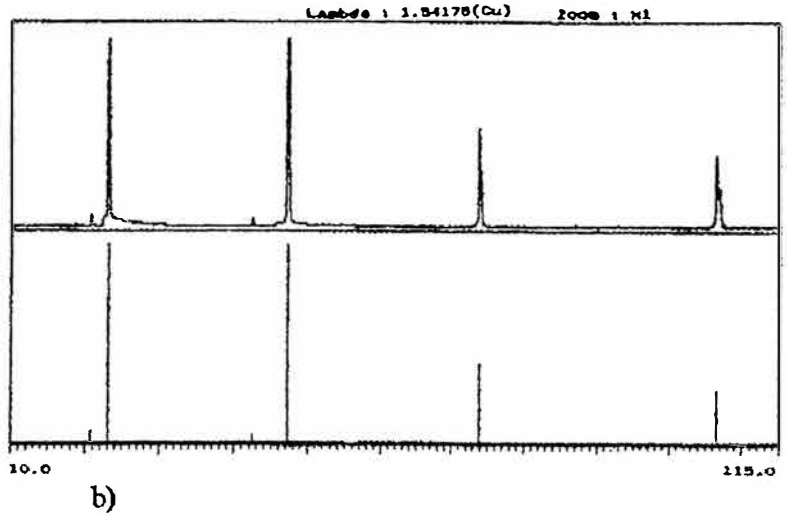

b)

Fig.3. X-ray diffraction patterns for the same {100} plane of a cubic single crystal before (a) and after (b) experiment. During experiment the crystal stopped showing neutron emission.

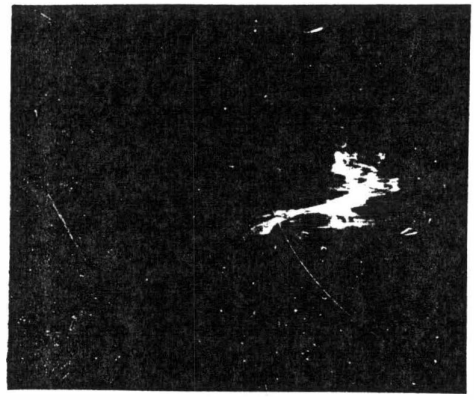

Fig.4. Typical topogram for the {100} plane of a cubic sodium tungsten bronze single crystal before experiment. Positive result at 4σ.

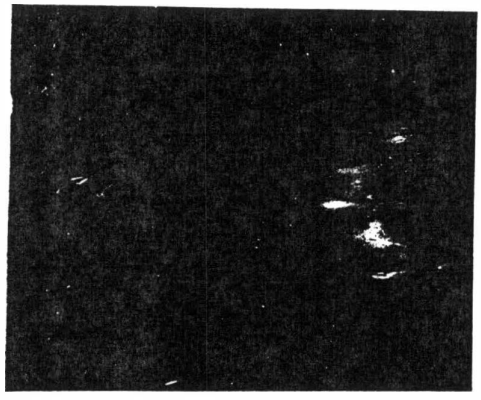

Fig.5. Typical topogram for the {100} plane of a cubic sodium tungsten bronze single crystal before experiment. No positive result.

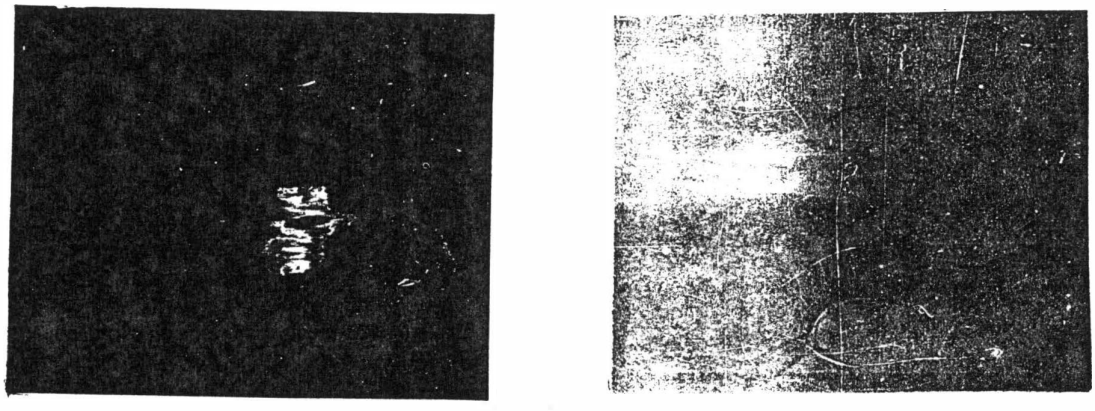

a b

Fig.6. Topograms for the same {100} plane of a single crystal before (a) and after (b) experiment.
During the experiment the crystal stopped showing neutron emission.

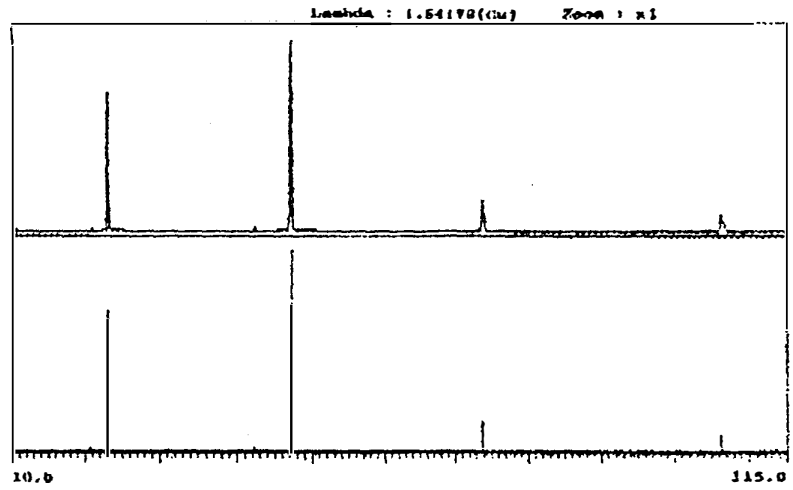

Fig.7. Typical X-ray diffraction pattern for the {100} plane of a cubic sodium tungsten bronze single crystal grown from imperfect seed (before experiment). No positive result.

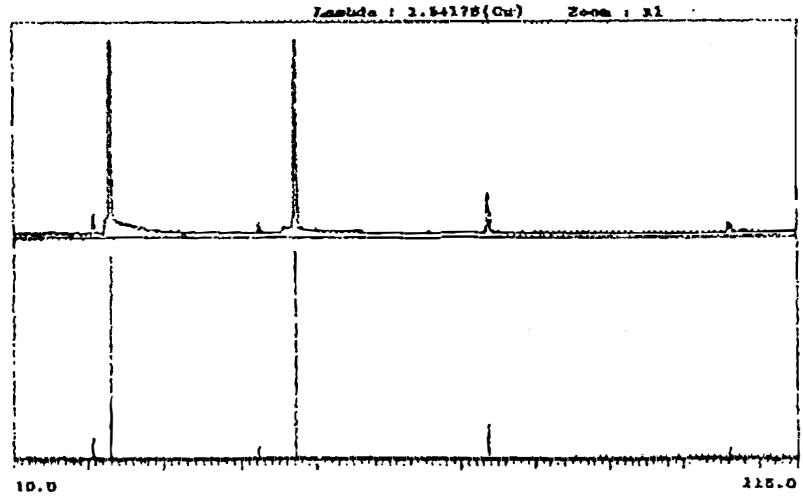

Fig.8. Typical X-ray diffraction pattern for the {100} plane (subjected to polishing and etching) of a cubic tungsten bronze bronze single crystal before experiment. No positive result.

Fifth International Conference on Cold Fusion
9-13 April, 1995 - Monte Carlo, Monaco
ICCF5 ©1995

Search for ^4He Production from Pd/D_2 Systems in Gas Phase

E. BOTTA[a], R. BRACCO[b], T. BRESSANI[a], D. CALVO[a], V. CELA[b], C. FANARA[a], U. FERRACIN[b], F. IAZZI[c]

[a] Dipartimento di Fisica Sperimentale dell'Universita' and I.N.F.N., Sezione di Torino I-10125 Torino (Italy)

[b] FIAT COMPES I-10152 Torino (Italy)

[c] Dipartimento di Fisica del Politecnico and I.N.F.N., Sezione di Torino I-10129 Torino (Italy)

Abstract

We describe the performances of an apparatus consisting of a cell containing a Pd sheet loaded with D_2 in gas phase coupled to a high resolution Q-mass spectrometer. The loading ratio α = D/Pd is increased by applying a constant electric field along the Pd sheet. α is carefully measured by means of the electric resistance variation and of the thermodynamic parameters. In one experiment a signal corresponding to ^4He production was observed.

1. Introduction

Since 1989 our Group (TOFUS-INFN Torino) is strongly engaged in the search of unambiguous signals of nuclear ashes from Cold Fusion devices. Our first effort was oriented towards the design, construction and operation of a rather sophisticated neutron spectrometer. The method we adopted to detect neutrons was double scattering among two segmented hodoscopes of plastic NE110 scintillators (60 elements in total). Time-of-flight and localization techniques allowed us to achieve an energy resolution of 1.0 MeV FWHM for 2.5 MeV neutrons, an efficiency of 2.5 10^{-4} and a powerful and reliable rejection of background due to cosmic rays and of environmental noise. Performances and technical details are given in Refs. [1÷4]. By means of this spectrometer we studied the neutron emission from cells containing Ti and Pd shavings loaded with D_2 in gas phase and submitted to thermal cycles. Temperatures, pressures and loadings were adjusted in such a way to cross a phase transition line during a cycle. 2.5 MeV neutron emission was observed in different runs, with a maximum statistical significance of 5σ [5÷6].

However, the measured neutron fluxes (from ~1 to ~0.1 neutrons/s·gr) were very low, fully inconsistent with the excess power reported by several other experiments. We decided then to concentrate our further efforts on the detection of ^4He, which seemed to be the nuclear ash produced at a rate consistent with the excess power [7÷9]. To this purpose we designed and constructed an experimental device able to measure on-line the ^4He content of gas mixtures from Cold Fusion cells by means of high resolution Q-mass spectrometry. We report in the following the performances of the experimental set-up, the characteristics of the cell and finally the results so far obtained.

2. Experimental set-up

Fig.1 shows a sketch of the apparatus. The purpose of the design was to perform all the operations (filling of the cell, use of calibrated volumes, H_2 and D_2 reduction by means of Ti getter to enhance the ^4He percentage, gas spilling from the cell to the spectrometer, ..) with one circuit. All the components were of Stainless Steel. In such a way we reduced at minimum the possibility of contamination of ^4He from atmosphere, which seemed to be a critical point in other experiments [7,9]. Since we had to operate with different parts of the circuit at once, pressures and temperatures were monitored by several gauges (K-type thermocouples (±1°C), Pt thermoresistances (±0.5% in the range 0÷100 °C) and cold cathode pressure transducers (±5%)).

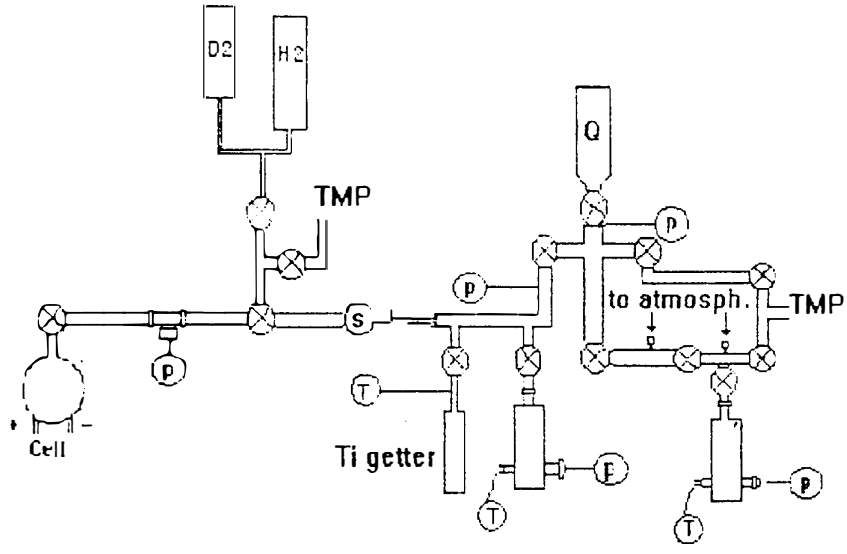

Fig.1 Scheme of the experimental set-up (p=pressure gauges, T=temperature gauges, TMP=turbomolecular pump, S=leak valve, Q=spectrometer)

The volumes of the different parts of the circuit were carefully measured by means of gas expansions from a 300 cc calibration volume. Error on each volume is less than ±2%. Vacuum in the circuit was maintained by means of a turbomolecular pump (TMP), and was typically 10^{-6} mbar.

The Q-mass spectrometer is an ULVAC HI-RESOM 2SM, able to analyze masses of gases both in high resolution and low resolution modes. In the first mode the mass resolution at M/e=4 is $M/\Delta M$ = 200 (10% P.H.). Fig.2 shows the peaks corresponding to $^4He^+$ and D_2^+, obtained with a calibration mixture. When used to analyze the gas composition from a Cold Fusion cell, the D_2 (or H_2) percentage, which is overwhelming, must be drastically reduced before immission into the spectrometer. To this purpose we used a getter pump, filled with 24 g of Ti sponge, well activated under vacuum and at ~ 600 °C before use. We measured in several runs the efficiency

of such a device and we found that after about 30 minutes all the content of D_2 (or H_2) was absorbed, within the precision limit due to the residual pressure.

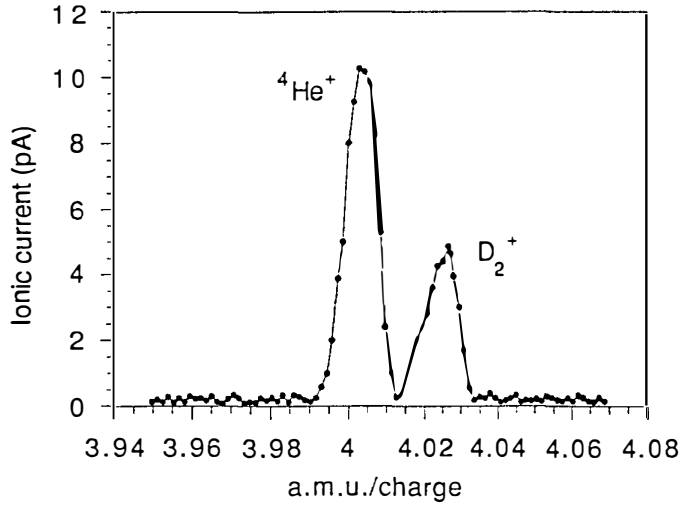

Fig.2 - Peaks due to $^4He^+$ and D_2^+ obtained with a calibration mixture.

3. The Cold Fusion cell

The cell was machined in Al. We used Pd sheets, supplied by Goodfellow (PD000262, 99.95% purity), of dimensions $(8 \cdot 1 \cdot 5 * 10^{-3})$ cm^3. At NTP, the maximum loading ratio α = D/Pd that can be reached is 0.67. Among the methods suggested to increase locally α beyond the thermodynamical limit, electromigration seems to be quite effective. It has been in fact known since long time [10] that protons embedded in a Pd lattice migrate and accumulate near the cathode when a weak electric field is applied through the metal. To this purpose we clamped the Pd sheet among two massive Cu electrodes and an intense electric current (up to 200 A) could circulate in the sheet. To ensure a better electric contact and also in order to have a well defined surface barrier, both ends of the Pd sheet were gold plated (6÷15 μm thickness) for a length of 1.5 cm. The effective surface of Pd exposed to the D_2 atmosphere was then 10 cm^2. From the value of the specific resistance of Pd at $\alpha = 0$ it is easily seen that with a current of 50 A circulating in the sheet the potential drop between the electrodes is 1.25 V, corresponding to an electric field of 0.25 V/cm. Higher fields could be more effective, but the temperature increase due to Joule heating of the sheet is prohibitive for maintaining a high value of α. Thermal dissipation was ensured by clamping in contact the free lateral surfaces of the Pd sheet with the lateral surface of the cell, cooled by a thermostatized (± 0.5°C) water flow on one side, by a massive Al heat dissipator on the other side. Aluminum surfaces were anodized (~ 20 μm thickness) in order to ensure a good electric insulation. The temperature at the center of the Pd sheet was continuously monitored by a K-type thermocouple (±1°C). The temperature of the gas in the cell was continuously monitored by a Pt thermoresistance (±0.5% in 0÷100 °C range) and its pressure was measured by an absolute pressure gauge (±0.1% F.S.).

Fig.3 shows the increase ΔT of the Pd sheet temperature with respect to the temperature of the water for different values of the circulating current. It can be seen

that at 120 A ΔT is ~ 100 °C, and the Pd was rapidly desorbing D_2. Following a long experimental study, we decided to use currents not exceeding 70 A. The measurement of α is of paramount importance in Cold Fusion experiments. It can be measured by means of thermodynamical parameters of the gas (p, T, V), or by the variation of the resistance of the Pd sheet. The ratio $R(\alpha)/R(0)$ at constant T is a bell-shaped function of α, well parametrized by the fifth order polynomial: $(1 + 3\alpha - 15.13\alpha^2 + 44.16\alpha^3 - 49.12\alpha^4 + 17.58\alpha^5)$ [11].

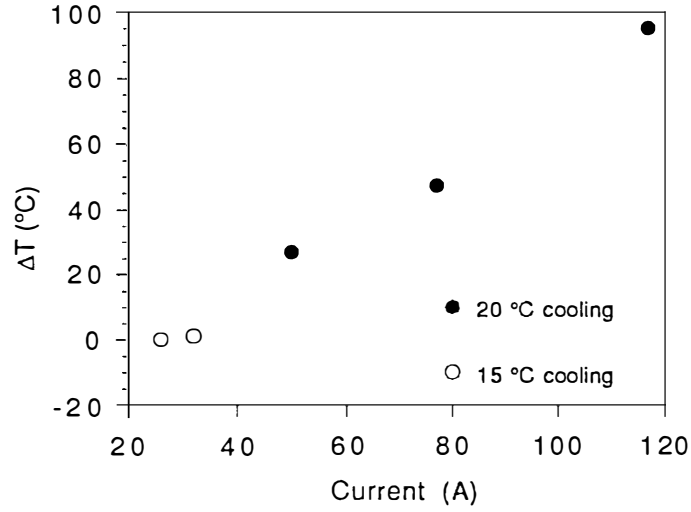

Fig.3 - Increase of the temperature of the Pd sample as a function of the circulating current.

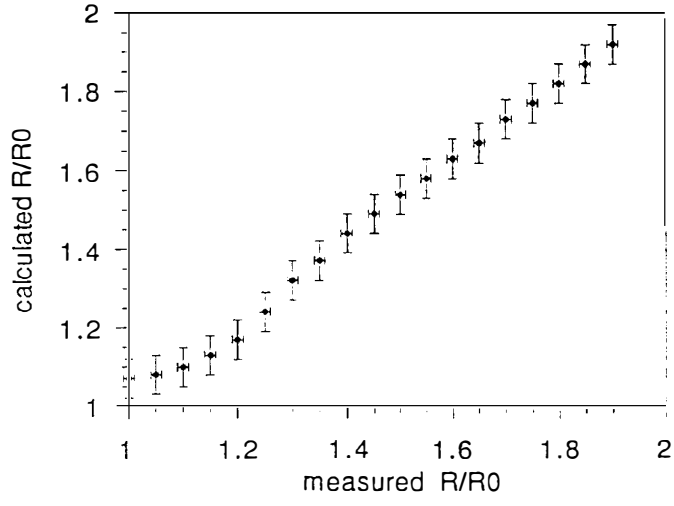

Fig.4 - Correlation between the measured values of $R(\alpha)/R(0)$ and the calculated ones (see text).

We used both methods to determine α in our experiment. Fig.4 shows the correlation between the measured values of $R(\alpha)/R(0)$ and those evaluated by means of the polynomial, in which the values of α were taken from the thermodynamical measurements. Within the errors, a satisfactory agreement is observed.

However we notice that both measurements provide α integrated over the full volume of the sheet, including the gold plated ends. At present we do not have direct measurements able to ascertain local enhancements of α. To this purpose a simple model taking into account the absorption , the diffusion and the mobility under application of the electric field of the deuterons into the Pd lattice was developed [12]. The prediction of the model was that α integrated was very slowly increasing with time whereas locally α could reach values exceeding 1, at the cathode, after about one week.

An indirect proof of this behaviour was that two Pd sheets broke just near the cathode, at high currents, and two others showed a local darkening, due to the carbonization on a small Vetronite insulator in contact with the cathode, after long runs at low current. For these four cases we had evidence for a local increase of temperature near the cathode.

4. Experimental results

Table 1 summarizes the conditions corresponding to the different runs, employing five different Pd sheets. The first three sheets were used mostly to study the effect of the different parameters, in particular the electric field, on α. We reached the following conclusions:

1) electromigration seems to be effective both in getting a faster loading of D_2 into Pd below $\alpha = 0.67$ and in exceeding the above value;
2) the effect is more evident with the increase of the pressure;
3) the temperature of the Pd sample must not exceed 70°C;
4) surface treatment helps the loading of D_2.

Pd Sheet N.	Vol. Lxlxδ cm^3	Surface Treatm.	Gold Thick.	Run Time (hour)	P Imm. (bar)	Max α	Analysis of Gas	^4He Excess
1	7.99x0.99 x47*10^{-4}	N	Y 15 μm	74.5	1.117	0.48	N	
2	7.99x0.99 x47*10^{-4}	N	Y 15 μm	91.5	1.566	0.67	N	
3	8.0x1.0 x52*10^{-4}	N	Y 6 μm	1159	1.63	0.74	N	
4	8.0x1.0 x52*10^{-4}	N	Y 6 μm	504	1.696	0.67	Y	N
5	7.98x0.96 x50*10^{-4}	Y HNO_3	N	699	1.564	0.69	Y	Y

Table 1. Summary of the runs.

Fig.5 shows the results of two runs. In the first one (a) the application of the current seems very effective in the last part of the run, after a short period during which we performed some rapid variations of the electric field (not shown in Fig. 6a). However,

α integrated did not reach the thermodynamical limit of 0.67. In the second one (b) the electric field was applied after a long time, during which the sample of Pd was loaded up to $\alpha = 0.67$. At this time, the application of an electric field of 0.25 V/cm produced a constant increase of α, up to a final value of 0.75, corresponding to a $\Delta\alpha/\Delta t$ of $(6.9\pm0.2) * 10^{-4}$ hour^{-1}. At a certain time (during a week-end) the acquisition system

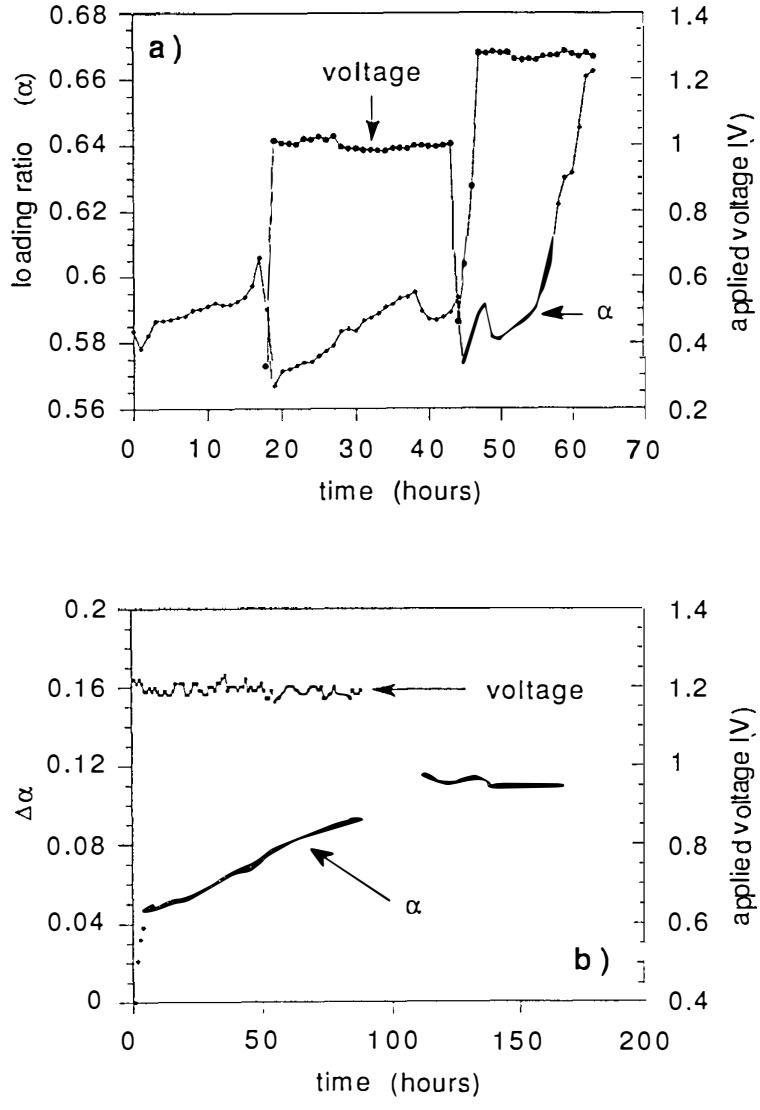

Fig.5 : a - Measured values of α (lower curve) and of the applied voltage (upper curve) as a functions of time.

: b - Measured values of α beyond the thermodynamical limit $\alpha = 0.67$ (lower curve) and applied voltage (upper curve) as a function of time.

went down, and we do not have the record. After restart, and switch off of the electric field, α kept constant at 0.75 for more than two days.

For the last two samples, we performed an analysis also of the ^4He content in the gas of the cell after ~ 500 hours of run. The second sample showed at the end a signal corresponding probably to the production of ^4He. Fig.6 shows the spectrometer scan around M/e=4, before and after the immission of the gas from the cell. It can be seen

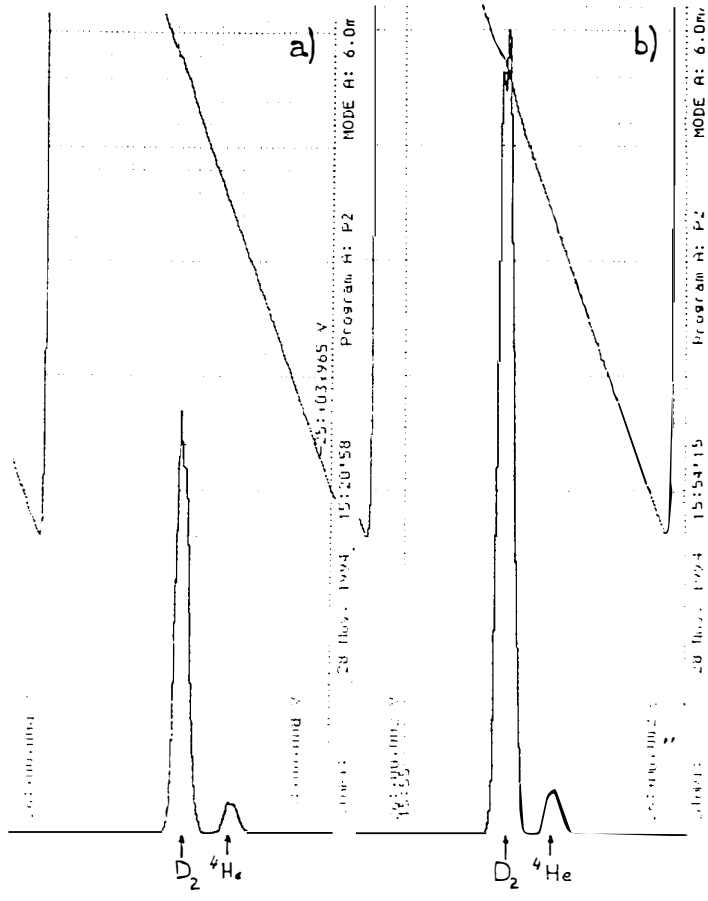

Fig.6 - Spectrometer scan around M/e=4 before (a) and after (b) the analysis of the gas sample from the cell.

that the peak corresponding to ^4He is increased by 25-30%, whereas the residual pressure is lower by ~ 15%. We remind that in mass spectrometers the net number of ions present is proportional to the ratio peak/(residual pressure). We may exclude contamination from the atmosphere. Scans in the low resolution mode, performed before and after the immission, showed that all the peaks corresponding to higher values of M/e were at same level or lower. Apart the obvious case of D_2^+, $^4He^+$ was the only one showing an increase. However the circumstances of having a significant background even before the immission is somehow disturbing.

In the hypothesis that the 25% increase of the peak is real, it would correspond to ~ $3*10^{10}$ ^4He atoms in the analysis volume of the Q-mass spectrometer and to $7.5*10^{16}$ ^4He atoms in the total volume of the cell, in the very semplified hypothesis that the ratios of the partial pressure of ^4He to the total pressure in the cell volume and in analysis volume are the same.

The above number of the ^4He atoms must be considered as un upper value, since the effect of the different pumping rate of the TMP for different gases (even a few units) has not been taken into account. For this reason we have not quoted errors, and we will not do it in the following.

Converting the numbers of ^4He ions into power due to the reaction d+d -> ^4He+23.8 MeV, we obtain an average value of about 1 watt for three days, too weak to be signalled by an increase of temperature of the cooling water of the cell. The average specific power is 25 watt/cm^3. However, since the profile of α along the Pd sheet is expected to be peaked near the cathode, and we may quite reasonably expect that Cold Fusion occurs in regions with high α, specific powers larger by at least one order of magnitude may be deduced.

The neutron spectrometer was active during these runs. No significant peak corresponding to 2.5 MeV neutrons was observed. The upper limit is 0.4 neutrons s^{-1} gr^{-1} at 1 σ level. The ratio $^4He/n$ is then larger than 10^{12}.

We stress again that all the above considerations follow from the hypothesis that the observed increase of the ^4He peak is not an instrumental artifact, a possibility that looks remote but cannot be excluded.

4. Conclusions

First round of runs of a novel Cold Fusion cell, with gas loading of D_2 assisted by electromigration, looks very promising. The cell is directly coupled in vacuo to a high resolution Q-mass spectrometer. In one experiment production of ^4He was observed. Improvements on the cell design (higher pressure of the loading gas, control of the temperature at both ends of the Pd sheet) were performed and we intend to start a new series of runs, both with H_2 and D_2, to confirm without doubts our observation.

Acknowledgments

We ackowledge Dr. Eng. F. Lanfranco for his continuous encouragement.

References

1. G.C.Bonazzola et al.,"A Large Area Neutron Detector Based on Double Scattering" *Nucl. Instr. Meth.*, **A299**, 25 (1990).
2. M.Agnello et al.,"Improvement of the TOFUS Apparatus", *The Science of Cold Fusion*, Conf. Proc. 33, 249, SIF, Bologna (1991).
3. F.Benotto et al.,"The Trigger of the TOFUS Detector", *IEEE Trans. Nucl. Sci.*, 39, 838 (1992).
4. M.Agnello et al.,"Performances of a Method of Reconstructing the Energy of Neutrons Detected by a Double Scattering Spectrometer", *IEEE Trans. Nucl. Sci.*, 39, 1270 (1992).
5. T.Bressani et al.,"Observation of 2.5 MeV Neutrons Emitted from a Titanium-Deuterium System", *Il Nuovo Cimento*, **104A**, 1413 (1991).
6. E.Botta et al.,"Measurements of 2.5 MeV Neutron Emission form Ti/D and Pd/D Systems", *Il Nuovo Cimento*, **105A**, 1663 (1992).
7. M.H.Miles et al.,"Heat and Helium Production in Cold Fusion Experiments", *The Science of Cold Fusion*, Conf. Proc. 33, 363, SIF, Bologna (1991).
8. E.Yamaguchi and T.Nishioka."Direct Evidence for Nuclear reactions in Deuterated Palladium", *Frontiers of Cold Fusion*, 179, Universal Academy Press, Tokyo (1993).
9. D. Gozzi et al.,"Excess Heat and Nuclear Product Measurements in Cold Fusion Electrochemical Cells", *Proceedings: Fourth International Conference on Cold Fusion*, **1**, 2-1, EPRI, Palo Alto (1994).
10. A. Coehn, *Z. Elektrochem.*, **35**, 676 (1929).
11. M.C.H.McKubre, private communication
12. C.Fanara et al., private communication

Fifth International Conference on Cold Fusion
9-13 April, 1995 - Monte Carlo, Monaco
ICCF5 ©1995

High Energy Phenomena in Glow Discharge Experiments

A.B. Karabut, S.A. Kolomeychenko, I.B. Savvatimova

Scientific Industrial Association "Luch"
24 Zhelesnodorozhnaya St., 142100 Podolsk, Moscow Region.
Russian Federation

Abstract

The experimental results of the nuclear product registration are presented in this paper. In our previous experiments with glow discharges in deuterium [1, 2,3] excessive heat release, neutron, gamma and charged particle emission have been observed. New data on emission of radiation (neutrons, gamma and x-rays, heavy charged particles, fast electrons) and on electric processes near the cathode provide clearer understanding of the specific nuclear processes involved into the reported observations. A possible mechanism for the initiation of these reactions is suggested.

1. Introduction

Two accepts of the research were important. There were authenticity of experimental results, use various kinds of physical measurements, what is important for to reveal possible mechanism of high energy process.

2. Methods

A glow discharge device [3] filled with deuterium, hydrogen or inert gases was used. Cathodes were made of Pd, Zr, Nb, Mo and other materials. The typical gas pressure in the chamber was 2-10 Torr, the discharge voltage 200-600 V and the discharge current 5-100 mA. A schematic diagram of the experimental device is given in Fig. 1.

Gamma measurement

The gamma-measuring system consisted of a liquid-nitrogen cooled Ge-Li detector, amplifier and AMA-3 multiscaler on-line with a microcomputer. Detector signals were accumulated by the multiscaler and then recorded digitally. The measuring procedure included gamma background registration before the experiments and gamma spectra registration during and after the experiments. The registration time for one spectrum was 10^4-10^5 s. The system was repeatedly calibrated against reference sources (^{241}Am, ^{235}U, ^{22}Na, ^{60}Co, ^{40}K, ^{208}Tl).

Recently we upgraded detector lead shielding significantly and focused on the gamma counting over extended periods up to 65 hours after

discharge termination. This approach excludes a noise from electric pick-ups, provide more counts for channel, and, therefore, better signal-to-background ratio.

It appeared that 80-90 percent of radiation is emitted from the vacuum chamber itself rather than from the cathode. We measured this residual induced activity in two steps. First, gamma spectrum was registered after discharge termination, and background was registered after 3 day (or more) break in the experiments. Then all counts were summed over the energy range from 60 to 1500 keV. The obtained results (Fig. 2) clearly indicate that residual activity signals stand out above all background fluctuations for Pd-D_2 system as well as for Pd-H_2, Zr-D_2, Pd-Ar systems.

Long-term (15-65 hours) gamma measurements after discharge termination were carried out in a variety of experiments. It was found that for a number of the cathode materials the gamma emission intensity stands out above background by 20-30% in the range of 50-1500 keV(Fig. 3a,b,c). The effect is well reproducible. The estimated intensity of the radiation is 10^2-10^3 s^{-1} within 10-15 hours after discharge switch-off. This residual radiation fades away in 2-4 weeks and the background spectrum goes back into its initial state. The radiation of this type is not observed after runs with certain cathode materials, for example Ag-D2 (Fig. 3d).Spectra, registered after discharge in Pd-H2, Pd-Ar, Ag-H2 systems are presented in Fig. 4.

Spectra, registered in run-time and after discharge termination, were processed by specially developed software. First, the spectrum was converted into energy units and normalized to account for the transducing efficiency of the detector and the geometrical factor. Background, treated in the same way, was subtracted from the spectrum. Randomly occurring negative overshoots were set equal to zero. Steady repeated patterns were considered to be gamma lines. In the background-corrected spectrum, lines were separated and selected by amplitude and width. Lines appearing at the same points on the energy scale over several spectra (from experiments with similar parameters) were selected. Then gamma lines were identified against databases of gamma emitting nuclides. One database contained a large block of data over the whole Periodic table [4]. Lines with energies close to the energies of exited levels of Pd nuclides are observed in all registered spectra.

Following the method, reported in [7] for short-lived isotopes, we constructed possible nuclear reactions with β^- and β^+ decays. Some of the elements (e.g., Cd, In, Sb, Sn), which could be involved into these reactions, were detected by direct methods [6].

Neutron registration

The results of the neutron registration were reported in our early works [1,2]. The following methods were used: beta activation of Ag, nuclear reactions (^{3}He and ^{10}B detectors), recoil proton registration in photoemulsion.

In the recent experiments average values of neutron production were registered over longer run-times of 10^3-10^4 s. Four ^{3}He detectors were used. They were placed into the moderator which thickness varied from 5 to 12 cm for different detectors. It appeared, that neutron signals varied from 5

to 20 V, while the gamma signals from ^{60}Co with E~1.3 MeV were about 1V. To minimize the noise, the counter discriminated only signal above 2.5 V.

The system was calibrated against a Pu-Be source (10^4 s^{-1}).The average rate of neutron production stands out above a background noise in a great variety of experiments. The experimental conditions with corresponding values of neutron production are presented in the Table 1. Increase in the neutron production within 10-30 minutes after discharge termination is observed repeatedly in these experiments.

TABLE 1

NEUTRON PRODUCTION VS. EXPERIMENTAL CONDITIONS

Cathode material and working gas	Neutron production ± 3n, s^{-1}			
	10-15 mA	20-30 mA	50-60 mA	after switch-off
Pd, H_2	8-10			10-11
Pd, D_2	12-14	11-12	11-12	10-12
Zr, H_2	6-7	5-6		8-9
Zr, D_2	10-11	11-12	11-12	10-11
W, H_2	8-9	□	□	
W, D_2	5-6	6-8	10-12 (100 mA)	5-6
Nb, H_2	5-6	□		
Nb, D_2	5-6	9-11	9-11	5-6

In some experiments with the specially designed cathodes the neutron counter indicated values corresponding to the neutron production of 10^4 s^{-1} with short "neutron flashes" up to 10^7 s^{-1}. But we are not sure yet that neutrons are responsible for such signals.

Heavy charged particles registration

Previously we registered charged particles by CR-39 polycarbonate track plates and by SSB detector with a set of degrading foils [3]. Recently we used two channel measuring system providing more reliable results. The system included two semiconductive Si-Au detectors, one with 10 μ Al screen, the other with 18 μ Al screen. The signals from the detectors were fed into the system, consisting of two preamplifiers, two amplifies (BUI-3K), two multiscalers (AMA-3). The signals after amplifier were visually controlled using an oscilloscope (S9-27). The signals were occasionally washed out by the noise, when generation of high voltage pulses began under certain conditions. We did not record the signals in this case. Control experiments were conducted to evaluate the influence of an optical and electric noise on the signal. In these experiments the detector window was shielded by 2 mm sapphire plate or 0.1 mm aluminum foil. Noise signals corresponded to energies less than 300 keV for all experimental conditions.

Both channels register the signal simultaneously. Type and energies of particles are determined by the energy shift between the two spectra. Judging by the recorded spectra, He, Li, B, C nuclei with energy of 5-6 MeV are observed (Fig. 5,6,7,8).

Registration of fast electrons

We used x-ray film RT-1V with various degrading screens to register x-rays and fast electrons. The films were exposed during run-times of 4000-15000 s. The film exposure was analyzed using a densitometer. In our experiments the film exposure can be caused by gamma, x-ray or fast electron emission. The results are still preliminary and the contribution of each specific component is not evaluated yet, but the results of the probe measurements (see below) indicate presence of electrons

The x-ray films were placed inside and outside the vacuum chamber. Inside the chamber the films were placed at the upper flange, at the bottom flange and in the middle of the chamber, so that they faced the cathode. For these films we applied as attenuating screens the following materials: 70-80 μ black paper, 6 μ polymeric film coated with 2 μ aluminum, aluminum (0.1, 1, 2, 3 mm), 2 mm lead. Outside the chamber films were placed on the bottom and upper flanges, and on the chamber wall. For these films an attenuator consists of 5 mm steel (chamber wall).

The films placed inside the chamber show two types of exposure: uniform exposure and local spots. The reason for the uniform exposure can be diffusive emission of gamma rays or electrons. For the film with step screen (aluminum plate with thickness of 1,2,3 mm) greater exposure is observed under thicker layer of the attenuator. This multiplication effect can be associated with 200-300 keV gamma rays or with fast electrons with energies up to 1 MeV. Intense diffusive exposure was found under aluminum-coated polymeric film (2 μ Al + 6 μ polyester), with no exposure under black paper. This is a good indication of the intense emission of x-rays or 5-20 keV electrons.

The spot film exposure can be caused by electron beams. Energy of the beams depends upon the cathode material and the working gas. The beams pass through 100 μ aluminum in the case of palladium cathode (Fig. 9a), but the same screen stops the beams completely, when Nb cathode was used (Fig. 9b). Such beams can be electrons with energy from 200 to 500 keV. In the case of Zr cathode the beams penetrate through 5 mm steel of the chamber wall, and 2 mm lead, placed behind x-ray films, increases the film exposure significantly (Fig. 10). Such beams can consist of electrons with energies ranging from hundreds of keV to units of MeV.

The exposure spots are clear and non diffused in spite of long-term exposure (up to 15000 s). This indicates that quite intensive beams are emitted within short-term intervals. The other peculiarity of the beams is anisotropy. Most of the beams propagate upwards from the cathode, diverging in the 60° cone.

Electric probe measurements

Electric probe measurements were conducted to study high voltage pulses of a short duration which are generated in the discharge area. The consisted of Mo cylinder placed in quartz tube with one end open, the probe was placed at 1 mm from the cathode. The spacing between anode and cathode was 2-5 mm.

Probe, anode or cathode voltages were applied to a dual trace digital oscilloscope (S9-27) through a low inductance voltage divider. Current in the cathode circuit was measured by the same oscilloscope with a low inductance shunt. The maximum time resolution was 10^{-8} s.

The voltage divider was 490 KOhm metal-film resistors placed in series. Dividers of the described type were mounted using insulators at the bottom and upper flanges in the close vicinity of the probe, anode, cathode electric leads. Special tests were done to verify active character of the divider impedance.

It appeared that high voltage pulses are generated during glow discharge operation in most of the experiments. This effect is observed in deuterium and other gases. Pulse generation starts when current exceeds some critical value. Spontaneous separate pulses and batches of pulses are observed. The batch typically contains 10^2 pulses. The generation rate and the pulse amplitude depend on the cathode material. The pulse generation rate increases with increasing current density and reached 10^3 pulses per second in the case of Pd-D. The probe voltage reached $0.23.10^6$ V in pulses and corresponded cathode current bursts were tens of amperes. Leading edge was 35-40 ns and independent of the sort of gas (H2,D2,Xe,Ar).

Discussion

Judging by the time dependence of probe and cathode voltages and cathode current, the registered pulses are generated by the spontaneous release of bunches of 0.01-0.23 MeV electrons. It is estimated that there are 10^8-10^{11} electrons in a bunch. The line character of the probe voltage spectrum indicates that electrons have fixed energies and can be conversion electrons.

Another evidence of fast electron presence is blackening of x-ray film placed outside the chamber (Fig. 5). The part of the film covered by lead shielding shows nonuniform blackening, while the rest of the film is not exposed. It can be interpreted as multiplying of secondary gamma emission in the lead due to the bombardment by fast electron beams.

The energies of the registered electron beams correlate with the first nuclear levels, specific to the cathode material. For Nb cathode (E=30.4 keV) the beams are completely stopped by 0.1 mm aluminum, in the case of Pd (E= 280, 433, 511, 556 keV) they partially penetrate through the same screen. For Zr cathode (E= 919, 934, 1760 keV) electrons pass through 5 mm steel.

A possible mechanism of conversion electron release may operate in the following way. In a high density ion flux in a glow discharge, energy can be transferred from low energy ions (0.1-100 eV) into nuclei in the cathode material step-by-step in nonelastic collisions. It is necessary that nuclear levels (from low levels of neutron resonance type with energies of tens of eV) would have a lifetime longer than the period between two successive ion impacts. The resulting metastable excited levels of Pd release their energy (~500 keV) by conversion electrons and partially by a small amount of gamma rays.

This suggestion is confirmed by experiments with Ar and Xe where high voltage generation and x-ray film exposure are also observed. By our

estimation 0.1-10 per cent of the discharge power is transferred according to this mechanism. It means that under a flux of 10^{17} ion/sec 10^{10}-10^{12} excited to MeVs energy nuclei of Pd arise per second. Other possible variant can be suggested the phenomenon opposite to Mossbauer effect. Energy of oscillations of atomic lattice in local part cathode material (about 10÷8-10÷11 atoms) is transfered to one nucleus at resonance.

Under certain concentration of the excited nuclei in the cathode material and density of implanted deuterium up to 10^{22} cm^{-3} some nuclear reactions can occur, such as described in [5]. Earlier we supposed the possibilty of occurrence of nuclear reactions (5). But in experiments it has observed very few gamma-radiation (10÷7-10÷8) and a large amount (10÷15-10÷16) the impurities of individual elements (Na,Mg,Zn,Ni...) and much of excess heat. Hypothetically it can be explained by two reasons: 1- only stable isotopes are formed. 2- forming by-products transfer the energy and pulse some to atoms crystalline lattice of the cathode material (just as in Mossbauer effect).

Acknowledgment

Thanks to P. Hagelstein (M.I.T.), who participated in our experiments in January 1994, for helpful cooperation and fruitful criticism.

References

1. Karabut A.B., Kucherov Ya.R., Savvatimova I.B. Pisma v GETF (Sov. Tech. Phys. Lett.), v. 16, release 12, 1990, p 53-57.
2. Karabut A.B., Kucherov Ya.R., Savvatimova I.B. The Investigation of Deuterium Nuclear Fusion at Glow Discharge cathode. Fusion Technology, December 1991, v.20, #4, part 2, p. 924.
3. Karabut A.B., Kucherov Ya.R., Savvatimova I.B. Nuclear Product Ratio for Glow Discharge in Deuterium. 1992. Physics Letters A, 170, p.265.
4. F. W. Walker, J. R. Parrington, F. Feiner. Chart of the Nuclides. General Electric, San Jose, 1988.
5. Karabut A.B., Kucherov Ya.R., Savvatimova I.B. Possible Nuclear Reactions Mechanisms at Glow Discharge in Deuterium. Frontiers of Cold Fusion, Proc. of the Third International Conf. on the Cold Fusion, October 21-25,1992, Nagoya, Japan, University Academy Press, Inc., Tokyo, Japan, p165-168
6. Savvatimova I.B., Karabut A.B., Kucherov Ya.R. Cathode Material Change after Deuterium Glow Discharge Experiments. Proc. of the 4th International Conf. on the Cold Fusion, December, 1993, Hawaii, USA (to be published).
7. Karabut A.B., Savvatimova I.B., Kucherov Ya.R. Possible Products of Nuclear Reactions under Glow Discharge in Deuterium..Report on the the 4th International Conf. on the Cold Fusion, December, 1993, Hawaii, USA.

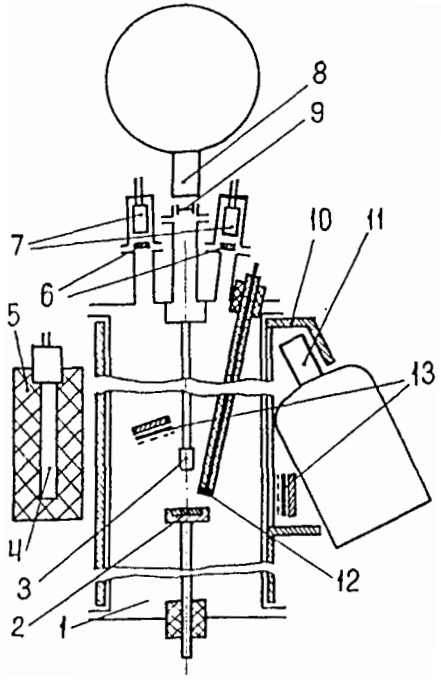

Fig. 1. Expermental device: 1-vacuum chamber, 2-cathode, 3-anode.4-He3 neutron detector, 5-moderator, 6-windows with attenuating fois, 7-Si-Au detectors, 8Si-Li detector, 9-Be window 10-lead shielding, 11-Ge-Li detector, 12-probe 13-x-ray film.

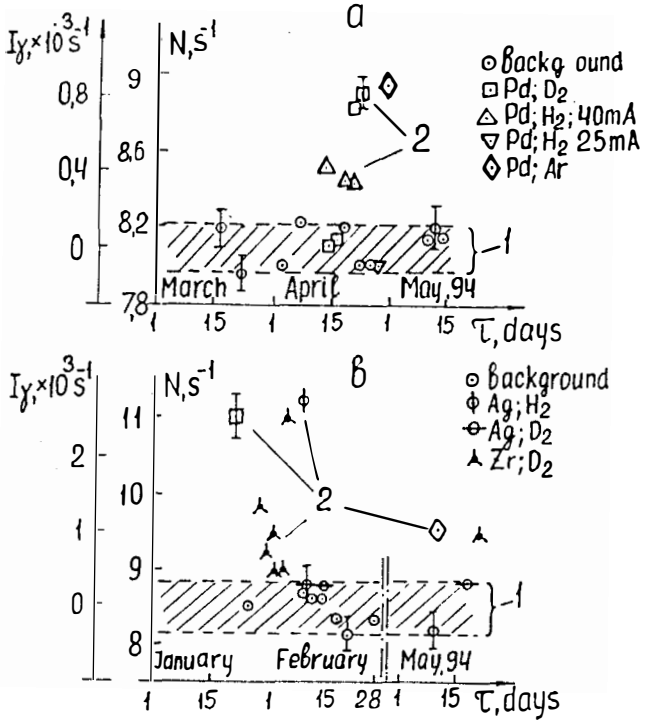

Fig.2. Gamma activity induced in the chamber after runs. N- total sum of the detector couts in the range 60-1500 keV. Iγ -calculated intensity of gamma emission. a-1,6 keV per channel, b-0,8 keV per channel.

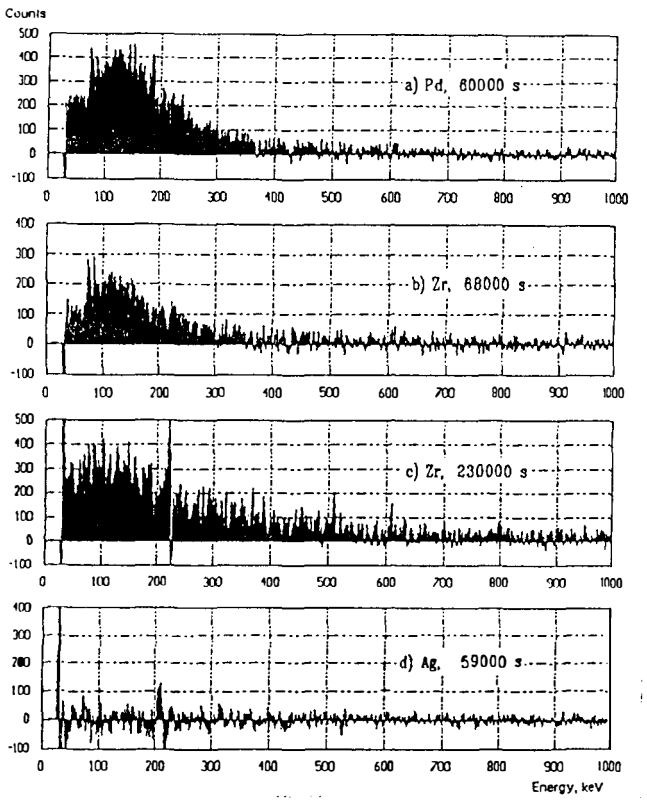

Fig.3. Background-corrected gamma spectra registered after discharge termination in the experiments with different cathodes (0,8 keV per channel).

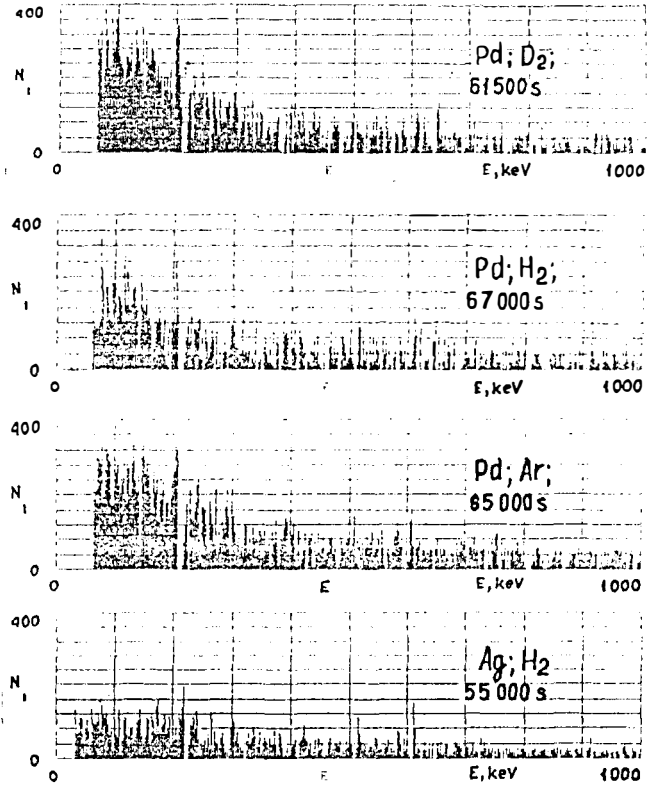

Fig.4. Background-corrected gamma spectra registered after discharge termination in the experiment with different cathodes and gases (1,6 keV per channel).

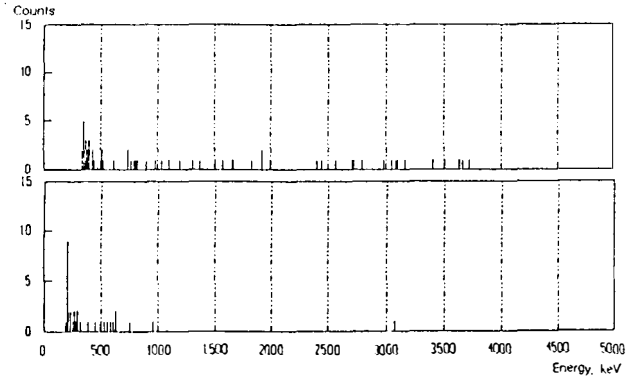

Fig.5. Spectra of heavy charged particles registered with different aluminum screens a- 10- μ, b- 18 μ, (total efficiency of Si-Au detector is 10-4). Pd cathode, D2, current 25 mA, time 1400 s.

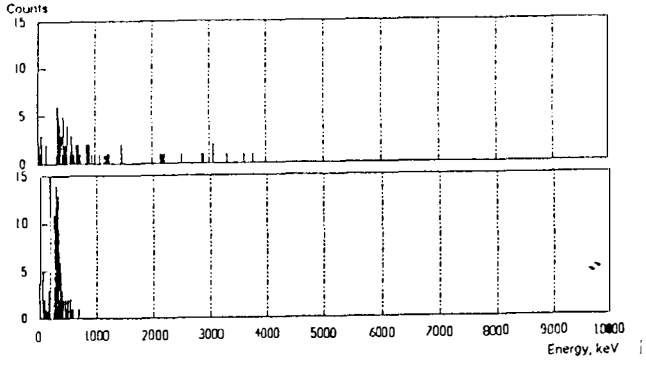

Fig.6. The same as above. Current 25 mA, time 1040 s.

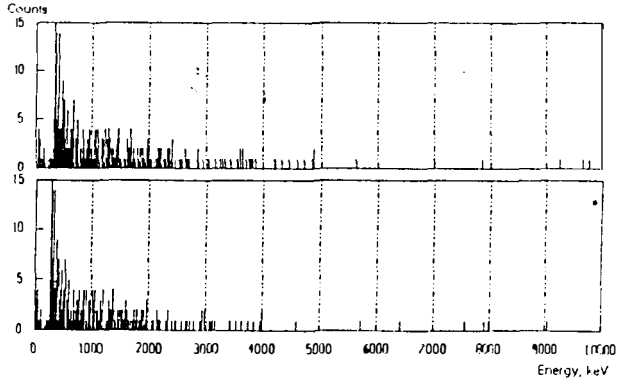

Fig.7. The same as above. Current 30 mA, time 1500 s.

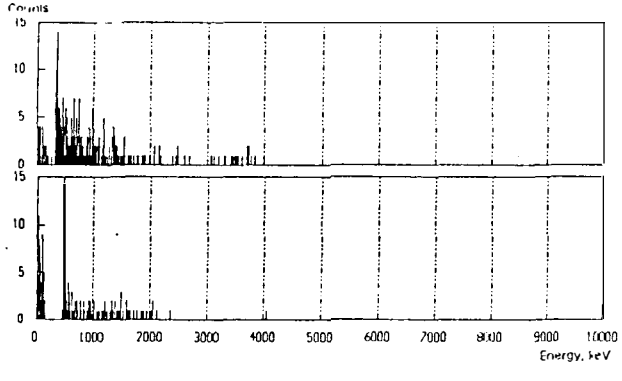

Fig.8. The same as above. Current 30 mA, time 2650 s.

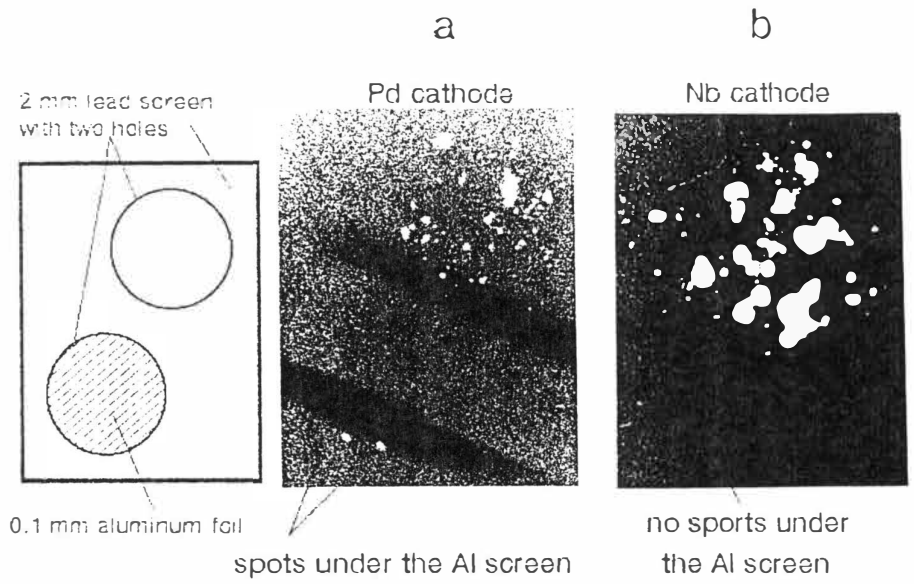

Fig. 9. Positive images of the films exposed inside the chamber with varios screens.

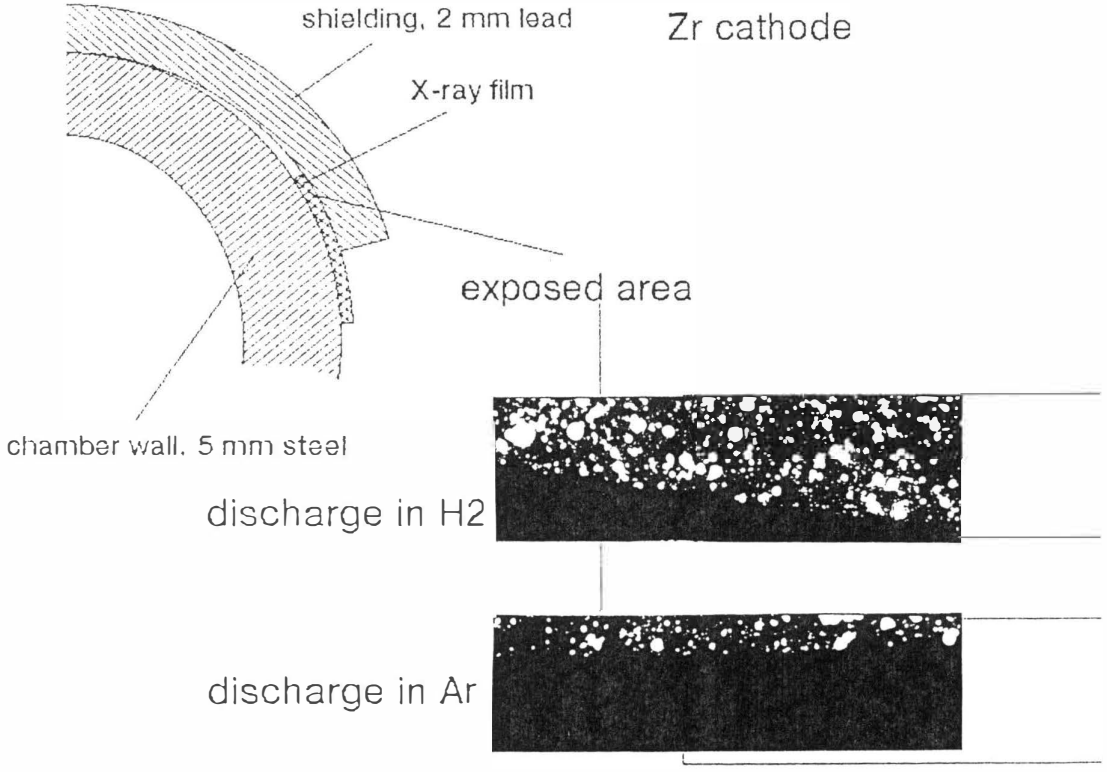

Fig. 10. Schematic diagram of registration of radiation emission outside er c an x-ray the the chamber using an x-ray films and positive images of the films.

Fifth International Conference on Cold Fusion
9-13 April, 1995 - Monte Carlo, Monaco
ICCF5 ©1995

D_2 release process from deuterated palladium in a vacuum

K. SHIKANO, H. SHINOJIMA, and H. KANBE
NTT Basic Research Laboratories
Nippon Telegraph and Telephone Corporation
3-1, Morinosato-Wakamiya, Atsugi-si, Kanagawa 243-03 Japan

Abstract

To enhance reproducibility of the phenomena taking place in deuterated palladium, we studied in detail the change in surface temperature, electrical resistance, and D_2 pressure during the release of D_2 from deuterated palladium in a vacuum. As a result, we categorized the temperature changes into three different types that were independent of coating materials. In almost all experiments, the resistance decreased and the D_2 pressure initially increased briefly and then gradually decreased in the D_2 release process. We also tried to simulate the temperature changes by calculating the balance between Joule heat and heat dispersion.

1. Introduction

Nuclear products of d-d reactions, such as ^{4}He, and an increased temperature have been observed when D_2 is released from deuterated palladium by the vacuum method[1]. To make these phenomena more reproducible and to make the reaction mechanism clear, we studied in detail the change in surface temperature, electrical resistance, and D_2 pressure during the D_2 gas loading into palladium, as well as the release of D_2 from deuterated palladium in a vacuum. Measurement of electric resistance during loading and release of D_2 was confirmed to be useful in monitoring the loading ratio. We measured the changes in surface temperature, electrical resistance and D_2 pressure during the D_2 release process and found that the temperature changes could be categorized into three different types. We also tried to simulate the changes in surface temperature by calculating the balance between Joule heat and heat dispersion such as enthalpy of D_2 release, radiant heat, and heat conduction.

2. Experiment

Figure 1 shows the samples preparation process. Samples were 30 x 30 x 1mm Pd plates. They were slightly etched by aqua regia and preheated at 400℃ for 2 hr in a vacuum before being loaded with D_2 gas in a chamber at room temperature or an elevated temperature. The loading ratio (D/Pd) was 0.60 - 0.65. One side of each deuterated plate was coated with manganese oxide or silicon nitride, and the other side was coated with a metal film (Au or Ag) . The sample was then placed in a vacuum chamber and heated by injecting currents while the chamber was evacuated by a turbo-molecular pump. Sample temperature, electrical resistance, and D_2 pressure were measured by thermocouples, the four-point probe method, and a vacuum gauge, respectively, as shown in Fig. 2.

3. Results and discussion

Availability of electrical resistance measurement

Figure 3 shows typical curves of electrical resistance and D_2 pressure during loading to Pd. Electrical resistance increases as D_2 pressure decreases during loading, and reaches a constant value after loading. The end of loading process can be determined by measuring electrical resistance. Figure 4 shows the dependence of the electrical resistance ratio (R/R_0) on the loading ratio (D/Pd) calculated from variations of D_2 pressure and Pd weight. As shown in the figure, the R/R_0 increases with an increase of D/Pd, and the

electrical resistance measurement was available to monitor the loading ratio in D_2 loading and release process.

Change in surface temperature, electrical resistance and D_2 pressure

Figures 5 a), b), and c) show electrical resistance and D_2 pressure during D_2 release caused by flowing electric current through the sample in a vacuum. In almost all experiments, after current started to flow, the resistance decreased, while the D_2 pressure initially increased briefly and then gradually decreased in the D_2 release process. However, we found that the temperature changes could be categorized into three different types and are independent of coating materials. In the first type, the temperature increases exponentially with time and reaches a constant value determined by the balance between Joule heating and heat dispersion. In the second type, the temperature rises above the balanced temperature after remaining low for several hours, and the pressure simultaneously falls. This change is similar to that reported before[1]. In the third type, there are some peaks in temperature that do not correlate with pressure. After these experiments, almost all samples were found to be bent. We also found that the surface temperature of Pd without loading increases as a simple exponential function of time and reaches a constant value, as shown in Fig. 5 d). This temperature change was the same in almost all samples in reheating by flow of electric currents after D_2 release.

Simulation of surface temperature changing

To find an explanation for the temperature changes, we tried to simulate the surface temperature change phenomenon by heat balance between Joule heat, enthalpy of D_2 release, radiant heat, and conduction of heat . The heat balance in this case is expressed as Eq. (1).

$$Cm(dT/dt) = [\text{Joule heat}] - [\text{radiant heat}] - [\text{conduction of heat}] - [\text{enthalpy of } D_2 \text{ release}]$$
$$= I^2[R_0\{1+a(T-T_0)\}(1+x)+R_S] - \varepsilon\sigma(T^4-T_n^4)S - k_0(1+10^{-3})(T-T_n)$$
$$-c\Delta H_d(x/t_h)\exp(-E_a/k_BT) \qquad (1)$$

C: specific heat, m: weight of Pd, R_0: resistance at temperature T_0, a: temperature coefficient of resistance, R_S: series resistance in the circuit, ε: emissivity, σ: Stephan-Boltzmann constant, T_n: chamber temperature, S: surface area of Pd, $k_0(1+10^{-3})$: temperature dependence thermal conductivity, ΔH_d: enthalpy of release, x: loading ratio ($=x_0 - {}_0{}^t x dt$), t_h: gas release time, $c\exp(-E_a/k_BT)$: temperature dependence of release process ($c=1.48\times10^5$, $E_a=0.434$ eV), k_B: Boltzmann constant.

Numerical solution using the Runge-Kutta-Gill method was used to simulate the temperature change. Figure 6 shows the typical results of simulation for changes of temperature, loading ratio (D/Pd), and electrical resistance ratio (R/R_0) under the condition of variable initial D/Pd and enthalpy of release (ΔH_d). It is found that the temperature changes depend on initial loading ratio (D/Pd), although reached temperatures determined by the heat balance are same, as shown in Fig. 6 a). In the case of Pd without loading (D/Pd = 0.0), the temperature change of Pd can be simulated, although the constant value that was calculated was different from the experimental result (Fig. 5 d). However, reproducing other temperature changes of deuterated Pd was difficult even though the D_2 release process was added to the experiments. We cannot explain these temperature variations. To make an accurate simulation, we must study the behavior of D_2 on the surface and measure the contact resistance change between the Pd and electric current probes in bending Pd. In addition to the above experiments, the same experiments should be performed for H_2 and the results compared with those of D_2.

4. Conclusion

We studied in detail the changes in surface temperature, electrical resistance, and D_2 pressure during the D_2 gas loading and D_2 release processes. As a result, we confirmed that the electrical resistance measurement can be used to monitor the loading ratio in D_2 loading and release processes. We also found that the electrical resistance and D_2 pressure initially increased briefly and then decreased gradually in D_2 release process in almost all experiments, while the temperature changes could be categorized into three different types and were independent of coating materials. We also tried to simulate the surface temperature changes by calculation of heat balance between Joule heat and heat dispersion. We concluded that the surface temperature change of Pd without loading could be simulated, but other temperature changes were difficult to simulate. We found that to explain temperature changes, the contact resistance change between Pd and electric current probes must be measured in bending Pd and the results of experiments for H_2 should be compared with those of D_2. We retained measurements of nuclear reaction products during the release of D_2 for future studies.

Reference

1) E. Yamaguchi and T. Nishioka, "Direct Evidence for Nuclear Fusion Reactions in Deuterated Palladium," *Proceedings of the Third International Conference on Cold Fusion*, Nagoya, October 21-25, 1992, p. 179, Universal Academy Press, Inc. (1993).

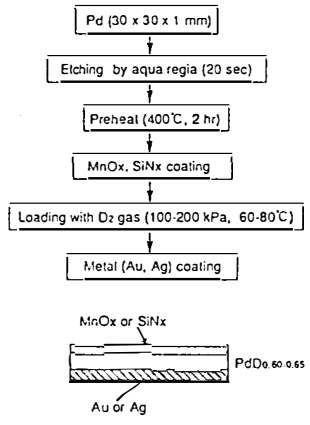

Fig. 1 Preparation of samples

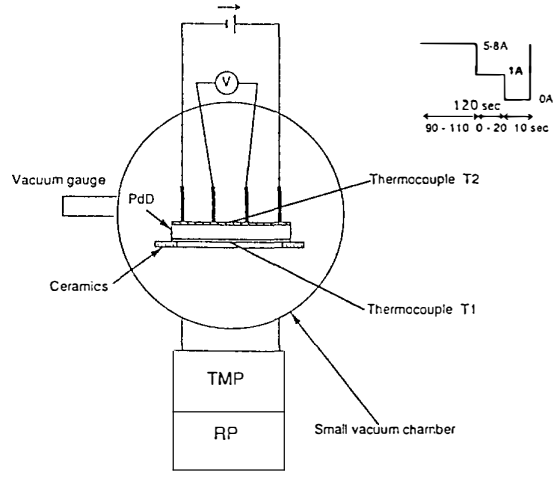

Fig. 2 Measurement system

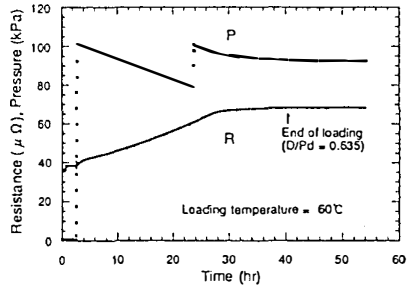

Fig. 3 Typical curves of electric resistance and D_2 pressure in loading to Pd

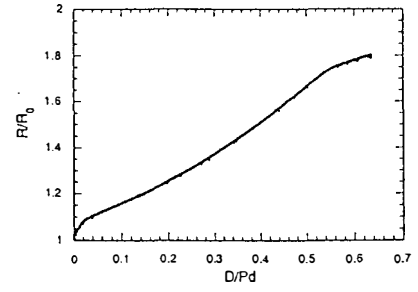

Fig. 4 D/Pd vs. R/R0

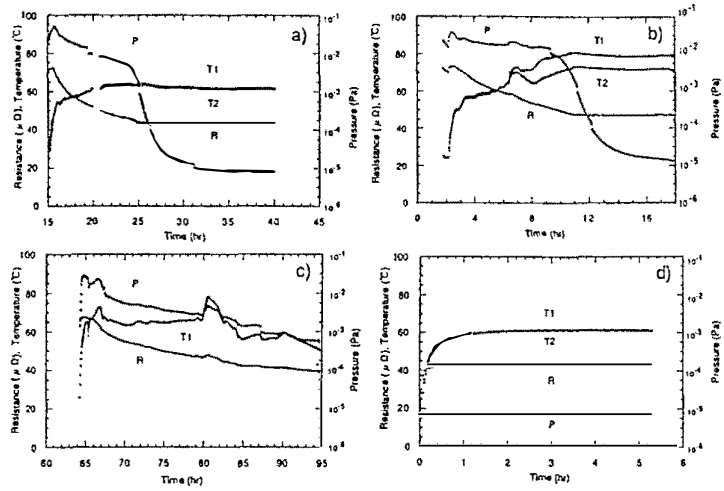

Fig. 5 Typical curves of the surface temperature, electrical resistance and D2 pressure during D2 release process in a vacuum.
(a) Type 1 (Sample: Pd), (b) Type 2 (Au/Pd/Au),
(c) Type 3 (MnOx/Pd/Ag), (d) Pd without loading.

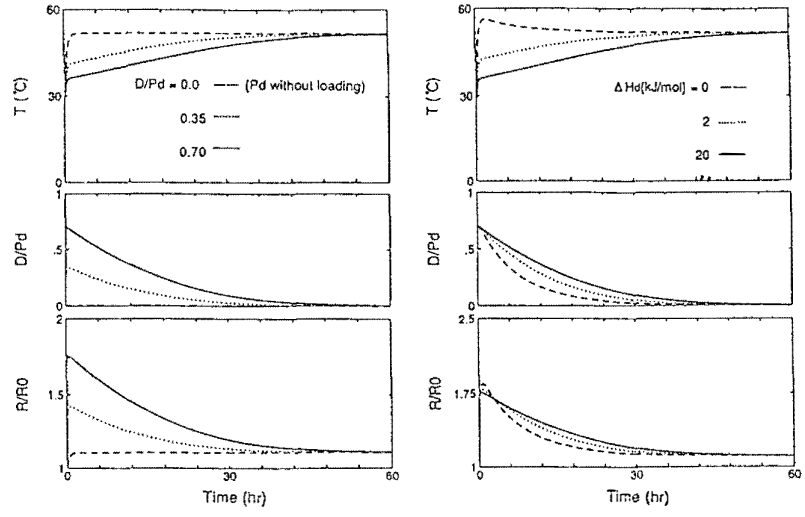

a) Dependence of temperature change on initial loading ratio (ΔHd is 20 kJ/mol)

b) Dependence of temperature change on ΔHd (Initial loading ratio is 0.70)

Fig. 6 Results of simulation by electric current flow at 7A

Fifth International Conference on Cold Fusion
9-13 April, 1995 - Monte Carlo, Monaco
ICCF5 ©1995

Studies of d-d Reactions in Deuterated Palladium by Using Low-Energy Deuterium Ion Bombardment

Hiroyuki SHINOJIMA, Takashi NISHIOKA,
Koji SHIKANO, and Hiroshi KANBE

NTT Basic Research Laboratories
3-1 Morinosato-Wakamiya Atsugi-Shi,
Kanagawa 243-01 Japan

1. Abstract

The cross sections and branching ratios of d+d reactions were measured as a function of deuteron energy by using low-energy deuterium ion bombardment. The branching ratio of d(d,^{3}He)n to d(d,p)t were found to be one to one at energies from 2.5 keV to 20 keV in the CM frame. The reation rate of d(d,p)t at 2.5 keV was four orders of magunitude less than that at 20 keV. These energy dependences were good agreement with those extrapolated from measurements of the d+d reaction which was derived by the high-enegy (mega-electron-volts) deuterium ion bombardments.

2. Introduction

E. Yamaguchi and T. Nishioka detected ^{4}He from deuterated palladium metals by using an "in vacuo" method,[1] thus indicating the possibility of nuclear fusion reactions occurring in condensed matter. However, the mechanism of the ^{4}He production from palladium metals has not yet been clarified, because it is confirmed in the high-energy region of deuterons that two reactions, d(d,p)t and d(d,^{3}He)n, are dominant in d+d reactions, and that the branching ratio (ρ) of d(d,p)t to d(d,^{3}He)n was one to one. Futhermore, the reaction cross section of producing ^{4}He is theoretically (and has been experimentally confirmed to be) less than 10^{-7} of those for d(d, p)t and d(d,^{3}He)n in the energy range above a few tens of kilo-electron-volts. It is very important to study d+d reactios in the low-energy region less than a few tens of kilo-electron-volts to clarify the possibility of ^{4}He production from palladium metals. The energy dependences of ρ and the cross sections in the low-energy region have not been examined experimentally.

We therefore measured the deuteron energy dependence of the branching ratios (ρ) and of the reaction rates by bombarding deuterated palladium metals with deutrons.

3. Experiment

The target sample was prepared by using the same procedures used in the ^{4}He-detection experiments.[1] One side of the deuterated palladium plate was coated with a 10-nm-thick MnO_x film and the other side was coated with a 100-nm-thick Au film in order to reduce D_2-release from the sample in vacuum. The loading ratio (D/P_d) was about 0.65. The experimental setup is shown in Figure 1. We bombarded deuterated palladium plates with deuterium ions (D^+,D_2^+) accelerated by 5 to 40 kV. The beam currents of D^+ and D_2^+ were about 10 μA and 17 μA, respectively. The deuterium beam was bombarded on the MnO_x side, and the beam diameter at the

sample position was 3 mm. Si-SSDs (solid states devices) and TPS-451S (Aloka Ltd.) were used for measuring charged particles and neutrons, respectively. The active thicknesses of the two SSDs were 300 μm and 100 μm, and the active area of each SSDs was 300 mm^2. The active area of the neutron detector was 20 cm^2. The conversion rate of the neutron detector was 5400 counts/μSV. The branching ratio (ρ), and the rates of d(d,p)t and d(d,^{3}He)n reactions were measured, as a function of the deuteron energy (E_d) in the CM frame, from 2.5 keV to 20 keV.

4. Results and Discussion

The energy spectrum of the charged particles detected during the deuteron bombardments at E_d=10 keV is shown in Fig. 2, and Figs. 3 and 4 show the energy dependence of the branching ratio obtained by comparing the proton and triton counts and by comparing the ^{3}He and netron counts, respectively. Each branching ratio was one to one throughout the deuteron energy range from 2.5 keV to 20 keV.

Figure 5 shows the energy dependence of the reaction rate (Γ_p (E_d)), which corresponds to the cross section ($\sigma_p(E_d)$) of d(d, p)t. This reaction rate Γ_p is propotional to the number of protons produced by d(d, p)t reaction at the incident deuteron flux of 1.0×10^7 counts/s, and at E_d=2.5 keV is four orders of magunitude less than that at E_d=20 keV. Note that this energy dependence can be achieved by the extrapolation of d+d reactions in the high-enegy region[2].

Figure 6 shows the deuteron energy dependence of d(d,^{3}He)n-reaction cross section. The cross section was estimated in the assumptions that the distribution and concentration of deuterons in the palladium metal were uniform and that all incident deuterons reacted in the region from the surface of the palldium to the deuteron penetration-depth at the energy. The cross section at E_d=5 keV is two orders of magunitude less than that at E_d=20 keV. This energy dependence of d(d,^{3}He)n cross section corresponded to the energy dependence of Γ_p.

Open circles and open triangles shows the experimental results obtained by using D^+ and D_2^+ beam, respectively in Fig. 3, 4, 5, 6. There was no difference between the experimental results for D^+ and D_2^+ bombardment if the incident deuteron energy was identical. The cluster effect,[3] so-called "cluster impact fusion," related to the bombardment of D_2^+ was not observed in the present work.

In conclusion, we investigated the d+d reaction driven by the deuteron bombardments with ion currents of a few tens of microamperes in the deuteron energy range above 2.5 keV. The cross sections and branching ratios of the fusion reaction did not differ from the values extrapolated from higher-energy bombardments. The new nuclear phenomena observed in condensed matter, however, remain to be studied.[4,5] We have to continue investigating d+d reactions in dense matter in the low-energy region (E_d < 2.5 keV). Accompanying high-resolution/high-sensitivity detection of ^{4}He/neutrons will give futher information on these reactions.

References

1. E. Yamaguchi and T. Nshioka, 1993, Frontiers of Cold Fusion, 170.
2. A. Krauss, H. W. Becker, H. P. Trautvetter, C. Rolfs and K. Brand, 1987, Nucl. Phys. **A465**, 150.
3. R. J. Beuhler, G. Friedlander, and L. Friedman, 1989, Phys. Rev. Lett. **63**, 1292.
4. J. Kasagi, K. Ishii, M. Hiraga and K. Yoshihara, 1993, Frontiers of Cold Fusion, 209.
5. S. Ichimaru, 1993, Rev. Mod. Phys., **65**, 255.

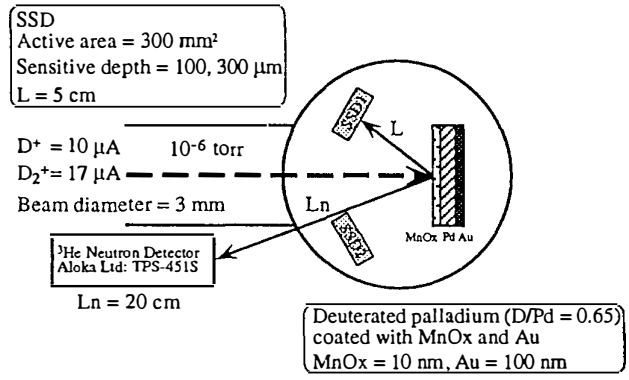

Figure 1. Experimental setup.

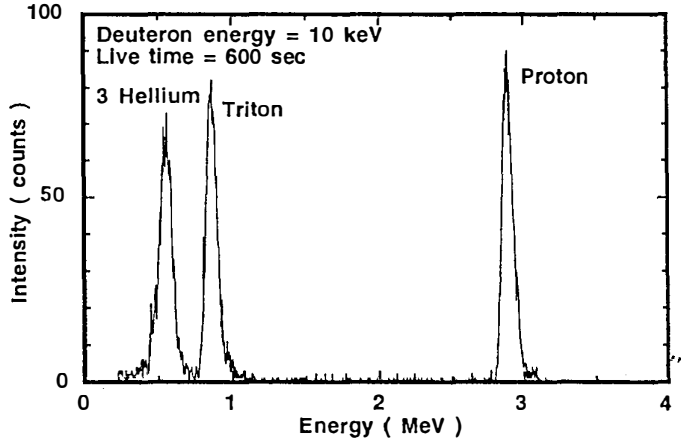

Figure 2. Energy spectrum in d+d reactions.

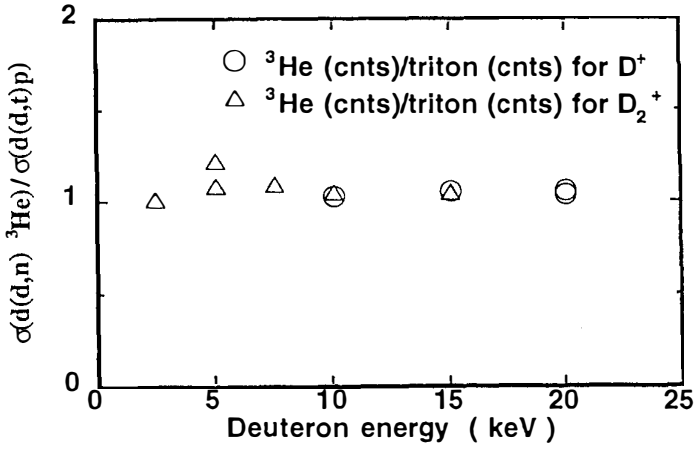

Figure 3. Energy dependence of the branching ratio obtained from proton and tritoncounts.

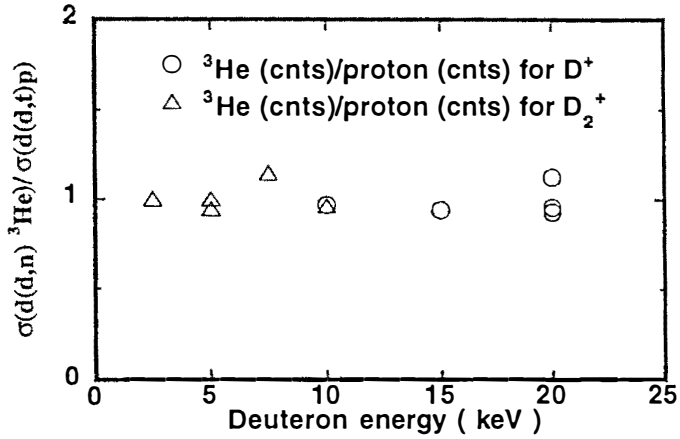

Figure 4. Energy dependence of the branching ratio obtained from ^{3}He and neutron counts.

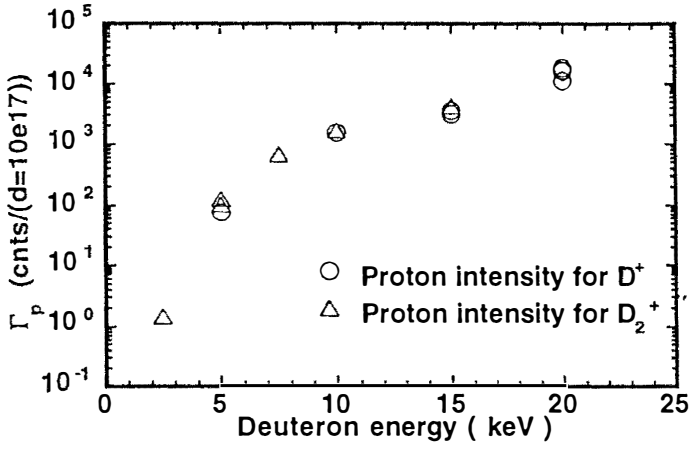

Figure 5. Energy dependence of the reaction rate Γ_p.

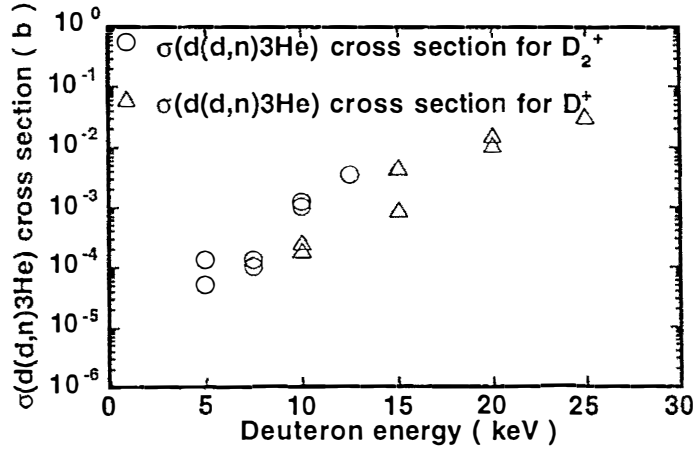

Figure 6. Energy dependence of the cross section.

Fifth International Conference on Cold Fusion
9-13 April, 1995 - Monte Carlo, Monaco
ICCF5 ©1995

Neutrons Observations in Cold Fusion Experiments

Lino DADDI
Accademia Navale - Gruppo Fisica
LEGHORN - 57100 Italy

Abstract

This report is a review of the most convincing observations of neutrons in Cold Fusion history up to recent experiments in which neutrons were so numerous and long-lasting so as to allow activation of thermal detectors. Lately neutrons were observed also by using natural hydrogen. A more complete review is published elsewhere [1].

1. Introduction

In the experiments conducted with deuterium, the measurement of neutrons, attributed to the reaction

$$D + D = {}^3He + n \qquad (1)$$

and therefore with energy of 2,45 MeV, has presented difficulties since the very first experiments in 1989 due to the scarcity and/or irregularity of the emission.

The fact that the neutron emission is weak even when the excess heat is rather high compels us to suppose that (1) holds true, however, in a minority of reactions; it seems therefore necessary to consider separate the cause of the heat and that of the neutrons.

The reaction could be different from (1) : Takahashi[2] has measured neutron emissions at energy between 3 and 7 MeV; Karabut [3] has obtained neutrons with energy up to 17 MeV from glow discharge in deuterium and, recently, Manduchi/Mengoli[4] have observed neutron emission (of energies > 2.45 MeV) from application of d.c current to Pd deuteride. In the electrolysis of D_2O in presence of tritium Stukan[5] has observed hard neutrons ascribable to the cold fusion T+D.

Although experiments have been reported in which the emission appears constant in time [6-9], irregularity is the most frequent characteristic of neutron production in cold fusion: the neutrons are often grouped in bursts of varied composition and duration.

2. Neutrons 1989-1995

Subsequently to the first communications of 1989 many groups have detected neutron intensities well above the background. We limit ourselves to an exemplification of experiences in which neutron generation is many times the statistical error σ_B on background.

ELECTROLYTIC LOADING

Measurement of reaction neutrons - Neutron spectrometry presents difficulties with this type of loading, because the electrolytic solution and the possible thermostatic bath slow down the neutrons. However, Takahashi[2] in pulsed electrolysis with a heavy water LiOD solution has measured neutron emissions at 2.45 MeV (but also at energy between 3 and 7 MeV).

Measurement of neutrons after thermalization - Sanchez[10], during heavy water electrolysis with a Ti cathode has measured for several hours, with a BF_3 detector, counting rates up to 10^5 n/s . Palibroda[11] has worked in electrolysis with a palladium cathode and a solution with an addition of thiourea; various neutron emissions have been recorded which, after thermalization, reached 300 times the background and lasted up to 12 hours. Fujii[12] has worked with a 0.1 mol/dm^3 LiOD solution in heavy water. Utilizing ^{3}He counters he has found neutron bursts up to 135 σ_B.

GASEOUS LOADING

Measurement of reaction neutrons - Botta/Bressani[13] have applied a time of flight spectrometer to the Ti/D system; neutrons of 2.45 MeV energy have been found in the excess of 5 σ_B compared to the background. Manduchi/Mengoli[14] have utilized the technique of gaseous loading of deuterium on Pd with decreasing temperature from 900°C to 20°C. The neutron measurement was effected with a NE213 (100 cm^3) spectrometer; significant quantities of neutrons have been observed especially in the temperature intervals in which the deuterium was more actively absorbed by the metal. Neutrons also are produced following loading with natural hydrogen.

Measurement of neutrons after thermalization - Manduchi/Mengoli[15] have, among other things, sought confirmation of Scaramuzzi's experiment of 1989, by producing many cycles of deuterium charging and discharging on titanium: for about two weeks they periodically found neutron emission, measured as thermals, for approximately 10 times σ_B.

ELECTRIC DISCHARGES IN DEUTERIUM GAS

This type of experiment, already begun in 1989[16,17], appears efficacious in the production of neutrons, but the reaction rate is not in general sufficient to produce a measurable excess heat. Only in the work of Kucherov[18], favorably characterized also by the maximum neutron emission (with activation of ^{107}Ag and ^{109}Ag) related to the minimum d.d.p. employed (< 500 V) , have 50 W been appreciated.

Long[19] experimented with the glow discharge between Pd-deuterated electrodes, obtaining reactions in the metallic film deposited on the glass of the bulb. The neutrons, measured with a recoil-proton scintillation detector, reached the average rate

of several hundred per second. With metals other than Pd the neutrons were more numerous (10^4 n/s) and long-lasting, so much so as allow the radioactivation of indium and iridium.

DIFFERENT TECHNIQUES AND / OR MATERIALS

Lyakhov[20] has found that the combined action of cavitation and electrolysis on a titanium surface determines a reproducible neutron emission (0.6 n/s) with bursts of 10^3 n/ms.

Bittner[21] employs a mixed method, in that it involves electrolytic deuteration of palladium and subsequent degassing through heating; the emission of neutrons (of approximately 2.5 MeV) took place mainly during the degassing phase, at high temperature, for about an hour.

The Piantelli's technique [22,23], which uses natural hydrogen, allows a generation of $>10^6$ n/s (radioactivity was induced in Au,In and Mn) besides of significant anomalous excess heat. Then this "Siena experiment" [24,25,26] is to be considered as the most sure acknowledgement, up to date, of the nuclear cold fusion hypotesis.

Manduchi-Mengoli [4] have founded strong neutron emission (30÷40 n/s) correlated with the migration of deuterium; the energy was > 2.45 MeV for 80% of the total.

Wada[27] reports emission of 2.45 MeV neutron bursts with temperature rise from palladium by means od simple exposure to D_2 gas in a closed glass bulb.

3. Transmutations

The finding of particular nuclides might be an indirect signal that neutron generation has taken place.

Coupland[28] reports that in the superficial layers of Pd electrodes the isotopic ratio $^6Li/^7Li$ appeared very reduced (from 0.08 to less than 0.05) after having been used by Pons and Fleishmann. The anomaly may be interpreted as the consequence of reactions of the ^6Li with thermal neutrons whose cross section (n,α), as is known, is very large (945 barn).

Other nuclides are presumably created by the transmutation of species originally composing the crystalline lattice. Rollison[29], in mass-spectrometric observations of the deuterated Pd, has found an increase (from 27 % to 40 %) in the abundance of the ^{106}Pd isotope (^{105}Pd abundance undergoes a corresponding reduction).

Karabut [3] has measured a γ-ray emission attributed to ^{109m}Pd ($T_{1/2}$= 4.7 min). Recently the production of silver has been observed, in particular by Dash[30], who believes that the $^{108}Pd\ (n,\gamma)^{109}Pd$ capture has taken place followed by decay into stable ^{109}Ag , with half life $T_{1/2}$ = 13.7 h. Obviously also the original impurities (for example Ag, Au and Pt) as well as the Pt of the anode, transferred in part onto the cathode in the course of experiments of electrolytic loading, may undergo transmutations[31]. In particular ^{196}Pt (relative abundance 25.3% in the natural element) through reaction (n,γ) would give place to ^{197}Pt which would become stable ^{197}Au after beta decay.

4. What activates the neutron channel ?

The examination of the works mentioned so far does not seem yet to furnish a final evidence about what could be the modes which activate the neutron channel, but in many cases non-equilibrium conditions appear necessary; the temperature seems important.

Loading ratio - It is known that many experiments indicate for Pd a loading ratio x = 0.85 as the threshold for the production of excess heat; for neutrons some authors have reported as useful decidedly inferior values. Shani[32] sealed the Pd sample destined to emit neutrons when the D/Pd ratio had been brought to a value of .6. In addition Long has indicated the condition x > .3, while from Bittner's graphs[21] neutrons still seem to be emitted when, during degassing, the ratio had been reduced to about .66. Iwamura[33], who with ^{3}He detectors observes neutron emission during degassing, claims to load to the maximum value of x = .66, while Nakada[34] recognizes a requisite value of x=.77 and, lately, Garg[35] has indicated useful x values from 0.4 to 0.7 in a variety of gas loading experiments.

For D/Ti systems Algueró[36] recommends the critical value x=1.95, which is attained in only a thin layer close to surface (few microns) during D_2O electrolysis.

Stratifications - In the Iwamura's and Algueró's experiments the phenomena seem to concentrate on the deposited superficial layer. Other experiments, as well, seem to indicate that the generative processes of neutrons are produced in correspondence to thin stratifications. Nakada[37] has proved that the formation of Pd-Li layers in the surface region favours the anomalous deuterium accumulation, with neutron emission.

Catalytic hypotheses - Some researchers affirm that the stochastic character of the emissions of neutron bursts suggests a catalytic nature, for which such episodes may be induced by neutrons or by other particles of the environmental background. From such a viewpoint the experiment described by Shani[32] seems interesting: in a high-neutron background environment (0.05 counts/s/cm^2) a 2.45 MeV neutron peak was observed, while in a low background environment (0.0002 counts/s/cm^2) there was no peak. The idea of catalysis is sustained also by Gluck [38] and by Kozima[39] who adduces as a clue the fact that the phenomena of cold fusion appear markedly less frequent in heavily shielded environments.

5. Conclusions

Neutrons were observed in many laboratories. The most frequently measured neutron energy is 2.45 MeV of the D+D reaction; reported higher energies need further confirmations. The isotopic shifts would also deserve careful examination.

Experiments seem to support the firm belief that excess heat is generated by principales nuclear events accompanied by less frequent reactions which produce neutrons.

References

1. L.DADDI - "Neutrons in Cold Fusion Experiments", *Proceedings of the IV° Workshop on the Status of Cold Fusion in Italy, Siena 1995* - Editor B.Stella
2. A.TAKAHASHI et al. "Emission of 2.45 MeV and Higher Energy Neutrons from D_2O-Pd Cell under Biased-Pulse Electrolysis", *J.Nucl.Sci.Technol.* - **27**,663 (1990) - also : *Abstract No.207 ICCF5*
3. A.B.KARABUT et al. "Nuclear Product Ratio for Glow Discharge in Deuterium" *Phys.Lett.A* **170**,265 (1992)
4. G.MENGOLI et al. "Neutron Emission from Transient and/or Steady-non-Equilibrium States of Pd Deuterides" *Abstract No. 310 ICCF5*
5. R.A.STUKAN "The Effect of Tritium on Hard Emission Generation During the Electrolysis of Heavy Water" *Abstract No.313 ICCF5*
6. A. TAKAHASHI "Neutron Spectra and Controllability by Pd-D Electrolysis Cell With Low-High Current Pulse Operation" *The Science of Cold Fusion* , Bologna 1991 (pag.93)
7. T.BRESSANI et al. "A Study of the Neutron Emission from Ti Loaded with D in Gas Phase by Means of a Time-of-Flyght Spectrometer" *The Sci. of Cold Fusion* , Bologna 1991 (pag.105)
8. M.PRELAS et al. *J.Fusion Energy* **9**,309 (1990)
9. Y.ARATA and Y.C.ZHANG "Cold" Fusion in a Complex Cathode" *Frontiers of Cold Fusion* ICCF3, Tokyo 1993 (pag 441)
10. C.SANCHEZ et al. "Cold Fusion during Electrolysis of Heavy Water with Ti and Pt Electrodes" - *Proc. Understanding Cold Fusion Phenomena , Varenna 1989* -**Vol.24** (pag.29)
11. E.PALIBRODA and P.GLUCK "Cold Nuclear Fusion in Thin Foils of Palladium" *J.Radioanal. Nucl. Chem.Lett.* **154**,153 (1991)
12. Y.FUJII, M.TAKAHASHI et al. "Anomalous Neutron Bursts in Heavy Water Electrolysis - *The Science of Cold Fusion"* , Bologna 1991 (pag.81)
13. E.BOTTA, T.BRESSANI et al. "Measurement of 2.5 MeV Neutron Emission from Ti/D and Pd/D Systems" - *Nuovo Cimento* **105-A**, 1663 (1992)
14. C.MANDUCHI et al. "Anomalous Effects During the Interaction of Subatmospheric D_2 (H_2) with Pd from 900°C to Room Temperature" *Nuovo Cimento* **107A**, 171 (1994)
15. G.MENGOLI et al. "Neutron Emission from the Interaction of D_2 with either Ti or Pd Based Alloys" *Proc. Rome Workshop on Status of Cold Fusion in Italy,Rome 1993* (pag.68)
16. N.WADA et al. *Jpn.J.Appl.Phys.* **28**,L2017 (1989)
17. R.H.XIONG et al. "The Detection of Neutrons in Discharge Device with Palladium Electrode and Deuterium Gas" *ICCF2 Abstr.*(pag.42) - *Proc.Conf.of Cold Fusion Beijing* 1990
18. Y.KUCHEROV et al. "Calorimetric and Nuclear Products Measurements at Glow Discharge in Deuterium" *Fusion Facts* **5**,33 (1993)
19. H.Q.LONG et al. "New Experiment Results of Anomalous Nuclear Effect in Deuterium Metals Systems" *Proc.ICCF4 - Palo Alto* (1994) , Vol.3 (pag 24.1)

20. B.F.LYAKHOV et al. "Generation of Nuclear Fusion Products by the Combined Action of Cavitation and Electrolysis of a Titanium Surface in Deuterated Electrolytes" *Tech.Phys. (USA)* **38**,623 (1993)
21. M.BITTNER et al. "Observation of d-d Fusion Neutrons During Degassing of Deuterium-Loaded Palladium" *Fus.Technol.* **23**, 346 (1993)
22. F.PIANTELLI "Produzione anomala di energia in esperimenti con isotopi H e D adsorbiti da un particolare reticolo metallico" - *Atti Accad.Fisiocr. Siena* - **Serie XV-Tomo XII,**89 (1993)
23. S.FOCARDI et al. "Anomalous Heat Production in Ni-H Systems" - *Nuovo Cimento* **107-A**, 163 (1994)
24. S.FOCARDI "The Siena Experiment: heat excess, gamma rays" *Siena Workshop on the Status of Cold Fusion in Italy* - Siena 24-25 March 1995
25. F.PIANTELLI "Reproducible hydrogen loading of Nickel and evidences for heat production and nuclear effects" - *Siena Workshop on the Status of Cold Fusion in Italy* - Siena 24-25 March 1995
26. S.VERONESI "Gamma-Rays and neutron activation in the Siena Experiment" *Siena Workshop on the Status of Cold Fusion in Italy* - Siena 24-25 March 1995
27. N. WADA - "Nuclear Fusion in Solid Pd/D_2 Gas" - *Abstract No.335 ICCF5*
28. DR.COUPLAND et al. "Some Observations Related to the Presence of Hydrogen and Deuterium in Palladium", *Frontiers of Cold Fusion* ICCF3, Tokyo 1993, pag 275
29. D.R.ROLLISON et al, *Proc. IACCF1 - Salt Lake City* **1990** (pag.36)
30. J.DASH and D.DIMAN "Localized Melting and Microcomposition of a Pd Cathode after Electrolysis in Acidified Heavy Water" *Fusion Facts* **5**,12 (1993)
31. J.DASH et al. "Surface Morphology and Microcomposition of Palladium Cathodes after Electrolysis in Acidified Light and Heavy Water" *Fus.Technol.* **26(4T)**,299 (1994)
32. G.SHANI et al. "Evidence for a background neutron enhanced fusion in deuterium absorbed palladium", *Solld State Comm.***72**,53 (1989)
33. Y.IWAMURA et al. "Observation of Anomalous Nuclear Effects in D-Pd Systems" *Fus.Technol.* **26(4T)**,160 (1994)
34. M.NAKADA et al. "Energy of Neutrons Emitted in Heavy Water Electrolysis" *Frontiers of Cold Fusion* ICCF3, Tokyo 1993 (pag.173)
35. A.B.GARG et al. "Protocol for Controlled and Rapid Loading/Unloading of H_2/D_2 Gas from Self-Heated Palladium Wires to Trigger Nuclear Events" - *Abstract No.309 ICCF5*
36. M.ALGUERÓ et al. "An Interpretation of Some Post-Electrolysis Nuclear Effects in Deuterated Ti" *submitted to Fus.Technol.*
37. M.NAKADA et al. "A Role of Litium for the Neutron Emission in Heavy Water Electrolysis" *Frontiers of Cold Fusion* ICCF3, Tokyo 1993 (pag.581)
38. P.GLUCK "Why Technology First" *Infinite Energy* **1**,26 (1995)
39. H.KOZIMA "A Phenomenological Model of the Cold Fusion in Pd(Ti)-D System" ICCF4 *Abstracts* (T 2.5)

Session 4

Theory and Modelling

Fifth International Conference on Cold Fusion
9-13 April, 1995 - Monte Carlo, Monaco
ICCF5 ©1995

Setting Cold Fusion in context: a reply

Giuliano Preparata
Dipartimento di Fisica – Universitá di Milano
INFN – Sezione di Milano

Abstract

This talk consists of three parts: the first on the "pathological" nature of Cold Fusion (CF) phenomena, the second on a wide theoretical effort based on the new ideas of QED coherence in matter, and the third replying to explicit criticisms to my work.

The "pathological" Science of Cold Fusion

Six years after the momentous announcement of March 23, 1989 the world of Science is still divided: a large majority that regards Cold Fusion (CF) an eminent example of "pathological" science, a small battered minority that still carries on with very limited means, both financial and, alas, intellectual, struggling for the survival of the grandiose dream that Fleischmann and Pons (FP) brought to mankind that now distant spring day of 1989.

Why did it go this way? Why a phenomenology[1] that has found so many diverse confirmations by several different experimental groups, has failed to convince such a large number of scientists, that have turned their back on this fascinating field?

I believe we must try to give an honest answer to these important questions, for if we fail to understand why so many of our colleagues perceive CF as a pathological form of science, we are doomed to remain marginal even if we will able, as in fact we are doing, to make substantial progress.

It seems to me that the basic reason why CF is almost universally considered "pathological", is that it is so at odds with deeply rooted expectations based on the generally accepted picture of condensed matter and nuclear physics, that it requires the established scientist an almost heroic effort even

[1]Throughout this talk I shall confine myself to the Pd/D system pioneered by FP, i.e. I shall not attempt to overcome the "Pd/D barrier" of CF.

to bring himself to look into such a bizarre set of physical phenomena (the situation is of course different for the scientists that live somewhat at the margin of Academia, and this has been part of the problem of CF).

Without a well defined frame that can accomodate the strange looking facts of CF, indeed its "miracles", the natural reaction of scientists is at best to ignore those facts, at worst to believe them the result of some kind of fraud. And, of course, we have seen all that. But, instead of moralistically condemning such attitudes (which in truth have caused us no minor suffering), as I have just stressed, we should try to put ourselves in the shoes of the many colleagues with whom, before that fateful day of the spring of 1989, we had a perfectly reasonable kind of relationship.

Confronted with the experimental landscape of CF, what do they see? The following "monstruosities":

i) the deuterons, that are well known to crowd a Pd cathode in a heavy water electrolytic cell, and to accomodate in the octahedral sites of its lattice, are supposed to undergo nuclear fusion at rates hundreds of orders of magnitude higher than what one expects in the D_2-molecule, where the deuterons are located even closer.

ii) not only do the deuterons (supposedly) fuse, defying all known condensed matter physics, but they would do so following a nuclear physics path, that is completely at variance with the known path, for which the two reactions

$$D + D \rightarrow n\ (2.45\ \text{MeV})\ +^3\text{He}\ (0.82\ \text{MeV}) \qquad (1)$$

$$D + D \rightarrow p\ (3.02\ \text{MeV})\ +^3\text{H}\ (1.01\ \text{MeV}) \qquad (2)$$

have each a branching ratio close to 50%.

Countless papers, books, sermons etc. have been written and uttered to admonish us all about the senseleness of what the CF scientists pretended to have experimentally demonstrated, and how their refusal to repent and recant jeopardized, indeed discredited the whole scientific community. By the way, the tones and the practices of the keepers of scientific orthodoxy in the CF debate have been remarkably close to those of the critics and enemies (mostly churchmen) of the Renaissance science, who finally saw the better part of Bruno, Galilei and their followers. And indeed, in the present frame of understanding both condensed matter and nuclear physics, there is no way to reconcile the above two "monstruosities" with the huge body of knowledge that is based upon the dominating paradigm. Thus, let us make a little investment in philosophy (a most abhorred and derided intellectual enterprise by the normal scientist[2] of today) and try to characterize the deep roots of the paradigm, for without it not only are we

[2]I am using this term in the technical sense of T. Kuhn [1].

condemned to a permanent and futile warfare and misunderstanding with our colleagues, but we will also remain unaware of the remarkable revolution that the "monstruosities" of CF are bringing about in modern science.

If one wishes to characterize with a single concept the paradigm, I believe the best of all is : Asymptotic Freedom (AF). The concept of AF, as far as I know, was first explicitly discussed in 1973 [2] within the then consolidating Standard Model (SM) of particle physics: it denotes the property of a non-abelian gauge theory (Quantum Chromo Dynamics (QCD)) to become (almost) free from interactions when probed at space-time distances which become asymptotically negligible with respect to the sizes ($\simeq 10^{-13}$ cm) of the strongly interacting particles (the hadrons). This peculiarity, which was proven within perturbation theory, has become enormously influential, due to the apparently natural solution it engenders of the unexpected simple structure of the cross sections of highly inelastic scattering of leptons off protons and neutrons (Deep Inelastic Scattering (DIS)). Besides its seemingly high predictive power in DIS, I believe that AF owes its universal acceptance to what appears to me as an unconscious psychological attitude, that pervades our advanced societies, which has to do with the jealousy for our privacy: the wish to become "asymptotically free", when we choose to go far from the "madding crowd"; the final triumph of the individual over the constraints of collective life. To see this now highly popular dislike of collectivism supported and corroborated by a rigorous result in (perturbative) Quantum Field Theory (QFT) must have certainly enhanced the belief that perturbation theory is a very good tool to describe the interactions among different levels of reality, involving far away space-time scales. The irony of all this, as I thoroughly pointed out in the last several years [3], is that just within the theory (QCD), that has led to a rigorous perturbative demonstration af AF, there has arisen the most spectacularly paradoxical notion of all modern physics, that of the **confined** quark. For those who are not very familiar with all this, let me only point out that the quark is the only known constituent of (hadronic) matter that is **essentially inseparable** from the matter it constitutes, i.e. nobody has ever been able, by any physical means, to take the quarks out of the particles (hadrons) of which they are, allegedly, constituents. It so appears that, as far as the quarks are concerned, they **are not asymptotically free**, in the sense that under no circumstances can we realistically talk of the individual quark, for unless a quark finds in the close environment partners to compensate its colour charge, it is condemned to disappear in an all embracing, sticky (recall that the quanta of the colour fields are called "gluons") vacuum. Thus the physical reality (or better unreality) of the quark discredits the notion of AF, just in the theoretical framework where this concept was first introduced and perturbatively proved.

But as far as condensed matter physics is concerned, within the pre-

vailing electrostatic picture of interactions, that we may call the "Electrostatic Meccano", AF is a true property of the QFT describing it, and its expectations coincide with those of the physics community. Thus according to AF it does not make any sense that the nuclear physics of deuterons, with its space-time scales six orders of magnitude smaller than the space-time scales of the lattice, be any different in vacuum than in the Pd-lattice. Any attempt to concoct, through some quantum-mechanical trick[3], an explanation of the CF phenomenology that stays within the tenets of the paradigm must necessarily fail, for AF is deeply rooted in the paradigm — I daresay it is the paradigm — and there can be no doubt that AF rules out CF altogether.

I believe that it is the poor understanding of this general implication of the paradigm that is responsible on one hand for the criticism of the majority of the scientific community of the "pathological" nature of CF, and on the other of the inanity, worse the outright falsehood, of most of the many theories of CF that have been proposed in the last six years.

But before introducing a new paradigm that avoids the narrow confines of AF (which I shall do in the next Section), I wish to conclude this Section with a small observation on "pathological science". As well known CF has been associated in its "pathology" with another subject that caused a scientific scandal in the seventies, the "polywater" affair. Unlike the discoverers of CF, the discoverer of "polywater" — Deryagin — finally recanted, conceding that the water that is found in very thin quartz capillaries is not a new strange phase of water but some kind of gel containing a sizable fraction of solved silica. This admission was hailed with relief and the deep rewarding feeling that scientific rationality had finally triumphed over unsound scientific claims and deductions. But, should it have really been so hailed? I doubt it, for, if not "poliwater", Deryagin had discovered the incredible fact that pure water (a collection of small, rather featureless molecules) is able to attack and dissolve a material that can stand the strongest chemical agents. Is this understood within the paradigm? A reply to this simple question would be highly appreciated.

Curing the "pathologies": QED coherence in matter

In the introductory Section I have tried to explain that the "pathological" nature of the science of CF, as perceived by the large majority of the scientific community, lies in fact not in the wide experimental body of knowledge

[3] Another unhappy aspect of the dominating paradigm is the subjectivism of the Copenaghen interpretation of Quantum Mechanics, imbibed of irrationalism. Irrationalism that very often is played against whoever asks embarassing questions about the physical bases of universally accepted but extremely obscure quantum mechanical developments (such as, for instance, the BCS "theory" of cold superconductivity and the Mössbauer effect).

that reproducibly has been accumulated throughout the world in the last six years, but rather in the intellectual framework — the paradigm — that dominates not only in physics, but in chemistry and biology as well.

When dealing with condensed matter phenomena the normal[4] scientist is led by the paradigm to expect that the constituents of condensed matter (atoms, molecules) are bound together by the same kind of forces that bind the elementary building blocks of molecular physics, namely electrons and ions/nuclei. As we know well, these forces are all of electrostatic nature, and have the fundamental property of extinguishing themselves at distances larger than a few $\mathring{A}$'s. This property stems from the well known fact that condensed matter at scales of just a few $\mathring{A}$'s is neutral. Thus the long range part $(1/r)$ of the Coulomb interaction[5] is ineffective (Debye screened) at distances that exceed a few atomic radii. The mental picture of condensed matter, that the paradigm suggests to the normal scientist, is that of a huge **electrostatic Meccano**, where the electrostatic two body (local) interactions are the nuts and bolts that keep the pieces of the Meccano — atoms and molecules — glued together to form the enormously complicated structures of condensed matter: crystals, glasses, hydrogen-bonded liquids etc. In this picture macroscopic order, that we contemplate often with marvel in matter, both living and inanimate, is the outcome of the juxtaposition of the pieces of the Meccano through the holding action of the electrostatic nuts and bolts. But just as the Meccano picture supports, with the aid of properly designed blueprints, the possibility of building meaningful, ordered structures, when all this is cast in the necessary quantum mechanical framework, where all nuts and bolts must be somewhat loose, in obeyance of the Heisenberg principle, it becomes highly implausible that such looseness, compound over about 10^{24} (the Avogadro number) elementary systems may result in macroscopic structures with the kind of stability and strength that we observe in condensed matter. And as a matter of fact, I know of no solvable theoretical model that achieves macroscopic order through short range interactions[6].

But there are more specific reasons not to believe in the **electrostatic Meccano**; just to mention a few: the Mössbauer effect, ferromagnetism, superfluidity, superconductivity, catalysis, experimental realities for which there exists only "kinematical" theoretical frameworks, based on "self-consistency" , the deep "dynamical" reasons being always postponed to some demiurgical

[4]see footnote on page 4

[5]It is thus very surprising to find that the most popular theory of the quantized Hall effect is based on a Hamiltonian for the electrons' system whose interaction term is the pairwise Coulomb interaction.

[6]The usual objection that I hear to this contention is, of course, in terms of the Ising model. However (i) the Ising model is formulated on a lattice, thus on an "a priori" ordered structure, (ii) I know of no successful application of the Ising model to any realistic system.

future computation/simulation.

It is for the keen unsatisfaction with the present state of affairs that a few years ago (1987), having completed a long and difficult analysis of the Quantum Chromo Dynamics (QCD) ground state [4], in search for an explanation of the peculiar confinement property of quarks, I started on a research programme to investigate the possibility that also for QED in condensed matter systems the ground state (the vacuum) show the highly non-trivial structure that in QCD explains the paradoxical confinement behaviour of quarks. This research quickly met with unhoped for success, and, as I explained in a series of lectures already in February 1989 [5], the idea[7] that the transverse electromagnetic field in the ground states of condensed matter is well described by an infinite set of quantum harmonic oscillators in their minimum energy states (the perturbative vacuum) is just simply wrong, for it is based on an approximation (the slowly varying envelope approximation) that, though fully valid in Laser physics, is totally inapplicable in systems that are cold and dense enough. And if the ground state of the e.m. field in condensed matter is in general the perturbative QED ground state, this must mean the doom of the paradigm, for it systematically ignores an important, indeed a fundamental actor of the dynamical drama of matter. And if the ground state of a piece of matter, as the paradigm envisages, is not the loose structure where the elementary matter systems and the e.m. field each perform their zero-point quantum oscillations chaotically and independently, what is it, really?

The answer, as widely and thoroughly discussed in a book that is due to appear soon [7], is disarmingly simple: it is a laser-like state where matter and field oscillate in phase on a frequency that is characteristic of the particular atomic/molecular species that make up a particular piece of matter. But there are two fundamental differences:

i) the laser-like state, being the ground state, is accessed **spontaneously** without any pump nor optical cavity, when it is below a critical temperature and above a critical density;

ii) no e.m. radiation can escape from such a state for, being it the ground state, this would violate energy conservation.

It turns out that with the kind of "oscillator strengths" (matter - e.m. couplings), and the kind of densities ($\left(\frac{N}{V}\right) \simeq 10^{22} \div 10^{23}$ cm^{-3}) typical of the atomic/molecular systems of condensed matter the critical temperatures are usually very high ($\simeq$1000 K) and the critical densities are usually well below 10^{23} cm^{-3}. Thus such states are predicted by QED to occur very frequently, as indeed they do! It should be abundantly clear, at this

[7] As forcefully argumented by P.W. Anderson in an influential book on condensed matter physics [6].

moment, that the doom of the paradigm, implied by such new developments, demands that it be replaced by the new approach, that is based on a solid (through well defined approximations) analysis of the ground states of QED in condensed matter systems [5]. We may call this new approach the electrodynamic Network (EN), for it involves the multitudes of atoms/molecules of a macroscopic piece of matter in an intricate dynamical interplay mediated by a large amplitude (classical) e.m. field.

One of the basic aspects of the EN, that being very conterintuitive is most difficult to visualize, is the peculiar behaviour of the matter systems, which comprise well defined quantum wave fields, the matter wave fields. When we concentrate our attention upon the elementary matter systems it seems completely natural to think that when in the ground state they are in the lowest state of excitation, for this appears to be a straightforward consequence of energy minimization. This, in fact, turns out to be generally wrong for, due to the phase coherence between the matter field and the e.m. field, energy is minimized when both the electromagnetic and the matter fields are in an excited state, the (negative) interaction energy being sufficient to bring the value of the total energy below that of the perturbative ground state, where both e.m. field and matter are indeed in their ground states.

As I have stressed [8,9] time and again to the CF community since the first paper published in May 1989, the ground state of a piece of matter, say a Pd rod, is so crowded with large coherent e.m. fields that the idea that AF should hold there does not seem at all reasonable. Indeed one should carefully evaluate (and this has been done in successive steps [9]) if and in which way the expectations of AF are violated. However, one thing can already be said with certainty: AF is not a general property of the coherent ground states of QED in condensed matter. Thus, from a purely conceptual standpoint, in the new approach the "pathologies" of CF are completely cured, for they are all based on a general property, AF, that does not hold in a large class of physical solutions of QED, the coherent ground states (CGS). At this point one may conclude that the " pathology" of CF is in fact in the eye of the beholder!

In an article written together with M. Fleischmann and S. Pons [10] an articulate discussion was presented of the strange behaviour of Hydrogen in a metal matrix such as Pd, arguing that, even ignoring the phenomena of CF, what is well known since long about the way Hydrogen enters and diffuses in Pd is totally at odds with the paradigm, and its qualifying AF. In particular, the high potential barrier ($\simeq$ 30 eV) that a D_2-molecule must overcome before entering the Pd-lattice (where, according to a series of fascinating experiments of A. Coehn [11], Hydrogen is found in the ionized state) is something that within the paradigm has never found any sensible explanation. This and the many other mysteries that still remain to be un-

raveled in the Palladium/Hydrogen system, as we have argued in Ref. [10], should be another warning signal that one does have to go beyond the paradigm, even ignoring (but how?) the dry and reproducible facts of CF.

Let me now devote the rest of this Section to paint a possible scenario of the Pd/D system at high loading (x =Pd/D), where the CF phenomena are known to occur. I shall do this in the framework of the new approach, whose conceptual bases have been described at length above, and whose calculational details have been worked out in several previous talks and reviews [12,13][8].

The Pd-lattice (a face centered cubic lattice) is the locus of several coherent dynamical processes, that give rise to coherent, collective plasma oscillations of the different elementary systems. Those in which we shall be mainly interested in are:

i) the coherent plasma of the Pd-ions;

ii) the coherent plasma of the d-electrons;

iii) the coherent plasma of the conduction electrons.

These plasmas realize an energetic gain with respect to the (mono)atomic high temperature gas, and such gain constitutes the previously ill-recognised "raison d'être" of the crystalline structure of the metal. When the Pd-lattice is entered by the Hydrogen (and its isotopes D,T) atoms one finds that the electrons go to augment the conduction band, and the (partially screened) nuclei arrange themselves in particular sites (octahedral and tetrahedral) (See Fig. 1), where they perform coherent, collective plasma oscillations. Again, it is the energy gain that is associated with the latter plasma oscillations that justifies the incorporation of Hydrogen by the Pd-lattice, that in fact turns out to be exothermal ($\simeq$ 15 Kcal/mole). Thus in the Pd/H system there is another all important plasma:

iv) the coherent plasma of the (partially screened) H (D,T) nuclei.

As explained in Ref. [13] there are two types of H plasmas, according to the sites the H-ions occupy: the β-plasma in the octahedral sites, and the γ-plasma in the tetrahedral sites. I have shown (and a more refined calculation [14] confirms it) that for $x \leq x_o$ ($x_o \simeq 0.7$) it is the β-plasma that realizes the ground state, while for $x > x_o$ the γ-plasma possesses the minimum (free) energy. Thus on a purely theoretical basis it was concluded that a (second order) phase transition (from the β-phase in the octahedral sites to a new phase, called γ-phase, in the tetrahedral sites should occur for $x \simeq x_o$. This prediction has now found many confirmations ranging from

[8]This reasonably exonerates me from repeating what can be found in easily accessible literature.

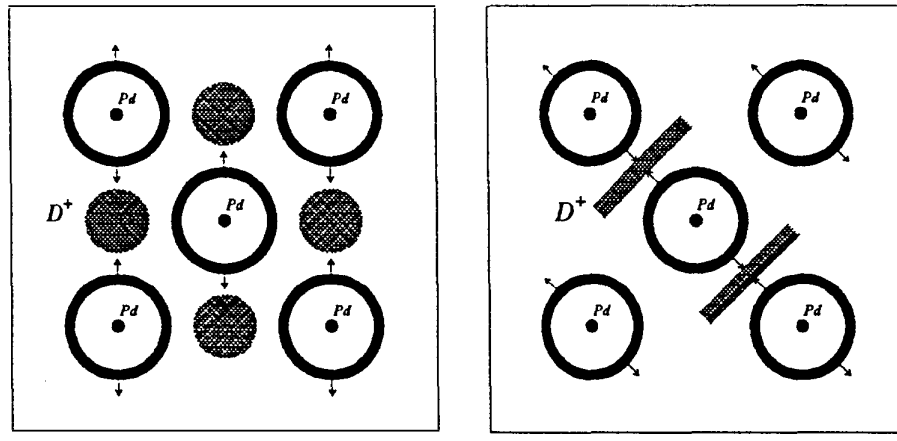

Figure 1: The octahedral sites (left) and the disks of the tetrahedal sites (right) in the (1,0,0) plane of the Pd lattice.

the measurement of the x-dependence of the diffusion coefficient [15], to the peculiar resistivity curve of the Pd/H system, which shows a maximum at $x_o \simeq 0.7$. The explanation of this latter well known fact is in the new approach quite simple and natural: the extra resistivity that, due to H incorporation, rises up to x_o and falls to zero for $x \to 1$, reflects the different scattering cross-sections that the H-ions have for the conduction electrons; in particular the decrease for $x > x_o$ indicates that in the γ-phase the H-ions are in a tightlier correlated state.

In the talk I have given at the ICCF4 [13] I posed two sets of questions, relevant to the H-loading of Pd (α) and to the CF phenomena proper (β). Let me recall them.

First the questions about Hydrogen (D) loading:

(α_1) Why and how does the process

$$D_2|_{gas} \to D + D|_{lattice} \tag{3}$$

proceed?

(α_2) why and how, in the lattice

$$D|_{lattice} \to D^+ + e^-, \tag{4}$$

D^+ and e^- enjoying a different, independent dynamics?

(α_3) why is D^+ so mobile at high x?

(α_4) what are the phases of Pd/D?

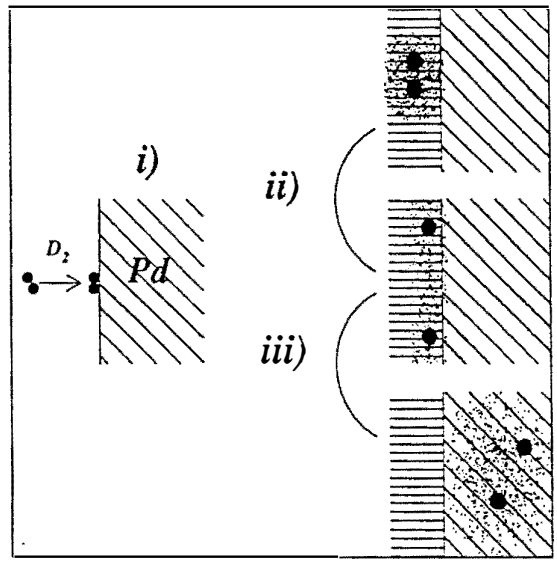

Figure 2: The steps of D_2 absorption by the Pd-lattice.

(α_5) what happens during electrochemical loading?

(α_6) why one observes "Heat after death" [16]?

As for the mechanisms of CF in the highly loaded Pd/D system, the relevant questions appear to be:

(β_1) how can one overcome the Coulomb barrier?;

(β_2) which is the main DD-fusion dynamics?;

(β_3) can we understand rarer processes: n,T,X-rays...?

Let me now briefly recall the answers.

(α_1) The process consist of two steps (see Fig. 2):

(i) the D_2-molecule is brought in contact with the Pd-surface; this step is governed by the gas chemical potential:

$$\mu_{D_2} = -\frac{T}{2}\left[19.3 + \frac{3}{4}\log\frac{T}{T_0} - \log\frac{p}{p_0}\right], \tag{5}$$

(ii) the D_2-molecule interact with the evanescent e.m. field associated with the different Pd-plasmas. It is the dispersive interaction of these coherent e.m. field that causes the tunneling of the D_2-molecule through the high barrier ($\simeq$ 30 eV) that separates it from the "shattered" state

$(2D^+ + 2e^-)$ in which it starts penetrating the Pd-lattice. Incidentally, the same kind of interaction must be at work when the coherent e.m. field of water [17] induce the NaCl (ionic) molecules of a crystal of salt to tunnel through their barrier (about 5 eV high) to become ions: Na^+ and Cl^-.

(α_2) The D^+'s and the e^-'s of the "shattered" deuterium surface state penetrate (almost) **independently** the Pd-lattice, for they belong to different plasmas, and there is an energetic gain to be part of the plasmas instead of remaining in the atomic configurations.

(α_3, α_4) It all depends on the different phases α- β- and γ- the D^+'s are in with increasing x. The α-phase is a disordered (gaslike) phase existing at $x < 0.1$; in this phase the diffusion coefficient is expected, and found, very small (see Fig. 3). The β-phase is an ordered (coherent) phase with the D^+'s oscillating in the octahedral sites. The (calculated [14]) x-dependence of the chemical potential μ for the β- and the γ-phase (the D^+'s in the tetrahedral sites) are reported in Fig. 4, which shows a cross-over at about x_0, implying that for $x < x_0$ the stable phase is the β-phase, while for $x > x_0$ it is the γ-phase to be stable. Recalling now that the diffusion coefficient is given by

$$D = \sigma x \frac{\partial \mu}{\partial x}, \tag{6}$$

where σ is Einstein's mobility, from Fig. 3 we may understand two major features of the D^+'s mobility in Pd:

(i) its fast increase with x;

(ii) its sharp discontinuity for $x \sim x_0$.

These deductions answer (α_3) and (α_4) completely. I should also remind you that the existence of the γ-phase, whose evidence is becoming compelling, was actually predicted on the grounds that CF **cannot** take place in the β-phase for:

(a) the D^+'s are too far away;

(b) only the tetrahedral sites can accomodate more that one D^+;

(c) only in the tetrahedral sites can the d-electrons of Pd effectively screen Coulomb repulsion.

This is another good example of the fact that the remarkable oddities of CF have just shed interesting light upon the dynamics of an ancient, well known system such as Pd/H.

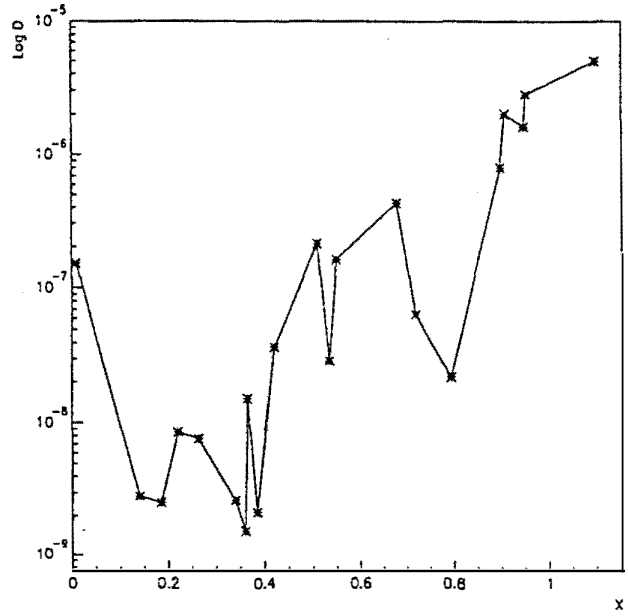

Figure 3: The diffusion coefficient of D in Pd as given by [15]

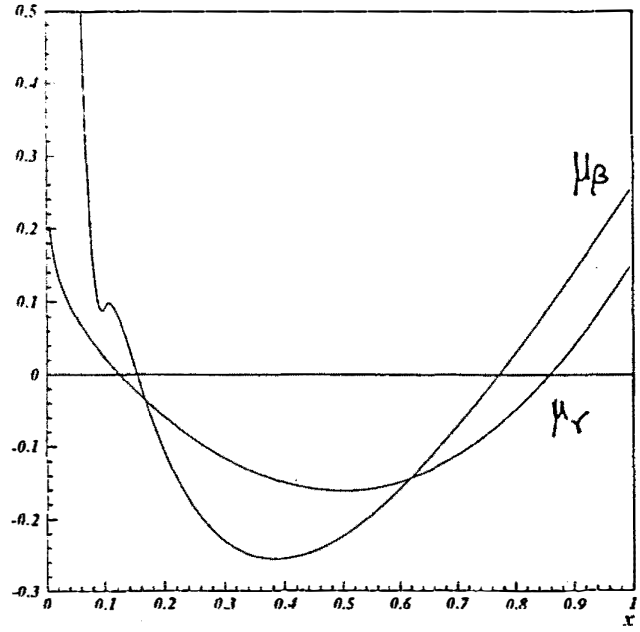

Figure 4: The chemical potential μ_β of the β-phase, compared with μ_γ of the γ-phase, as a function of x.

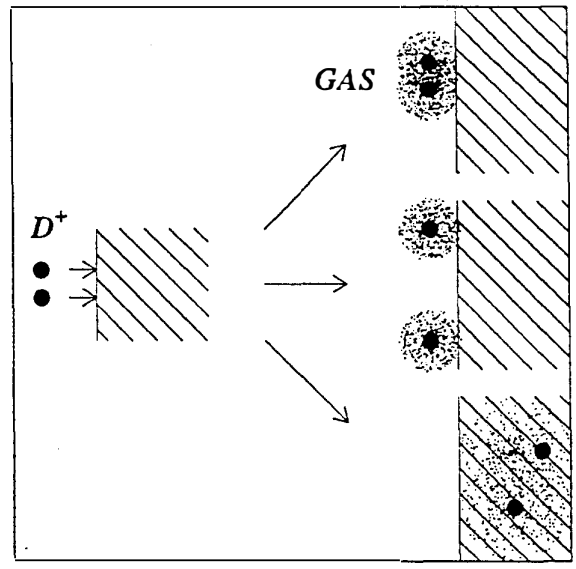

Figure 5: The different fates of D^+'s arriving at the Pd-cathode.

(α_5, α_6) The description of electrochemical loading that our approach affords takes off from the three possible fates (depicted in Fig. 5) of the D^+-ions once they arrive at the cathode. How many of them will be able to enter the Pd-lattice, and load it at high x (the fundamental prerequisite for CF phenomena to occur), it depends on:

(i) how many D-atoms will combine on the Pd-surface and leave the premises as D_2-molecules, forming the well visible gas bubbles;

(ii) the chemical potential of the D's left at the surface.

In order to minimize the number of D-atoms that bubble out as D_2-molecules some kind of "muck", that forms during the electrolysis upon the surface, is certainly useful, for it hinders the free traffic of D-atoms on the surface and its consequent high recombination probability. As for the surface chemical potential a fairly detailed analysis of the ponderomotive effects due to the evanescent e.m. fields of the various plasmas of the Pd/D system has been presented at ICCF4 [13], showing interesting autocatalytic aspects. In fact, the surface, as well as the bulk chemical potentials acquire negative terms, whose absolute values increase with x, thus leading to large equilibrium x-values, quite far away from thermodynamical equilibrium.

As for "heat after death", the subtle interplay of surface and bulk chemical potentials at high x is capable to account for the strange observations reported by S. Pons at ICCF4 [16]

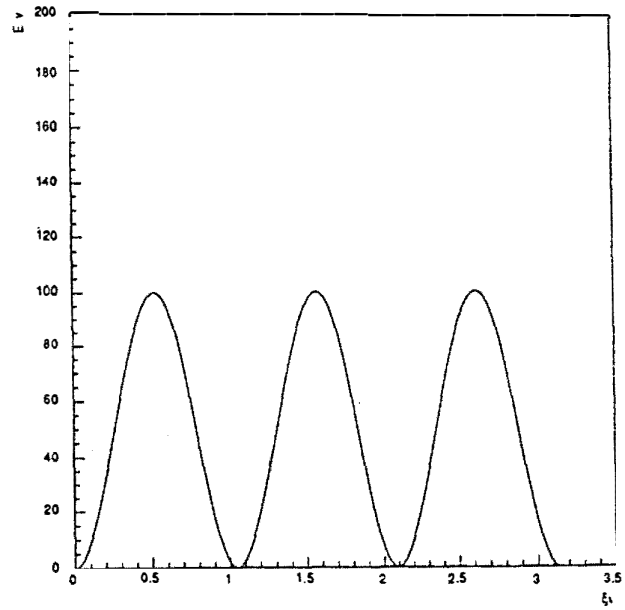

Figure 6: The electrostatic potential as seen by the D^+'s along the tetrahedral disks

Getting now to the CF phenomena in the highly loaded Pd/D system, I will now sketchily[9] answer the questions posed above in order.

(β_1) The screening that the plasma of d-electrons provides in the tetrahedral sites has been determined by calculating the electrostatic potential generated by them, which is reported in Fig. 6.

Introducing such screening potential in the Gamow barrier penetration amplitude ($\mu = \frac{m_D}{2}$ is the reduced mass of the D-D system)

$$\eta_G \sim \exp\left\{-(2\mu)^{1/2}\int_{r_N}^{r_0} dr'[V(r') - E]^{1/2}\right\}, \tag{7}$$

yields

$$\eta_G(\mathrm{Pd}) \sim 10^{-22\pm1}, \tag{8}$$

some thirty orders bigger than the amplitude in the D_2-molecule $\eta_G(\mathrm{DD}) \sim 10^{-51}$. This very strong screening is enough to yield rates for the purely incoherent processes (the only one that takes place in vacuum)

$$\Gamma_{INC} = |\eta_G|^2\Gamma_{NUCL} \simeq 10(x-1)\ \text{fusions/sec cm}^3, \tag{9}$$

where the $(x-1)$ factor takes into account the threshold at $x = 1$, a strict prediction of this approach.

[9]Again, extended answers are found in the ICCF4 talk [13]

(β_2, β_3) The main fusion path is not, of course, the incoherent one, that is the only fusion mechanism in the vacuum, and would be the only one in Pd as well, should AF hold, as dictated by the paradigm.

The new approach, in fact, predicts that the strong e.m. fields that crowd the lattice, once the barrier is penetrated, couple the extra D-nuclei (i.e. those in excess of $x = 1$) to the wave-field comprising all deuterons within a coherence domain[10], of the size of a few microns. Due to the N_{CD} factor, arising from coherence, and the strength of the e.m. fields, the nuclear dynamics becomes strong and fast, leading to the nuclear ground state ^{4}He with high probability and in a very short time. This is why:

(i) the main fusion channel is

$$D^+ + D^+ \rightarrow {}^4He + \text{energy in Pd};$$

(ii) the energy released to the Pd-lattice brings the various coherent fields in excited states that relax with their particular times ($\frac{2\pi}{\omega}$, ω is the oscillation frequency) in various forms:

a) e.m. radiations of all frequencies,

b) exotic nuclear photo-reactions, including neutrons from the photofission of D,

c) heat, i.e. phonons.

(iii) in regions where the coherence is partial, we may have different, weaker and longer pathways (Fig. 7), which may explain the odd $\left(\frac{n}{\Gamma}\right)$ ratios that have been observed.

(iv) a (semi)quantitative calculation of the main fusion channel on the case of "minimal" coherence (i.e. coherence over only one CD) yields for $x \sim 1.1$ rates of the order of kW/cm^3 Pd. Much higher rates are expected for higher x-values and more extended coherence.

To conclude this Section, I believe I may state with confidence that on the basis of the accumulated body of observations and of the theoretical work done so far:

(α) a good, predictive, sound theory of the "pathologies" of CF can be based on the general laws of QED, liberated at last from the crippling constraints of Asymptotic Freedom;

(β) the science of CF is just in its infancy, other promising systems, besides the Pd/D are now coming to the fore and even in the Pd/D system there

[10]As I have explained, almost "ad nauseam" on several different occasion, the minimum space domain in which the matter and the e.m. fields are coherent is the Coherence Domain (CD), whose size is the wave-length of the e.m. field.

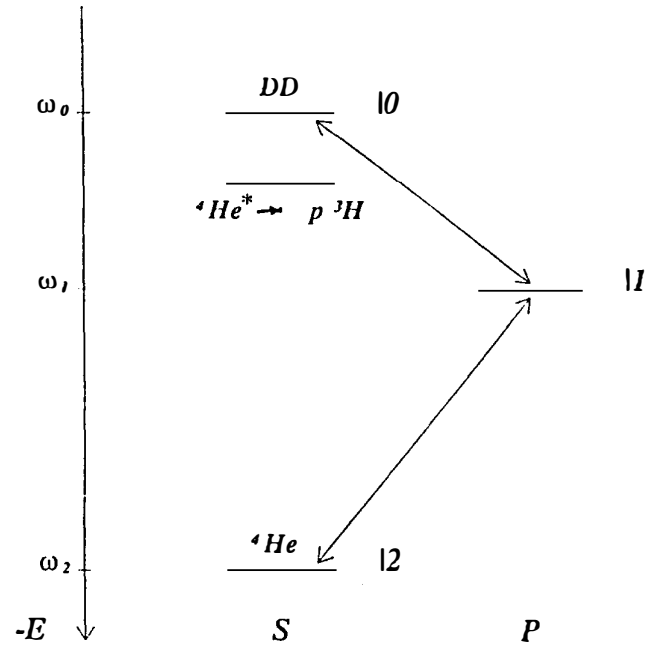

Figure 7: The level diagram for the states involved in the dynamical evolution described in the text. Also reported is Schwinger's $^4He^*$.

are large areas of experimentation where a new chemistry, a new condensed matter and a new nuclear physics are very likely to emerge, fostered by the power and the simplicity of the new, coherent approach.

What's wrong with this?: a reply to my critics

I may concede that I never, since my long scientific militance in the camp of CF, expressed so explicitly to this community the need for the drastic paradigm shift that the CF phenomenology demands. The new approach — QED coherence in matter[11] — just realizes such paradigm shift by identifying in the neglect of the transverse e.m. field in condensed matter a fatal drawback of the dominant paradigm and of its fundamental consequence: Asymptotic Freedom. In hindsight this was a mistake, for very few scientists (fortunately Fleischmann among them) have perceived the logical cogency of the various deductions that form the body of an in principle (to go from principle to practice will require substantially more work) **complete theory** of CF, both with regard to the fascinating problems of Hydrogen loading in a metal matrix such as Pd, and to the CF phenomena in such metal/D systems.

As a matter of fact what in my work most people have incorrectly understood, and criticized, is a collection of more or less "imaginative" models to **fix** the various "miracles" of CF, that to a closer scrutiny within the frame of prejudices and constraints of the paradigm end up (is it so surprising?) to violate one or other of its tenets.

I shall illustrate this important point by analyzing and answering the most explicit critiques[12] that have been levied against my work, which appear in the ICCF4 Proceedings [18], and in a review article published in a recent issue of the International Journal of Theoretical Physics [19].

The hostile attitude of the authors toward my work is betrayed by their complaint that Dicke, the inventor of Superradiance, is never mentioned in the CF papers. As mentioned in a footnote above, though Dicke's Superradiance leads to ordered quantum states of matter and radiation that have some common feature with those of QED coherence in matter, their distinctive feature of producing coherent e.m. radiation (like in a laser) is just orthogonal to the e.m. field trapping within matter, that gets realized in the new approach when the density of the atomic/molecular systems is

[11] In a first stage I gave this approach the name of Superradiance, as a due homage to the pioneering work of R.H. Dicke. This was a mistake, for my generosity has been maliciously taken as a plagiarism. But more of this in a moment.

[12] To be fair, I should credit these critics the basic honesty of speaking out their disagreement: a practice that is less and less popular in the contemporary scientific world, for it exposes the critic himself to critiques. The more frequent and safer practice makes use of gossips and of anonymous referee reports.

large enough and their temperature low enough. It is just for these reasons that Dicke has been fully mentioned in other papers and lectures, his work being totally unrelated to the subtle phenomenology of CF.

Their hostility is further displayed in their accusing me of conceptual errors, that they do not care to argue, and of "a number" of numeric and analytic mistakes, of which they discuss only a minor one (about a factor of 5 in a Gamow amplitude $\sim 10^{-21}$, whose evaluation can clearly not be more accurate than one order of magnitude!).

But, enough with such pettiness; their really strong critique has to do with the large screening potential ($V_{screen} \sim 100$ eV at the bottom of the well) derived in Ref. [9], and further refined in subsequent calculations [14]. Incidentally, without such screening there is no (known) way to understand how CF phenomena could happen.

Having taken the original calculation to mean that the Z electrons of the Pd atom surround the D^+-ion at distances of the order of the Fermi-Thomas radius for a Z electron atom, they conclude that all this violates basic physics, for "a solid would collapse if such close equilibrium screening were possible".

Their turn of arguments would not be blatantly incorrect if the screening electrons (only the d-electrons, as realistically done since march 1990 [9]) were in static orbits around the Pd-nucleus. But, as stressed time and again, such electrons comprise a plasma performing wide plasma oscillations, that realize an energy gain. In such state, due to the strong correlations among them, the electrons do not behave incoherently and individually, as they do in the atom, but follow their collective dynamics, which endows them with much sharper localization properties, as if their effective mass (their inertia) were in fact larger than in the "asymptotically free" limit. For the sake of visualization only, one may think that the electrons tend to mimic the physics of μ-catalysis. Clearly, the misunderstanding has its origin in the critics' lack of perception that QED coherence in matter does change the paradigm, whose conceptual schemes are totally inadequate to penetrate collective behaviour, that, instead, is at the root of the new approach.

Finally the critique [18] that I violate the laws of physics "in trying to insure a large enough time for the existence of a large charge density on the sides of a crack". Again it is their poor understanding of the paradigm shift that is realized by the new approach that blurs the critics' perception of what I am trying to do in the different field of "fractofusion". The coherent e.m. fields that in the form of evanescent waves fill the crack of a mechanically stimulated solid may have rather large lifetimes, and it is they, and not a large density of electrostatic charges that are responsible for the acceleration (under appropriate conditions) of the charged particles that move across the cracks.

These are the only critiques that I find in the literature to the body of

my work on CF, and so my reply should end here.

But, in the CF community, there are other more serious critiques, or better (worse!) the widespread belief that we do not, after six years, possess the correct intellectual means to understand CF. This refrain occurs over and over in all published literature, which most of the time ignores all that has been done in the new approach since March 1989. What kind of answer can I give to such vast majority of believers of CF, but skeptics of CF theory? I have thought a lot about ths problem, that I have always seen as a major obstacle to quick progress in this fascinating field. Philosophy, or better epistemology, clearly has not worked, for the conceptual superiority of the new approach should have convinced my colleagues to invest some of their time to try and understand it, and contribute better critiques to the development of the associated research program. The discussion it affords of general different and subtle mechanisms that give a completely coherent picture of the CF phenomena in the Pd/D system also has had little impact due, I presume, to the philosophical barrier just described. Let me try a new (though at this time subliminal) way. I can tell you with a reasonable degree of confidence that proceeding on the road built by the new approach through CF land one should be able to reproducibly achieve powers in the order of 100 kW/cm^3 Pd.

It is reasonable that all this will be common knowledge by the time of ICCF6.

References

[1] T. Kuhn, *The Structure of Scientific Revolutions* (Chicago Univ. Press, Chicago, 1962).

[2] D.J. Gross, F. Wilczek, *Phys. Rev.* **D9** (1973) 1343.

[3] G. Preparata, *Nuovo Cim.* **107A** (1994) 2657.

[4] G. Preparata, *Nuovo Cim.* **96A** (1986) 366.

[5] G. Preparata, in "*Problems of Fundamental Modern Physics*", R. Cherubini, P. Dalpiaz and B. Minetti eds. (World Scientific, Singapore, 1990).

[6] P.W. Anderson, *Basic Notions of Condensed Matter Physics* (Benjamin-Cummings, Menlo Park (Ca), 1984).

[7] G. Preparata, *QED Coherence in Condensed Matter* (World Scientific, Singapore, 1995).

[8] T. Bressani, E. Del Giudice, G. Preparata *Nuovo Cim.* **101A** (1989) 845.

[9] G. Preparata, *Proc. First Annual conference on Cold Fusion*, Salt Lake City, Utah, March 28-31 (1990) 130.

[10] M. Fleischmann, S. Pons, G. Preparata, *Nuovo Cim.* **105A** (1992) 763.

[11] A. Cohen, *Z. Electrochem.* **35** (1929) 676.

[12] G. Preparata, *Towards a theory of Cold Fusion Phenomena*, Proc Rome Workshop of Cold Fusion in Italy, B. Stella ed. (Roma, 1993).

[13] G. Preparata, *Transactions of fusion technology*, **26** (1994) 397.

[14] G. Preparata and F. Taddei, in preparation.

[15] G. Mengoli et al., *J. Electroanal. Chem.* **57** (1989) 350.

[16] M. Fleischmann, S. Pons, *Transactions of fusion technology*, **26** (1994) 87.

[17] R. Arani et al., *QED coherence and the therodynamics of water*, preprint MITH 93/3 (Milano 1993).

[18] M. Rabinowitz et al., *Transactions of fusion technology*, **26** (1994) 3.

[19] V.A. Chechin et al., *Int. Journ. Theor. Phys.* **3** (1994) 617.

Fifth International Conference on Cold Fusion
9-13 April, 1995 - Monte Carlo, Monaco
ICCF5 ©1995

Solving the Puzzle of Excess Heat without Strong Nuclear Radiation

Xing Zhong LI*
Department of Physics, Tsinghua University
Beijing 100084, CHINA
*Current address: Dept. of Chem., Univ. of Hawaii, Honolulu, HI 96822-2275, USA

Abstract

Five experimental evidences show that the excess heat is from a nuclear source with a life-time of 10^4 seconds. This life-time is shown to be related to the barrier penetration number, θ, in terms of the resonance penetration theory. The boson nature of the deuteron ion (D^+), and the deuteron energy band structure in lattice play the critical roles in filling the corresponding narrow resonance energy level. Prof. J. Huizenga's challenge of three miracles[1] is answered, and "excess heat" without strong nuclear radiation is a reasonable phenomenon. It predicts: (1) there must be a critical loading ratio; (2) the greater the grain size and the activation energy are, the better the reproducibility.

1. Introduction

After six years of studies on the "cold fusion" phenomenon, two facts are established: (1) Under certain conditions there is "excess heat" of several watts per cubic centimeter of palladium; (2) There are no commensurate neutrons, tritons, or γ-radiation in parallel with the "excess heat" which is of non-chemical origin. The regression is that: instead of using the neutron signal to convince people to believe there is any nuclear reaction, we attempt to explain that these two facts are due to the existence of a long life-time nuclear resonance state inside a lattice.

Early in 1928, Gamow proved that the life-time of an α-radiation nuclide, τ_α, was determined by the Coulomb barrier penetration number, θ.[2] At that time the α-particle after disintegration was a free-moving particle , and $\tau_\alpha \propto \theta^2$. Now the penetration of the Coulomb barrier happens in a reverse direction and in a different environment: the lattice confined deuteron penetrates the Coulomb barrier and enters a resonance state. The life-time of this resonance state, τ_{xh}, is determined by the θ again, but $\tau_{xh} \propto \theta$. Now τ_{xh} is linearly proportional to the θ due to the discrete nature of the energy level of the lattice confined deuteron which is different from the continuum of the free-moving deuteron.

We will start from the experimental evidences of this long life-time state (section 2); then, we calculate this life-time based on the nuclear resonance theory (section 3). In order to fill this resonance state, this theory requires a critical loading ratio which is another well-established experimental fact in the past five years (section 4). Finally, we discuss the famous challenge of three miracles (section 5), and the conclusion (section 6).

2. Evidences for Long Life-time State

The strongest evidence is from the "heat after death".[3] The boiling-to-dry electrolytic cell was kept at about 100 °C for three hours without any power input. It clearly showed that the "excess heat" source was inside the palladium deuteride. The reliable calorimetric calculation proved that the energy released in this 3 hours was 20 times greater than the heat of combustion possibly released by the deuterium stored in this system. This was a nuclear active state with a life-time of 10^4 seconds.

The second evidence is from the "heat after life".[4] The SRI electrolytic cell was a closed cell. It was not driven to boil. However, when the electrolysis was shut down, and input power was zero, the system did not cool down as a source-free system. The flow-calorimeter clearly recorded that there was an energy source inside the system. The first peak of the "excess power" was about 100 mW (the accuracy and the precision of that experiment was ±10 mW), and the width of that peak was about 3 hours again. The energy released in these three hours was also about 10 times greater than the heat of combustion possibly released by the deuterium available in the palladium electrode. This was again a nuclear active state with a life-time of 10^4 seconds.

During the ICCF-5, J.P. Biberian's "excess heat" data [5] showed that after the shut down of the input power, the "excess heat" continued for 3–4 hours. Although there was no palladium lattice, an $AlLaO_3$ single crystal provided the lattice confined deuterons. Once again the life-time of that "excess heat" source was of the order of 10^4 seconds.

In the "Critical Review of the 'Cold Fusion' Effect",[6] E.Storms talked about the replacing time of the palladium deuteride. When he put the deuteron-loaded electrode into the light water cell, he observed the "excess heat" continuing for the first several hours. He called this time the replacing time, because he considered that when the deuteride was replaced by hydride, the "excess heat" was supposed to stop. From another point of view, this showed that the life-time of the nuclear active state was again of the order of 10^4 seconds.

After my talk in ICCF-5, M.Eisner of the University of Houston was so kind as to give me his 1989 data for the "excess heat".[7] It clearly showed that the width of the first "excess power" peak after the shut down of the electrolysis was once again of the order of 10^4 seconds.

It was not realized that the answer to Prof. J.Huizenga's challenge of three miracles has been indeed implied in this long life-time of nuclear active state.

3. Theory of Resonance Penetration for Lattice Confined Ions

The life-time of a quantum mechanical state, τ, is related to the width of its energy level, Γ, by the uncertainty principle:

$$\tau \approx \frac{\hbar}{\Gamma} \tag{1}$$

The width of the energy level can be expressed by the imaginary part of the wave number, k^i, through the identity:

$$\Gamma = \mathrm{Im}U \equiv \frac{\hbar^2}{m} k^r k^i \tag{2}$$

Here $\mathrm{Im}U$ is the imaginary part of the potential well U, k^r and k^i are the real and imaginary part of the wave number k, respectively. $k^2 \equiv \frac{2m}{\hbar^2}(E-U)$. E is the total energy of the relative motion of the two deuterons. When the energy E coincides with the energy level inside the nuclear well, $(k^r a) \approx O(1)$. Here a is the size of the nuclear well. However

$$\left|k^i a\right| \approx O(\theta^{-1}) \tag{3}$$

for this resonance. Here θ is defined as

$$\theta \equiv \exp[\int_a^b \sqrt{\frac{2m}{\hbar^2}(U-E)}dr] \tag{4}$$

and θ^{-2} is just the famous Gamow barrier penetration factor. Equation (3) has been rigorously proved for the square well case, [8] and for the arbitrary potential configuration.[9] Here we just explain why the imaginary part of the wave number, k^i , should be such a small number in order to have a resonance penetration. As we know, when $k^i < 0$, k^i determines the damping of the wave function. The wave e^{-ikr} will be damped by a factor of $\exp[-\left|k^i a\right|]$ when the wave propagates through a length of a. On the other hand the Coulomb barrier suppresses the amplitude of the penetrating wave function by a factor of θ^{-1}. In order to use the resonance effect to build-up the wave amplitude to its initial value in terms of the constructive interference between the reverberating wave and the penetrating wave, we need at least θ-times reverberation before the wave is damped. So we need $\left|k^i(\theta a)\right| \le O(1)$, or $\left|k^i a\right| \le O(\theta^{-1})$.

Consequently, sustituting k^r and k^i in eq.(1) and (2), we have the life-time for "excess heat"

$$\tau_{xh} \approx \frac{ma^2}{\hbar}\theta \tag{5}$$

For the d+d interaction, m≈10^{-24}g., $a \approx 10^{-13}$ cm, $\theta \approx 10^{27}$, [10,11] we have $\tau_{xh} \approx 10^4$ sec. The theory just gives the correct order of magnitude of the life-time of the nuclear active state.

4. Bose Condensation and the Critical Loading Ratio

Such a long life-time state corresponds to a very narrow energy level in the order of 10^{-19} eV. This is the reason why we could not observe this resonance level in any low energy beam-target experiment.[12] Because the beam energy distribution is much wider than the width of the resonance energy level, it is an analogy to using a screw driver to detect a tiny crack in a brick wall. The crystal lattice assists in observing this narrow resonance in two ways: (1) the trapped deuteron ion in the lattice well is sitting on a discrete energy level with very narrow width also; (2) the periodical structure of the lattice well creates an energy band for the trapped deuteron ions. Then, we have a bunch of needles to detect the single tiny crack on the brick wall. The number of the energy levels (needles) in this band is determined by the grain size, L (i.e. the size of the periodical structure, or the coherent length), and the size of the primitive cell in the palladium lattice, δ (i.e. the size of the PdD molecule). When $\delta \approx 3\text{Å}$, L≈ 60μ, we have roughly $(L/\delta)^3 \approx 10^{16}$ energy levels inside a deuteron energy band. On the other hand the deuteron energy band width, Γ_B, is determined by the size of the primitive cell as:

$$\Gamma_B \le \frac{\hbar^2}{2m}\left(\frac{1}{\delta}\right)^2 \approx 10^{-3}\text{eV} \tag{6}$$

Thus, the energy difference between each neighboring energy level inside the band is about 10^{-19} eV. Hence, if the whole band is occupied by the deuterons; then, the whole population has the chance to be in resonance penetration of Coulomb barrier, as long as the energy band is adjusted to a level in resonance with the nuclear energy level. When $(L/\delta)^3 << 10^{16}$, we have much less chance to have resonance penetration of the Coulomb barrier due to the difficulty in matching the narrow nuclear energy level with the lattice energy level.

Now the question is: how can we populate the deuterons into this energy band ? We need the Bose-Einstein condensation. Experiment has shown that hydrogen solved in palladium acts like an ion,[13] so deuteron should act like a boson. If the deuterons are totally free-moving particles like a gas inside the palladium; then, the critical density for Bose-Einstein condensation is about[14]

$$n_c = 2.612\left(\frac{mk_BT}{2\pi\hbar^2}\right)^{3/2} \approx 8.5\times10^{24}\ \text{cm}^{-3} \tag{7}$$

It is much higher than the maximum possible deuteron density inside the palladium ($\approx 6.8\times10^{22}$ cm^{-3}). However, the experiment has also shown that the hydrogen solved in palladium is not a free-moving gas. In order to explain the anomalous diffusion behavior of the hydrogen in the palladium, we must assume that there is a component of trapped hydrogen ions (localized).[15] If we assume an energy spectrum as that in Fig.1,

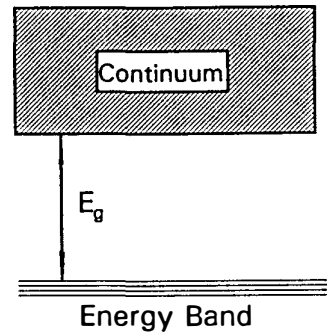

Fig.1 Energy Band Structure in Palladium Deuteride lattice

then the critical density for Bose-Einstein condensation would be

$$n_{cg} = n_c \exp(-\frac{E_g}{k_BT}) \tag{8}$$

Using $n_{cg}\approx 6.8\times10^{22}$ cm^{-3} (corresponding to critical loading ratio$\approx$1), T=300 K, we have

$$E_g = -k_BT\log(\frac{n_{cg}}{n_c}) \approx 125\ \text{meV} \tag{9}$$

this number is very close to the activation energy for hydrogen in palladium.[15]

In fact this condensation model gives a good reason for the critical loading ratio. If the deuteron density is lower than this critical density n_{cg}, then, there will be no enough population in the low lying energy band, and less chance for resonance penetration.

5. Nuclear Surface Absorption and $0^+\rightarrow0^+$ Forbidden Transition

The low energy beam-target experiments have established a fact that the strong interaction will annihilate the penetrating deuteron wave after several reverberations. When one assumes the reaction rate

$$\Lambda = A|\Psi(0)|^2 \tag{10}$$

low energy experimental data show that $A = 1.5\times10^{-16}\text{cm}^3\,\text{sec}^{-1}$.[16] Considering that the volume of the deuteron-deuteron nuclear interaction is the order of 10^{-39} cm^3, we know that the life-time of the deuteron-deuteron strong interacting system is the order of 10^{-23} sec, i.e. the order of the reverberation time. Then, one may ask the reason why the built-up wave function in the resonance case is not annihilated by this strong interaction .

In fact, the strong absorption in the nuclear well is concentrated on the surface region as suggested by the nuclear optical model.[17] The reaction "constant", λ, is not a constant inside the nuclear well; hence, the reaction rate, Λ, should be

$$\Lambda = \int \lambda(r)|\Psi(r)|^2 d^3\vec{r} = \int \lambda_V(r)|\Psi_V(r)|^2 d^3\vec{r} + \int \lambda_S(r)|\Psi_S(r)|^2 d^3\vec{r} \qquad (11)$$

Here, the subscripts, V and S, denote the volume and surface, respectively. $\lambda_V(r)$ is much smaller than $\lambda_S(r)$ by a factor of θ^{-1}. When there is no resonance, $|\Psi_V(r)| \approx |\Psi_S(r)|$; then, the reaction happens mainly in the surface region of the nuclear well, and the life-time is the order of the reverberation time. When the energy reaches the resonance level, the wave function, $\Psi_V(r)$, builds up due to the constructive interference between the penetrating wave and the reverberating wave. $|\Psi_V(r)| \approx \theta|\Psi_S(r)| >> |\Psi_S(r)|$ .Hence,

$$\int \lambda_V(r)|\Psi_V(r)|^2 d^3\vec{r} \approx \int \frac{1}{\theta}\lambda_S(r)|\theta\Psi_S(r)|^2 d^3\vec{r} >> \int \lambda_S(r)|\Psi_S(r)|^2 d^3\vec{r} \qquad (12)$$

The life-time of the state is determined by the core part of the wave function, and is greater than the reverberation time by a factor of θ.

In other words, the strong interaction annihilates only the deuteron wave near the nuclear surface. The deuteron wave function can still be built up inside the core of the nuclear well where the absorption due to strong interaction is weak. Physically, the absorption (i.e. deuteron loses its identity) only happens in the region where the nuclear force (the derivative of the nuclear potential) is large. Inside the nuclear core, although the nuclear well is deep, the nuclear force is weak there. So the deuteron wave can survive inside the core of the nuclear well.

In contrast to the short range of the nuclear force, the electromagnetic interaction is a kind of long range force. One may ask the reason why the electromagnetic force does not annihilate the long life-time state . This is due to the symmetry of the system. The symmetry of the wave function of the d+d system is determined by their orbital motion and their spin motion. At the low incident energy, only the S-wave (orbital angular momentum l = 0) is dominant inside the core of the nuclear well. So the symmetry for the orbital motion is symmetric about the exchange of the two deuterons. Then, the spin motion part of the wave function should be symmetric also in order to keep the symmetry of the total wave function which is necessary for a boson-boson indistinguishable particle system. The spin for each deuteron is 1, the resultant angular momentum may be 0,1, or 2. Since the state of resultant spin 1 is anti-symmetric about the exchange of the two deuterons, it is not an allowable state. The resultant spin should be 0 or 2.[18] Consequently, the possible total angular momentum and parity for the d+d system is 0^+, or 2^+. If the resonance state takes the 0^+; then, it should be stable against the electromagnetic interaction. Because the ground state for d+d system is 0^+ (helium-4), and the spin for photon (the electromagnetic quantum) is 1,

it is forbidden to have a $0^+ \rightarrow 0^+$ electromagnetic transition due to the conservation of the angular momentum.

What we have to figure out is the mechanism through which the excited d+d system transfers the energy to the lattice system in a slow time scale.

6. Conclusion: Thunder without Lightning is OK

Based on above-mentioned discussion, we have seen that the long life-time nuclear active state may be created after the resonance penetration of Coulomb barrier in the d+d system in terms of the lattice confined deuterons. This is a resonance state which cannot be observed in a low energy beam-target experiment. This resonance state will not emit strong nuclear radiation (neutron, triton, or γ radiation). This is just the answer to Professor J.Huizenga's challenge of three miracles. Only the chemists have a better chance to discover this nuclear active state in terms of calorimeter, because there is no strong nuclear radiation.

Although it is a long life-time slow reaction, it is still a practically useful energy source. Even if only one thousandth of the deuterons inside the palladium are involved in this state, the "excess power" is of the order of 1 kW per cubic centimeter of the palladium. This is about the same as that in a fuel rod of a fast fission breeder reactor.

In these two meanings, we say that thunder without lightning is O.K. This theory predicts that if we could produce the palladium with greater grain size and greater activation energy, it should be easier to reproduce the "excess heat" experiment.

Acknowledgments

This work is under the project of the State Commission of Science & Technology, and the Natural Science Foundation of China. Many thanks to Mr. Karl Chang, the co-founder of the VeriFone Inc., for his generous support, and to Professors D.Yount, G.Andermann, B.Liebert, and Dr. B.Liaw for their hospitality during author's visit to the Univ. of Hawaii. Professor M.Fleischmann's personal contribution is critical for this work to be presented at ICCF-5.

List of Symbols

a=size of the nuclear well, cm

A=experimental bulk reaction constant, $cm^3 sec^{-1}$

b=classical turning point of Coulomb barrier, cm

d=deuteron

E=total energy of relative motion, erg.

$\hbar$=Planck constant divided by 2π, erg·sec

k, k^i and k^r=wave number, its imaginary and real part, cm^{-1}

k_B=Boltzmann constant, erg·K

L=grain size in crystal, cm

m=mass of deuteron, g

n_c=critical density for Bose condensation of free-moving particles, cm^{-3}

n_{cg}= critical density for Bose condensation of particles with energy gap in spectrum, cm^{-3}

r =radial coordiante, cm

T=temperature, K

U=potential energy, erg

ImU=imaginary part of the potential energy, erg

Γ= width of energy level, erg

Γ_B=width of energy band, erg
δ=size of the primitive cell of a crystal, cm
λ=reaction constant, sec^{-1}
λ_V=reaction constant in core region of the nuclear well, sec^{-1}
λ_S=reaction constant in surface region of the nuclear well, sec^{-1}
Λ=reaction rate, sec^{-1}
θ=square root of the reciprocal of Gamow factor
τ=life-time of an energy level, sec
τ_{xh}=life-time of the resonance state releasing "excess heat"
Ψ=wave function, $cm^{-3/2}$

References

1.J.R.Huizenga, "*Cold Fusion: The Scientific Fiasco of the Century*", p.112,University of Rochester Press (1992).
2.G.Gamow, "Zur Quantentheorie des Atomkernes." *Zeitschrift fur Physik*, 51, 204 (1928).
3.S.Pons & M.Fleischmann, "Heat after death", *Proceedings: Fourth International Conference on Cold Fusion*,Decmber 6-9,1993, Lahaina, USA, Vol.2, p.8-1(1994).
4.M.C.H.McKubre, et al.,"Loading, Calorimetry, and Nuclear Investigation of the D/Pd System", *Proceedings: Fourth International Conference on Cold Fusion*, Decmber 6-9,1993, Lahaina, USA,Vol.1, p.5-26(1994).
5.J.P.Biberian,"Excess Heat Measurement in $AlLaO_3$ Doped with Deuterium", ICCF-5, paper No.205(1995).
6.E.Storms,"A Critical Overview of Cold Fusion", ICCF-5, paper No.101(1995).
7.M.Eisner,"The Serendipitous Design and Execution of an Early Experiment which Confirmed Heat in the Fleischmann-Pons Effect",ICCF-5, paper No.212(1995).
8.X.Z.Li, "Tunneling the Coulomb Barrier via Lattice Confined Ions", submitted to *Physics Letters A*,(1995).
9.X.Z.Li, "Revisit to Gamow Factor", ICCF-5, paper No.403,(preprint,1995).
10. S.E.Koonin, and M.Nauenberg, "Calculated Fusion Rates in Isotopic Hydrogen Molecules." *Nature*, 339, 690(1989).
11.Ya. B. Zel'dovich, S.S.Gershtein, "Nuclear Reactions in Cold Hydrogen, I. Mesonic Catalysis", *Soviet Phys. Usp.* 3, 593 (1961).
12. F.E.Cecil, and G.M.Hale, "Measurement of d-d and d-^{6}Li Nuclear Reactions at Very Low Energies." in the "*The Science of Cold Fusion.*" Edited by T.Bressani, E.Del Giudice and G.Preparata, SIF, Bologna, p.271 (1991).
13.A.H.Verbruggen, et al., *Phys. Rev. Lett.* 52, 1625 (1984).
14.C.Kittel, and H.Kroemer, "*Thermal Physics*", 2-nd ed., p.281, Freenman, New York (1980).
15.Y.Fukai, "*The Metal-Hydrogen System*", p.212, Springer Verlag, Berlin (1993).
16.F.W.Fowler, G.R.Caughlan, & B.A. Zimmerman, *A. Rev. Astr. Astrophys.* 5, 525-570 (1967).
17.H.Feshbach, "*Theoretical Nuclear Physics*", Wiley & Sons, Inc.,Boston, p.488(1992)
18. D.M.Brink, and G.R.Satchler, "*Angular Momentum*", 3-rd ed., p.35, Oxford Science Publications (1993).

Fifth International Conference on Cold Fusion
9-13 April, 1995 - Monte Carlo, Monaco
ICCF5 ©1995

Uncertainties of Conventional Theories and New Improved Formulations of Low-Energy Nuclear Fusion Reactions

Yeong E. KIM and Alexander L. ZUBAREV
Department of Physics, Purdue University
West Lafayette, IN 47907-1396, U.S.A.

Abstract

We examine uncertainties of conventional theoretical estimates for low-energy nuclear fusion cross-section $\sigma(E)$ and fusion rate $\langle\sigma v\rangle$. Using new formulations based on the optical theorem and the radial distribution function, we derive new improved formulae for $\sigma(E)$ and $\langle\sigma v\rangle$. Our results of the optical theorem formulation for $\sigma(E)$ indicate that a near cancellation of the Gamow factor can occur if the imaginary part of the effective nuclear interaction in the elastic scattering channel has a very weak component with a long finite interaction range. Uncertainties of conventional estimates of the electron screening effect for $\sigma(E)$ are also examined and a new alternative formulation is proposed. Finally, based on a solution of three-body Schrödinger equation and the optical theorem formulation, we derive a new formula for three-body fusion cross-section and rate and compare its predictions with conventional estimates and also with the recent experimental data for three-deuteron fusion reaction.

1. Introduction

In this paper, we examine uncertainties of conventional theoretical estimates and propose new improved formulations of low-energy nuclear fusion reactions. Since the 1989 announcements of nuclear fusion at room temperature in palladium (Pd) [1] and titanium (Ti) [2] electrolytic cells using heavy water (D_2O), there have been persistent claims of observing the cold fusion phenomena. Most of the reported experimental results are not reproducible at a desirable level of 100% [3]. However, there are a few experimental results which appear to be 100% reproducible [4,5]. There have been many theoretical models proposed to explain the cold fusion phenomena. Most of those theoretical models claiming to have explained the phenomena appear far from having accomplished their claims [6,7].

In section 2, we present a new alternative theoretical formulation of low–energy nuclear fusion reactions based on the optical theorem [8], which is much less model–dependent than previous theoretical approaches. In section 3, we describe and compare our new improved formula with the conventional one for the fusion cross-section. In section 4, we show that some of the cold fusion phenomena may be justified theoretically if the imaginary part of the effective nuclear interaction in the elastic channel has a very weak component with a long finite interaction

has a component with a long finite range. A new modified general formula for nuclear fusion rate in high-density plasma is derived in section 5. In section 6, we discuss uncertainties of the conventional theoretical estimates of low-energy fusion rates due to electron degrees of freedom. We propose an alternative formulation for investigating the electron screening effect, which avoids this difficulty. In section 7, we show that there is a very serious difficulty associated with non-square integrability in the conventional formula. In section 8, we describe a derivation of a new formula for three-body fusion cross-section and rate, and compare its predictions with the conventional estimates and also with the recent experimental data for $D+D+D \rightarrow p+n+{}^4\mathrm{He}$ reaction [5]. Section 9 contains a summary and conclusions.

2. Optical Theorem Formulation of Fusion Reactions

For the elastic scattering cross-section $\sigma^{(e\ell)}(E)$, we introduce the partial wave expansion $\sigma^{(e\ell)}(E) = \sum_\ell (2\ell+1)\sigma_\ell^{e\ell}$ where $\sigma^{(e\ell)}$ is related to the elastic partial wave scattering amplitude $f_\ell^{(e\ell)}$ by $\sigma_\ell^{(e\ell)} = |f_\ell^{(e\ell)}|^2$ where $f_\ell^{(e\ell)} = f_\ell^c + e^{2i\delta_\ell^c} f_\ell^{N(e\ell)}$ with $f_\ell^{N(e\ell)} = (S_\ell - 1)/2ik$ and the ℓth partial wave S-matrix given by S_ℓ. Hence, $\sigma_\ell^{(e\ell)}$ can be written as

$$\sigma_\ell^{(e\ell)} = |f_\ell^{(e\ell)}|^2 = \sigma_\ell^c + \sigma_\ell^{\mathrm{int}} + \sigma_\ell^{N(e\ell)} \tag{1}$$

where $\sigma_\ell^c = |f_\ell^c|^2 = 4\pi \sin^2\delta_\ell^c/k^2$ (Rutherford scattering), $\sigma_\ell^{\mathrm{int}} = -2\pi Re\ [(S_\ell - 1)(e^{2i\delta_\ell^c} - 1)]/k^2$ (interference term), and $\sigma_\ell^{N(e\ell)} = |f_\ell^{N(e\ell)}|^2 = \pi|S_\ell - 1|^2/k^2$ (nuclear scattering).

For reaction cross-section, we have $\sigma^{(r)} = \sum_\ell (2\ell+1)\sigma_\ell^{(r)}$ where $\sigma_\ell^{(r)} = \pi(1 - |S_\ell|^2)/k^2$. Using $\sigma_\ell^{(r)} + \sigma_\ell^{N(e\ell)} = 2\pi(1 - ReS_\ell)/k^2$, and $Imf_\ell^{N(e\ell)} = (1 - ReS_\ell)/2k$, we obtain the optical theorem for two-potential scattering case as

$$Imf_\ell^{N(e\ell)} = \frac{k}{4\pi}\left(\sigma_\ell^{(r)} + \sigma_\ell^{N(e\ell)}\right) \tag{2}$$

which is a rigorous result.

For low energies, $f_\ell^{N(e\ell)} \propto e^{-2\pi\eta}/k$ and hence $\sigma_\ell^{N(e\ell)} = |f_\ell^{N(e\ell)}|^2 \propto e^{-4\pi\eta}/k^2$. Since $\sigma_\ell^{(r)} \propto e^{-2\pi\eta}/k^2$, we have $\sigma_\ell^{(r)} >> \sigma_\ell^{N(e\ell)}$ at low energies, and hence we can write eq. (2) as

$$Imf_\ell^{N(e\ell)} \approx \frac{k}{4\pi}\sigma_\ell^{(r)} \tag{3}$$

which is still a rigorous result at low energies. We note that eqs. (2) and (3) are for non-radiative nuclear reactions and need to be modified for radiative nuclear reactions.

In terms of the partial wave T-matrix, T_ℓ, the elastic nuclear scattering amplitude, $f_\ell^{N(e\ell)} = (S_\ell - 1)/2ik$, can be written as

$$f_\ell^{N(e\ell)}(E) = -\frac{2\mu}{\hbar^2 k^2}\langle\psi_\ell^c|T_\ell|\psi_\ell^c\rangle \tag{4}$$

where ψ_ℓ^c is the ℓth partial wave regular Coulomb function and μ is the reduced mass. Using the low energy optical theorem eq. (3) with eq. (4), we obtain the ℓth partial-wave (fusion) reaction cross-section $\sigma_\ell(E)(=\sigma_\ell^{(r)}(E))$ as

$$\sigma_\ell(E) \approx \frac{4\pi}{kE}\int_0^\infty \psi_\ell^c(r)U_\ell(r,r')\psi_\ell^c(r')drdr' \tag{5}$$

where $E = \hbar^2k^2/2\mu$ and $U_\ell(r,r') = -Im\langle r|T_\ell|r'\rangle$ with T_ℓ representing the ℓth partial wave contribution of the T-matrix operator. The total cross-section $\sigma(E)$ is given by $\sigma(E) = \sum(2\ell+1)\sigma_\ell(E)$. It is important to note that our optical theorem formulation of nuclear reactions, eq. (3), can be applied to both non-resonance and resonance reactions using the T-matrix given in eq. (4). In reference [8], we have shown that $U(r,r')$ has a separable form for the case of two open channels (elastic and fusion).

3. New Fusion Cross-Section Formula and the Effective Potential Range

It is shown in reference [8] that $Im\langle r|T_\ell|r'\rangle$ for $\ell = 0$ case and hence $U_0(r,r')$ in eq. (5) are separable for the two-channel case. Therefore, for estimating the S-wave cross section, $\sigma_0(E)$, for the two-channel case, we can parameterize $U_0(r,r')$ in eq. (5) by two parameters λ (strength/length) and β^{-1} (range) in a separable form as

$$U_0(r,r') = \lambda g(r)g(r') \tag{6}$$

where λ is expected to be a slowly varying function of E for the non-resonance case. (For the case of resonance reactions the energy dependence of λ can be parameterized by the Breit-Wigner expression.) For $g(r) = e^{-\beta r}/r$, the integral in eq. (5) can be carried out analytically using eq. (6) and the exact form $\psi_0^c(r)$ $= C_0(\eta)M_{i\eta,\frac{1}{2}}(2ikr)/2i$, where $C_0^2(\eta) = 2\pi\eta/(e^{2\pi\eta}-1)$ and $M'_{i\eta,\frac{1}{2}}$ is the Whittaker function. The result is

$$\sigma_0(E) = \frac{4\pi\lambda}{kE}\left[\int_0^\infty dr\psi_0^c(r)e^{-\beta r}/r\right]^2 = \frac{4\lambda\pi^2}{E}R_B\frac{(e^{-2\phi\eta}-1)^2}{(e^{2\pi\eta}-1)}e^{4\phi\eta} \tag{7}$$

which for the low-energy case reduces to

$$\sigma_0(E) = \frac{\tilde{S}_0(E)e^{4\phi\eta}}{E}\,e^{-2\pi\eta} \tag{8a}$$

with

$$e^{4\phi\eta} = \exp\left[4\alpha\frac{\mu c^2}{\hbar c}\left(\frac{Z_aZ_b}{k}\right)\tan^{-1}\left(\frac{k}{\beta}\right)\right] \tag{8b}$$

where $\phi = \tan^{-1}(k/\beta)$ and $\tilde{S}_0(E) = 4\pi^2\lambda R_B$ with $R_B = \hbar^2/(2\mu Z_aZ_be^2)$. Since the energy dependence of V_0 and β is expected to be weak, $\tilde{S}_0(E)$ depends weakly on

energy. Numerical results of eq. (8b) will depend on the unknown range parameter β^{-1}, which needs to be determined either from experimental data or from reliable microscopic calculations.

The use of $g(r) = e^{-\beta r}$ leads to

$$\sigma_0(E) = \frac{4\pi^2\lambda}{ER_B}\left(\beta^2 + k^2\right)^{-2}\left(e^{2\pi\eta} - 1\right)^{-1} e^{4\phi\eta} \tag{9}$$

while, for $g(r) = re^{\beta r}$, we obtain

$$\sigma_0(E) = \frac{4\pi^2\lambda}{ER_B^3}\left[(2R_B\beta + 1)^2/\left(\beta^2 + k^2\right)^4\right]\left(e^{2\pi\eta} - 1\right)^{-1} e^{4\phi\eta} \ . \tag{10}$$

The use of a more general form for $g(r) = e^{-\beta r}\left(\Sigma_{i=0}^{N} c_i r^i\right)$ in eq. (6) also leads to the same enhancement factor $e^{4\phi\eta}$. Therefore, the enhancement factor $e^{4\phi\eta}$ is independent of shape of the separable function $g(r)$ used in eq. (6). The enhancement factor $e^{4\phi\eta}$ can be applied to both light nuclei reactions (small Z_a and Z_b) but also to heavy ion reactions (larger Z_a and Z_b) such as sub–barrier heavy ion fusion where $e^{4\phi\eta}$ can be very large.

Our derivation of eq. (8a) is the first derivation of the Gamow factor based on the optical theorem, and is much more rigorous than other previous derivations, most of which are based on the barrier transmission coefficient derived in the WKB approximation. Our new extra exponential factor, $e^{4\phi\eta}$, eq. (8b), in eq. (8a) is obtained together with the Gamow factor from our derivation and can be regarded as a modification of the Gamow factor affecting it only at low energies, or as a part of the S-factor if we still wish to keep the conventional formula eq. (11). In any case, the new exponential factor has a sound theoretical foundation as the above nearly model-independent derivation clearly shows. Furthermore, the energy dependence of this new extra exponential factor depends on the range parameter, inverse of beta (β^{-1}). If the range is small, this factor is nearly energy independent as experimental data for some low–energy reactions show. If the range is longer, the new extra exponential factor can provide an enhancement of the "S-factor" or the cross-section over the conventional values at low energies, and thus could give a reasonable explanation of the experimental data referred to below [9-12]. Therefore, it is important to determine the range of the imaginary part of the effective potential in the elastic channel for each nuclear reaction from experiment and/or from reliable microscopic calculations.

For non–resonance reactions, it is customary to extract the S–factor, $S(E)$, from the experimentally measured $\sigma(E)$ using the following formula

$$\sigma_G(E) = \frac{S(E)}{E} e^{-2\pi\eta(E)} \tag{11}$$

where $\eta(E) = Z_a Z_b e^2/\hbar v$, $e^{-2\pi\eta(E)}$ is the Gamow factor representing the probability of bringing two charged nuclei to zero separation distance, and $S(E)$ is

expected to be a slowly varying function of E. Recent results for $\sigma(E)$ from laboratory beam experiments for nuclear reaction involving light nuclei at low energies (> 3 keV) show that the extracted $S(E)$ increases toward lower energies instead of being a constant extrapolated from higher energy data, indicating a possibility of the importance of the electron screening. However, recent theoretical calculations [13,14] of the electron screening effect yield limiting values which are much smaller (by $\sim 1/2$) than those extracted from the experimental data for reactions ^{3}He$(d,p)^4$He [9,10], ^{6}Li$(p,\alpha)^3$He, ^{6}Li$(d,\alpha)^4$He, ^{7}Li$(p,\alpha)^4$He [11], ^{10}B$(p,\alpha)^7$Be, and ^{11}B$(p,\alpha)^7$Be [12]. This discrepancy between the experimental data and the theoretical estimate for the electron screening effect is not understood at present. Because of the importance of accurate low–energy cross–sections for bare nuclei needed for astrophysical problems, it is very important to understand and resolve the discrepancy. If we identify $\tilde{S}_0(E)$ in eq. (8a) as $S(E)$ in eq. (11), $e^{4\phi\eta}$ in eq. (8a) is a new enhancement factor for S–factor $S(E)$ in eq. (11).

Since $\phi = \tan^{-1}(k/\beta) = \pi/2$ and $e^{4\phi\eta} = e^{2\pi\eta}$ in the limit of $\beta \rightarrow 0$, a (near) cancellation of the Gamow factor $e^{-2\pi\eta}$ can occur if the interaction range β^{-1} is large (or β is small). Therefore, it is important to investigate a possibility that the interaction range is finite but large (i.e., long finite range). One example is a long range potential which can arise from Coulomb interaction as an electric polarization potential in the real part of the effective potential in the elastic scattering channel at low energies due to the electric polarizability of the target [15-19].

The effective potential V for scattering of a charged projectile from a target with an extended charge distribution can be written as

$$V = V^S + V^C + V^{pol} \tag{12}$$

where V^C and V^S are Coulomb and strong interactions, respectively. The polarization potential in the adiabatic approximation is given by

$$V^{pol}(r) \approx \frac{\alpha_e e^2}{2R_B r^4}\ , \quad r >> R_B \tag{13}$$

where α_e is the electric polarizability of the target and R_B is the Bohr radius of the target plus the projectile, $R_B = \hbar^2/(2\mu Z_a Z_b e^2)$. If we denote the S–factor, S, corresponding to the case of no polarization potential ($V^{pol} = 0$, and $V = V^S + V^C$) and the polarization S–factor, S_p, for the case including V^{pol} ($V = V^S + V^C + V^{pol}$), perturbation calculations [15-18] yield $|S_p/S - 1| < 10^{-3}$, and show that V^{pol} has negligible effects for fusion reactions involved in stellar nucleosynthesis [19]. Even though V^{pol} has a long range, it is the real part of the effective potential, and hence it does not contribute to the enhancement factor $e^{4\phi\eta}$ in eq. (8a) which is due to a finite range interaction in the imaginary part of the effective potential.

Using the observed value of the deuteron polarization $\tilde{\alpha} = \alpha_e/R_B = 0.63$ fm^3 [19], we can show that $V^{pol}(R_B) \approx 10$ eV. To obtain an upper bound of $|S_p/S - 1|$, we can use the following expression

$$\left|\frac{S_p(E)}{S(E)} - 1\right| < \left|e^{2\pi(\eta(E+V_{pol}(R_B)) - \eta(E))} - 1\right| . \tag{14}$$

For the $d+d$ reaction with $E = 2$ keV, eq. (14) yields $|S_p(E)/S(E) - 1| < 10^{-2}$. In laboratory beam experiments, the electron screening effect needs to be taken into account using the screening energy, which is known to be larger than $V^{pol}(R_B) \approx 10$ eV. Therefore, the effect of the polarization potential may be negligible for low–energy fusion reactions. This example shows that the contribution of the real part of the effective potential to the reaction cross–section behaves drastically different from that of the imaginary part of the effective potential.

Interaction range of the imaginary part of the effective potential in the elastic channel for nuclear fusion reactions at low energies has not been investigated previously, although there are some examples of the imaginary part of the effective potential with a long finite interaction range involving Coulomb excitation. When inelastic channels due to Coulomb excitation of the target nucleus to excited states become open at higher energies, a dynamic polarization potential results from the long–range Coulomb potential. For the case of a quadrupole excitation, the dynamic polarization potential has an imaginary part with an asymptotic behavior of r^{-5} at large distances [20]. For nuclear fusion reactions involving charged nuclei, rearrangement or fusion is involved in the exit channel, and hence it may be reasonable to expect that a long range interaction may result as an imaginary part of the effective potential due to the long–range Coulomb potential involved in nuclear fusion reactions. Therefore it is suggestive that the imaginary part may also have a component with a long finite range interaction for some nuclear systems at low energies. If the imaginary part of the effective potential or $g(r)$ in eq. (6) has a form

$$g(r) = e^{-\beta_1 r}/r + \Lambda e^{-\beta r}/r \tag{15}$$

with $\beta < \beta_1$, the second term could be dominant over the first term even if $\Lambda << 1$. In the limit of $\beta \to 0$, $\phi = \tan^{-1}(k/\beta) = \pi/2$ and $e^{4\phi\eta} = e^{2\pi\eta}$ which can cancel the Gamow factor $e^{-2\pi\eta}$ in eq. (8a). Although at present we have not succeeded to prove theoretically the existence of a long finite interaction range ($\beta \approx 0$) for $\Lambda e^{-\beta r}$ from our quantum mechanical derivation of the imaginary part of the effective potential [8], the possibility of the existence of term $\Lambda e^{-\beta r}$ with $\beta \approx 0$ and hence a near cancellation of the Gamow factor at low energies cannot be ruled out theoretically. A near cancellation of the Gamow factor at low energies may provide an explanation for anomalous fusion products (new isotopes and enhanced isotope abundances) reported in some recent experiments [3]. Therefore, it is important to investigate both theoretically and experimentally the possibility of existence of the long finite range ($\beta \approx 0$) interaction for the imaginary part of the effective potential.

4. Possible Scenarios for Cold Fusion

Since we cannot rule out the possibility of (near) cancellation of the Gamow factor $e^{-2\pi\eta}$ by the enhancement factor $e^{4\phi\eta}$ in eq. (8a), we investigate possible scenarios for cold fusion based on such hypothetical near cancellation of the Gamow factor. We examine $d + d$, $d + Pd$, and $p + Pd$ as examples in this section.

For the observed neutron counting rate of $(4.1 \pm 0.8) \times 10^{-3}\text{s}^{-1}$ claimed by Jones et al. [2], the fusion rate is 0.41 s^{-1} after neutron detection efficiency of $\sim$ 1% is taken into account for 3 g of Ti. Since the Ti density is 4.5 g/cm^3 and its

molar weight is 47.9 g/mole, the observed fusion rate is

$$R^J_{\rm exp} = 0.615/{\rm sec} - {\rm cm}^3({\rm deuterons}) \approx 1.0/{\rm sec} - {\rm cm}^3(d's) \tag{16}$$

where we have assumed the deuteron density n_D to be $n_D = n_{Ti}/2 = 2.83 \times 10^{22}/{\rm cm}^3 \approx 3 \times 10^{22}/{\rm cm}^3$. The observed fusion rate claimed by Fleischmann and Pons is larger than $R^J_{\rm exp}$ by a factor of $\sim 10^{10}$,

$$R^{FP}_{\rm exp} \approx 1.0 \times 10^{10}/{\rm sec} - {\rm cm}^3({\rm deuterons}) \ . \tag{17}$$

To include the electron screening effect, we assume $E = E_{sc}$ where E_{sc} is the screening energy given by Thomas–Fermi model [21]

$$E_{sc} = 30.7 Z_a Z_b \left(Z_a^{2/3} + Z_b^{2/3}\right)^{1/2} \ {\rm eV} \ . \tag{18}$$

For $d+d$ reactions, $E_{sc} = 43.4$ eV, while $E_{sc} = 5.25$ keV for $d + Pd$ and $p + Pd$. Corresponding velocities, $(v/c) = \sqrt{2E/\mu} = \sqrt{2E_{sc}/\mu}$, are 0.3×10^{-3}, 2.4×10^{-3} and 3.3×10^{-3}, for $d+d$, $d+Pd$, and $p+Pd$ reactions, respectively. The observed fusion rate, $R_{\rm exp}$, is related to the cross–section $\sigma(E)$ by $R_{\rm exp} = n_a n_b \langle \sigma v \rangle / (1+\delta_{ab})$. For $E = E_{sc} = 43.4$ eV or 5.25 keV, $\langle \sigma v \rangle$ can be approximated by $\langle \sigma v \rangle = \sigma v$ and hence $R_{\rm exp} \approx n_a n_b \sigma v/(1+\delta_{ab})$ or $\sigma \approx R_{\rm exp}(1+\delta_{ab})/n_a n_b v$. Using $\sigma(E)$ given by eq. (8a), we obtain

$$\Lambda e^{4\phi\eta} e^{-2\pi\eta} \approx \frac{(1+\delta_{ab}) R_{\rm exp} \mu c^2}{2 n_a n_b c \tilde{S}_0(E)} \left(\frac{v}{c}\right) \tag{19}$$

where we have used $g(r)$ given by eq. (15) with $\beta << \beta_1$. From the extrapolation of higher energy $d+d$ fusion data, $S(0)$ in eq. (23) is known to be $S(0) \approx 50$ keV–b for $D(d,p)^3{\rm H}$ or $D(d,n)^3{\rm He}$ reactions. For $d+d$ reactions with $\tilde{S}_0(E) \approx S(0) = 50$ keV–b, we obtain 0.2×10^{-30} and 0.2×10^{-20} for $\Lambda e^{4\phi\eta} e^{-2\pi\eta}$, with $R^J_{\rm exp}$ and $R^{FP}_{\rm exp}$, respectively. For $d + Pd$ reaction, assuming $\tilde{S}_0(E) \approx 50$ keV–b, we obtain 1.6×10^{-30} and 1.6×10^{-20} for $\Lambda e^{4\phi\eta} e^{-2\pi\eta}$, with $R^J_{\rm exp}$ and $R^{FP}_{\rm exp}$, respectively, while for $p + Pd$ reaction with the assumed value of $\tilde{S}_0(E) \approx 50$ keV–b, $\Lambda e^{4\phi\eta} e^{-2\pi\eta} = 1.2 \times 10^{-30}$ and 1.2×10^{-20}, respectively, for $R^J_{\rm exp}$ and $R^{FP}_{\rm exp}$.

$R^J_{\rm exp}$ and $R^{FP}_{\rm exp}$ can be explained if we can assume large values of β^{-1}. The use of very small value of $\Lambda = 10^{-14}$ will preserve the conventional description of nuclear fusion reactions at higher energies greater than 1 keV for $d+d$ and greater than 1 MeV for $d + Pd$ and $p + Pd$. To obtain the claimed value of $R^J_{\rm exp}$ with $\Lambda = 10^{-14}$, we need $\beta^{-1} = 1633$ fm, 693 fm, and 686 fm, while $\beta^{-1} = 4275$ fm, 1881 fm, and 1845 fm for $d + d$, $d + Pd$, and $p + Pd$ fusion reactions, respectively, are needed to obtain $R^{FP}_{\rm exp}$. Larger values of β^{-1} for $d+d$ case compared with smaller values of β^{-1} for $d + Pd$ and $p + Pd$ cases imply that $d + Pd$ and $p + Pd$ fusion reactions may be more favorable than $d + d$ fusion reaction. Another interesting aspect of $d+Pd$ and $p+Pd$ reactions is that the final fusion product can be unstable

with a finite lifetime, which may help to explain "heat after death" phenomenon [22] and absence or lower level of X–rays and bremsstrahlung radiation.

The anomalous large ratio of T/n from $D(d,p)T$ and $D(d,n)^3$He claimed by many authors [3] can be explained by assuming that β^{-1} for the $D(d,p)T$ channel is larger than β^{-1} for the $D(d,n)^3$He channel. However, since bremsstrahlung radiation and other expected effects are not observed in many of the electrolysis fusion experiments [3], $D(d,p)T$ and $D(d,n)^3$He may not be occurring in these experiments. Other possibilities are now numerous, since our results with the electron screening effect using E_{sc} (eq. (18)) show a surprising result that the fusion cross–section for nuclei with larger values of Z can be comparable or much greater than that for nuclei with smaller Z, contrary to the commonly accepted belief otherwise. There are many possible candidate fusion reactions involving Pd with different Q values which produces no neutrons. For ${}^APd(d,p)^{A+1}Pd$, Q values are 5.21 MeV (A = 102), 1.48 MeV (A = 104), 7.72 MeV (A = 105), 3.71 MeV (A = 106), 7.27 MeV (A = 107), 6.88 MeV (A = 108), and 3.08 MeV (A = 110). For tritium producing ${}^APd(d,t)^{A-1}Pd$ reactions, Q values are 2.55 MeV (A = 105) and 0.32 MeV (A = 107). If X–rays and/or bremsstrahlung radiation are not observed or are at a very low level in the electrolysis experiments [3], all of the above fusion reactions involving Pd isotopes are ruled out except possibly ${}^{107}Pd(d,t)^{106}Pd$ reaction which have a small value of Q = 0.32 MeV, and hence we need to look for other candidate fusion reactions with small values of Q, including those involving impurity isotopes in electrolysis experiments. Examples of other possible fusion reactions with small Q values are ^{102}Pd(^{7}Li,^{6}Li)^{103}Pd (Q = 0.531 MeV), ^{108}Pd(^{14}N,^{15}N)^{107}Pd (Q = 0.102 MeV), ^{110}Pd(^{6}Li,^{5}Li)^{111}Pd (Q = 0.089 MeV), ^{110}Pd(^{10}B,^{12}B)^{108}Pd (Q = 0.254 MeV), and ^{110}Pd(^{19}F,^{21}F)^{108}Pd (Q = 0.136 MeV). Other possibilities with different sets of nuclei in the initial and final states are to be explored.

If the claimed results of excess heat with no accompanying radiation are confirmed at a level of $\sim$ 100% reproducibility, and if there are no candidate fusion reactions with Q values small enough to be consistent with the radiationless results, then we may need to investigate some unconventional mechanisms [3,6,7] involving collective excitations of Pd clusters and/or Pd crystals, in addition to the near cancellation of the Gamow factor discussed in section 3. The radiationless results may turn out to be independent of and decoupled from the mechanism described in this section and section 3.

5. New Modified Formula for High-Density Plasma Fusion

In this section, a new modified general formula for the high density nuclear fusion rate is described. For a given relative velocity $v = v_{ij} = |\vec{v}_i - \vec{v}_j|$ between the i*th* and j*th* particles and fusion cross–section $\sigma(v_{ij})$, the fusion rate per unit volume, R_f, is expected to be proportional to $P(\vec{r}_i, \vec{v}_i; \vec{r}_j, \vec{v}_j) v_{ij} \sigma(v_{ij})$ where P is the probability of finding the i*th* particle at $\vec{r}_i$ with $\vec{v}_j$ and the j*th* particle at $\vec{r}_j$ with $\vec{v}_j$. For a given one–body phase space (density) distribution, $\rho(q_\ell, p_\ell) = \rho(\vec{r}_i, m_i\vec{v}_i)$, one possible choice for P is, suppressing m_i, $P(\vec{r}_i, \vec{v}_i; \vec{r}_j, \vec{v}_j) = \rho(\vec{r}_i, \vec{v}_i)\rho(\vec{r}_j, \vec{v}_j)$ which is valid for a collisionless ideal or low–density gas but may not be valid for a high–density

gas. The separability of the phase–space distribution $\rho(\vec{r}_i, \vec{v}_i) = n(\vec{r}_i)f(\vec{v}_i)$ is assumed, where $f(\vec{v}_i) = (m_i/2\pi kT)^{3/2} \exp(-m_i v_i^2/2kT)$ is the Maxwell–Boltzmann (MB) velocity distribution for a system in thermal equilibrium. With the above assumptions, we can write R_f as

$$\begin{aligned} R_f &= \frac{1}{(1+\delta_{ij})V_r^2} \int d^3r_i \int d^3r_i \int d^3v_i \int d^3v_j P(\vec{r}_i, \vec{v}_i; \vec{r}_j, \vec{v}_j) v_{ij} \sigma(v_{ij}) \\ &= \frac{1}{(1+\delta_{ij})V_r^2} \int d^3r_i \int d^3r_j \int d^3v_i \int d^3v_j n(\vec{r}_i) n(\vec{r}_j) f(\vec{v}_i) f(\vec{v}_j) v_{ij} \sigma(\vec{v}_{ij}) \end{aligned} \tag{20}$$

where V_r is the system volume.

After transforming the ith and jth particle coordinates into the relative and center of mass (CM) coordinates, and integrating the CM coordinates, eq. (20) reduces to ($r = |\vec{r}_i - \vec{r}_j|$)

$$R_f^{new} = \frac{n_i n_j}{(1+\delta_{ij})V_r} \int d^3r \int d^3v \; g(r) f(\vec{v}) v_0 \sigma(v_0) \tag{21}$$

using the assumption that the pair number density $n(\vec{r}_i)n(\vec{r}_j)$ is related to the radial distribution function $g(r)$ by $n(\vec{r}_i)n(\vec{r}_j) = n_i n_j g(r)$ with n_i and n_j representing the average number densities. $g(r)$ is defined as the number of particles, on the average, in the volume $4\pi r^2 dr$ centered about a given particle divided by the number that would be in the same volume if the system behaved as an ideal gas [23]. $g(r)$ can be calculated from a molecular dynamics simulation [23].

Since $\sigma(v_0)$ is experimentally measured with v_0 representing the asymptotic relative speed v_0 in the potential free region ($V(r) = 0$), we must use $v_0\sigma(v_0)$ instead of $v\sigma(v)$ in eq. (21), where v_0 and v are related by the total pair energy (E_0) conservation, $E_0 = \mu v_0^2/2 = \mu v^2/2 + V(r)$ with the reduced mass μ.

For a collisionless ideal gas ($V(r) = 0$), we have $v_0 = v$ and $g(r) = 1$, and hence R_f^{new}, eq. (21), reduces to the conventional fusion rate formula: $R_f^{new} \rightarrow R_f^{conv}$, where

$$R_f^{conv} = \frac{n_i n_j}{1+\delta_{ij}} \int d^3v \; f(\vec{v}) v\sigma(v) \; . \tag{23}$$

R_f^{new} becomes substantially different from R_f^{conv} at lower temperatures.

6. Uncertainties for the Electron Screening Effect

We investigate non-adiabatic effects in the quantum mechanical description of the electron screening effect for nuclear reaction rates. At low energies, the fusion reaction cross-sections of charged nuclei can be also written as

$$\sigma(E) = G(E)|\psi_E(0)|^2/v \tag{24}$$

where $G(E)$ is the so-called astrophysical factor, which embodies the nuclear aspects of the process, E and v are the collision (kinetic) energy and the relative nuclear velocity, respectively, $\psi_E(0)$ is the wave function at the origin, and $|\psi_E(0)|^2 = (2\pi\alpha c/v)\exp(-2\pi\alpha c/v)$. At low energies, the behavior of $\sigma(E)$ is dominated by Coulomb repulsion between the nuclei. In cold fusion and laboratory beam experiments the ion is incident on a target consisting mostly of neutral atoms or molecules, and hence incident ions can recombine, partially or totally, with the electrons they encounter while moving through the target. As a consequence, the final nuclear collision, which leads to nuclear fusion, occurs while the nuclei are surrounded by one or several electrons. These electrons become more deeply bound in the Coulomb field of the unified nuclei, and transfer kinetic energy to the internuclear degree of freedom. Therefore, the cross-section measured in the laboratory beam experiments are not equal to the cross-section for bare nuclei. Recent results for $\sigma(E)$ from laboratory beam experiments for nuclear reactions involving light nuclei at low energies (> 3 keV) show that the extracted $S(E)$ increases toward lower energies instead of being a constant extrapolated from higher energy data, indicating the importance of the electron screening. However, recent theoretical calculations [13, 14] of the electron screening effect based on the adiabatic Born-Oppenheimer approximation (the united atom model with the screening energy, 15.7 $Z^{7/3}$ eV) yield limiting values which are much smaller (by $\sim 1/2$) than those extracted from the experimental data for reactions ^{3}He$(d,p)^4$He [9,10], ^{6}Li$(p,\alpha)^3$He, ^{6}Li$(d,\alpha)^4$He, and ^{7}Li$(p,\alpha)^4$He [11]. This discrepancy between the experimental data and the conventional theoretical estimate for the electron screening effect is not understood at present.

We will now examine the united atom approximation for low-energy $d + de$ reaction. For this case we need to calculate

$$|\psi_E(0)|^2 = \int |\psi_E(\vec{r},\vec{\rho})|^2 d\vec{\rho}|_{r=0} \, . \tag{25}$$

For the total $d+de$ energy $\epsilon = E - |E_{1s}| = (E - 13.6\text{ eV})$ where $\vec{r} = \vec{r}_{d_1} - \vec{r}_{d_2}, \vec{\rho} = \vec{r}_e - (\vec{r}_{d_1}+\vec{r}_{d_2})/2$, we assume that $\psi(\vec{r},\vec{\rho})$ in eq. (26) is the solution of the Schrödinger equation

$$\left(-\frac{\hbar^2}{2\mu}\Delta_r - \frac{\hbar^2}{2m_e}\Delta\rho + \frac{e^2}{r} + V(\vec{r},\vec{\rho})\right)\psi = \epsilon\psi \, , \tag{26}$$

where

$$V(\vec{r},\vec{\rho}) = -\left(\frac{e^2}{\left|\vec{\rho}-\frac{\vec{r}}{2}\right|} + \frac{e^2}{\left|\vec{\rho}+\frac{\vec{r}}{2}\right|}\right) \tag{27}$$

and μ is the reduced mass of deuteron, $\mu = M_d/2$, with the deuteron rest mass M_d.

Let us introduce an operator $\hat{H}$,

$$\hat{H} = -\frac{\hbar^2}{2m_e}\Delta\rho - \frac{2e^2}{\rho} \tag{28}$$

and the eigenfunction $\psi_n(\vec{\rho})$ satisfying

$$\hat{H}\psi_n(\vec{\rho}) = E_n\psi_n(\vec{\rho}) \ . \tag{29}$$

We expand the solution of eq. (26) in terms of $\psi_n(\vec{\rho})$ as

$$\psi(\vec{r},\vec{\rho}) = \sum F_n(\vec{r})\psi_n(\vec{\rho}) \tag{30}$$

where $F_n(\vec{r})$ satisfy

$$-\frac{\hbar^2}{2\mu}\Delta F_n(\vec{r}) + \frac{e^2}{r}F_n(\vec{r}) + \sum V_{nm}F_m = (\epsilon - E_n)F_n(\vec{r}) \ . \tag{31}$$

For the case of $L = 0, \ell_r = \ell_\rho = 0$, we have

$$-\frac{\hbar^2}{2\mu}\frac{d^2F_n}{dr^2} + \frac{e^2}{r}F_n + \sum_m \tilde{V}_{nm}F_m = (\epsilon - E_n)F_n \tag{32}$$

where

$$\tilde{V}_{nm} = \left\langle \psi_n|\tilde{V}|\psi_m \right\rangle \ , \quad \tilde{V}(r,\rho) = 2e^2\begin{cases} 0 \ , & \rho \geq r/2 \\ \dfrac{1}{\rho} - \dfrac{2}{r} \ , & r/2 \geq \rho \end{cases} \ . \tag{33}$$

If we restrict to the case of $n = 1$ and $m = \epsilon$ (continuum state) and neglect $V_{\epsilon n\neq 1}$ and $V_{\epsilon\epsilon'}$, eq. (32) reduces to

$$-\frac{\hbar^2}{2\mu}\frac{d^2F_1}{dr^2} + \tilde{V}_{11}F_1 + \int \tilde{V}_{1\varepsilon}F_\varepsilon d\varepsilon + \sum_{n\neq 1}\tilde{V}_{1n}F_n = (\epsilon - E_1)F_1 \tag{34a}$$

$$-\frac{\hbar^2}{2\mu}\frac{d^2F_\varepsilon}{dr^2} + \tilde{V}_{\varepsilon 1}F_1 + \frac{e^2}{r}F_\varepsilon = (\epsilon - \varepsilon)F_\varepsilon \ . \tag{34b}$$

In terms of solutions, F_1 and F_ε, of eq. (34), the probability integral in eq. (25) can be written as (see Appendix A)

$$|\psi_E(0)|^2 = \int |\psi_E(\vec{r},\vec{\rho})|^2 d\vec{\rho}|_{r=0} \approx \left|\frac{F_1(r)}{r}\right|^2_{r=0} + \int \left|\frac{F_\varepsilon(r)}{r}\right|^2 d\varepsilon\Big|_{r=0} \tag{35}$$

where $|F_1(r)/r|^2_{r=0}$ corresponds to the conventional united atom approximation

$$|\psi_E^{U.A.}(0)|^2 = \left|\frac{F_1(r)}{r}\right|^2_{r=0} \tag{36}$$

while the other term $\int |F_\varepsilon(r)/r|^2 d\varepsilon|_{r=0}$ corresponds to the non-adiabatic correction term. For the low-energy case of $E \lesssim 10$ eV, our estimates of eqs. (35) and (36) using solutions F_1 and F_ε, of eq. (34) yield the ratio (see Appendix A)

$$\frac{|\psi_E(0)|^2}{|\psi_E^{U.A.}(0)|^2} \gtrsim 10 \tag{37}$$

which indicates the importance of the non-adiabatic contribution for the electron screening effect. We are extending our calculation of the ratio, eq. (58) to higher energies, $E \lesssim 10$ keV.

7. Non-Square Integrability for the Electron Screening Effect

In this section, we show that there is a very serious difficulty associated with the conventional formula for nuclear fusion rate in the presence of electron degrees of freedom due to non-square integrability of the probability integral $|\psi_E(0)|^2$ in eq. (24), which has been ignored in previous theoretical calculations. The probability integral in eq. (24) is written as $|\psi_E(0)|^2 = (2\pi\alpha c/v)\exp(-2\pi\alpha c/v)$ representing the probability of bringing two charged nuclei to zero separation distance in the absence of electrons. We will consider ^{3}H$(d,n)^4$He reaction for simplicity and use the three-body $d + e +$ ^{3}H (det) initial state. The probability integral $|\psi_E(0)|^2$ in eq. (24) for this case is

$$|\psi_E(0)|^2 = \int |\psi_E(\vec{r},\vec{\rho})|^2 d^3\rho|_{r=0} \tag{38}$$

where $\psi_E(\vec{r},\vec{\rho})$ is the det wave function with $\vec{r} = \vec{r}_d - \vec{r}_t$ and $\vec{\rho} = \vec{r}_e - (m_d\vec{r}_d + m_t\vec{r}_t)/(m_d + m_t)$. We demonstrate that the integral in eq. (38) is not square-integrable over ρ, when $\psi_E(\vec{r},\vec{\rho})$ is the exact solution of the three-body rearrangement scattering problem involving more than three bodies (five bodies, d, e^-, t, ^{4}He, and n for ^{3}H$(d,n)^4$He reaction) and more than one channel in the final state.

If $\psi_E(\vec{r},\vec{\rho})$ in eq. (38) is replaced by an approximate adiabatic representation as customarily done in previous conventional theoretical estimates, then the probability integral in eq. (38) may be square-integrable. However, the square-integrability of eq. (38) with use of an approximate solution for $\psi_E(\vec{r},\vec{\rho})$ is meaningless, if eq. (38) is proven to be not square-integrable when the exact solution for $\psi_E(\vec{r},\vec{\rho})$ is used.

For ^{3}H$(d,n)^4$He reaction, $d+(e^-,t) \longrightarrow (e^-,{}^4\text{He})+n+Q$ and $d+(e^-,t) \longrightarrow e^- + {}^4\text{He} + n + Q$, Schrödinger equation and Hamiltonian can be written as

$$\left(\tilde{E} - \tilde{H}\right)|\tilde{\psi}\rangle = 0\,, \quad \tilde{E} = \begin{pmatrix} E & 0 \\ 0 & E+Q \end{pmatrix}, \quad \tilde{H} = \begin{pmatrix} H_{det} & V_{det,e^4\text{He}n} \\ V_{e^4\text{He}n,det} & H_{e^4\text{He}n} \end{pmatrix} \tag{39}$$

with $H_{det} = T_r + T_\rho + V_{de} + V_{et} + V_{dt}$ and $H_{e^4\text{He}n} = T_{r'} + T_{\rho'} + V_{e^4\text{He}} + V_{^4\text{He}n}$. $T's$ are kinetic energy operators, $\vec{r} = \vec{r}_d - \vec{r}_t$, $\vec{r}\,' = \vec{r}_n - \vec{r}_{^4\text{He}}$, $\vec{\rho} = \vec{r}_e - (m_d\vec{r}_d + m_t\vec{r}_t)/(m_d + m_t)$, and $\vec{\rho}\,' = \vec{r}_e - (m_n\vec{r}_n + m_{^4\text{He}}\vec{r}_{^4\text{He}})/(m_n + m_{^4\text{He}})$. H_{det} and $H_{e^4\text{He}n}$ are the channel Hamiltonians for the det and e^4Hen channels, respectively. For $\vec{\rho} \to \infty$ and $r < b$ (b is the nuclear interaction range), eq. (39) can be written as

$$\begin{aligned} &\left[E + \frac{\hbar^2}{2\mu}\frac{d^2}{d\rho^2} + \frac{\hbar^2}{2M}\frac{d^2}{dr^2} + \frac{2}{r} - V_{dt}(r)\right]\psi_{det}(r,\rho) = \\ &r\rho \int d\Omega_{\vec{r}} d\Omega_{\vec{\rho}} V_{det,e^4\text{He}n}(\vec{r},\vec{r}\,')\psi_{e^4\text{He}n}(\vec{r}\,',\vec{\rho})d\vec{r}\,' \,. \end{aligned} \tag{40}$$

From behavior of the asymptotic solution $\psi_{det}(0,\rho \to \infty)$ of eq. (40), we show the non-square-integrability of eq. (38) in the following.

We can show (see Appendix B)

$$\psi_{det}(0,\vec{\rho}) \approx \sum_n C_n \frac{d^{2n}}{d\rho^{2n}} y(\rho) \tag{41}$$

where $y(\rho) = \rho \int d\Omega_{\vec{\rho}} \psi_{e^4\mathrm{He}n}(0,\vec{\rho})$ and C_n are constants. Therefore, if $\psi_{e^4\mathrm{He}n}(0,\vec{\rho})$ is not square-integrable, then $\psi_{det}(0,\vec{r})$ is also not square-integrable due to eq. (40). To show $\psi_{e^4\mathrm{He}n}(0,\vec{\rho})$ is not square-integrable, we use the following approximation, $\psi_{e^4\mathrm{He}n}(0,\vec{\rho}) \approx e^{i\vec{k}_\epsilon \vec{r}} \phi_{\vec{k}}(\vec{\rho})$, where $\phi_{\vec{k}}(\vec{\rho})$ is the $(e,{}^4\mathrm{He})$ Coulomb function for positive energy $\hbar^2 k^2/2m_e$, $k_\epsilon = m_e v_\epsilon$, and v_ϵ is the recoil velocity of ^{4}He as calculated from the momentum conservation. We have

$$\lim_{\rho\to\infty} y(\rho) \sim \frac{1}{k k_\epsilon \rho} \sum_{\ell m} (-1)^\ell e^{i\delta_\ell^c} \times$$

$$\times \sin\left(k\rho - \frac{\ell\pi}{2} - \eta\ell n 2k\rho + \delta_\ell^c\right) \sin\left(k_\epsilon r - \frac{\ell\pi}{2}\right) Y_{\ell m}(\hat{k}_\epsilon) Y^*_{\ell m}(\hat{k}) \ .$$

Because any $d^{2n}y(\rho)/d\rho^{2n}$ is a linear superposition, only two functions $g_1(r)$ and $g_2(r)$ are needed

$$\frac{d^{2n}y(\rho)}{dr^{2n}} = \alpha^{(n)} g_1(\rho) + \beta^{(n)} g_2(\rho) \tag{42}$$

where

$$g_1(\rho) = \frac{1}{\rho} \sum_{\ell m} (-1)^\ell e^{i\delta_\ell^c} \sin\left(k\rho - \frac{\ell\pi}{2} - \eta\ell n 2k\rho + \delta_\ell^c\right) \sin\left(k_\epsilon \rho - \frac{\ell\pi}{2}\right) Y_{\ell m}(\hat{k}_\epsilon) Y^*_{\ell m}(\hat{k})$$

and

$$g_2(\rho) = \frac{1}{\rho} \sum_{\ell m} (-1)^\ell e^{i\delta_\ell^c} \cos\left(k\rho - \frac{\ell\pi}{2} - \eta\ell n 2k\rho + \delta_\ell^c\right) \cos\left(k_\epsilon \rho - \frac{\ell\pi}{2}\right) Y_{\ell m}(\hat{k}_\epsilon) Y^*_{\ell m}(\hat{k}) \ . \tag{43}$$

For $\rho \to \infty$, we obtain the final result $\psi_{det}(0,\rho) = \alpha g_1(\rho) + \beta g_2(\rho)$ which leads to the non-square-integrability of eq. (38).

Since the conventional definition $\sigma(E)$ given by eq. (24) has difficulties associated with non-square integrability of eq. (38), we introduce an alternative formulation. For the previous example of $^3\mathrm{H}(d,n)^4\mathrm{He}$, we need to solve eqs. (39) under the boundary condition in $e^4\mathrm{He}n$ channel [1],

$$\psi_{e^4\mathrm{He}n} \sim \sum_\beta T^{(\beta)} \phi_\beta(\vec{r}_{e^4\mathrm{He}}) U^+\left(\vec{K}_\beta, \vec{R}\right) \tag{44}$$

for $R \to \infty$ where $r_{e^4\mathrm{He}}(R)$ is the relative distance between e and ^{4}He (e^4He and n). U^+ is the outgoing wave between $(e,{}^4\mathrm{He})$ and n, with a momentum K_β, and β indicates the quantum numbers of $(e,{}^4\mathrm{He})$ atomic states including continuum states. $T^{(\beta)}$ is given by

$$T^{(\beta)} = \left\langle e^{-i\vec{K}_\beta \vec{R}}, \phi_\beta(\vec{r}_{e^4\mathrm{He}}) | V_{e^4\mathrm{He}n,det} | \psi_{det} \right\rangle + \left\langle e^{-i\vec{K}_\beta \vec{R}}, \phi_\beta(\vec{r}_{e^4\mathrm{He}}) | V_{^4\mathrm{He}n} | \psi_{e^4\mathrm{He}n} \right\rangle \ . \tag{45}$$

Since it is very difficult to calculate $T^{(\beta)}$ given by (45), we use some approximations.

(i) The coupling interaction $V_{e^4\mathrm{He}n.det}$ may be replaced by $V_{^4\mathrm{He}n.dt}$ (bare nuclei) since electrons are not expected to affect the nuclear rearrangement process significantly. For example, we can use some sets of the interaction $\left\{V_{dt}, V_{^4\mathrm{He}n}, V_{dt,^4\mathrm{He}n}\right\}$, which reproduce the experimental data.

(ii) From (45), we see that $\psi_{e^4\mathrm{He}n}$ is needed only for $r' \lesssim b$ (where b is the range of $^4\mathrm{He} - n$ interaction). For this internal region of r', $\psi_{e^4\mathrm{He}n}$ may be expanded in terms of some basis functions.

With these approximations, we can define σ as

$$\sigma \sim \textstyle\sum_\beta |T^{(\beta)}|^2 \tag{46}$$

We are using this alternative formulation for investigating the electron screening effect.

8. Three-Body Fusion Reactions

Recently, energetic protons ($\lesssim$ 17 MeV) and α particles ($\lesssim$ 6.5 MeV) have been observed in experiments in which deuterated Ti target is bombarded with 150 keV deuteron beam [5]. The observed proton and α-particle energy spectrum cannot be explained with existing two-body fusion reactions but is consistent with a three-body fusion reaction, $d + d + d \rightarrow p + n + {}^4\mathrm{He}$ [5]. The observed rate $R^{(3)}$ is $\sim 10^{-6} R^{(2)}$ where $R^{(2)}$ is the observed fusion rate for $D(d,p)T$ with 150 keV deuteron beam, i.e., $R^{(3)}/R^{(2)} \approx 10^{-5}$. However, the conventional theoretical estimate for $R^{(3)}/R^{(2)}$ is $\sim 10^{-17}$ [5] or much less, and hence the observed value of 10^{-6} for $R^{(3)}/R^{(2)}$ is anomalous. In this section, we describe the 3d fusion cross-section $\sigma^{(3)}(E)$ and rate $R^{(3)}(E)$ based on the optical theorem and a solution of three-body Schrödinger equation.

The scattering problem for three particles ($3 \rightarrow 3$) has been investigated in the context of the formal scattering theory [25-29]. The hyperspherical harmonics (h.h.) expansion method was first introduced in 1935 by Zernike and Brinkman [30] but has not been used until 1960 for the few-body bound-state problem [31-33]. More recently, it has been used for the ($3 \rightarrow 3$) scattering problem [34-39].

For the 3d fusion reaction, we consider two-channel case,

$$d + d + d \longrightarrow \begin{cases} d + d + d \\ p + n + {}^4\mathrm{He} \quad (Q = 21.62 \text{ MeV}) \end{cases} . \tag{47}$$

Three–body Schrödinger equation in the elastic channel is (we suppress the spin and isospin degrees of freedom for simplicity)

$$-\frac{\hbar^2}{2m}\left(\nabla_{\vec{x}}^2 + \nabla_{\vec{y}}^2\right)\Psi(\vec{x},\vec{y}) + V\Psi(\vec{x},\vec{y}) = E\Psi(\vec{x},\vec{y}) \tag{48}$$

where $\vec{x} = \sqrt{\frac{1}{2}}(\vec{r}_2 - \vec{r}_3)$, $\vec{y} = \sqrt{\frac{2}{3}}\left[\frac{1}{2}(\vec{r}_2 + \vec{r}_3) - \vec{r}_1\right]$, $V = V^C + V^S = \left(V_{12}^C + V_{23}^C + V_{13}^C\right)$ $+ \left(V_{12}^S + V_{23}^S + V_{13}^S\right)$ with $V^S = V_{Re}^S - iV_{Im}^S$. We introduce the hyperspherical har-

monics expansion for $\Psi(\vec{x},\vec{y})$ as

$$\Psi(\vec{x},\vec{y}) = \sum_{K\ell_x\ell_y} \Psi_K^{\ell_x\ell_y LM}(\rho)\Phi_K^{\ell_x\ell_y LM}(\Omega)\,, \tag{49}$$

where $\rho^2 = x^2 + y^2$ (hyperradius), and

$$\Phi_K^{\ell_x\ell_y LM}(\Omega) = \sum_{m_x m_y} \langle LM|\ell_x m_n \ell_y m_y\rangle \bar{\Phi}_K^{\ell_x\ell_y m_x m_y}(\Omega)$$

with $\bar{\Phi}_K^{\ell_x\ell_y m_x m_y}(\Omega) \propto Y_{\ell_x m_x}(\hat{x})Y_{\ell_y m_y}(\hat{y})$. If we write $\Psi_K^{\ell_x\ell_y LM}(\rho) = U_K^{\ell_x\ell_y LM}(\rho)/\rho^{5/2}$, eq. (48) reduces to

$$\frac{d^2U_k^{\ell_x\ell_y LM}(\rho)}{d\rho^2} + \left[\frac{2mE}{\hbar^2} - \frac{(K+3/2)(K+5/2)}{\rho^2}\right]U_K^{\ell_x\ell_x LM}(\rho) = \frac{2m}{\hbar^2}V_{KK'}^{\ell_x\ell_y,\ell'_x\ell'_y}U_{K'}^{\ell'_x\ell'_y,LM}(\rho) \tag{50}$$

where

$$V_{KK'}^{\ell_x\ell_y,\ell'_x\ell'_y} = \langle\Phi^{\ell_x\ell_y LM}|V|\Phi^{\ell'_x\ell'_y LM}\rangle\,. \tag{51}$$

For $K = 0(\ell_x = 0, \ell_y = 0, L = 0)$ case (known as "true" [28] or "democratic" state [35]), eq. (50) reduces to

$$\frac{d^2U}{d\rho^2} + \left(k^2 - \frac{15/4}{\rho^2}\right)U = \frac{2m}{\hbar^2}\tilde{V}U\,, \tag{52}$$

where $\tilde{V} = \tilde{V}^C + \tilde{V}^S$ with $\tilde{V} = V_{00}^{00,00}$. For $\tilde{V} = \tilde{V}^C$(i.e. $\tilde{V}^S = 0$), the solution of eq. (52) is

$$U^C(\rho) = C(k\rho)^{5/2}e^{-ik\rho}M\left(\frac{5}{2} - i\eta, 5, 2ik\rho\right), \tag{53}$$

where M is the Whittaker function and $C = 2^{3/2}e^{-\pi\eta/2}|\Gamma\left(\frac{5}{2} + i\eta\right)|/\Gamma(5)$.

In terms of T-matrix, the $K = 0$ elastic 3d nuclear scattering amplitude, $f_{3B}^{(e\ell)}$, can be written as

$$f_{3B}^{(e\ell)} = -\frac{2m}{\hbar^2 k^{7/2}}\langle U^C|T|U^C\rangle\,. \tag{54}$$

Using the optical theorem [39], $\sigma_r = \sqrt{2\pi}\left(\pi^2/k^{5/2}\right)Im\left(f_{3B}^{(e\ell)}\right)$, and eq. (54), we obtain the following expression for the 3d fusion cross-section,

$$\sigma^{(3)}(E) = \sigma_r \approx \frac{2m}{\hbar^2 k^6}\pi^2\sqrt{2\pi}\int_0^\infty U^C(\rho)W(\rho,\rho')U^C(\rho')d\rho d\rho' \tag{55}$$

where $W(\rho,\rho') = -Im\langle U^C|T|U^C\rangle$. If we parameterize $W(\rho,\rho') = -Im\langle U^C|T|U^C\rangle = \lambda g(\rho)g(\rho')$ with $g(\rho) = e^{-\beta\rho}\rho^{3/2}$, we obtain

$$\sigma^{(3)}(E) \approx \lambda\frac{2m}{\hbar^2 k_3}\pi^2\sqrt{2\pi}C^2\frac{(4!)^2}{(\beta^2+k_3^2)^5}e^{4\phi\eta_3} \tag{56}$$

where

$$|C|^2 = \frac{1}{36}\left(\frac{9}{4}+\eta_3^2\right)\left(\frac{1}{4}+\eta_3^2\right)\frac{\pi e^{-2\pi\eta_3}}{1+e^{-2\pi\eta_3}} \ . \tag{57}$$

Other quantities in eqs. (56) and (57) are $\phi = \tan^{-1}(k_3/\beta)$, $k_3 = (2mE/\hbar^2)^{1/2}$, $\eta_3 = 1/(2k_3R_B^{(3)})$, $R_B^{(3)} = \hbar^2/(2mZ_{eff}e^2)$, $Z_{eff} = 16/(\pi\sqrt{2}) \approx 3.6$, and $\lambda = V_0/a^4$.

We note that $\sigma^{(3)}(E)$ in eq. (56) has a dimensionality of the 5th power of length $[L^5]$ since $f_{3B}^{(e\ell)}$ has a dimensionality $[L^{5/2}]$ expected from the solution, $\Psi(\rho) = e^{i\vec{k}\cdot\vec{\rho}} + f_{3B}^{(e\ell)}e^{ik\rho}/\rho^{5/2}$, while two-body fusion cross-section $\sigma^{(2)}(E)$ has a dimensionality of $[L^2]$. For comparison, we use eq. (11) for the 2d cross-section

$$\sigma^{(2)}(E) \approx \frac{S^{(2)}(E)}{E}e^{-2\pi\eta_2} \ . \tag{58}$$

Since Kasagi et al. [5] observed energetic protons and α particles indicative of $d+d+d \rightarrow p+n+{}^4\mathrm{He}$ reaction only when deuteron concentration in the TiD_x target reaches $x > 1.2$, we can assume that some fraction f of deuterons in the TiD_x are mobile when x becomes greater than 1.2 with mobile deuteron number density $fn_D = fn_{Ti}/2 \approx f(3\times10^{22})/\mathrm{cm}^3$. For these mobile deuterons fn_D, the number of deuteron pairs we can form with mobile deuterons per unit volume is $(fn_D)^2/2 + f(1-f)n_D^2/2 = fn_D^2/2$. The incident deuteron can now interact with one of these deuteron pairs and can form a "true" or "democratic" three-body state, leading to $d+d+d \rightarrow p+n+{}^4\mathrm{He}$ fusion with the cross-section described by $\sigma^{(3)}(E)$, eq. (56). The 3d fusion probability $P^{(3)}$ is then given by

$$P^{(3)}(E_d) = fn_D^2\int_0^{E_d}\frac{\sigma^{(3)}(E_{cm}^{(3)})}{|dE/dx|}dE \tag{59}$$

compared with the 2d fusion probability $P^{(2)}$ given by [40]

$$P^{(2)}(E_d) = n_D\int_0^{E_d}\frac{\sigma^{(2)}(E_{cm}^{(2)})}{|dE/dx|}dE \tag{60}$$

where dE/dx is the stopping power for d in the target T_iD_x, and E_d is the laboratory kinetic energy of the incident deuteron.

To make an order of magnitude estimate for the ratio $\left(P^{(3)}/P^{(2)}\right)$, we approximate the ratio as

$$R = \frac{P^{(3)}(E_d)}{P^{(2)}(E_d)} \approx fn_D\frac{\sigma^{(3)}(E_{cm}^{(3)})}{\sigma^{(2)}(E_{cm}^{(2)})} \tag{61}$$

where $E_{cm}^{(3)} = (2/3)E_d$ and $E_{cm}^{(2)} = E_d/2$. In eq. (56), λ (or V_0 and a for $\lambda = V_0/a^4$) and β are parameters to be determined from theory and/or experiment. In the following, we assume $V_0 \approx 10$ MeV, $a = 2\ fm$, and $\beta = 0.065\ fm^{-1}(\beta^{-1} = 15fm)$. For the $2d$ fusion cross-section $\sigma^{(2)}(E)$, we use eq. (58) with $S^{(2)}(E) \approx S_0 \approx 50$

keV–b. For $f = 0.1$, we obtain the following results for R. R (in units of 10^{-6}) = 0.40, 0.42, 0.42, 0.40, 0.38, and 0.36 for E_d = 100, 110, 120, 130, 140, and 150 keV, respectively, which is comparable with the results of $R_{\rm exp} \approx (1-3) \times 10^{-6}$ within an order of magnitude.

It is known that the asymptotic behavior of the real part of the effective potential is $1/\rho^3$ [41]. However this long-range asymptotic dependence does not apply to the imaginary part. Therefore, the use of a small value of $\beta^{-1} = 15\ fm$ is reasonable.

The quantum number K is closely related to the impact parameter. In terms of classical orbits, a large value of K implies that three particles cannot come close together. For $K = 0$, all three particles seem to converge to or diverge from a scattering center [42]. Therefore the $K = 0$ "true" (or "democratic") three-body state is important for the three-body fusion reaction.

If the experimental data of Kasagi et al. [5] is conclusively determined to be due to $d + d + d \rightarrow p + n +$ ^{4}He fusion by future p–^{4}He coincidence measurements by Kasagi et al. and independently by other groups, the experimental result and its theoretical understanding based on "true" (or "democratic") three-body state may have very important implications for nucleosynthesis and stellar evolutions, since there are possibilities that other three-body fusion reactions may be involved in astrophysical problems, such as pycnonuclear triple-alpha fusion [43-45].

9. Summary and Conclusions

We have examined uncertainties due to many approximations made in the conventional theoretical formulations of low-energy nuclear fusion reactions, and presented new improved formulations which avoid some of these approximations. Some of the new formulations lead to unexpected results. One striking result is a possibility that a near cancellation of the Gamow factor (or "Coulomb barrier transparency" (CBT)) can not be ruled out completely at present. Another surprising result is that the large value of the 3d fusion rate recently observed in the laboratory beam experiment [5] may be justified theoretically in terms of a solution of the quantum mechanical three-body problem. Since there are still a great deal of uncertainty and absence of reliable reproducibility at a desirable level of $\sim 100\%$ for reported anomalous effects [3], it is at present premature to make definitive tests and comparisons of the predictions of our new improved formulations with the experimental data [3].

Appendix A

Let us rewrite eq. (34b) in an integral form

$$\left.\frac{F_\epsilon(r)}{r}\right|_{r\rightarrow 0} = \frac{2\mu}{\hbar^2}\Gamma(1+\eta_\epsilon)\frac{X(r)}{2k_\epsilon r}\int_r^\infty Y(r)V_{\epsilon 1}(r)\frac{F_1(r)}{r}rdr \qquad (A1)$$

where η_ϵ is the Sommerfeld parameter for $(d+d)$

$$\eta_\epsilon = \frac{1}{2k_\epsilon R_B}\ , \quad k_\epsilon = 2\mu\,\frac{\epsilon - E_{1S} - E}{\hbar^2} \qquad (A2)$$

R_B is the Bohr radius $R_B = 14.4123 fm$ for $(d+d)$, and $X(R)$ and $Y(r)$ are the Whittaker functions

$$X(r) = e^{-k_\epsilon r}(2k_\epsilon r)M(1+\eta_\epsilon, 2, 2k_\epsilon r)$$

and

$$Y(r) = e^{-k_\epsilon r}(2k_\epsilon r)U(1+\eta_\epsilon, 2, 2k_\epsilon r)\ . \qquad (A3)$$

We assume $F_1(r)$ to be the regular Coulomb function with energy $E + E_{scr}$ where E_{scr} is the screening energy. We will integrate (A1) from $r = 0$ to $r = \rho_B$, where $\rho_B = 0.529 \cdot 10^{-8}$cm. If $k_\epsilon^2 \rho_B R_B << 1$ and $k_E^2 \rho_B R_B << 1$ for $k_\epsilon^2 = (2\mu/\hbar^2)(\varepsilon - E_{1S} - E)$ and $k_E^2 = 2\mu(E + E_{scr})/\hbar^2$, we can use the following approximation [46]

$$\frac{X(r)}{2k_\epsilon r} \approx L_1(r) + \frac{(k_\epsilon r)^2}{6} L_2(r) \qquad (A4)$$

$$\Gamma(1+\eta_\epsilon)Y(r) = H_1(r) - \frac{1}{3}k_\epsilon^2 r R_B H_2(r) \qquad (A5)$$

$$\frac{F_1(r)}{r} = C\left[L_1(r) - \frac{(k_E r)^2}{6} L_2(r)\right] \qquad (A6)$$

where

$$|C|^2 = \frac{2\pi\eta_E}{e^{2\pi\eta_E} - 1}\ , \quad \eta_E = \frac{1}{2k_E R_B}\ , \qquad (A7)$$

$$L_n(r) = n!\left(\frac{r}{R_B}\right)^{n/2} I_n\left(2\left(\frac{r}{R_B}\right)^{1/2}\right) \qquad (A8)$$

and

$$H_n(r) = \frac{2}{(n-1)!}\left(\frac{r}{R_B}\right)^{-n/2} K_n\left(2\left(\frac{r}{R_B}\right)^{1/2}\right) \qquad (A9)$$

Using eqs. (A4)–(A9),

$$\psi_\epsilon(\rho) \approx \frac{1}{\hbar}\frac{\sqrt{2m_e}}{(\rho_{B/2})^{1/2}}\sqrt{\frac{\rho_B}{2\rho}} J_1\left(\sqrt{\frac{16\rho}{\rho_B}}\right) \quad (\text{for } \epsilon \approx 0) \qquad (A10)$$

and

$$\psi_{1S}(\rho) = 2\left(\frac{\rho_B}{2}\right)^{-3/2} e^{-2\rho/\rho_B} \qquad (A11)$$

we can calculate $V_{\epsilon 1}(r)$ in eq. (A1) which we can integrate over ϵ from $\epsilon = 0$ to $\epsilon' = 10$ eV to obtain $F_\epsilon(r)/r|_{r\to 0}$ from eq. (A1). (Eqs. (A4) – (A10) are valid for $\epsilon < 10$ eV.) Our numerical estimate yields

$$\int_0^{\epsilon'} \left|\frac{F_\epsilon(r)}{r}\right|^2_{r\to 0} d\epsilon \approx 6.4|C^2|\ . \qquad (A12)$$

Using eq. (A12) and the following relation for $\epsilon' \approx 10$ eV

$$\int_0^{\epsilon'} \left|\frac{F_\epsilon(r)}{r}\right|^2_{r=0} d\epsilon < \int_0^{\infty} \left|\frac{F_\epsilon(r)}{r}\right|^2_{r=0} d\epsilon$$

we obtain eq. (37) for the very low-energy case of $k_\epsilon^2 \rho_B R_B << 1$ and $k_E^2 \rho_B R_B << 1$.

Appendix B

Consider a set of functions $\varphi_n(r)$ satisfying

$$\int_0^b \varphi_n^*(r)\varphi_m(r)dr = \delta_{nm} \quad \text{and} \quad \int_0^b \varphi_n^*(r)\left(-\frac{\hbar^2}{2\mu}\frac{d^2}{dr^2} + V(r)\right)\varphi_m(r)dr = E_n\delta_{nm} \tag{B1}$$

where E_n are positive numbers.

We can represent the solution of the equation (64) in a form

$$\psi_{det}(r,\rho) = \sum_n \psi_n(\rho)\varphi_n(r) \; . \tag{B2}$$

Using (40) and (B1) we obtain

$$\left(k_n^2 + \frac{d^2}{d\rho^2} + -\frac{2\mu}{\hbar^2}\cdot\frac{2}{\rho}\right)\psi_n(\rho) \approx \gamma_n y(\rho) \; , \quad B \leq \rho \leq \infty \tag{B3}$$

where B is a sufficiently large distance in the asymptotic region and

$$\gamma_n = \frac{2\mu}{\hbar^2}\int_0^b \varphi_n(r) r V_{det,e^4\mathrm{He}}(\vec{r},\vec{r}\,') \cdot d\Omega_{\vec{r}} d\vec{r}\,'$$

with $k_n^2 = 2\mu(E - E_n)/\hbar^2$. Let us introduce a Green's function satisfying

$$\left(k_n^2 + \frac{d^2}{d\rho^2} + \frac{2\mu}{\hbar^2}\frac{2}{\rho}\right)G(\rho,\rho') = \delta(\rho - \rho') \; . \tag{B4}$$

The solution of (B4) is given by

$$G(\rho,\rho') = \lambda_n \begin{cases} (f_1(\rho) + \delta_n f_2(\rho))f_2(\rho'), \rho \leq \rho' \\ f_1(\rho)(f_1(\rho') + \delta_n f_2(\rho')), \rho' \leq \rho \end{cases} \tag{B5}$$

where λ_n is defined in terms of $f_1(\rho) = G_0(\rho) + iF_0(\rho)$ and $f_2(\rho) = G_0(\rho) - iF_0(\rho)$ as $(F_0(\rho)(G_0(r))$ is the regular (irregular) Coulomb function)

$$\lambda_n[f_1'(\rho)(f_1(\rho) + \delta_n f_2(\rho)) - f_1(\rho)(f_1'(2) + \delta_n f_2'(\rho))] = 1 \tag{B6}$$

and δ_n is determined by boundary conditions at $\rho = B$. The solution $\psi_n(\rho)$ of eq. (B3) can now be written as

$$\psi_n(\rho) = \lambda_n \gamma_n \Big[f_1(\rho) \int_B^r (f_1(\rho') + \delta_n f_2(\rho')) y(\rho') d\rho' + (f_1(\rho) + \delta_n f_2(\rho)) \int_r^\infty f_1(\rho') y(\rho') d\rho' \Big] \tag{B7}$$

For $r \geq B$ with a large value of B, we can obtain asymptotical expressions for $f_1(\rho)$ and $f_2(\rho)$ as $f_1(\rho) = e^{i(k_n\rho - S_n \ell n 2k_n\rho + \eta_n)}$ and $f_2(\rho) = e^{-i(k_n\rho - S_n \ell n 2k_n\rho + \eta_n)}$ where $Imk_n > 0$, $S_n = 2e^2/\hbar v_n$, $v_n = \hbar k_n/\mu$, $e^{2i\eta_n} = \Gamma(1 + iS_n)/\Gamma(1 - iS_n)$.

For large values of ρ and B, we can rewrite (B7) as

$$\psi_n(\rho) \approx \delta_n \lambda_n \gamma_n \Big[f_1(\rho) \int_B^\rho f_2(\rho') y(\rho') d\rho' + f_2(\rho') \int_\rho^\infty f_1(\rho') y(\rho') d\rho' \Big] \tag{B8}$$

Using $f_1(\rho) \approx \frac{1}{ik_n} f_1'(\rho)$ and $f_2(\rho) \approx -\frac{1}{ik_n} f_2'(\rho)$, we obtain

$$\begin{aligned} & f_1(\rho) \int_B^\rho f_2(\rho') y(\rho') d\rho' + f_2(\rho) \int_\rho^\infty f_1(\rho') y(\rho') d\rho' \\ & \approx -\frac{2}{ik_n} y(\rho) + \frac{1}{k_n^2} \Big(f_1(\rho) \int_B^\rho f_2(\rho') y''(\rho') d\rho' + f_2(\rho) \int_\rho^\infty f_1(\rho') y''(\rho') d\rho' \Big) \end{aligned} \tag{B9}$$

for $\rho \to \infty$. Eq. (B9) leads to the following generalization,

$$\begin{aligned} & f_1(\rho) \int_B^\rho f_2(\rho') y^{(N)}(\rho') d\rho' + f_2(\rho) \int_\rho^\infty f_1(\rho') y^{(N)}(\rho') d\rho' \\ & \approx -\frac{2}{ik_n} y^{(N)}(\rho) + \frac{1}{k_n^2} \Big(f_1(\rho) \int_B^\rho f_2(\rho') y^{(N+2)}(\rho') d\rho' + f_2(\rho) \int_\rho^\infty f_1(\rho') y^{(N+2)}(\rho') d\rho' \Big) \end{aligned} \tag{B10}$$

From (B2), (B8), (B9), and (B10), we obtain eq. (41).

References

1. M. Fleischmann, S. Pons and M. Hawkins *J. Electroanal. Chem.*, **261**, 301 (1989); for some corrections see *J. Electroanal. Chem.*, **263**, 187 (1989).

2. S. E. Jones, E. P. Palmer, J. B. Czirr, D. L. Becker, G. L. Jensen, J. M. Thorne, S. F. Taylor and J. Rafelski, *Nature*, **338**, 737 (1989).

3. See references in *Transaction of Fusion Technology*, **26**, (1994), Proceedings of the 4th International Conference on Cold Fusion, December 6–9, 1993, Lahaina, Mauii, Hawaii.

4. Y. Arata and Y.-C. Zhang, in Proceedings of the Japanese Academy, Series B, Vol. 70, ser. B. no. 7 pp. 106-111 (1994).

5. J. Kasagi, K. Ishii, M. Hiraga and K. Yoshihara, in Proceedings of the 3rd International Conference on Cold Fusion, Nagoya, 1992, edited by H. Ikegami (Universal Academy Press, Inc., Tokyo 1993) p. 209; J. Kasagi, T. Ohtsuki, K. Ishii, and M. Hiraga, to be published in *J. Phys. Soc. Jpn.* (1995).

6. M. Fleischmann, S. Pons and G. Preparata, *Nuovo Cimento*, A, **107**, 143 (1994).

7. V. A. Chechin, V. A. Tsarev, M. Rabinowitz and Y. E. Kim, *International J. Theor. Phys.*, **33**, 617 (1994).

8. Y. E. Kim and A. L. Zubarev, "Optical Theorem and Effective Finite-Range Nuclear Interaction for Low-Energy Nuclear Fusion Reactions," Purdue Nuclear Theory Group Report PNTG-95-1, to be published.

9. S. Engstler et al., *Phys. Lett.*, **B202**, 179 (1988).

10. G. Blüge et al., *Zeitschrift für Physik*, A **333**, 219 (1989).

11. S. Engstler et al., *Phys. Lett.*, B **279**, 20 (1992); *Zeitschrift für Physik*, A **342**, 471 (1992).

12. C. Angulo et al., *Zeitschrift für Physik*, A **345**, 231 (1993).

13. L. Bracci et al., *Nucl. Phys.*, A **53**, 316 (1990).

14. T. D. Shoppa et al., *Phys. Rev.*, C **48**, 837 (1992).

15. A. I. L'vov, *Few-body Systems*, **2**, N28 (1987).

16. V. V. Levashev, *Phys. Lett.*, B **214**, 443 (1988).

17. Gy. Bencze, *Phys. Lett.*, **202**, 289 (1988).

18. V. P. Pupyshev and O. P. Solovtsova, *International J. of Mod. Phys.*, A **7**, 2713 (1992).

19. N. F. Ramsey, B. J. Malenka and U. E. Kruse, *Phys. Rev.*, **91**, 1162 (1953).

20. W. G. Love, T. Terasawa and G. R. Satchler, *Nucl. Phys.*, **A291**, 183 (1977).

21. J. F. Ziegler, J. P. Biersack and U. Littmark, The Stopping and Range of Ions in Solids (Pergamon Press, New York, 1985).

22. S. Pons and M. Fleischmann, *Transaction of Fusion Technology*, **26**, 87 (1994).

23. J. P. Hansen and I. R. McDonald, Theory of Simple Liquids, Academic Press, Orlando, 1986

24. M. Kamimura, *AIP Conference Proceedings*, **181**, 330 (1988).

25. E. Georjuoy, *Philos. Trans. R. Soc. Lond.*, A, **270**, 197 (1971).

26. J. J. Nuttall, *J. Math. Phys.*, **12**, 235 (1971).

27. S. P. Merkuriev, *Theor. Mat. Fiz.*, **8**, 235 (1971).

28. R. G. Newton, *Ann. Phys. (N.Y.)*, **74**, 324 (1972); R. G. Newton and R. Shtochamer, *Phys. Rev.*, A, **14**, 642 (1976).

29. R. D. Amado, *Phys. Rev.*, C, **12**, 1354 (1975).

30. F. Zernike and U. C. Brinkman, *Proc. K. Ned. Akad. Wett.*, **38**, 161 (1935).

31. L. M. Delves, *Nucl. Phys.*, **9**, 391 (1959); **20**, 275 (1960).

32. F. T. Smith, *Phys. Rev.*, **120**, 1058 (1960).

33. Yu. A. Simonov, *Sov. J. Nucl. Phys.*, **3**, 461 (1966).

34. K. K. Fang, *Phys. Rev.*, C, **15**, 1204 (1977).

35. R. I. Jibuti and K. I. Sigua, Preprint IF AN GSSR 31-YaF (1977).

36. J. Raynal and J. Revai, *Nuovo Cimento*, **68A**, 612 (1970).

37. R. I. Jibuti and N. B. Krupennikova, The method of hyperspherical functions in the quantum mechanics of several bodies, Tbilisi, Metsnierba (1984).

38. R. I. Jibuti, Few-body problems in Physics, Proc. of the Ninth European Conf., ed. L. D. Faddeev and T. I. Kopaleishvili, World Scientific (1985) p. 284.

39. R. I. Jibuti and Ya. Keserashvili, *Czech. J. Phys.*, B, **30**, 1090 (1980).

40. Y. E. Kim et al., *Mod. Phys. Letters*, B **5**, 941 (1991).

41. A. M. Badalyan and Yu. A. Simonov, *Sov. J. Nucl. Phys.*, **3**, 1032 (1966).

42. E. W. Schmid and H. Ziegelmann, The Quantum Mechanical Three-Body Problem, Vieweg, Braunschweig, Germany, 1974.

43. A. G. W. Cameron, *Astrophysics. J.*, **130**, 916 (1959).

44. E. E. Salpeter and H. M. van Horn, *Astrophysics. J.*, **155**, 183 (1969).

45. S. Schramm, K. Langanke, and S. E. Koonin, *Astrophysics. J.*, **397**, 579 (1992).

46. J. D. Jackson and J. M. Blatt, *Rev. Mod. Phys.*, **22**, 77 (1950).

Fifth International Conference on Cold Fusion
9-13 April, 1995 - Monte Carlo, Monaco
ICCF5 ©1995

The Ion Band State Theory

T. A. Chubb and S. R. Chubb
Oakton International Corporation
5023 N. 38th Street
Arlington VA 22207 USA

Abstract

We have previously explained[1-3] how the occupation of ion band states by hydrogen (H) and deuterium (D) in palladium deuteride PdD and possibly Ni can result in radiationless fusion. The explanation includes a number of assumptions about the governing conditions associated with the process. As a consequence of these assumptions we predicted[1-3] important excess heat phenomena (loading requirements, by-products, etc.) of Cold Fusion (CF) that were subsequently observed[4,5]. Although the governing ideas are based on mainstream solid state physics ideas, the underlying theory "seems" to have "evaded" a number of potential problems that have bothered many people concerning CF. As we have explained recently[6,7], as a result of these solid state physics effects, discontinuous changes in momentum and singularities in the effective kinetic energies associated with H or D that may occur through the occupation of ion band states provide a means for eliminating the phenomena that seemingly are omitted by the theory. In this paper we clarify the origin of these effects and their relationship to questions that have been raised associated with our treatment of the Coulomb barrier.

1. Introduction

The ion band state theory of radiationless fusion, which is based on mainstream many-body physics of the solid state, "seems" to have "evaded" a number of potential problems that have bothered many people concerning CF. An important reason for this is that the theory is based on the conventional assumption of solid state physics that all of the charged particles in the problem are forced to occupy a finite volume of space. As a consequence, the particles are bound to the solid, and the rules of bound (as opposed to unbound) state quantum mechanics apply. Important consequences of this fact include the possibility of discontinuous changes in momentum (through wave function cusps, for example) at points where electrostatic repulsion or attraction becomes infinite. Immediate consequences of this result include the possibility of large variations in deBroglie wavelength over small spatial domains (since the momentum may become discontinuous), significant particle-particle overlap at isolated locations by same charge charged particles, and the breakdown of the rules and underlying mathematics of conventional Gamow tunneling theory.

The paper explains, using a concrete example, the solid state physics rationale for dealing with the Coulomb barrier, based on energy minimization, in the particular context in which ion band state occupations may occur. Because in a realistic solid periodic symmetry plays an important role in defining kinetic energy in ion band states, and because electron screening requires that all ions be neutralized not only within each unit cell but effectively outside a small screening volume, in such a situation, in determining the

minimum energy of potentially interacting ion band state (IBS) deuterons (D^+), the Coulomb repulsion between two IBS D^+'s is altered by the crystalline environment. In particular this repulsion is reduced by a factor $1/N_{cell}$, where N_{cell} = the total number of unit cells within the crystal.

A second important point brought out in the paper is that the underlying symmetry that results from periodic order, which is responsible for this dependence on crystal size, also plays a pivotal role in defining the potential avenues for reaction, once IBS D's overlap. In particular, in any potential nuclear reaction, the potential stable channels for reaction are directly coupled to the requirement that periodic symmetry be maintained. This leads to the additional requirements that predominantly only ground state to ground state nuclear transitions be allowed in which the location of each initial or final state nucleus is described by an ion band state, and that potential reaction products be released in regions outside periodically ordered domains (for example at cracks, interfaces and surfaces of heat-producing crystals). These requirements also explain why high energy particles are not released and can be used in a self-consistent manner to explain a number of materials preparation procedures: e.g. the choice of host material, loading requirements, the choices of crystal size, and the role of temperature in the generation of excess heat.

2. Mainstream Physics

The ion band state theory of radiationless fusion is based on mainstream many-body physics. Experimental/theoretical support for the theory is provided by Puska et al.[8] and Astaldi et al.[9], where it is have shown that the excited surface states of H and D on Ni and Cu are ion band states. In *Nature* magazine Nieminen states that "What is good enough of electrons is good enough for protons, their chemical counterparts 2000 times more massive"[10]. Cassella[11] invokes 3-dimensional band states to explain neutron scattering results in $NbH_{.003}$.

There is a thermodynamics rationale[12] for populating ion band states in PdD_x as $x \rightarrow 1$. A major component of system chemical potential is lattice strain energy[13]. Ideally, when an ordered compound such as low temperature PdD is forced to take on additional D, the added D must either force a localized expansion of the lattice or go into a band state. Forcing a localized lattice expansion is a highly endothermic process. Thus ion band state occupation is thermodynamically favored over a range of δ in $PdD_{1+\delta}$ at low temperature. However, too large a value of δ increases the energy level of the band state, which can lead to a two phase PdD + Pd_3(vacancy)D_4 superlattice[14]. At ambient temperature, occupation of ion band states can be expected at values of x somewhat less than 1.

3. How Band States Form

One experimental situation that leads to band state occupation in PdD_x is illustrated schematically in Fig. 1. Fig. 1 is a 1-dimensional pictorial representation of the Pd lattice in which the valleys represent the octahedral sites for interstitial D atoms and the hills are the saddle points separating the stable locations. The figure illustrates conditions presumed to exist after prolonged electrolysis has created a polarized surface passivation barrier through which D^+ ions have been plated so as to raise the D chemical potential of the electrode. The figure shows ~90% of the interstitial sites occupied by localized "chemical" D occupations. However, at the above-equilibrium chemical potential it is postulated that a small 10^{-6} - 10^{-4} fraction (= the value of δ in $PdD_{1+\delta}$) of the ions are excited to higher energy states that are able to rapidly tunnel through the saddle points that separate locally confining potential wells. The ions then see the lattice as a whole. The new boundary conditions enable the ions to assume lattice symmetry. They become band state ions. The

ion band state theory says that radiationless fusion involves only interactions between band state ions, i.e.. none of the chemical interstitials or lattice ions serve as nuclear reactants or products.

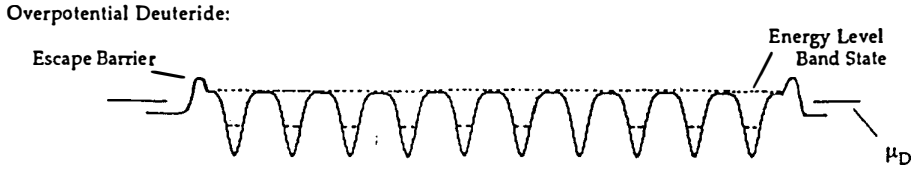

Fig. 1 Representation of PdD_X under conditions that enable D^+ band state occupation.

4. Unbroken Lattice Symmetry

Why does being in a band state make a difference? One answer is found in the insights of P. W. Anderson[15]. Anderson presents a hierarchy of scientific disciplines, with each discipline distinguished by the physical laws or processes that play a major role within the discipline. In solid state, many-body physics, the important processes are dominated by a requirement of periodic order (unbroken lattice symmetry). In contrast, in all chemical processes within a solid, lattice symmetry is broken. Reactions between band state ions are governed by unbroken lattice symmetry. We now show how this principle when combined with electron screening leads to a reduced Coulomb barrier to fusion.

5: The Coulomb Barrier in Bound Systems

To understand how being in a band state can affect the Coulomb barrier, it is first necessary to understand how the Coulomb barrier is expressed in confined particle systems. By a confined-particle system we mean a system in which the particles are bound by having negative energy, i.e. they cannot escape to ∞. Such systems are described by wave functions ψ such that $\psi \to 0$ as $r \to \infty$. The physics of the Coulomb barrier problem is contained in the 2-particle problem, as discussed below.

Consider the 2-ion-in-a-crystal problem. The stationary state wave equation is

$$\{- h^2/2m\ [\nabla_1^2 + \nabla_1^2\ ] + e^2/r_{12} + V_{lattice}(\mathbf{r}_1,\mathbf{r}_2)\}\ \Phi(\mathbf{r}_1,\mathbf{r}_2)\ = E\ \Phi(\mathbf{r}_1,\mathbf{r}_2) \qquad (1)$$

where $\phi(\mathbf{r}_1,\mathbf{r}_2)$ is a 2-ion wave equation in 6 variables x_1, y_1, z_1, x_2, y_2, z_2, and the derived variable $r_{12} = |\mathbf{r}_1-\mathbf{r}_2|$ = separation between ions. We have assumed no electron screening. To study the barrier problem it is necessary to change coordinates to $\mathbf{r}_{cm} = (\mathbf{r}_1+\mathbf{r}_2)/2$, $r_{12} = |\mathbf{r}_1-\mathbf{r}_2|$. When it is assumed that the electrostatic interaction between the lattice and the center of mass motion of each pair is very different than the comparable ion-ion electrostatic interaction $V_{lattice}(\mathbf{r}_1,\mathbf{r}_2) \approx V'_{lattice}((\mathbf{r}_1+\mathbf{r}_2)/2)$. (For metals in which screening lengths are considerably less than the lattice spacing, this is a good approximation) Then, it is permissible to write $\phi(\mathbf{r}_1,\mathbf{r}_2) = \Psi(\mathbf{r}_{cm})\ g(r_{12})$, and Eq. 1 becomes

$$\{- h^2/2m\ [1/2\nabla^2_{\mathbf{r}_{cm}} + 2\ \nabla^2_{r_{12}}\ ] + e^2/r_{12} + V'_{lattice}\}\ \Psi(\mathbf{r}_{cm})\ g(r_{12})\ = E\ \Psi(\mathbf{r}_{cm})\ g(r_{12})\ .(2)$$

Here, $\Psi(\mathbf{r}_{cm})$ defines an amplitude at each point in the crystal and $g(r_{12})$ is a "dimming" function which decreases the amplitude of $\Psi(\mathbf{r}_{cm})$ as $r_{12} \rightarrow 0$. $\mathbf{r}_{cm}$ and r_{12} are independent degrees of freedom. With suitable normalization $g(r_{12})$ can have values between 0 and 1. If $g(r_{12}) \rightarrow 0$ as $r_{12} \rightarrow 0$, there is a total Coulomb barrier against ion-ion overlap, which precludes nuclear reaction. If $g(r_{12})$ remains finite as $r_{12} \rightarrow 0$, then wave function overlap exists and fusion is allowed.

The role of the dimming function in determining overlap is illustrated by the well-known two-electron solution of the helium atom[16]. In Fig. 2 we show how the amplitude of the 2-electron wave function varies as $r_{12} \rightarrow 0$. Fig. 2 shows the case where both electrons are equidistant from the He nucleus. When the electrons are on opposite sides of the nucleus, $\Theta = 180^\circ$ or -180° and $g(r_{12}) = 1$. When the electrons are on top of each other, $\Theta = 0^\circ$ and $r_{12} = 0$. $g(r_{12})$ then has its minimum value. Since $g(r_{12}) \neq 0$, there is finite wave function overlap. If the electrons had the nuclear property of deuterons, they would fuse.

6. Cusp Condition

Fig 2 also illustrates an important property of charged point particles. The r_{12} dependency of the 2-particle wave function has a cusp at $r_{12} = 0$. The helium atom wave function (assuming infinite nuclear mass) is

$$\{-\hbar^2/2m_e\,[\nabla_1^2 + \nabla_1^2] + e^2/r_{12} + V_{\text{central field}}\}\,\Phi(\mathbf{r}_1,\mathbf{r}_2) = E\,\Phi(\mathbf{r}_1,\mathbf{r}_2). \quad (3)$$

The singularity of e^2/r_{12} at $r_{12} = 0$ must be canceled by a singularity in the kinetic energy term if the equation is to be bounded, as required by the right hand side. This requires that

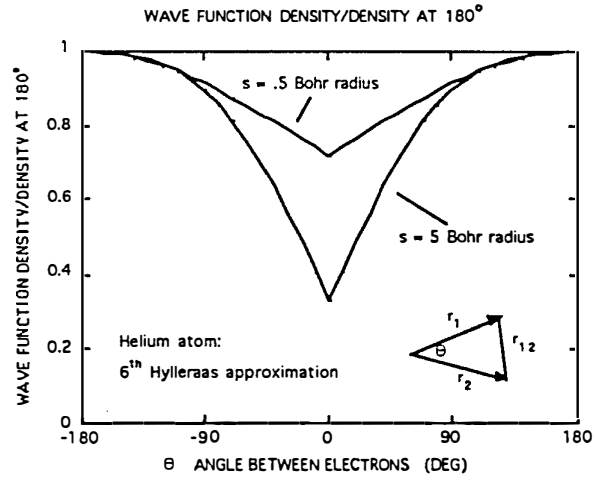

Fig. 2 Amplitude of helium ground state 2-electron wave function on the surfaces of 2 spheres for which s = constant. Values have been normalized with respect to the peak values, which occur when the 2 electrons are on opposite sides of the nucleus. Nature uses a cusp at $r_{12} = 0$ to compensate for the infinite electrostatic potential existing at this condition. The values at $\theta = 0$ measure the degree of electron-electron overlap.

$d/dr_{12}\ \phi(r_1,r_2)$ must be discontinuous if non-zero, and the discontinuity in slope must have the proper value to cancel e^2/r_{12}. This condition is called the cusp condition. The amplitude b of the cusp shown in Fig. 2 is determined by system energy minimization. The variational method used by Hylleraas, which minimizes kinetic energy plus potential energy, determined the amplitude of b for the two cases shown in Fig. 2.

7. Principles Determining Wave Function Overlap

Two principles combine to effect a reduction in Coulomb barrier for band state ions. The first principle is that of unbroken lattice symmetry. The second principle is that of electron screening. The principle of unbroken lattice symmetry requires that each unit cell of a crystal must be equivalent, i.e. the 2-ion wave function must have the same amplitude distribution in each unit cell. Functions meeting this requirement are Bloch functions ψ such that $|\psi(\mathbf{r} + \mathbf{R}_{Bravais})| = |\psi(\mathbf{r})|$, where $\mathbf{R}_{Bravais}$ is any lattice vector $\mathbf{R}_n$. The Bravais lattice vectors locate sets of periodically equivalent points of the lattice. Electron screening is a property of metallic conductors. In metals there are itinerant electrons, which have much higher mobility than the ions. As a result, each ion present in the lattice is always surrounded by negative charge provided by the electrons, such that the ion's Coulomb field is always canceled outside a small partially screened volume. As a result, ions in different unit cells of a crystal do not repel each other.

The eigenstates of band state ions are spatially distributed wave functions which contribute a fractional charge e/N_{cell} to each unit cell of the host crystal, where N_{cell} is the number of unit cells in the crystal. It is, however, possible to expand Bloch wave functions in terms of a sum of virtual (i.e. short-lived) states called Wannier functions[16]. These virtual states can be viewed as snapshots of the system and show undivided ions located in randomly selected unit cells. The time independent eigenstate can be calculated as the average of all the virtual state snapshots. This procedure provides a picture of the effect of electron screening. Sometimes the snapshots show both ions in a single unit cell. Under these conditions the unit cell occupations are of the form

0 0 0 0 0 0 2 0 0 0 ..... 0 0 0 0 0 0 0

(Here, 0's represent "empty unit cells, while the "2" represents a doubly occupied site.) In this case the Coulomb repulsion potential between band state ions is e^2/r_{12}. However, most of the snapshots show the ions in different unit cells,

0 0 0 1 0 0 0 0 .... 0 0 1 0 0 ... 0 0 0 0 0

In this second case the Coulombic repulsion potential is 0. The average-over-snapshots Coulombic repulsion potential is $e^2/(r_{12}\ N_{cell})$. This snapshot-averaged potential is that which applies to the electron-screened-ion-in-a-lattice problem.

8. The Eigenstate

We can now write the stationary state wave equation for 2 screened D^+ ions in a periodic lattice,

$$\{-\hbar^2/2m\ [\nabla_1^2 + \nabla_1^2] + e^2/(r_{12}\ N_{cell}) + V_{lattice}\}\ \Phi(r_1,r_2) = E\ \Phi(r_1,r_2) \qquad (4)$$

This equation is consistent with unbroken lattice symmetry. The resulting wave function has both unbroken lattice symmetry and cusps at equivalent locations in each unit cell. Each point-particle interaction occurs simultaneously at periodically equivalent points. The solution is time-independent and describes the stationary state of the system.

We have carried out an energy minimizing variational analysis of a cusp-containing wave function describing the 2-ion case[11]. The value of b that minimizes the sum of kinetic and potential energy at large N_{cell} is

$$b = 2/\pi \ (m_D/m_e) \ (r_{sc}/a_o) \ 1/N_{cell} \qquad (5)$$

The analysis shows that the cusps have negligible amplitude at large N_{cell} ($N_{cell} = \sim 10^5$)). As a result the $D^+_{band} + D^+_{band}$ interaction has no Coulomb barrier against fusion. a_o is the Bohr radius.

9. Relation to QEDCM

The ion band state theory is consistent with the QEDCM[17] picture of a non-perturbative ground state (NPGS). This idea, which also has been applied in the study of critical phenomena[18], is based upon the notion that the ground state has preferential length scales associated with it which distinguish it from asymptotically free states (associated with higher energy) where preferential length scales are not present. In fact, the ion band state theory, as well as the more general problem associated with the physics of bound charged particles in a periodically ordered system, is governed by a self-consistent quantum field theory called Local Density Theory (LDT), in which the length scales and boundary conditions are all treated on an equal footing, governed by a single requirement: that energy be minimized, based upon the known rules of quantum mechanics.

In practice, the associated theory is also similar to the QEDCM picture in that the ground state does exhibit coherence at periodically equivalent points. However, the associated coherence does not result from the inference of the QEDCM plasma-like oscillations that result from variations in the zero of energy. In the ion band state theory, the coherence occurs as a natural consequence of unbroken lattice symmetry, particle exchange, and the properties of the many-body wave function. A fundamental difference is that the wave functions for the particles associated with the QEDCM plasma are described using the Gamow tunneling factors and formalism and do not incorporate particle-exchange, while the ion band state theory wave functions, which do incorporate particle-exchange, are derived by minimizing the energy in a situation that incorporates the boundary conditions of bound particles. As a consequence, the ion band state theory does allow for the possibility (through wave function cusps and other discontinuous changes in the momentum) of changes in kinetic energy that not only are not possible in the QEDCM plasma but which are dictated by the rules of Quantum Mechanics. A second important point is that the starting point of the ion band state theory, LDT, is a well-tested, self-consistent Quantum Field Theory that has been applied quite well for accounting for the electronic structure and dynamics of charge transport in transition metals and for PdD in particular, and that a key element in the success of this theory has been a treatment of kinetic energy that incorporates these kinds of discontinuous changes in momentum.

10. Reaction Possibilities: Guiding Principles

Band theory was invented to explain important anomalies associated with charge and heat transport in ordered, metallic solids. In particular, during the early days of quantum mechanics, it was discovered from conductivity measurements in these kinds of solids, that the effective mean free path of electrons between collisions is many orders of

magnitude larger than the one appropriate in classical, semi-classical, and even quantum mechanical (free electron approximation) modeling of conductivity. Beginning with Bloch, it was discovered that by including periodic order in the kinematics and statistics associated with quantum transport, these anomalies in mean free path not only could be explained, but that meaningful parameterizations of electronic structure, based on the notion of energy bands, could be applied to a large range of problems associated with ordered solids, in general, including insulators, semi-metals, and semi-conductors, as well as metals.

Beginning in the early 1960's, important computational and formal developments occurred, which have provided a means for relating macroscopic phenomena associated with charge and heat transport to a considerably more detailed, microscopic theory, from which these transport phenomena are deduced as a natural, semi-classical limit. In terms of understanding reaction possibilities in general in solids, and the associated implications for cold fusion, these facts have important implications: 1) the presence of periodic order may significantly alter the manner in which charge "moves" within a solid, 2) the locations of individual "particles" within a solid may be altered in manner in which the reaction site may appear (depending upon how the locations are measured) to be in a number of seemingly impossibly different locations at once, and 3) the kinetic energies and momenta of the "particles" may discontinuously change without altering their energies.

Beginning in the 1970's, through the use of LDT and modern computational methods, and by making comparisons of calculated results with application of modern experimental spectroscopic techniques (ultra-high-vacuum photo-emission, x-ray photoemission, etc.), we have obtained a quantitative understanding at a very fine level of detail of the underpinnings of the microscopic theory, and means for quantifying our knowledge of the role of kinetic energy in particular in the microscopic theory. Specifically, considerable progress has occurred in our understanding of most of the ordered metallic lattices, and in particular, in the study of PdD and Pd, and in the study of 3d and 4d transition metals. In the process of accomplishing this we have obtained an understanding of three important factors: 1) the rapid screening of charges in the local electrostatic environments present in these materials by electrons, 2) the presence of periodic order, and 3) (from a calculational viewpoint) the importance of obtaining self-consistent results. Extremely important points are that each of these factors plays an important role in determining the kinetic energy of the individual "particles", that the kinetic energies of "particles" that occupy band states are very different than the kinetic energies of non-band state "particles", and that when particles occupy band states, the reaction possibilities are strongly affected by kinetic energy.

An important assumption of our application of these ideas to the ion band state problem and the potential nuclear reaction possibilities, is that the associated situation is adequately described within this context. As a consequence, throughout, it is assumed that the dominant electrostatic problem is described using "self-consistent", single-particle theory, in a manner that does not invalidate the assumptions that govern the validity of this approach. As we have discussed elsewhere, the underlying dynamics of the many-body system is initialized by the single-particle band states. An important point is that from this starting point, the limitations of the single-particle representation provide constraints on the many-body physics. In particular, a form of "Born-Oppenheimer" separability is always required, in which the motion of the center of mass of each ion band state nucleus (either H, D, ^{3}H, or ^{4}He) is always constrained to be independent of the motions of the individual nucleons contained within each nucleus. In practice, this constraint restricts considerably the potential channels for nuclear reaction. However, not only is this requirement consistent with the underlying assumptions that the potential modes of interaction are the result of relatively "small" perturbations of the ground state, it also is consistent with a potentially more important result: in the crystal lattice, ion-band-state-mediated reactions occur in a manner in which it becomes impossible to identify either in the initial state or in

the final state the precise location where the center of mass of the reaction is located. A second important consequence is that potential nuclear reactions cannot significantly disrupt the underlying crystalline environment, either by destroying periodic order, or by requiring that energy be transferred to the solid in such a large amount locally that the underlying assumptions of the band theory and associated theory of transport phenomena become invalid. A final important point is that these assumptions not only can be quantified but also provide a rationale for understanding a number of results: 1) why ^{4}He is the predominant reaction product (which we predicted prior to measurements), 2) why the ^{4}He should be found at low-energy outside heat-producing crystals, 3) the role of loading and electronic structure in radiationless fusion, and 4) why no high energy particles are released in the phenomena. Elsewhere[3], we have provided a detailed discussion of each of these predictions. It should be emphasized that each of these results follows from requirements that make the underlying picture valid, not as a consequence of theory. In other words, the assumption that ion-band-state-mediated reactions are at work requires that each of these effects be present, not the reverse.

In particular, implicit in the ion band state picture are the ideas of the "time-averaged" picture associated with the Bloch state picture and the occupation of Bloch states in a manner that minimizes energy. Important consequences of this are that: to minimize energy, a macroscopically small number (much less than N_{cell}) of ions occupy ion band states, and the resulting possibilities for nuclear reaction do not perturb the environment in a significant manner. When it is in fact impossible to determine the location of the center of mass of a particular nuclear reaction because the center of mass of each initial state and final state nucleus is in a band state, on the average, as we have previously discussed[2,3], each reaction occurs at all of the periodically equivalent locations in the solid. Heat release is then fractional: each D+D$\rightarrow^4$He reaction releases an amount of energy Q=23.8 MeV/N_{cell} (= 0.23 eV, for $N_{cell}=10^9$) in each unit cell. In the remainder of the paper, we will quantify a number of factors related to the point concerning the reasons that ^{4}He is found outside the crystals at low energy. To understand these factors, it is necessary to examine a number of points associated with ion band state transport.

11. Band Transport Theory

Modern Band State transport theory is based upon applying the Greens function methods derived by Kadanoff and Baym[20], which were extended by Langreth and Wilkins[21] to the many-body physics associated with the single-particle, band state solutions that are appropriate in a solid. A fundamentally important point is that the relevant many-body physics of charge transport is converted through this procedure from a Greens function that describes the evolution of charge in the microscopic theory, to a semi-classical limit in which a Boltzmann transport equation such as

$$J_e(\mathbf{x}) = e/\hbar \sum_i g(\mathbf{x},\mathbf{k}_i) \quad \nabla_{\mathbf{k}}\varepsilon(\mathbf{k})$$

can be used to quantify the relationship between the underlying microscopic dynamics and the macroscopic properties. Here $J_e(\mathbf{x})$ is the current density, $\mathbf{x}$ is macroscopic position vector, which extends over the whole solid, $g(t,\mathbf{x},\mathbf{k})$ is the Boltzmann "particle" distribution function, $\mathbf{k}$ is the wave vector, and the $\varepsilon(\mathbf{k})$ are the energy eignevalues. To understand the role of periodic order in this process it is important to recognize its role in the underlying microscopic theory, as expressed in the solutions of the single-particle band state equations.

In modern band state theory, these solutions most often are derived based upon the single-particle LDT[19] band theory. In practice these equations are derived as a subsidiary step in the problem of minimizing the total energy of the solid. In particular, in LDT, energy is minimized as part of a two step procedure in which, first, the charge distribution of all the electrons and nuclei is calculated self-consistently, based upon a prescribed choice of geometry, and then the geometry is varied until the minimum energy is obtained.

The single-particle (Kohn-Sham) band theory equations are used during the process of calculating the self-consistent charge density. Specifically, the initial charge density is used to construct a potential $V_{lattice}$ based upon the trial geometry, which is defined by the spacing and orientation of the collection of periodically positioned nuclear centers. The band theory equations in turn are used to determine the density. With respect to the transport problem, important points are that $V_{lattice}$: 1) includes all of the electrostatic interactions from electrons and positive nuclear centers, and 2) is a periodic function of each of the Bravais lattice vectors $\mathbf{R}_n$, that separate any of the periodically positioned nuclear centers. Because $V_{lattice}$ is periodic, $V_{lattice}(\mathbf{r} + \mathbf{R}_n) = V(\mathbf{r})$. Using this potential, the eigenstates (Ψ), and eigenvalues (ε) of an effective Schroedinger equation (the single-particle, Kohn-Sham equation) are constructed. In solving this problem, important simplifications are made possible by assuming that the geometry is periodic. The significance of this symmetry is that it means that each eigenstate Ψ may be selected as a Bloch state $\Psi_{\mathbf{k}}$, defined by the wave-vector $\mathbf{k}$ and the Bloch condition

$$\Psi_k(\mathbf{r} + \mathbf{R}_n) = e^{i\mathbf{k}\cdot\mathbf{R}_n}\,\Psi(\mathbf{r}) \quad . \tag{6}$$

Each eigenvalue (also called a band energy) is also a function of the wave vector $\mathbf{k}$, namely, $\varepsilon = \varepsilon(\mathbf{k})$. This provides a method for solving the effective single-particle Schroedinger equation, which for electrons is

$$H_{sp}\Psi_k(\mathbf{r}) = [-\hbar^2/2m_e\nabla^2 + V_{lattice}(\mathbf{r})]\,\Psi_k(\mathbf{r}) = \varepsilon(\mathbf{k})\,\Psi_k(\mathbf{r}) \tag{7}$$

Once these equations are solved, the density $\rho(\mathbf{r})$ is constructed[19]. It is important to note that because $V_{lattice}$ is a periodic function of $\mathbf{R}_n$, its Fourier transform is defined by a discrete set of vectors (called reciprocal lattice vectors)$\mathbf{G}_n$, such that $\mathbf{R}_n\cdot\mathbf{G}_m$ is an integer multiple of 2π, for any values of m and n. As a consequence of this, $\varepsilon(\mathbf{k}) = \varepsilon(\mathbf{k}+\mathbf{G}_m)$, for any value of m. An important result of this fact is that during any interaction involving Bloch states, it is possible for discrete values of momentum, given by $\hbar\mathbf{G}_n$, to be transferred to and from the lattice without effecting the energy of the individual states, while preserving periodic order. These energy conserving processes in which momentum is changed, which are called UmKlapp processes, were first identified by Peierls[22] as being important in the low temperature behavior of electrical conductivity. Because they provide a means for allowing a non-zero momentum-change interaction between different forms of quasi-particles that possess lattice symmetry (band state, phonons, etc.), at low temperature, they also provide a means for coupling surface phenomena with bulk phenomena in which minimal disruption of periodic order occurs.

Important points are: 1) the kinetic energy is treated in a manner consistent with the underlying boundary conditions, 2) the charge distribution and the lattice geometry are allowed to vary in a manner consistent with minimizing the energy, subject to the constraint that periodic order is maintained, and 3) exchange and correlation effects associated with the effects of occupying particular portions of the underlying many-body wave function are

treated in an approximate manner that becomes exact in the limit of small electron separation (a limit that applies quite well in transition metals).

Because the LDT energy is constrained to be stationary with respect to variations of the electron density, it follows that when small numbers of deuterium ions (and their electrons) are injected into any periodic host, the resulting energy may be constrained to be stationary with respect to variations in the densities of either injected ions or electrons provided both the ions and electrons occupy band states and variations in ion band state density are constrained to be independent of electron band state density, and provided the ion band states are derived using the negative of the Coulomb potential associated with Eq. 7 and the approximation that ion band state-ion band state exchange effects are negligible. The basis for the argument follows from continuity of the total energy with respect changes in density, and the fact that infinitesimal variations can occur when macroscopically small numbers of charged particles occupy band states.

We have previously summarized the underlying many-body physics that makes possible overlap between ion band states[2,3]. The potential for overlap follows from the fact that the many-body state is constructed by forming the product of occupied single-particle band states, each of which has overlap (as a consequence of Eq. 5) with every equivalent lattice site in the crystal. An important point, however, is that overlap alone does not provide a means for understanding how reaction can occur. To understand how reaction might occur, it is important to understand how reactions occur within solids. Here, an extremely important point is associated with the manner in which charge and energy are transferred within a solid and the significance of the Kadanoff-Baym procedure.

In particular, Kadanoff and Baym (as shown by Langreth and Wilkins) observed that there exists a natural procedure for relating the angular frequency representation G_o of the single-particle Greens function associated with an arbitrary single-particle Hamiltonian H_{sp} and the comparable Greens function G to a macroscopic quantity, called the Wigner function, G_W, which, in the case of ordered solids, asymptotically approaches the solution of the Boltzmann equation that is used to describe charge and heat transport. In particular, G_o is directly related to solutions of the Kohn-Sham equations through the relationship

$$G_o(\mathbf{r},\mathbf{r}',z) = \sum_{\mathbf{k},\lambda} \frac{\Psi_{\mathbf{k}}(\mathbf{r})\Psi_{\mathbf{k}}^*(\mathbf{r}')}{\hbar z - \varepsilon_\lambda(\mathbf{k})} \quad , \tag{8}$$

where z is any complex frequency and the sum is over all wave vectors $\mathbf{k}$ and all bands λ. The corresponding equation describing G_w is

$$\frac{\partial G_w}{\partial t} + \dot{\mathbf{k}} \cdot \nabla_{\mathbf{k}} G_w = 0 \quad , \tag{9}$$

where

$$\dot{\mathbf{k}} = -\nabla_{\mathbf{x}} \varepsilon(\mathbf{k}) + \text{external forces} \quad . \tag{10}$$

Here, G_W may be interpreted as the probability of a charged particle occupying a band state with energy $\varepsilon(\mathbf{k})$ at the position $\mathbf{x}$. In the general periodic solid case including disruptions in period order, $\mathbf{x}$ is any integer multiple of any Bravais lattice vector. In the case of G_o, where order is assumed, the differentiation of $\varepsilon(\mathbf{k})$ with respect to $\mathbf{x}$ only alters the eigenvalue through changes in the wave function at the boundaries of the lattice where periodic order is lost. When additional effects (phonons, additional lattice imperfections,

and additional many-body effects) are included, the resulting expression for the single particle Greens function analog of G_o solves a "Dyson's equation" in which time-dependent modifications, through collision processes, are required. These effects in turn can be related to a Boltzmann equation in which an additional term of the form

$$\dot{\mathbf{x}} \nabla_{\mathbf{x}} G$$

is added to the left side, where

$$\dot{\mathbf{x}} = \nabla_{\mathbf{k}} \varepsilon(\mathbf{k}) \quad ,$$

and a complicated hierarchy of terms are included on the right side. The important point is that all of the many-body physics can be captured in G and G_o.

A second important point, however, is that in the case of Eq. 9, an avenue exists through modifications of the eigenvalue at the boundary of the solid for changing the Greens function associated with a particular charged species (be it electrons or ions in band states) without significantly altering the underlying periodic order within the solid. A second important point is that the quantities $\dot{\mathbf{k}}$ and $\nabla_{\mathbf{x}} G$ may change discontinuously through Umklapp processes. These are processes in which the wave vector changes discontinuously by a reciprocal lattice vector, and physical momentum is transferred to the crystal as a whole.

We believe that a potentially dominant mode for reaction at low-moderate temperature involves the situation in which the energy release of $D_{band} + D_{band} \rightarrow {}^4He_{band}$ results in a shift of the electrostatic zero of the solid and an accompanying Umklapp-process-mediated momentum transfer (through lattice recoil), manifesting itself through a shift in the chemical potentials of ion band state ^4He and D. Because a constant shift of the potential is a periodic function and because all of the initial and final state contributions occupy band states, the densities of each are periodic and the perturbations to the electrostatic potential are all periodic functions, and are all small on a per unit cell basis. In such a situation, the dominant modes for interaction will be through effective neutralization of ^4He with boundary region electrons. These will manifest themselves through variations both in $\nabla_{\mathbf{x}} \varepsilon(\mathbf{k})$ and in gradients of the chemical potential at the boundaries of the crystal through the quantities $\dot{\mathbf{k}}$ and $\nabla_{\mathbf{x}} G$.

12 WHY Cusps and Discontinuities in Momentum Invalidate Gamow Theory

In the 1-dimensional Gamow approximation the r_{12} dependence of the two particle wave function can be represented by $\phi(r_{12}) \propto \exp(i\phi(r_{12}))$, in which

$$\phi(r_{12}) = \int_{\infty}^{r_{12}} k(x)\, dx \text{ , where } \quad k(x) = \sqrt{\frac{2m}{\hbar^2}(E\text{-}V(x))} \quad . \tag{11}$$

Away from the classical turning point (defined by k(x)=0) this formula is valid provided $|dk/dx| << |k(x)|^2$, while near the turning point a relationship between the second and first derivatives is used to identify the appropriate (connection formula) forms of the wave function that apply asymptotically far from the turning point, based on the premise that $k(x)^{1/2}$ is continuous and continuously differentiable on either side of the classical turning

point. When the first derivative of $\phi(r_{12})$ becomes discontinuous, $k(r_{12})$ is discontinuous so that $|dk/dx| \rightarrow \infty$. Then, Eq. 11 is not valid for any value of k. Also, because k is neither continuous nor continuously differentiable at a cusp, one cannot identify an appropriate form of the wave function that matches the Gamow function in the vicinity of the cusp, nor apply the conventional connection formula.

References

1. S. R. and T. A. Chubb, "Lattice Induced Nuclear Chemistry", in *AIP Conf. Proc.* **228**, 691(eds. S.E.Jones et al., AIP, NewYork, 1991).
2. T. A. Chubb and S. R. Chubb, "Cold Fusion as an Interaction between Ion Band States", *Fusion Technology*, **20**, 93 (1991).
3. S. R. Chubb and T. A. Chubb, "Ion Band State Fusion: Reactions, Power Density, and the Quantum Reality Question", *Fusion Technology.* **24**, 403 (1993).
4. M. H. Miles and B. F. Bush , "Search for Anomalous Effects Involving Excess Power and Helium during D_2O Electrolysis Using Palladium Cathodes", in *Frontiers of Cold Fusion.*, H. Ikegami, Editor, (Universal Academy Press, Tokyo, 1993), p. 189.
5. M.C.H. KcKubre et al., in *Frontiers of Cold Fusion.*, H. Ikegami, Editor, (Universal Academy Press, Tokyo, 1993), 3. K. Kunimatsu et al., ibid,31.
6. T.A. Chubb and S.R. Chubb, "Wave Function Overlap and Nuclear Reactions in D+ ion Band State Matter". submitted to *Fusion Technology.*.
7. T. A. Chubb and S. R. Chubb, "Wave Function Overlap Behavior of D^+ Ion Band State Matter", submitted to *Phys. Rev. Lett.*
8. M. J. Puska, R. M. Nieminen, M. Manninen, B. Chakraborty, S. Holloway, and J. K. Norskov, "Quantum Motion of Chemisorbed Hydrogen on Ni Surfaces", *Phys. Rev. Lett.* **51**, 1081 (1983).
9. C. Astaldi, A Bianco, S. Modesti, and E. Tosatti, "Vibration Spectra of Atomic H and D on Cu(110): Evidence of H Quantum Delocalization", *Phys. Rev. Lett.* **68**, 90 (1992).
10. R, Niemenen, "Hydorgen atoms band together", Nature 356,289 (1992).
11. R. C. Casella, "Theory of excitation bands of hydrogen in bcc metals and of their observation by neutron scattering", *Phys. Rev. B* **27**, 5943 (1983).
12. E. Wicke and H. Brodowsky, "Hydrogen In Palladium and Palladium Alloys," *Hydrogen in Metals II,* p. 73., G. Alefield and j. Volkl, Eds., Springer , Berlin (1978).
13. Y. Fukai and N. Okuma, "Formation of Superabundant Vacancies in Pd Hydride under High Hydrogen Pressures", *Phys. Rev. Lett.* **73**, 1640 (1994).
14. P. W. Anderson, "More Is Different", *Science* **177**, 393 (1972).
15. E. A. Hylleraas, Zeit. f. Phys. **54**, 347 (1929). F. Seitz, *The Modern Theory of Solids* (McGraw-Hill, New York, 1940), pp. 227-234.
16. J. M. Ziman, *Principles of Theory of Solids*, (Cambridge University Press, London, 1972).
17. G. Preparata, "Cold Fusion '93: Some Theoretical Ideas", *Trans. Fus. Tech.* **26**, 397.
18. ShangKeng MA, "Modern Theory of Critical Phenomena", (W. A. Benjamin, Inc. Reading, MA, 1976), 561 pp.
19. P. C. Hohenberg and W. Kohn, *Phys. Rev. B*, **138**, 864 (1964). W. Kohn and L. J. Sham, *Phys. Rev. A*, **140**, 1133 (1965).
20. L. P. Kadanoff and G. Baym, *Quantum Statistical Mechanics* (Benjamin, New York, 1962).
21. D. C. Langreth and J. W. Wilkins, "Theory of Spin Resonance in Dilute Magnetic Alloys", *Phys. Rev. B* **6**, 3189 (1972).
22. R. E. Peierls, *Ann. Phys (5)* **12**, 154 (1932).

Fifth International Conference on Cold Fusion
9-13 April, 1995 - Monte Carlo, Monaco
ICCF5 ©1995

Update on Neutron Transfer Reactions

Peter L. HAGELSTEIN
Massachusetts Institute of Technology
Research Laboratory of Electronics
Cambridge, Massachusetts 02139

Abstract

We discuss progress in our studies of two new basic physical mechanisms that may be relevant to recent experiments that exhibit anomalies in metal hydrides and deuterides.

Anomalous energy transfer from phonon modes to the constituents of a lattice may occur through frequency-shifting phonon modes that are highly excited. The energy transfer is $\Delta E = N\hbar\delta\omega$, where N is the number of phonons in the modes, and $\delta\omega$ is the frequency shift of the phonon modes. A phonon laser can provide a large N; a finite frequency shift can be produced in a lattice with a phonon bandgap and with impurity vacancy modes that occur in the phonon bandgap. We propose that exothermic desorption in a metal hydride pumps a surface phonon laser.

We propose that neutrons can hop in a lattice, by analogy with electron hopping. Neutron hopping in crystalline silicon has been analyzed, and found to be unobservable; neutron hopping in lighter nuclei should lead to observable gamma emission. Neutron hopping in lighter nuclei, combined with anomalous energy transfer, is a candidate route to account for anomalous excess heat and tritium production.

1. Introduction

We have considered a number of possible theoretical approaches over the that past several years that may be relevant to a description of the anomalies that have been reportedly observed in metal hydrides and metal deuterides.[1] The primary experimental claims at this point include: [1] excess energy production in electrochemical experiments at a level that could not possibly be chemical (with essentially no associated radiation); [2] tritium production, without secondary neutron emission (the tritium, if real, must be born nearly stationary); and [3] neutron emission. There also exists claims of experimental evidence in support of

[4]He production, host lattice activation, x-ray emission, gamma emission, and beta emission.

Many involved in the experimental efforts mentioned above hold that the existence of the anomlies is now proven; many involved in mainstream physics research (and most of the scientific community) hold that none of the anomalies are real. This difference of opinion appears to be a stable feature of the field, and there appear to be no prospects to resolve the differences any time soon. In our research, we take the experimental claims for which the evidence seems to be strongest, and study theoretical mechanisms that appear to be relevant. While the nature of the experimental claims excludes many possible mechanisms and reactions, they unfortunately do not generally make positive statements that would clearify reaction pathways or underlying mechanisms.

For any theory to begin to be relevant to claims of this sort, two fundamental issues must be addressed: [1] there must be a mechanism that allows for the transfer of a large amount of energy from the atomic scale to the nuclear scale; and [2] there must also be a mechanism that will allow nuclei to react in the most general sense. The second point is usually cast in terms of overcoming the Coulomb barrier, but in light of the discussion in the present work, this is too restrictive. Our studies have consequently focused on mechanisms for anomalous energy transfer, and also on new nuclear reaction pathways involving charge neutral reactants for which no Coulomb barrier problem occurs.

2. Anomalous Energy Transfer

We have considered during the past several years the possibility of anomalous energy transfer with the phonon modes in a lattice. Basic energy transfer mechanisms with vibrational modes in molecules and solids were understood in the 1930s; the creation and destruction of phonons in a lattice was described by Lamb[2] and later by Mossbauer[3]; frequency-shifting of phonon modes in the molecular case was described by Duschinsky[4]. Anomalous energy transfer through the creation and destruction of phonons does not appear to be feasible; instead, we have examined energy transfer by frequency shifting phonons that are already present.[5] In this case, the energy transfer is

$$\Delta E = N\hbar\delta\omega \tag{1}$$

where N is the number of phonons present, and where $\delta\omega$ is the associated frequency shift.

For this energy to be anomalously large, we require a large number of phonons N to be present (which could be developed by a phonon laser, for example). We also require a lattice with special properties: it must have a phonon spectrum that contains a band gap, and phonon modes must jump a band gap due to a modification of the lattice at a single site. Many metal hydrides contain a band gap between the acoustic and optical phonon modes; the basic theory for how

phonon modes are altered due to mass or force constant changes at a single site was studied by Dawber and Elliott[6].

This mechanism alone appears to be capable of producing anomalies if the appropriate conditions can be met. For example, phonon gaps may be produced in metal hydrides if host lattice vacancies occur at impurity levels. In this case, processes that alter the number of host lattice vacancies can mediate anomalous lattice energy transfer. We have computed decay rates for this general process for a variety of recoil and nuclear decay channels.[7] For example, lattice-induced recoil of deuterons will lead to *dd*-fusion reactions with predicted neutron production rates that are in the general range of those claimed in experiments. This general mechanism could in principle produce anomalous alpha and beta decays; the associated reaction rates are reported in Ref. 7.

3. Proposed Surface Phonon Laser

Anomalous energy transfer through the route described in the last section presupposes the existence of a large number of phonons per mode N; we know that this could be produced by a phonon laser. Phonon lasers are known, and phonon lasing on acoustic modes up to 0.87 THz has been reported in the literature.[8] The energy exchange mechanism that we are interested in requires the existence of an optical phonon laser that operates near 6-8 THz.

Phonon lasers are in many ways analogous to optical lasers, as both require the development of a population inversion (or else the development of parametric gain). There exist few proposals for driving an optical phonon laser, although it would be reasonable to expect that optical pumping of impurities in a low temperature transparent crystal could be extended to optical phonons. Such techniques are not readily extended to metal hydrides, and the requirement that gain be developed at room temperature makes the problem far more severe since the optical phonon lifetimes are expected to be quite short (on the order of a picosecond) under these conditions.

We have recently proposed that exothermic desorption of a metal hydride can be used to drive a surface phonon laser.[9] If we consider the potential for molecular hydrogen near a clean metal surface,[10] we note that molecular hydrogen is not stable at the surface and is in fact pushed away (see Figure 1). Hydrogen in the metal can be either at lower or higher energy than the molecular energy. In the case that the energy is higher, so that the desorption is exothermic, then the situation becomes in some sense a phonon analog of an excimer laser.

Phonons can stimulate the desorption, and some of the desorption energy will go into the phonon modes that initially caused the desorption; in the event that the desorption is exothermic, then there exists the possibility of stimulated phonon emission and phonon gain. The hydrogen desorption from PdH probably becomes exothermic near a loading of 0.83; the situation is expected to be similar for desorption from PdD.

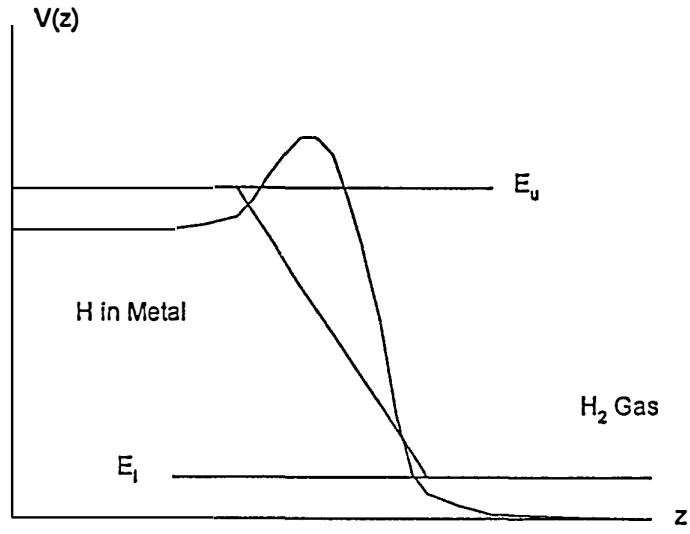

Figure 1. Schematic energy of H_2 minimum potential energy surface near a metal hydride surface.

Quantum desorption models have been studied in the literature (see for example Ref. 11). A basic description relevant to the present discussion could be developed starting from

$$\hat{H} = \sum_i \epsilon_i \hat{b}_i^\dagger \hat{b}_i + \sum_{\mathbf{k}} \epsilon_{\mathbf{k}} \hat{c}_{\mathbf{k}}^\dagger \hat{c}_{\mathbf{k}} + \sum_{\sigma,\mathbf{q}} \hbar\omega_{\mathbf{q},\sigma} \hat{a}_{\mathbf{q},\sigma}^\dagger \hat{a}_{\mathbf{q},\sigma} + \sum_{i,j,\mathbf{k}} \left[V_{i,j,\mathbf{k}}(\hat{a}, \hat{a}^\dagger) \hat{c}_{\mathbf{k}}^\dagger \hat{b}_i \hat{b}_j + h.c. \right] \quad (2)$$

This model includes hydrogen atoms at site i, free molecular hydrogen with momentum $\mathbf{k}$, phonon modes indexed by $\mathbf{q}$ and σ, and phonon-dependent desorption and adsorption terms. A linearization of the desorption potential in the phonon mode operators results in a Hamiltonian that can describe a one-phonon laser amplifier.

Perhaps the simplest quantitative estimate for the desorption flux required to sustain such a phonon laser comes from a balance between surface phonon creation and destruction; net gain is present when more phonons are generated than destroyed. If we imagine that a surface phonon mode is initially very highly excited, so that a significant fraction of the desorption power is converted to stimulated phonon power, then the threshold condition is equivalent to the statement that as many phonons are generated as destroyed. For surface optical phonons modes, the number of phonons required in this example is perhaps on the order of unity per atom participating; consequently the number of phonons destroyed per unit time is the product of the mode volume V, the relevant density n, and the destruction

rate $1/\tau$. The number of phonons generated per unit time is the product of the exothermic desorption flux J_{des}, weighted by the number of phonons generated per desorption event $\overline{N}$, and mode surface area A. We obtain

$$\overline{N} J_{des} A = \frac{nV}{\tau} \tag{3}$$

The required desorption flux for normal surface optical phonon modes obtained from this argument is very high, on the order of 10^{28} molecules/cm^{2}sec. Such a desorption flux is not sustainable, even on a microscopic timescale, either by conventional diffusion or by thermodynamically-forced diffusion.[12]

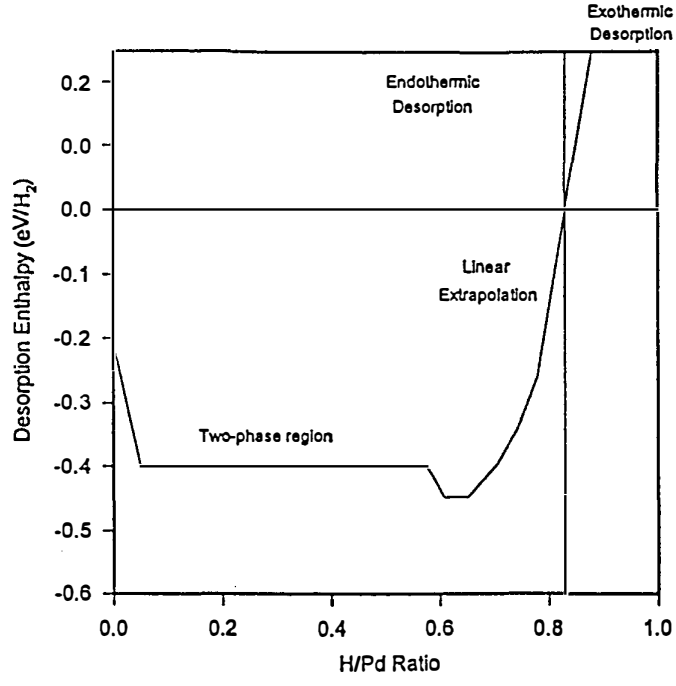

Figure 2. Estimated desorption energy for PdH versus loading.

Inspection of equation (3) indicates that the constraint on the desorption flux in the case of an impurity mode can in principle be lower by a dilution factor. For example, host lattice vacancies at the per cent level has been proposed to lead to an "impurity" optical phonon band within the PdD phonon band gap. The participating deuterium atoms are those within a cell containing a vacancy, which occurs at a reduced density; consequently, the threshold desorption current should be considerably less (on the order of 10^{26} molecules/cm^{2}sec). If a dominant mode of release of molecular deuterium from the surface of a highly loaded cathode is through local explosive exothermic desorption events that last on the order of a nanosecond, then such events may be sufficient to drive an optical phonon laser on dilute impurity modes.

The existence of such a mechanism would be critical for the operation of the physical mechanisms under discussion in section 2, and in the following sections. In addition this type of mechanism appears to be consistent with recent correlation of excess heat with flux discovered recently by the SRI group.[13]

4. Neutron Hopping

While there have been several proposals for mechanisms that may lead to enhanced screening of the Coulomb potential between nuclei, we have abandoned fusion reaction mechanisms generally (as candiates for heat and tritium production) in the belief that the amount of screening required is nonphysical. Our deliberations have driven us through a string of relatively exotic reactions, finally reaching a new class of reactions that may all be classed under the generally heading of "neutron hopping" reactions.[14] It is well known that electrons hop in solids, and the basic model that describes this hopping can be applied almost directly to examine the possibility of neutron hopping.

The neutron mixed valence Hamiltonian that describes the coupling between bound and continuum neutron states is

$$\hat{H} = \sum_{\mathbf{k},\sigma} \epsilon_{\mathbf{k}} \hat{c}^{\dagger}_{\mathbf{k},\sigma} \hat{c}_{\mathbf{k},\sigma} + \sum_{i,\sigma} \epsilon_d \hat{d}^{\dagger}_{i,\sigma} \hat{d}_{i,\sigma} + \frac{1}{2} U \sum_{i,\sigma} \hat{n}_{i,\sigma} \hat{n}_{i,-\sigma}$$
$$+ \sum_{i,\mathbf{k},\sigma} \left[V_{\mathbf{k}} e^{-i\mathbf{k}\cdot\hat{\mathbf{R}}_i} \hat{c}^{\dagger}_{\mathbf{k},\sigma} \hat{d}_{i,\sigma} + V^{*}_{\mathbf{k}} e^{i\mathbf{k}\cdot\hat{\mathbf{R}}_i} \hat{d}^{\dagger}_{i,\sigma} \hat{c}_{\mathbf{k},\sigma} \right] \tag{4}$$

Neutron hopping is only expected in nuclei with s-wave valence neutrons and two neighboring stable isotopes; elements which satisfy this requirement include: hydrogen, helium, silicon, cadmium, tin, tellurium and xenon.

We recently investigated neutron hopping in silicon, in the hopes of developing an experiment that would exhibit the effect cleanly. The basic idea is that $2s$ neutrons from ^{29}Si would hop among neighboring ^{28}Si nuclei, and from time to time be captured by ^{29}Si to make ^{30}Si; this capture process would lead to a gamma at 2.1 MeV. Crystalline silicon has a diamond lattice structure, which consists of two interpenetrating FCC lattices. Virtual neutrons originating from one FCC sublattice are Bragg scattered by the other and delocalized; the gamma emission rate for this structure is obtained from fourth order perturbation theory

$$\Gamma = -\frac{2}{\hbar \epsilon_D^4} \mathrm{Im} \left\langle \hat{V}_{13} \hat{V}_{32} (E - \hat{H}_2)^{-1} \hat{V}_{23} \hat{V}_{34} (E - \hat{H}_4)^{-1} \hat{V}_{43} \hat{V}_{32} (E - \hat{H}_2)^{-1} \hat{V}_{23} \hat{V}_{31} \right\rangle \tag{5}$$

In this formula, state 1 refers to a ^{29}Si valence neutron on the first sublattice, state 2 refers to a ^{29}Si valence neutron on the second sublattice, state 3 refers to a free neutron, and state 4 refers to a gamma captured ^{30}Si neutron; the interaction potentials $\hat{V}_{ij}$ are of the form of given in the neutron mixed valence Hamiltonian.

This gamma emission rate can be evaluated approximately (after much algebra); we obtain in the high temperature limit

$$\frac{\Gamma}{^{29}\mathrm{Si}} \approx \frac{V_0^6 N_B^4 \gamma}{\epsilon_D^4 \delta \epsilon_M^2} f[^{28}\mathrm{Si}] f[^{29}\mathrm{Si}] e^{-\Delta\epsilon/kT} \tag{6}$$

where V_0 is the volume-averaged nuclear matrix element (about 20 meV), N_B is the number of Brillouin zones contributing (about 30 near the melting point), γ is the capture rate for a free virtual neutron (about 2.5 sec^{-1}), ϵ_D is the neutron binding energy (8.47 MeV), and $\delta\epsilon_M$ is the lattice energy transfer in the Mossbauer limit (uncertain, but perhaps on the order of 10^{-10} eV). The f factors are fractional site occupation probabilities. The exponential factor comes about from destructive interference of the continuum Bragg waves, limited by the requirement that the virtual neutron scattering generates no phonons; the effective energy barrier is

$$\Delta\epsilon \approx \frac{a^2 kT}{< |\mathrm{u}|^2 >} \longrightarrow \frac{2Ma^2(k\Theta_m)^2}{9\hbar^2} \approx 22 \text{ eV} \tag{7}$$

where a is the lattice constant (2.715 Å), $< |\mathrm{u}|^2 >$ is the mean square thermal center of mass displacement, M is the nuclear mass of ^{28}Si, and Θ_m is the Debye temperature (about 525 K). This relation may also be written as

$$\Delta\epsilon \approx \frac{1}{3} M\omega_0^2 a^2 \tag{8}$$

where ω_0 is the characteristic vibrational frequency.

The gamma emission rate in this case is unfortunately too small to be observable. The emission rate is highest near the melting point (1683 K); the prefactor is respectable ($\sim 10^{-13}$ sec^{-1}), but the exponential (due to destructive interference of the Bragg waves) reduces the rate by more than 60 orders of magnitude.

Consequently, we turn to the question as to whether the effect would be observable in other systems. Upon inspection of the various factors that make up the effective energy $\Delta\epsilon$ for the diamond lattice structure, it appears that only two quantities are of importance: the nuclear mass and Debye temperature. Lighter nuclei could exhibit in principle a much greater effect. Of the candidate elements with outer s-wave neutrons, by far the most interesting candidate is hydrogen: virtual neutron originating from deuterium have the best chance of being delocalized by Bragg scattering from nearby protons in an ordered lattice. This argument assumes that the relevant nuclear matrix element (which we have not yet computed for deuterium) is of comparable magnitude. For example, the vibrational frequency ω_0 for the deuterons in PdD is roughly the same as for the silicon nuclei in crystalline Si (the lattice structure is that of NaCl, so that a somewhat different proportionality may occur); the barrier energy $\Delta\epsilon$ in this case should be much less.

If these arguments are correct, then we would expect that a metal hydride that is loaded with a mixture of deuterium and hydrogen would exhibit neutron hopping if heated suddenly, as a thermally-induced bulk effect, with an effective

energy on the order of an electron volt. The presence of the effect should be observable through gamma emission. Computations of this process are ongoing.

5. Neutron Hopping Coupled with Anomalous Energy Transfer

For the past several years we have examined various approaches to the problem of neutron hopping to an inequivalent nucleus coupled with the lattice energy transfer mechanism. A neutron hopping onto a nucleus generally will lower the phonon mode frequency, which leads to an energy transfer that has the wrong sign for heat production. We proposed that impurity modes due to host lattice vacancies could shift up through a recoil upon neutron capture that reduced the number of vacancies. While it seemed to be clear that the energy transfer through frequency shifting could be driven by a neutron transfer in principle, the frequency shifting mechanism leaves the lattice in a state which cannot use the same phonons for subsequent energy transfers.

This problem is in general serious. If phonons were used only once then lost, then the maximum efficiency would be much less than one; the experimental claims for heat production are larger than this. We have proposed earlier that the phonons could be frequency-shifted back down by a Raman process, and replaced when lost by phonon gain. While this may be possible in principle, it is by no means compelling.

Here we propose a speculative alternate solution that may have some advantages. We propose to couple an exothermic neutron hopping reaction with an endothermic lattice-induced decay process, and then require that the phonon distribution not be changed significantly during the combined process. Such a mechanism could be repeated without a loss of phonons; it has the additional advantage that the reaction rate for the coupled process will be faster than the rate for the neutron hopping part of the reaction alone, since the lattice-induced processes are so fast.

For example, we consider a virtual neutron that originates from a deuteron, resonantly Bragg scatters off of nearby protons in a metal hydride, and then lands on ^{28}Si with enough recoil to dislodge it so as to change the number of host lattice vacancies. If the process were conservative so far, then the lattice would be highly excited and unstable against a rapid decay of the host lattice, the fastest of which would be lattice-induced alpha decay of a low Z nucleus. Since the lattice decay is so fast, it is reasonable to couple it with the preceding reaction as a second order process,[7] which need not conserve energy in the intermediate state. The associated decay rate of a deuteron through this route can be computed from

$$\Gamma = -\frac{2}{\hbar\epsilon_D^4\Delta\epsilon_L^2}\mathrm{Im}\left\langle \hat{V}_{13}\hat{V}_{32}(E-\hat{H}_2)^{-1}\hat{V}_{23}\hat{V}_{34}\hat{V}_{45}(E-\hat{H}_5)^{-1}\hat{V}_{54}\hat{V}_{43}\hat{V}_{32}(E-\hat{H}_2)^{-1}\hat{V}_{23}\hat{V}_{31}\right\rangle \tag{9}$$

In this formula, $\Delta\epsilon_L$ is the energy excess determined by the difference in neutron

binding energies of the donor and acceptor nuclei, taking into account the energy transfer with the lattice:

$$\Delta\epsilon_L = |\epsilon_A| - |\epsilon_D| - N\hbar\delta\omega \tag{10}$$

and state 5 includes the results of the lattice-induced decay.

This mechanism is currently the focus of our theoretical investigations. While we have not yet evaluated this rate in detail, certain aspects of the reaction rate appear at this point to be plausible. We expect the total reaction rate to be perhaps of the form

$$\frac{\Gamma}{D} \sim \frac{V_H^6 V_{Si}^2 N_B^4}{\epsilon_D^4 \Delta\epsilon_L^2 \delta\epsilon_M^2} f[\mathrm{D}] f[\mathrm{H}] f[^{28}\mathrm{Si}] e^{-\Delta\epsilon/kT} e^{-\theta} \sum_i \gamma_i \tag{11}$$

The prefactor here is reduced from that encountered in the last section by $V_{Si}^2/\Delta\epsilon_L^2$; the fractions f can be on the order of unity; the effective energy $\Delta\epsilon$ ought to be less than 1 eV. The probability that the appropriate recoils occur, and that the coupling between the initial, intermediate and final lattices is phonon conservative, will appear as an exponential damping factor (taken to be $e^{-\theta}$ here, the magnitude of which is presently unknown). Finally, the lattice-induced decay gives rise to a very large rate γ_i (on the order of 10^{20} sec^{-1} for each nucleus i in the lattice that is capable of causing a useful phonon mode gap jump; this results in a potential increase in the total rate over the results of the previous section.

One interesting feature of this type of theory is that it does not require that the lattice actually has the very large number of phonons required for a complete exchange of the reaction energy. Since the intermediate state is now virtual, and the final state lattice does not have the reaction energy (it is in the fast alpha in this case), the requirements on the lattice are now much reduced. Two requirements are seemingly apparent however: (1) given the combinatorial number of available phonon states, the lattice states with frequency-shifted phonon modes had best have large coupling matrix elements and be well separated in energy to avoid destructive interference effects; and (2) given the fast (psec) decoherence time of the optical phonon modes, unless phonon gain is present on the gap jumping modes, the number of atoms that can take place in the final alpha decay process will be limited. Further study of this mechanism will determine the applicability of the theory to experiments reporting heat and tritium production.

6. Conclusions

We have reviewed key aspects of our theoretical approach to account for anomalies claimed in recent experiments with metal hydrides. We have focused on two new physical effects: [1] lattice energy transfer by frequency shifts of phonon modes, and [2] neutron hopping. Neither of these mechanisms has been proven experimentally, yet we contend that both effects are predicted from quantum mechanics.

Specific results that are new since ICCF4 include: [1] a proposal for a surface phonon laser driven by exothermic desorption; [2] that neutron hopping should lead to second order gamma emission as a thermally-induced bulk effect; [3] the observation that Bragg scattering of virtual neutrons by the internal unit cell structure is important (especially for nuclei with outer *s*-wave neutrons); [4] the conclusion that the primary donor or acceptor nuclei for heat or tritium production must involve outer *s*-wave neutron orbitals; [5] that neutron hopping should work much better with light nuclei; [6] that the energy exchange with the lattice during a neutron hop in the Mossbauer limit is nontrivial and must be included properly. The formula for second order gamma emission, as well as the theory outlined in section 5 constitute new theoretical results.

We conclude that there exist routes within conventional theory both for anomalous energy transfer and for a new class of reactions based on neutron hopping. The theory outlined in section 5 describes excess heat and tritium production mechanisms, perhaps similar to the experimental claims; further calculations and comparisons with experiment are required to determine whether it is correct in detail. The phonon laser route to energy transfer outlined in sections 2 and 3 can result in neutron, alpha, beta and gamma production, also perhaps relevant to the experimental claims. The neutron hopping/gamma emission process outlined in section 4 is a bulk effect, and may be more easily verifiable experimentally.

Quantitative predictions specific to the various metal hydrides for thermally-induced second order gamma emission will soon be available; these predictions can be tested experimentally, and can be used to prove or disprove a major part of the present theory. Heat production according to the theory of section 5 a neutron transfer from deuterium to silicon, and a low Z alpha decay; this can be proven or disproven through measurements of silicon isotopic ratios, and detection of the alpha decay products.

Acknowledgements

This work was supported in part by EPRI, by ENECO and by the MIT EE&CS Department.

References

1. As discussed, for example, in more than 20 experimental papers presented at this conference.

2. W. E. Lamb, "Capture of Neutrons by Atoms in a Crystal," *Phys. Rev.*, **55**, 190 (1939).

3. R. L. Mossbauer, "Kernresonanzfluoreszenz von Gammastrahlung in Ir^{191}, *Z. Physik.*, **151** 124 (1958).

4. F. Duschinsky, "Zur Deutung der Elektronenspektren mehratomiger Molekule," *Acta Physiochemica (URSS)*, **7**, 521 (1937).

5. P. L. Hagelstein, "A Possible Mossbauer Effect in Neutron Capture," *Hyperfine Interactions*, **92**, 1059 (1994).

6. P. G. Dawber and R. J. Elliott, "The Vibrations of an Atom of Different Mass in a Cubic Crystal," *Proc. Phys. Soc.*, **81**, 483 (1963).

7. P. L. Hagelstein, "Lattice-Induced Atomic and Nuclear Reactions," *Trans. Fusion Tech.*, **26**, 461 (1994).

8. P. Hu, "Stimulated Emission of 29-cm^{-1} Phonons in Ruby," *Phys. Rev. Lett.*, **44**, 417 (1980).

9. P. L. Hagelstein, "Proposed Novel Optical Phonon Laser Pumped by Exothermic Desorption," *Bull. APS*, **40**, 808, (1995).

10. J. Harris, "On Vibrationally-Assisted Dissociation of H_2 at Metal Surfaces," *Surface Science*, **221**, 335, (1989).

11. E. Goldys, Z. W. Gortel and H. J. Kreuzer, "Desorption Kinetics Mediated by Surface Phonon Modes," *Surface Science*, **116**, 33 (1982).

12. C. Bartolomeo, M. Fleischmann, G. Larramona, S. Pons, J. Roulette, H. Sugiura, "Alfred Coehn and After: the α, β, γ of the Palladium-Hydrogen System," *Trans. Fusion Tech.*, **26**, 23 (1994).

13. M. C. H. McKubre, S. Crouch-Baker, S.I. Smedley, and F. L. Tanzella, "The Measurement of Excess Power in the D/Pd System under nearly Isothermal Conditions," presented at ICCF5 (this conference); (1995).

14. P. L. Hagelstein and S. Kaushik, "Neutron Transfer Reactions," *Proc. ICCF4*, vol. 1, 10-1 (1994).

Fifth International Conference on Cold Fusion
9-13 April, 1995 - Monte Carlo, Monaco
ICCF5 ©1995

The Electron Catalyzed Fusion Model (ECFM) Reconsidered with Special Emphasis Upon the Production of Tritium and Neutrons

R.T. BUSH
Physics Department, California State Polytechnic University
3801 W. Temple Avenue, Pomona, CA 91768, USA

ENECO, Inc., Salt Lake City, Utah
Proteus Processes and Technology, Inc., Denver, Colorado

Abstract

The author's ECFM ("Electron Catalyzed Fusion Model") first presented at the ICCF-4 is re-examined with special reference to the production of tritium and neutrons. The model is of some interest in that it is the first model to fit excess power-vs-loading fraction data of McKubre et al. (SRI International/EPRI) and, independently, that of Kunimatsu et al. (IMRA). Of special note is that the peak of the theoretical curve of tritium production versus loading fraction, which is related to that for neutrons by a branching ratio scaling factor, is found to be at a fractional D/Pd loading of approximately 0.825, which is in good agreement with the empirical value of 0.83 announced at the ICCF-5 by Iwamura et al.(Mitsubishi) for both tritium and neutrons. It is of interest then that this theoretical ECFM tritium production curve arises essentially from purely statistical mechanical considerations involving the deuteron occupation of the three-dimensional interstitial lattice, rather than arising from the details of a specific nuclear mechanism. The model shows why tritium is ordinarily not observed when excess heat is being observed. For the neutron-to-triton branching ratio a theoretical lower limit $(r/R)^{12}$ results (r is the protonic charge radius and R is the deuteronic charge radius.) yielding a value of 2×10^{-9} in agreement with the empirical value of 2×10^{-9} for the neutron-to-triton branching ratio.

1. Introduction: Review of the ECFM

The author's ECFM[6]("Electron Catalyzed Fusion Model") employs collapsed electron orbits catalyzing genuine cold fusion reactions between deuterons within the Pd. The orbital collapse is hypothesized to be the result of the weakening of the zero point field induced by the cathodic environment, as explained in reference (6). It is based upon work of Boyer[1,2] and Puthoff[3] according to which, on the basis of "stochastic electrodynamics" (SED), the electronic ground state of an electron in an atom is a dynamic state in which the energy radiated away by the accelerating electron is compensated for by stimulated absorption from the zero point electromagnetic field. The ECFM has been highly successful at fitting data on excess power versus loading fraction, S, for the data of McKubre et al.[4], (SRI International/EPRI)]as shown in Fig. 1, and for the data of Kunimatsu et al.[5] (IMRA)].

Fig. 1

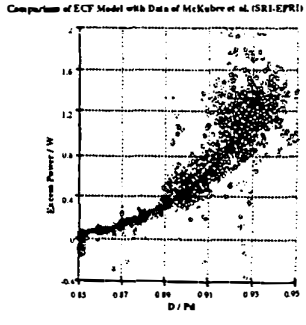

Fig. 2

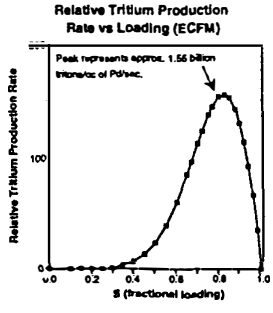

2. Statistical Mechanical Picture: Tritium /Neutron Production vs Heat Production

Much of the dependence in the ECFM of the formulas for power or particle production upon S (fractional loading) arise from strictly statistical features of the deuteron occupation of the interstitial lattice. To that extent the S-functionality is independent of a specific nuclear mechanism and therefore exploitable. Thus, the experimental corroboration of such nuclear mechanism nonspecific behavior would provide additional proof that the phenomenon is genuine.

Consider a 1-dimensional interstitial lattice configuration:

(Key: • represents an interstitial D, o represents an empty interstitial site.)

o • o • o • o • o • o • o .... etc. (1)

(1) represents a hypothetical one dimensional lattice configuration for which no cold fusion occurs due to a lack of nearest-neighbor D's.

Clearly, then, any expression for excess power will contain a factor that is a function of loading fraction, S, and arises strictly from the statistical mechanical picture accounting for the different possible interstitial lattice configurations that can contribute to cold fusion. Quoting from ref.(6) we make the distinction in the context of the model between the situation for heat production and that of triton production (At this stage we merely note that neutron production is linked to triton production in the ECFM via a branching ratio.): "We hypothesize that the cold fusion reaction $D + D \rightarrow He^4 + 24$ MeV occurs for lattice configurations with nearest-neighbors on either side to produce a "sideways charge polarization" of the D's with protons directly opposite neutrons so that collisions are highly "guided" (lattice assisted anti-Tokamak regime):

o • • • o + o • • • • o + o • • • • • o + ... etc. (2)

(S^3) (S^4) (S^5)

Thus, each D near the center of these configurations sees a nearest-neighbor D on either side. It is further hypothesized that tritium and neutrons result from the opposite situation; viz. the oscillatory collision of two nearest-neighbor D's isolated from their neighbors for which charge polarization favors neutronic components of the D's facing each other, thus heavily favoring tritium production via $D + D \rightarrow T + p + 4.03$ Mev as an Oppenheimer-Phillips type nuclear reaction :

o • • o + o • • o • • o + o • • o • • o • • o +. . . .etc. (3)

$(1-S)^2\ S^2$ $(1-S)^3\ S^4$ $(1-S)^4\ S^6$

For He^4 production the configurations in (2) yield a sum of probabilities (dependent upon fractional occupation, S):

$$p = S^3 + S^4 + S^5 + \ldots \text{ etc.} \quad (4)$$

that, when combined with other considerations, leads to an expression for excess power production given by

$$P_{exc} = (26.0) \cdot \{[(2-S)(1-S)]\ S^3\} \cdot (e^{\theta/T} - 1)^{-1} \cdot 10^{[23.6 - (24.774)\ S^{1/12}]} \quad (5)$$

3. Tritium Production on the Basis of the ECFM

From (3) the sum of the probabilities is

$$p = (1-S)S^2 + (1-S)^3 S^4 + (1-S)^4 S^6 + \ldots \text{ etc.} \quad (6)$$

Ref. (6) shows that this leads to the following

$$N(S,T) = (6.789 \times 10^{12}) \cdot S(1-S)[1 - (1-S)^2 S^3] \cdot (e^{\theta/T} - 1)^{-1} \cdot 10^{[23.6 - (24.774)\ S^{1/12}]} \quad (7)$$

(Tritons/cm^3/sec)

Fig. 2 shows a graph of triton production rate (tritons/cm^3 of Pd·sec) based upon (7) for a temperature of 60C showing a peak value of about 1.6 x 10^9 tritons/(cm3 of Pd.sec.). A computer study of the S-dependent part of (7) shows that the peak of the production curve is located at about S=0.825. This is of some interest since it was reported by Iwamura et al.[7] (Mitsubishi) at the ICCF-5 that tritium production was maximized at about S=0.83. (Presumably the uncertainty in their experimental result would put this in reasonable agreement. with S=0.825.) In a second ICCF-5 paper Iwamura et al.[8] reported that neutron emission was also maximized at about S=0.83. This feature is of special interest here since the ECFM simply relates neutron production to triton production via a branching ratio; i.e., the theoretical neutron production curve is simply a uniformly scaled down version for that of tritium.

In their abstract, Iwamura et al.[7] note that they had "previously reported that neutron emissions and tritium production were observed even with low deuterated palladium metals (D/Pd = 0.66). It is expected that the yield of nuclear products will increase using highly deuterated palladium metals (D/Pd = 0.8), since it has been widely recognized that anomalous nuclear effects are related to the D/Pd ratio." In this regard, note from Fig. 2 that the theoretical tritium (or neutron) production rate at S=0.66 would be about half of what it is at the peak of about S=0.83. Additionally we note from Fig. 2 that the curve plunges more steeply with S to the right of the peak than to the left. It is this latter feature that accounts for two general observations: (1)Tritium production is rarely observed simultaneously with excess heat production [Recall that excess power grows with increasing values of S above about 0.8.] (2)Neutron emission decreases as excess power increases. With regard to (2) note that Takahashi et al. [9] (Osaka University) in their ICCF-5 abstract state that "the neutron emission rate was about 2n/s at most and appeared to decrease when the excess heat rates increased, as was the case for our 1922 experiments." The present author[10] has reported observing a decrease in the emission rate of thermal neutrons as excess heat increases. Finally the neutron emission rate reported by Takahashi et al.[9] of about 2n/s is apparently in reasonable agreement with the prediction of the ECFM, which is now shown: Note from Fig 2 the value of 1.55 billion tritons/ cc of Pd.sec. Multiplying this by the theoretical branching ratio of 1.64 x 10^{-9} given in the next section yields a neutron production rate of about 2.54 neutrons/cc of Pd.sec. [In reference (6), Fig. 8 shows the theoretical tritium production vs S (ECF Model) for three different temperatures (100C, 600C, and 1200C) and emphasizes that the production peak does not shift with temperature, but remains fixed at about S=0.825.]

4. Neutron Production

Based upon the ECFM[6], neutron production is given by N in (7) multiplied by an appropriate branching ratio highly favoring (T,p)-production over (He^3,n)-production. The author[11] has derived an extreme limiting branching ratio based upon charge polarization considerations, which reduces to a good approximation to

$$BR = (r/R)^{12} \tag{8}$$

where r is the protonic charge radius, and R is the deuteronic charge radius.

Substituting $r = 0.8\text{x}10^{-13}$ cm, and $R = 4.31\text{x}10^{-13}$ cm, from DeBenedetti[12], yields

$$BR = 2 \text{ x } 10^{-9}, \tag{9}$$

which compares well with the best experimental value[13] for the smallest branching ratio given by about

$$(BR)_{exp} = 2 \text{ x } 10^{-9}. \tag{10}$$

Acknowledgments

ENECO, Inc. (Salt Lake City, UT), and especially **Fred Jaeger** (CEO) is greatly appreciated for funding my participation in the Monaco Conference(ICCF-5), and for its encouragement and support of the Cal Poly cold fusion program. **Proteus Processes and Technology, Inc.** (Denver, CO) are thanked for their encouragement and support of my research In particular, **Joe Ignat** (CEO) and **Ron Flores** are especially thanked in this regard. **Tim Shoemaker (Head)** and **Jeanne O'Neill** of the Cal Poly (Pomona) College of Science Instructional Support Center are appreciated for their help with the preparation of the poster and this paper. **James Djunaedy**, Cal Poly undergraduate (electrical engineering major), is thanked for some number crunching.

References:

1. Boyer, Phys. Rev. D., **11**, 790 (1975).
2. Boyer, Phys. Rev. D, **11**, 809 (1975).
3. Puthoff, "Ground State of Hydrogen as a Zero-Point-Fluctuation Determined State", Phys. Rev. D, **35**, 3266 (1987).
4. McKubre, Crouch-Baker, Riley, Smedley, and Tanzella, "Excess Power Observations in Electrochemical Studies of the D/Pd System; the Influence of Loading, Proc. ICCF-3, Universal Academy Press, Inc. (Tokyo), 5 (1993).
5.Kunimatsu, Hasegawa, Kubota, Imai, Ishikawa, . Akita, and Tsuchida (IMRA), "Deuterium Loading Ratio and Excess Heat Generation during Electrolysis of Heavy Water by a Palladium Cathode in a Closed Cell Using a Partially Immersed Fuel Cell Anode", Proc.3-ICCF, 31 (1993).
6. Bush, "A Unifying Model for Cold Fusion",Transactions of Fusion Technol.,December 1994, **26**, No. 4T, p.431.
7.Itoh, Iwamura, Gotoh, and Toyoda, "Observation of Nuclear Products Under Vacuum Condition from Deuterated Palladium with High Loading Ratio, Proc. ICCF-5, Monte Carlo, April 9-13, 1995.
8. Iwamura, Gotoh, Itoh, and Toyoda, "Characteristic X-ray and Neutron Emissions from Electrochemically Deuterated Palladium", Proc. ICCF-5, Monte Carlo, April 9-13, 1995.
9. Takahashi, Miyamaru, Inokuchi, Chimi, Ikegawa, Kaji, Nitta, Kobayashi, and Taniguchi, "Experimental Correlation Between Excess Heat and Nuclear Products," Proc. ICCF-5, Monte Carlo, April 9-13, 1995.
10.Bush and Eagleton, "Neutron Emission from Electrolytic Cells: Correlation With Current Density," Poster at ICCF-2, Como, Italy, June 31-July 4, 1991.
11.Bush, " 'Cold Fusion': The Transmission Resonance Model Fits Data on Excess Heat, Predicts Optimal Trigger Points, and Suggests Nuclear Reactrion Scenarios," Fusion Technol., **19**, 313 (1991).
12.DeBenedetti, Nuclear Interactions, John Wiley & Sons, New York (1966).
13.Storms, Los Alamos National Laboratory, Personal communication, June, 1990.

Fifth International Conference on Cold Fusion
9-13 April, 1995 - Monte Carlo, Monaco
ICCF5 ©1995

A Model for the Impurity Promotion and Inhibition of the Excess Heat Effects of Cold Fusion

R. T. BUSH
Physics Department , California State Polytechnic University, 3801 West Temple Avenue, Pomona, CA 91768, USA
ENECO, Inc., Salt Lake City, Utah
Proteus Processes and Technology, Inc., Denver, Colorado

Abstract

A theoretical[2] model describes impurity promotion and inhibition of the heavy water[1] and light water[3,4] excess heat effects of cold fusion based upon the influence on the magnetic properties of Pd and Ni, respectively, of alloying with different metals. For Ni (light water case), promoters, in increasing order of efficiency, are predicted to be Cu, Zn, Al, and Sn. Inhibitors, in increasing order of efficiency, are predicted to be Co, Fe, and Mn. Ag, Au, and Cu are indicated as promoters in the case of Pd (heavy water case). Empirical evidence impacting the model will be presented in another paper (ref. 5) in these Proceedings.

1. Introduction: Basis for the Promotion-Inhibitor Model for the Light Water Excess Heat Effect

Let us hypothesize that cold nuclear reactions have cross-sections highly sensitive to the relative spin orientation of the two reacting particles. In particular, if the product particle has a smaller spin than either of the reacting particles, an anti-parallel configuration of the spins of the approaching particles is hypothesized to be relatively favorable for the reaction as compared to a parallel spin configuration. Thus, an applied magnetic field and magnetization of the Ni cathode material, both of which tend to align the reactant particle spins, tends to diminish the light water excess heat effect. [An important exception to this would be in those cases where the excess heat effect is enhanced via magnetic resonance. Thus, if the excess heat effect is stimulated by employing microwave radiation in the magnetic resonance method to produce spin flips (e.g. Letts[6] and Piantelli & Focardi[7] with Piantelli's experiment as a variation of the Letts experiment), then the presence of a magnetic field with concomitant magnetization of the Ni is necessary.)]

We additionally hypothesize that promotion or inhibition of the magnetic susceptibility of the Ni can be achieved by adding impurities suggested by band theoretic considerations for magnetism.

2. Promotion of the Excess Heat Effect:

Band theory shows that the ferromagnetism of Ni in the solid state is associated with holes, i.e. vacancies, in the electronic d band, with the number of holes in the d band of Ni producing a saturation moment per atom of 0.6 Bohr magnetons per atom. (In this, and what follows, the treatment of the magnetic susceptibility of the transition metals such as Ni, Fe, Pt, and Pd, follows that presented by Mott and Jones[8,9,10] in their classic reference, *The Theory of the Properties of Metals and Alloys*.)

Thus, suppose that Cu is alloyed with Ni, where Cu has one more electron per atom than Ni; Mott and Jones[8] point out that Cu-Ni alloys possess "a face-centered cubic lattice with no superstructure for all compositions," so that "if a nickel atom is replaced by a copper atom in an alloy, we may suppose that the lattice is unaltered except that an extra electron is added." Since, band theoretic considerations show that the d band density of states is much greater than the s band density, this extra electron annihilates one of the holes. Thus, for the case of a 60% alloy, all the holes are filled and Ni's ferromagnetism should disappear. So, for an alloy fraction f of Cu with

Ni less than 0.60, the number of holes, N_h in the d shell for the solid is given by

$$N_h(f) = 0.6\text{-}f \qquad (1)$$

The figure, which is based upon one in Mott and Jones[9], portrays this situation with the atomic moment in Bohr magnetons per atom shown as 0.6 for a 0% alloy falling to 0.0 for a 60% alloy. [The plot is equivalent to plotting $N_h(f)$ in (1) versus f.] (Of course, it is not clear that 60% would be the optimal percentage "impurity" to use because of the fact that Ni is known to be a better absorber of hydrogen than Cu.)

Atomic Moment vs. Percent Impurity

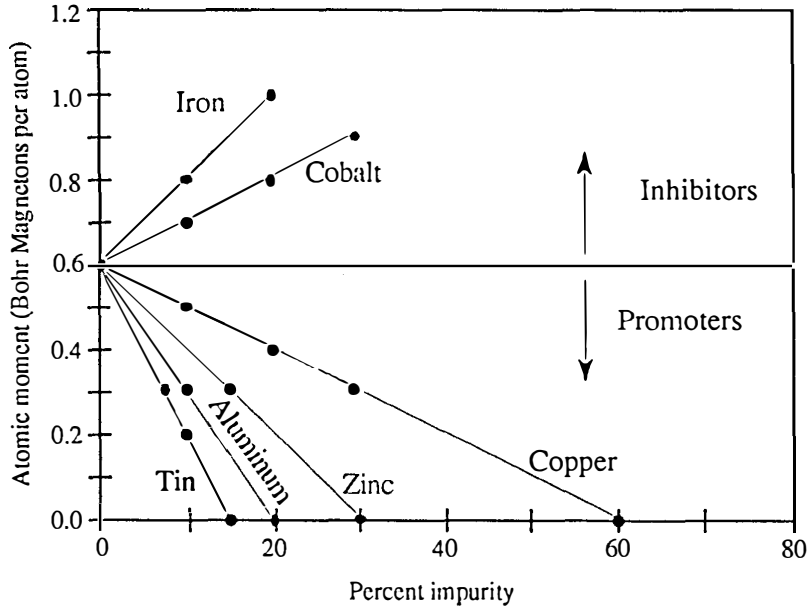

Cu has an excess of electrons per atom of +1 over Ni. For the general case of the number of electrons per atom outside that of an inert gas given by n_e, the formula in (1) is generalized to the following:

$$N_h(fn_e) = 0.6 - (n_e - 10)\, f, \qquad (2)$$

where $n_e = 10$ is the number of electrons for Ni outside the closed Ar shell. Thus, for n_e greater than 10, we have the impurity promoters of excess heat as portrayed in the figure and in order of increasing effectiveness as Cu ($n_e = 11$), Zn (12), Al (13), and Sn (14). Of these, Sn, with the largest n_e value should be the most effective per percent of alloy with Ni. Thus, it would be interesting to try a 15% alloy of Sn with 85% Ni corresponding to f = 0.15 and the theoretical extinction percentage of 15% for the curve for Sn in the figure.

3. Inhibition of the Excess Heat Effect:

If the metal to be alloyed with Ni has fewer than 10 electrons (Ni case) outside an inert gas shell, the value of $(10 - n_e)$ in (2) will be negative and the magnetic susceptibility enhanced. Examples are Co ($n_e = 9$), Fe(8), and Mn(7). Curves for Co and Fe are shown in the figure, and clearly these are predicted by the model to be impurity inhibitors of the light water excess heat effect in the case of Ni.

4. Application to the Case of Palladium as a Cathode Material:

According to Mott and Jones[10], the strongest paramagnetism of Pd is quenched for about a 55% alloy of Au in terms of numbers of atoms, which gives evidence that there are about 0.55 holes per atom in the 4d band of Pd producing the paramagnetism in comparison to the 0.6 holes in the 3d band of Ni. Au, Ag, and Cu, all of which have one more electron outside of a closed inert gas shell (the Xn shell for Au, The Kr shell for Ag, and the Ar shell for Cu) than does Pd, are, thus, predicted on the basis of the model to be approximately equally effective impurity promoters of cold fusion. (For this same reason, Au and Ag might function about as effectively as Cu as impurity promoters in the case of Ni, assuming that the lattice considerations introduce no major complexities in alloying with Ni.) In support of this, the curves of magnetic susceptibility versus % alloy for all three metals with Pd have been found to be very similar. (However, Ag would have an additional advantage since, as is well-known, Ag functions also to prevent "microcracking" of Pd under the influence of deuterium. The latter process is known to be able to significantly reduce the stoichiometry of the deuterium by leaking it to the surface.)

Additional evidence that there are about 0.55 holes per Pd atom in the 4d shell, and that these produce the strong paramagnetism of Pd, is the fact that the magnetic susceptibility of Pd drops to zero for a deuterium, or hydrogen, stoichiometry of about 0.55. Thus, since hydrogen is absorbed much more strongly by Pd than it is by Ni, it appears that while the impurity considerations of this model (hydrogen not taken as an impurity) may be significant for Pd, they are probably much more important for the light water case of Ni. (Absorbed hydrogen would, of course, also reduce the ferromagnetism of Ni since presumably the hydrogen becomes ionized when it enters the lattice with the one electron per hydrogen atom free to fill a hole in the 3d band associated with the Ni lattice.)

Conclusion

Recent experimental findings at Cal Poly (Pomona)provide strong preliminary support for the author's model. In this regard, please see the Proceedings contribution of reference 5.

Finally, this phenomenon of excess heat effect promotion and inhibition elucidated by band state theoretic considerations sheds an additional light on the entire area of cold fusion research.. It provides dramatic additional evidence for the excess heat effects first elucidated by Fleischmann and Pons[1] , by Mills[3], and by the author[4].

Acknowledgments

Hal Fox, Director of the Fusion Information Center , (Salt lake City, Utah) is thanked for soliciting the original form of my model for the Minsk Conference Proceedings. ENECO, Inc. (Salt Lake City, Utah),and especially Fred Jaeger (CEO), is greatly appreciated for funding my participation in the Monaco Conference (ICCF-5), and for generally encouraging and supporting the Cal Poly cold fusion research program. Proteus Processes and` Technology, Inc. is thanked for its encouragement and support of my work. In particular, Joe Ignat (CEO) and Ron Flores, are especially thanked in this regard. Tim Shoemaker (Head) and Jeanne O'Neill of the Cal Poly (Pomona) College of Science Instructional Support Center are appreciated for help with the preparation of the poster and this paper.

References

1. Fleischmann and Pons,"Electrochemically Induced Nuclear Fusion of Deuterium", *J. Electroanal. Chem.*, **261**, 301 (1989).
2. Bush, "Impurity Promotion and Inhibition of the Excess Heat Effects of Cold Fusion," accepted for publication in the Minsk Conference Proceedings (1994).
3. Mills and Kneizys, "Excess Heat Production by the Electrolysis of an Aqueous Potassium Carbonate Electrolyte and the Implications for Cold Fusion," *Fusion Technol.*, **20**, 65 (1991).
4. Bush, "A Light Water Excess Heat Reaction Suggests that 'Cold Fusion' May Be 'Alkali-Hydrogen Fusion'", *Fusion Technol.*, **22**, 301 (1992).
5. Bush and Eagleton, "Experimental Evidence Supporting a Model for Impurity Promotion of a Light Water Excess Heat Effect," Proc. ICCF-5, Monte Carlo, Monaco, April 9-13, 1995.
6. Bockris, Sundaresan, Lettts, and Minevski, "Triggering of Heat and Sub-Surface Changes in Pd-D Systems," Proc. ICCF-4, Maui,December 6-9, 1993, Vol. 2, p.1.
7. Focardi, Habel, and Piantelli, "Anomalous Heat Production in Ni-H Systems," *Il Nuovo Cimento*, **107**, January, 1994.
8. Mott and Jones,*The Theory of the Properties of Metals and Alloys*, p. 196, Dover Publications, Inc., New York, N.Y.(1958).
9. Ibid., 197.
10. Ibid., 199.

Fifth International Conference on Cold Fusion
9-13 April, 1995 - Monte Carlo, Monaco
ICCF5 ©1995

NUCLEAR PROCESSES in TRAPPED NEUTRON CATALYZED MODEL for COLD FUSION

KOZIMA Hideo and WATANABE Seiji
Department of Physics, Faculty of Science, Shizuoka University
836 Oya, Shizuoka 422, JAPAN

Abstract

Results are given of detailed calculations of 1) probability of channeling for particles generated in $n-d$ and $n-p$ fusion reactions, 2) fusion probability of a triton generated in $n-d$ fusion with a deuteron and 3) fusion probability of a deuteron accelerated by $n-d$ elastic collision with another deuteron. A lot of neutrons are generated in a successive reactions of $d-d$ fusion reactions triggered by a trapped thermal neutron enough to explain experimentally observed anomalous excess heat, neutron bursts and tritium anomaly in optimum situations. The results confirms the preliminary estimations used in the previous works.

1. Introduction

There has been observed Cold Fusion Phenomenon in various materials. Those materials are divided into two categories; (1) Materials containing mainly a lot of deuterium (let us call them "deuterides" hereafter) and (2) Materials containing mainly a lot of hydrogen ("hydrides").

We had proposed a model (Trapped Neutron Catalyzed Model for Cold Fusion, TNCF model)[1~4] to explain cold fusion phenomenon and the model could give a consistent qualitative understanding of experimental facts in the phenomenon even though not quantitative.

The reactions having connection with the model are written down as follows:

$$n + p = d\ (1.33\ \text{keV}) + \gamma\ (2.22\ \text{MeV}) \quad (1)$$
$$n + d = t\ (6.98\ \text{keV}) + \gamma\ (6.25\ \text{MeV}) \quad (2)$$
$$p + d = {}^3\text{He}\ (5.35\ \text{keV}) + \gamma\ (5.49\ \text{MeV}) \quad (3)$$
$$d + d = {}^3\text{He}\ (0.82\ \text{MeV}) + n\ (2.45\ \text{MeV}) \quad (4)$$
$$= t\ (1.01\ \text{MeV}) + p\ (3.02\ \text{MeV}) \quad (5)$$
$$= {}^4\text{He}\ (76.0\ \text{keV}) + \gamma\ (23.8\ \text{MeV}) \quad (6)$$
$$t + d = {}^4\text{He}\ (3.5\ \text{MeV}) + n\ (14.1\ \text{MeV}) \quad (7)$$
$$d + {}^3\text{He} = p\ (14.68\ \text{MeV}) + \alpha\ (3.67\ \text{MeV}) \quad (8)$$

Here, it is useful to give attention to a fact about the difference of fusion cross sections of Res. (1) and (2). The cross sections of these reactions depend on the energy E of the thermal neutron and increase as $\mathrm{E}^{-1/2}$ with decrease of the energy. This fact means low temperature is advantageous to realize Cold Fusion for the same

density of trapped thermal neutron. Fusion cross section of Re. (1) for a neutron with the energy 25 meV is about 3×10^{-1} barns and that of Re. (2) for the same energy is about 6×10^{-3} barns[5]. So, a thermal neutron is easier to fuse with a proton than with a deuteron by a factor 50.

Some characteristics of the Cold Fusion phenomenon in deuterides and hydrides are pointed out as follows.

(1) Cold Fusion in deuterides.

Once Re. (2) occurs in deuterides between a trapped thermal neutron and a deuteron in the sample, the generated triton and photon will give several effects on the sample. The attenuation lengths ell_{att} of 6.25 MeV and 2.22 MeV photons in relevant metals are given as follows: 8.0 (Ti), 3.4 (Ni) and 2.2 (Pd).

If the sample is large enough to attenuate the photon (2 cm for Pd metal), the sample will be heated drastically as observed by rare experiments[6]. In samples with smaller linear dimensions, the photon will come out from the sample[7] and excess heat will be resulted from other particles generated in reactions induced by the triton. In Ti/D system, however, the attenuation length is too long ($\sim$8 cm) to heat usually used samples drastically and no remarkable excess heat has been observed hitherto.

The triton generated in Re. (2) will be observed in the remains as tritium[8,9]. In an optimum situation, the triton will make fusion reaction with a deuteron in the sample to generate ^{4}He and a high energy neutron with energy 14.1 MeV according to Re. (7). ^{4}He generated in this reaction will be observed as helium atom[10,11]or as alpha particle.

The high energy neutron will have two effects; the neutron itself will be observed coming out from the sample[7,12,13] or the neutron will make predominantly elastic collisions with deuterons in the sample. A deuteron accelerated by an elastic collision with the neutron will obtain enough energy to make a fusion reaction with another deuteron in the sample by Res. (4) or (5) (Detailed calculation will be given later).

When the neutron generated in Re. (7) loses almost all its energy by the elastic collisions with deuterons, the neutron contributes to Re. (2) together with the neutron generated in Re. (4). In an optimum situation where Res. (2), (7) and (4) occur successively (a chain reaction), there will be generated a lot of neutrons[14] and a neutron burst will be observed[7~9,15] (Detailed calculation will be given later).

(2) Cold Fusion in Hydrides[4].

Once Re. (1) occurs in hydrides, a deuteron and a photon are generated. The generated photon can heat the sample effectively when it has enough dimension to attenuate the photon[16,17]. The deuteron also contributes to heat the sample losing its energy by elastic collisions with charged particles in the sample. The deuteron can make fusion reaction Re. (3) to generates ^{3}He which will contribute to heat the sample and also be measured in hydrides.

The larger cross section of Re. (1) compared with that of Re. (2) is favorable for

stationary heat generation for hydrides. It is possible to say that we will obtain excess heat generation linearly depending on the number of trapped thermal neutrons in a sample. This prediction should be checked experimentally.

On the other hand, the successive reactions feasible in deuterides are absent in hydrides. It is possible to conclude that there are neither neutron bursts nor explosive excess heat generation in hydrides by TNCF mechanism.

(3) Direct evidence for the effect of thermal neutrons in Cold Fusion

Recent private communication[18] reported interesting observation in KD_2PO_4 single crystal. When background neutrons were increased artificially to 100 times the natural one, the enhancement factor (No. of neutrons in the transition region/No. in others) increased from 4 to 25. This result shows that the effect of thermal neutron is nonlinear to its density suggesting a productive effect (chain reactions).

Similar effect of thermal neutrons have been investigated several times until now. The first one was done in 1989[19]. Others were done after then with much care[13,20].

Inexistent results of the Cold Fusion phenomenon[21] were also obtained including Kamiokande experiment in 1992 (in Japan) showing that there are no Cold Fusion without background neutrons.

These data clearly support TNCF model directly.

(4) Irreproducibility

Irreproducibility of Cold Fusion phenomenon (especially gigantic excess heat, neutron burst and tritium anomaly), the remarkable controversial problem throwing a big question to all scientists, had been explained in TNCF model as a result of stochastic processes working in samples to realize the optimum condition to make feasible the Cold Fusion (trapping of thermal neutron, realization of chain reactions, etc.).

The direct supports from experiments with controlled thermal neutron[13,18,20] and the self-consistent interpretation of the whole experimental results except absence of high energy photons show that something true is in TNCF model. The question about the absence of the high energy (6.25 and 2.22 MeV) photons might be related with a fact that the absorption coefficient of a photon in many materials has a minimum at a range from 1 to 10 MeV of the photon energy. A critical review of experimental data given by E. Storms[22] is useful to overlook whole range of the Cold Fusion phenomenon.

We will give some detailed calculations about nuclear processes in TNCF model in this paper.

2. Neutron Mössbauer Effect and Neutron Band

Among the mechanisms responsible neutron trapping, the neutron Moessbauer effect is the one concerned with individual nucleus. As explained in a previous paper[3], a nucleus with a mass number A and even atomic number Z around 26 in a crystal lattice is responsible neutron Mössbauer effect, which works as a mechanism

to confine neutrons effectively in the lattice (M-mechanism). The trapped neutron by this mechanism is free from its short life time about 900 seconds of the isolated neutron.

The momentum change of the nucleus in the emission and absorption of a neutron is pertinent with the lattice, while the difference between energy levels in the nucleus with $(A + 1)$ and Z is pertinent with energy levels in the nucleus.

A neutron with an energy 5.33 eV has the same momentum as that of a photon with energy 100 keV which corresponds to photons usually used in the Mössbauer resonance technique. Thus, ordinary crystal can give rise to the neutron Mössbauer effect for neutrons with energies less than 100 keV including the thermal energy (0.025 eV). The neutron Mössbauer effect is legitimated by analogy with the photon Mössbauer effect.

This mechanism of neutron trapping depends on the dynamic character of the local lattice around the pertaining nucleus. In an inhomogeneous material where the Cold Fusion occurs, the dynamical characteristics of the lattice varies place to place. To keep the M-mechanism effective, the size of the locally homogeneous region should have a minimum value. On the other hand, to have a long trapping time T of the neutron in the material, it is desirable to make the total volume of the locally homogeneous region as large as possible.

A compound nucleus (A+1,Z) has another effect on the neutron trapping – a neutron band in the crystal. A Bloch state composed of individual nuclear state (real and virtual) just like the exciton band in oxides or 4f band in rare earth metals will be formed to trap neutrons effectively with an elongated life time.

3. Channeling

There is a propagation of a neutral or a charged particle through crystal without energy loss, i.e. the channeling[23,24]. The channeling occurs when the de Broglie wave length of the particle is short compared with the lattice constant of the crystal and the propagation vector makes a small angle with a crystal axis or a crystal plane[24]. In our case, it occurs when the propagation is around a specific crystal direction (OHS line) through interstitial sites (a channeling axis).

Once a thermal neutron makes a fusion reaction with a deuteron or a proton in an material occluding it, particles generated in the reaction have appropriate energies to channel through the material where the crystal lattice is ideal. High energy triton or deuteron generated in Re. (2) or (1) makes collision with deuteron or proton effectively to fuse with it, shown as follows.

A charged particle can propagate through a channel with a radius r_0 when the angle ψ between its momentum and a channel axis is smaller than a critical angle ψ_{cr}. The ψ_{cr} for a particle with an energy E and a charge Z_1e through a lattice composed of atoms with nuclear charge Z_2e is given by following formulae:

$$\psi_{cr,1} = \sqrt{\frac{2Z_1Z_2e^2}{Ed}}, \quad (E > E'), \tag{9}$$

$$\psi_{cr,2} = \sqrt{\frac{Ca_{TF}\psi_{CR,1}}{\sqrt{2}d}}, \quad (E < E'), \tag{10}$$

where $E' = 2Z_1Z_2e^2d/a_{TF}^2$, $C \simeq \sqrt{3}$ and the Thomas-Fermi atomic radius a_{TF} for this case is given by

$$a_{TF} = 0.8853a_0(Z_1^{1/2} + Z_2^{1/2})^{-2/3}.$$

The parameter d in the above formulae is a distance of matrix atoms along the channel axis.

For the triton with an energy of 6.98 keV, $E/E' < 1$ and $\psi_{cr,2} = 0.105$ rad. A triton which is generated by Re. (2) can propagate along one of twelve main channels through the site where was a deuteron with a probability of 3.3 %. On the other hand, the deuteron which is generated by Re. (1) can propagate along one of twelve main channels with a probability of 7.6 % according to similar estimations. Those probabilities increase with the decrease of particle energy.

Now, we proceed to individual reactions between particles.

4. Tritium Production Rate in Deuterides

As is explained in Section 1 and is well known in the neutron physics[1,5], the fusion cross section of a neutron with a deuteron increases rapidly with the decrease of the impinging neutron energy ε, while the elastic scattering cross section remains constant about 3.2 barns under $\varepsilon = 1$ MeV. The ratio of two cross sections is about 10^{-6} at $\varepsilon = 10^6$ eV and is 10^{-3} at $\varepsilon = 10^{-3}$ eV.

To interpret rare experimental results where observed tritium anomaly, we must be aware of a fact that detections of neutron and tritium are usually not simultaneous. So, we may assume in this case that one or other trapping mechanisms are very effective and a lot of neutrons are trapped in the sample. Then the fusion reaction Re. (2) will occur to produce a lot of triton which will make an effective collision to accelerate deuterons when propagating along an OHS line or to lose energy by the Coulomb interaction with charged particles in the lattice and to remain in the sample.

By the head-on elastic collision of a triton with a static deuteron, the triton lose its 12/25 of the initial energy. The accelerated deuteron makes a collision with another deuteron. If a deuteron with an energy of $(12/25) \times 6.98 = 3.35$ keV propagate along an OHS line in a cylinder with a cross section πr_0^2, it induces about two $d-d$ fusions in 10^{-4} second with occluded deuterons generating one triton by the reaction Re. (5) in an infinite sample[2] in an optimum situation, where r_0 is the radius of the channel. At the same time, the deuteron generates one neutron by Re. (4). Considering the average fusion length of about 8×10^3 cm, we obtain 10^4 neutrons per second in a sample with a size $1 \times 1 \times 1$ cm^3 with 8000 reactions Re. (4) per second.

This mechanism results in two effects: 1) When the trapping mechanisms work effectively for higher energy neutrons in a sample with enough inhomogeneity, the

neutrons lose energy effectively and are trapped as a warm or cold neutrons to fuse with deuterons according to Re. (2) and many tritons are generated. 2) When the trapping mechanisms for higher energy neutrons don't work well, the 2.45 MeV neutrons propagating along an OHS line to make sequential neutron-breeding-process generating many neutrons to be observed (as discussed in the next section).

In some experiments[8,25,26] the first mechanism would be predominant and the tritium is generated by a chain reaction Res. (4) and (5) interposed by the $t-d$, $n-d$ and $d-d$ elastic collisions. In the experiment[25], a part of neutron bursts preceding the tritium emission would be stored effectively as trapped neutrons in the sample. After a neutron burst, the sample became the second type by effects of the fusion products including heat and the trapped neutron could worked to initiate the chain reaction generating a lot of tritium to give $t/n \sim 10^6$. In the other experiment[26], there was no neutron burst above the background and the trapped neutrons would be the initiator of the chain reaction to generate a lot of tritons of the order of $t/n \sim 10^4$.

5. Neutron Breeding Rate

The neutron breeding rate is calculated starting from one neutron with an energy 2.45 MeV (or 14.1 MeV) emitted along a OHS line (channeling direction). The neutron makes collisions with deuterons on the line and the recoiled deuterons generate five (or six) neutrons by Re. (4) in 10^{-6} seconds in an infinite sample. In this calculation, simplifications were made assuming 1) the particles always propagate on an OHS line and 2) an amount of energy transferred by elastic collisions is that of the average one with rigid spheres collision model.

It is also assumed arbitrarily that one out of five (or six) neutrons with energy 2.45 MeV generated in Re. (4) is possible to start another propagation along an OHS line to produce five (or six) neutrons again to continue the reaction forever. In this optimum situation, one $n-d$ reaction generates neutrons about 10^6 per second and the neutrons are emitted from the sample if the trapping of high energy neutrons is not effective. This is a story only occurs in an optimum situation achieved very rarely in samples and corresponds to very rare, irreproducible events giving experimental results with neutron bursts[8,15].

6. Conclusion

It is difficult to prove the occurence of the Cold Fusion phenomenon in materials from the first principles because the physics in it include statistical property. The estimations given above illustrate a possibility of the occurence of the Cold Fusion phenomenon in the presence of abundant thermal neutrons in materials pertinent with the phenomenon and possibilities of the existence of many neutrons in appropriate materials had been shown in the preceding papers[1~4]. The photon with energy of 6.25 MeV (or 2.22 MeV) has been measured rarely[7] and should be a target of future enthusiastic experiments.

References

1. H. Kozima, " Trapped Neutron Catalyzed Fusion of Deuterons and Protons in Inhomogeneous Solids", *Proceedings of ICCF 4*, **4**, p. 5-1, Electric Power Research Institute, California, USA, 1994; and *Trans. Fusion Tech.* **26**, 508 (1994). And also "Trapped Neutron Catalyzed Model for Cold Fusion", *Cold Fusion Source Book*, EPRI, Salt Lake City, Utah, USA (to be published).

2. H. Kozima and S. Watanabe, "t-d and d-d Collision Probability in the Trapped Neutron Catalyzed Model of the Cold Fusion", *Proceedings of International Symposium "Cold Fusion and Advanced Energy Sources"* (May 24-26, 1994, Minsk, BELARUS.)(in Russian) p. 299.

3. H. Kozima, "Neutron Mössbauer Effect and the Cold Fusion in Inhomogeneous Materials", *Nuovo Cimento* **27A**, 1781 (1994).

4. H. Kozima, "On the Cold Fusion in Ni-H System", *Cold Fusion* **8**, 5 (1995).

5. T. Nakagawa, T. Asami and T. Yoshida,"Curves and Tables of Neutron Cross Sections", *JAERI-M 90-099, NEANDC(J)-153/U INOC(JPN)-140/L* (July, 1990).

6. M. Fleischmann and S. Pons, "Electrochemically induced Nuclear Fusion of Deuterium", *J. Electroanal. Chem.* **261**, 301 (1989).

7. H. Long, S. Sun, H. Liu, R. Xie, X. Zhang and W. Zhang, "Anomalous Effects in Deuterium/Metal Systems", *Frontiers of Cold Fusion* p.447, ed. H.Ikegami, Universal Academy Press (Tokyo), 1993. H. Long, R. Xie, S, Sun, H. Liu, J. Gan, B. Chen, X. Zhang and W. Zhang, "The Anomalous Nuclear Effects Inducing by the Dynamic Low Pressure Gas Discharge in a Deuterium/Palladium system", *ibid.* 455 (1993).

8. R.K. Rout, M. Srinivasan, S. Shyam and V. Chitra, "Detection of High Tritium Activity on the Central Titanium Electrode", *Fusion Tech.* **19**, 391 (1991).

9. T. N. Claytor, D. G. Tuggle and S. F. Taylor, "Evolution of Tritium from Deuterided Palladium Subject to High Electrical Currents", *Frontiers of Cold Fusion* p.217, ed. H.Ikegami, Universal Academy Press (Tokyo), 1993.; S. F. Taylor, T. N. Claytor, D. G. Tuggle and S. E. Jones, "Search for Neutrons from Deuterated Palladium Subject to High Electric Currents", *Proc. Fourth Intern. Conf. on Cold Fusion*, Lahaina, Maui, Dec. 6 - 9, 1993, Vol. **3**, p.17, EPRI TR-104188..

10. E. Yamaguchi and T. Nishioka, "Direct Evidence for Nuclear Fusion Reactions in Deuterated Palladium", *Frontiers of Cold Fusion* p.179, ed. H.Ikegami, Universal Academy Press (Tokyo), 1993.

11. M. H. Miles and B. F. Bush, "Heat and Helium Measurements in Deuterated Palladium", *Trans. Fusion Tech.* **26**, 156 (1994).

12. A. De Ninno, A. Frattolillo, G. Lollobattista, G. Martinio, M. Martone, M. Mori, S. Podda and F. Scaramuzzi, "Evidence of Emission of Neutrons from a Titanium-Deuterium System", *Europhys. Lett.* **9**, 221 (1989).

13. B. Stella, M. Corradi, F. Ferrarotto, V. Milone, F. Celani and A. Spallone, "Evidence for Stimulated Emission of Neutrons in Deuterated Palladium", *Frontiers of Cold Fusion* p.437, ed. H.Ikegami, Universal Academy Press (Tokyo), 1993.

14. S.E. Jones, E.P. Palmer, J.B. Czirr, D.L. Decker, G.L. Jensen, J.M. Thorne, and S.E. Tayler, "Observation of Cold Nuclear Fusion in Condensed Matter", *Nature* **338**, 737 (1989).
15. E.Yamaguchi and T.Nishioka, "Cold Nuclear Fusion induced by Controlled Out-Diffusion of Deuterons in Palladium", *Jpn. J. Appl. Phys.* **29**, L666 (1992).
16. S. Focardi, R. Habel and F. Piontelli, "Anomalous Heat Production in Ni-H System", *Nuovo Cimento* **107A**, 163 (1994).
17. U.S. Pat. No. 5,318,675 "Method for Electrolysis of Water to form Metal Hydride and No. 5,372,688 "System for Electrolysis of Liquid Electrolyte"; and Report by V. Lapuszynski, "The Patterson Power Cell^{TM}", *Cold Fusion*, **7**,1 (1995).
18. A. G. Lipson and D. M. Sokov "Amplification of the Neutron Flux Transmitted through KD_2PO_4 Single Crystal at the Ferroelectric Phase Transition State", *ICCF 5 Book of Abstract* (April 9 - 13, Monte-Carlo, Monaco), Page 320 (1995); *JETP* (in Russian), **76**, 1070 (1993) and *J. Tech. Phys. Lett.* (in Russian), **20**, 46 (1994).
19. G. Shani, C. Cohen, A. Grayevsky and S. Brokman, "Evidence for a Background Neutron enhanced Fusion in Deuterium absorbed Palladium", *Solid State Comm.* **72**, 53 (1989).
20. F. Celani, A. Spallone, L. Liberatori, F. Croce, L. Storelli, S. Fortunati, M. Tului and N. Sparvieri, "Search for Enhancement of Neutron Emission from Neutron-Irradiated, Deuterided, High-Temperature Superconductors in a Very Low Background Environment", *Fusion Tech.* **22**, 181 (1992).
21. S. E. Jones, D. E. Jones, D. S. Shelton and S. F. Taylor, "Search for Neutron, Gamma and X-Ray Emission from Pd/LiOD Electrolytic Cells: A Null Results", *Trans. Fusion Tech.* **26**, 143 (1994).
22. E. Storms, "A Critical Review of the "Cold Fusion" Effect", *Fusion Techn.* (to be published).
23. V. I. Visotskii and R. N. Kuz'min, "Kanalirobanie Neitral'nib Tyastiz i Kbantob b Kristallaxa", *Uspehi Phizityeskix Nauk* (in Russian) **162** (1992) 1.
24. D. S. Gemmell, "Channeling and related effects in the motion of charged particles through crystals", *Rev. Mod. Phys.* **46**, 129 (1974).
25. P.K. Iyengar and M. Srinivasan, Proc. First Annual Conf. Cold Fusion, Salt Lake, 1990 cited in M.Srinivasan, *Current Science* **60** (1991) 417.
26. M. Nakada, T. Kusunoki and M. Okamoto, "Energy of the Neutrons Emitted in Heavy Water Electrolysis", *Frontiers of Cold Fusion* p.173, ed. H.Ikegami, Universal Academy Press (Tokyo), 1993.; T. Sato, M. Okamoto, P. Kim, Y. Fujii and O. Aizawa, "Detection of Neutrons in Electrolysis of Heavy Water", *Fusion Tech.* **19**, 357 (1991).

Fifth International Conference on Cold Fusion
9-13 April, 1995 - Monte Carlo, Monaco
ICCF5 ©1995

Collision Between Two Deuterons in Condensed Matter: IonTrap Mechanism

V. Violante,
ENEA Dip. Energia, Settore Fusione,Centro Ricerche Frascati,
C.P. 65 - 00044 Frascati, Rome (Italy)

A. De Ninno
ENEA, Dip. Innovazione, Settore Fisica Applicata, C.R. Frascati,
C.P. 65 - 00044 Frascati, Rome (Italy)

Abstract

In this paper is studied the behaviour of ions confined by means of quadrupolar electro-dynamic containment around palladium lattice tetrahedral sites. Ion confinement in a quadrupolar trap is known to be strongly influenced by the initial conditions and trap parameters. The considered system is a lattice ion trap for deuterons, supposing that over a certain concentration they occupy the tetrahedral sites. The electron motions seem to have a dominant role in the dynamics of two deuterons moving around such lattice sites. A mathematical model allows us to describe, with a computer simulation, the deuteron dynamics and reveals an approach mechanism that could strongly decrease the mean distance between two positive charges embedded in a lattice.

1. Model description

Over the past forty years, several authors have investigated electro-dynamic containment of charged particles in a quadrupole trap [1-3]. Our intention in this paper is to develop a preliminary classical study of the dynamics of two deuterons moving within the Pd lattice space around tetrahedral sites, by considering a remarkable similarity between the above mentioned quadrupole radio-frequency traps and the palladium lattice structure. Several features of the palladium-hydrogen system indicate that the hydrogen isotopes (e.g. deuterium) exceeding the atomic ratio x=D/Pd=0.8 have a distinctive kind of interaction with the host lattice. Experimental data [4] indicate that above threshold (x=0.8) the D diffusion coefficient increses steeply by almost two order of magnitude. A suddenly increase of the diffusion coefficient is expected if the energy barrier between two allowed positions decreases. The decrease of the energy barrier could be due to deuterons moving, for x>0.8, from the octahedral sites to the tetrahedral ones. In the following we will assume that over the threshold x=0.8 at least a fraction of deuterons moves from octahedral sites to tetrahedral ones [5,6]. In the proposed model the authors suppose that the alternating signal of a lattice radio-frequency trap can be generated by the motion of electrons close to te Fermi energy. The electron motion can be traced back to an oscillating electronic cloud that produces an electric field. Fig. 1 shows the palladium lattice cell. The octhaedral sites are in the middle between the vertex of the cubic structure. The tetrahedral sites, that could be available for deuterons above x=0.8 [5,6] belong to the intersection between the (101) and the $(10\bar{1})$ planes. We can imagine a similarity between a quadrupolar ion trap and the system shown in Fig.1. It can be shown [5] that the e.m.

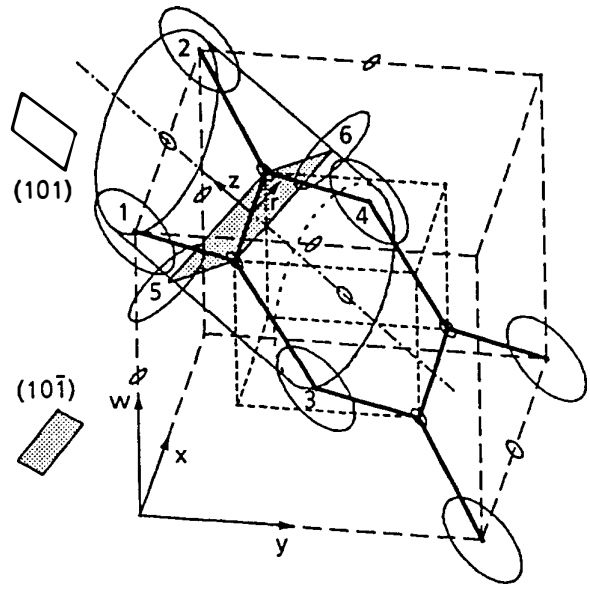

Fig.1 Palladium-Deuterium lattice cell.101 plane and its orthogonal plane $(10\bar{1})$ (dashed area). A similarity can be envisaged between the quadrupolar ion trap and the system shown in the figure. Cylindrical symmetry of the "lattice ion trap"

coupling of oscillators minimize the energy, i.e. the collective motion of N identical oscillators is amplified if compared with to their incoherent interaction. We start considering electronic clouds oscillations having the same phase and the same orientation in both planes (in their coherence domain). For simplicity's sake we consider that the charges acting in the (101) plane are the midway between Pd atoms 1 & 2, and 3 & 4 (see Fig.1) and the charges acting in the $(10\bar{1})$ plane are just the atoms 5 and 6. A simplified two–dimensional representation of the system can be carried out considering the projection in the w-y plane of the spatial electronic cloud oscillations around the Pd atoms. We see that their displacements in both (101) and $(10\bar{1})$ planes are oscillations of the charge density (see Fig.2a, 2b) producing an alternating potential difference that generates an electric field. Then E^{101} and $E^{10\bar{1}}$ in the [101] and [$10\bar{1}$] directions respectively, are the effective components of the electric field for ions dynamics. If we suppose that the electron clouds move at random, then as the oscillation direction moves away from the plane direction (see Fig. 2b) the oscillating charge density decreases within the plane and therefore also the signal across the plane is reduced. This effect can be described by introducing a random factor (ranging between zero and one) in the peak signal. The electric field in each plane acheives its maximum value when it is minimum in the other one and vice-versa because of the orthogonality between the planes: the maximum value of the peak signal for one plane is obtained when the oscillation takes place along the plane direction itself, as can be seen in Fig 2a. Such a situation leads to sinusoidally time varing forces whose strengths are proportional to the distance from a central origin. The trap can be considered to have cylindrical symmetry as shown in Fig.1. The expression for the alternating signal can be derived from the circular symmetric potential distribution [1]. For the system under consideration the field intensities can be obtained by differentiating the potential distribution (and introducing both the coefficients taking into account the effective value of the peak signal in both planes due to the oscillation direction and the possible

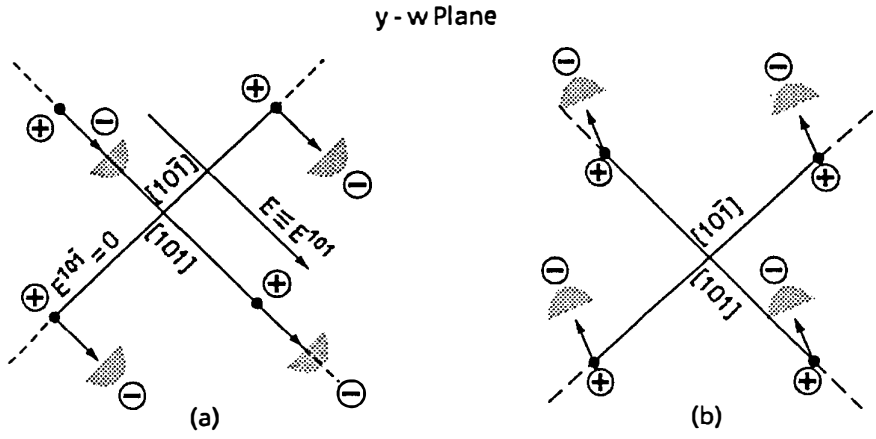

Fig. 2 (a,b) Two-dimensional representation of the alternating signal

shift).Let $E_z = E^{101}$ and $E_r = E^{10\bar{1}}$ then:

$$E_r = -(1-\alpha)V_{acr}\cos(\Omega t + \frac{3}{2}\pi)\frac{r}{r_0^2}$$
$$E_z = 2\alpha V_{acz}\cos(\Omega t + \phi)\frac{z}{r_0^2} \qquad (1)$$

where V_{acr} and V_{acz} are the r and z ([10$\bar{1}$] and [101] directions respec-tively) peak values of the alternating signal having angular frequency Ω, r_0 is the trap characteristic length (the radius or the length from the simmetry point that are equal in this case), r and z are the relative coordinates of two deuterons moving in the trap, α is a random number, ranging between 0 and 1 taking into account the direction of oscillation, and φ is a random phase shift that is equal to zero if we imagine collective organized oscillations of the electronic clouds (α and φ can also change after a time interval of the order of the oscillation period).Considering both the coordinates, and introducing the following dimensionless variables $\bar{r} = \frac{r}{r_0}; \bar{z} = \frac{z}{r_0}; x = \frac{\Omega t}{2}$, the balance of the forces leads to:

$$\frac{d^2\bar{r}}{dx^2} = -\frac{2}{m\Omega^2 r_0^2}\frac{dE_b}{d\bar{r}} + \frac{4}{m\Omega^2}\bar{r}[e^2\frac{1}{(r^2+z^2)^{3/2}} + \frac{(1-\alpha)eV_{acr}}{r_0^2}\cos(2x+\frac{3}{2}\pi)]$$
$$\frac{d^2\bar{z}}{dx^2} = -\frac{2}{m\Omega^2 r_0^2}\frac{dE_b}{d\bar{z}} + \frac{4}{m\Omega^2}\bar{z}[e^2\frac{1}{(r^2+z^2)^{3/2}} - \frac{2\alpha eV_{acz}}{r_0^2}\cos(2x+\phi] \qquad (2)$$

where e is the electron charge. The terms on the right side of Eq. (2) are due to the damping force, the Coulomb interaction and to the trap force respectively. The damping force could be evaluated as the gradient of the energy barrier whose shape is unfortunately unknown. Therefore in this preliminary description the damping term in the Eqs.(2) is simply evaluated as average gradient of the energy gap $\Delta E_b / r_0$ (being ΔE_b

the energy barrier,~0.2 eV). The initial conditions have to be included to describe the relative position of the two deuterons, travelling towards the trap, and their initial velocity. The frequency of the alternating signal can be evaluated by means of the approximation to an ideal electron plasma [5]. In this calculation we shall assume, as mentioned above, that only the electrons close to the Fermi level (4d-5sp bands) partecipate to the oscillations ($n = 6.8\times10^{23}$). The peak value of the alternating signal can be calculated on the basis of the electric field, in the classical approximation, associated with the plasma oscillation: $V_{acr,z} = 4\pi ne\eta^2$; where η is the maximum distance between the positive and negative centres of charge during the oscillations: i.e. the distance between the Pd atoms (here η =2.83 Å and $V_{acr,z} \sim 10^3$ V).

2. Results and Conclusions

The computer simulation allows us to investigate the system's sensitivity to the initial conditions and to obtain a preliminary correlation between the lattice state and the *collision* between two deuterons. The lattice cell parameters used in the simulation have been obtained from the lattice constant for the β phase. The **Fig. 3** shows the evolution of the distance between two deuterons versus the dimensionless time α=constant and φ=0. Fig 3a shows the situation when it is considered a Coulomb interaction, whereas Fig. 3c shows the analogous by considering a Thomas-Fermi screened potential. The closest approach, within the investigated time interval is ~0.1 Å but after one *collision* one of the particles escapes from the trap. Fig. 3b shows the distance evolution (assuming a Coulomb potential) with a different choice of the initial conditions. In this case no *collision* occurs. Figure 4a shows the evolution of distance between the two deuterons vs the dimensionless time by assuming the same conditions as the case described by Fig. 3b, whereas the Fig. 4c shows the situation by considering an electron plasma density reduced of 10%. We can see (in the enlargement of the *collision* region) that because of the reduction of the plasma frequency and of the peak value of the signal (see Eqs (6) and (8)) the minimum distance of approach increases. This effect is not negligible in terms of nuclear interaction probability. Thus this analysis reveals that an increase of the Deuterium/Palladium loading ratio, with an associated increase of the electron plasma density plays an important role in the *collision* event. Fig 4b show the situation with the same initial condition of the case described by Fig. 3b but assuming a T.F interaction potential. From the numerical calculations it results that, under the same conditions, the minimum distance between deuterons increases if the electron clouds oscillate with a time dependent orientation (even if it is always of the order of 0.1 Å). The components of the electric field (1) are still valid in this case because the time domain has been divided in sub-intervals where α is constant. In this case the integration is carried out taking as initial condition for each sub-interval the final condition of the previous one. Even if the calculated distances between the deuterons can only be considered indicative, the model gives the interesting result that, the deuterons, because of the electronic oscillations within the Pd lattice, can approach each other up to distances of the order of a fraction of one angstrom; therefore overlapping deuteron wave functions can be obtained at low energy in condensed matter under a variety of scenarios and hypotheses concerning the trap mechanism. Also, the calculations show that the two nucleus remain close together for a time long compared with the nuclear reaction time (~10^{-15} s against ~10^{-21} s). In addition to the cases discussed here, several other boundary conditions have been used giving similar behaviour of the deuterons. The combined effects of the trap force, the trostatic interaction, non linearity, and the damping produce, under proper conditions, an interesting effect of *collisions* between the particles. Besides it is possible that a nuclear

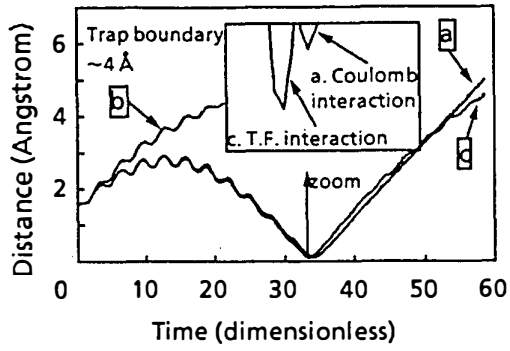

Fig. 3 evolution of the distance between two deuterons (α=constant, φ=0). Fig 3a (Coulomb interaction), Fig. 3c (Thomas-Fermi screened potential). In both cases the initial dimensionless coordinates are r(t=0)=0.001, z(t=0)=1.1, and the initial dimensionless relative velocity components are r'(t=0)= =0.001 and z'(t=0) =0.12. Fig. 3b shows the distance evolution (assuming a Coulomb potential) with a different choice of the initial conditions: r(t=0)=0.001, z(t=0)= 1.1, r'(t=0)=0.125, z'(t=0) = 0.12.

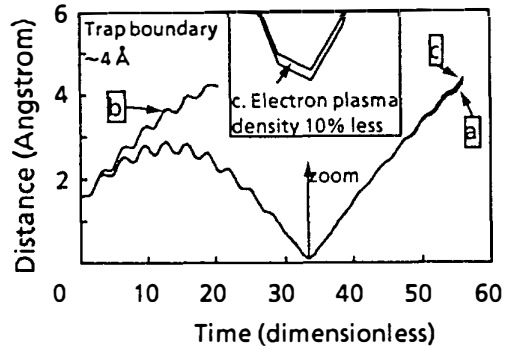

Fig. 4a evolution of distance between the two deuterons (conditions of Fig. 3c), whereas the Fig. 4c shows the situation with an electron plasma density reduced of 10%. Fig. 4b show the situation with the same initial condition Fig. 3b but assuming a T.F interaction potential.

reaction could proceed in matter differently from in vacuum, if coupling with a radiation field in the nuclear transition probability is taken into account. Furthermore we observe that the condition for close approach between two particles is produced by proper values of the plasma electrons density, cell trap geometry and lattice state; therefore it is not impossible that a similar dynamics can be obtained by using host materials different from palladium. The model highlighs that a face centred lattice plays a fundamental role in deuteron confinement and dynamics. It should be observed that the proposed mechanism is not necessarily a bulk mechanism but can take place also in a material region very close to the surface, within several hundred angstroms. Quantization should be carried out among the future developments.

References

1. R.F. Wuerker, H. Shelton, R.V. Langmuir, "Electrodynamic Containment of Charged Particles", *J. of Appl. Phys.*, **30**, 3, 342 (1959)
2. J. Hoffnagle, R.G. De Voe, L. Reyna, R.G. Brewer, "Order-Chaos Transition of Two Trapped Ions", *Phys. Rev. Letts* **61**,3, 255 (1988).
3. R.G. Brewer, J. Hoffnalge, R.G. De Voe, L.Reyna, W. Henshaw, "Collision Induced Two Ions Chaos", *Nature*, **344**, 305 (1990).
4. G. Mengoli, M. Fabrizio, "Surface and Bulk Effects in the Extraction of Hydrogen from Higly Pd Sheet Electrodes", *J. Electr. Anal. Chem.*, **350**, 57 (1993).
5. G. Preparata, Cold Fusion '93: Some Theoretical Ideas, Transactions of Fusion Technology Vol. **26** (Dec. 1994) 397-407.
6. R.A. Oriani,The Physical and Metallurgical Aspects of Hydrogen in Metals. Transactions of Fusion Technology, **Vol.26**, (Dec. 1994) 235-266.

Fifth International Conference on Cold Fusion
9-13 April, 1995 - Monte Carlo, Monaco
ICCF5 ©1995

ON ONE OF ENERGY GENERATION MECHANISM IN UNITARY QUANTUM THEORY

Lev G. Sapogin
Department of Physics, Technical University (MADI),
Leningradsky prospect 64, A-319, 125829, Moscow, Russia

It is now a well established fact that in Cold Nuclear Fusion (CNF) only a small portion of heat results from nuclear reactions, the rest being of a mysterious origin. In this connection Prof. Peter Hagelstain writes in [1]: "Some say that this heat can be explained easily by elementary chemical reactions, phase changes, or battery-like storage effects. I have trouble with these explanations". For instance, nickel electrolysis in light water produces the same amount of energy as that of palladium in heavy water. Besides, we have to consider a no less mysterious phenomenon of sonoluminescence, that was discovered in Russia in 1933 by S.N.Rzhevkin. At first sight these phenomena seem to bear no correlation. But Julian Schwinger, the Nobel Laureate and profound research worker, has drawn parallels between cold fusion and sonoluminescence in his continuous technical publication on both topics. He notes in [2]: "Like Cold Fusion, sonoluminescence "should not exist", but it does. This now well established phenomenon occurs when ultrasonic sound, beamed into liquid, causes bubbles to oscillate stably - to expand and contract regularly - and also to emit regular pulses of light".

But one is positively struck by the heat generator built by Dr.Yu.S.Potapov (Kishinev, Moldavia), which produces in water cavitation bubbles, generating 12 kWt of heat on 4 kWt of electric energy.

This is achieved by the aid of a centrifugal pump that runs light water thought a tube with a number of special attachments. Similar, though less effective results, have been obtained in the USA by James Griggs [3]. The reactions taking place in the abovementioned cases can be explained neither in chemical nor in nuclear terms. Moreover, Potapov's system is now in production and used for heating homes. There is no doubt that the described phenomena can be viewed as "new physics" and it is impossible to describe them within the laws of conventional science.

Below it will be shown that Unitary Quantum Theory (UQT) allows one to explain all these seemingly unrelated effects. UQT was developed in 1970-1988 and its validity is proved by the fact that at a limited number of cases the theory results in both the Dirac's equations and the relativistic equation of Hamilton-Jacobi. Moreover, the solution of approximate UQT equation has yielded the electric charge value and that of the fine structure constant with reasonable exactness, the result being achieved for the first time in theoretical physics [6-14].

The solution allowed to formulate one more approximate equation for the oscillating charge particles model which gives promising results in dealing with the deutons interaction problem (the basic CNF problem) [4,5] .

Let us consider more closely, as it was done in [4,5], the particle's behavior in a potential well. The equation describing this process can be expressed in the following way:

$$\ddot{x} = \mathrm{GRAD}\, U(x)\, \mathrm{COS}^2(t\dot{x}^2/2 + x\dot{x} + f0) \qquad (1)$$

where U(x) is a potential and x, $\dot{x}$, t, f0 - a coordinate, velocity, time and initial phase correspondingly. This equation manifests a number of peculiarities. Having integrated it once, we arrive at

$$\dot{x}^2 = 2W(x,t) \qquad (2)$$

where W(x,t) is some time-dependent complex potential not amenable for analytical expression even for the simplest U(x). Therefore nothing can be said about the integrals of motion. Equation (1) behaves very peculiarly in translation - invariance conditions. It doesn't exist in common case but manifests itself at translations divisible by $\mathcal{R}_c$. That means that 2 classes of solutions are available: for the first class the laws of energy and momentum conservation are valid, while for the second class they are not.

Numerical computation for the parabolic well yields solutions of 4 types that result from different initial conditions. Similar results can also be obtained for other potentials [4].

1. The stable standard periodic solutions are obtained only for definite discrete energy E values equal to $(n+1/2)\hbar w$ at n=0,1,2... and at definite values of x, $\dot{x}$, f0. Trite solutions of the same kind are available in conventional quantum mechanics and will not be analyzed in this paper.

At other initial conditions 3 more types of solutions arise:

2. The particle performs complex oscillations of a diminishing amplitude. Sometimes at certain x, $\dot{x}$, f0 values the process starts at an increasing amplitude with its consequent decrease. At this point the particle charge and mass approach zero and after some rather long period of time the former ceases to exist altogether. This is not surprising because in UQT the particle is defined as a periodically emerging and disappearing wave packet. Its complete disappearance means that the packet's harmonic constituents have scattered so far from each other that the packet itself ceased to exist, its energy given away to the vacuum, smeared out throughout the entire space, manifesting itself only in the form of vacuum fluctuations. Let us call this solution "a crematorium".

3. The particle performs complex oscillation with an increasing amplitude, yet sometimes the process can develop with an initial short-time decrease in the amplitude. In doing so the particle's energy can increase indefinitely, if the potential well's parameters do not change. Physically this means that the particle takes energy from vacuum fluctuations but the mechanism of this process, of how it does so can be deduced only from equation (1). Let us call this solution "a maternity home".

4. There is also a diffusion solution, in which the particles tunnel into the potential gap wall. This solution is similar to that of the particle's behavior at the potential step, whence the particle in the course of considerable period of time can penetrate deep into the step. Periodic and irregular oscillations determine the energy discrete and continuous regions, respectively.

From a purely esthetic point of view it is desirable that the quantity of energy (matter) disappearing in the "crematoria" should be equal to that emerging from the "maternity homes". But I am not yet in a position either to prove or disprove it.

Solutions 2 and 3 are incompatible with conventional quantum mechanics, whence solution 4 corresponds to exponentially decaying (damping out) wave function tail at large x values.

If the system contains a number of identical wells, all the decisions of type one will be identical for them and that's the reason why the discrete energy levels are easily traced out in the experiment. But there will be no discrete levels for solutions of type 2 and 3 because each individual decision will possess its own peculiarities. The availability of these solutions can be perceived only through integral effect - either the energy release or drastic charge, or mass variation in the system, being in itself a very specific phenomenon.

Let's take a more close look at intriguing solutions 2 and 3.

I was aware of them as far as 2 years ago, which can be seen in [5, p.98]. But I was afraid to discuss the matter in my publications in the absence of reliable experimental data. Even now I am in mortal fear lest my reasoning turns out to be erroneous. But the situation has since changed and one can say now with certainty, that within UQT in quantum processes the energy and momentum conservation laws have grown from local to a global one, i.e. in individual processes the energy and momentum are not conserved, but may be taken from or given away to the vacuum. Nevertheless there exist some range of phases when the energy and momentum are preserved locally. Being summed up throughout all phases for a large number of particles the resulting energy and momentum turns out to be conserved as is shown by calculations in [5, page 93].

The experiments show, that in individual quantum processes at high energies the local energy and momentum conservation laws and conservation laws for the lepton and barion numbers are well observed. But the same is not true at small energies at least on account of ambiguity correlation [7,14]. Nevertheless the idea of global (not only local) energy conservation law is invisibly present in all quantum mechanics, it is by no means a new one. From physical viewpoint it simply means that in steady-state solutions with fixed discrete energies, the velocity of a particle reflected at the wall is equal to that of the impinging one. If the particle speed decreases upon each reflection this corresponds to the "crematorium" solution, in case it increases we face the "maternity home" alternative.

The "crematorium" solution should not be confused with the familiar phenomenon of particles' decay - it is an absolutely new and very slow process taking place at small energies. It possesses no analogs in conventional quantum physics.

The "maternity home" solution (3) has been proved by reliable experimental data for any small cavity in a metal or ceramics-made sample, or likewise a water bubble with enclosed free particles and can be viewed as a well. This can explain both sonoluminescence and the emission of heat in nickel, palladium and ceramics. The theory allows for the samples to crack because of the ressure exerted on their walls due to energy growth, the energy generation being immense in the installations of Dr.Y.S.Potapov and J.Griggs. It would be extremely helpful to create an electrically isolated system emitting great amounts of heat in order to measure its charge, which is expected to vary in the course of energy generation. This would serve as an additional proof of the picture of the phenomena described above.

Thus the excessive energy is taken from the vacuum, but this does not occur for nothing because in the neighboring wells some part of the matter would disappear. In other words, one is under the impression that a new mechanism for the direct conversion of matter into energy has been discovered. This energetic phenomenon is entirely pollution-free and thousand times more effective then that of nuclear reactions. It is for the future to prove it.

Now let's take a bit of philosophy. The Local Energy Conservation Law (LECL) in individual processes follows directly from Newton's equations under the condition of uniformity of time. It would be naive to think that his local definition will remain unchanged. The trend in modern physics now is to treat the LECL, especially in theory, as a conclusion of secondary importance from the motion equation (integrals of motion). Some physics confine LECL within the limits of the first law of thermodynamics others as D.Blokhintsev maintain that "it is highly probable that the development of new theory will make LECL change its form" [15].

F.Engels wrote in "Nature Dialectics" "...no physicist regards essentially the LECL as an eternal (ever-lasting) absolute law of Nature, the law of spontaneous transformation of matter motion forms and the quantitative stability of this motion throughout all its transformations". But many research workers are of a different opinion as M.P.Bronshtein [16] who wrote; "The ECL is one of the fundamental laws of Newton mechanics. Yet, Newton himself had never ascribed to his law the uniform character, which it possesses in reality. The reasons for such erroneous treatment of the ECL on Newton's part are extremely interesting...".

The idea to treat the ECL in quantum mechanics equally with the second law of thermodynamics as a static law, being true only in average cases and unsuitable to individual acts, goes back to [15] E.Schrodinger , and later to N.Bohr, H.Kramers, I.Slater and G.Gamov. L.Landau had called it "a beautiful Bohr's idea" [15]. Yet, later it was rejected by the authors themselves. It should be noted that this idea did not follow from the quantum theory equations. But the brilliant idea still remains one, even being reject by the person to whom it had occurred. In fact, it may simply turn out to be premature. Eventually,all the cosmologist's dream of having a process explaining why throughout the entire Universe there are some places where energy emerges, being extinguished in the others. It is interesting that solution 3

gives one an opportunity to set a very small initial fluctuation, which then will accumulate energy and turn into a particle.

One has to accept the truth regardless of it's source. Therefore I will conclude with the words of F.Engels. "But when the solar system completes its life-path and shares the fate of everything finite, when it falls victim to death. What then? Thus we come to the conclusion that the heat emitted into world space should have an opportunity by some miraculous way, which it will be the task of future science to define, to turn into some other form of motion, in which it can accumulate again and start functioning. In this case the main difficulty becomes obsolete, the one obstructing the reverse change of dead suns into a red hot nebula".

One can expect that having read this paper some high-brow theoreticians will assume attitude of persons being witness to some childish tactlessness. But in the course of physics' development it was experimentation that had always been the main judge.

I'd like to express my gratitude to N.V.Famina, the attractive translator of the article. I am equally thankful to Drs. F. Jager, O.Finodeyev, V.A.Boichenko, O.I.Kasakov, I.V.Kulikov, F.Mair and Yu.G. Rudoy for taking part in the discussion and practical help in my work.

References

1. Hagelstain. "A plethoria of 'miracles'".Cold Fusion vol.1, No.3, p.22, 1994
2. Schwinger. "Cold Fusion: Does it have a future?". Cold Fusion. vol.1, No.1, p.14, 1994
3 Rothwell, Mallove."The hydrosonic pump: An excess energy device?" Cold Fusion. vol.1, No.2, p.26, 1994.
4. Sapogin. "Deuteron interaction in unitary quantum theory", "On the mechanisms of cold nuclear fusion". Proceedings: Fourth International Conference on cold fusion.Vol.4: Theory and special topics papers. TR-104188-V4. July 1994 (Hawaii)
5. Sapogin. "Deuterium interaction in unitary quantum theory", "On the mechanism of cold nuclear fusion". Cold Fusion Source Book. International Symposium on Cold Fusion and Advanced energy sources. Belarusian State University. Minsk, Belarus, May 24-26, 1994
6. Sapogin. "Unitary Field and Quantum Mechanics." Investigation of systems. (in Russian, Vladivostok, Academy of Science), No. 2, p. 54, (1973).
7. Sapogin. "On Unitary Quantum Mechanics." Nuovo Cimento. vol. 53A, No. 2, p. 251 (1979)
8. Sapogin."An Unitary Quantum Field Theory", Annales de la Fondation Louis de Broglie. vol. 5, No.4, 285 (1980)
9. Sapogin. "A Statistical Theory of Measurements in Unitary

Quantum Mechanics." Nuovo Cimento. vol. 70B, No.1, p.80 (1982).
10. Sapogin. "A Statistical Theory of the Detector in Unitary Quantum Mechanics." Nuovo Cimento. vol. 71B, No.3, p. 246 (1982).
11. Boichenko, Sapogin."On the Equation of the Unitary Quantum Theory." Annales de la Fondation Louis de Broglie. vol. 9, No. 3, p.221 (1984).
12. Sapogin, Boichenko. "On the Solution of One Nonlinear Equation."Nuovo Cimento. vol. 102B, No.4, p.433 (1988).
13. Sapogin, Boichenko. "On the Charge and Mass of Particles in Unitary Quantum Theory." Nuovo Cimento.vol.104A,No.10, p.1483 (1991).
14. Sapogin. "Clear-cut picture of micro worlds".Technic for the young (in Russian) No.1, p.41 (1983).
15. Blokhintsev. Collection of scientific methodological works in physics.(in russian). State University of Moscow,1993.
16. Bronshtein. The matter structure.(in russian). Moscow,1935.

Fifth International Conference on Cold Fusion
9-13 April, 1995 - Monte Carlo, Monaco
ICCF5 ©1995

Optimization of Output in a Cold Fusion Generator

Robert Indech and Ruvin Karshenboym
IPD Associates
3642 Cedar Corners, Norcross, Ga. 30092 USA

Abstract

Progress has been made in the production of excess heat from a cold fusion generator based upon the combination of deuterium ions within a metallic matrix. Drawing from fundamental considerations, this paper identifies for optimization those quantities and methods which would tend to increase the heat production. An analogy to hot fusion is presented, followed by theory of the PONS cell. Methods to increase fusion output are introduced with a detailed theoretical analysis of the effective kinetic temperature generated for deuterium ion under an electric field in a porous material.

1. Introduction: Similarity to Hot Fusion

In a light ion hot fusion reactor, deuterium (D) and tritium (T) are magnetically bottled and interact together to form helium (He) and its isotopes. Two major forces are at work: a electrostatic repulsion force between the two protons, and a short range strong nuclear attraction force between all protons (P) and all neutrons (N). Considering the P and N as "hard balls", the minimum separation distance between nuclei is two times the P radius. The net force is attractive until a larger unstable equilibrium distance and is repulsive after that distance. The quantity of work required to bring the two nuclei together is simply the force from the equilibrium separation distance to infinity integrated over distance. This work is derived from the initial momentum of the ion, which is a function primarily of temperature. Thus, when two ions are on a collision course, fusion will occur when their initial relative velocity exceeds a certain minimum which is sufficient to overcome the electrostatic repulsion force mediated by the strong nuclear attraction force. Clearly, the nuclear attraction force increases linearly with the number of possible nuclear interactions: If a P-P interaction force is arbitrarily set at "1", then a P-D interaction would be set at "2", D-D interaction would be set at "4", D-T at "6", and T-T at "9". As the total amount of charges remains constant, the interaction temperature decreases as the atomic number increases. For example, a D-D reaction may occur at approximately $3x10^8$°K, a D-T reaction at $3x10^7$°K and a T-T reaction at $3x10^6$°K.

2. Theory of Electrolytic "PONS" Cell

The objective of cold fusion is to experience these types of reactions at 300°K. In the PONS type electrolytic cell[REF 1], D gas ions form on the surface of palladium electrode and diffuse into the metal lattice. When two D ions coexist in one metal lattice cell at the same time, and their relative velocity is sufficient to overcome the net electrostatic barrier, then fusion occurs. It is noted that the velocity of the ions in the gas follows a Boltzman probability distribution of velocity curve. Intrinsic in this

design is the realization that the electronic fields of the metal lattice shield a major part of the natural electrostatic repulsion of the two ions. That some shielding occurs is undisputed; the extent of the shielding is difficult to calculate and is disputed to be sufficient for the fusion process to occur at essentially room temperature.[REF 2]

3. Methods to Increase Fusion Output

To increase the rate of nuclear fusion increase the probability of reactant contact per unit time or for each reactant contact and/or increase the probability of reaction.[REFS 3]

3.1. To increase the probability of reactant contact, one may:

A. Increase the local density of reactant.

1. One method would be to increase the pressure of the entire system. Practical considerations are the strength of the reactant vessel.

2. A second method would be to preload the metallic lattice with D ions until the ratio of ions to lattice cells reaches a certain fraction.[REF 4] While this method will cause reaction initiation, the D ion concentration will decrease in the steady state.

3. Another method would be to increase the net velocity of the ions through the lattice. Physically increasing the temperature would increase the binary diffusion rate, producing this result. The practical limitation in the PONS (wet) system is not to exceed the boiling point of the water. In a D gas--metal system, one could operate at much higher temperatures, radically increasing the diffusion rate and hence the local density of reactant.[REF 5]

B. Decrease the presence of any nonreacting interfering species

1. The system must be purged of all non-reacting chemicals. The lattice may be internally cleaned of absorbed hydrogen by thermal vacuum outgassing and other methods. The surface of the system must be cleaned continuously with no biological or physical coatings impeding the diffusion of the deuterium ions.[REF 6]

C. Increase the presence of the most highly reacting species. ,

1. As T is more reactive than D, methods to increase the density of T within the lattice would tend to increase reaction rates.

3.2. To increase the probability of reaction, one may:

Given two charged ions, the major obstacle to combination is their mutual electrostatic repulsion. Thus, either decrease the repulsion or give the ions sufficient velocity to break through the repulsion barrier.

A. To decrease the repulsion, surround the positive ion with a dense electronegative field.

1. The field could emanate from the metallic lattice. Thus, selection of a metallic lattice which tends to have a high local electronegativity or high dielectric constant would increase reaction rate.[REF 7] Lattices of palladium, titanium and nickel have been shown to produce excess heat. A lattice of perovskite ceramic have been successful by some researchers.

2. The field could emanate from a singular unusual charged cloud, such as a mu-meson.[REF 8] The mu-meson, an atomic entity with the charge of an electron and 200 times its density, closely surrounds the ion, allowing sufficient shielding for proven fusion at room temperature. However, this atomic entity is short lived and takes more energy to produce that is derived economically from the fusion reaction.

3. The field could emanate from point defects in a metallic lattice. Local defects show a remarkable concentration of electric field which could lead to local fusion generation at that point. However, the immense quantity of local heat generated by such fusion events would tend to cause disruption of the point defect, and self-extinguishment of the reaction. Perhaps this method could account for some of the irregular times of occurrences of fusion reported by some authors. Selection of a metal with many point defects and grain boundaries may enhance this method of increasing reaction rate.

4. The field could emanate from an artificial external source.

A. An electron cloud could be generated similar to that in old-styled radio tubes and the D gas would be placed within that cloud.

B. Selective bombardment of D within the metal lattice with high energy focused electromagnetic waves would increase the field density.

B. To increase the velocity of contact, certain steps could be taken.

1. Increase the individual temperature of the ion. There is a severe limitation on this method by the wet ion-metal system over that of gas ion-metal system.

2. Accelerate the ion by placing it within an electric field.

A. The electric field could be placed across the metal or ceramic in a binary gas-metal/ceramic system. From electron transport theory inside a metal, consider the movement of an ion of charge "Q" along a free path across a pore diameter "A" under the influence of an electric field, "E". Consider that the ion's velocity at its point of origin at the entry to one side of the pore is zero, and that the ion subsequently loses all electric field induced momentum by impaction at the other side of the pore. Letting "V_f" be the final ion velocity, "m_i" being the mass of the ion, "t_f" be the total flight time, "a" being the acceleration, "T_k" being the effective kinetic temperature, and "k" being Boltzman's constant. The effective kinetic temperature "T_k" is defined conventionally as the equivalent gas temperature of a set of ions moving at an average velocity "V_f". The equations governing the motion of this ion would be:

$$Q \cdot E = m_i \cdot a \ , \quad A = .5 \cdot a \cdot t_f^2 \ , \quad v_f = a \cdot t_f \ , \quad .5 \cdot m_i \cdot v_f^2 = 1.5 \cdot k \cdot T_k \ , \quad T_k = \frac{2 \cdot A \cdot Q \cdot E}{3 \cdot k}$$

Question: For an electric field of 5×10^5 Volts/meter, and a pore size of 10 microns, what would be the effective kinetic temperature?

$$T_k = \frac{2 \cdot 10^{-5} \cdot 1.6 \cdot 10^{-19} \cdot 5 \cdot 10^5}{3 \cdot 1.38 \cdot 10^{-23}} = 3.9 \cdot 10^4 \, K$$

This magnitude of electric field cannot be supported in a metal. It can be supported in a semiconductor with the properly chosen material properties. Even allowing for other inefficiencies in the accelerating flight path due to field interaction with the lattice ions, an electric field could produce, at room temperature, an effective kinetic temperature, which, magnified by shared lattice electronegative field, would

allow light ion fusion. Like the electron beam hitting the interior of a television tube, the total quantity of energy transferred to the ion is small compared to the overall thermal energy of the lattice, and therefore that overall lattice temperature does not substantially rise due to the electric field alone. Certain researchers have observed transient fusion effects which are difficult to repeat. These effects could well be due to lattice defects, which are themselves lost due to the intense local energy generated at a point at the site of ion fusion. Current research in our laboratory utilizes an apparatus with these electric fields.

Placement of any electric field across a metal is difficult as its resistivity is low, leading to excess current flow. Alternatively, an electric field could be placed on an insulator, essentially creating a capacitor. One might construct an ion-insulator system. In a capacitor, there is a large surface charge and no movement of electrons within the material. The insulator may not be able to provide the proper amount of local electron sharing required to local electrostatic shielding, although some research groups have noted positive results for certain high temperature ion-ceramic systems.

B. The electric field could be placed upon a semiconductor. Thus, one would have a ion-semiconductor system. Many natural materials, such as germanium and silicon, are semiconductor by nature, and may allow both the presence of the electric field and the proper amount of internal electrostatic shielding for fusion to occur.

C. The electric field could be directly acting upon the ion.

1. One method is to produce deuterium ions by electric or X-ray ionization and then accelerating them in an electric field in vacuum, letting them impact a metallic lattice system. The ion would gain sufficient velocity but only at the surface of the metal, as the ion would transfer much of its kinetic energy to the lattice upon contact, essentially losing all of it within a few atomic layer depths. Further, the impact itself would tend to damage the surface of the lattice.

2. Another method is to accelerate the ion by electric field and increase the ion density through magnetic pinch effect to increase the reaction rate.

4. THE PROOF IS IN THE PUDDING

The public will accept cold fusion as a viable energy source when they can see a totally closed system producing usable power. It is good for individual researchers to produce sophisticated calorimeter results of excess heat production, but unless this heat can be translated into usable power, and the power utilized to prime, sustain and power the instrumentation for the reaction, the public will remain skeptical.

We have experimented with a novel design to extract heat from a boiling reaction chamber and convert it directly to electricity. In this design, a matched heat pipe is connected to a metallic thermal reservoir, itself connected to thermoelectric modules with cooling fins. At present, the unit efficiency is low, on the order of 1.5-2%, but better convection cooling, a higher reaction temperature, and a lower cooling temperature will increase this figure substantially. Obvious advantages are no observable moving parts, no danger of overload, and no necessity of continuous adjustment or calibration.

REFERENCES:

1. Bockris et al., "A Review of the Investigations of the Fleischmann-Pons Phenomena," *Fusion Technology* 18, p.11-31(Aug. 1990).

2. Handel, "Intermittency, Irreproducibility, and the Main Physical Effects in Cold Fusion," *Fusion Technology* 18, p.512-517 (Nov. 1990).

3. Rafelski et al., "How Cold Fusion Can Be Catalyzed," *Fusion Technology* 18, p.136-142 (Aug. 1990).

4. Yao et al., "Observation of Cathodic Charging on a Palladium Electrode in Heavy Water," *Journal of Material Science Letters* 9, p.228 (1990).

5. Aiello et al., "Nuclear Fusion Experiment in Palladium Charged by Deuterium Gas," *Fusion Technology* 18, p.115-119 (Aug. 1990).

6. Nimtz and Marquardt, "A Proposal for a Lukewarm Nuclear Fusion," *Fusion Technology* 18, p. 518 (Nov. 1990).

7. Shohoji, "Unique Features of Hydrogen in Palladium Metal Lattice: Hints for Discussing the Possible Occurrence of Cold Nuclear Fusion," *Journal of Material Science Letters* 9, p. 231-232 (1990).

8. Jones, "Engineering Issues in Muon-Catalyzed Fusion," *Fusion Technology* 8(1)2B, p.1511-21 (July 1985).

Fifth International Conference on Cold Fusion
9-13 April, 1995 - Monte Carlo, Monaco
ICCF5 ©1995

Two–dimensional Proton Conductors

William S. Page
Daneliuk & Page

May 7, 1995

1 Introduction

An enormous literature has developed on the subject of the abnormal mobility of protons in aqueous solutions. Eigen and De Maeyer in 1958 [1] may have been among the first to observe that "The proton transport in hydrogen-bonded media is completely different from normal ionic migration and corresponds more to electronic transport processes in semi-conductors. ... Phenomenologically, the ice crystal may be considered as a 'protonic semi-conductor' with an intrinsic (thermal) distribution of the charge carriers (protons) between a 'valence' band (H-bonded H_2O) and a 'conduction' band (excess protons fluctuating in H-bonds). As an elementary particle the proton has much more in common with the electron than any other ion, the radii of which are of completely different order of magnitude.". Eigen and De Maeyer describe a "protonic rectifier" based on "The combination of two crystals, one doped with a proton donor (HF, F^- being almost immobile) and the other one with an acceptor ($LiOH$, NH_3, Li^+ or NH_4^+ being immobile)...".

The bond structure of ice (and to a large extent liquid water as well) involves two protons (hydrogen atoms) per oxygen atom in a 3-dimensional, approximately tetrahedral structure, i.e. the oxygen atoms occupy the corners of a tetrahedron while the hydrogen atoms form the bonds between pairs of oxygen atoms along the edges of the tetrahedron.While each oxygen atom is surrounded by four hydrogen atoms, each primitive cell of the lattice is occupied by an H_2O molecule as expected. Similar to the electrons in conventional semiconductors, in pure water almost all of the hydrogen is in the "valence" band state. Each oxygen atom has two loosely bound hydrogen atoms which form hybrid hydrogen "orbitals" with four tetrahedrally coordinated neighboring oxygen atoms. Defects in this structure are classified as L-defects (empty hydrogen bonds, expressed in molecular terms as the hydroxyl ion OH^-) and D-defects (doubly occupied hydrogen bonds, expressed in molecular terms as the hydronium ion H_3O^+). An L-defect can also be described as a "proton hole" in the valence band, while a D-defect corresponds to a proton in a conduction band.

Thermal disruptions of the lattice structure give rise to a small number of defects in this structure. In some cases two hydrogen atoms may occupy a single hydrogen-bond creating a D-type defect. In pure water, each D-type defect is accompanied by a corresponding L-type defect. It is the movement of these defects which give rise to the protonic conductivity of water.

In the case of substitutional impurities such as ammonia NH_3 the N atom is an H-donor. The extra H atom does not fit into the regular hydrogen bond structure and there is therefore an excess of D-type defects. The result is that these extra protons are relatively free to hop from one already occupied hydrogen bond to the next In the case of substitutional impurities such as hydrogen fluoride HF the F atom is an H-acceptor – introducing "holes" in the structure. One of its structurally-expected hydrogen bonds is empty and there is therefore an excess of L-type defects over pure water. It is now the absence of a proton in a hydrogen bond that moves throughout the lattice.

Water with an excess of D-defects is called a D-type electrolyte (analogous to N-type electron semiconductor). Water with an excess of L-defects is call an L-type electrolyte (analogous to P-type electron semiconductor). Both L-type and D-type electrolytes are good proton conductors. L/D-type junctions produce proton current diodes with properties similar to their electron counterparts. In particular such diodes display rectification (unidirectional current flow), high values of thermoelectric power, and may display luminescence under forward bias due to recombination of L and D-defects. Such effects as thermoluminescence of ice following irradiation [10] and sonoluminescence of water [9] may be related to L/D recombination.

These structural considerations when applied to ice seem straight forward [5]. It also turns out, however, that liquid water to a very large extent retains this tetrahedrally coordinated structure locally. In fact, both ice and liquid water depart from this ideal 3-dimensional structure in fairly subtle and random ways that give rise to the beautiful fractal patterns of snow flakes and frost. It may well be appropriate to treat water as a substance with a "fractal" fractional dimension with liquid water having a dimension between 1 and 2 and ice having a dimension between 2 and 3. In the simplified calculations in this paper we will, however, use only 1-dimensional models.

2 Band States

The detailed structure of the periodic potential that the hydrogen nuclei encounter is the result of the overlap of electron orbitals and Coulomb interactions. Due to the electronic structure of the oxygen atoms, the electrons are all very tightly bound to the oxygen centers. In comparison to the protons, the electrons are not free to move and do not appreciably take part in electrical conduction. Because both the oxygen and hydrogen nuclei are so much more massive than the electrons we can neglect the motion of the electrons and approximate the interaction between hydrogen and oxygen simply in terms of the generalized Morse potential [7]. Analogous to the treatment of electrons in conventional solid state physics, we can describe the quantum motion of hydrogen in many solids and liquids as solutions of the many-body wave equation which take the form of energy bands. In any situation in which a particle moves in a periodic potential, the energy states of that particle are constrained to occur in "bands", i.e. groups of closely spaced discrete energy levels separated by "gaps" or forbidden energies. Each band contains the same number of states - equal to the total number of unit cells in the "lattice", i.e. the number of potential wells in the periodic structure. The gaps between bands arise from Bragg scattering conditions applied to the De Broglie waves of the particles. This has significant implications for the mechanical, thermal and electrical properties of hydrogen-bonded materials.

The lowest energy band is called the valence band. It is the valence band that is responsible for the structural stability of the material. Since protons are spin 1/2 particles, Fermi's exclusion principle allows two such particles (in opposite spin states) to occupy each energy level. In the case of water each unit cell (molecule) contributes two protons to the valence band. Therefore, as in the theory of electronic semi-conductors, we can see qualitatively that at absolute zero temperature water should be a proton insulator. All the potentially mobile protons would be in the valence band and this band would be full - a moderate potential difference is not able to change the energy level of (that is, to accelerate) these protons. At 0° K, the higher energy bands (the conduction bands) are all empty. As the temperature is increases, a small number of the protons from the valence band can be excited across the energy gap into the conduction bands.

As a first step in looking at the structure of water from the point of view a protonic semi-conductor we will estimate the magnitude of the energy gaps between the first few energy bands.

3 Morse Potential

Ignoring the detailed motions of the electrons, as in the theory of diatomic molecules, we can approximate the interaction between an excess hydrogen atom and a structural water molecule in the lattice in terms of the Morse potential [3]:

$$U_r(r) = -D_0 + D_0(1 - e^{(-a(|r|-r_e))})^2$$

where D_0 is the energy required to completely dissociate the $H_2O - p$ bond, a is the asymmetry parameter and $r[e]$ is the equilibrium value of r_p, the distance between the p and the centre of mass of the H_2O in H_3O^+.

We will consider the movement of a proton along a linear chain of water molecules. Taking account of the overlapping potential from the five nearest neighbors of each water molecule, the approximate potential energy barrier along the chain can be written as

$$F(x) = \sum_{k=-5}^{5} U_r\,(x + k\,d_{OO})$$

where d_{OO} is the mean Oxygen-to-Oxygen distance along the chain.

Bockris and Reddy[3] give the value of D_0 as the total hydration energy of a proton or about 266 kcal/mole or $11.543eV$. From spectroscopy studies, r_e for water (liquid) is estimated as 0.98 Angstroms and the oxygen to oxygen spacing is approximately $d_{OO} = 2.92$ Angstroms. By an iterative numeric procedure we can determine the value of the asymmetry parameter $a = 1.29455$, such that we obtain the approximate observed value of the cohesive energy of water.

It can be shown using these parameters that there is a significant departure of the potential $F(x)$ from the commonly employed harmonic oscillator potential. It is this difference which gives rise to the particular distribution of the hydrogen band gaps in water discussed below.

4 Band Gaps

In the "almost free" approximation, the size of the energy gap between the proton valence and proton conduction bands is given by degenerate perturbation theory as twice the value of the corresponding Fourier coefficient of the lattice potential (Burns, p257 [2]). The coefficients of the discrete Fourier transform of the lattice potential are given by

$$T(n) = \frac{\int_{-d_{OO}/2}^{d_{OO}/2} F(r)\, e^{\left(-2\,\frac{i\pi nr}{d_{OO}}\right)}\, dr}{d_{OO}}$$

for $n = 0, 1, 2, \ldots$

$T = [-4.8185, 11.297, 6.6585, 3.6722, 2.2436, 1.4942, 1.0607, .7898, .61, .48492, .39449]$

(The first band corresponds to $n = 1$).

Gosar and Pintar [6] estimate that the width of the energy bands as 2.2×10^{-3} eV which is much narrower than the band gaps. Note, however, that due to the asymmetry of the lattice potential, the width of the band gaps drops quickly as the energy level increases.

It is interesting to compare the spectrum of light emitted during sonoluminescence with the width of the proton band gaps. One speculative theory on the origin of sonoluminescence is that the alternating compression and de-compression cycles induced by the sound waves excite protons into the upper proton conduction bands. These protons lose energy and relax back to the valence band in quanta determined largely by the size of the band gaps. If this is the case, a cut-off in the luminescence spectrum will be found in the ultraviolet region at approximately 22.6 eV, that being the size of the lowest and largest band gap.

5 Two-Dimensional Proton Conductors

Stern and Howard [8] describe n-channel Metal-Oxide-Semiconductor Field Effect Transistors (n-MOSFET) in the following terms:

> An n-type inversion layer is produced at the surface of a p-type semiconductor when the energy bands near the surface are bent down enough that the bottom of the conduction band lies near or below the Fermi level. This band bending can be introduced by applying an electric field to the surface, in a configuration like that shown in FIG 1, ...
>
> The electric field associated with an inversion layer is strong enough to produce a potential well whose width in the z direction, the direction perpendicular to the surface, is small compared to the wavelengths of the carriers. Thus the energy levels of the electrons are grouped in what we call electric sub-bands, each which corresponds to a quantized level for motion in the z direction, with a continuum for motion in the plane parallel to the surface.

One of the aspects that makes this configuration interesting and useful as a amplifying device is that the density of charge carriers in the inversion layer can be controlled by the intensity of the electric field. The carrier density, in turn affects how the valence and conduction bands are populated as well as the Fermi energy. When the Fermi level is at or above the bottom of the conduction band, protons become highly mobile.

We would like to suggest that it is possible to produce a protonic semi-conductor analogue of this device. Further, as for a two dimensional electron gas, the density of energy states is a constant and the Fermi energy is proportional to the hydrogen atom density. Therefore, hydrogen density in the inversion layer increases with the strength of the applied potential and the kinetic energy of the hydrogen atoms increases more rapidly than Coulomb potential energy. It may therefore be possible to "tune" the occupation of the conduction band states so as increase the possibility of inelastic scattering due to matching lattice and nuclear states such as suggested by [11] in relation to a possible theory of the "cold fusion" phenomena.

The same two-dimensional effect is also expected in the so-called electrical double-layer central to much of electrochemistry. Bockris and Reddy [3] provide a detailed discussion of the structure of the electrical double-layer at the electrode-electrolyte interface. It may come as a surprise that there is considerable similarity between the charge distribution in MOSFETs and the structure of the double-layer. As a result we expect that the protons trapped in the approximately linearly varying electric field of the double-layer will have dynamics similar to the two-dimensional proton gas.

Good two-dimensional proton conduction and possible cold fusion effects have been reported in some crystal structures such as sintered oxygen deficient oxides $SrCe_{0.95}Yb_{0.05}O_{3-\alpha}$ [12], hydrogen uranyl phosphate $HUO_2PO_4 \cdot 4H_2O$ (HUP), and hydronium β''-alumina. Hydronium β''-alumina [4] is prepared by ion exchange in concentrated sulfuric acid with sodium β''-alumina. Despite the β''- designation, β''-alumina is not new crystalline form of alumina, rather it is a compound in which

consists of a structural backbone of close-packed $Al-O$ "spinel blocks" connected by $Al-O-AL$ columns with intervening ions suchs a Na^+ or H_3O^+. Sodium β''-alumina is also a good sodium ion conductor.

6 Conclusions

The possibilities for constructing devices that utilize the protonic semi-conductor properties of water and similar materials seem numerous. In particular, the quantum mechanical properties of hydrogen nuclei confined to a two-dimensional surface created by a potential gradient may give rise to novel proton/deuteron transport properties. These might include the possibility of matching lattice resonant states with nuclear states resulting in cold fusion.

The close analogy between electronic semi-conductors and protonic semi-conductors (as exemplified by aqueous electrolytes) makes it possible to transfer much of the enormous literature and theoretical results on semi-conductors to the behavior of protons in solution. This may well be a new and very fruitful area of research.

References

[1] Eigen M., De Maeyer L. "Self-dissociation and protonic charge transport in water and ice" Proc. Royal Soc. (London) Series A, v247, p505, 1958.

[2] Burns G., "Solid State Physics" Academic Press, 1985.

[3] Bockris J.O'M. and Reddy A.K.N. "Modern Electrochemistry" Plenum Press, 1970.

[4] Farrington G.C. and Briant J.L. "Hydronium Beta" Alumina: A Fast Proton Conductor" Mat. Res. Bull., v13, p763, 1978.

[5] Fletcher "The Chemical Physics of Ice" Cambridge University Press, 1970.

[6] Gosar P. and Pintar M. "H_3O^+ Ion Energy Bands in Ice Crystals" Phys. Stat. Solidi, v4, p675, 1964.

[7] Pauling L. and Wilson E. "Introduction to Quantum Mechanics" McGraw–Hill, 1935.

[8] Stern F. and Howard W.E. "Properties of Semiconductor Surface Inversion Layers in the Electric Quantum Limit" Phys. Rev. v163 (n3), p816, 1967.

[9] Putterman S.J. "Sonoluminescence: Sound into light" Scientific American, v272, n2, p46, February 1995.

[10] Grossweiner L. and Matheson M. "Fluorescence and Thermoluminescence of Ice" Journal of Chemical Physics, v22, n9, p1514, 1954.

[11] Li X. "The 3-Dimensional Resonance Tunnelling in Chemically Asisted Nuclear Fission and Fusion Reactions" Proceedings of the Fourth International Conference on Cold Fusion, ICCF4, v4, p2-1.

[12] Mizuno T, Enyo M, et. al. "Anomalous Heat Evolution from $SrCeO_3$ - type Proton Conductors During Absorption/Desorption of Deuterium in an Alternating Electric Field" Proceedings of the Fourth International Conference on Cold Fusion, ICCF4, v2, 14-1.

Fifth International Conference on Cold Fusion
9-13 April, 1995 - Monte Carlo, Monaco
ICCF5 ©1995

Centripetal de Broglie Wave Fields Connected to Particles at Rest Explain Cold Fusion and the Particle-Wave-Duality.

Olof SUNDEN
113 Rue d'Arbere, F-01220 Divonne, France.

1. Abstract

The controversy about Cold Fusion "CF" depends on the fact that the phenomena discovered are not in agreement with present physical theories, like QM and QED. The aim of this paper is to show that a. Time-Space-Oscillation `TSO' connected to matter is a physical perspective able to explain CF and the Particle-Wave-Duality, even able to propose technical means for further development. According to this perspective a particle -even at rest- is joined to a real, centripetal TSO, a 'de Broglie oscillation', instead of a mathematical Schrödinger wave function1). This TSO-field propagates with velocity c toward a focus, where the particle is created as a flickering wave vertex, that can push an instrument trigger. Particles and nuclides including their Coulomb barriers, thus become endowed with phase dependency and a centripetal wave field, that can interfere in slits. This explains the Particle-Wave Duality and why the Coulomb barrier can be tunneled under certain phase conditions.. This TSO-perspective further hints at nuclear reactions of a 'centripetal' kind different from those based on 'translational collisions', described by present high energy physics. It is worth consideration because it gives accurate accounts for physical constants, particle masses and charges, while the nuclides appear as focal resonance-shells, able to arrange acc. to Mendelejev.

2. Introduction

Present physics has been successful in accounting for its own mathematical images of matter, as quarks and gluons. But it has failed in accounting for real matter, for the nuclides. Various efforts to solve their wave functions have not given a useful image of matter. Neither has physics explained the riddle at its heart, the Particle Wave Duality nor Cold Fusion. Thus, the search for a more powerful physical perspective is justified in order to unveil the riddles of time-space-matter. The one presented here is not a new whim. It is in fact the very first scientific idea of time-space-matter, expressed by the Pythagoreans (Parmenides and Zenon of Elea) 2500 years ago. They considered time-space-matter as a. unified manifestation, caused by an oscillation between "the spheres" of time and space, that caused matter, including life and mind, to condense at the foci. This idea was not understood outside the Pythagorean esoteric sect, but it was scornfully rejected by Aristotle and finally eradicated as a heinous gnosticism by the Church in the 4th century AD [2].

3. The Universe - A System of 'De-Broglie' Time-Space-Oscillators.

If this out-cast-idea is considered in the light of present physical knowledge and experiences, a. remarkable, consistent world view appears. It yields causal and accurate accounts; 1) for Relativity and QM, 2) for our physical constants, 3) for all forces as phase shifts between time and space and 4) for an incessant 'gentle fission' of neutrons into protons and electrons with correct masses and charge only by aid of the TSO-arnplitudes plus c and nut simple arithmetic relations [3]. See Table.

The consideration of particles and nuclides as focal resonance-shells endows them and their Coulomb barriers with a phase dependency ($f=10^{24}\ s^{-1}$), due to which barrier-tunneling becomes possible for particles, when close to the phase of 'non-existence'. Huge translational velocities and extreme temperatures may not be Nature's only means to break the Coulomb barrier and cause nuclear fusion. Particles and nuclides can exchange energy and even fuse gently, if their centripetal TSO-waves are close to coincide and they are in the same phase. Then there is no initial translational energy and momentum to be conserved, which results in less active by-products (gamma-photons and neutrons) [4]. The consideration of nuclides as focal resonance shells enables the elaboration of a Mendelejev Periodic Table for nuclides, based solely on geometric principles. A Pauli exclusion principle is not required. In this way light is shed on present CF-phenomena, and those elements are identified (Pd, Ti, Ni, Be?), which can serve as Coulomb-shields and catalytic templates in CF.

4. Hidden Variables and Geometric Relations Revealed by TSO.

If Reality is described as a multitude of "De Broglie"-TS-oscillators [5], one has to specify the inherent energy of the unit oscillator, its wave length and amplitude components A_L and Aw. Considerations show, that an oscillator energy Eo, identical to the mass energy $Em=mnc^2$ of the neutron, yields the most accurate description. So we can depart from the known equations for mass energy and for harmonic oscillators acc. to (1a) and we then obtain the values given in (1b).

$$Em=mnc^2=hc/\lambda=Eo=mn\omega^2AL^2/2 \quad (\omega=2\pi c/\lambda) \qquad (1a)$$

$$\lambda=h/mc=13,19595x10^{-16}m \quad \text{and} \quad AL=\lambda/\pi\sqrt{2}=h/m(\pi c\sqrt{2})=2,970134x10^{-16}m \qquad (1b)$$

So the cosmic TS-oscillation toward the focus can be described by X the Compton wave length and by A_L a longitudinal constant amplitude component of 'time' here expressed in meter. But a transversal width or space component Aw is also required, forming a time-space-amplitude A_LAw. Aw has to start at the horizon as a space quantum ($Aq=2,226x10^{-56}m$, Eq. 13) and grows along the path by transfer of time quanta until it at the focus reaches its maximum $Aw\approx A_L$, forming a 'square' $Ao^2= A_LAw$. Inside the nucleus, Aw is finally transmuted to a time empl. AT, creating the conjugate realm of space - and of QM! The assumption that $Aw\approx A_L\approx 2,971x10^{-16}$ is correct only to 3 digits.

In order to endow quantum limitations to the 'classical oscillator' used here, the Planck length LP and time TP are introduced, Eqs 8-9). At first sight the Planck length seems not to have any connection to TSO. However, Eqs 10-11) show, that there exists a, profound not yet uncovered geometric relation between A and the Planck length LP, Also the oscillative force Fo, Eq. 3) appears as a geometrical phase shift it-2. By aid of this numerical relation the value of $Aw=2,97148x10^{-16}$ finally obtained, Eq. 4). These surprising numerical relations are the very key to a physics based on the TS-oscillation. They seem to violate our dimensional rules, but in fact they bring us into a physical system, where only time (inverse space) appears as the fundamental unit and dimension. In Eqs 15-20) some further implications of TSO are displayed, which show that our physical constants are geometrically related by recurrent factors ($\pi c\sqrt{2}$) and ($\pi^2 c$), and that A_L (time) and Aw (space) are differently related to mass, Eqs 1b & 4). It is surprising that the constants we know with least accuracy, G and h plus the size of 'universe' (the TS-oscillator) Y, appear with highest accuracy, Eqs 21-23) because they are determined by π, c and $Ao^2=A_LAw=8,825700x10^{-32}M^2$ Eq. 6).

5. Centripetal Nuclear Reactions - versus Translational Ones.

The fact that the mass relation $m_n/m_e=1838,4$ "without reason" appears in Eq. 12) as a factor $A=10^{24}(\pi\sqrt{c})^{-1}=1838.4$ ($10^{16}L_P$) has special bearing upon CF. At heart, it tells us that protons and electrons can be incessantly formed by centripetal fissions of neutron-oscillators ($n \Rightarrow p^+ + e^-$). But where is the mass difference 0,76 MeV, the neutrino and the gamma-radiation, required by present physics? And what about conservation of angular momentum, spin, parity, etc? Here the problem must be called in question. Do centripetal, catalytic nuclear transmutations incessantly occur at the nuclides without showing the conservation nuts and the reaction signs we are used to observe?

In the TSO-perspective it is plausible, that the phenomena connected with a centripetal neutron fission to proton and electron depend on a reorganization of the time-space-amplitude AwA_L before the Aw-component is transformed to time inside the nucleus. It can in simplified terms be described as follows. First a "strip" 1,4($10^{16}L_Pw$) wide and 1838.4 ($10^{16}L_{PL}$) long separates from the space amplitude Aw and adds to the time amplitude A_L, which thereby increases to $A_{LE}=1839,8(10^{16}L_{PL})=2,97239x10^{-16}m$, Eq. 14), while Aw decreases to 1837($10^{16}L_Pw$), an integer of the quantum. Then a second strip 1($10^{16}L_Pw$) wide and 1839,8($10^{16}L_Pw$) long separates, forming the electron with charge. As mass depends on Aw, Eq. 5) the neutron mass is based on the unchanged Aw=1838,4($10^{16}L_Pw$), Eq. 15-16), the electron on Aw=1($10^{16}L_Pw$), Eq. 17), the proton on the residual 1836($10^{16}L_Pw$), Eq. 18-19). Thus the first dissociated strip 1,4($10^{16}L_Pw$), directly transferred to time A_L, never appears as mass. As charge depends on A_L, Eq. 20), it instead causes an increase of $A_L \Rightarrow A_{LE}$ and causes charges to appear. So in a centripetal TSO-perspective not even $E=mc^2$ seems always to be true!

6. Conclusions

In the TSO-perspective, CF is a centripetal fusion of deuterons or protons, a concentric super-position of their time-space-waves, when they mutually are in the same phase and subject to an intense centripetal pressure, but free from any intense translational momentum. A translational or linear momentum will probably destroy the symmetry, necessary for a centripetal nuclear reaction, while an oscillative centripetal pressure may be of advantage, because it contributes to minor phase adjustments of the reactants. A bold prediction is that centripetal nuclear reactions will be favoured at temperatures close to 0°K, when thermal movements cease. Perhaps the world exists as it does due to en equilibrium between centripetal and translational energies. At low temperatures centripetal nuclear reactions are favoured and at extreme high temperatures translational ones, while in between only the gentle and incessant nuclear reaction occurs around complex nuclides ($n \Rightarrow p^+ + e^-$)

The phase and symmetry conditions thus required for CF, can be achieved by a symmetrical and 'Coulomb shielding' adhesion of two deuterons to a heavy 'template nuclide' having a radius of maximal 4 wave-lengths (the N-shell) and the utmost shell with 4 free positions for adhered deuteron-units. The Mendelejev nucleon matrix indicates that such nuclides are Pd, Ti, Ni and Be?. Then the heavier nuclide can function both as a. Coulomb shield and a catalytic template for fusing two symmetrically adhered deuterons. A requirement is that the two deuterons are exactly in the same TSO-phase and opposite (π) to that of the template-nuclide. Only then they can overcome the phase dependent Coulomb barrier to the template nuclide, only then the template nuclide can shield them from each other, and only then the fusion product (^{4}He) can separate from the template, as it is π out of phase to the template nuclide and can not fuse permanently with it. This phase-accordance will occur occasionally, but will be difficult to reproduce and control technically.

Another way to achieve these phase and symmetry conditions would be to use the sono-luminescence technique, i.e. to apply ultrasonic sound to gas microbubbles in water or heavy water, preferably in a "capillary" equipment. Also here we meet the requirement on phase unanimity, that makes the process occasional. But with an immense amount of bubbles in a limited reactor volume it seems possible to keep the reaction continuous. A test with ultra-sound applied to a capillary reactor continuously supplied with a liquid helium-hydrogen mixture at ≈0°K is proposed.

7. Cosmological and Futurity Aspects.

In CF-articles, the idea of halo-neutrons, virtual- and di-neutrons has frequently appeared [6,7]. As the unit TSO-oscillator is based on the energy of the neutron, a justified question is if TS-oscillations are possible, which are not focused and thus not appear as mass at certain points in space. This seems possible, if two neutrons are 'destructively' superposed on each other with a phase difference of π. But then they do not 'exist' according to present physical teachings!

This is true as far as we can not know of them, they do not emit light, and without energy focused to a point in space, we can not detect them. Nevertheless they and their energy may exist, non-localized and distributed over whole our universe. They are then identical to the missing, dark, matter of the universe and the cause of the zero-point energy. In fact their energy is nowhere and at the same time everywhere. It appears as real however, at every place, where a. centripetal focusing can be arranged. New matter with detectable mass is born once a di-neutron is centripetally focused in space. When a gamma-photon is transmuted to an electron-positron pair at the surface of a heavy nuclide, we observe a similar centripetal focusing of energy to a. point. The energy of the gamma photon is originally translational, not focused, but due to the centripetal action of the heavy nuclide the photon is focused to a point and thus materialized.

The technical path to the energy of the future may be our ability to arrange centripetal focusing of energy and particles, not our ability to achieve huge translational velocities by means of immense accelerators or extreme temperatures. The centripetal fusion of deuteron around Pd-nuclides may thus be e. first step on a new evolutionary path. The discovery of CF by Fleischman and Pons in combination with the pathological scorn showered upon them by the physical establishment may in the long run be of advantage. These events have made the future path more discernible to us.

Units and symbols used.

m = mass. $m_n = 1,67495 \times 10^{-27}$ kg	m_n, m_p, m_e = masses n, p, e
c = $2,997925 \times 10^{8}$ ms^{-1}	A, A_o, A_L, A_w, A_{LE} = amplitude components
G=grav. const.=$6,672 \times 10^{-11}$ Nm^{2}kg^{-2}	$A_L A_w = A_o^2$ = "time-space-amplitude"
h = Planck const. =$6,6262 \times 10^{-34}$ Js	A_w/A_L=k="space-time-elasticity"
λ=Compton wave-length =$13,19595\ 10^{-16}$m	acc=$A\omega^2$=oscill. acceleration ($\omega = 2\pi c/\lambda$)
$L_{Po}^2 = Gh/2\pi c^3 = 261,1378 \times 10^{-72}$m^2	F_o=oscillative (strong) force $F_o = m \times acc.$
$L_{Po} = 16,15977 \times 10^{-36}$m the Planck length	$T_{Po} = L_{Po}/c = 5,3903 \times 10^{-44}$m
$A_q = (L_{Po}/2\pi)^2/A_w$=quantum ampl.of transfer	$D = 10^{16} A_o/L_{Po}$=dissociation. $n \Rightarrow p^+ + e^-$
$Y = A_o^2/(L_{Po}/2\pi)^2$ "size" of oscillator/universe	$e^{\pm}$ = elementary charge

Physical units and relations revealed by the TSO-perspective.

$\mathbf{E_n = mc^2 = hc/\lambda = E_o = m\omega^2 A_L^2/2}$	$\lambda = 13,19595 \times 10^{-16}$ [m]		(1a)
$A_L = h/m_n(\pi c\sqrt{2})$	$A_L = 2,970134 \times 10^{-16}$ [m] $A_T = A_L/c$		(1b)
$\omega^2 = (2\pi c/\lambda) = 2c^2/A^2$	$acc = A\omega^2 = 2c^2A/A^2 = 2c^2/A_w$!		(2)
$\mathbf{F_{osc} = m_n \times acc. = 2m_n c^2 A_w = 0,1013211 \times 10^7}$	$\mathbf{F_{osc} = 10^7/(\pi^2)}$!		(3)
$\mathbf{A_w = 10^{-7} m_n (\pi c\sqrt{2})^2}$	$\mathbf{A_w} = 2,971480 \times 10^{-16}$ [m]		(4)
$F_o A_w/2 = F_o A_w$ (eff.)$= mc^2 = 10^7 A_w/2(\pi^2)$	$m = 10^7 A_w/(\pi c\sqrt{2})^2$		(5)
$A_L A_w = A_o^2 = 10^{-7} h\ (\pi c\sqrt{2})$ [m]	$A_o^2 = 8,825700 \times 10^{-32}$ $A_o = 2,970806 \times 10^{-16}$ [m]		(6)
$k = A_w/A_L = 10^{-7}\ m^2(\pi c\sqrt{2})^3/h = 1,00044$	$\sqrt{k} = A_o/A_L = 1,00022$ ($k_{el} = 1,00050$)		(7)
$L_{Po}^2 = Gh/2\pi c^3 = 261,1378 \times 10^{-72}$[m^2]	$L_{Po} = 16,15976 \times 10^{-36}$[m] ($T_{Po} = L_{Po}/c$)		(8)
$L_{Pw} = \sqrt{k} L_{Po} = 16,1633 \times 10^{-36}$[m]	$L_{PL} = L_{Po}/\sqrt{k} = 16,1560 \times 10^{-36}$[m]		(9)
$A_o^2 = 10^{48} L_{Po} T_{Po}/(\pi^2) = 10^{48} L_{Po}^2/(\pi^2 c)$	$L_{PL} = 10^{-24} A_L(\pi\sqrt{c})$		(10)
$A_o^2/L_{Po}^2 = 10^{48}/(\pi^2 C)$	$A_o^2/L_{Po}^2 = \mathbf{0,033797104 \times 10^{40}}$		(11)
$10^{-16} A/L_P = 10^8/(\pi\sqrt{c}) = D$ (n-fission)	$D = 10^8/(\pi\sqrt{c}) = \underline{1838,40} = m_n/m_e$		(12)
$A_q = (L_{PL}/2\pi)^2/A_w$	$A_q = 2,2260 \times 10^{-56}$ [m]		(13)
$A_{LE} = 10^{16} L_{PL} 1839,8 = 10^{32} L_{PL}/1837(\pi^2 c)$	$A_{LB} = 2,97239 \times 10^{-16}$[m]		(14)
m_n(kg)$= 10^7 A_w/(\pi c\sqrt{2})^2$	$m_n = 1,674952 \times 10^{-27}$kg	(1,674953)	(15)
m_n(MeV)$= 10^{19}\ A_w/\sqrt{10}$ approxim.	$m_n = 939,65$ MeV	(939,56)	(16)
$m_e = 10^{-1}\ A_o(\pi\sqrt{c})/(\pi c\sqrt{2})^2$	$m_e = 0,91090 \times 10^{-30}$ kg	(0,91091)	(17)
$m_p = 10^{-1}\ A_w \underline{1836}(\pi\sqrt{c})/(\pi c\sqrt{2})^2$	$m_p = 1,67275 \times 10^{-27}$ kg	(1,67265)	(18)
m_p(MeV)$= 10^{19} A_w 1836(\pi\sqrt{c})/\sqrt{10}$	m_p(MeV)$= 938,4$ MeV	(938,28	(19)
$e^{\pm} = 10^{40} A_{LE} T_{Po} = 10^{16} A_{LB} A_o(\pi/\sqrt{c})$	$e^{\pm} = 16,0221 \times 10^{-20}$ As	(16,0219)	(20)
$h = 10^7\ A_L A_w/(\pi c\sqrt{2}) = 10^7 A_o^2/(\pi c\sqrt{2})$	$h = 6,626184 \times 10^{-34}$ Js	(6,6262)	(21)
$G = 10^{-55}(\pi c\sqrt{2})^3(\pi c^2) = 10^{37} A_q c$	$G = 6,671882 \times 10^{-11}$	(6,672)	(22
$Y = A_o^2/(L_P/2\pi)^2 = 10^{48} 4/c$ (= A_L/A_q)	$Y = 1,334256 \times 10^{40}$ (λ)	$1,761 \times 10^{25}$ [m]	(23)

References

1) Jammer M. *The Philosophy of QM* p.44-54. John Wiley & Sons (1974)
2) Guthrie W.K. *A History of Greek Philosophy* p 300 Cambridge Univ. Press (1962-75)
3) Sunden O. "Time-Space-Matter..." *III Intern. Conf. on Space & Time* St. Petersburg (1994)
4) Sunden O. "Centripetal de Broglie waves explain..." *Cold Fusion* No 6 (1995).
5) De Broglie L.Journ. de Physique May 1927 and Bohm D. Cauality and Chance R&K (1957)
6) Hagelstein P. "A plethora of Miracles" *Cold Fusion Magazine* No 3 (1994)
7) Illert C. "Discovered halo nuclei" and Moon D. "Testing a theory" *Cold Fusion* No 6 (1995).

Session 5

Cathode Loading and Materials

Fifth International Conference on Cold Fusion
9-13 April, 1995 - Monte Carlo, Monaco
ICCF5 ©1995

MATERIALS/SURFACE ASPECTS OF HYDROGEN/ DEUTERIUM LOADING INTO Pd CATHODE

J. Minato, T. Nakata, S. Denzumi, Y. Yamamoto, A. Takahashi, H. Aida, Y. Tsuchida, H. Akita, and K. Kunimatsu
IMRA JAPAN CO. LTD.
2-3-6 Techno-Park Shimonopporo Atsubetsu-ku
Sapporo 004 Japan

ABSTRACT

Electrolytic hydrogen and deuterium loading into Pd and Pd-Rh alloys have been investigated applying various modes of surface modification: thiourea on Pd and Pd-Rh, Pd black on Pd and Pd-Rh and Pd-Rh deposit on Pd. From these systematic data role of the bulk and surface properties of the cathode in determining the maximum loading has been discussed. The cathode loading is improved for Pd and Pd-Rh with a surface modified by thiourea and Pd modified by Pd-Rh deposit, while reduction of the cathode loading was observed when the surface of the Pd-Rh alloy cathode was modified by Pd-black. These results show clearly importance of controlling the surface catalytic property of the cathode in controlling and improving the maximum cathode loading. It has been found that $D/Pd \geqq 0.95$ can be achieved reproducibly in electrolyte solutions containing thiourea at high concentrations. However, electrolysis in solutions containing thiourea can be conducted successfully only when the anode and cathode are separated by an ion exchange membrane in order to avoid the consumption of thiourea by anodic oxidation at the anode.

Application of partial deload/reload cycles to a Pd cathode in 1M-LiOD has led to improvement of cathode loading to the value between 0.9 and 0.95, but implication of such effects is not well understood yet in terms of the bulk and the surface properties of the cathode.

INTRODUCTION

Despite the well referred importance of attaining and maintaining high cathode loading in the generation of excess heat in the Pd/LiOD systems, no reproducible ways to achieve D/Pd> 0.95 has been known to date. It has been believed that there are some good Pd materials, the nature of which is unknown, which would guarantee such high loading under certain electrolysis conditions. While nature of such materials are scarcely understood, optimization of electrolysis conditions which leads to the highest loading for a given Pd material has been a target in the investigations of certain research groups. The effects of ordinary electrolysis conditions such as current density, cathode overvoltage and temperature, the difference between the acidic and alkaline solutions, isotope effect observed between the light water and the heavy water systems, cation effect observed in LiOH, NaOH, KOH and $(CH_3)_4NOH$, and surface modification by catalytic poison such as thiourea at its low concentrations have been fairly well understood [1].

Optimization of such ordinary electrolysis conditions, however, has been still unsatisfactory in achieving cathode loading higher than 0.95. The cathode material and its preparation as well as pretreatment is probably a key area to achieve successful loading. The issue is closely related to a fundamental question: " Is the successful loading determined by the bulk property of the palladium or the surface characteristics ? " The well known pretreatment of palladium samples by vacuum annealing followed by chemical etching in aqua regia has been successful in achieving cathode loading higher than 0.9 [2, 3, 4, 5]. But such combined pretreatment may change both the bulk as well as the surface properties of the palladium sample, and it is difficult to elucidate the role of the surface and bulk properties separately.

The purpose of the present report is to give some answer to the above question as to the respective role of the surface and the bulk property of the palladium in determining the high cathode loading. For this purpose we have conducted experiments to determine cathode loading of palladium and palladium-rhodium alloy in either 1M-LiOD or 2.8M-H_2SO_4 and 2.8M-D_2SO_4 by modifying their surfaces in various ways. The surface of the cathode was modified by thiourea, Pd/Pd deposited film and Pd-Rh deposited alloy film and their effect on the cathode loading was monitored. The results were interpreted in terms of the respective roles of the surface and the bulk properties on the cathode loading.

EXPERIMENTAL

Measurements of the cathode loading were conducted either in fuel cell type closed cells by monitoring the gas (D_2) pressure as described elsewhere [6] or in open cells by monitoring the electrical resistance change of the Pd cathode. The resistance change is defined as ratio R/R_0 where R and R_0 are the cathode resistance with and without absorbed hydrogen or deuterium respectively, and they were measured by AC four terminals method using a NF or HP milli-Ohm meter with 1kHz AC probe current of 1mA amplitude. The relation between R/R_0 and H/Pd or D/Pd to convert the measured resistance change to cathode loading were determined in a series of experiments in fuel cell type closed cells measuring simultaneously the cathode loading from gas pressure and the resistance change.

The surface modification by thiourea was possible in the limited concentration range only below 0.6 mM in fuel cell type closed cells due to its poisoning action on the fuel cell anode at higher concentrations [1]. In open cells, however, thiourea in the electrolyte is electrochemically oxidized at the platinum anode and its bulk concentration is reduced during electrolysis. The effect of surface modification is no longer maintained under such conditions. We have developed electrolysis method to separate the anode and the cathode compartments by an ion-exchange membrane which is practically impermeable to thiourea during a certain electrolysis period. It has been found that the cation exchange membrane Nafion can be successfully applied for such purposes in acidic electrolytes. We have conducted H(D)/Pd measurements of a Pd foil, 5mm × 20mm × 50 μm, in 2.8M-H_2SO_4 and D_2SO_4 with up to 1M-thiourea in a Pyrex glass cell separated to two compartments by a Nafion membrane which is held on a glass flange as shown in Fig. 1. The Pd foil was annealed in vacuum at 850℃ for 2 hours and then etched in freshly prepared H_2SO_4/HNO_3 mixture for ten minutes.

The surface of the Pd rod electrode was modified in two ways either by electrodepositing Pd-black or by forming a thin film of Pd-Rh alloy in order to see the effect of surface catalytic properties of Pd on the cathode loading. A thin film of Pd-Rh alloy was formed on the Pd surface by electrodepositing rhodium followed by alloying the surface region for 4 hours at 800℃ in a vacuum oven. The Pd-Rh alloy was selected because of its high electrolytic loading of deuterium at the rhodium concentration between 5-10%. It was thought that the results of electrolytic loading into such Pd cathode with a modified surface will answer to two questions: Is the good loading of the bulk Pd-Rh alloy due to its bulk property or the surface property ? Can we improve the

loading characteristics of Pd by adding a new surface with better catalytic properties ? The answers to such questions would be very useful in establishing the respective roles of the surface and the bulk of the cathode.

Modifying the cathode surface by Pd-black would be also useful in knowing the role of the catalytic property of the surface for the cathode loading. The deposition of Pd-black was conducted in 1M-HCl containing $PdCl_2$. A relatively smooth surface and rough one were prepared by controlling concentration of $PdCl_2$, and the surface area of the deposits were measured by conducting cyclic voltammetry between 0.4 V and 1.5 V(RHE).

RESULTS AND DISCUSSION

1. Cathode loading and the resistance change

Figures 2 and 3 show the relation between resistance ratio, R/R_o, and the cathode loading , H/Pd and D/Pd, measured for a ϕ 2mm×50mm Pd rod(99.99% up, Johnson Matthey) in fuel cell type closed cells in 1M-LiOH and LiOD containing 0.6mM-thiourea. The low cathode loading region was investigated potentiostatically allowing the loading process to reach steady state in order to avoid building up of non-steady state distribution of hydrogen/deuterium which affects the measured resistance of the cathode. The high cathode loading region was investigated either galvanostatically in 1M-LiOH or potentiostatically in 1M-LiOD after the potentiostatic measurements in the lower cathode loading region. Figure 4 presents a set of data recorded in 1M-LiOD with 0.6mM-thiourea to show the sequence of the applied overvoltage, current response, resistance ratio R/R_o and D/Pd measured from the gas (D_2) pressure in the curse of an entire measurement which took for this case over 5 months. The Pd electrode was set at 800mV/RHE to avoid deuterium absorption as well as electrochemical oxidation of thiourea at the palladium electrode before onset of deuterium loading which was initiated at 200mV/RHE for 10 days. The overvoltage was lowered to 100mV, 50mV and 0V spending 40, 20 and 30 days at each value to allow the absorption to reach equilibrium. As seen in Fig. 4, however, the absorption equilibrium was not reached in these time span at the positive overvoltages, but only at 0 mV the resistance ratio and the D/Pd reached steady value of 0.75 which is indicative of absorption equilibrium at the reversible hydrogen electrode potential under D_2 gas of ca 6atm. In the negative overvoltage region, however, the resistance ratio as well as D/Pd reached their respective steady value, and decrease of the resistance ratio accompanied by increase of D/Pd was observed up to the current density of 120mA/cm^2. Although the absorption equilibrium was not

established at positive overvoltages, we can assume that there is little concentration gradient of absorbed deuterium inside the Pd electrode in view of the electrode diameter, 2mm, and the time span spent during the measurement. This is an important point as such concentration gradient (decrease) from the Pd surface to its interior could give rise to a lower resistance than the value corresponding to homogeneous deuterium distribution in the Pd electrode [7].

The present results thus obtained spending 5 months are almost in agreement with the previous data reported by various groups [8, 9, 10, 11] as shown in Figs. 2 and 3. Because the data of the cathode loading was available up to H/Pd and D/Pd around 0.9 in the present study, curve fitting was applied by using a fifth order polynomial to obtain the relation between R/R_o and the cathode loading between 0.9 and 1.0. The extrapolated curves are almost consistent with the data reported by Baranovsky et [10] al under high pressure of hydrogen and deuterium. It is important to mention the difference between the R/R_o vs D/Pd relation to be employed in our study and the similar relation frequently employed by the group at SRI [12, 13, 20]. Figure 5 compares the three curves to show the R/R_o vs D/Pd relation, which show that all the three curves almost coincide at D/Pd=0.9, below which our curve gives higher D/Pd than other two curves reported by SRI, while lower D/Pd by a few percent would be obtained above D/Pd=0.9. It is confusing a little bit for different groups to apply different calibration curves in the calculation of D/Pd from the measured R/R_o, and it is necessary to keep this in mind when interpreting cathode loading data obtained by resistance measurements.

2. Effect of surface modification by thiourea

Figure 6 shows a series of R/R_o data for a Pd foil in 2.8M-D_2SO_4 containing thiourea, $(NH_2)_2C=S$, of 0, 0.3mM. 3mM, 30mM, 300mM and 1M measured at 20℃ for a series of applied electrolysis current density up to 500mA/cm^2. Upon addition of thiourea the initial peak of R/R_o becomes more prominent with its increasing concentration and the R/R_o value becomes lower for a given current density. Magnification of the initial change of the R/R_o for the series of concentrations at 30mA/cm^2 shown in Fig. 7 demonstrates the marked effect of surface modification by thiourea. Figure 8 shows dependence of D/Pd on current density for a series of 2.8M-D_2SO_4 containing up to 1M-thiourea, and it demonstrates marked effect of thiourea to give D/Pd of 0.96 at 500mA/cm^2 in a solution containing 1M-thiourea. Dependence of the cathode loading on the concentration of thiourea at a constant current density, 500mA/cm^2, is shown in Fig. 9 both for H_2SO_4 and

D_2SO_4 solutions, which shows a systematic effect of surface modification by thiourea on the cathode loading, and H/Pd of 0.99 can be achieved according to this data. The current dependence of H/Pd is shown in Fig. 10, which again demonstrates marked improvement of the cathode loading upon addition of thiourea in 2.8M-sulfuric acid.

The data presented in Figs. 6-10 to show the marked effect of the surface modification by thiourea strongly suggests that the cathode loading can be controlled primarily by modifying the surface property of the cathode. Although we do not know the microscopic mechanism of the surface modification, deactivation of the Tafel step to recombine two adsorbed deuterium atoms to form a molecule is certainly what happens upon addition of thiourea. This is understood in terms of the overvoltage of the Tafel step, η_2, which is related to the chemical potential of absorbed hydrogen atoms according to the relation;

$$\mu_{H(abs.)} = \mu_{H_2} - 2F\eta_2.$$

Existence of the second term in the right hand side of the above equation demonstrates advantage of the electrolytic cathode loading compared to the gas phase loading for which we have the first term, chemical potential of the hydrogen gas, only. The advantage can be interpreted in terms of effective pressure or fugacity of the hypothetical hydrogen gas which is in equilibrium with the absorbed hydrogen to have the chemical potential given by the above equation [14].

$$P_{H_2}^*/P_{H_2} = \exp(-2F\eta_2/RT),$$

where P_{H_2} and $P_{H_2}^*$ are the actual pressure of the hydrogen gas in the electrolytic cell and the effective pressure operating under cathodic polarization.

It should be mentioned that thiourea acts as a catalytic poison of the Tafel step by adsorbing on the cathode surface, and the adsorption appears to be reversible, i.e., not chemisorption upon which adsorbed molecules usually decomposes to form a strongly adsorbed species. This is inferred from the fact that effect of thiourea cannot be maintained if the anode and the cathode compartments are not separated by the ion-exchange membrane. The Fig. 11 shows a typical example to show the gradual loss of the effect of thiourea during electrolysis in a cell which has the anode and the cathode in the same compartment. The decrease of the resistance ratio $R/R_\bullet$ after passing through the maximum upon applying electrolysis current, $50mA/cm^2$, is followed by the gradual increase due to desorption of absorbed hydrogen, which is more prominent in the sulfuric acid containing thiourea at lower

concentrations. Thiourea is electrochemically oxidized at the platinum anode leading to deterioration of the bulk concentration which causes desorption of the adsorbed thiourea molecules and simultaneously desorption of absorbed hydrogen atoms.

3. Surface modification of Pd-Rh alloy cathode by Pd-black

Pd-Rh alloy has better electrolytic hydrogen/deuterium loading characteristics than palladium as we reported at ICCF4. We have tried to find if the better cathode loading of the alloy is controlled by its bulk or the surface property. For this purpose we have conducted experiments applying surface modification by Pd-black to see if the cathode loading of the alloy could be maintained with a thin layer of the Pd-black on its surface. Measurements were conducted in a fuel cell type closed cells as described elsewhere. Pd-Rh(10atm.%) was selected for the experiments in view of its highest cathode loading characteristics of all the Pd-Rh alloy cathodes investigated up to 30atm% Rh [15]. A thin layer of the Pd-black was deposited in either 0.1wt% or 2 wt% $PdCl_2$ in 0.1M-HCl at 12.5mA/cm^2 for 15 min., the former being for obtaining high surface area and the latter smooth Pd-black deposited layer. In fact surface area of 429.2 cm^2 and 6.4 cm^2 were obtained in this manner for the geometrical surface area of 2.7 cm^2(ϕ 4mm×20mm), which were determined by conducting cyclic voltammetry between 0.4 V and 1.5 V in 0.5M-H_2SO_4. After loading experiments, however, these surface area changed to 150cm^2 and 12cm^2, respectively, i.e., the rougher surface became a little bit smoother and the smooth surface rougher.

Figure 12 compares the dependence of D/M(Pd+Rh) on overvoltage for Pd, Pd-Rh(10atm%), Pd-Rh(10atm%)/Pd(150cm^2) and Pd-Rh(10atm%)/Pd(12cm^2). Addition of the Pd-black layer on the surface degrades the loading characteristics of the alloy cathode according to these data, and D/M of the alloy with modified surface lies between Pd-Rh(10atm%) and Pd. The difference in the surface roughness of the Pd-black on the alloy surface has not caused significant change in the loading characteristics. It is interesting to note that dependence of the cathode loading on overvoltage presented in Fig. 12 show tendency to saturate at high overvoltage, i.e., higher than ca −800 mV. In other words, the increase of the total cathode overvoltage in this region is not contributing to increase in the cathode loading. This is interpreted in terms of the constituent overvoltage of the Tafel step which is almost invariant at high current densities despite the rapid increase of the total cathode overvoltage.The Tafel lines recorded for these cathodes simultaneously with the cathode loading are shown in Fig. 13, and indeed the slope of them become steeper at high current densities. The steep increase of the cathode

overvoltage is caused not by the increase of the overvoltage of the Tafel step but of the discharge step of the hydrogen evolution reaction in the alkaline solutions, which is discharge of water molecules combined with discharge of Li^+ ions according to the post-surface analysis of the Pd electrode as described later.

The data presented in Fig. 12 suggests clearly that the cathode loading is strongly influenced by the surface property of the cathode but at the same time the bulk property is still a key factor to determine the cathode loading.

4. Surface modification of Pd by Pd-Rh alloy film

We then tried to add a thin film of Pd-Rh alloy on a Pd surface to see if the loading characteristics of the Pd could be improved by modifying its surface with a Pd-Rh alloy film, which was formed by depositing Rh on the Pd surface in 0.5M-H_2SO_4 containing 1mM-$Rh_2(SO_4)_3$ at 12.5mA/cm^2 for 15 min. followed by annealing /alloying at 850℃ for 2 hours in vacuum. Figure 14 shows the Auger depth profile of Pd and Rh before (A) and after (B) the annealing treatment. Sputtering rate is 6 nm/min and 13 nm/min before and after 300 min, respectively. According to the depth profile the thickness of the Rh deposit is ca 600 nm, while alloying extends into the Pd substrate up to 3.1 μm after the annealing treatment with continuous change of Rh concentration from ca 30% near the surface to several % in this region. Figure 15 shows dependence of D/M on overvoltage for this Pd electrode with the modified surface, and we can see that the loading characteristics is greatly improved at high cathode overvoltage compared to Pd electrode, but is not as good as Pd-Rh(10atm%). The data presented in Fig. 15 again demonstrates importance of the surface catalytic property as well as bulk property of the cathode substrate to accommodate absorbed deuterium.

5. Surface modification of the cathode by electrolysis products in LiOD

It has been frequently recognized that the cathode surface is subjected to *in-situ* modification or contamination by electrolysis products such as Li or platinum deposits during electrolysis in LiOD. In many experiments conducted in cells made of pyrex glass the dissolution of the glass components inevitably leads to accumulation of such materials on the cathode and the anode surfaces. Effect of these *in-situ* modification of the cathode surface has not been understood to any satisfactory extent due to absence of systematic studies.

We have conducted a series of XPS and SIMS analysis of the surface and near surface region of Pd samples which have been

subjected to a long term loading experiments in 1M-LiOD in quartz cells at 20 ℃, D/Pd having been monitored by resistance measurements, and tried to relate the cathode loading data and the results of these surface analyses. Figure 16 presents a set of XPS spectra for a Pd sample taken after various sputtering times by Ar^+: 0, 60 and 300 sec, respectively, which shows almost no sign of Pd but strong Pt bands for the unsputtered sample. But as sputtering proceeds the Pt bands intensity decrease drastically with development of Pd bands dominating the entire spectrum. The ratio Pt/Pd on the surface was determined from the narrow spectra of Pt and Pd for six Pd samples, O-1 to O-6, and is summarized in Table 1. The ratio varies from sample to sample, the largest and the smallest values being 50.4 and 0.6, respectively. The data indicates that the surface of the Pd cathodes are heavily contaminated by platinum, the origin of which being most likely the platinum anode or the four Pt leads welded to the Pd cathode for the resistance measurements. It is possible to relate the large variation of the surface Pt/Pd ratio of the samples to their electrolysis history if we classify the samples to two groups: one having the Pt/Pd ratio smaller than 1 and the other with the ratio larger than 10. All the samples were initially subjected to cathodic polarization at 300mA/cm^2, but the following electrolysis history was quite different between the two groups of samples with the large and the small Pt/Pd ratio. Figure 17 presents typical electrolysis history of the two groups as represented by the change of cathode resistance ratio with the applied current density during electrolysis which lasted for nearly fifty days. The group of the samples with the large Pt/Pd ratio was subjected to repeated load/deload cycles as shown by A while the other group of Pd samples underwent an unexpected resistance increase around 25th days which is indicative of deloading and did not experience the repeated load/deload cycles as shown by B. Dissolution of platinum from the Pt anode would depend on the total length of time of electrolysis at 300mA/cm^2, which is in fact almost the same for the electrolysis histories A and B as shown in Fig. 17. This suggests that dissolution of platinum from the Pt anode cannot explain the large difference of the surface Pt/Pd ratio, while dissolution of platinum from the Pt leads welded to the Pd cathode during the repeated deloading conducted by applying +1.5 V to the cathode is more likely responsible to the larger surface Pt/Pd ratio.

Figures 18 and 19 show the depth profile of Li and Pt respectively observed by SIMS for the six Pd samples described above. Comparison of the depth profile of the Pd sample before electrolysis, O-7, with the others, O-1 to O-6, clearly demonstrates that these depth profiles of Li and Pt deposits have been developed near the surface during electrolysis, although the quantitative difference of these depth profiles among the six samples is not well

interpreted in terms of their electrolysis history. We can note that both Li and Pt concentration drops sharply within 20-30 nm from the surface and that their depth profiles are closely related to each other if we take samples O-1 and O-7 for example. The quantitatively close relation, however, is not well understood at the moment. The apparent presence of a maximum in the Li depth profile near the surface around 10-20 nm is probably either an artifact in the SIMS analysis due to adsorbed oxygen, as the primary ion being O_2^+, or due to loss of the surface Li upon washing by water after the electrolysis.

All the data shown in Figs. 16 and 19 and in Table 1 are indicative of heavy contamination of the surface region of the Pd cathode by Li and Pt deposits as previously reported by other groups [16, 17, 18], but interpretation of the loading data in terms of the surface contamination is not straightforward.

In the case of Li, however, comparison of the cathode loading data in 1M-LiOH and 1M-$(CH_3)_4NOH$, which is alkali metal free alkaline solution, clearly demonstrates, as shown in Fig. 20, however, that presence of the lithium deposit in the surface layer is not contributing to improving the cathode loading since the data observed in the lithium-free system is as good as or even better than the cathode loading in LiOH [1].

The platinum deposit which accumulates on the cathode surface during electrolysis has been considered to reduce the cathode loading since it would catalyze the Tafel step to enhance hydrogen desorption out of the palladium cathode. Comparison of the loading data observed in the open cells with an Pt anode and fuel cell type closed cells is interesting in discussing the role of the surface contamination by Pt since in the latter cells the surface Pt/Pd ratio is much smaller than in open cells as shown in Table 2. Figure 21 shows results of such comparison of the cathode loading data for the JM Pd(99.99%up) pretreated by the same procedure: mechanical polishing, degassing in vacuum at 200℃ for 3 hours, and chemical etching in freshly prepared HNO_3/H_2SO_4 mixture for 10 min. The results show, however, that D/Pd in open cells is a few % higher than in the fuel cell type closed cells, i.e., the less contaminated system by platinum gave rise to lower cathode loading. We can conclude that the surface contamination by platinum is not playing a key role in the series of present loading experiments. Presumably there is some other unknown factors which are playing more important role in suppressing the maximum loading level than the surface contamination by platinum.

6. Improvement of the cathode loading by load/deload cycles

Improvement of cathode loading by repeated load/partial deload cycles was reported recently for Pd wires with palladized surface which were subjected to preloading in gas phase before electrolytic loading [19]. But because determination of the cathode loading was conducted volumetrically by using water filled manometer, two possible sources of error are envisaged: firstly, the apparent increase of cathode loading detected volumetrically may be due to hydrogen or deuterium trapped in internal voids or micro cracks created by the load/deload cycles, secondly contamination by H_2O from the manometer the rate of which was estimated as 0.13% a day could contribute to the apparent D/Pd increase during the load/deload cycles which lasted for 1-2 weeks.

The effect of repeated deload/reload cycles was also indicated for a Pd rod of 3 mm diameter with a smooth surface more recently by applying resistance measurements [20], although the detailes of the study was not reported.

We have conducted similar measurements to see the effect of applying load/deload cycles on the cathode loading in open cells made of quartz glass. In order to avoid the problems described above, however, the cathode loading was monitored by resistance measurements which would not be affected by increase of absorbed hydrogen or deuterium trapped in the internal voids or micro cracks, while the cell was kept purged by dry boil-off nitrogen above the electrolyte solution to avoid H_2O contamination the level of which was determined by NMR before and after the loading experiments.

Figure 22 presents a typical example to show the resistance change of the JM Pd(99.99%up) cathode and electrolysis current during the entire period of experiment to see the effect of load/deload cycles. The current density was increased in a step wise manner up to 1 A/cm^2 and then decreased to zero at which deloading proceeded for 5 days until D/Pd decreased down to 0.572, and then reloading was conducted at 0.3 A/cm^2. By this first deload/reload cycle the D/Pd at 0.3 A/cm^2 reached 0.919 while it was 0.893 before applying such cycle. The cycle was repeated for several times as shown in Fig. 22 and further improvement of the cathode loading was recorded. Figure 23 presents result of such deload/reload procedure for two samples, which shows that the effect of such deload/reload cycles observed for the two samples almost saturated after applying two cycles. The effect of the deload/reload cycles and the tendency for the effect to saturate was commonly observed for other Pd materials with different purities ranging from 99%up to 99.99%up and with different heat treatment, i.e., either cold worked or annealed at 850℃, from other sources, and the maximum D/Pd achieved after applying the deload/reload cycles lies between 0.90 and 0.95 which varies from sample to sample. The fact that the effect of deload/reload cycles is

commonly observed for Pd materials with different bulk properties especially with different heat treatments suggests that the cycle is giving rise to some change in the surface catalytic property to control the desorption of absorbed deuterium.

Because this was confirmed by the resistance change of the cathode the observed improvement of the cathode loading is not caused by trapping of hydrogen/deuterium in the internal voids or micro cracks possibly created in the cathode upon applying deload/reload cycles.

The deloading in the above experiments was conducted simply by switching off the electrolysis current for a few days, during which period the D/Pd decreased to around 0.6. We then tried to find effect of degree of deloading on the improvement of the cathode loading after reloading at 300 mA/cm^2. The degree of deloading was adjusted either by controlling the time at zero current before the reloading or by applying anodic current to the Pd cathode for a given time to enhance deloading. Figure 24 presents a set of data obtained for ten JM Pd samples which shows the relation between the D/Pd before reloading and the D/Pd after reloading at 300 mA/cm^2. The data suggests that it is necessary to deload the Pd cathode below D/Pd=0.6～0.7 for the effect of deload/reload cycle to develop and that the effect appears to increase as the cathode is more deloaded until D/Pd=0.40～0.6 is reached. What these findings mean is not clear at the moment, but it looks as if it were necessary for the cathode to go into the $\alpha \rightarrow \beta$ transition region during the deloading process for the effect of deload/reload cycle to start developing.

There is a problem in interpreting the data corresponding to complete or near complete deloading in Fig. 24 that Pd cathodes sometimes undergo irreversible change in its size when it is subjected to such heavy deloading. The estimation of D/Pd from the resistance measurements is no longer reliable when such change in the cathode size is accompanied with the deloading process. We checked actual size change of the cathode as a function of the cathode loading by measuring the change in the cathode length during the load/deload processes. Figure 25 presents a pair of data of two experiments using JM Pd rods(ϕ 2mm×40mm, 99.99%up) to show % change in cathode length with respect to the original one during the load and deload processes. We can note that the cathodes become longer as loading increases with different rates for a unit increase of D/Pd below and above D/Pd = 0.58 : 1% and 3.8%, respectively, while the cathode length is reduced almost linearly during the deloading process at the same rate, 3.8%, until the complete deloading. There is a marked hysteresis in the size change below D/Pd=0.58 and this would give rise to irreversible resistance change of the cathode if the cathode is deloaded below this level. In view of this results all the data presented in Fig. 24

for D/Pd before reloading below 0.2 would be suffering from the irreversible size change and the D/Pd after reloading for this region would be actually lower than plotted by at least ca 1.6 %.

The region above D/Pd=0.58 corresponds to the so-called β phase, in which the change of the cathode length is completely reversible as demonstrated in Fig. 26 for the three consecutive load/deload cycles above D/Pd=0.6. Apart from the reversible change it is interesting to note that the cathode becomes longer accompanied by increase of D/Pd as the cycle is repeated. This is an independent proof obtained by the monitoring of the cathode length to confirm the effect of deload/reload cycles on the loading. The rate of the length change in the β phase region is 3.8 % with respect to an unit increase of D/Pd, and this is close to the rate 4.4% predicted from the lattice constant data [21] assuming an uniform lattice expansion in the Pd cathode, as shown in Fig. 25, while the rate experimentally observed during the loading process below β phase region which is considerably smaller than the rate in the β phase suggests strongly that the cathode expands originally much more along the radial direction than the direction along the rod axis.

Finally NMR analysis of the 1M-LiOD used in the above experiments was conducted to see the level of contamination by light water which might affect the long term resistance measurements in the electrolytic cells as increase of H/D in the cathode would contribute to lowering its resistance, which will be interpreted misleadingly in terms of apparently higher cathode loading. Figure 27 shows a set of data to show the NMR analysis of 1M-LiOD before pre-electrolysis, after pre-electrolysis, after electrolysis in open cells, and after electrolysis in fuel cell type closed cells. The atomic ratio H/D in the electrolyte becomes slightly smaller after pre-electrolysis, but is markedly reduced after prolonged electrolysis in open cells, while no such reduction in H/D was not observed in the fuel cell type closed cells. These results confirm effectiveness of pre-electrolysis and electrolysis in open cells in reducing the light water level in the electrolyte due to the preferential hydrogen evolution at the Pd cathode, while in the fuel cell type closed cells no such reduction is to be expected as the evolved hydrogen goes back to the electrolyte by electrochemical oxidation at the fuel cell anode. In conclusion the improvement of the cathode loading by applying the deload/reload cycles is not an artifact caused by light water contamination during the long term electrolysis.

Practically it is very important to maintain the improved cathode loading at high current densities as the high D/Pd at high current densities is the necessary condition for the excess heat generation according to the previous data of various groups [13, 22, 23]. Figure 28 presents an example to show the dependence of

D/Pd on current density before and after the improvement of the cathode loading by applying the deload/reload cycles. The improved cathode loading is maintained at high current densities giving rise to a new dependence of D/Pd on current density. Addition of 100 ppm Al appears to improve the cathode loading at higher current densities as reported before [20].

In conclusion the improvement of the cathode loading by applying the deload/reload cycles could be an effective way to establish the necessary condition for excess heat generation.

7. Cathode loading in 1M-LiOH

We conducted H/Pd measurements in 1M-LiOH in order to understand the problem encountered in achieving the high cathode loading in 1M-LiOD is really specific to the heavy water system. Two experiments were run for this purpose in similar cells made of quartz glass using JM Pd(ϕ 2mm×40mm, 99.99%up) cathodes which were mechanically polished, cleaned, chemically etched, and degassed in the same procedure as described already. Figure 29 presents a pair of data to show change of the cathode resistance ratio with the applied current density. Electrolysis was initiated at 30 mA/cm^2, upon which the resistance ratio goes through a sharp maximum as predicted from Fig. 2 and becomes a steady value around 1.5. With further increase of the current density the ratio goes down continuously, which is indicative of further increase of the cathode loading. Figure 30 presents dependence of H/Pd on current density determined from the data in Fig. 29. H/Pd of 0.97 is achieved at 500 mA/cm^2, and it is very likely that higher loading would be achieved at higher current densities as there is little tendency for H/Pd to saturate.

The data in 1M-LiOH strongly suggests that the difficulty encountered in the cathode loading in LiOD is really specific to the heavy water system as reported before [3].

8. Conclusion

There are still unknown factors related to the bulk and/or surface properties of the cathode to control its maximum loading by deuterium. We have found out at least two systems which guarantee the cathode loading higher than 0.95, the one being Pd-Rh alloys containing 5-10 atm% rhodium and the other Pd in 2.8M-D_2SO_4 containing 1M-thiourea. The deload/reload cycles certainly improves the cathode loading to get it higher than 0.9 but less than 0.95.

The results reported in the present study strongly indicate that the surface property of the palladium cathodes essentially controls

the maximum loading level apart from modifying the bulk property by alloying with rhodium. The detailed picture of such surface to enhance the cathode loading, however, is not clear yet at the molecular level.

References

1. H. Akita, Y. Tsuchida, T. Nakata, A. Kubota, M. Kobayashi, Y. Yamamoto, N. Hasegawa, N. Hayakawa and K. Kunimatsu, Proceedings of ICCF4, vol. 1 p 21-1, Electric Power Res. Inst. Palo Alto California, 1994.
2. T. A. Green and T. I. Quickenden, J. Electroanal. Chem., 368(1994)121.
3. T. A. Green and T. I. Quickenden, J. Electroanal. Chem., 389(1995)91.
4. M. C. H. McKutre, R. Rocha-Filho, S. I. Smedley, F. Tanzella, S. Crouch-Baker, T. O. Passell and J. Santucci. Proceedings of ICCF2 "The Science of cold fusion" p 419, T. Bressani, E. Del Guidice and G. Preparata (Eds.) SIF Bologna, 1991.
5. H. Okamoto, T. Sano, Y. Oyabe, T. Terazawa and T. Ohi, ICCF5 Book of abstracts p 505, Monte-Carlo, Monaco 1995.
6. K. Kunimatsu, N. Hasegawa, A. Kubota, N. Imai, M. Ishikawa, H. Akita, and Y. Tsuchida, Proceedings of ICCF3 " Frontiers of Cold Fusion" Ed. by H. Ikegami, Universal Academy press Inc. 1993, p 31.
7. T. Nakata, A. Kubota and K. Kunimatsu, Abstracts of '93 Fall meeting of the Japanese Electrochem. Soc., Fukuoka p 255. Abstracts of the 61st annual meeting of the Japanese Electrochem. Soc., Sendai, p 309.
8. T. B. Flanagan and F. A. Lewis, Z. Physik. Chem., 27(1961)104.
9. J. C. Barton, F. A. Lewis and I. Woodward, Trans. Faraday Soc., 59(1963)1201.
10. B. Baranowski, F. A. Lewis, W. D. Mcfall, S. Filipek and T. C. Witherspoon, Proc. Royal Soc. London A 386(1983)309.
11. A. W. Szafranski and B. Baranowski, Phis. Stat. Sol. (a) 9(1972)435.
12. M. C. H. Mckubre, R. C. Rocha-filho, J. Chao, B. Chexal, T. Passel and J. Santucci, Proc. of the 1st Ann. Conf. on Cold Fusion 1991 p 20.
13. M. C. H. McKbre, S. Crouch-Baker, R. C. Rocha-Filho, S. I. Smedley and F. L. Tanzella, T. O. Passel. and J. Santucci, J. Electroanal. Chem., 368(1994)55.
14. T. Maoka and M. Enyo, Electrochim. Acta, 26(1981)607.
15. Y. Yamamoto, N. Hayakawa and K. Kunimatsu, Abstracts of '94 Fall meeting of the Japanese Electrochem. Soc., Yokohama, p 183.
16. O. Yamazaki, H. Yoshitake, N. Kamiya and K. Ota,

J. Electroanal. Chem., 390(1995)127.
17. M. Nakada, T. Kusunoki, M. Okamoto and O. Odawara, Proc. of the ICCF3 "Frontiers of Cold Fusion" Ed. by H. Ikegami, Univ. Acad. Press Inc. 1993 p 581.
18. D. R. Coupland, M. L. Doyle, J. W. Jenkins, J. H. F. Notton, R. J. Potter and D. T. Thompson, Proc. of ICCF1 p 299.
19. F. G. Will, K. Cedzynska and D. C. Linton, J. Electroanal. Chem., 360(1993)161.
20. M. C. H. McKubre, B. Bush, S. Crouch-Baker, A. Hauser, N. Jevtic, S. Smedley, M. Srinivasan, F. Tanzella, M. Williams, and S. Wing, Proc. of ICCF4 vol. 1 5-1.
21. J. E. Schirber and B. Morosin, Phys. Lett. B 12(1975)117.
22. M. C. H. Mckubre, S. Crouch-Baker, A. M. Riley, S. I. Smedley and F. L. Tanzella, Proc. of ICCF3 "Frontiers of Cold Fusion" Ed. By H. Ikegami Univ. Acad. Press Inc. 1993 p 5.
23. N. Hasegawa, N. Hayakawa, Y. Tsuchida, Y. Yamamoto and K. Kunimatsu, Proc. of ICCF4 p 3-1.

Table 1 Surface Pt/Pd ratio determined from the XPS narrow spectra of Pd cathodes(JM 99.99% up, ϕ 2mm × 40mm) after prolonged electrolysis in 1M LiOD in open cells made of quarz glass.

	O-1	O-2	O-3	O-4	O-5	O-6
Pt/Pd	50.4	11.6	0.8	11.0	12.7	0.6

Table 2 Surface Pt/Pd ratio determined from the XPS narrow spectra of Pd cathodes after long term electrolysis in 1M LiOD in fuel cell type closed cells.

	F-1(white spot)	F-1(black spot)	F-2(white spot)	F-2(black spot)
Pt/Pd	0.27	0.05	0.19	0.02

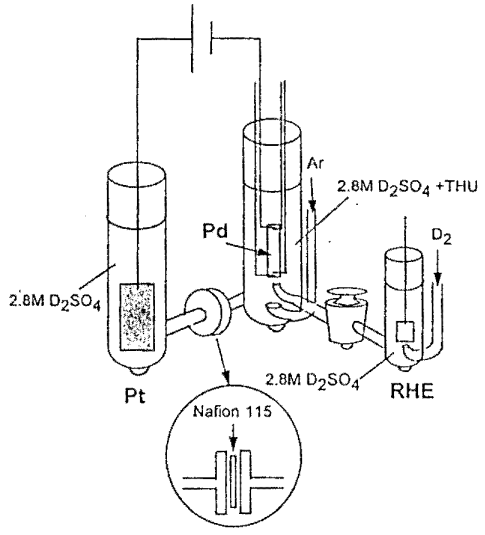

Fig. 1 Electrolysis cell to separate the cathode and the anode compartments by cation exchange membrane Nafion 115.

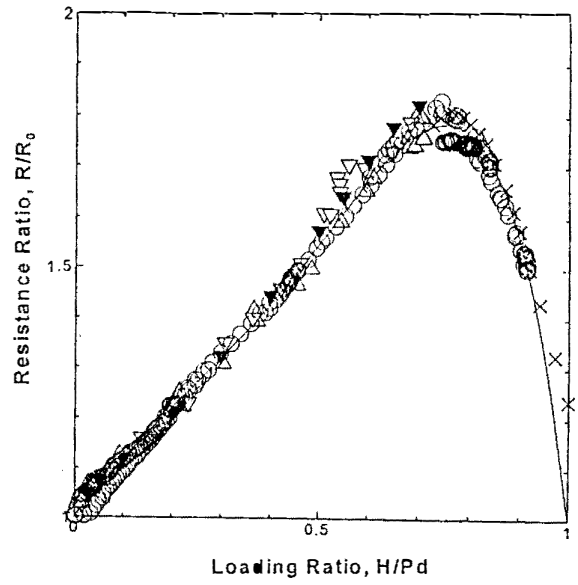

Fig.2 Cathode resistance ratio vs. H/Pd relationship obtained in the present study in 1M-LiOH at 20° C (○), Lewis et al., 25° C (△▽▼), Baranowski et al., 25° C (×).

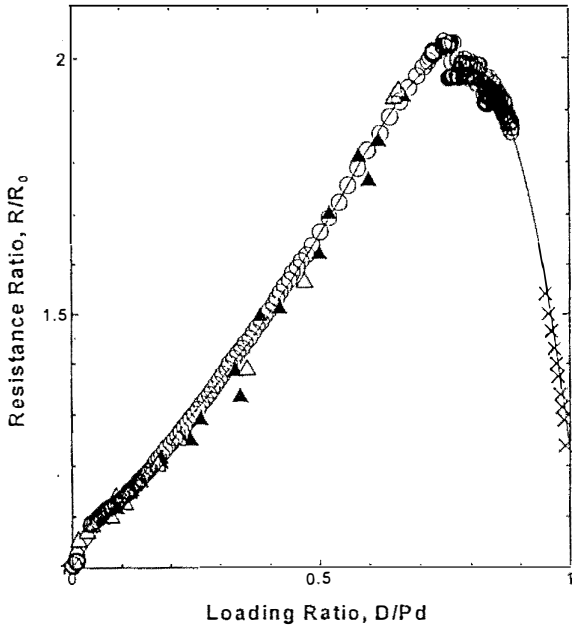

Fig.3 Cathode resistance ratio vs. D/Pd relationship obtained in the present study in 1M-LiOD containing 0.6mM thiourea at 20° C (○), Sieverts & Danz, 25° C (▲), Flanagan & Lewis, 25° C (△), Baranowski et al., 25° C (×).

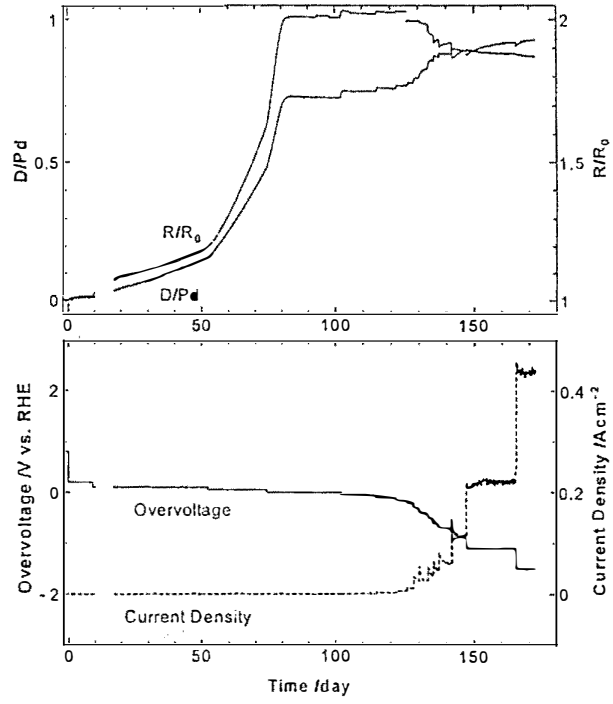

Fig.4 Change of R/R_0, D/Pd, cathode overvoltage and current density during the long term electrolysis using a Pd cathode (JM ϕ2mm×50mm, 99.99% up) in 1M-LiOD containing 0.6mM thiourea.

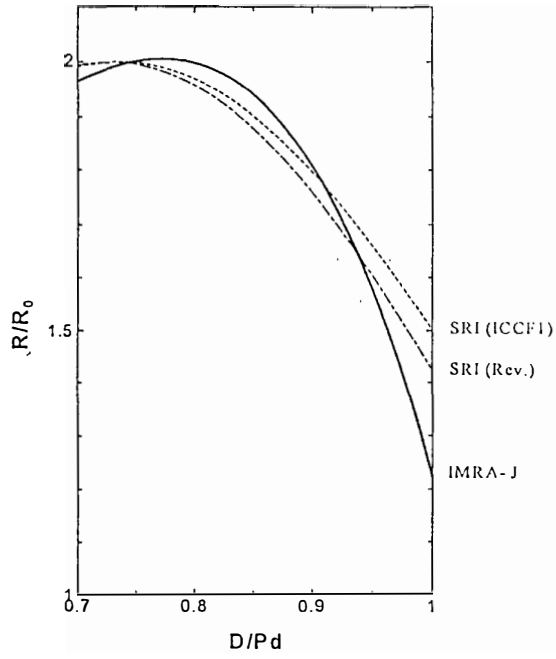

Fig.5 Cathode resistace ratio, R/R_0, vs. D/Pd for the cathode loading higher than 0.7: SRI(ICCF1), SRI(Revised) and IMRA Japan curves.

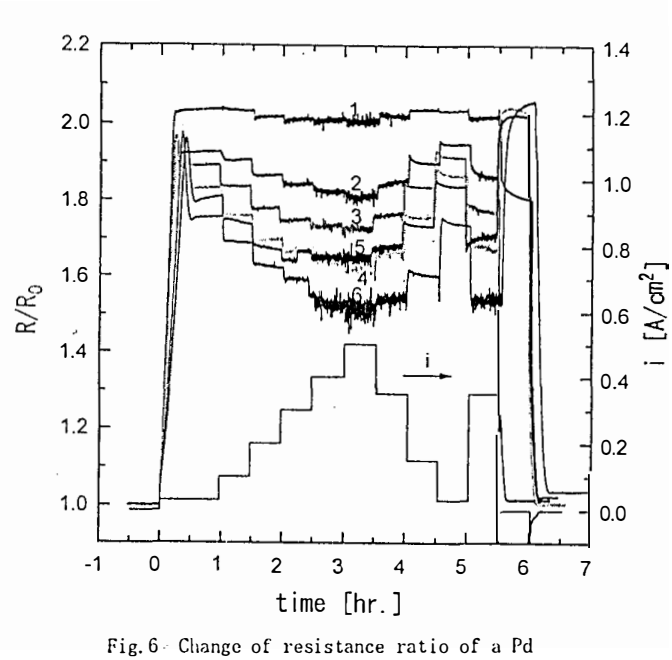

Fig. 6 Change of resistance ratio of a Pd foil cathode (5mm×20mm×50 μm) with applied current density in 2.8M-D_2SO_4 containing thiourea at 20℃. Concentration of thiourea: 0(1), 0.3mM(2), 3mM(3), 30mM(4), 300mM(5), 1M(6).

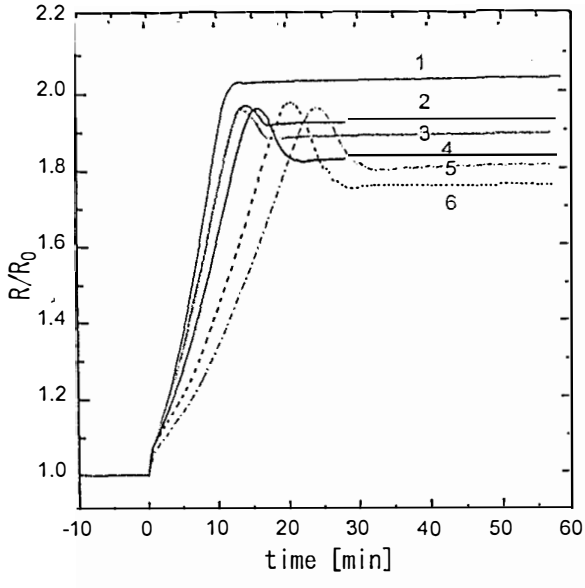

Fig.7 Initial stage of Fig.6 to show change of resistance ratio with time at 30mA/cm^2.

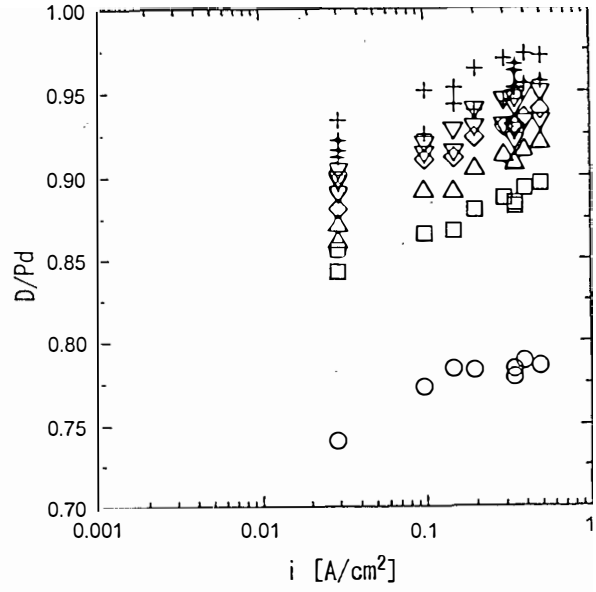

Fig. 8 Dependence of D/Pd on current density for the Pd foil cathode in 2.8M-D_2SO_4 containing thiourea. Concentration of thiourea: 0mM(○), 0.3mM(□), 3mM(△), 30mM(◇), 300mM(▽), 1M(+). The D/Pd in pure D_2SO_4 was determined electrochemically by integrating the anodic dissolution current.

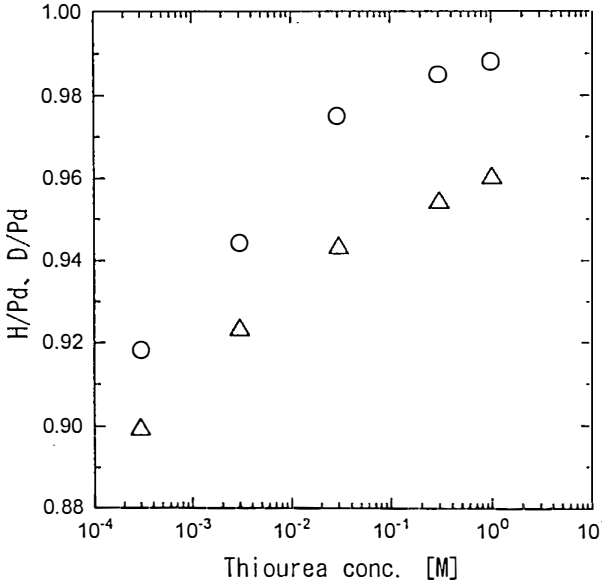

Fig. 9 Dependence of H/Pd and D/Pd on thiourea concentration for the Pd foil cathode at 20℃ and 0.5A/cm^2 in 2.8M-H_2SO_4(○)and D_2SO_4(△).

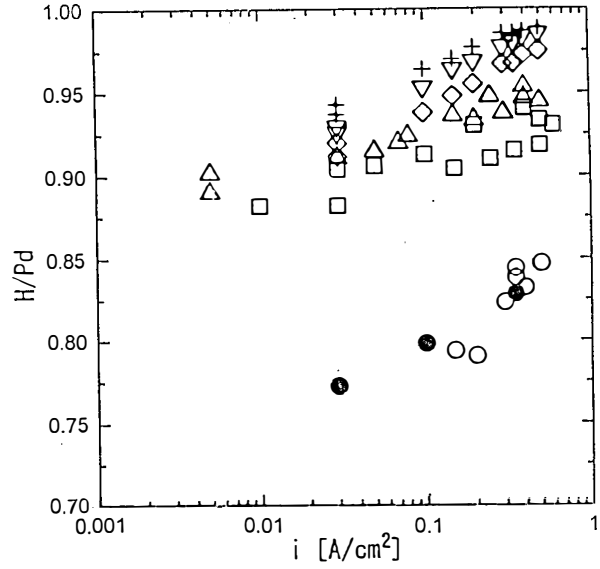

Fig. 10 Dependence of H/Pd on current density for the Pd foil cathode at 20℃ in 2.8M-H_2SO_4 containing thiourea. Concentration of thiourea: 0(○ , ●), 0.3mM(□), 3mM(△), 30mM(◇), 300mM(▽), 1M(+). The data points ● were determined electrochemically by anodic oxidation of the absorbed hydrogen.

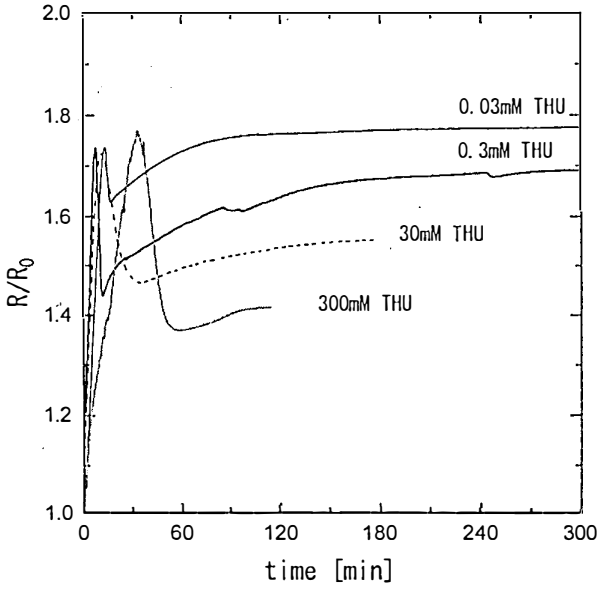

Fig. 11 Change of resistance ratio with time for the Pd foil cathode in 0.5M-H_2SO_4 containing thiourea observed at 20℃ in a electrolysis cell with the Pd cathode and Pt anode in the same compartment.

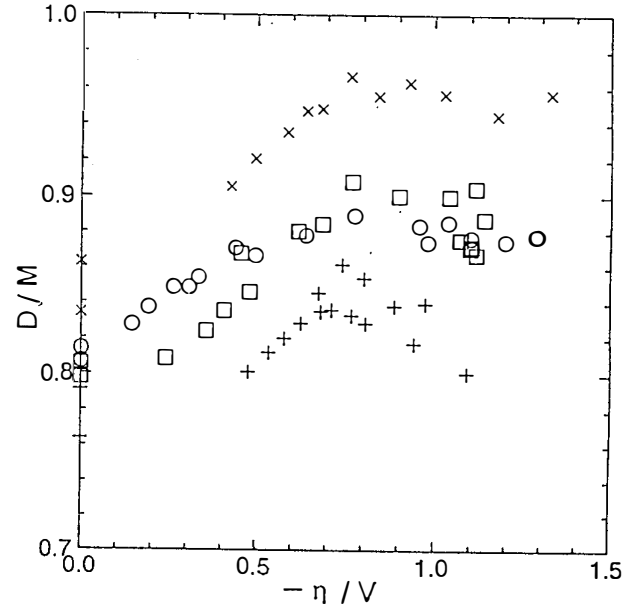

Fig. 12 Dependence of D/M on cathode overvoltage observed at 10℃ in 1M-LiOD for ϕ4mm Pd(+), Pd-Rh(10at%)(×), Pd-Rh(10at%)/Pd(150 cm^2)(○), Pd-Rh(10at%)/Pd(12cm^2)(□).

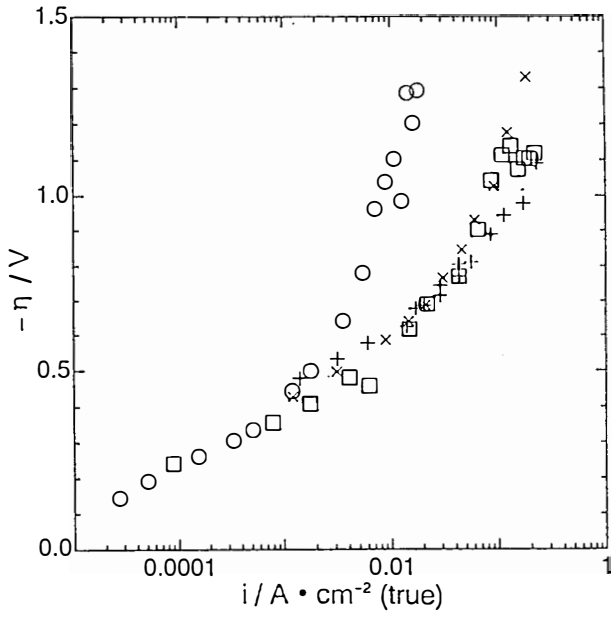

Fig. 13 Tafel lines observed in 1M-LiOD at 10℃ for ϕ 4mm Pd, Pd-Rh and Pd-Rh/Pd alloys. The notations are the same as Fig. 12.

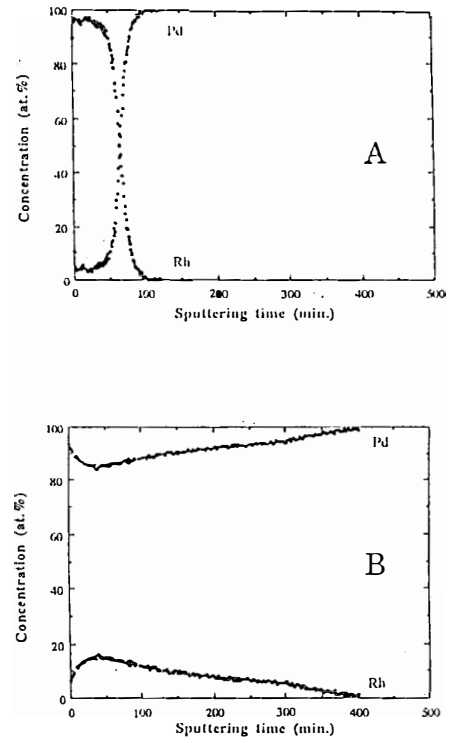

Fig. 14 Auger depth profile of Pd and Rh of the Pd cathode with a electrodeposited Rh film before (A) and after (B) annealing at 850℃ for 2 hours in vacuum.

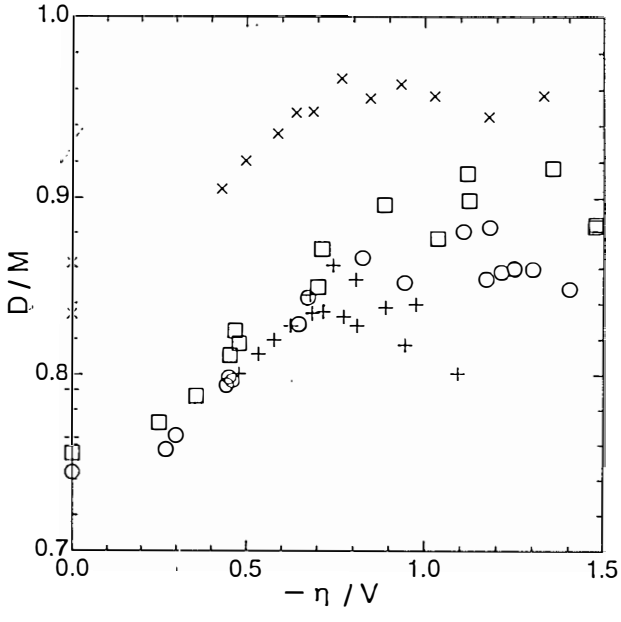

Fig. 15 Dependence of D/M on cathode overvoltage observed in 1M-LiOD at 10℃ for ϕ 4mm Pd(+), Pd-Rh(10 at%)(×), Pd/Pd-Rh(○,□).

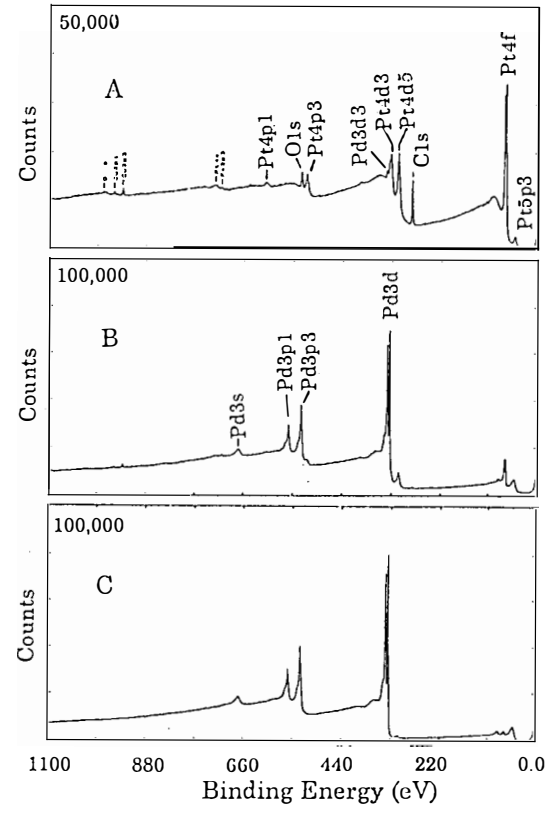

Fig. 16 Change of XPS spectra of a Pd cathode surface with sputtering time: 0 (A), 60 sec (B), 300 sec (C). The Pd cathode was subjected to a long term electrolysis in 1M-LiOD in an open cell with a Pt anode.

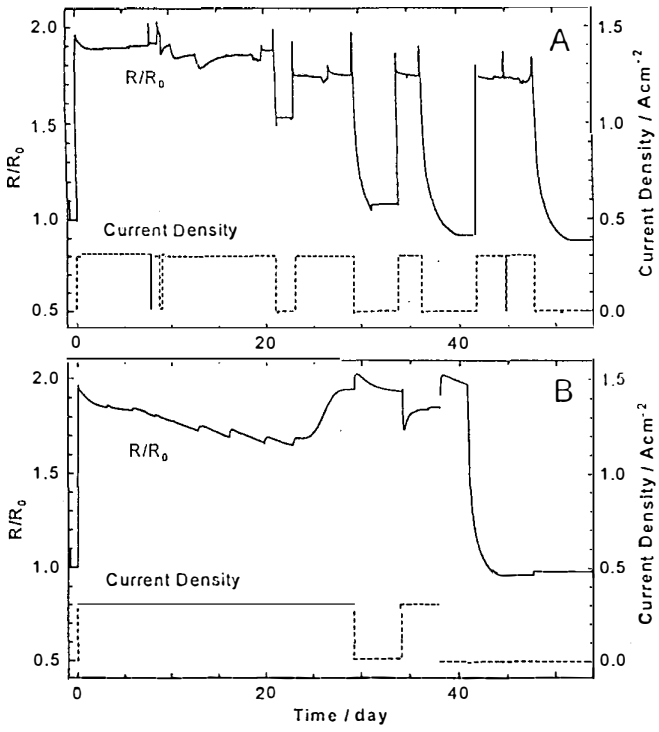

Fig.17 Change of resistance ratio of the Pd rod cathodes (JM, ϕ2mm×40mm, 99.99% up) and current density during the electrolysis in 1M-LiOD at 20° C in open cells. A: Pd with surface Pt/Pd ratio higher than 10, and B: Pd with surface Pt/Pd ratio lower than 1.0

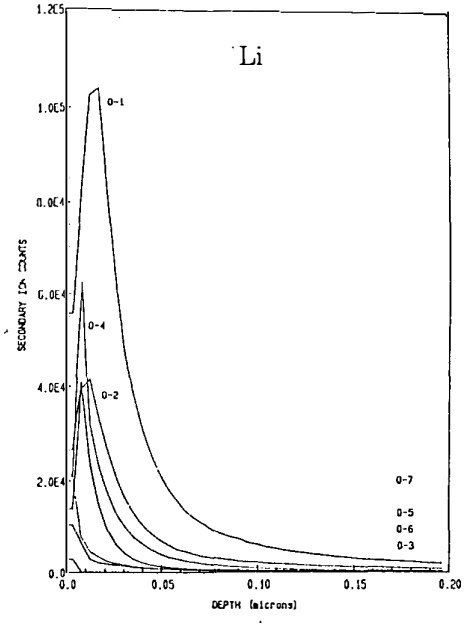

Fig. 18 SIMS depth profile of Li for Pd rods (JM, ϕ 2mm × 40mm, 99.99%) before electrolysis (O-7) and subjected to long term electrolysis in 1M-LiOD in open cells (O-1—O-6).

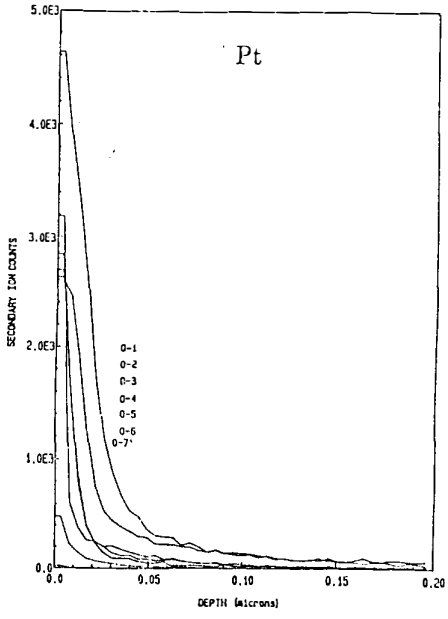

Fig. 19 SIMS depth profile of Pt for Pd rods. The notation is the same as Fig. 18.

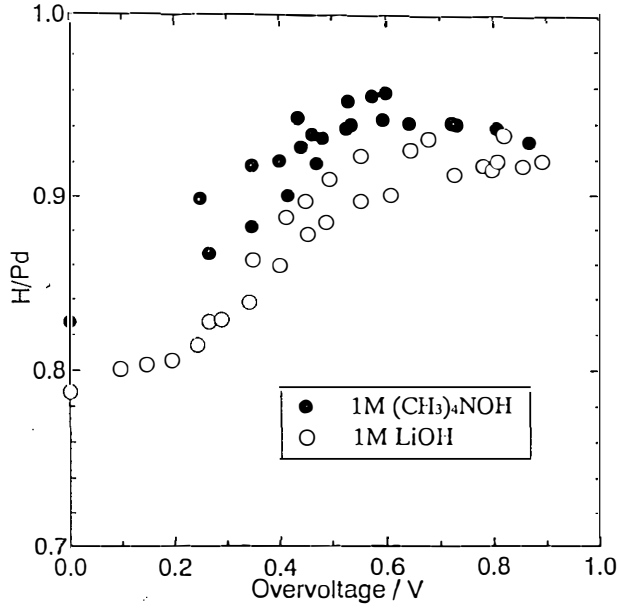

Fig.20 Comparison of overvoltage dependence of H/Pd for ϕ4mm Pd(TNK, 99.9% up) observed in 1M-LiOH(○) and 1M-$(CH_3)_4NOH$(●) at 10℃.

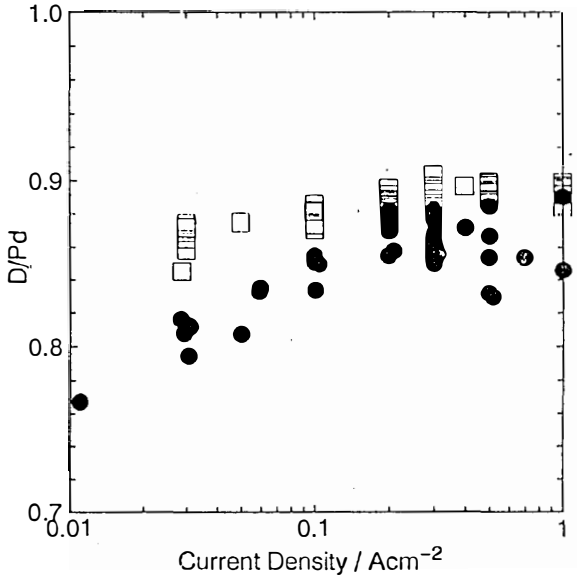

Fig.21 Comparison of D/Pd observed for 6 Pd cathodes in open cells(□) and 5 Pd cathodes in fuel cell type closed cells (◑) in 1M-LiOD at 20℃. Pd rods: φ2mm × 40mm, JM 99.99 %up

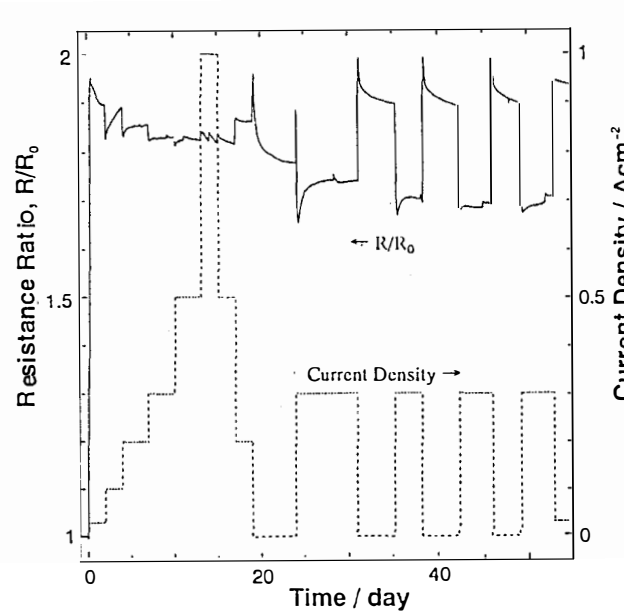

Fig.22 Change of cathode resistance ratio and current density during the electrolysis in 1M-LiOD at 20℃ to see the effect of deload/reload cycles on the cathode loading

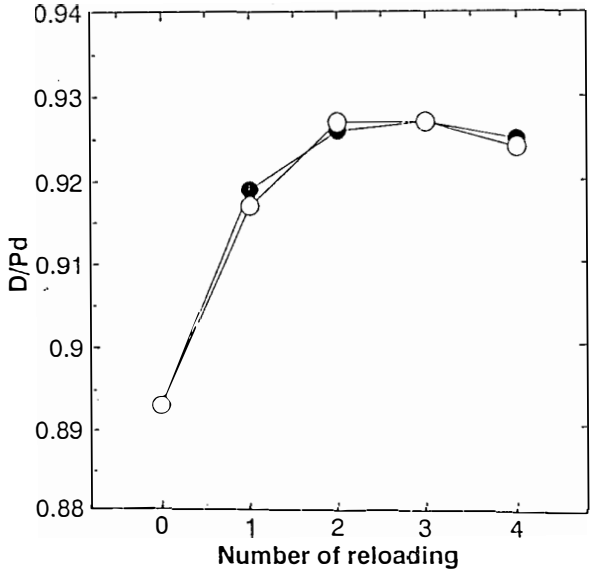

Fig.23 Dependence of D/Pd after reloading on the number of deload/reload cycles observed for two Pd cathods in 1M LiOD at 20℃ in open cells.

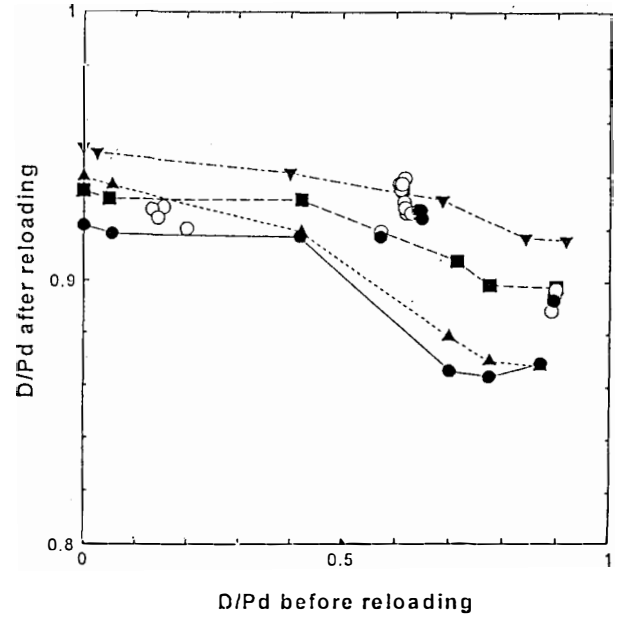

Fig.24 The effect of degree of deloading on D/Pd after reloading at 300mA/cm^2 of the ten JM Pd rods (φ2mm×40mm) in 1M-LiOD at 20° C.

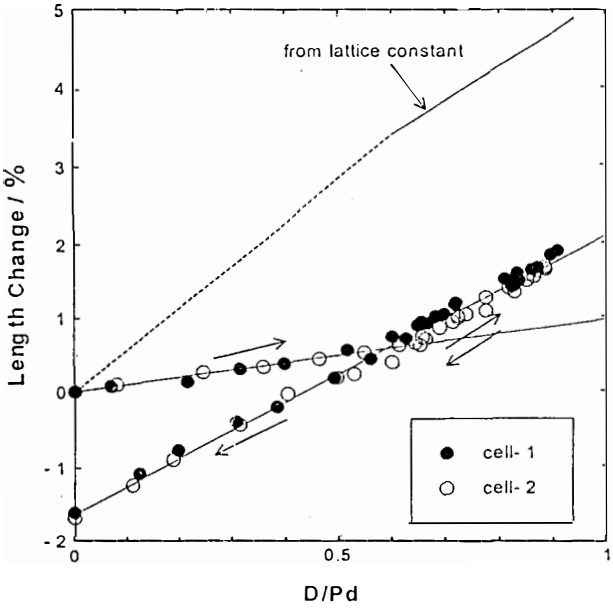

Fig.25 Dependence of change in cathode length on D/Pd observed for the two Pd rod cathodes (JM, ϕ2mm×40mm, 99.99% up) in 1M-LiOD and the change in length calculated from the lattice constant data assuming uniform expansion of the palladium lattice.

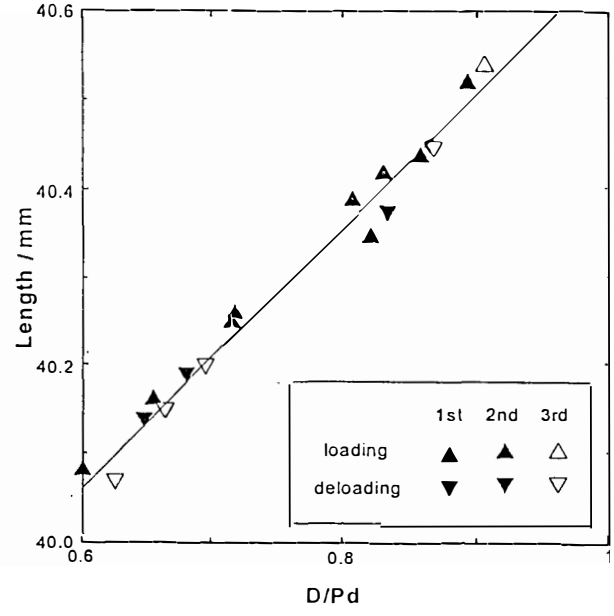

Fig.26 Change of the cathode length during the three consecutive load-deload-load cycles in the β phase region.

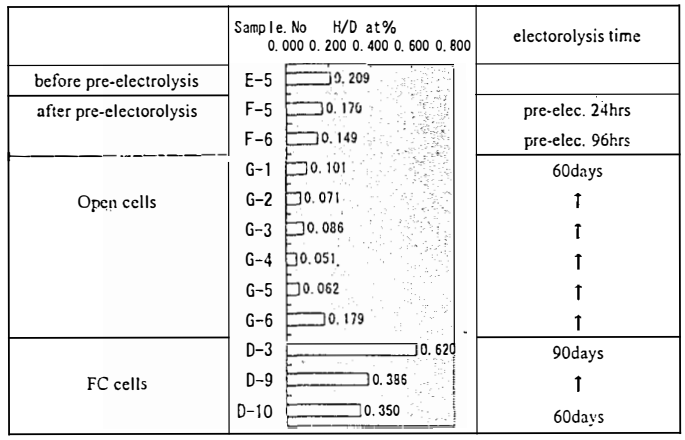

Fig.27 Results of the NMR analysis of H/D ratio in 1M LiOD before and after pre-electorolysis, after electrolysis in open cells for 60 days, and after electrolysis in fuel cell type closed cells for 60 and 90days.

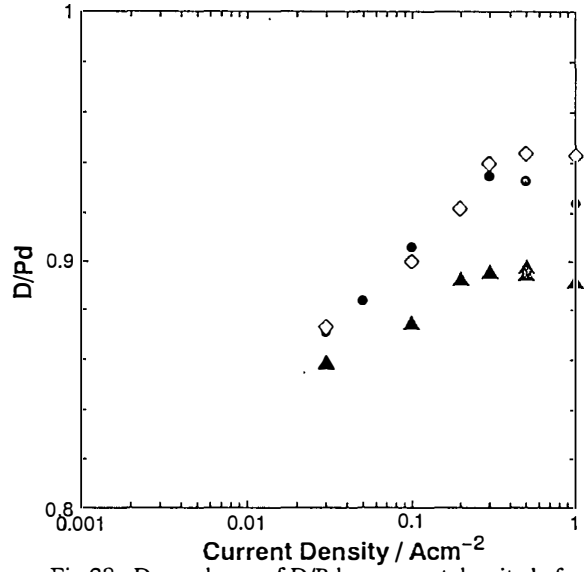

Fig.28 Dependence of D/Pd on current density before applying deload/reload cycles(▲), after the cycles(●) and with 100ppm Al after the cycles(◇) observed for a JM Pd rod (ϕ 2mm × 40mm,99.99 up) in 1M-LiOD at 20℃

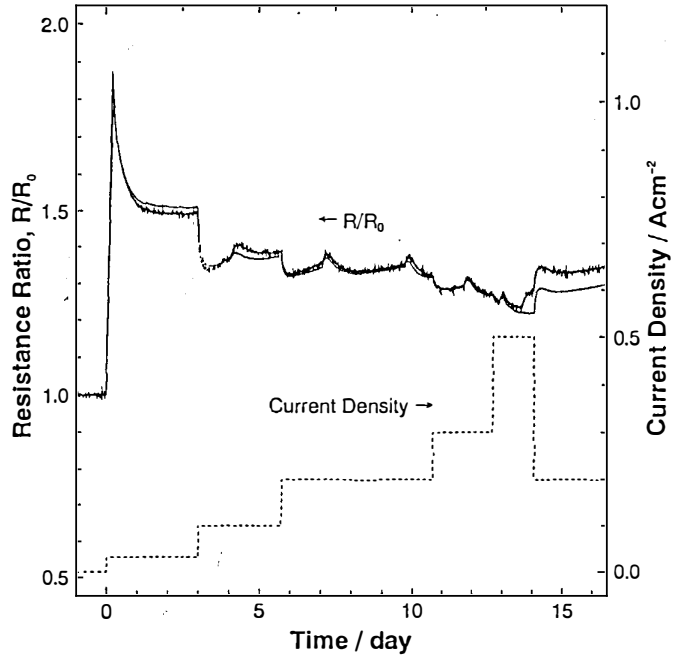

Fig.29 Change of the cathode resistance ratio and applied current density observed for JM Pd rods in 1M-LiOH at 20℃.

Fifth International Conference on Cold Fusion
9-13 April, 1995 - Monte Carlo, Monaco
ICCF5 ©1995

Numerical simulation of deuterium loading profile in palladium and palladium alloy plates from experimental data obtained using μs pulsed electrolysis.

Francesco CELANI*, Alessandra PETROCCHI*, Antonio SPALLONE*,
Paolo TRIPODI*, Daniele Di GIOACCHINO*, Misa NAKAMURA*,
Paolo MARINI**, Vittorio Di STEFANO**,
Giuliano PREPARATA***, Marco VERPELLI***,

* INFN, Laboratori Nazionali di Frascati, via E.Fermi 40, 00044 Frascati (Italy).

**SKITEK, IRI, Pomezia (Italy)

***Dipartimento di Fisica, Universita` di Milano, Via Celoria 16, 20133 Milano (Italy)

Abstract

Various palladium cathodes have been studied to determine the influence of metallurgy and surface treatment on deuterium loading. In this paper we apply a numerical solution to the appropriate differential equation to calculate the time dependent local deuterium concentration inside the plates. We use experimentally determined deuterium coefficients for the α, β and γ phases [1].
We find the highest concentration gradient in the case of oxidized samples.

1. Introduction

The aim of this work is to find correlation between local deuterium concentration and bulk and surface characteristics of the cathodes used in pulsed electrolysis. A high peak current (about 15 A) and very short pulses (800 ns) generator has been used to perform electrolysis in 0.3 N LiOD-D_2O solution.
We tested pure palladium, palladium-silver, palladium-cerium and palladium-yttrium alloys, to see if a higher hardness (Ag) or the addition of a rare earth (Ce, Y), that has a high capability of absorbing deuterium, could be useful for increasing D/Pd ratio.
We also tried to verify if a surface oxidization treatment [2] influences the local concentration of deuterium. In fact, during the electrolysis, the PdO reduces and the area of active surface increases because of the formation of nanocrystals of palladium[3]. The flow calorimeter used for this experiment and our method to measure in situ the deuterium absorption rate in the metallic plate (25x25x1 mm) have already been described elsewhere [4],[5]. We used absorption rate data to assign boundary conditions of the diffusion equation. The numerical integration of this equation allows us to figure the time dipendent concentration profiles of deuterium in the plates.

2. Methods

We described the deuterium motion in metal as due to the diffusion only and we integrated [6] the parabolic partial differential equation in one space variable:

$$\frac{\partial U(x,t)}{\partial t} = \frac{\partial}{\partial x}\left[\mathfrak{D}\ (U(x,t))\ \ \frac{\partial U(x,t)}{\partial x} \right]$$

where : U = D/Pd value, x = space, t = time ,$\mathfrak{D}$ = diffusion coefficient . $\mathfrak{D}(U)$ is obtained fitting data from experimental measuraments of the diffusion coefficent.
For the boundary conditions we have chosen :

$$J(t) = \mathfrak{D}(U(x,t)) \frac{\partial U}{\partial x}$$

where J(t) is the deuterium current flowing through the plate surfaces. We calculated this current as the number of moles entering the plate for second for square centimeter.
In the following we compare the results of these measurements for pure Pd and oxidized Pd, for $Pd_{90}Ag_{10}$ and oxidized $Pd_{90}Ag_{10}$, for PdCe (Pd 99.9x %,Ce 0.0x %) and oxidized PdCe, for PdY (Pd 99.9x %, Yttrium 0.0x %) and oxidized PdY.
As concerning as the concentration profiles obtained by our numerical method we show the D/Pd ratio vs the thickness for each plate at different time steps of the loading process. It has to be noticed that for Pd alloys and oxidized samples we can show just a qualitative trend because we used the same values of the diffusion coefficent we used for pure palladium.

3. Results

Palladium plates

At the beginning of the loading the absorption rate of oxidized palladium shows a plateau that is absent in the pure one (fig. 1a). Only after 15 X10^4 s the PdO absorption rate values become less than for Pd. Meaning of this trend is that the loading efficiency is higher for treated palladium.
The difference between the values of the concentration profiles in the two samples (fig 1b) is not very evident. Absolute maximum value of loading ratio is the same (~1.1) for both plates.

PdAg alloy plates

As for the PdO, the oxidized PdAg sample shows a higher löading efficiency respect to the not treated PdAg (fig. 1c).The initial value of its absorption rate is higher than in PdO. After $7X10^4$ s the PdAgO absorption rate become less than for the PdAg. A consequence of this trend is that the concentration profiles of PdAg and PdAgO become less and less different (fig. 1d).
Absolute maximum value of loading ratio is the same (~0.8) for both plates.

PdCe alloy plates

The deuterium loading efficiency of not treated plate is the least among all the samples. The absorption rate of the oxidized sample is very high at the beginning of the experiment (fig. 2a) and after $13X10^4$ s it becomes equal to the PdCe.
The D/Pd ratio is higher near the surface during the first hours of the experiment (fig.2b).
Absolute maximum value of loading ratio is higher in oxidized palladium alloy (~0.9) than in not treated one (~0.6).

PdY alloy plates

Also in this case the treated sample shows an initial high absorption rate but without any plateau (fig. 2c). After $17X10^4$ s the PdYO absorption rate becomes less than the PdY.
The difference between the behavior of the concentration profiles of the two plates is less than in the case of the PdCe samples (fig. 2d).
Absolute maximum value of loading ratio is the same for both plates (~1.1).

4. Conclusions

The oxidization surface treatment is determinative to obtain a high loading efficiency. In PdCe the difference between treated and not treated sample is very clear also in the concentration profiles. In the case of PdYO we obtained high value of absorption rate but for the shortest time, while in PdO the value of the absorption rate has remained high for the longest time. The oxidized palladium sample has also reached the highest final value of D/Pd rate.

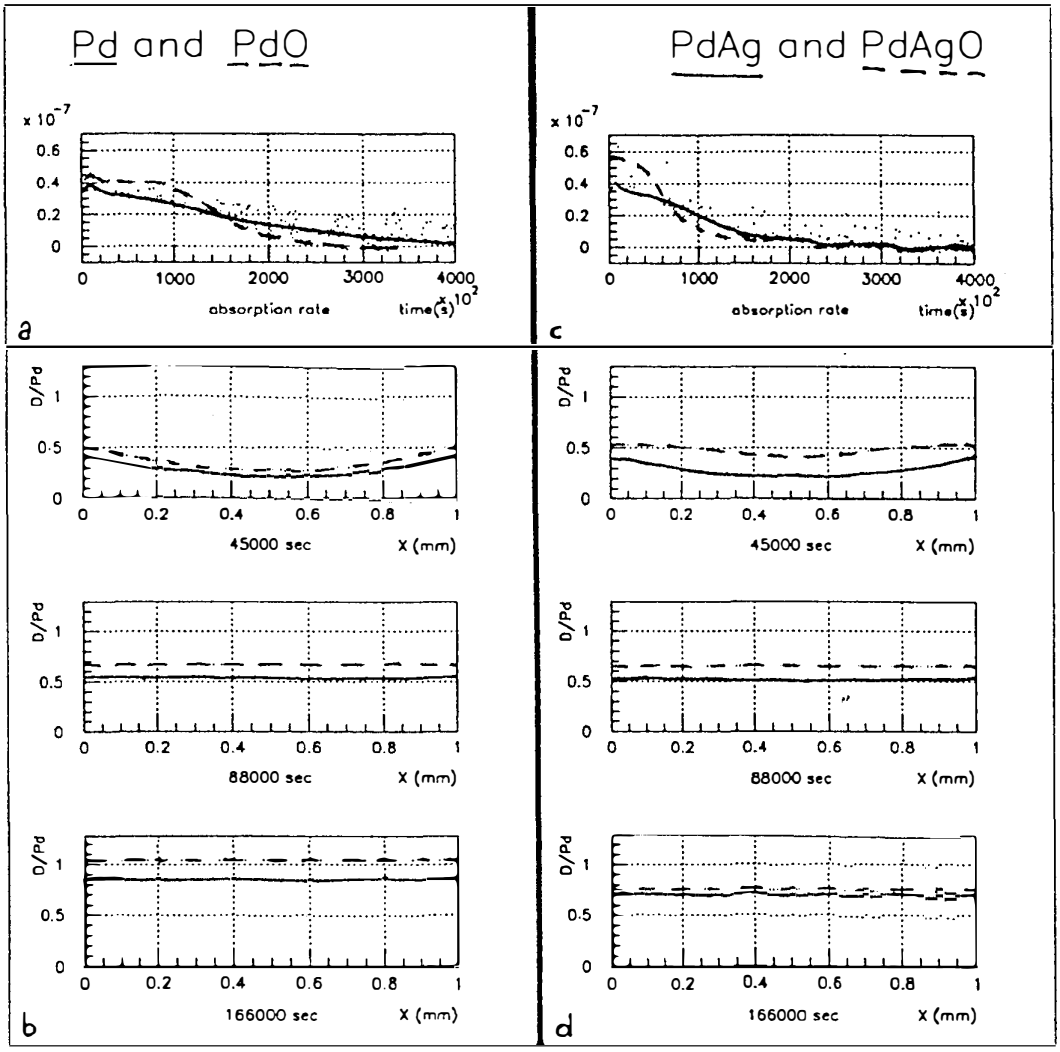

fig. 1a : Absorption rate (in moles per unit area per second) versus time for Pd (full line) and Pd oxidized plates (broken line).

fig. 1b : Concentration profiles vs the depth of Pd (full line) and PdO (broken line) plates (at 45000, 88000, 166000 s after the beginning of the experiment).

fig. 1c : Absorption rate (in moles per unit area per second) versus time for PdAg (full line) and PdAg oxidized plates (broken line).

fig. 1d : Concentration profiles vs the depth of PdAg (full line)and PdAgO (broken line) plates (at 45000, 88000, 166000 s after the beginning of the experiment).

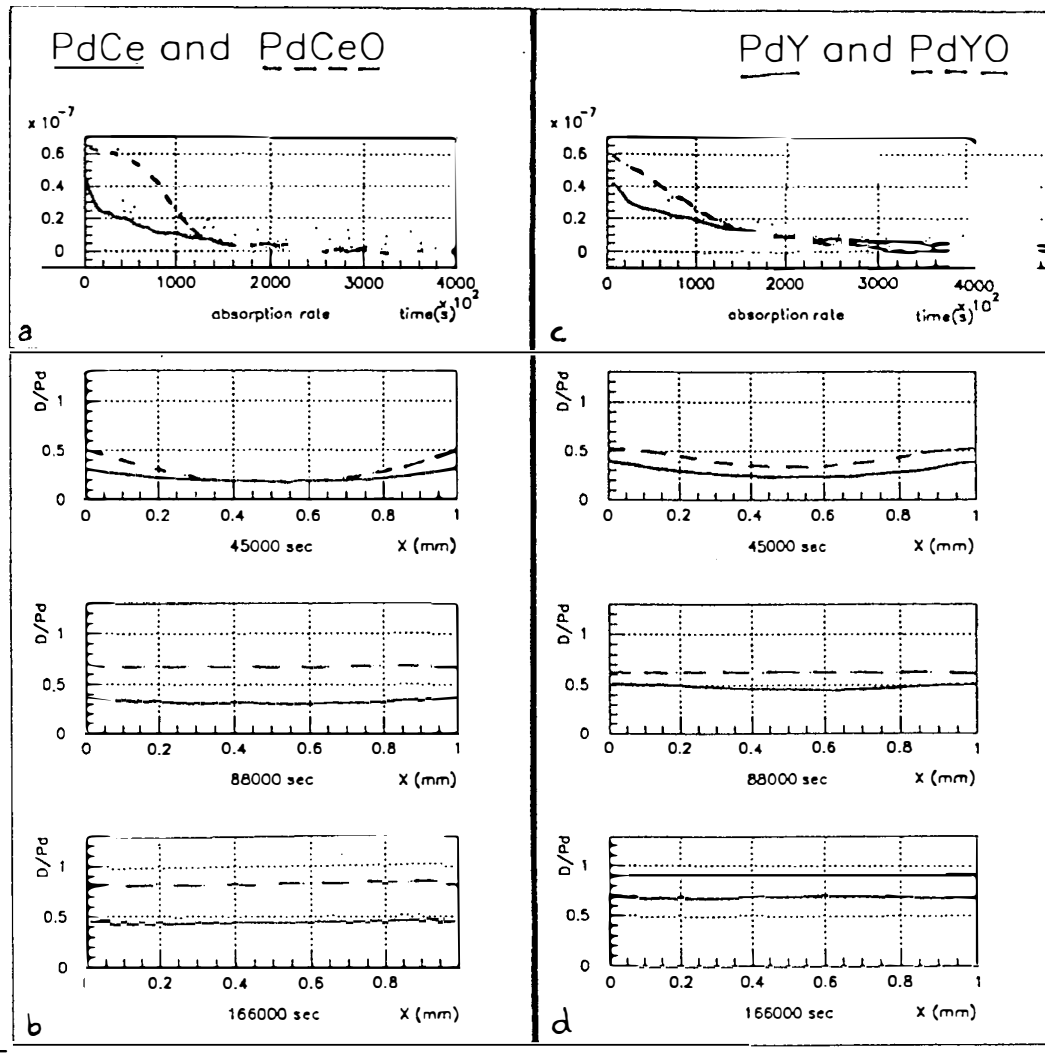

fig. 2a : Absorption rate (in moles per unit area per second) versus time for PdCe (full line) and PdCe oxidized plates (broken line).

fig. 2b : Concentration profiles vs the depth of PdCe (full line) and PdCeO (broken line) plates (at 45000, 88000, 166000 s after the beginning of the experiment).

fig. 2c : Absorption rate (in moles per unit area per second) versus time for PdCe (full line) and PdCe oxidized plates (broken line).

fig. 2d : Concentration profiles vs the depth of PdY (full line)and PdYO (broken line) plates (at 45000, 88000, 166000 s after the beginning of the experiment).

References

[1] Mengoli G., Fabrizio M. et al., ICCF5 Proceedings (1995)
[2] Celani et al., ICCF5 Proceedings (1995)
[3] Sato et al.,Jpn. J. Appl. Phys., **32**, 5095 (1993)
[4] Celani et al. , ICCF4 Proceedings, (1994)
[5] Celani et al., Fusion Technology, publishing (1995)
[6] Nag Fortran Library routine document (D03PGF subroutine) (1991)

Fifth International Conference on Cold Fusion
9-13 April, 1995 - Monte Carlo, Monaco
ICCF5 ©1995

Study of deuterium charging behaviour in palladium and palladium alloy plates, changing surface treatments, by μs pulsed electrolysis.

Francesco CELANI*, Antonio SPALLONE*,Paolo TRIPODI*,
Alessandra PETROCCHI*, Daniele Di GIOACCHINO*
Paolo MARINI**, Vittorio Di STEFANO**
Marco DIOCIAIUTI***, Alfredo MANCINI****,

* INFN, Laboratori Nazionali di Frascati, via E.Fermi 40, 00044 Frascati (Italy).

**SKITEK, IRI, Pomezia (Italy)

***ISS, Via Regina Margherita 5, 00100 Roma (Italy)

****ORIM S.R.L., Via Concordia 65, 62100 Macerata (Italy)

(*)

Abstract

A systematic study about deuterium loading in palladium has been performed. Palladium cold worked plates and palladium alloy plates have been used as comparison. A proper plate surface oxidation has been performed and anomalous absorption rates have been measured. A high peak current (15 A), short width pulse (duration 1 μs) electrolysis technique has been used to test all chatode plates and it is visible that this technique permits to reach very high D/Pd loading values (around 1/1 or even more for palladium). At the beginning of the loading, in close relation with the anomalous absorption rate, a bump of excess heat has been measured in two similar oxidized surface palladium plates.

All these tests show that the loading is completely reproducible.

1. Introduction

It is commonly accepted that very high Deuterium concentration into a Palladium lattice is required to produce Cold Fusion effects as well as extra heat production or nuclear radiation emission. For this reason a standard loading technique has been improved particularly with electrolytic system.

Since three years we have been using this special pulsed electrolytic loading technique testing Palladium plates (25x25x1 mm). Many plates have been tested and an optimization, looking at the loading parameters (absorption rate, overvoltage), has been reached. Indeed, a preliminary study has been performed to observe in which way the status of the electrode surface can modify the absorption dynamics.

(*) All Palladium plates were kindly provided by:
IMRA Material, Japan, which supported partially this work.

The tests show that high loading is not a sufficient condition to produce measurable excess heat.

2. The Experimental Set-Up

The experimental apparatus has been shown in a previous paper[1] and it consists in a flow cooling calorimeter (fig. 1.a) in which there is a special turned Pt wire as anode having inside the Pd plate (fig. 1.b). The cooling system is composed by a double coil, a water bath (17 °C) and a peristaltic pump (flow typically at 1 ml/s).The linearity of the operating range of this calorimeter is from 0.5 up to 150 W (1.5 KW maximum power), depending from the cooling flow from 0.5 to 10 ml/s. The produced electrolytic gases are collected in a close volume (150 cm^3) and periodically some electrovalves are open to permit to these gases to go outside quickly. The variation of the pressure is continuously measured and recorded. All physical parameters (time, temperatures, pressure, cell voltage and current, reference voltage of a pseudo R.H.E.) are continuously monitored and acquired by a computer.

The electrolysis is powered by a complex electronics gated system to produce a very high peak current (fig. 2.a). A fast power pulser circuit, triggered by pulse generator, discharges a capacitor to the electrodes of the cell during a selected time (timing): the repetition rate of this discharging process is selectionable. During the pulsing a proper circuitry acquires the voltage and current generated. During the discharge, with an integrator circuit, is possible to measure the total electric charge (or the mean current) and the total electric energy (or the mean power) dissipated by the cell. An other proper circuitry, measuring (gate enable) during the inter-pulsing, permit to have the cathode and the floating reference wire voltages: in such a way it is possible to estimate the Tafel over-potential and to understand the difference between Tafel and Volmer region. The circuitry (fig. 2.b) works in 2 stages: firstly the capacitor charges slowly (τ about 10 μs) from the voltage supply, secondly the fast electronics switch (gated by the trigger pulse) connects the charged capacitor to the cell electrodes, producing a very high current (Imax about 150 A) in a short time (from 0.2 to 0.5 μs). Because the time pulse width (typically less than 1 μs) is much less than the discharging mean time (τ typically of 7 μs), in first approximation we can say that, during the pulse, the electrolytic cell is applied to a constant voltage generator (the 2 μF capacitor having Vmax about 200 V) so that the electric charge transferred from the capacitor to the cell is around a few percent of the total electric charge cumulated by the capacitor (at maximum of 400 μC). This pulse can be generated with a repetition rate of 0.5 up to 20 KHz.

3. The Experimental Procedure

Strong motivations lead to use a pulse electrolysis instead of constant current electrolysis:

- It is possible to generate a very high current density value to the cathode (even if in a very short time but taking in account to repeat the pulse at enough high frequency to avoid the deloading process).
- The gaseous recombination (Tafel region) at the cathode is strongly reduced providing a very high loading efficiency (Volmer region) during the first charging up (very low production of gas bubbles permitting to have a very fine measurement of absorbed moles).
- It is possible to measure the cathode voltage during the inter-pulse avoiding the power supply noise (possibility to estimate the over-potential).

- Non-equilibrium conditions are produced at the cathode surface (because of the fast electric field applied to the voltage "double layer" between the electrode and the ionic solution).
- The reproducibility of the loading is guarantied by the repeatability of the pulse (also is possible to tune up the pulse to have an optimization of the process parameters).

All the plates were tested in these operating conditions: pulse time width about 0.5 μs (pulse rise time around 100 ns), pulse repetition rate about 5 KHz, peak voltage at 50 V and peak current at 15 A (e.g., mean current is about 60 mA, peak power is 750 W and mean power around 1.5 W). During this pulse the charge transfered is about 13 μC and the electric energy is around 375 μJ.

Some plates were specially treated by the following procedure: heating to about 700 °C with an oxidizing flame during a processing time of some minutes. After this heat treatment the plates show a thin surface oxide layer (less than 0.5 μm) having a high chemical resistance to the concentrated nitric acid attack. These plates, after this treatment, are not more supposed to be cold worked.

4. The Deuterium Loading

Some blank tests were performed using the Gold plates of the same size of Pd plates. This test shows a very small Deuterium absorption at the beginning of the charging up (maximum value of absorbed Deuterium is less than $3 \cdot 10^{-3}$ Moles, corresponding at less than 0.05 of D/Au) and vanishing in a few hours (less than 600 C of electrolytic charge). This absorption is explainable by the cell materials (solution, polyethylene, Teflon, heather, etc.). In the calculation we took into account this small effect and made appropriate corrections to the data.

The results for pure "cold worked" Pd plates (I65 and I85) are shown in figures 3.a,b. The absorption rate (fig. 3.a,b left side) must be intended as the amount of Deuterium moles absorbed by Palladium per surface unit and per time unit. The evolution in the time (or electrodes flowed electric charge equivalent) of the absorption is typically decreasing closing to the zero in a few days (roughly 5 days or 25000 C equivalent). The D/Pd loading ratio (fig. 3.a,b right side), at the saturation, reaches values around 1 or more (the cumulative experimental errors are roughly ±10%). The very similar absorption shapes show that this process can be enough reproducible.

The results for oxidized surface Pd plates (I63 and I340) are shown in figures 4.a,b; also in this case the absorption shapes and the D/Pd curves are very similar indicating a good reproducible grade. It is clear, comparing to the previous figures, that the absorption dynamics at the beginning of the charging up is quite different: the absorption is roughly flat for long time (5000 C or about 1 day) for both the plates. It means that the PdO surface layer has modified the absorption process in such a way that the ingoing Deuterium does not see an increased concentration during the time of this anomalous process. Obviously, when the plate reaches an high concentration of Deuterium the absorption drops down in a faster way to slowly vanishing at saturation level.

Some Pd alloys has been tested to better understand the role that some other different metals (sometimes present as impurities) can play in these absorption processes. A PdAg (90% / 10%) alloy has been used (fig. 5.a: I120 plate). The behavior of this plate is not different in respect to the pure Pd shown if we take in account that the useful Pd material is reduced by 10% of the total plate: Silver is known to be not a Deuterium absorption material, but it increases the hardness of the Pd plate. This PdAg plate has been surface oxidized according to the standard procedure and his behavior is shown in figure 5.b (I118 plate): the high value shoulder of absorption rate

is still present but the D/Pd ratio does not increase (because the high Ag percent in this alloy).

Also a PdCe (99.9% + 0.1%) alloy has been used (fig. 6.a: I418 plate). It is known that the element Ce (Cerium) is a strong Hydrogen absorption inhibitor (even at low concentration) as is visible in the previous figure of D/PdCe. It is evident that the oxidized PdCe surface increases the loading ratio (fig. 6.b: I419 plate), moreover the typical oxidization shoulder is visible at the absorption rate.

Also a PdY (99% + 1%) alloy has been used (fig. 7.a: I613 plate). The Y (Yttrium) is a good Hydrogen absorption element (as well some rare earth) and the loading ratio is quite high but not much higher than pure Pd plates results. Still the PdY oxidized surface shows the "oxidation effect" looking at the absorption rate (fig. 7.b: I614 plate) and the loading ratio does not appear to be increased by this treatment (however it is still higher than 1). In this case the presence of Y does not help the plate to overcome the loading respect to the pure Pd plate.

5. Excess Heat Results

As reported[2], it seems to be a strong correlation respect to the oxidized surface and an increasing of excess heat appearing during the flat high absorption rate at beginning of the loading (fig. 8.b,c: plates I63 and I340). In similar condition we did not detect a similar effect using a pure Pd plate (fig. 8.a: plate I65). In such a way, the surface dynamic seems to play an important role for the excess heat increasing. The alloys tested did not show similar effects even if we have to say that we operated at a few watts of input power (roughly 1.5 W), too close at the lower operating limit range of the calorimeter (about 0.5 W).

Conclusion

We can remark that pulsed electrolysis (at very high peak current) can be a "sufficient" condition to over-load Pd Plates: in this condition the plate metallurgy is not a constrain anymore.

Pd alloys are not necessary to have Pd overloading (in particular if pulse electrolysis is used) and it seems advisable to use just Pd.

Pd treated surface (as well as oxidized surface) strongly modifies the absorption dynamic influencing the loading parameter; furthermore it seems to involve particular dynamic to increase the heat production. We can say that the absorption rate seems to be more indicative parameter concerning the D/Pd ratio.

Finally, a bulk condition to generate excess heat is not a necessary condition, and surface dynamic can be a more important condition to realize heat production.

References

1. F.Celani, A.Spallone, P.Tripodi et al. "High power μs pulsed electrolysis for large deuterium loading on Pd plates."
   Transactions of Fusion Technology, Vol. 26, Dec. 1994, pg. 127-137.

2. F.Celani, A.Spallone, P.Tripodi et al. "Reproducible D/Pd ratio over 1 and excess heat correlation by μs pulse high current electrolysis."
   Publishing on Fusion Technology, summer 1995.

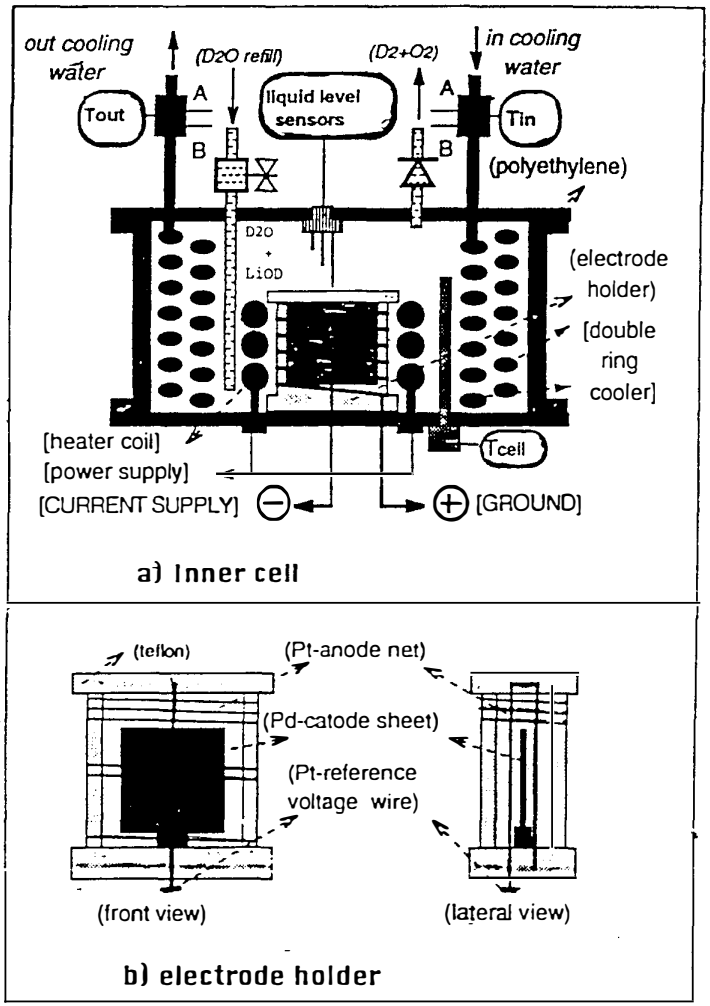

Fig. 1 - Inner cell design and electrode holder.

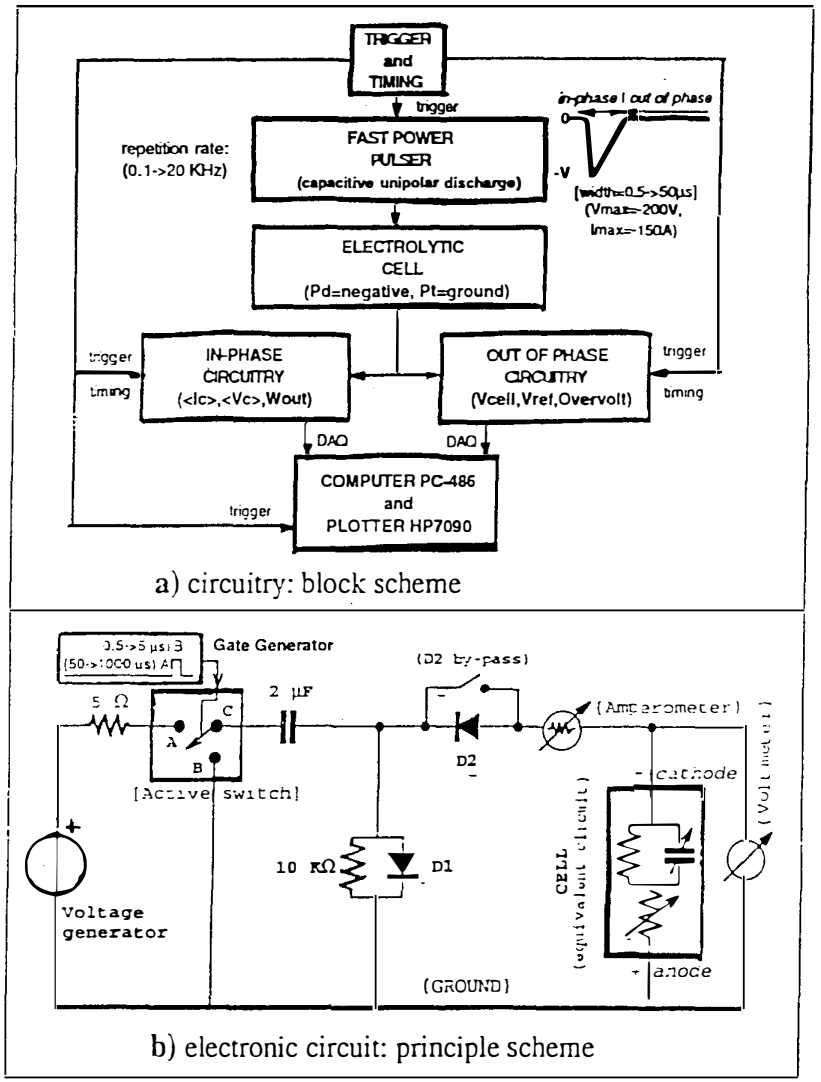

Fig. 2 - High power pulse circuitry.

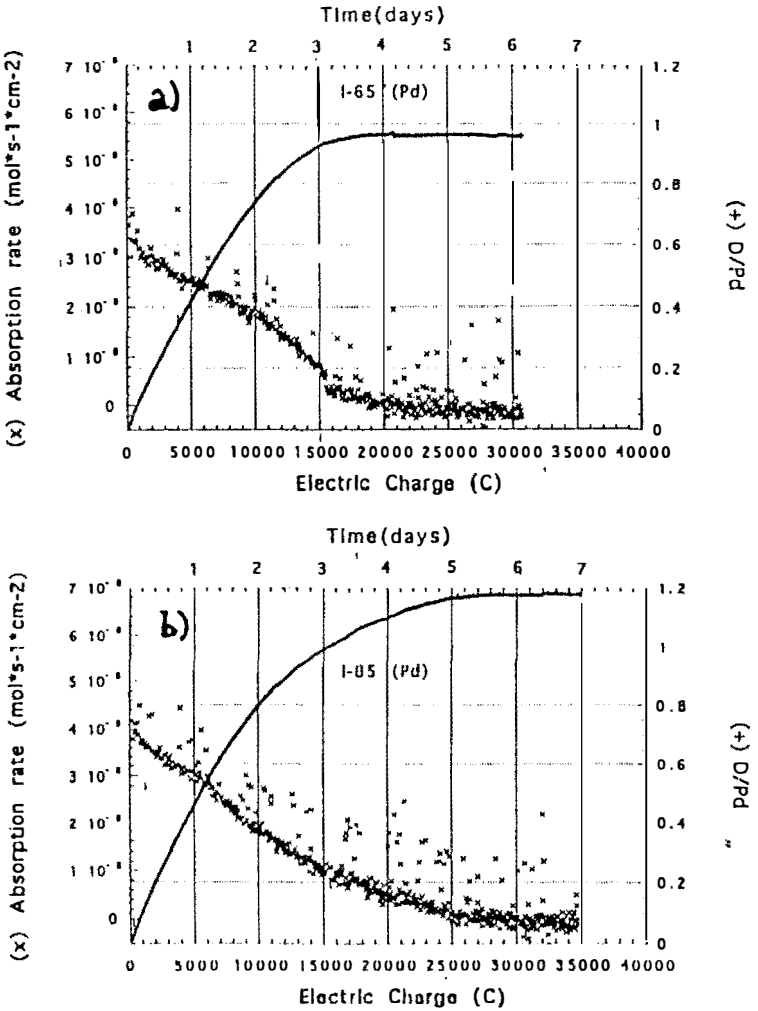

Fig. 3 - Pure palladium (no surface treatment)
a) Plate I-65
b) Plate I-85

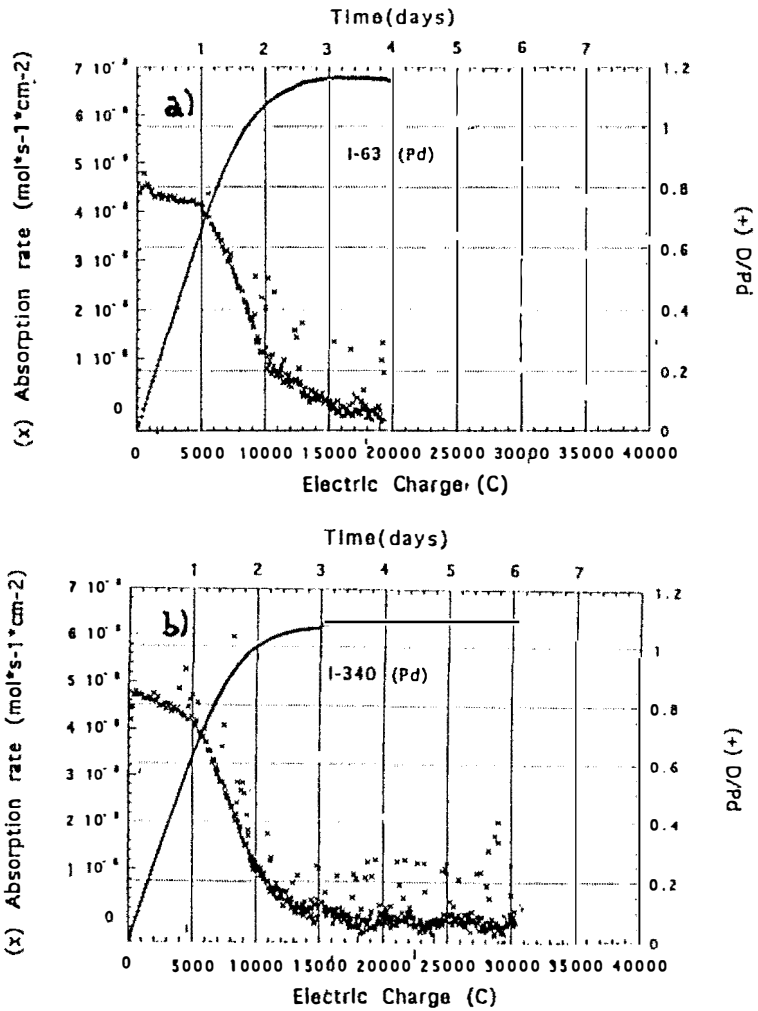

Fig. 4 - Pure palladium (oxidized surface)
a) Plate I-63
b) Plate I-340

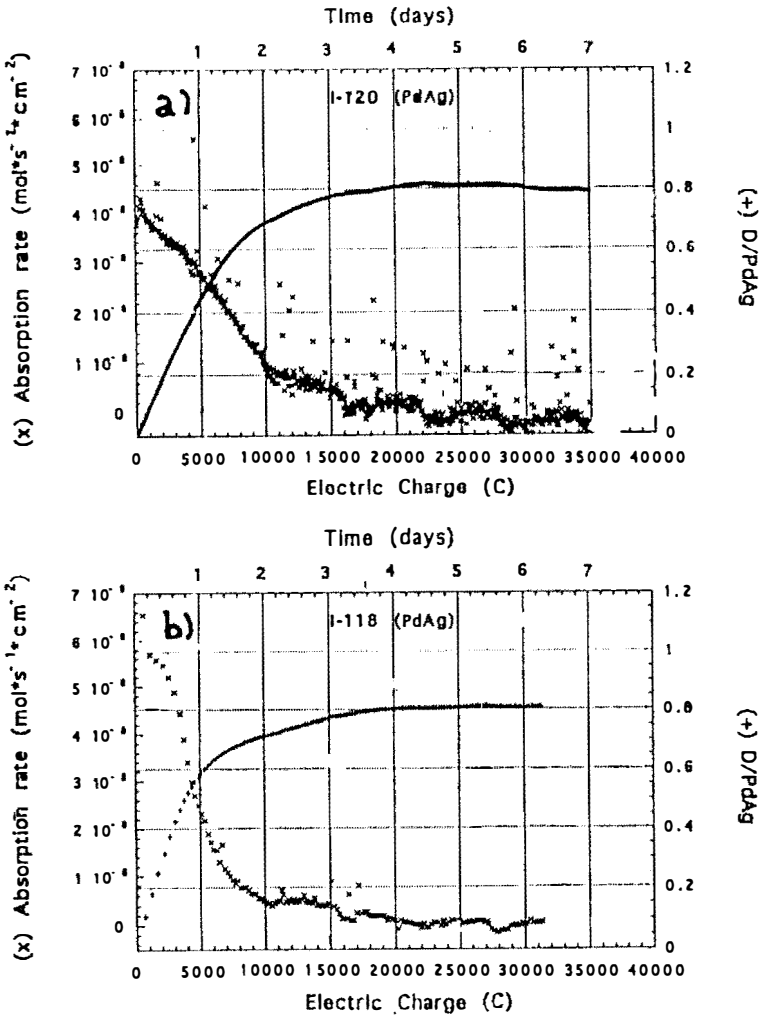

Fig. 5 - Palladium Silver alloy
a) Plate I-120 (no surface treatment)
b) Plate I-118 (oxidized surface)

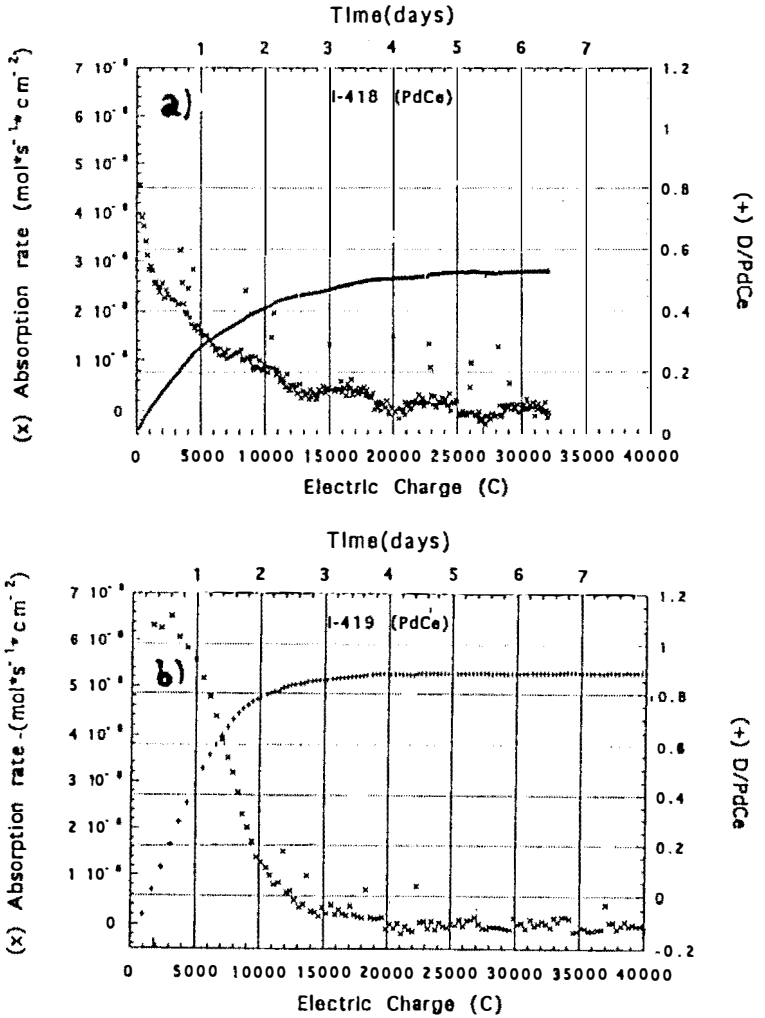

Fig. 6 - Palladium Cerium alloy
a) Plate I-418 (no surface treatment)
b) Plate I-419 (oxidized surface)

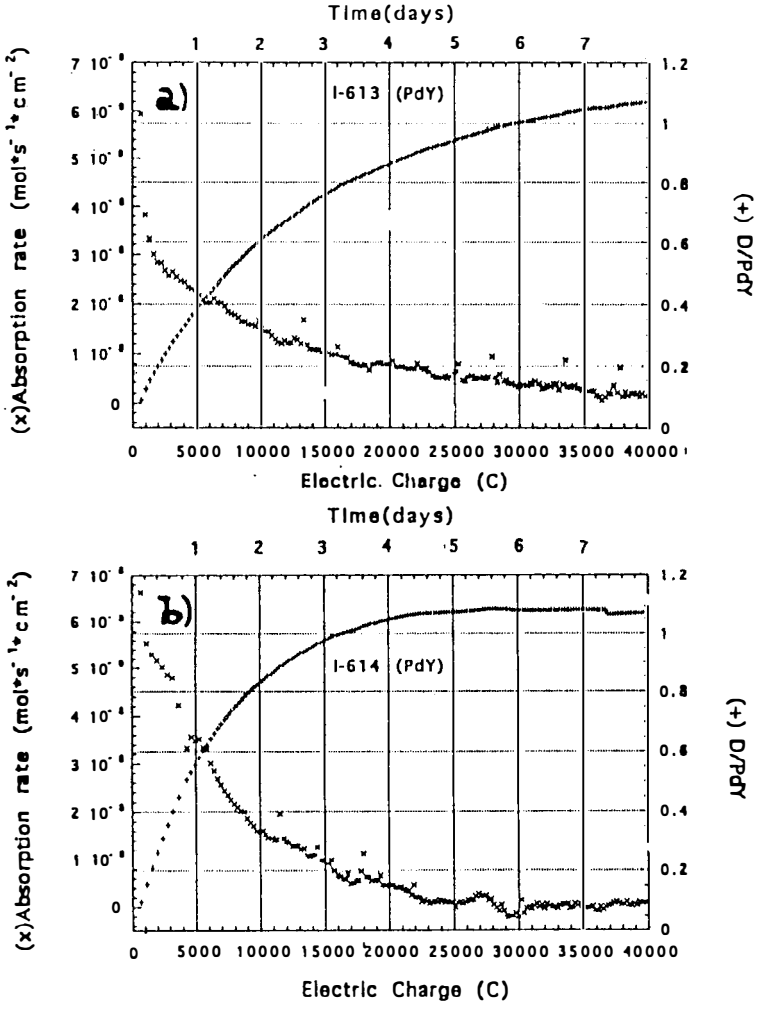

Fig. 7 - Palladium Yttrium alloy
a) Plate I-613 (no surface treatment)
b) Plate I-614 (oxidized surface)

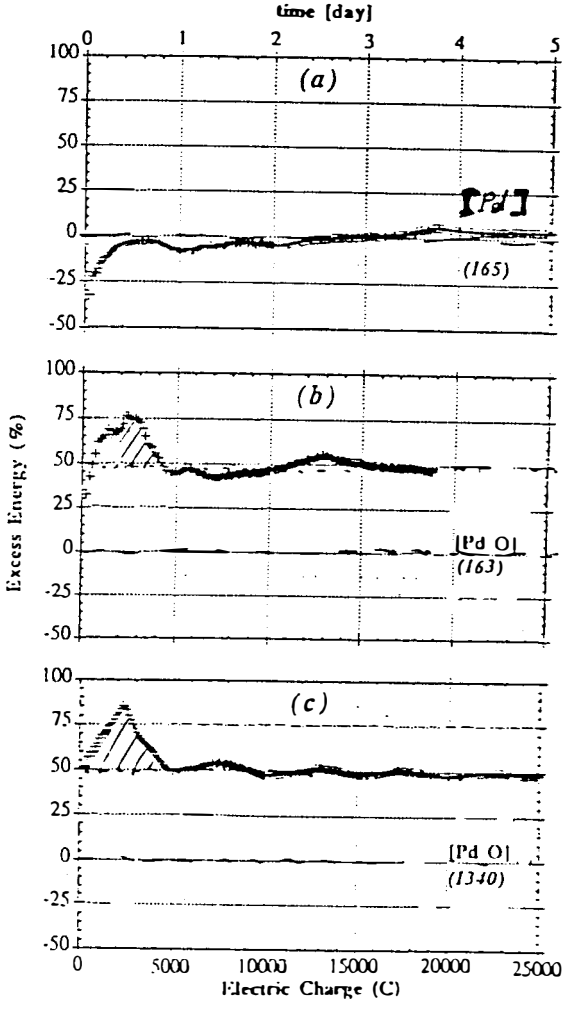

Fig. 8 Pd plates: Excess energy variation (%) vs time and electric charge. All data refer to the Au controls.

Fifth International Conference on Cold Fusion
9-13 April, 1995 - Monte Carlo, Monaco
ICCF5 ©1995

Approach to Obtain Higher Deuterium Loading Ratios of Palladium Cathodes

Hikaru OKAMOTO, Toshiyuki SANO, Yosuke OYABE,
Toshihisa TERAZAWA, and Tamio OHI

IMRA MATERIAL R&D CO., LTD.
5-50 Hachiken-cho, Kariya, Aichi, 448 JAPAN

Abstract

Deuterium loading ratios in the electrolytic palladium cathodes are measured by the electric resistance method. Many kinds of palladium rod are prepared and their loading ratios are determined during our standard electrolysis procedure. Some palladium cathodes are provided with additional treatments to change surface conditions. As the results, it is found that the deuterium loading ratio is very sensitive to palladium surface conditions. For example, when a palladium sample of which surface is modified by aqua regia, the loading ratio as high as D/Pd $\approx$ 0.95 is obtained at 200 mA/cm^2 of electrolytic currents, which can hardly be achieved with an ordinary palladium cathode rod.

1. Introduction

Since the announcement of cold fusion in 1989 [1], a number of attempts have been made to address the reproducibility of excess heat production. M. McKubre and coworkers of SRI [2] reported that a correlation existed between an excess heat reproducibility and D/Pd loading ratios and suggested that the loading ratio should exceed 0.85 to generate excess heat. They also showed that the amount of excess heat increased exponentially or to the square, with the difference of the loading ratio above the threshold, D/Pd=0.85. Furthermore, they claimed that if the loading ratio is attained to D/Pd$\geqq$1, excess heat would be observed with a 100 % reproducibility.

It is known, however, very difficult to attain such a high loading ratio as to exceed 0.90. The present paper reports on studies on some relationship between material properties and the loading ratios to achieve higher loading ratios of deuterium in the palladium.

2. Experimental

2.1 Preparation of Palladium Cathodes

A typical process of producing palladium cathode rods used mostly in our loading experiments, is shown in Figure 1. Palladium lumps from Tanaka Kikinzoku Kogyo (99.95 % Pd) were melted and cast into a rod (50 mm in diameter) in the air. Calcium-

boride (CaB_6) powder was added into the molten palladium to remove dissolved oxygens. The rod was homogenized at 750 ℃ for 2 hours under the vacuum ($<5 \times 10^{-4}$ Torr), and then swaged into a wire of 2 mm in diameter. The wire was cut to pieces of 50 mm in length and they were annealed at 850℃ for 4 hours in the vacuum ($<5 \times 10^{-4}$ Torr). After the rods were cooled down to the room temperature in the vacuum, they were polished with diamond slurry (0.5 μm in diameter) for 30 minutes.

Impurity content of the palladium rods are shown in Table 1, which was detected by Inductively Coupled Plasma Spectrometry (ICP). The content of 200-250 ppm boron by weight, is due to CaB_6 addition.

The palladium rods produced by the above-mentioned process are described as "Standard palladium cathodes" hereafter. With respect to the deuterium loading, those standard cathodes were compared with other palladium cathodes processed by a different method from the standard procedure.

2.2 The Experimental System

The deuterium loading into palladium rods was performed by the electrolysis method, and in-situ measurements of the loading ratios were made with the resistance method.

The electrolytic cell used in the present loading experiments is shown in Figure 2, where the casing of the cell is made of tetrafluoroethylene (FEP) not to be corroded by the electrolyte of 1M LiOD solution. The anode is made of platinum mesh (99.9 % Pt), 20 mm in diameter. and 60 mm in length, and palladium rods (99.9 % Pd), 2 mm in diameter, and 50 mm in length, were used as the cathodes. Five nickel leads 0.5 mm in diameter were spot welded to the cathode. Two of the leads were welded to each end-face of the rod, which served to deliver currents along the rod to measure its electric resistance. Other two leads were welded to the rod at the positions ca. 3 mm from each end of the cathode, to measure the voltage drop along the palladium cathode. The last lead was welded to the position ca. 1.5mm from the upper end of the cathode to derive electrolytic currents.

Loading experiments were performed in an electrolyte of 1.0 M LiOD produced by dissolving a lithium metal piece (Aldrich, 99.9 % Li) in the heavy water, D_2O (ISOTEC, 99.9 %). Throughout the loading experiments, the electrolytic cell was immersed in a water bath maintaining a constant temperature at 25 ± 1 ℃. Electrolyte temperatures were measured with a thermocouple (K type).

In-situ measurements of the cathode resistance were made by using the standard four-probe technique, as already described. The measurement was automated to take data at every 2 minute interval with Milliohmmeter (Yokogawa-Hewlett-Packard, Ltd. HP 4338), which delivered alternative currents (1kHz, typically 10 mA) through the cathode rod . The electrolysis was operated with a galvanostat.

The value of measured resistance was adjusted to the value of the resistance at

25.0 ℃ and the resistance ratio ,R/R_0, was calculated, where R_0 was the resistance of the palladium cathode without hydrogen loadings. The relative resistance ratio ,R/R_0, was plotted versus loading ratios, D/Pd, at 298 K . The calibration curve was the one employed by M. McKubre and coworkers[2].

3. Results and Discussion

A. Effect of the current patterns

It has been often suggested that an electrolytic current pattern of the electrolysis would play a crucial role in the phenomenon of "cold fusion" [3,4], and that this current pattern would also affect the deuterium loading in the palladium cathodes. M. McKubre et al. [5] reported that they achieved high loading ratios by step-up electrolysis and periodic stripping of a cathode surface with a reversed polarity for deloading.

As the first step in the construction of our palladium rods evaluation system, we had to decide the electrolytic current pattern to obtain higher loading ratios. A step-up electrolytic current pattern included an anodic stripping; started with a low constant current, then stepped-up to a higher current and reversed the current polarity for a short time at a low current, was employed in the present experiments. Furthermore, a constant electrolytic current pattern (at 200 mA/cm^2) was examind.

Figure 3 shows a different behavior of deuterium loading into a palladium cathode. "Standard palladium cathodes" were used in this case.

In the step-up electrolysis, at the initial stage of the constant current electrolysis ($20mA/cm^2$), the R/R_0 value increased to near 2.0 and then began to decrease. It means that the deuterium loading ratios went beyond 0.75 and the further decrease of R/R_0 values indicated the increase of deuterium loading ratios. The maximum loading ratio increased as the electrolytic currents were increased, finally, attained to 0.91

In the high constant current electrolysis, at the beginning of the constant current electrolysis of $200mA/cm^2$, the R/R_0 value started to decreased through the first peak ($R/R_0=2$) as well as the step-up electrolysis. The decrease stopped to the 1.9 of R/R_0 and the further decrease was not observed and eventually the maximum deuterium loading ratio attained to 0.85 at most.

From these results, we had selected the step-up electrolytic current pattern for evaluating our palladium rods.

In addition, the alternating polarity method was also examined in the present experiments. And, it was found that the loading ratios after such anodic stripping of some palladium cathodes were observed to get higher than those before the anodic stripping. Typical results of the anodic stripping are shown in Figure 4, which are not always reproducible even under the same electrolytic condition. It is uncontrollable for us at present. Accordingly the palladium cathodes are electrolyzed by the step-up current pattern included an anodic stripping and evaluated with the maximum loading

ratio before the anodic stripping.

The maximum loading ratio of many "Standard" palladium cathodes were measured to exhibit D/Pd= 0.90 ± 0.01 before the anodic stripping which was still not good enough according to the SRI criterion for the better excess heat generation.

B. Effect of Processing on Deuterium Loading Ratio

Effects of unidentified characteristics of those processed palladium rods on the deuterium loading ratios were investigated from the following two points of view.

One is that a certain processing to a palladium rod surface seems to influence its bulk properties. Another is that the processing will change and control only some surface conditions.

The maximum deuterium loading ratio of each palladium rod before the anodic stripping was considered to be governed by its bulk properties.

Experimental results are summarized in Table 2. When the purity of palladium rods, or some processing such as casting and annealing, which might change their bulk properties, were modified, their maximum deuterium loading ratios were observed still not to exceed that of Standard.

Further treatments were added, such as polishing, etching by aqua regia, heating to a high temperature, etc. to a standard palladium rod with an expectation of some effect on the deuterium loading ratio. These results are summarized in Table 3.

Eventually two effective surface treatments were identified to produce higher loading ratios than the standard palladium rods without treatment ; etching by aqua regia and high temperature annealing in the vacuum for a long time.

(i)Etching process by aqua regia

Aqua regia was prepared from HNO_3 (WAKO, highest grade, HNO_3 70 %) : HCl (WAKO, highest grade, HCl 30 %) = 1 : 4, volumetric ratio. The standard palladium rods were etched by aqua regia immediately after preparing the aqua regia for a definite time and rinsed by pure light water. To remove hydrogen gas absorbed in these samples during the etching, these samples were heated at 200 ℃ in a low vacuum condition ($\sim 10^{-2}$ Torr) for 24 hours.

Figure 5 shows the resistivity changes during electrolysis of the standard palladium rods etched for a different length of time. At the initial stage of the electrolysis, at 20 mA/cm^2, a rapid decrease of the resistivity was observed and followed by an increase. This is a peculiar feature to the palladium cathode etched by aqua regia and the cathode will indicate a rapid deuterium absorption and desorption at each change of electrolytic currents. The etched palladium rods were observed to attain higher loading ratios than the standard palladium rods, and the maximum deuterium loading ratios of the palladium rods etched by aqua regia for 10 minutes could attain to D/Pd = 0.95.

The chemical etching by aqua regia can be expressed as a chemical oxidization of palladium. From resistivity changes of electrochemically oxidized palladium rods, some additional studies were made on the effect of such chemical oxidation on the deuterium loading. Prior to the electrolysis, the standard palladium rod were oxidized by the anodic oxidation at the electrolytic current density of 20 mA/cm^2 for 20 hours, and the result is shown in Figure 6.

The palladium oxide formed on the surface by the anodic oxidation was found to reduce to show a metallic palladium surface as soon as the cathodic electrolysis is started. Apparently the color of the palladium rod was observed to turn into a dark black color with the anodic-cathodic polarization cycle, which may indicate a morphology change on the surface.

However, the maximum deuterium loading ratio of palladium with anodic oxidation was so small that the deuterium loading ratio was less than 0.75. From the result, we concluded that the anodic oxidation has no effect on the improvement of deuterium loading ratios such as shown by the chemical oxidation by aqua regia.

(ii)Heat treatment in vacuum at high temperature

Influence of heat treatments in the vacuum at high temperatures on the deuterium loading ratio was studied. The standard palladium rods were heated in a vacuum (5×10^{-5} Torr) at 1000 ℃ for 24 hours. (or 1200 ℃ for 24 hours) before the electrolysis.

Figure 7 shows the loading characteristics of those heat-treated palladium electrodes (1000 ℃ in the vacuum for 24 hours). Temporal changes of the resistivity of these palladium rods were gentle, that is to say, the deuterium absorption rate was rather slow, but the maximum deuterium loading ratio was attained to the value as high as 0.94.

It is conceived that the heat treatment can affect not only on surface properties, but also bulk properties. The heat-treated palladium rods were polished to remove surface layers, which might affect loading characteristics. Figure 8 shows loading characteristics of those of the heat-treated ones.

It will be conclusively important observation that resistivity changes of those heat-treated palladium rods are observed to show the same resistivity charactaeristics when their surface is polished. Thus we can conclude that the surface condition of palladium is a more crucial factor to control the deuterium loading than its bulk properties.

4. Conclusions

1) To achieve a higher deuterium loading ratio of palladium cathodes the step-up electrolysis must be adopted.

2) The deuterium loading characteristics is influenced and controlled the surface condition of palladium cathode rather than its bulk properties.

3) The deuterium loading ratios as high as 0.95 can be obtained by two simple treatments. They are etching by aqua regia and heating in vacuum at 1000 ℃ for 24hrs. With the above two treatment, each loading characteristics was observed not same with each other, but both treatments are observed to improve the maximum deuterium loading ratios in palladium cathodes, which were higher than that with the standard palladium rods.

References

1. M.Flischmann, S.Pons and M.Hawkins, *J.Electroanal. Chem.*, **261**(1989) 301.
2. M. C. H.McKubre, R.C.Rocha-Filho, S.Smedley, F.Tanzella, J.Chao, B.Chexal, T.Passell and J.Santucci, *Proc. 1st Annu.Conf. on Cold Fusion*, Salt Lake City, National Cold Fusion Institute, UT, 28-30, March 1990.
3. Celani, F., A. Spallone, P.Tripodi, A.Nuvoli, A.Petrocchi, D.Di Gioacchino, M.Boutet, P.Marini and V.Di Stefano, "High Power μs Pulsed Electrolysis for Large Deuterium Loading on Palladium Plates" , *Proc. Fourth International Conference on Cold Fusion*, Lahaina, Maui, Dec. 6-9, 1993. EPRI TR-104188-V1(1994), p.22.
4. Takahashi.A, A.Mega, T.Takeuchi, H. Miyamaru, and T.Iida, "Anomalous Excess Heat by D_2O/Pd Cell Under L-H Mode Electrolysis" , *Proc. Third International Conference on Cold Fusion,* October 21-25, 1992, Nagoya Japan, "Frontiers of Cold Fusion" , (H. Ikegami, ed), p.79.
5. M.McKubre, B.Bush, S.Crouch Baker, A.Hauser, N.Jevtic, S.Smedley, F.Tanzella, M.Williams, and S.Wing, "Loading, Calorimetric and Nuclear investigation of the D/Pd System" , *Proc. Forth International Conference on Cold Fusion,* Lahaina Maui, Dec. 6-9, 1993, EPRI TR-104188-V1, P.5.

Table 1. Elemental analysis of standard Pd.

(ppm)

Element		Pt	Au	Ag	Al	B	Ca	Cd	Cr	Cu	Fe	Mg	Pb	Si	Ti
Raw material		<10	<10	7	-	-	3	-	-	6	<10	<1	-	<1	-
Casting Pd	Upper part	<10	<10	4	53	240	37	-	-	3	50	<1	-	1	<5
	Lower part	<10	<10	3	30	200	5	10	<1	5	10	<1	-	10	-

This analysis was carried out by ICP.

Table 2. Various Pd material and its maximum deuterium loading ratio before anodic stripping.

Parameters		Number of Samples	Average	Range of $(D/Pd)_{max}$ 0.85 0.90 0.95
Standard Pd		14	0.90	
Purity	99.99 %	2	0.89	
	99.5 %	2	0.88	
Casting	Melted in vacuum	4	0.89	
Annealing in vacuum	Unannealed	2	0.88	
	550 °C for 2 hr	3	0.86	
	1000 °C for 24 hr	3	0.89	

All Pd rods were polished by diamond slurry for 30 minutes to have same surface condition.

Table 3. Maximum deuterium loading ratio with Standard Pd before anodic stripping.

Parameters		Number of Samples	Average	Range of $(D/Pd)_{max}$ 0.85 0.90 0.95
Standard Pd		14	0.90	
Polishing	Unpolished	3	0.87	
	Polished for 4 hr	2	0.89	
	Polished by argon plasma	2	0.88	
Etching by aqua regia	Etched for 20 sec.	2	0.92	
	Etched for 3 min.	3	0.93	
	Etched for 10 min.	7	0.94	
Heat treatment in vac.	1000 °C for 24 hr	3	0.94	
	1200 °C for 24 hr	2	0.93	

Surface treatments were added on Standard Pd rods except for unpolished.

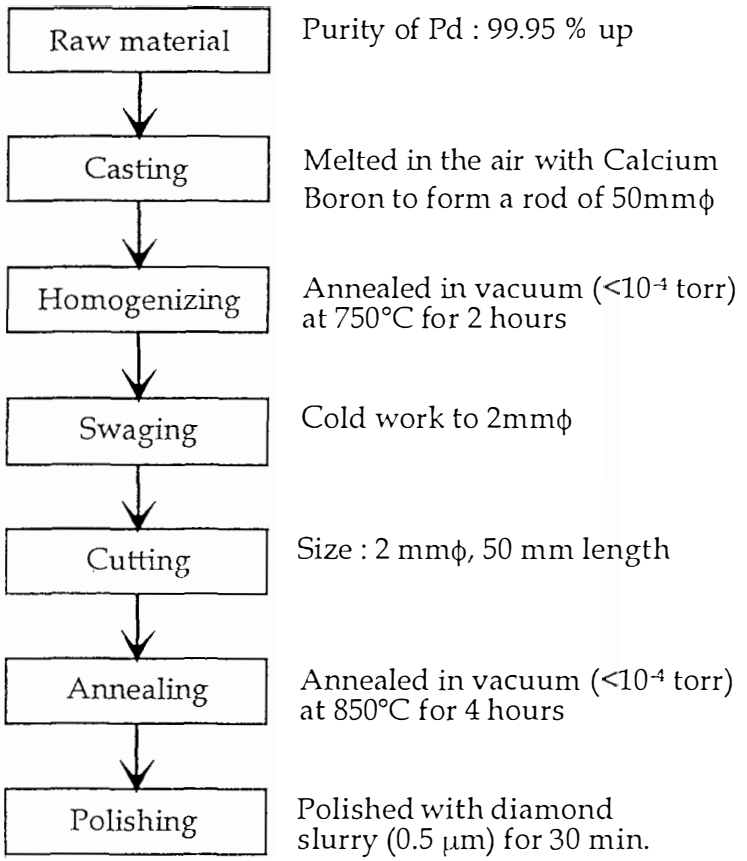

Figure 1. Process of Standard Pd electrode.

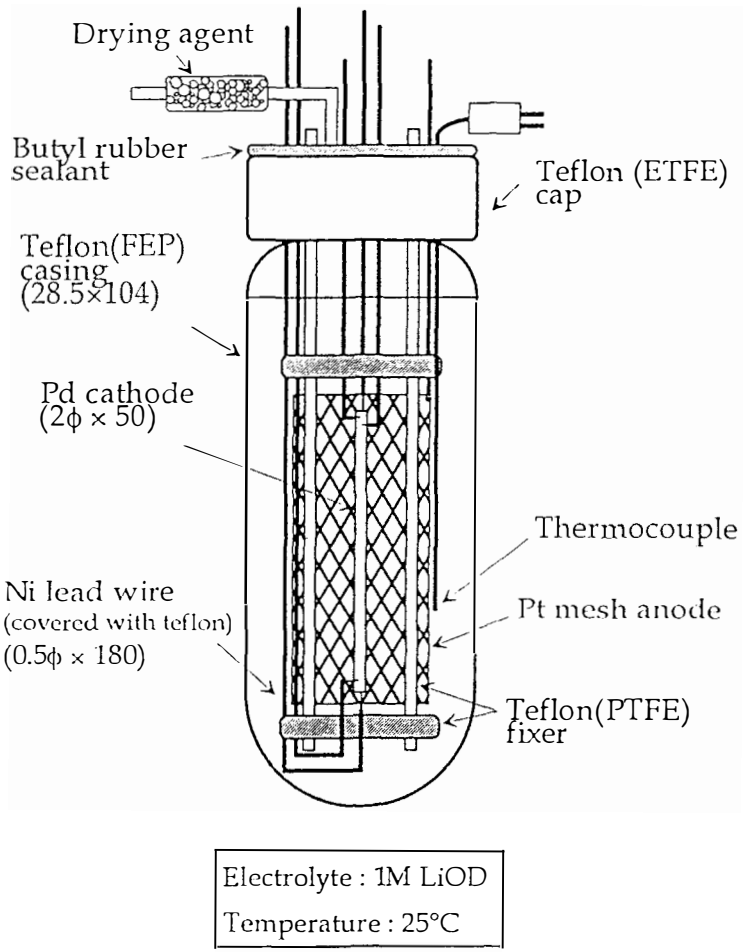

Figure 2. Electrochemical cell for Pd resistance measurements.

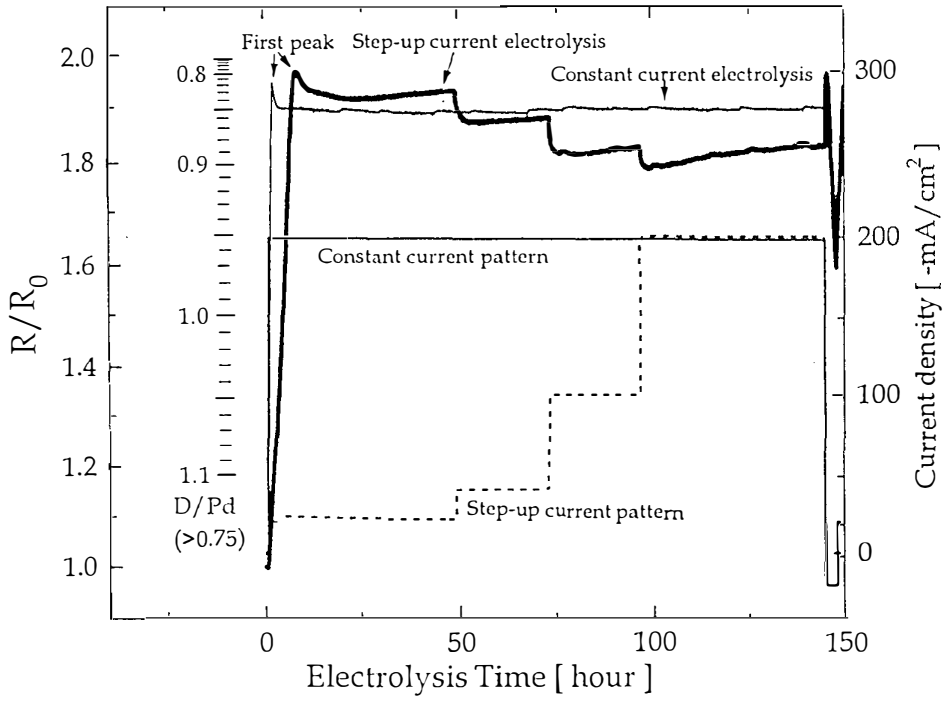

Figure 3. Effect of the current pattern on the loading ratio.

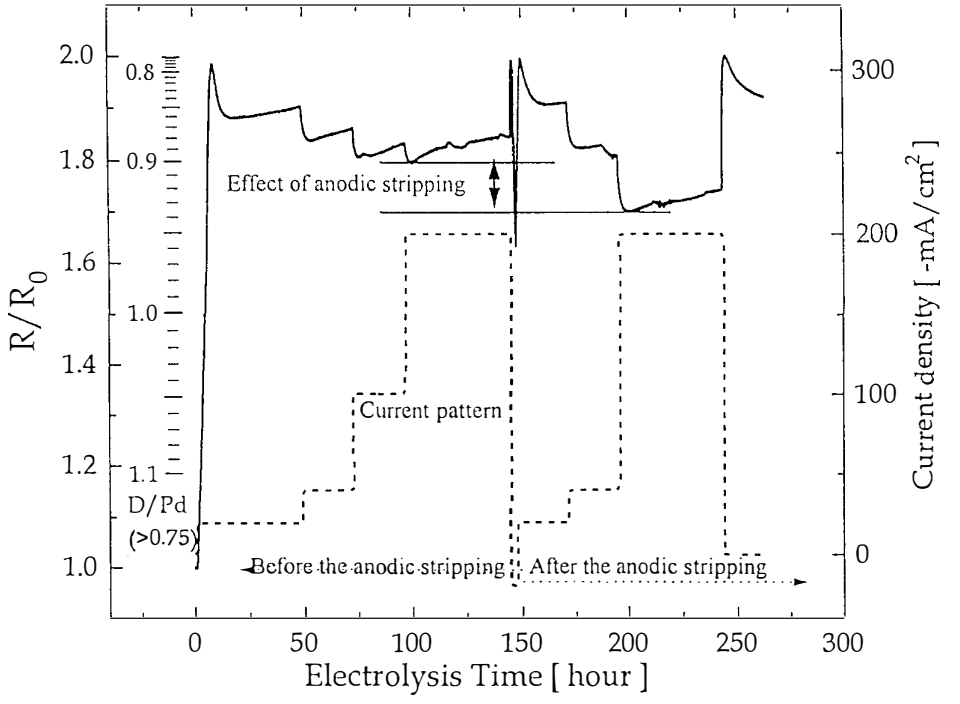

Figure 4. Effect of anodic stripping.

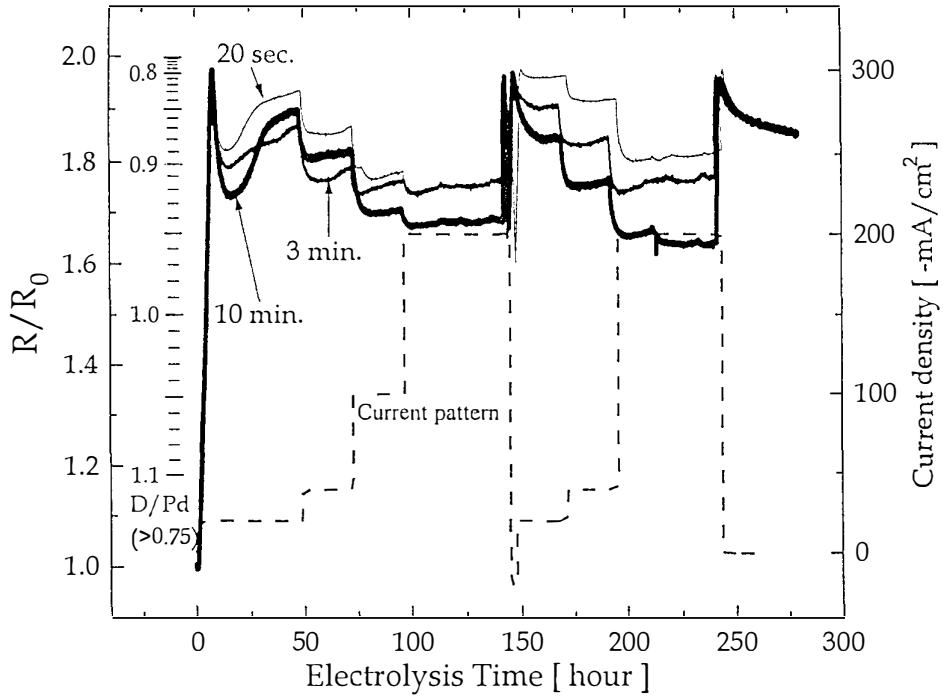

Figure 5. Effect of etching time by aqua regia for a different period of treatment.

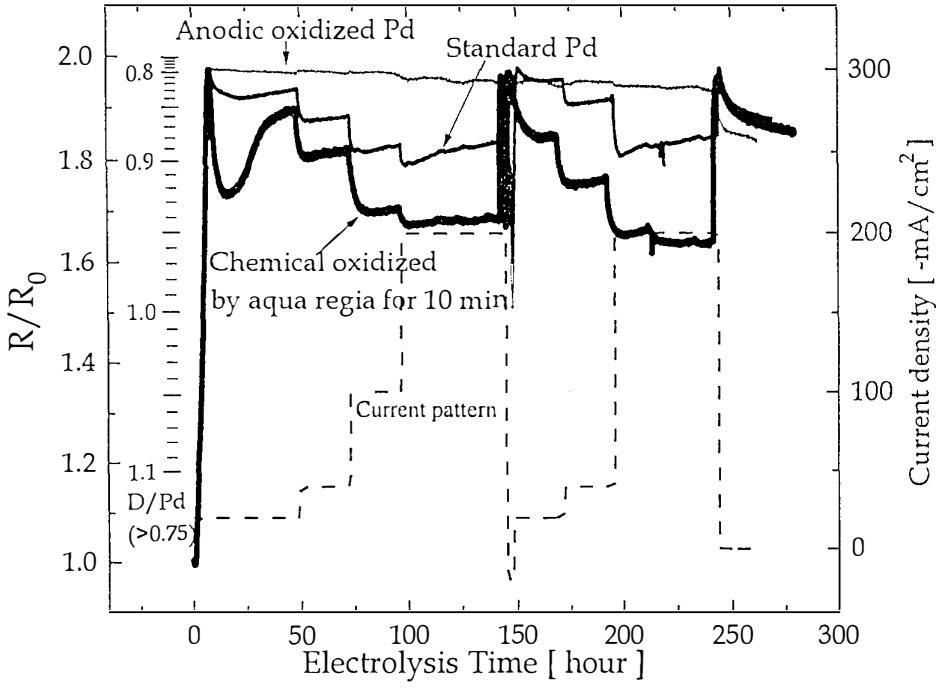

Figure 6. Effect of electrochemical oxidation.

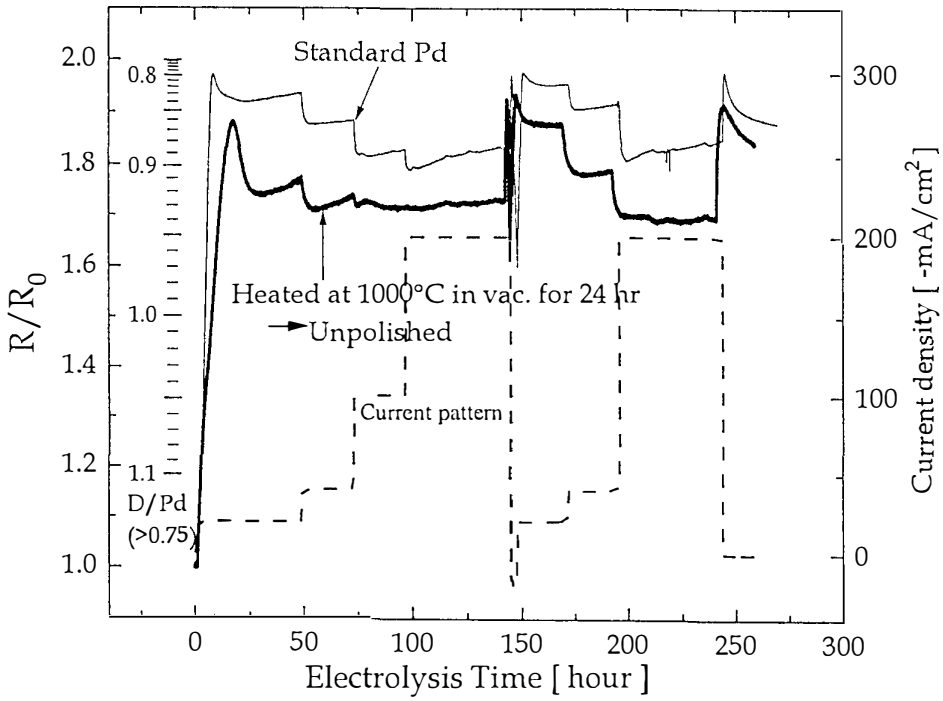

Figure 7. Effect of heat treatment in the vacuum.

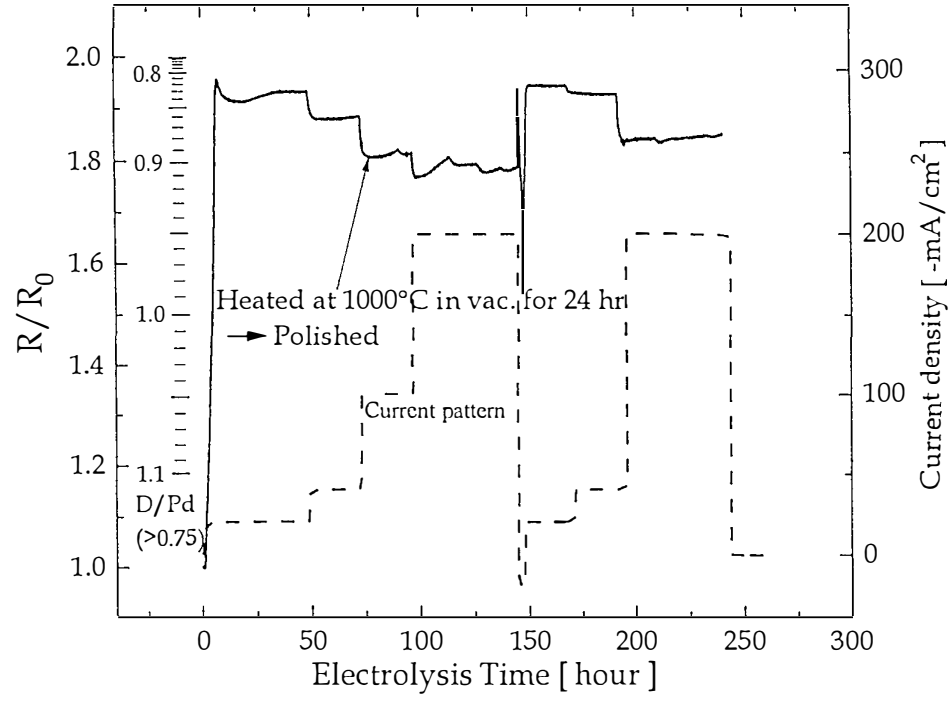

Figure 8. Effect of polishing after heat treatment in the vacuum

Fifth International Conference on Cold Fusion
9-13 April, 1995 - Monte Carlo, Monaco
ICCF5 ©1995

Some Thermodynamic Properties of the H(D)-Pd system

S. CROUCH-BAKER, M. C. H. McKUBRE and F. L. TANZELLA,
Energy Research Centre,
SRI International,
Menlo Park, CA 94025, U.S.A.

Abstract

In any discussion of the origin, measurement or description of the anomalous power producing process which occurs in connection with the electrochemical loading of deuterium into palladium, knowledge of the thermodynamic behaviour of the system is clearly of importance. More particularly, since the formation of highly loaded palladium is implicated as a necessary (but itself insufficient) condition for the observation of anomalous power, thermodynamic considerations relating to the attainment of high loadings are of interest. Here, it is intended to review, at a general level, those aspects of the thermodynamic nature of the H(D)-Pd system, both equilibrium and non-equilibrium, which appear to bear most directly on the question of excess power production in relation to the attainment of high loadings.

1. Introduction

Although considerable effort has been expended in the study of the H(D)-Pd system,[1,2] relatively little attention has been paid to the thermodynamic properties of compositions within the β (α′) phase, in particular for $x > 0.8$. In the context of excess power production in the D-Pd system, this deficiency is particularly unfortunate since the attainment of loadings higher than about 0.85 appears to be *one* of the criteria necessary for its observation.[3-6]

Experimentally, the reproducible attainment and maintenance of electrochemical loadings larger than about 0.85 have proven to be more challenging than might be expected from cursory inspection of earlier literature and, presently, much of the effort in the "new hydrogen energy" field is devoted to this issue. Clearly, in order to understand fully the calorimetric behaviour of the H(D)-Pd system at elevated loadings (i.e. elevated values of the H(D) *chemical potential*, at modest temperatures and pressures[3]), a number of thermodynamic issues must be addressed. A number of such issues are discussed briefly here; although both hydrogen and deuterium alloys are described, the data cited are for H-Pd (at 298 K) unless otherwise indicated.

2. Non-ideality in the H(D)-Pd system

Any description of the thermodynamic properties of the β phase must take into account the fact that it is a non-ideal solution of hydrogen in palladium. Thus the thermodynamic state functions vary not only with temperature and pressure (or

volume), but also with *composition*. The chemical potential of hydrogen in palladium may be written as:[7]

$$\mu = \mu^0 + R\,T \ln \frac{x}{1-x} + \mu^{ex} \qquad (1)$$

where the term μ^{ex} is introduced to account for deviations from ideal solution behaviour. For didactic purposes at least, it is found convenient to regard the dissolved hydrogen as electronically screened protons. This leads to the decomposition of μ^{ex} into two (additive) terms: Firstly, an "elastic" term due to the dilation of the lattice on occupation by hydrogen. This term is increasingly negative with increasing x (very approximately linearly so) corresponding to a net attractive interaction between the screened protons. Secondly, an "electronic" term which reflects the rise in the Fermi level due to the electrons associated with the dissolved hydrogen. This term is increasingly positive with increasing x, increasing relatively slowly for $x < 0.6$ as the high density-of-states 4d band is occupied, but more rapidly, and approximately linearly, at higher loadings as electrons are forced to enter the low density-of-states 5s band (for a detailed account, see Ref. 2). For compositions in the β phase ($x > 0.6$) the electronic term dominates, leading to a linear variation of μ with x, as has been observed experimentally for both H and D, at least up to $x = 0.8$.[8,9]

The non-ideal nature of hydrogen in palladium has several consequences of interest in the context of loading. For example, the dependence of chemical potential on loading contributes directly to the Fick's law diffusion coefficient,

$$D_F = M\,x\,\frac{\partial \mu}{\partial x} \qquad (2)$$

Recent measurements on the H-Pd system reveal that D_F increases with x in the β phase[10] indicating that the rapid rise of μ with loading offsets the anticipated drop in mobility with increased octahedral site occupancy (however, contrary data have been reported[11]).

Another quantity of interest is the (relative) partial molar enthalpy of absorption in the β phase, ΔH_r. This is the enthalpy change for the *constant temperature* process

$$\tfrac{1}{2}\,H_2\,(p^0, T) \rightarrow [H]\,(x, p, T) \qquad (3)$$

By considering ΔH_r to be a function of volume and composition, we may derive the following compositional dependence[2,12]

$$\Delta H_r = \Delta H_r(x=0) - \frac{V_H^2\,K\,x}{V_{Pd}} + \int_0^x \left(\frac{\partial \Delta H_r}{\partial x}\right)_V dx \qquad (4)$$

The second and third terms on the right-hand-side of Eqn. 4 behave analogously to the elastic and electronic contributions, respectively, to the chemical potential. In Fig. 1, the quantity "$\Delta H_r - \Delta H_r(x=0) - p\,V_H$" is plotted schematically versus loading, together with its "elastic" and "electronic" components.[13] (Qualitatively, the behaviour of this

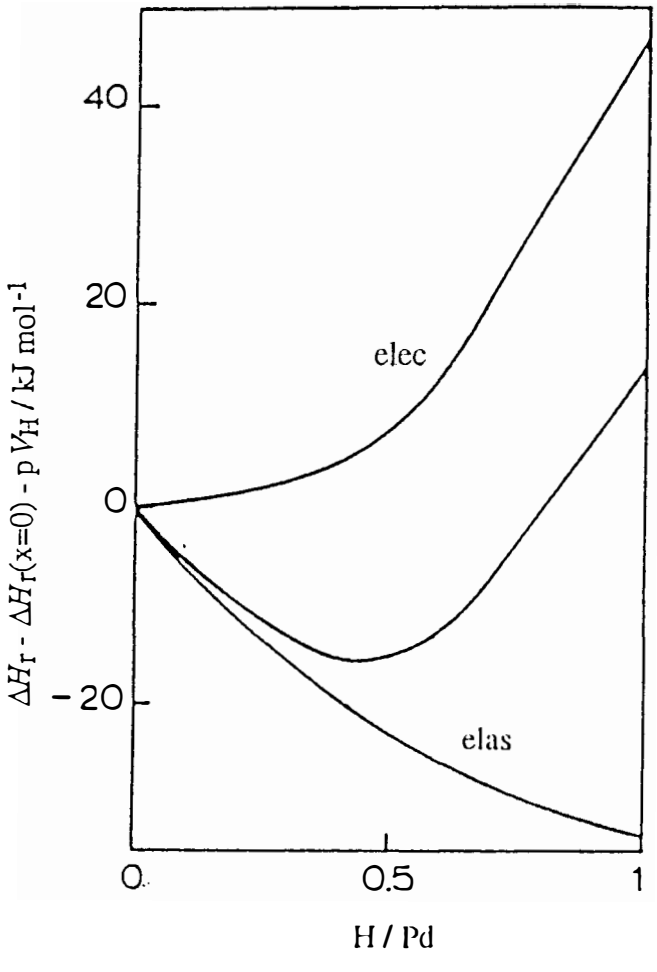

Figure 1. Compositional dependence of elastic and electronic contributions to relative partial molar enthalpy. Adapted from Ref. 13.

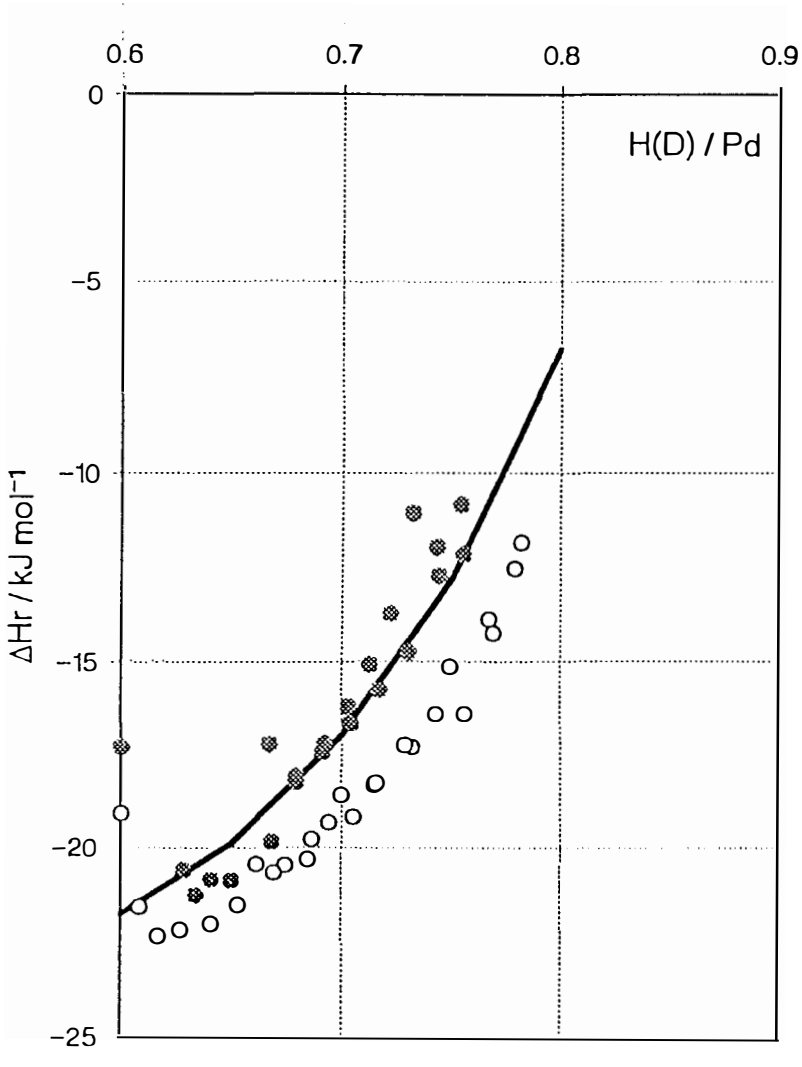

Figure 2. Relative partial molar enthalpies: calorimetrically determined, H (open circles), D (filled circles); calculated, H (line). Data from Refs. 9 and 14.

quantity is the same as that of ΔH_r itself since the additional terms are either relatively small or constant). At low loadings, the partial molar enthalpy of absorption is exothermic, due to the dominance of the negative elastic contribution. However, similar to the behaviour of the chemical potential, in the β phase region the electronic term dominates, causing the relative partial molar enthalpy to become more positive with increasing loading. The results of a detailed statistical thermodynamical calculation of ΔH_r for *hydrogen* are shown in Fig. 2.[14] It is apparent that, unless a phase change occurs in the region $0.8 < x < 1.0$, ΔH_r is expected to become endothermic somewhere in this interval. In Figs. 1 and 2, it should be noted that the existence of the two-phase region for $x < 0.6$ has not been explicitly recognized; this is often the case in modelling studies based on equations such as (1) and (4). For increasing loading in the two-phase region, the molar enthalpy change is independent of composition and approximately -19 kJ mol^{-1} for H-Pd and -17 kJ mol^{-1} for D-Pd.[9]

Calorimetrically measured values of ΔH_r are shown for both hydrogen and deuterium in Fig. 2.[9,15] Although these data do not extend to particularly high loadings, they are in broad, if not exact, agreement with theoretical predictions. It is of interest to note that the exothermic / endothermic transition is expected to occur at a lower loading for deuterium than for hydrogen. It should be remarked that experimental values of ΔH_r are available in the literature for $x > 0.9$.[16] However, other researchers have questioned these data[17] and they are not included here.

Since direct calorimetric measurement of ΔH_r at high x may be difficult, it is of interest to see if other experimental data may be used to derive ΔH_r values. From elementary thermodynamics we may derive

$$\Delta H_r = T\,(V_H - {}^1/_2\,V_{H_2})\left(\frac{\partial p}{\partial T}\right)_x - \frac{R\,T^2}{2}\left(\frac{\partial \ln f_{H_2}}{\partial T}\right)_p \qquad (5)$$

where the first term on the right-hand-side is the partial molar enthalpy change for the process

$${}^1/_2\,H_2\,(p, T) \rightarrow [H]\,(x, p, T) \qquad (6)$$

This is a negative quantity at accessible pressures. The second term corresponds to the molar enthalpy change (a positive quantity) for the process

$${}^1/_2\,H_2\,(p^0, T) \rightarrow {}^1/_2\,H_2\,(p, T) \qquad (7)$$

This latter process is well-characterised thermodynamically; thus calculation of ΔH_r is essentially a matter of determining the pressure-compositions isotherms over a range of temperatures at high loadings.

For a finite change in loading at constant temperature (involving the production or consumption of hydrogen gas at 1 atm.), the total enthalpy change is given by

$$\Delta H(x_1 \rightarrow x_2) = \frac{1}{x_2 - x_1}\int_{x_1}^{x_2} \Delta H_r\,dx \qquad (8)$$

Furthermore, the total energy change, $\Delta U(x_1 \rightarrow x_2)$, and $\Delta H(x_1 \rightarrow x_2)$ differ by no more than about 1 kJ mol^{-1}, for loadings up to approximately unity.

3. Gas-phase vs. electrochemical loading

Gas-phase and electrochemical loading differ thermodynamically in two important respects: Firstly, with respect to the value of μ for a given loading; secondly, with respect to the ease of measurement of μ (and, hence, the loading) for each loading method. In what follows, it is assumed that metallurgical considerations do not intervene to lower the loading below that (maximum) value which corresponds to the thermodynamic state of surface adsorbed hydrogen atoms, i.e. in the electrochemical steady-state, the metal is internally in equilibrium. Furthermore, for ease of expression, only acidic conditions are considered in the electrochemical case; the following arguments are unchanged for loading in basic solutions. Finally, during electrochemical loading, it is assumed that the ambient hydrogen pressure is 1 atm.

The essential differences between gas-phase and electrochemical loading are illustrated in Fig. 3. In this figure, H_a represents a surface-adsorbed hydrogen atom, while H_i represents dissolved hydrogen. In gas-phase loading, a state may be reached where the environing hydrogen gas, surface adsorbed hydrogen atoms, dissolved hydrogen atoms and any hydrogen gas formed in voids within the metal are in equilibrium. In this case, the loading at a given temperature is determined by the fugacity of the environing hydrogen gas (or hydrogen partial pressure, at pressures less than about 100 atm.). In the electrochemical case, on the other hand, the steady-state does not necessarily correspond to equilibrium between the environing hydrogen gas and the surface adsorbed hydrogen atoms. Hence, the sample experiences a hydrostatic pressure of 1 atm. regardless of the chemical potential of surface adsorbed hydrogen atoms. (Note, however, that any gas formed in voids within the metal is in chemical equilibrium with the dissolved hydrogen, leading to pressurized voids). Thus, *at a given loading*, the chemical potential of dissolved hydrogen loaded electrochemically, $\mu(p^0\ x)$, is related to the chemical potential obtained in gas-phase loading, $\mu(p, x)$, by

$$\mu(p^0, x) = \mu(p, x) - \int_{p^0}^{p} V_H \, dp \qquad (9)$$

This difference, although conceptually important, is generally small numerically. In other words, those physical properties of gas-loaded and electrochemically loaded palladium which are dependent of the chemical potential of hydrogen will differ only negligibly; for example, the pressure generated within voids in the metal when loaded electrochemically will be slightly less than that generated under gas-phase loading, for the same loading. As an aside, we note that a situation similar to electrochemical loading exists in so-called *gas phase atomic loading*, Fig. 3. Here, hydrogen atoms are generated continually in the gas phase from molecular hydrogen using a hot wire. These hydrogen atoms are not equilibrated with the molecular hydrogen, i.e. are formed with an elevated chemical potential, and are thus capable of causing high loadings, as has been demonstrated experimentally.[18] We speculate that the ultrasonic cavitation of water in the presence of a palladium substrate (where hydrogen atom generation is known to occur[19]) will have similar consequences.

The following question naturally arises: can we, in an electrochemical experiment, infer the loading of a palladium cathode from the measured cathode

a) Gas phase loading - chemical equilibrium

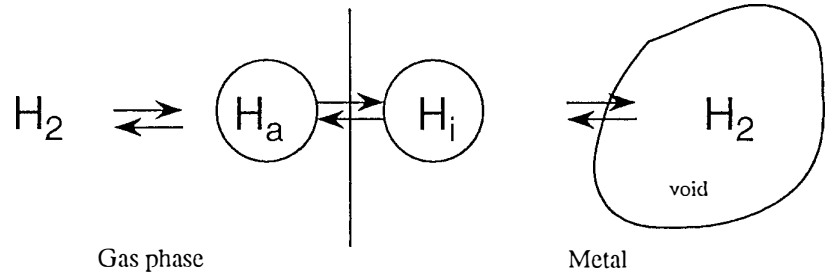

b) Electrochemical loading - steady-state

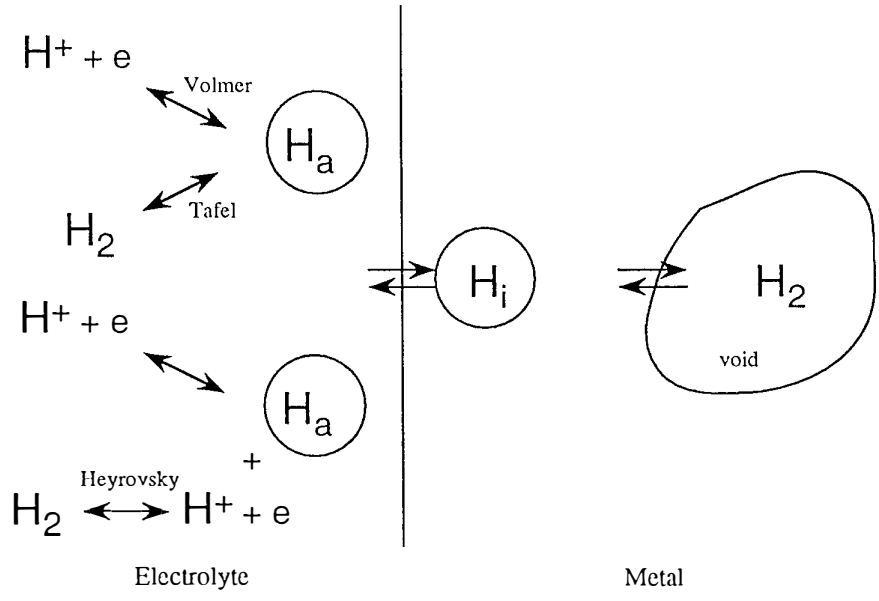

c) Gas phase atomic loading - steady state

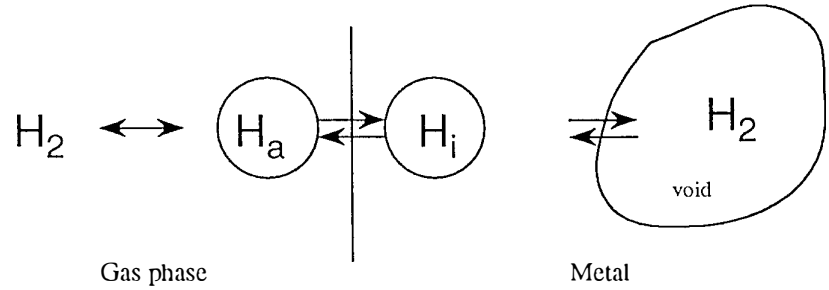

Figure 3. Loading mechanisms

overvoltage? In gas-phase loading, knowledge of the hydrogen pressure and the temperature are sufficient to determine the palladium loading at equilibrium. Thus gas-phase loading is generally not suitable for achieving very high loadings due to the experimental difficulties caused by the enormous pressures involved. In electrochemical loading, on the other hand, while it is possible to generate overvoltages at a palladium cathode which are, in principle, sufficient to raise the chemical potential of the dissolved hydrogen to values necessary for loadings approaching unity (greater than 35 kJ mol^{-1} or 0.35 eV for H), it is *not* possible to convert a measured overvoltage directly into a loading without detailed knowledge of the electrochemical reaction mechanism. This subject has been discussed extensively in the literature[20-23] and only the key points are summarized here.

In general, two *extreme* cases may be recognized:

(i) For an electrochemical reaction in which the electron transfer (Volmer) step has a relatively small - in the limit, zero - affinity (i.e. is in a state of "quasi-equilibrium"):

- The dissolved hydrogen is not equilibrated with the environing hydrogen.
- High loadings are possible (the chemical potential of dissolved hydrogen is directly proportional to the (negative) overvoltage measured with respect to a standard hydrogen reference electrode, η).
- Metal voids are pressurized, leading potentially to cracking and blistering.

(ii) For an electrochemical reaction in which the hydrogen atom recombination (Tafel) step is in quasi-equilibrium:

- The dissolved hydrogen is equilibrated with the environing hydrogen.
- High loadings are not possible (the chemical potential of dissolved hydrogen is given directly by the environing gas pressure and is not related to the overvoltage).
- Metal voids are not pressurized.

It is important to realise that the two cases described above represent the upper and lower limits of a spectrum of possible behaviour (a third possibility, that of an atom-ion recombination (Heyrovsky) step in quasi-equilibrium, is similar to case (ii) in that it is not condusive to high loadings); in practice, the situation will be somewhere in between such that only a *fraction* of the measured overvoltage is used to determine the chemical potential of dissolved hydrogen. This fraction is determined by the affinity distribution between the various elementary steps, which is turn is decided by the relative values of the forward and reverse reaction rates for each step. Thus, ultimately, the loading / overvoltage (or loading / current) functionality is determined by kinetic factors. Traditional electrochemical procedures may be used to induce a functionality which corresponds more closely to (the desirable) case (i) than (the undesirable) case (ii) above; for example, the addition of thiourea, which is known to increase the affinity of the Tafel step (i.e. the overvoltage at constant current under case (i) conditions), thereby preventing it reaching a state of quasi-equilibrium, and hence enhancing the loading.[24,25]

In the event that the kinetic properties of the system are such that, in the limit, case (i) behaviour is observed (or, in the general case, that the affinity of the Volmer step is independent of overvoltage), a simple relationship may be derived for the dependence of loading on overvoltage (or current). Under case (i) conditions (referred to in the electrochemical literature as "fast discharge / slow recombination"),

$$- F \eta = \mu - \mu^* \qquad (10)$$

where μ^* is the chemical potential of dissolved hydrogen with no applied overvoltage (i.e. that value corresponding to the environing hydrogen pressure). Up to loadings of about 0.8 (and perhaps beyond, although data are lacking), μ varies linearly with loading, as discussed above, and, hence

$$\eta = A\,x + B \tag{11}$$

where A and B are constant at a given temperature. Further, if Tafel's law is obeyed, the loading is expected to vary logarithmically with the current. Experimental verification of these relationships has been obtained,[5] even at loadings well above those at which the linear μ, x dependence has been observed empirically.

4. Effect of temperature on loading

The results obtained above may be used to address the question: how does the loading of a palladium sample vary with temperature? In the general case, we may write:

$$\left(\frac{\partial x}{\partial T}\right)_p = \left\{\left(\frac{\partial \mu}{\partial T}\right)_p - \left(\frac{\partial \mu}{\partial T}\right)_{x,p}\right\} \Big/ \left(\frac{\partial \mu}{\partial x}\right)_{T,p} \tag{12}$$

In the case of gas-phase loading, where equilibrium exists between the sample and the environing hydrogen, the first partial differential term on the right-hand-side of Eqn. 12 may be expressed in terms of the properties of the environing hydrogen, giving

$$\left(\frac{\partial x}{\partial T}\right)_p = \Delta S_6 \Big/ \left(\frac{\partial \mu}{\partial x}\right)_{T,p} = \Delta H_6 \Big/ T\left(\frac{\partial \mu}{\partial x}\right)_{T,p} \tag{13}$$

where ΔS_6 and ΔH_6 are the partial molar entropy and enthalpy changes, respectively, of the reaction in Eqn. 6. These are negative quantities, leading to the expected result that, in gas-phase loading, raising the temperature at constant pressure will lower the loading. Note that Eqn. 13 is a mathematical statement of Le Chatelier's principle.

In the case of electrochemical loading, where, if high loadings are to be obtained, the sample is not in equilibrium with its environment, Eqn. 13 may not be employed. Instead, we may utilize Eqn. 10 in order to cast the first partial differential term on the right-hand-side of Eqn. 12 into a more convenient form, and write

$$\left(\frac{\partial x}{\partial T}\right)_{p^0} = \left\{-F\left(\frac{\partial \eta}{\partial T}\right)_{p^0} + \Delta S_r\right\} \Big/ \left(\frac{\partial \mu}{\partial x}\right)_{T,p^0} \tag{14}$$

where ΔS_r is the partial molar entropy change of the reaction in Eqn. 3, a negative quantity. Eqn. 14 is valid for case (i) conditions, described in Sect. 3. (Of course, case (ii) conditions correspond to Eqn. 13). In the (likely) event that an intermediate case is encountered, an additional partial differential must be added to the bracketed term in Eqn. 14 in order to include the temperature dependence of the reaction affinity for the Volmer step. Thus, in the case of electrochemical loading, a number of (ultimately) kinetically-determined factors enter into the determination of $(\partial x/\partial T)_{p^0}$, the sign and magnitude of which are difficult to predict. Under case (i) conditions, in order to ensure that the loading increases as a result of a temperature step, the overvoltage must

increase (become more negative) at constant current. The magnitude of this increase is given by Eqn. 14 if ΔS_r is known. Practically, an increasing overvoltage with increasing temperature (at first sight, an unlikely situation) might correspond to an increasingly "poisoned" recombination step (either atom-atom or atom-ion); for example, due to a change in electrode surface composition with increasing temperature. Finally, it will be noted that the value of ΔH_r is important in this context only to the extent that it contributes (partially) to ΔS_r.

5. Concluding remarks

The present discussion has centered on the properties of highly loaded compositions in the H(D)-Pd system. Unfortunately, a general absence of pertinent empirical data hampers a definitive development of many of the areas of inquiry dealt with here. In order to fully understand the properties of the highly loaded H(D)-Pd system, considerable experimental work is required in order to determine basic thermodynamic parameters for $x > 0.8$. This is particularly important if the possibility of new phase formation at elevated loadings cannot be discounted.

Acknowledgments

The financial support provided by the Institute of Applied Energy and the New Energy and Industrial Technology Development Organization (Japan) and the Electric Power Research Institute (U.S.A.) is gratefully acknowledged.

List of Symbols / Nomenclature

μ = chemical potential of dissolved hydrogen
μ^0 = a standard chemical potential
D_F = Fick's law diffusion coefficient
M = mobility
ΔH_r = (relative) partial molar enthalpy of absorption
$\Delta H_r(x=0)$ = as above, at infinite dilution
ΔH = enthalpy change
ΔU = energy change
V_H = partial molar volume of hydrogen
V_{Pd} = molar volume of Pd
V_{H2} = molar volume of gaseous H_2
x = loading ratio, H(D)/Pd
R = gas constant
[H] = dissolved hydrogen
T = absolute temperature
p = total pressure
p^0 = 1 atm. pressure
f_{H2} = hydrogen fugacity
K = bulk modulus of PdH_x
F = Faraday's constant

References

1. Lewis, *The Palladium Hydrogen System*, Academic Press, London, New York (1967).
2. Wicke and Brodowsky, "Hydrogen in Palladium and Palladium Alloys", *Hydrogen in Metals II*, ed. Alefeld and Volkl, Topics in Applied Physics, vol. 29, p. 73, Springer-Verlag, Berlin (1978).
3. Fleischmann, Pons and Hawkins, J. Electroanal. Chem., **261**, 301 (1989); **263**, 187 (1989).
4. McKubre, Crouch-Baker, Riley, Smedley and Tanzella, "Excess Power Observations in Electrochemical Studies of the D/Pd System: the Influence of Loading", *Frontiers of Cold Fusion*, ed. Ikegami, Frontiers Science Series no. 4, p. 5, Universal Academy Press, Tokyo (1993).

5. Kunimatsu, Hasegawa, Kubota, Imai, Ishikawa, Akita and Tsuchida, "Deuterium Loading Ratio and Excess heat Generation during Electrolysis of Heavy Water by a Palladium Cathode in a Closed Cell Using a Partially Immersed Fuel Cell Anode", *ibid.*, p. 31.

6. McKubre, Crouch-Baker, Rocha-Filho, Smedley, Tanzella, Passell and Santucci, J. Electroanal.Chem., **368**, 55 (1994).

7. Wagner, Z. Physik. Chem., **A193**, 386, 407 (1944).

8. Wicke and Nernst, Ber. Bunsenges. Phys. Chem. **68**, 224 (1964).

9. Flanagan, Luo and Clewley, J. Less Common Metals, **172-174**, 42 (1991).

10. Mengoli, Fabrizio, Manduchi and Zannoni, J. Electroanal. Chem., **350**, 57 (1993).

11. Majorowski and Baranowski, J. Phys. Chem. Solids, **43**, 1119 (1982).

12. Fukai, *The Metal-Hydrogen System*, Springer Series in Materials Science 21, Springer-Verlag, Berlin (1993).

13. Hemmes, Salomons, Griessen, Sanger and Driessen, Phys. Rev. B, **39**, 10606 (1989).

14. Flanagan and Lynch, J. Phys. Chem., **79**, 444 (1975).

15. Kuji, Oates, Bowerman and Flanagan, J. Phys. F: Met. Phys., **13**, 1785 (1983).

16. Baranowski, "Metal-Hydrogen Systems at High Hydrogen Pressures", *Hydrogen in Metals II*, ed. Alefeld and Volkl, Topics in Applied Physics, vol. 29, p. 157, Springer-Verlag, Berlin (1978).

17. Feenstra, Griessen and de Groot, J. Phys. F: Met. Phys., **16**, 1933.(1986).

18. Oates and Flanagan, Nature, **231**, 19 (1971).

19. Suslick, "Homogeneous Sonochemistry", *Ultrasound - Its Chemical, Physical and Biological Effects,* ed. Suslick, p. 123, VCH Publishers, New York (1988).

20. Andrews and Ubbelohde, Proc. Roy. Soc., **A253**, 6 (1959).

21. Van Rysselberghe, "Some Aspects of the Thermodynamic Structure of Electrochemistry", *Modern Aspects of Electrochemistry*, ed. Bockris, p. 1, Plenum, New York (1966).

22. Bockris and Subramanyan, Electrochimica Acta, **16**, 2169 (1971).

23. Maoka and Enyo, Electrochimica Acta, **26**, 607, 615 (1981).

24. Bockris and Conway, Trans. Faraday Soc., **45**, 989 (1949).

25. Akita, Tsuchida, Kubota, Kubota, Kobayashi, Yamamoto, Hasegawa, Hayakawa, Kunimatsu, "Electrolytic Hydrogen/Deuterium Absorption into Pd, Pd-Rh and Pd-Ag Alloys in Fuel Cell Type Closed Cell", *Proceedings: Fourth International Conference on Cold Fusion*, EPRI TR-104188-V1, p. 21-1, Electric Power Research Institute, Palo Alto, (1994).

Fifth International Conference on Cold Fusion
9-13 April, 1995 - Monte Carlo, Monaco
ICCF5 ©1995

AN EXPERIMENTAL METHOD TO MEASURE THE RATE OF H(D)-ABSORPTION BY A Pd CATHODE DURING THE ELECTROLYSIS OF AN AQUEOUS SOLUTION: ADVANTAGES AND DISADVANTAGES

M. ALGUERO, J.F. FERNANDEZ, F. CUEVAS AND C. SANCHEZ
Dpto. Física de Materiales, C-IV. Facultad de Ciencias. Universidad Autónoma.
Cantoblanco 28049. Madrid. Spain

Abstract

An experimental set up to measure the rate of H(D) uptake by a Pd cathode during the electrolysis of an aqueous electrolyte has been built and its behavior is analyzed. The experimental procedure is based on the pressure changes that take place within a closed electrolytic cell during the hydride (deuteride) formation. Calibration of the system has been done by accomplishing electrolysis with two Pt electrodes and the error sources have been studied. A protocol to be used in Pd hydrogenation (deuteration) is defined. Finally, the advantages and disadvantages of this experimental method against measurements of the Pd electric resistance variations are briefly discussed.

1. Introduction

It has been shown [1-3] that neither thermal nor nuclear effects are expected during the electrolysis of a heavy water electrolyte with a Pd cathode unless a D/Pd≥ 0.8-0.9 is reached and sustained for a prolonged time, i.e. more than a week. On the other hand, the amount of deuterium that a Pd cathode absorbs, has been shown to depend on both, the characteristics of the electrolysis, i.e. electrolyte, electrodes arrangement, electrolytic current, temperature, etc. and the structural features of the sample bulk and surface [2-5]. Data on the final values of D/Pd with a well established electrolytic configuration and sample metallurgy are scattered and often contradictory [4,5]. It has been also pointed out that once a D/Pd≥0.9 has been reached it seems to decrease with time during prolonged electrolysis at high current densities [2,4,6].

We have built up an experimental set up to measure the rate of hydrogen (deuterium) absorption by a Pd cathode during the electrolysis of an aqueous solution. The technique deals with the amount of gas evolved during the electrolysis. The pressure in a closed electrolytic cell is allowed to raised up to a fixed value at which an electrovalve is opened and closed. The difference between the number of gas molecules evolved in a period of time, and the number of them that should have been evolved, according to the electric charge that has passed in the same period through the cell, is a direct measure of the H(D) absorbed by the cathode (in absence of other sinks or sources

of gas). Similar set ups have been used successfully by other groups in cold fusion research [5,7].

The experimental set up has been tested by carrying out several electrolyses of a light water electrolyte with two Pt electrodes. The role played by the different parameters relevant to the set up has been defined, as well as a protocol to be used in Pd loading experiments.

2. Experimental

The set up we have built up (Fig.1) comprised a closed electrolytic cell (1), an U-shaped glass manometer (2), a deposit with $CaCl_2$ (3), an electrovalve (4), and an electronic circuit (5) that opens the electrovalve. Later on a pre-deposit of water (6), and a thermostatic bath to control the temperature of the electrolyte (7), were added. At overpressures, ΔP, below a fixed value, ΔP_f, the electronic circuit is opened and the electrovalve is closed. The pressure in the cell raises during electrolysis due to gas evolution. When the overpressure in the cell reaches ΔP_f, the level of mercury in the open arm of the manometer reaches two Pt wires, and close the electronic circuit that opens the electrovalve, what allows the accumulated overpressure to disappear. The level of mercury goes down opening the circuit, and so, closing the electrovalve. The circuit is able to keep the electrovalve opened for a certain time, t_r, after this switching. The time between two openings, t_i, is recorded in a PC. Experimental data collected during an electrolysis are a series of times, $\{t_i\}$.

The number of moles, Δn_o, of both $H(D)_2$ and O_2 needed to increase the pressure in the free volume of the electrolytic cell, V, in ΔP_f, at temperature T is given by eq.(1). On the other hand, the number of moles, Δn, of both $H(D)_2$ and O_2, that are evolved in a period of time, t_i, between two openings of the electrovalve, during an electrolysis accomplished in galvanostatic conditions at current I is given by eq.(2), where N_A is the Avogadro's number and e the electronic charge.

$$V\Delta P_f = \Delta n_o RT \qquad (1)$$

$$\Delta n = \left(\frac{I}{2N_A e} + \frac{I}{4N_A e} \right) t_i \qquad (2)$$

The difference, Δn_i, between Δn and Δn_o, that occurs during an electrolysis accomplished with a Pd cathode, is the number of moles of H(D) that have been absorbed by the cathode in the period t_i. The whole amount of H(D) absorbed during an electrolysis is the sum of the series $\{\Delta n_i\}$. The free volume, V, is not constant during an electrolysis but it diminishes due to the electrolyzed water and so, t_i increases with time in a linear fashion at constant electrolytic current.

3. Results

3.1. Qualitative aspects of the set up

A great number of the electrolyses accomplished were devoted to understand and solve the problems we readily faced.

. Both H_2O and Hg were tested as filling liquids of the manometer. H_2O was not operative because its evaporation. Hg also presented shortcomings. Its surface became oxidized during electrolysis so a small amount of an organic compound was put above the Hg surface to prevent it.

. The linear increase of t_i was bigger than it should be by considering the loss of H_2O by electrolysis. It was also observed that bubbles were often formed in the glass line. Both observations were related to the evaporation of the electrolyte induced by the dessecator ($CaCl_2$). The pre-deposit of water (6) was placed to minimize this effect.

. It was also found that some gases (air, H_2. O_2) were absorbed and released by the electrolyte. These phenomena were specially present at the beginning of the electrolysis and whenever a sharp change of the electrolyte temperature took place. The thermostatic bath was placed to eliminate the second possibility. The electrolyte behavior at the beginning of the electrolysis will be discussed in the next paragraph.

3.2. A quantitative analysis of the initial transients

Following the inclusion of the pre-deposit of water and the thermostatic bath, a more systematic program of measurements was designed. Three sets of electrolyses of a LiOH 0.1M electrolyte using Pt foils as electrodes were done. The whole volume of the system was 2000cc. All the components (Hg, electrolyte, $CaCl_2$, and the water within the pre-deposit) were renewed before each electrolysis. Table 1 summarizes the conditions at which the electrolyses were accomplished. The time the electrovalve (4) remained open after the closing of the circuit (5) was fixed in the three sets as 3.4 s. This time allows a good equilibration of the mercury in the two arms of the manometer (2).

Fig.2 shows $\{t_i\}$ for electrolysis 6.$\{t_i\}$ values fit very well to an expression with 6 parameters of the form $\{a + b\tau_i - c\ \exp(-d\tau_i) + f\ \exp(-g\tau_i)\}$, in which τ_i is the electrolysis time at which t_i was recorded. The linear increase is due to the water loss by electrolysis and by evaporation, whenever the pre-deposit is not placed. The two exponential terms describe a transient in t_i that is produced by the release and the absorption of different gases by the electrolyte. The ten electrolyses have been fitted to such an expression and the parameters have been evaluated.

Fig.3 (a) shows the parameter **a** for the ten electrolyses. **a** is the time, t_1, elapsed between switching the current on and the first opening of the electrovalve. It is given by eq.(1-2) with the initial free volume, V=2000cc-V_e. The continous lines in Fig.3 (a) are the expected values according to eq.(1-2). The error bars are the errors associated with the expected values, calculated from the errors of T, V_e, ΔP_f and I. A good agreement is reached between **a** from $\{t_i\}$ and the expected values. This was a essential pre-requisite for the feasibility of the experimental set up. Fig.3 (b) shows the parameter **b**, the slope of the linear increase in t_i. The dashed line in Fig.3 (b) is the expected value of **b** considering only the effect of electrolysis. The pre-deposit was not placed in sets 1 and 3 and **b** from these sets is clearly above the dashed line. The pre-deposit was placed in set 2 and **b** from it is well around the dashed line, so, it is clear the importance of the pre-deposit of water to minimize the effect of electrolyte evaporation.

Fig.4 shows the two parameters, **c** and **d**, of the first initial transient for the ten electrolyses. They do not show a clear dependence on I, although they seems to change with the volume of electrolyte, V_e. This transient is due to a release of gas from some of the components of the system. We have related it to a release of the air solved initially

in the electrolyte. This effect strongly depends on the previous history of the aqueous solution.

Fig.5 shows the two parameters of the second initial transient, **f** and **g**, for the ten electrolyses. Both show a clear dependence on I, so it seems that it is likely due to a $H(D)_2$ and O_2 absorption by the electrolyte. The pre-exponential factor, **f**, follows a I^{-1} behavior, as expected in a process that is related to the amount of gas evolved by electrolysis that is solved in the electrolyte. The parameter **g** increases as I increases, i.e. the transient is faster when the gas evolution rate is faster.

Both initial transients must be taken into account in an electrolysis with a Pd cathode. If they are not considered an uncertainty of 5-10% in the evaluation of the mean H(D)/Pd, $\overline{H(D)/Pd}$ is introduced. However the corresponding parameters present a behavior quite irreproducible that makes their evaluation really complicated. Therefore we searched for any procedure to eliminate the initial transients in t_i. We have found that they do not appear if an adequate mixture of $H(D)_2$ and O_2 is bubbled through the electrolyte prior to the electrolysis. A similar conclusion has been reached by other authors [1].

4. Discussion

The evaluation of the amount of H(D) absorbed by the Pd cathode is accomplished by summing all the Δn_i. It is important to be aware that any error in the determination of Δn_o, uncertainties in V_e, or ΔP_f, is repeated in a systematic way in each of the contributions. On the other hand it has been shown that the initial transients must be suppressed by a previous bubbling through the electrolyte. We have accomplished it by locating three Pt electrodes in the closed cell besides the Pd one. A pre-electrolysis is accomplished with two of the Pt electrodes, while the Pd is anodically polarized against the third Pt to avoid its hydrogenation (deuteration) during this step. It allows to avoid the initial transients whether the cell is not opened before the loading experiment and to evaluate "in situ" Δn_o from the series $\{t_i\}$ recorded during the pre-electrolysis.

To finish, the advantages and disadvantages of our experimental set up and related ones, either sealed cells with recombination catalyzers [3] or cells that are dinamically opened and closed [5,7], against electric resistance measurements are briefly discussed.

A main disadvantage of this set up, which is not presented by resistance measurements, appears in relation to its use in "Excess Heat" measurements: its strong response to changes of temperature in the electrolyte. A sharp change in temperature produces a release (whether T increases), or an absorption (whether T decreases) of gases from or by the electrolyte. A calibration of this effect is needed to avoid an uncertainty of a few % in the evaluation of the $\overline{H(D)/Pd}$ during an "Excess Heat" experiment.

It presents two clear advantages against resistance measurements. (1) It has been pointed out [8] that the relation ρ(H(D)/Pd), where ρ is the resistivity, changes significantly from one sample to another. Moreover, these relations can change in a unique sample whether it suffers irreversible structural changes during its loading. It is

well known that the electric resistance presents hysteresis during sequential loadings and deloadings. The $\overline{H(D)/Pd}$ evaluation from measurements of gas evolution is not affected by the structural properties of the cathodes. (2) ρ measurements do not give the $\overline{H(D)/Pd}$ as a function of the electrolysis time, but they only give a final value, when a stationary situation has been reached. It has been shown in [4,9] that the existence of gradients of H(D) in the Pd cathode do not allow a proper evaluation of $\overline{H(D)/Pd}$ from ρ. In contrast, the set up in our lab allows to obtain $\overline{H(D)/Pd}$ vs. t curves during the electrolysis, and so, to make a study of the rates of H(D) absorption by Pd. This is likely the main advantage of volumetric techniques since published data on rates of H(D) absorption during electrolysis of aqueous solutions with Pd cathodes are even more scattered than data on final H(D)/Pd, when a stationary situation has been reached.

5. Conclusions

It has been tested an experimental set up to measure the rate of H(D)-absorption by a Pd cathode during the electrolysis of an aqueous solution. It has been shown that some cautions proposed in this paper must be taken. The set up allows not only to measure final H(D)/Pd, but to record $\overline{H(D)/Pd}$ vs. t curves during electrolysis.

6. Acknowledgments

Thanks are given to Mr. C. Palazuelo and Mr. A. Bergas for their technical assistance. Financial support from Spanish DGICYT (PB 33-0266) is acknowledged.

7. References

[1] K. Kunimatsu, N. Hasegawa, A. Kubota, N. Imai, M. Ishikawa, H. Akita and Y. Tsuchida. "Frontiers of Cold Fusion", ed. H. Ikegami. Universal Academy Press inc. Tokyo (1993). 31-45.

[2] M.C.H. McKubre, S. Crouch-Baker, R.C. Rocha Filho, S.I. Smedley, F.L: Tanzella, T.O. Passell and J. Santucci. J. Electroanal. Chem., 368 (1994) 55-66.

[3] F.G. Will, K. Cedzynska and D.C. Linton. J. Electroanal. Chem. 360 (1993) 161-176.

[4] T.A. Green and T.I. Quickenden. J. Electroanal. Chem. 368 (1994) 121-131.

[5] S. Nezu and T. Sano. Transactions of fusion tech. 26 (Dec.1994) 69-73

[6] K. Ota, H. Yoshitake, A. Yamazaki, M. Kuratsuka, K. Yamaki, K. Ando, Y. Iida and N. Kamiya. Transactions of fusion tech. 26 (Dec.1994) 138-142.

[7] F. Celani, A. Spallone, P. Tripodi, A. Nuvoli, A. Petrocchi, D. di Gioacchino, M. Boutet, P. Marini and V. di Stefano. Transactions of fusion tech. 26 (Dec.1994) 127-137.

[8]B. Baranowski, S. Filipek and W. Raczynski. Polish J. Chem., 68 (1994) 845-857.

[9]M.C.H. McKubre, S. Crouch-Baker, A.M. Riley, R.C. Rocha Filho, M. Schreiber, S.I. Smedley and F.L: Tanzella. Electrochemical Society Proceedings, Vol. 92-5, 269-286.

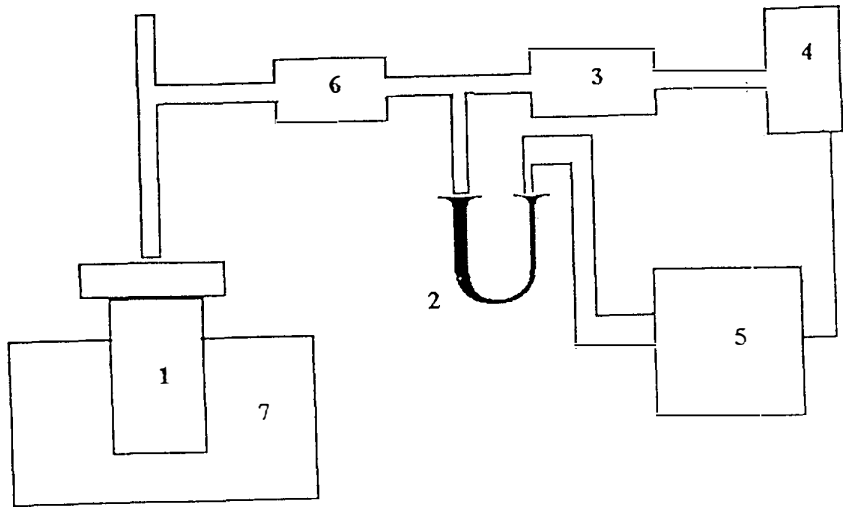

Fig.1 (1) Closed electrolytic cell. (2) U-shaped glass manometer. (3) deposit with $CaCl_2$. (4) electrovalve. (5) electronic circuit. (6) pre-deposit of water. (7) thermostatic bath

TABLE 1

Run	Set	t_e (h)	V_e (cc)	ΔP_f (torr)	T_e (K)	I (mA)
1	1	45	600±6	6.18±.06	294±1	400±1
2	1	45	600±6	6.18±.06	294±1	600±1
3	1	80	600±6	6.18±.06	294±1	800±1
4	2	24	1500±15*	7.16±.06	285±1	200±1
5	2	36	1500±15*	7.16±.06	285±1	400±1
6	2	20	1500±15*	7.16±.06	285±1	600±1
7	2	20	1500±15*	7.16±.06	285±1	800±1
8	3	50	1500±15*	6.189±.006	294±1	400±1
9	3	24	1500±15*	6.189±.006	294±1	600±1
10	3	45	1500±15*	6.189±.006	294±1	800±1

Table 1. t_e: time of electrolysis. V_e: volume of electrolyte. In electrolysis marked as * the electrolyte was stirred. ΔP_f: fixed overpressure. T_e: electrolyte temperature. I : electrolytic current. The pre-deposit of water was not placed in sets 1 and 3.

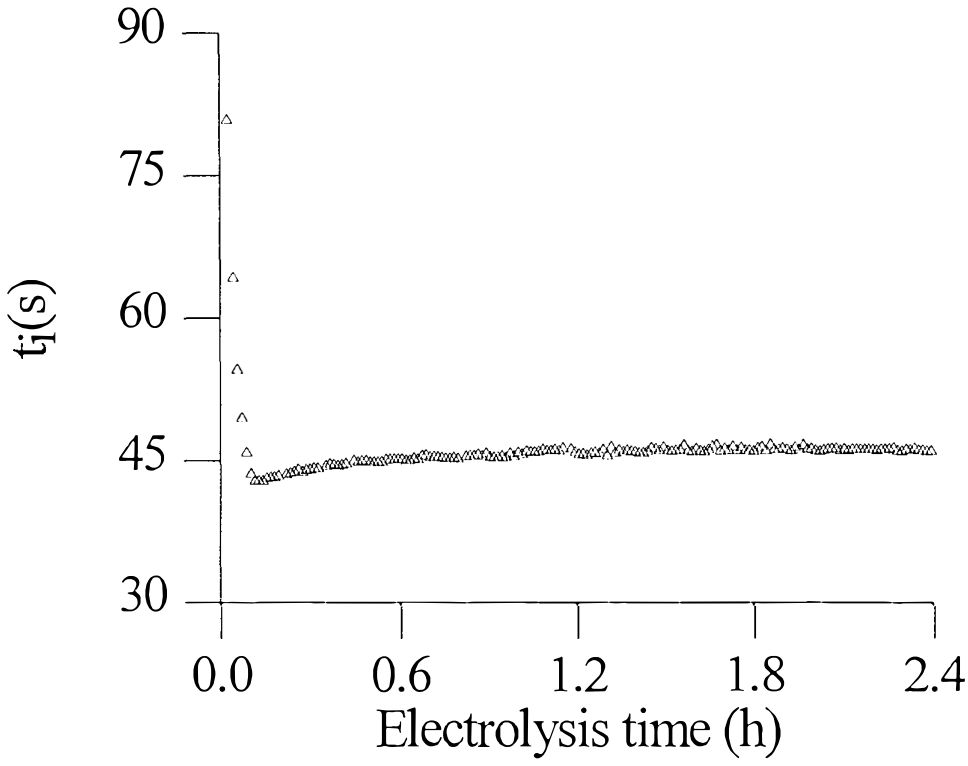

Fig.2 (t_i) in electrolysis 6. 2.4 first hours

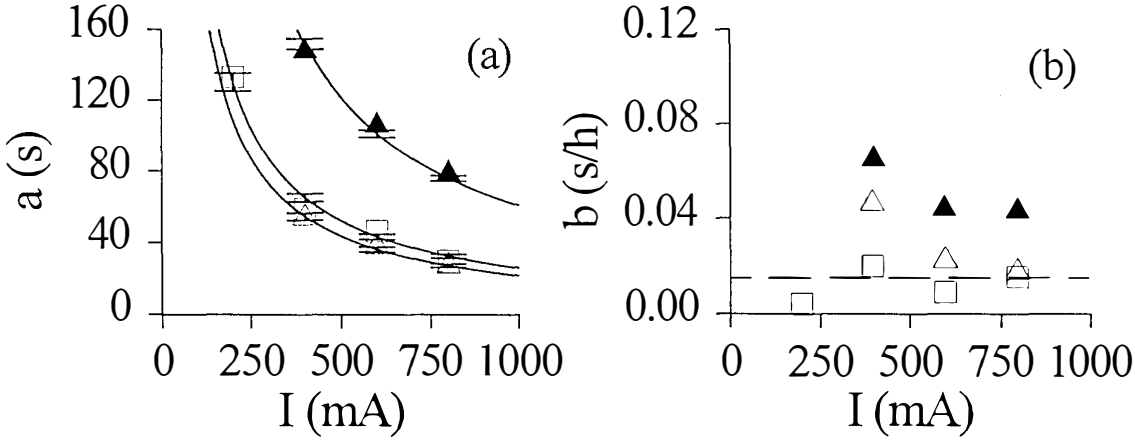

Fig.3 (a) a from the fittings of the 10 electrolyses. (b) b from the fittings of the 10 electrolyses. Set 1: black triangles. Set 2: open squares. Set 3: open triangles. The pre-deposit of water was not placed in sets 1 and 3

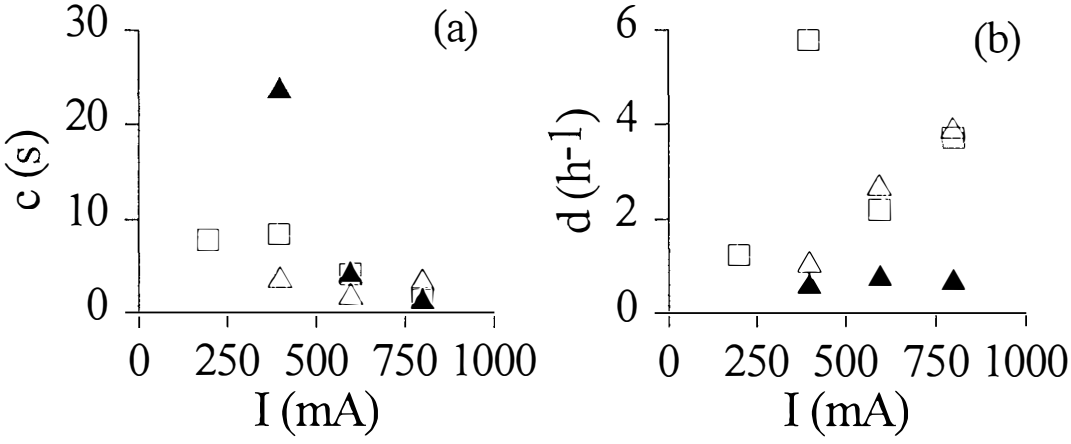

Fig.4 (a) c from the fittings of the 10 electrolyses. (b) d from the fittings of the 10 electrolyses. Set 1: black triangles. Set 2: open squares. Set 3: open triangles

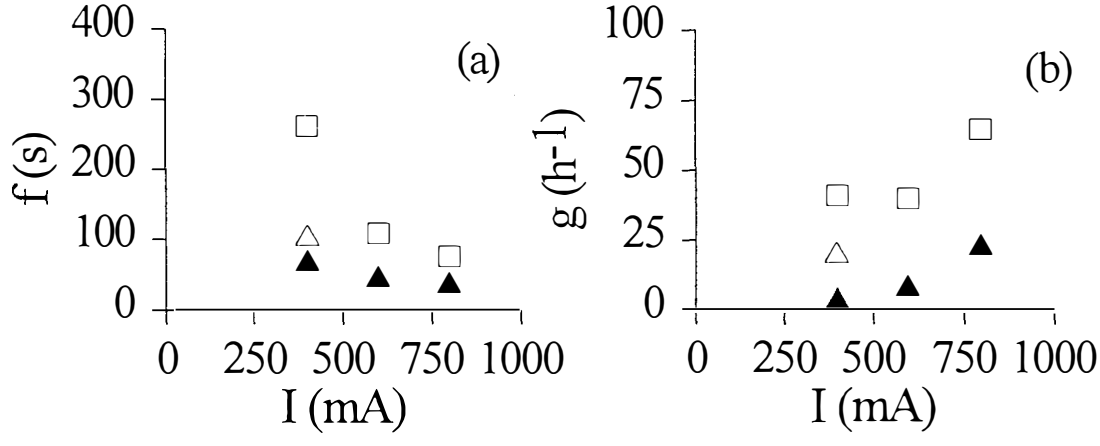

Fig.5 (a) f from the fittings of the 10 electrolyses. (b) g from the fittings of the 10 electrolyses. Set 1: black triangles. Set 2: open squares. Set 3: open triangles

Fifth International Conference on Cold Fusion
9-13 April. 1995 - Monte Carlo. Monaco
ICCF5 ©1995

Electrolytic Deuterium Absorption by Pd Cathode and a Consideration for High D/Pd Ratio.

Norifumi HASEGAWA, Masao SUMI, Masanori TAKAHASHI, Toshio SENJUH, Naoto ASAMI, Takeshi SAKAI* and Toshinori SHIGEMITSU*

R&D Center for New Hydrogen Energy, The Institute of Applied Energy
3-5, Techno Park 2-Chome, Shimonopporo, Atsubetsu-ku, Sapporo, Hokkaido 004, Japan.
*Nuclear Fuel Industries, Ltd.
950, Noda, Kumatori-Cho, Sennan-Gun, Osaka 590-04, Japan.

Abstract

Using several kinds of Pd electrodes, electrolysis were performed in " Fuel-Cell Type Closed Cell ". Initial deuterium absorption (D/Pd) at the first period of electrolysis of 50 mA/cm² current density. Maximum D/Pd during electrolysis and deuterium desorption were measured. Single crystal Pd electrode reached the highest initial deuterium absorption, D/Pd=0.89, and the highest Maximum D/Pd, 0.89, during electrolysis. Except single crystal one of high purity, more than 99.99%, Pd electrodes annealed at 850 ℃ reached the highest D/Pd, 0.87. And this electrodes showed excess heat of 13 % of input power.

The results of metallographical examinations of Pd electrodes after electrolysis suggest that the electrodes of high purity, annealed at 850 ℃, and machined & etched to remove surface defects will be preferable to reach higher D/Pd.

1. Introduction

It is often pointed out that high loading ratio (D/Pd) over 0.85 is necessary to get the excess heat generation with high reproducibility during electrolysis of heavy water by Pd electrode. Therefore it is important to make clear the parameters of Pd material that can increase the deuterium loading ratio.

In this study using several kinds of Pd electrodes, the effect of the metallographical characteristics of Pd material on the deuterium loading ratio were investigated.

This study has been conducted under the consignment of New Energy and Industrial Technology Development Organization (NEDO).

2. Experimental

2-1. Electrolysis cell

Fig.1. shows the electrolysis cell which has been used for this study. This cell is so called " Fuel-Cell Type Closed Cell " (1). A Pd cathode of 4 mm diameter and 20 mm length was set at the center of the pressure vessel, and surrounded by a gas diffusion electrode, Fuel Cell Anode. 50 cm³ of 1 M LiOD was filled in the cell, and the cell was pressurized by D_2 gas up to 9

Kg/cm².

D/Pd was estimated by the following equation (1);

$$D/Pd = 2(n_0 - n_1)/Pdmol$$

where n_0 is molarity of D_2 gas before electrolysis, and n_1 is molarity of D_2 gas at the present of the estimation.

Thermocouples are used to measure the temperatures of Pd rod and solution. Measuring these temperatures excess heat was estimated as the deviation from the calibration curve measured using Ni cathode.

2-2. Electrolysis condition

Fig.2. shows a typical history of current density and D/Pd during electrolysis.

At the beginning of electrolysis the current density was set at 50 mA/cm², and then the current density has been changed step by step after stable equilibrium reached.

An electrolysis has been performed for more than 30 days.

2-3. Pd Electrodes

Table.1. shows Pd electrodes used in this study. The electrodes of No.1 through No.12 in this table were made by TANAKA Kikinzoku Kogyo, and No.13, single crystal, was made from TKK-A Pd Material by Floating zone melting method in Ar gas atmosphere.

The effect on D/Pd by the following parameters were examined; purity of material, melting condition, cold work temperature, annealing, etching before electrolysis.

3. Results and Discussion

3.1. D/Pd

The last column in Table.1. shows initial D/Pd reached at the end of the first period of electrolysis at 50 mA/cm² current density and the maximum value of D/Pd during the electrolysis.

Except No.13, single crystal, there were not big differences in initial D/Pd; 0.77 ~ 0.83.

Single crystal reached the highest initial D/Pd, 0.89, in this study. Also single crystal reached the highest D/Pd, 0.89, during electrolysis.

The maximum values of D/Pd by the electrodes of No.1 through No.3, which were manufactured from Pd ingot made by in-air melting process, were a little lower than other electrodes manufactured from Pd ingot made by in-vacuum melting process.

No.12 in Table.1. reached the highest D/Pd, 0.87, during electrolysis except single crystal. This electrodes was manufactured from Pd ingot made by in-vacuum melting process and cold worked in room temperature and annealed at 850 ℃ for 4 hours by TANAKA K.K. and 3 hours by NHE.

3.2. Excess Heat

Fig.3. shows the relation between Cathode temperature and input power during the electrolysis of No.13, single crystal, in Table.1. Any excess heat was not observed.

Fig.4. shows the relation between Cathode temperature and input power during the electrolysis of No.12 in Table.1. 13 % of excess heat was observed.

Fig.5. shows the some results of excess heat related with D/Pd. In this figure two electrodes showed excess heat: one is NHE-B-B, No.12 in Table 1, and another is JM-Z, the electrode of which was made by Johnson-Mathey. The purity of these electrodes were more than 99.99 % and both electrodes were annealed at 850 ℃ after the final cold work.

3.3. Desorption of deuterium after electrolysis

Fig.6. shows the deuterium desorption from several electrodes just after electrolysis; No.1(TKK-A), 4(TKK-A-V-3N), 5(TKK-A-V-4N), and 13(TKK-A-S) in Table.1.

The desorption rate of single crystal was significantly lower than other electrodes which were not annealed after cold work. This means that absorbed deuterium can stay longer in single crystal. On the other hand deuterium desorption from the electrodes cold worked and not annealed was very rapid. This suggests that the electrodes with stable grains can hold more deuterium inside.

3.4. Metallographical Examination

Fig.7. shows the surface appearance of the single crystal before electrolysis. White spots on the surface were deoxidizer which were oozed out from inside the rod during floating zone melting. Fig.8. shows the surface appearance of the single crystal after electrolysis.

All spots of oxidizer were completely removed from the surface. Fig.9. shows stripes and grooves on the surface of the single crystal after electrolysis. These might be caused by the dislocation of lattice of crystal due to deuterium absorption.

Fig.10. shows internal defects of the single crystal after electrolysis. These might be caused by the deformation of the crystal due to deuterium absorption.

Fig.11. shows a crack on the surface of TKK-C electrode before electrolysis.

Fig.12. shows an inclusion of TKK-C electrodes. There were a lot of inclusions caused by deoxidizer used in the process of in-air melting of Pd.

Fig.13. shows the metallography of the cross section of Pd electrode not annealed after cold work. No grains were observed.

Fig.14. shows the metallography of the cross section of Pd electrode annealed after cold work. Annealed Pd electrode has stable grains.

4. Conclusions

4.1. Pd material

(1) Effect of the purity of the Pd electrodes upon D/Pd and excess heat during electrolysis has not been concluded only by this study. But the highest D/Pd by single crystal in this study suggests that Pd electrodes of higher purity and stable grains will reach higher D/Pd. Highly purified and annealed Pd will be preferable to reach higher D/Pd and reduce the dispersion of D/Pd.

But further investigations regarding the role of inclusion and the effect of impurities at grain boundaries will be necessary in order to conclude the effect of impurities upon D/Pd and excess heat.

(2) Several electrodes cold worked in liquid nitrogen did not bring out high D/Pd nor excess heat. We may be able to conclude that cold work temperature is not significant for higher deuterium absorption.

(3) Grain size and/or grain boundaries may be significant for higher D/Pd and the diffusion of D in Pd electrodes. The further studies regarding the effect of grains of Pd electrodes will necessary and important.

(4) Cracks on the surface of Pd must obstruct the higher deuterium loading. All of cracks should be removed before electrolysis. Machining and polishing of the surface of Pd electrodes should be necessary before electrolysis.

4.2. Excess Heat

Excess heat was observed in the two experiments. But further studies should be necessary to confirm the reliability and reproducibility of excess heat.

It will be also important to make clear the relation between excess heat and characteristics of Pd electrodes.

References

(1) K.Kunimatsu et al. " Deuterium Loading Ratio and Excess Heat Generation during Electrolysis of Heavy Water by a Palladium Cathode in a Closed Cell Using a Partially Immersed Fuel Cell Anode." 3rd International Conference on Cold Fusion, "Frontiers of Cold Fusion", ed. H. Ikegami, Frontiers Science Series No.4, p.31.

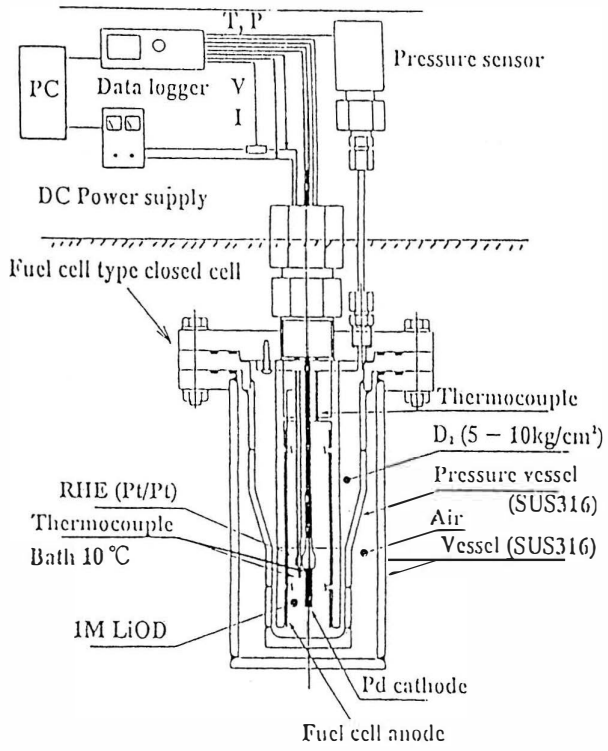

Fig.1. Fuel Cell Type Electrolysis Cell

Table.1. D/Pd at 50mA/cm^2 and max D/Pd during electrolysis

No.	Electrode Material	Purity of Pd	Melting	Cold Work Temp.	Anneal	Etching	D/Pd	
							50mA/cm^2	Max
1	TKK-A	>99.95	air	room temp.	—	—	0.80	0.81
2	TKK-C	>99.95	air	liq. N_2	—	—	0.78	0.79
3					850 ℃ (3hrs)	—	0.77	0.79
4	TKK-A-V-3N	>99.9	vacuum	room temp.	—	—	0.83	0.85
5	TKK-A-V-4N	>99.99	vacuum	room temp.	—	—	0.80	0.82
6					850 ℃ (3hrs)	—	0.83	0.84
7					—	×	0.80	0.82
8	TKK-C-V-3N	>99.9	vacuum	liq. N_2	—	—	0.82	0.85
9	TKK-C-V-4N	>99.99	vacuum	liq. N_2	—	—	0.79	0.81
10					—	×	0.80	082
11	NHE-B-A	>99.99	vacuum	room temp.	—	—	0.83	0.85
12	NHE-B-B	>99.99	vacuum	room temp.	850 ℃ (3hrs)	—	0.83	0.87
13	TKK-A-S	>99.99	(single crystal)		—	×	0.89	0.89

Note 1. All electrodes were pretreated in vacuum at 200 ℃ for 3hrs just before electrolysis except for No.3 & No.6.

Note 2. Etching was performed with aqua regia for 1 min. before the above pre-treatment.

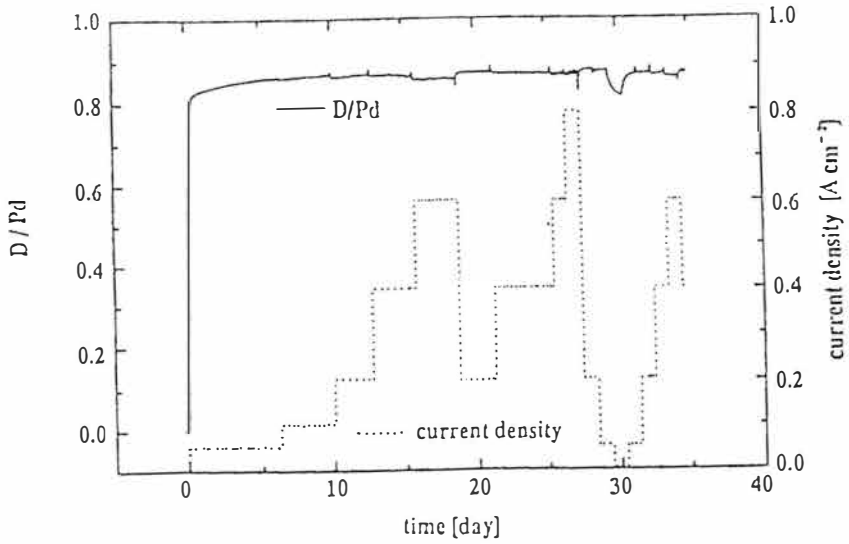

Fig.2. D/Pd and current density for Pd (NHE-B-B) in 1M LiOD

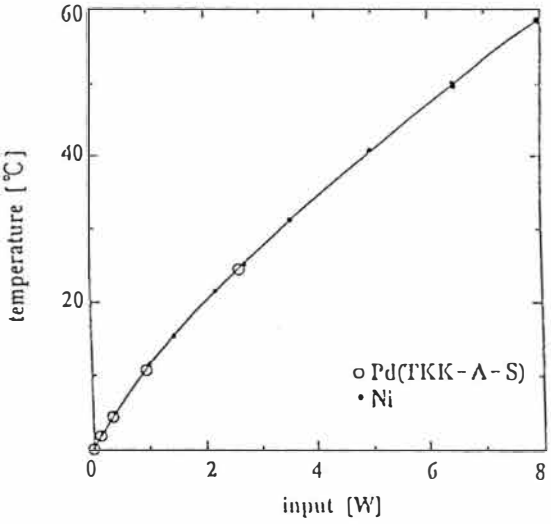

Fig.3. Cathode temperature vs. input power for Pd (TKK − A − S) in 1M LiOD

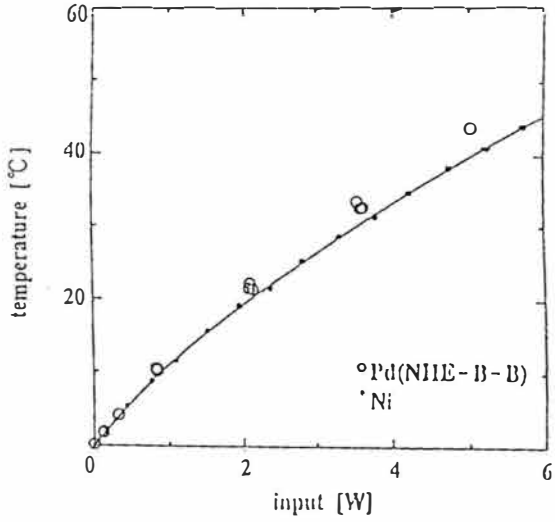

Fig.4. Cathode temperature vs. input power for Pd (NHE − B − B) in 1M LiOD

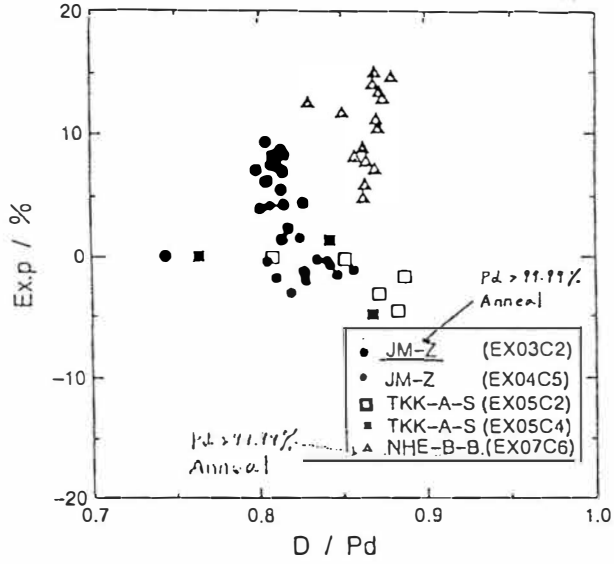

Fig.5. Excess heat vs. D/Pd for Pd cathodes in 1M LiOD

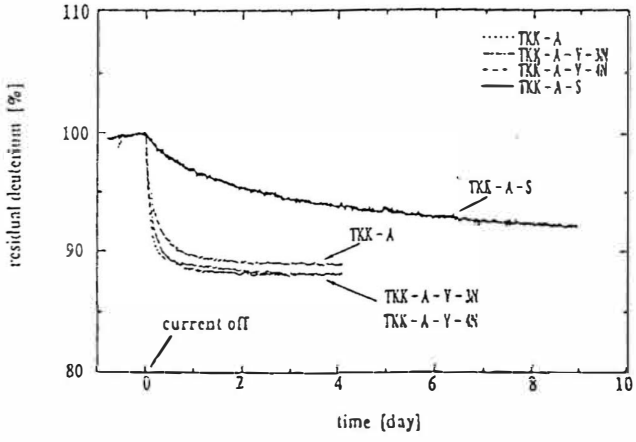

Fig.6. Desorption of deuterium after current interrupt

Fig. 7.

TKK-A-S(single crystal) : before electrolysis

Surface appearance

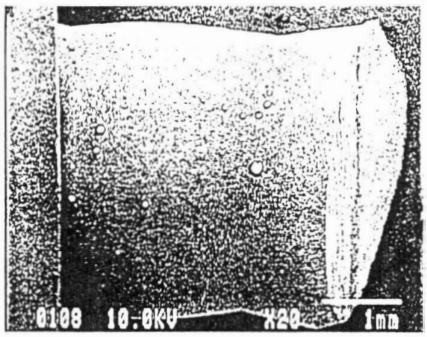

axial direction

Fig. 8.

TKK-A-S(single crystal) : after electrolysis

Surface appearance

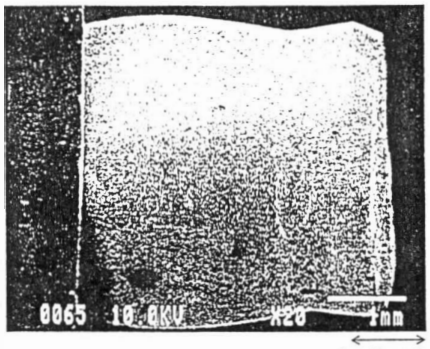

axial direction

Fig. 9. TKK-A-S(single crystal) : after electrolysis

Surface appearance

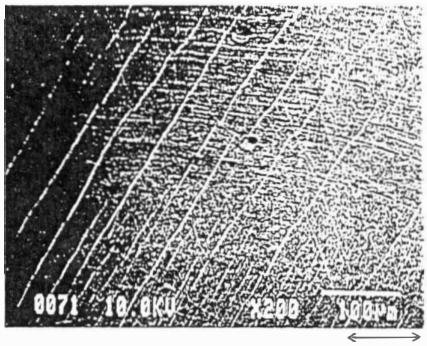

axial direction

Surface appearance

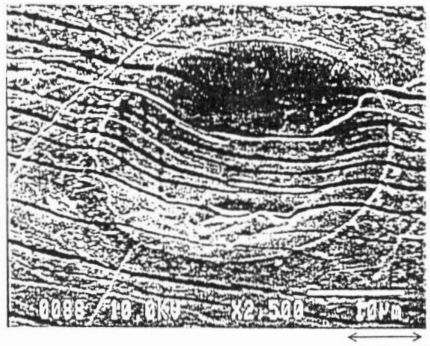

axial direction

Fig. 10. TKK-A-S(single crystal) : after electrolysis

Cross section

Defect like Blister

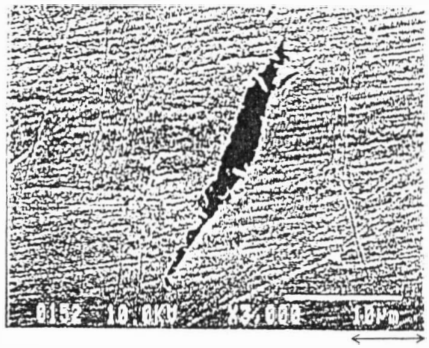

axial direction

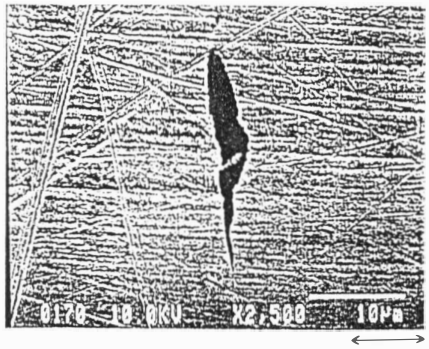

axial direction

Fig. 11. TKK-C :before electrolysis

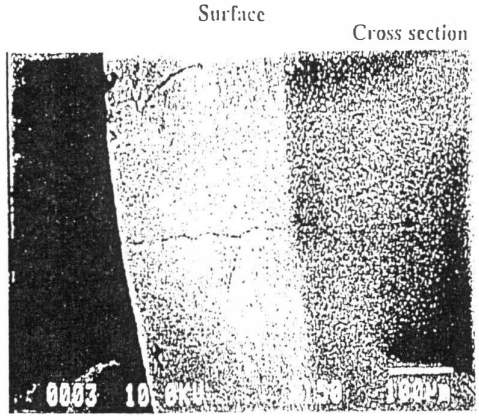

Fig. 12. TKK-C

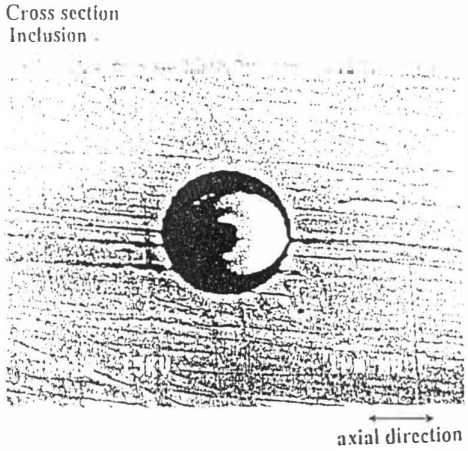

Fig. 13. Metallography of TKK-A-V-4N
(not annealed)

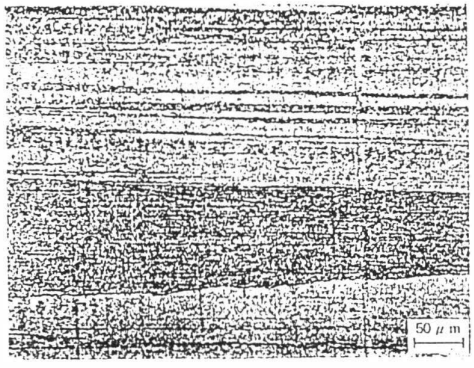

Fig. 14. Metallography of NHE-B-B
(annealed)

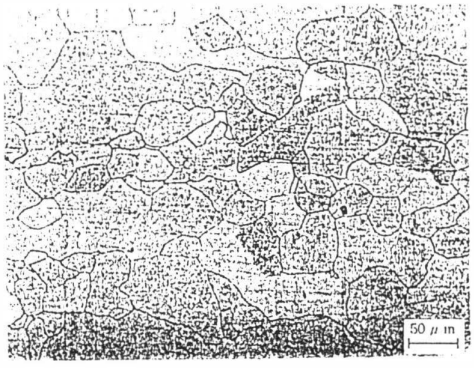

Fifth International Conference on Cold Fusion
9-13 April, 1995 - Monte Carlo, Monaco
ICCF5 ©1995

AN EXPERIMENTAL SYSTEM FOR "COLD FUSION" EXPERIMENTS WITH SELF-PRODUCED IODIDE TITANIUM FILMS

F.CUEVAS, J.F. FERNÁNDEZ, M. ALGUERÓ and C.SÁNCHEZ
Dpto. Física de Materiales C-IV. Facultad de Ciencias. Universidad Autónoma de Madrid. Cantoblanco 28049. Madrid. Spain.

Abstract

An experimental system has been developed to grow pure titanium films on tungsten substrates. The physicochemical properties of these films have been widely studied and ad hoc samples can be used for Cold Fusion experiments avoiding their contact with atmosphere. Different Cold Fusion experiments are proposed in a new experimental setup that allows deuterium gas loading of the film while electrical current is applied through them. Thus, an experimental configuration similar to an electrochemical loading is attained.

1. Introduction

Most of the Cold Fusion experimental work has been carried out without paying much attention to the physicochemical properties of the metal matrix, as they were usually run with commercial samples. However, the purity and structural properties of the matrix sample have a strong effect on its hydrogenation/deuteration behavior[1,2]. For example, gaseous impurities can reduce the maximum hydrogen uptake and influence the mobility of the hydrogen atoms. Therefore, we think that the lack of reproducibility in Cold Fusion experiments could be related to some non controlled characteristic of the metal matrix, as was evidenced by the dependence of reported results on the commercial batch production number[3]. Considering this scene, we have been working on the production of very pure titanium films of well-controlled characteristics to be used in Cold Fusion experiments.

2.Film Growth and Characterization.

Titanium films were grown by a modified Iodide Process. This technique is based on the thermal decomposition of TiI_4 vapors according to the overall reaction

$TiI_4 \leftrightarrow Ti + 4I$. Its major success comes from the fact that the obtained material is nearly free of oxygen, nitrogen and carbon, as these gases do not react with iodine.

In our experimental system, a flow of iodide vapors is passed over a tungsten ribbon filament (40x2x0.025 mm) electrically heated up to 1100-1500 ^{o}C and located in a Pyrex glass chamber. The quantity of titanium deposited mass is monitored on line by accurate measurements of the electrical resistance variations of the filament. The obtained samples have an average titanium mass of 60 mg to reach a final thickness about 200 μm. The films can be deposited at distinct filament temperatures and mass deposition rates, by suitable adjustment of the electrical current and TiI_4 vapor pressure. When the titanium deposition is finished, the filament chamber is sealed off. Thus, residual iodine and TiI_4 are taken away and the film is never exposed to the external atmosphere avoiding its superficial oxidation. A more detailed information about the sample preparation system is given elsewhere[4].

The obtained films were analyzed by EDAX (energy-dispersive analysis of X-rays) and XRD (X-Ray diffraction), and observed by SEM (scanning electron microscopy). Its hydrogenation behavior was also studied in an external system[5,6]. The main feature yielded by these analyses is the strong diffusion of the tungsten substrate into the deposited titanium films depending on the growth rate and temperature . Due to the tungsten diffusion the obtained films exhibit special physicochemical characteristics compared to pure titanium. It was determined by XRD that the high temperature crystallographic structure of titanium (β-titanium phase, BCC) is stabilized when tungsten exceeds a certain concentration (~8 at%) whereas the common α-phase (HCP) is presented when tungsten concentration is lower than this value. In relation to their hydrogenation behavior, a large hysteresis effect was observed in the β-δ plateau of the P-X diagram that increases as tungsten diffusion does. However, the hydrogenation kinetics of the films does not differ much from pure titanium as the diffusion coefficients of hydrogen in these films have been found to be, at most, an order of magnitude lower than that for pure titanium.

Finally, it is worthy to comment that the titanium deposition rate has also a significant influence on the morphological characteristics of the films. Slow deposition rates produce a very compact bulk structure and high crystallinity, while fast deposition rates can even develop macroscopically cavities inside the films.

3.Cold Fusion experimental setup and features.

Once the film has been grown, the filament chamber is joined to the "Cold Fusion" experimental setup, which is sketched in figure 1. Three different parts can be distinguished in this arrangement: the hydrogenation line, the neutron detection system, and the electrical control system of the sample.

The hydrogenation line, constructed in S.S (316) and Pyrex glass, behaves as a Sieverts type apparatus. The entire system can be evacuated to 10^{-6} torr by means of a turbomolecular pump and it is equipped with Pirani, Penning and Piezoresistive gauges and a quadrupole mass spectrometer (Balzers QMG 064). In the Pyrex line, a

magnetic striker is located to open the filament chamber after the system is evacuated. Several valves allow the entry of hydrogen or deuterium in the chamber by doses.

The neutron detection system comprises two liquid scintillator detectors: a BC501, properly shielded with a 10 cm thick wall of Pb, and a NE213. Far from the experiment, we have installed a BF_3 detector (2202D Alnor) to monitor possible variations of the neutron background. For the sample-detectors configuration our neutron detection efficiency is equal to 0.5%. Neutron energy and time spectra are eventually monitored in different MCA (Canberra).

The electrical control of the filament allows to pass an electrical DC current through the film while two tungsten wires (25 μm OD), welded at its edges, serve as two probes for determining the voltage drop in the film. This configuration constitutes a four probe system. The electrical current is applied by a DC power supply (Keenwood 2036D) which is operated manually or controlled by a function generator. In addition, an electrically heated furnace or a liquid nitrogen container can be placed around the filament chamber to attain temperatures from -196 to 300ºC. All the electrical and pressure parameters are finally monitored by a PC.

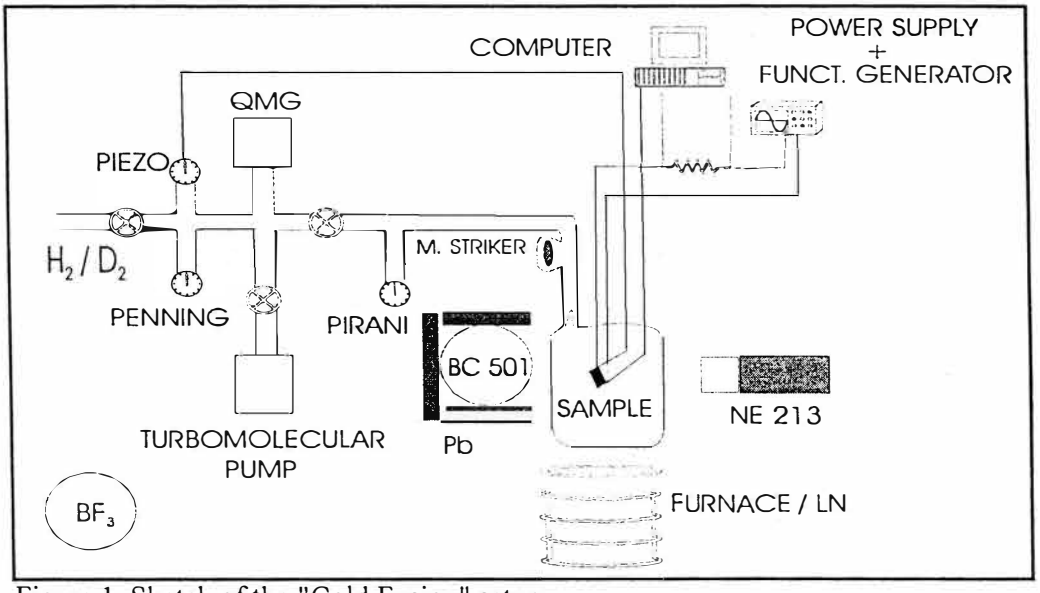

Figure 1. Sketch of the "Cold Fusion" setup.

This experimental system provides very interesting new highlights. Electrical currents up to 12 A can be passed through the sample that is heated up, in this way, to 1500°C. When using the external liquid nitrogen container, sample temperature is cooled down, at least, at -100°C. Hydrogen uptake is measured by the drop of the hydrogen pressure and is correlated with filament resistance variations. Besides, absorption and desorption cycles can be done under controlled rates by electrical heating of the samples. Nevertheless, as an electrical current can be passed through the

sample during its hydrogenation, this system resembles an electrochemical Cold Fusion experiment. This fact probably constitutes the principal highlight of this arrangement. In addition, hydrogen/deuterium diffusion coefficient can be made very similar to those attained in the Pd hydrogenation in electrochemical cells, by heating the Ti samples at 300-500°C. Furthermore, both β-Palladium hydride and δ-Titanium hydride present the same crystallographic structure (FCC) at these circumstances.

Considering the well-known physicochemical properties of the films described before it will be able to relate the possible nuclear reactions with their characteristics. In addition, it should be remarked that the presence of the tungsten substrate will proportionate good mechanical strength to the film during loading-unloading hydrogenation cycles as tungsten does not absorb appreciably hydrogen.

4. Summary

A novel experimental system for the production of titanium samples has been developed and it can be adapted to Cold Fusion experiments. This system provides a good control of the physicochemical properties of the metal matrix and produces films with low content of gaseous impurities even at a superficial level. A wide field of Cold Fusion experiments in the gas phase can be run with the described setup and, under certain circumstances, deuterium loading can be done in a very similar way to that used in electrochemical cells by applying electrical current to the films. We feel that all this scheme will help to obtain interesting and reproducible results in the very next future.

Acknowledgments

Thanks are given to Mr. F.Moreno and Mr. A. Bergas for their technical assistance. Financial support from Spanish DGICYT (PB 33-0266) is acknowleged.

References

1. Alefeld and Völkl, *Hydrogen in Metals II. Application-Oriented Properties*, p. 305, Springer Verlag, Berlin, Heidelberg, New York (1978).
2. Fukai, *The Metal-Hydrogen System, Basic Bulk Properties*. Springer Verlag, p.43, Berlin, Heidelberg (1993).
3. Ikegami, *Frontiers of Cold Fusion* ps 21,79. Universal Academy Press Icn., (1993).
4. Cuevas, Fernández, Algueró and Sánchez, "On the Necessary Experimental Conditions to Grow Titanium Films on Hot Tungsten Filaments Using Titanium Tetraiodide", to be published in J. Alloys and Compounds.
5. Cuevas, Fernández, Algueró and Sánchez, "The Influence of Tungsten Substrates on Hydrogen Absorption by Iodide Titanium Films", to be published in J. Alloys and Compounds.
6. Fernández, Cuevas, Algueró and Sánchez, "Influence of preparation conditions of titanium hydride/deuteride TiHx(Dx) ($x \approx 2.00$) on the specific heat around the δ-ε phase transition", to be published in J. Alloys and Compounds.

Fifth International Conference on Cold Fusion
9-13 April, 1995 - Monte Carlo, Monaco
ICCF5 ©1995

Protocol for Controlled and rapid Loading/ Unloading of H_2/D_2 Gas in Self Heated Pd Wires to Trigger Nuclear Events

A.B.GARG, R.K.ROUT, M.SRINIVASAN, T.K.SANKARNARAYANAN@, A. SHYAM and L.V. KULKARNI
Neutron Physics Division, @Chemical Engineering Division
Bhabha Atomic Research Centre
Trombay, Bombay 400 085, India

Introduction

It has now been established that during electrolysis of LiOD using Pd cathodes a threshold loading ratio of at least 0.85 needs to be achieved before excess heat production can be expected [1]. However for emission of neutrons and tritium and possibly charged particles and transmutation products too much lower D/Pd ratios, in the region of 0.4 to 0.7 appears to be adequate. This has been independently corroborated in a variety of electrolytic and gas loading experiments. It is not so much the magnitudes of the steady state loading ratio, but rather creation of non - equilibrium conditions which facilitates rapid migration/transport of deuterons within the Pd lattice that seems to be required. With this in view a systematic study has been undertaken using electrically self-heated 0.125 mm dia Pd wires in H_2/D_2 atmospheres to optimize the conditions under which rapid loading/unloading of H_2 or D_2 can be achieved. Pd wire was of 99.9% purity and was procured from Lieco Industries, USA.

Procedure for Loading

After a number of trial experiments the following protocol was established for optimum and rapid loading:

1. Measure initial wire resistance, namely R_o^* of the unannealed wire.
2. Heat wire to glow hot condition in air by ohmic heating. R_l/R_o, the ratio of resistance at glow hot condition to resistance at room temperature would be ~3.
3. Lower the current to < 100 mA and measure resistance in atmospheric air after wire cools down. This is the R_o value to be used for further studies. This may differ slightly from R_0^*.
4. Evacuate system to ~10^{-2}mb and heat wire to red hot condition. Current for red hot condition in vacuum would be much lower.
5. Introduce air under red hot condition of pd wire. This provides a thin oxide layer on the wire surface.
6. Evacuate once again.
7. Introduce H_2 or D_2 as required when wire is red hot. It reacts with oxide layer and activates surface. Measure resistance (R_{max}) after cooling.
8. A loading of approximately 0.6 corresponding to R_{max}/R_0 ~ 1.7 for H_2 or 1.85 for D_2 may be achieved within 2-3 minutes, provided activation of wire surface has taken place. Loading increases further to ~0.7 in another 30 minutes. For rapid loading the wire should be as hot as possible during step No.7. However increasing wire tempera-

ture unduly has the risk of accidentally burning out the wire.

Some typical parameters recorded in our experiments are:

Wire diameter	:0.125 mm
Wire length	:~ 100 mm
Annealed wire resistance R_0	:0.8 ohms
Resistance at red hot condition R_t	:2.5 ohms
Vacuum employed in chamber better than	:10^{-2} mb
H_2/D_2 gas filling pressures	:1-2 bars

Verification of (H(D)/Pd) Loading Ratio

On routine basis (a) Resistance Ratio [1] is used to infer the degree of loading. However to cross check the loading value, (b) Oil manometer technique and (c) Inert gas fusion technique were used in a few cases. All the three techniques were found to give comparable loading values.

Summary of main Results

1. We are able to load up to a H(D)/Pd value of 0.7 both in case of H_2 as well as D_2.
2. We do not find any difference in loading rate whether it is D_2 or H_2.
3. Loading is fast if the gas (H_2 or D_2) is introduced in the system when the wire is brilliantly hot. Because of good conductivity of hydrogen, wire temperature automatically falls below the threshold temperature for absorption in Pd, as soon as gas enters the chamber.
4. Since temperature at which wire gets unloaded is less in D_2 (110°C) than in H_2 (150°C), at a given filling pressure, current for deloading is lower for D_2 than for H_2 [3].
5. Loading rate is not particularly influenced by H_2 or D_2 gas pressure (at least in region of few tens of mb to 4 bars, which we have studied), but it is very sensitive to the pretreatment given to the wire.
6. Rate of unloading of a loaded Pd wire at room temperature in atmospheric air is found to be surprisingly slow .
7. If the wire surface is activated properly loading up to 0.6 or 0.7 can be attained with 100% reproducibility.

Hysteresis Studies

To get the hysteresis curve [2], following procedure is adopted:
1. Load the wire at particular gas pressure (1 to 2 bars) to the maximum extent possible (0.7 in our case).
2. Slowly increase the current in steps. Measure the resistance at each current step after wire temperature stabilizes.
3. At some value of current, resistance suddenly drops.
4. On increasing current further, at a particular current, wire resistance starts going up again. In this state wire is fully unloaded.
5. To obtain hysteresis curve now slowly decrease the current; observe that resistance

starts decreasing; at some value of current resistance begins to increase. This implies that wire has begun to load. The current at which wire starts loading in reverse part of cycle is less than in the forward half cycle.
6. Typical hysteresis curve obtained by us is shown in Fig 1.
7. Effect of temperature on loaded Pd wire at different hydrogen gas pressures is shown in Fig 2.

Procedure for Repeated Cycles of Loading/ Unloading

From the hysteresis curves corresponding to a given pressure select the lower and upper "safe" current values at which absorption and desorption will be rapid and assured. For the case of D_2 gas at 1.8 bars for example the lower and upper current values are 0.9 amps and 1.7 amps for loading and unloading respectively (See Fig.1). A simple and automatic switching device can be designed which will flip the current between these two values by shorting a precalculated resistance placed in series with the Pd wire. Since loading takes a longer time , it is recommended that more time be allowed in absorption mode than in desorption mode.

Applications and Conclusion

Having learnt to absorb/desorb H_2 or D_2 in a 100% reproducible and controlled manner in Pd wire, creating non-equilibrium conditions, following experiments have been carried out/are proposed to be carried out in our centre in search of anomalous nuclear effects:
1 Autoradiography: After loading the wire with H_2 or D_2 it was autoradiographed using medical X - ray photographic film. Every loaded wire is found to fog X - ray film. Typical autoradiographs are shown in Fig 3 & 4. Even a low loading of 0.1 fogs the film. This is the phenomena of PdH_x luminescence first reported by our group in 1991 [2]. Efforts to understand the cause for mechanism of fogging are continuing.
2. Charged particle emission: Solid State Nuclear Track Detectors (SSNTD) and surface barrier detector were employed to search for emission of charged particles if any from PdD_x wires subjected to repeated cycles of loading/unloading of deuterium. So far we have not detected any charged particles from self-heated Pd wires.
3 Tritium and neutron detection experiments are under way.

References

1. M.C.H Mckubre et al, "Isothermal flow calorimetric investigations of the D/Pd and H/Pd systems," *J . Electroanal. Chem.* ,386,55 (1994)
2. Lewis, *The palladium hydrogen system*, p. 118,Academic press, London,New York (1967)
3. R.K Rout et al, "Copious low energy emissions from palladium loaded with hydrogen or deuterium,"*Indian Journal of Technology*, 29,571,(1991)

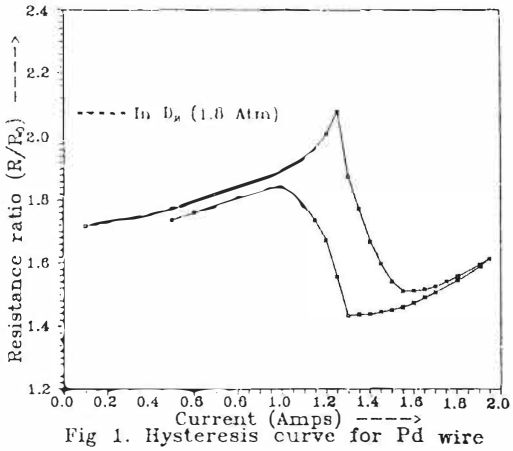

Fig 1. Hysteresis curve for Pd wire

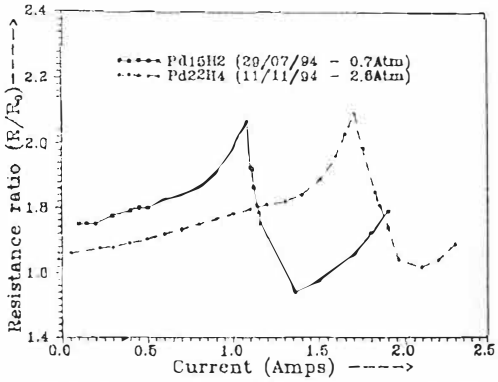

Fig.2 Temperature effect on a loaded Pd wire at different H_2 gas pressures

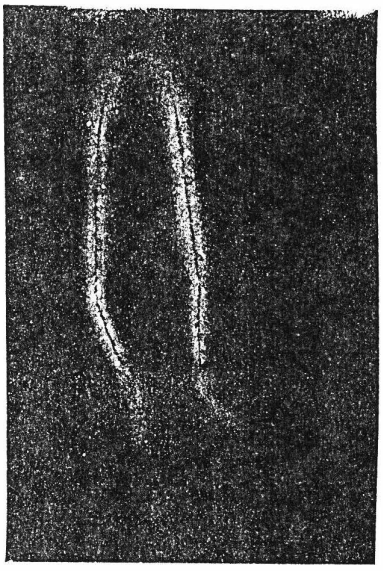

Fig 3. Autoradigraph of Pd hydride wire H/Pd ~0.65

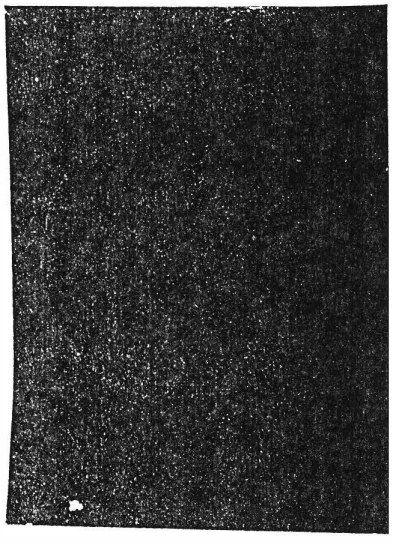

Fig 4. Autoradiograph of Pd hydride wire H/Pd ~0.6

Fifth International Conference on Cold Fusion
9-13 April, 1995 - Monte Carlo, Monaco
ICCF5 ©1995

Preliminary Results on the Variation of Electrical Resistance of a TiD_x Wire With Deuterium Concentration

V.K.Shrikhande†, T.C.Kaushik‡, S.K.H. Auluck‡, A. Shyam‡ and M.Srinivasan‡
†Technical Physics & Prototype Engineering Division,
‡Neutron Physics Division,
Bhabha Atomic Research Centre,
BOMBAY - 400 085 (India)

Abstract

Experiments have been carried out to study the variation and reproducibility of electrical resistance as a function of the deuterium concentration (D/Ti) in titanium wires. Deuterium loading is carried out in a series of steps by passing a D.C. current to ohmically heat the sample for some time in D_2 gas until a measurable quantity is absorbed. After every loading, the wire resistance and decrease in the gas pressure are measured *at room temperature* using a four probe resistance meter (±0.2% accuracy) and an oil manometer respectively.

Significantly, it is observed that an apparently simple property like electrical resistance is not easily reproducible. The preloading heat treatment and residual gases in high vacuum appear to play an important role on the behaviour of the resistance in TiD_x. The preliminary results also suggest that this property may not be useful in estimating the deuterium content in titanium.

1. Introduction

Titanium has been one of the materials in which occurrence of anomalous nuclear reactions have been reported after being loaded with deuterium either electrolytically[1-2] or otherwise[3-5] Exact origin of products such as neutrons and tritium which typically signify these reactions is not understood due to the fact that such experiments are still not reproducible even if materials are taken from the same stock and other conditions are apparently similar. It is therefore imperative to look for characteristics that distinguish such "identical" samples and affect the results.

Physical properties of titanium-hydrogen (deuterium) system are known to be highly sensitive to presence of oxygen[6]. Surprisingly there is no data (at least to our knowledge) on the variation of its electrical resistivity with ratio D/Ti at room temperature, although at high temperature (beta phase) such measurements have been reported earlier[6-8]. In the experiments reported here, attempts have been made to obtain such data and identify factors which may influence its behaviour. This type of data could possibly also yield a simple parameter which may be used to characterize the loading[9]. The experimental set up and procedure are described in the next section followed by the results, their implications and conclusions in subsequent sections.

2. Experimental Set up

The experimental set up used for deuterium loading is schematically shown in Fig.1. It consists of a glass reaction chamber (cell) having a provision for inserting the mounted sample on one side and connected to a silicon oil filled U-tube differential manometer on the other side. The system is connected to a high vacuum system and gas reservoir etc. through an isolation valve. Volume of cell as well as that of the remaining system are calibrated using a standard flask of known

capacity. At times, to produce ultrahigh vacuum (UHV), a glass bulb containing Cesium getter is fused to the cell (and pinched off prior to filling of deuterium gas) as indicated in the figure. Two tungsten feedthroughs are used to mount the sample inside the cell. A four probe resistance meter, having a built in 7.8 mA constant current power supply, is used to measure the electrical resistance with an accuracy of ± 0.2%. The low current ensures that during the resistance measurement temperature rise in the sample is not more than 2^{0}C.

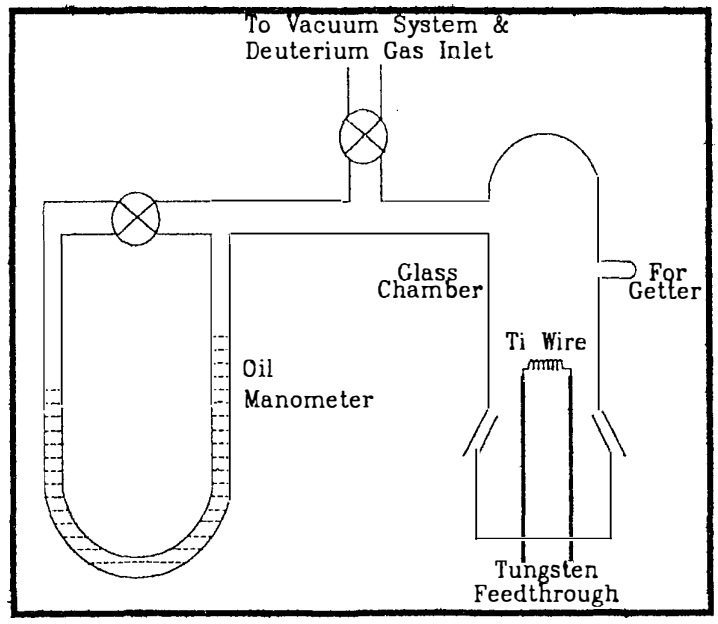

Fig.1. Schematic of The Gas Loading Set-up.

The titanium samples are taken in form of wires (Goodfellow Metals, 99.6% purity). They are cleaned in an acid mixture, weighed and spot welded to the tungsten feedthroughs. Initial resistance (R_{00}) of the free length of wire as well as that of joints and feedthroughs are then measured separately before the whole assembly is inserted into the cell.

The chamber is evacuated to a pressure of 10^{-6} mbar (high vacuum) or better (ultrahigh vacuum produced by the Cesium getter) and a D.C. current is passed through the wire for four minutes to activate it by resistive heating. After the current is switched off and wire cools down to room temperature, its preloading resistance (R_0) is measured. In a few samples, where heating and cooling cycles have been repeated a few times, R_0 has been defined as the value of resistance at the end of last cycle.

Deuterium gas (generated using a commercial Milton Roy cell) is filled into the chamber typically to a pressure of 250 mbars which is sufficient to ensure that the pressure drop on account of absorption remains insignificant. Deuterium loading versus resistance measurements are then conducted in a series of steps.

In every step, the wire is ohmically heated by passing a D.C. current for some time to allow an appreciable absorption of gas to occur and the current is then switched off. After the wire attains room temperature, its resistance (R_1) is measured. The corresponding loading ratio (D/Ti) is determined from the decrease in the chamber pressure (Δp) observed from the oil manometer. These steps are repeated until further absorption of gas becomes practically negligible.

3. Results and Discussion

The initial results obtained from the present series of experiments, which are still in progress, indicate several interesting aspects. During the initial heat treatment of samples in vacuum, the resistance at room temperature is found to increase after every cycle. A similar observation has been earlier reported by Powell and Tye[8], who have attributed it to possible oxygen pick up by titanium from the residual gases in vacuum. Such an effect can also arise due to generation of defects during rapid cooling of a material to room temperature. Since the number of defects should reach a limiting value, a few experiments have been carried out to check if the value of resistance stabilizes after a few cycles of heating and cooling in vacuum. The results are shown in Fig.2. where a trend to stabilize after about 10 cycles can be observed. The actual number of required cycles appears to vary from sample to sample.

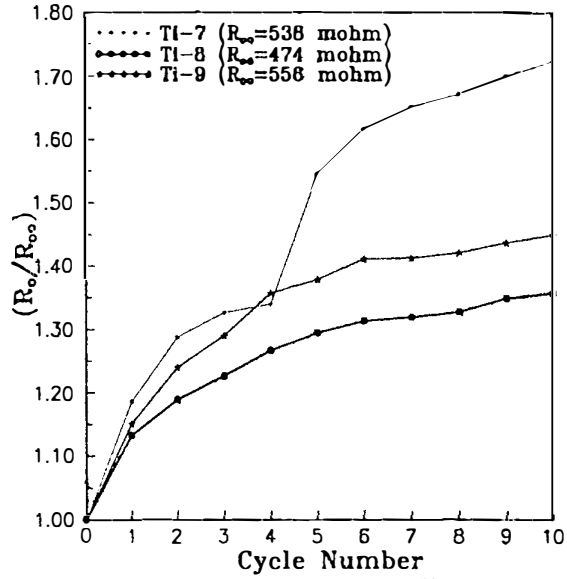

Fig. 2. Resistance Ratio Versus Heat Cycle For A Few Samples.

For most of the samples, the activation cycle has been restricted to just one. Variation of resistance with change in loading ratio (D/Ti) for some of the typical cases is displayed in Fig. 3 and Fig. 4. The samples, according to their experimental conditions may broadly be classified into three categories as noted below.

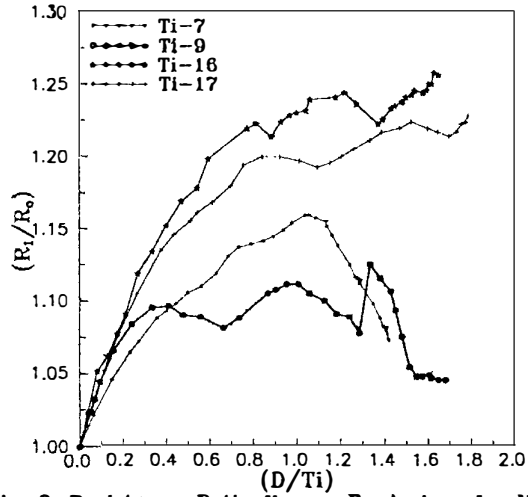

Fig. 3. Resistance Ratio Versus Deuterium Loading (Heat Treatment in 10^{-4} mbar Vacuum)

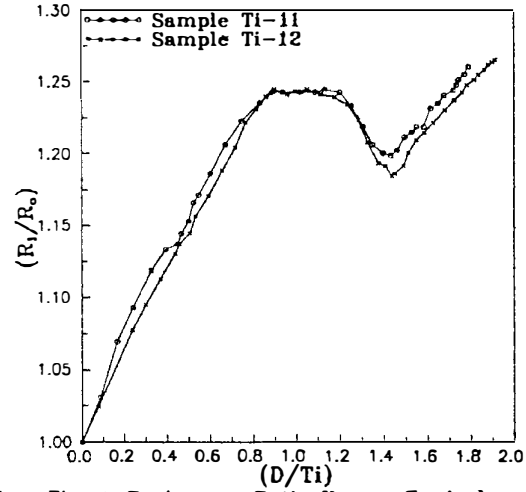

Fig. 4. Resistance Ratio Versus Deuterium Loading (Heat Treatment in UHV).

I.	(Sample **Ti-7 and Ti-9**)	Preloading treatment by repeated heating and cooling in high vacuum.
II.	(Sample **Ti-11 and Ti-12**)	Heat treatment in UHV for one cycle only.
III	(Sample **Ti-16 and Ti-17**)	Similar to Ti-11 and Ti-12 but in high vacuum.

From the results shown here, it is evident that only in case of samples Ti-11 and Ti-12, a reproducible behaviour of the resistance is obtained while an unpredictable trend is seen for other samples. This further supports the earlier indications of the samples being sensitive to the effect of residual background gases during initial heat treatment.

A difference in resistance variation is observed for samples heat treated only once (Ti-16, Ti-17) or more (Ti-7, Ti-9) in similar (ungettered) vacuum. While the resistance ratio (R_0/R_{00}) for former type of samples (Ti-16 & Ti-17) continues to increase beyond the D/Ti loading of 1.4, this ratio is found to decrease in case of samples like Ti-7, Ti-9 which have been heat treated more than once.

4. Conclusions

The results obtained so far in the present experiments imply that apparently similar samples may not yield identical results even for a well known property like electrical resistance. The residual gases and heat treatment conditions definitely appear to play an important role. The data is however to be considered preliminary in nature as various elaborate measurements are underway to cross-check it. Similar further investigations could help to identify many other factors that may affect such physical properties and possible occurrence of nuclear effects.

References

1. Menlove, Fowler, Garcia, Miller, Paccioti, Ryan and Jones, "Measurements of Neutron Emission From Ti and Pd in Pressurized D_2 and D_2O Electrolysis Cells", *J. Fusion Energy* 9, 494 (1990).
2. Krishnan, Malhotra, Gaonkar, Nayar and Shyam, "Observation of Cold Fusion in a Ti-SS Electrolytic Cell", *Fusion Technol.* 18, 42 (1990).
3. Ninno, Frattolillo, Lollobattista, Martinis, Martone, Mori, Podda, and Scaramuzzi, "Evidence of Emission of Neutrons From a Titanium Deuteride System", *Europhys. Lett.* 9, 221 (1989).
4. Menlove, Paciotti, Claytor, Maltrud, Rivera, Tuggle and Jones, "Reproducible Neutron Emission Measurements From Ti Metal in Pressurized D_2 Gas", *Proc. Anomalous Nuclear Effects in Deuterium/Solids Systems*, p. 287, American Institute of Physics, New York (1991).
5. Kaushik, Shyam, Srinivasan, Rout, Kulkarni, Krishnan, Malhotra and Nagvenkar, "Preliminary Report on Direct Measurement of Tritium in Liquid Nitrogen Treated Ti Chips", *Indian J. Technol.* 28, 667 (1990).
6. Mueller, Blackledge and Libowitz, *Metal Hydrides*, Chapter 8, Academic Press, New York (1968).
7. Ames and McQuillan, "The Resistivity - Temperature - Concentration Relationships in β-phase Titanium-Hydrogen Alloys", *Acta Metallurgica* 4, 602 (1956).
8. Powell and Tye, "The Thermal and Electrical Conductivity of Titanium and its Alloys", *J. Less Common Metals* 3, 226 (1961).
9. McKubre, Crouch-Baker, Rocha Filho, Smedley and Tanzella, "Isothermal Flow Calorimetry Investigations of the D-Pd and H-Pd System", *J. Electroanal. Chem.* 386, 55 (1994).

Fifth International Conference on Cold Fusion
9-13 April, 1995 - Monte Carlo, Monaco
ICCF5 ©1995

Boson Condensation Involved In Radiation-Less Fusion

II Spinodal Decomposition of Palladium/Palladium Deuteride System and the Andreev Effect

James T. WABER
Research Professor (Physics)

and

Ouliana L. EGOROVA-CHEESMAN
Chemical Engineering
Michigan Technological University
Houghton, Michigan. USA (49931)

Abstract

The palladium/palladium deuteride system has an immiscibility gap between two face centered cubic solutions which is the necessary condition for spinodal decomposition. The interface between the α and β phases will contain a high concentration of dislocations due to the coherency strains of the lattice prior to the actual separation and formation of the β phase, as deuterium is introduced.

Deuterium atoms will be trapped in these dislocations and the atomic diffusion significantly reduced.

The requirements of the Fujita-Watanabe theory of high temperature superconductivity are (a) near complete filling of the Brillouin Zone and nearby pockets and (b) optical phonons to bring about Cooper pair formation. The connection to Radiation-Less fusion, which has been more commonly known as Cold Fusion, was proposed by Waber and de Llano. It involves a small modification of the FW theory, namely that a Cooper pair of charged bosons replaces the electron holes of the Bardeen-Cooper-Schrieffer theory. Since deuterons are bosons, the dissociative separation i.e., ionization of the D atoms into two deuterons and two electrons mediated by an optical phonon (*a la* Yukawa) is reasonable. Further the requirements of the FW theory are met by Palladium dueteride.

Introduction

Because of the immiscibility gap in the Pd/PdD_x system, a two phase situation will occur. in general, the mixed phase will consist of alternative layers of metal and superconductor and will exhibit anomalous conductive behavior as a function of applied magnetic field. of the lattice.

Let us study the formation of palladium deuteride from the α-phase metal. The introduction of deuterium by diffusion yields a supersaturatd phase with Pd (D, X*) with the average concentration X* being greater than the equilbrium X_α value, at some point Z but less than X_β. The volume at Z is greater than the volume of the alpha phase. Consequently, the lattice will become dislocated in order to accomodate the coherence strain. As more dueterium is introdued into the lattice around Z. (Note that both phases are face Centered Cubic and enhanced diffusion can occur by *pipe difusion* along the edge dislocations. The latter effect is well known for the diffusion of interstitial elements like H, C, N, and B in FCC metals).

The little diagram will illustrate the stages in the process.

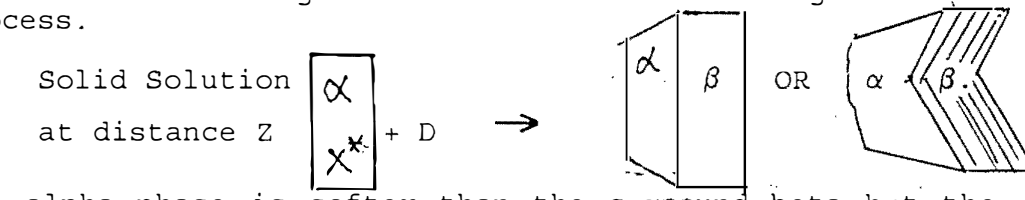

The alpha phase is softer than the compound beta but the beta phase is significantly larger than the parent alpha. The growth process cannot be discussed in any detail in this short manuscript. It suffices to say that the interphase boundary may not remain plane and twin boundaries in the beta phase may be involved. The situtaion contemplated here is sketched here, The details must await further investigation

2. Microstructure of Charged Specimens

The alpha form of palladium deuteride (hydride) is alternatively intermixed spatially with the compound form, PdD_x (where x is greater than 0.66). The photomicrograph of Rolison *et al.* [1] in Figure I, on the left hand side, shows parallel, thin-edged ridges at 5000x. These are crystallographicaly aligned in each grain. They can be readily interpreted as evidence of the two phase structuree On the right hand side they have interpreted the strucutre to be intertwinned.

There is a strong probability that twinning occurs on

the close packed planes of the lattice, namely on {111} planes, as it does in various copper alloys and austenitic stainless steels. Figure II is a metallographic sketch of the twinning in alpha brass. The situation is less clearly seen for austenitic stainless steel - only the twin boundaries are visible. Whether the structure is truly two phase or not can not be unequivocally determined from that study. However, the additonal possibility of twinning can not be dismissed by this study. Given that twinning does occur, blocks of material could be deformed as indicated in this small sketch and lead to surface relief,

D. Rolison *et al.*[2] have studied the morphological changes in polycrystalline palladium which occur on charging. Photomicrographs are presented in Figure III. Their stereogram is interpeted in Figure IV. On charging and the tilting of grains clustered around **<001>** surface normal is significant and they note that deuterium has a stronger effect than hydrogen. The grains with a **<hkl>** normal to the surface other than those near **<111>** are virtually inactive as shown in their stereograph.

The active slip planes are **{111} <110>** in FCC metals and so the dislocations lie in the **{111}** planes. A sketch of the deformed surface is indicated in Figure IV. Several grains are tilted and the surface is in relief.

3. Effect of Dislocations on Diffusion

Kircheim[3] has discussed the trapping of deuterium atoms in such edge dislocations as well as their mutual attraction. The hydrogen atoms with opposing spins attract each other and hence have an influence on the formation of Cooper-paired ion band states.

Oriani in his paper, commented on the significant enhanced concentration of hydrogen (isotopes) in dislocation cores due to the positive partial molar volume of hydrogen in palladium

The trapping of deutereium atoms or ions in dislocations is dempnstrated in Reference 3. Positron annihilation is a sensitive technique which has been used for determining the type and content of dislocations by Waber and colleagues in the case of iron single crystals.

Yong-Ki Park et al.[4] has measured the trapping of hydrogen in annealed and in charged palladium using positron annihilation. They also made Sievert's Law determinations. The positron lifetimes were 147 ± 2.8 psec for the bulk and ranged from 183 to 189 psec in cold rolled and annealed

specimens. Hydrogen charging reduced the percentage of positrons annihilating in the dislocations by 20 percent in the case of the cold rolled and by 16 percent for the quenched specimens. Such a reduction is the signature of hydrogen (isotope) trapping[5]. They also investigated the elimination of dislocations by annealing. It is a second order process. In addition, they studied the changes in the **R** parameter which had been developed by Lee *et al*[6] for this purpose. The value of 1.75 is consistent with proton trapping in dislocations. These dislocations apparently formed upon phase change. Isochronal annealing led to the formation of microvoids[2] with an estimated size of a few Ångstroms.

4. Hydrogen Diffusion Studies

The hydrogen diffusion measurements were made using the method of Devanathen and Stachurski.[7] Hydrogen (or deuterium) atoms are cathodically deposited on one face of the single crystal (or specimen) and anodically oxidized back to hydronium (deuteronium) ions at the parallel exit face. The equipment is shown in Figure V. Typical penetration curves[8] are presented in an accompanying paper and the figure will not be presented here. It shows the holdup or delayed diffusion of the hydrogen caused by the dislocations[9]. In run 1 of this figure, the metal has been polished. In successive runs, the same specimen was held for a short time and recharged. The annealed run which shown no holdup had been annealed at a high enough temperature until the dislocations had been annealed out. The traps are clearly deep and saturable. A proper theory of diffusion in the presence of reversible and irreversible traps has been published by Iino[10].

5. Effect of Mechanical Polishing on Diffusion Rates

In Figure VI, the effect of mechanically polishing the crystal with even a 0.50 micron alumina slurry, resulted in dislocations extending inward about 20 microns, whereas the usual mechanical polish produced more and deeper dislocations. Note that the distribution is logarithmic.

In the course of the investigation of the thermal removal of dislocations by annealing. It was observed that mechanical polishing would produce a thin layer about 50 microns thick of dislocations and in addition, these would reduced hydrogen diffusion.[11] In figure VII, the effect of the slow chemical removal of this thin layer is shown and in. Note that the diffusion (constant), through the 960 micron thick specimen increased 20-fold by the removal of the outer 50 micron surface layer (which had been produced by polishing only the entry side of the sample).

Without further detail, the effect of this thin layer is convincingly shown in another way. In the Arrhenius plot of Alefield and Völkl[12], which involves more than a hundred studies, our triangular point is the diffusion rate measured on a polished crystal of iron. By removing this dislocated layer, the diffusion rate of the same crystal increased at least tenfold and is represented by the square point. The latter lies slightly above their line fitted at higher temperatures. The rather large spread of the data below 300 C is probably due to the fact (a) that all the investigators had abraded or polished their specimens and (b) that the dislocations anneal out above 300°. This is a rather unexpected finding. This illustrates the importance of carefully preparing and annealing palladium test samples - drawn wire is clearly inadequate.

6. The Meissner Effect

In transverse electromagnetic fields, a superconductor has the form

$$|> = \exp\ (i\sum_q \alpha_q(t)\rho_q\ |G>$$
$$\alpha_q = \alpha^*_{-q}$$

The superconductor behaves like a system of charged (or free) bosons. If the external field is uniform, $\nabla\alpha(\mathbf{r},t)$ is a constant vector $\mathbf{K}$ and the wave function of the superconductor is

$$\left[A \sum_k (v_k/u_k)\ c^*_{k+1\uparrow}\ c^*_{-k+1\downarrow} \right]^{N/2} |0>$$

and all the pairs of electrons (and deuterons) have their total momentum increased by $2\hbar\mathbf{K}$ and the wave function is unchanged. For practical applications, the penerating depths of the fields in the Meissner Effect are comparable to the coherence lengths (which is of the order of lattice dimensions for such materials as palladium deuteride) and it is questionable whether it exists. At temperatures above the absolute zero, the quasi-particles exist at all times and are easily perturbed[13]. In Type II superconductors, alloying (or compound formation) κ leads to a mixed state. It was not until the work of Abrisikov[14] that the full implications of the negative energy regime was appreciated. Above H_{c2} in Figure VIII, the material is normal and below H_{c1}, there is the Meissner state. But in the intermediate regime, $H_{c1} < H < H_{c2}$ a mixed vortex state predominates. The dynamics of votrices for high T_c superconductors, is not trivial and is of technological importance.[15] It is intriguing to identify these vortices with the rotons (discussed in an earlier theoretical paper[16]) which were predicted by Feynman[17].

The schematic temperature-magnetic field phase diagram is presenteed in Figure IX.

7. The Arfeev Effect

The significance of the possible twinning in PdD_x is indicated. Cheikin and Chlustikov[18] observed superconductivity localized on twinning planes in 1981. More recently, this has attracted attention due to the occurrence of twinning planes in high T_c superconductors. Huzdina and Rulaevski proposed a phenomenological theory[19] and Arfeev has studied this theoretically.

The formation of a high T_c superconductor has been discussed by Waber and de Llano[20] in palladium deuteride as boson condensation. Their theory needs spin-paired deuterons which form Cooper Pairs in an ion band state. The coherence length of the eletronic Cooper pairs is of the order of 1-3Å but the mass of the deuterons reduces this to 30-40 Fermis.

8. Josepheson Junctions

It is proposed that deuterated palladium with $x \geq 0.66$, occurs as an intimate mixture of the superconductive state with the metallic state. Thus many Josephson junctions are formed. The multi-layered sandwich model which A. E. Andreev[21] proposed in 1967 is realized. Cooper pairs can leak through the semiconductor. In the sandwich, one electron from the semiconductor joins to form a Cooper pair at the superconductor interface [which could be a twinning or slip plane] and the resulting electron hole travels in the opposite direction to another interface and interacts there with a second Cooper pair annihilating it, but in doing so, frees a second electron to shoot across to the interface and form a new Cooper pair. This phenomenon has apparently now been observed with indium arsenide by Kroemer *et al.* [22] In a rising magnetic field, the resistance rises episodically. The unusual quantized magnetic effects which have been observed, have not been thoroughly explored.

Summary

The trapping of deuterium atoms or ions in edge dislocations is studied. These can form as a result of the two phase formation in the Pd/PdD_x system and the effort of one phase to remain coherent. The effect of polishing and the production of dislocations on hydrogen diffusion has been shown to lower the latter substantially in iron single crystals.

The microscopic evidence is that twinning can occur in charged palladium on {111} planes in an FCC lattice. The

dominant dislocation type is {111} <110> in the FCC lattice. The grains deformed most on charging Pd have their surface normals clustered around <001> with those near <111> being largely inactive. At room temperature, the Meissner effect is unlikely to be present. However, the Arfeev effect may lead to superconductivity concentrated on twinning planes and to a stable vortex temperature regime.

Acknowledgements

The interest of the U. S. Army Research Office in Research Triangle, N.C.is gratefully acknowledged and the encouragement of Dr. Robert Reeber is of inestimable value.

References

1. Debra R. Rolison, Wm. E. O'Grady, R. J. Doyle Jr. and Patricia P. P. Trzaskoma, "Anomalies in the Surface Analysis of Deuterated Palladium," *Proc. 1st Annual Conf. on Cold Fusion,* March 1988 Salt Lake City, UT pp 272-279.

2. D, Rolison,. Wm O'Grady, R. B. Doyle. Jr.and P.Tzraskova, "Anomalies in the Surface Analysis of Deuterated Palladium," *Proc. First Annual Conf. on Cold Fusion,* Salt Lake City, Ut, (1990) pp.272-279.

3. R. Kirkheim, "Interaction of Hydrogen with Dislocations in Palladium - II. Interpretation of Activity Results by Fermi-Dirac Distribution," *Acta Met,.* **29** 845-853 (1981)

4. Won Il Koh, Yong Ku Yoon and Yong Ki Park, "A Study on Palladium-Hydrogen Interaction by Positron Annihilation Technique" *First Pacific Rim Int'l Conf. on Advanced Materials and Processing* Edited by Changxu Shi, Hengde Li and Alexander Scott, (Minerals, Metals & Materials Society, Warrendale, Pa., 1992) pp 421-427.

3. Yong Ki Park, James T. Waber and C. L. Snead, Jr., "Reduction of the Trapping by Dislocated Single Crystals of Iron When Charged with Hydrogen," *3rd Int'l Conf. On Positron Annihilation* EditeD by P. C. Jan, R. M. Singra and K. P. Gopinathan, (World Scientific Publ. Singapore 1986) pp. 595-491

6. Jong Lam Lee, James T, Waber, Yong Ki Park and Jeff Th. M. de Hosson, "Stages in the Recovery of Deformed Single Crystals of Iron Studied by Positron Annihilation Techniques," *Proc. Int'l Conf. on Low Energy Dislocation Structures.* (Elsevier-Sequoia, Oxford. England (1986)

7. M. A. V. Devanathan, Z. Stachurski and W. Beck. " A Technique for the Evaluation of Hydrogen Embrittlement Characteristics of Electroplating Baths." *Jour. Electrochem. Soc.*, **110** 896 - 890 (1963)

8. See the thesis of Yong Ki Park, *Northwestern University*. Also Yong Ki Park, James T. Waber and L. C. Snead, Jr., "Reduction of the Trapping of Positrons in Dislocated Single Crystals of Iron When Charged with Hydrogen," *Seventh Int'l Conf. Positron Annihilation* Editors P. C. Jan, R. M. Singra and K. P. Gopinathan, New Delhi, India (World Scientific Publ., Singapore, 1986) pp. 589-591

9. Yong Ki Park, *Ph. D. Thesis*, Northwestern University (1986)

10. M. Iino, "A More Generalized Analysis of Hydrogen Trapping," *Acta Met.*, **30** 367-375 (1982)

11. James T. Waber and Yong Ki Park, "Dislocation Density Profile of Mechanically Polished Iron Single Crystals Determined by Positron Annihilation," *Jour. Mater. Science Letters*, **5** 183 (1986).
Jong Lam Lee, James T. Waber and Yong Ki Park, "The Effects of Mechanical Polishing on Hydrogen Diffusion in Iron Single Crystals" *Scripta Met.*, **20** 823-826 (1986)

12. G. Alefield and J. Völkl, "Hydrogen in Metals II" Springer Verlag, Berlin, Heidelberg 1978 ISBN 3-540-08883-0

13. G. Rickayzen, *"Link with Boson Theories,"* **Theory of Superconductivity** (Interscience Publ., New York, 1965) p.111

14. A. A. Abriskov, *Zh. Eksper. Teor. Fiz*, **32** 1442 (1957)

15. G. Burns, *Chap. 2,* **High Temperature Superconductivity,** Interscience Publ., Boston, (1992) pp. 25-26.

16. James T. Waber, "Solid States Boson Condensation in Cold Fusion," **Frontiers in Cold Fusion** Ed. H. Ikegami World Sci Press Sept. 1992 pp 627-630.

17. R. Feynman, "Superfluidity and Superconductivity" Rev. Mod. Phys.,**20** (1957) 205-318

12. H. S. Cheikin and I. N. Chlutikov, *Letters to Jour, Theor. Physics* **33** 176 (1981)

19. A. I. Huzdin and L. N. Bulaevski, *Letters to Jour. Theor. Physics*, **38** 118 (1981)

20. James T. Waber and Manuel de Llano, "Cold Fusion as Boson Condensation in a Fermi Sea," *Proc. Fourth Int'l Conf. on Cold Fusion*, Dec. 1993 **Paper 11-1**

21. A. F. Andreev, "Exotic Superconductivity of Twinning Planes," *Pis'ma Zhur. Eksp. Teor. Fiz. (USSR)*, **46** 463-465 (1987)

20. H. Kroemer, C. Nguyen and E. L. Hu, "Reflections in a Quantum Well." *Scientific Amer.*, Feb. 1994 p. 20

Figure I. Photmicrographs of Highly Etched, Characteristically Restructured Grains After Charging. In the Left Hand Side, one sees rugged, parallel, thin-edged ridges. On the Right Hand side, the Morphology can be Described as an Intertwinned Structure.

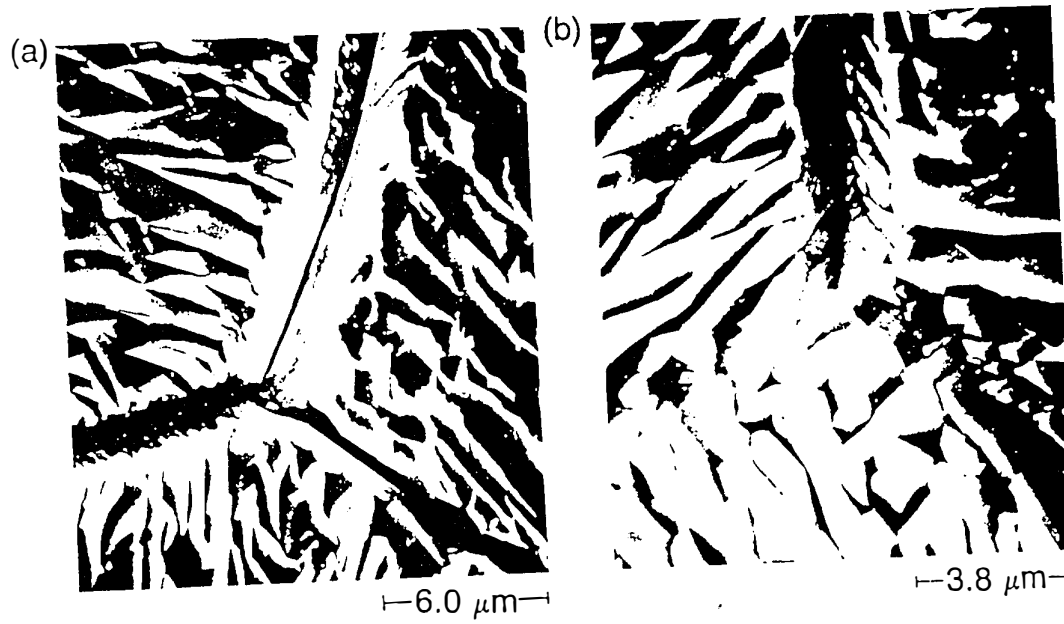

Figure II Metallographic Illustration of the Twinning in Alpha Brass

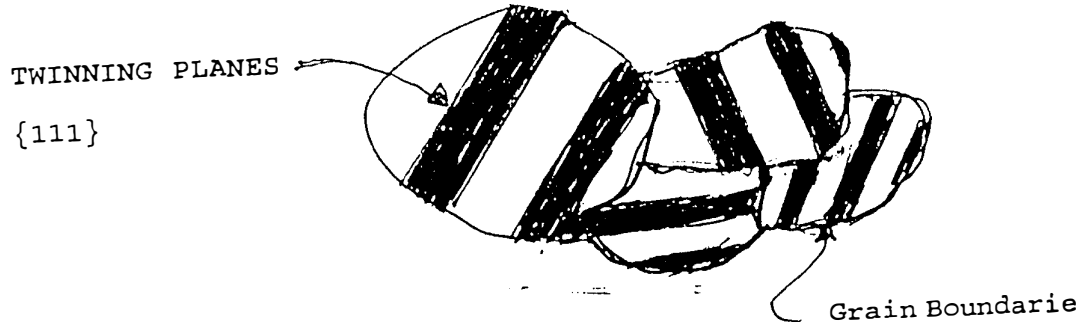

Figure III Photomicrographs Illustrating Intergranular Elevational Differeences in Palladium (a) after Charging and (b) after Fast Ion Bombardment

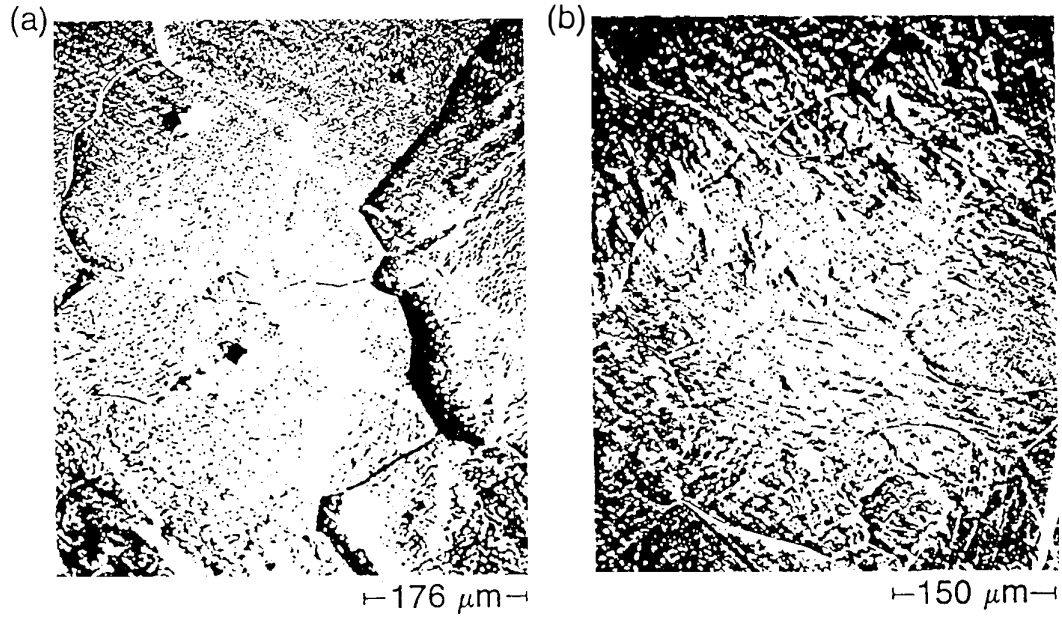

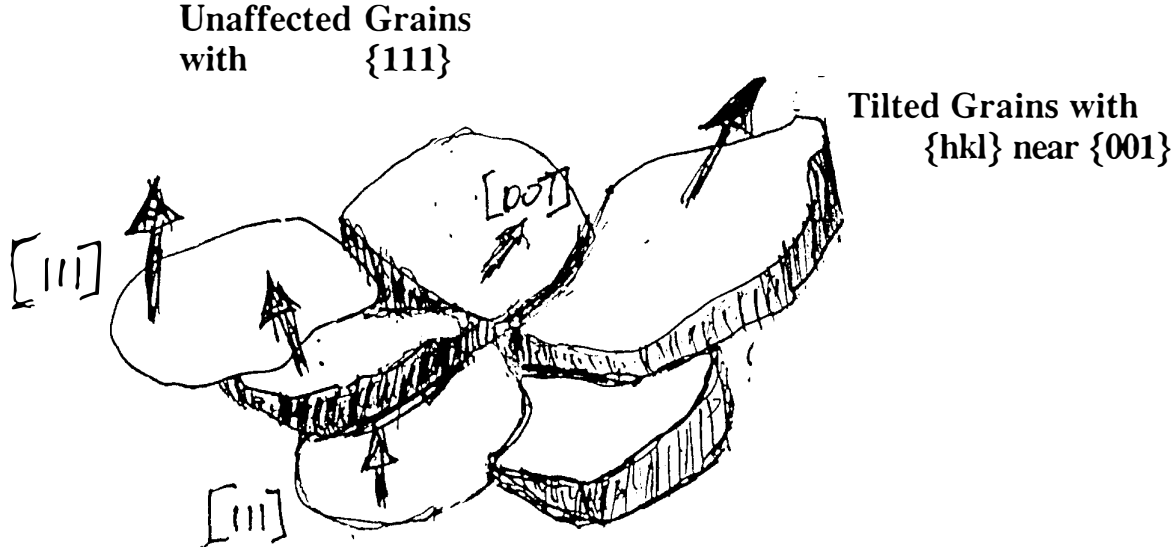

Figure IV. An Interpretation of the Stereographic Plot of D. Roleson *et al.* on Grain Tilting

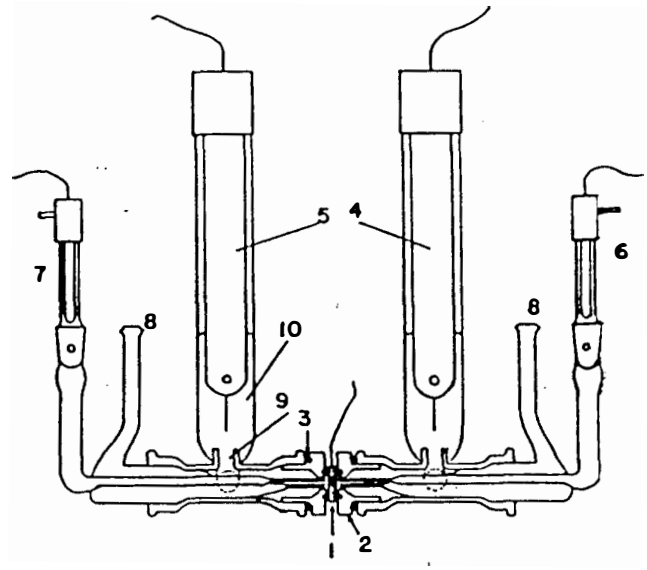

Figure V. The Apparatus for Charging and Discharging Iron Single Crystals. Also used for Measuring Hydrogen and Deuterium (or Ion) Penetration and Desorption.

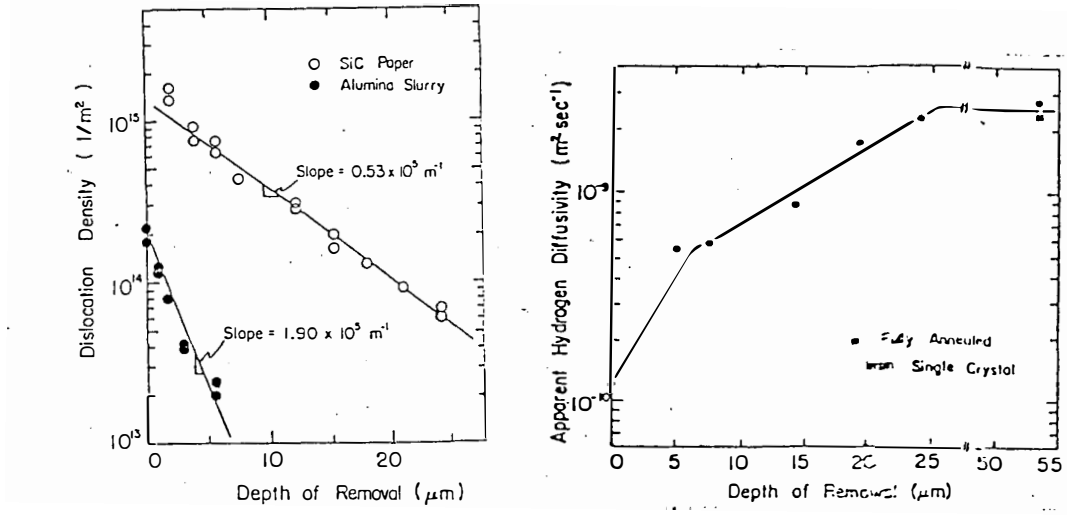

Figure VI. The Distribution of Dislocations Measured from the External Surface Produced by Mechanical Polishing.

Figure VII. Recovery of the Bare Diffusion Rate brought about by the Slow Removal of the Thin Laver Electrolytically.

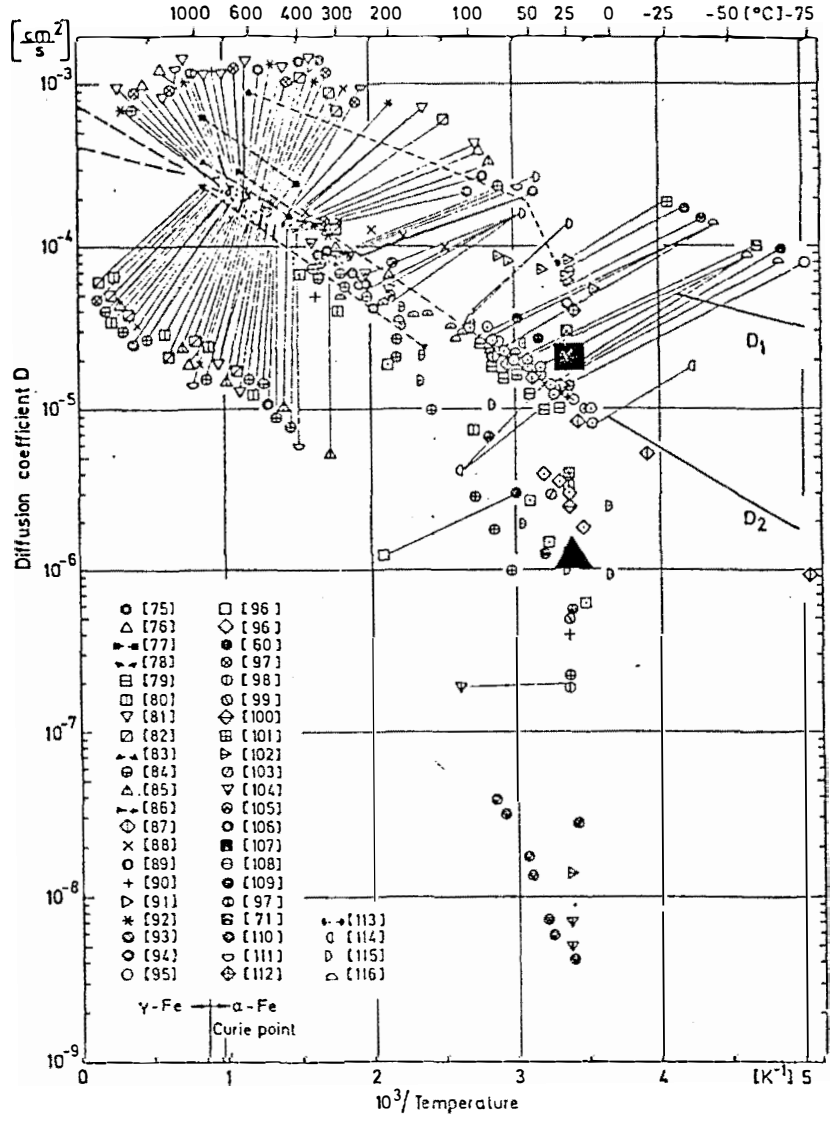

Figure VIII Diffusion coefficient of Hydrogen in α-Fe (2).
(■: hydrogen diffusivity in iron before mechanical polishing
▲: hydrogen diffusivity in iron after mechanical polishing.)

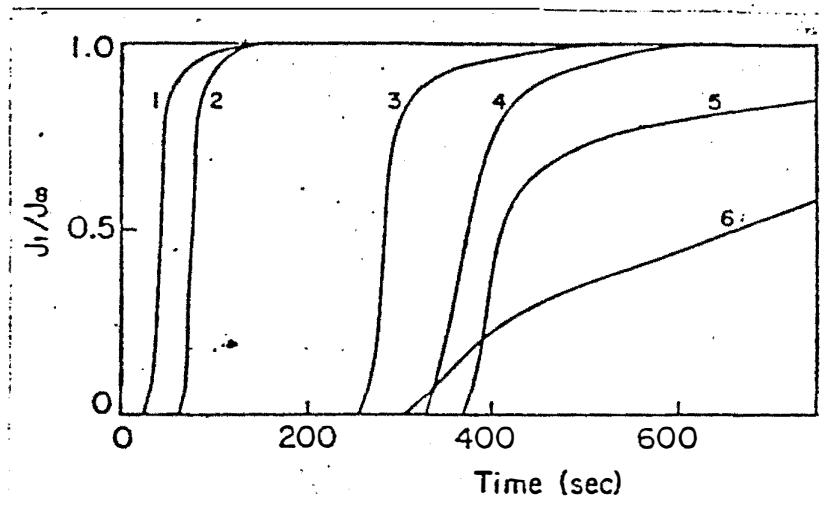

Normalized hydrogen permeability with holding time in air after first permeation (holding time : 1:840 s, 2:1610 s, 3:5190 s, 4:50400 s, 5:evolution for 50 min at 363K in vacuum 6:first polarization 6 strokes on grit 240.

Figure IX. Effect of Holding The Fully Charged Specimen at Roo Temperature. When Fully Degassed and the Dislocations Annealed Ou there is now Holdup. The long delay following mechanicall polishing.

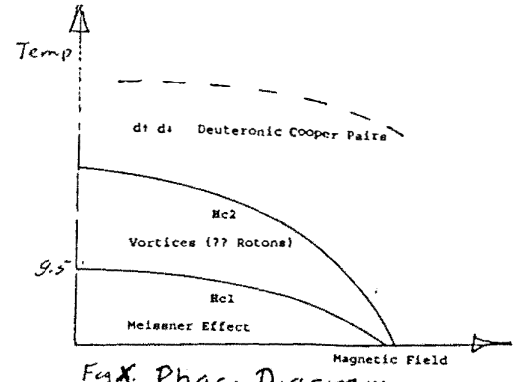

Fig X Phase Diagram

Session 6

New Developments, Approaches and Systems

Fifth International Conference on Cold Fusion
9-13 April, 1995 - Monte Carlo, Monaco
ICCF5 ©1995

Excess heat and Mechanism in Cold fusion reaction

Yoshiaki ARATA [1] and Yue-Chang Zhang [2]

1) Arata Hall Osaka University
2) Welding Research Institute Osaka University
(11-1,Mihogaoka, Ibaraki, Osaka, 567, Japan)

Abstract

The authors have proposed a new "Model" which can reasonably explain the existence of Cold Fusion Reaction and also verify the generation of tremendous excess energy in the DS-cathode. which is fifty thousand times higher than chemical reaction energy. The new model is named "Latticequake Model". Cold fusion is caused by high energitic deuterium similar to "hot" fusion.

Key words: Latticequake; cold fusion; molecular dynamics; excess heat; DS-cathode

1. Introduction

The authors pointed out that reactions in a Double Structure cathode (DS-cathode) contained with "Pd-black" continuously generated more than 5×10^4 times of excess energy expected in chemical reactions.[1] So far many researchers have reported on the excess heat generation and the evidence on the generation of nuclear-reaction products.[3] "Cold fusion", however, has not been generally accepted due to the lack of experimental evidences on the stable and/or continuous generation of large amount of excess heat or nuclear reaction products. Furthermore, poor reproducibility of the experimental data tended to obstacle the determination of conditions for the generation of nuclear reactions. Therefore the theoretical works devoted to explain the mechanisms involved in the cold fusion have been failed because of lack in their stand points based on the experimental results with sufficient reproducibility.

In the present paper, the authors would like to propose a new "model" and to clarify the justifications on the cold fusion.

2. Characteristics of DS-Cathode

The principle of the DS-Cathode is schematically depicted in **Fig. 1**. In moving deuterium from the Pd region A with a deuterium concentration of $[D_A^*]$ ($\equiv D/Pd$) to the other Pd region B, each separated by the space C, the problem to be considered here is what is the most appropriate way to get the concentration $[D_B^*]$ in the region B as high as possible.

Here we have considered to compare the following 4 possible ways as schematically illustrated in **Fig. 2**. First in the case of (a) where the space C is vacuum so that the concentration in the region B becomes $[D_B^*]=0$ and naturally results in the process in the case of (b). In other words, deuterium gas is diffused into the space C and the D2 gas pressure P_{D2} increases with time. So the concentration $[D_B^*]$ in the region B gradually increases to follow $[D_B^*] = a + b \log P_{D2}$ according to the Sieverts' law. Even with hydrogen gas the condition to achieve $[H_B^*]=0.9$ as shown in Fig. 2 requires the hydrogen pressure higher than at least ten thousand [atm], and approximately 30 times higher pressure is believed to be required to satisfy this condition with deuterium gas. therefore, as fas as experiments performed in the territory of the Sieverts' law, where the high pressure regime is preferred,As has been experienced by many researchers,it is impossible to realize a high concentration of deuterium. Accordingly, they should need a major break-through to get out of this law. Based on these facts, as has been presented by many reports, it should be absolutely unlike to observe the reaction products ($_2{}^4$He, $_1{}^3$T, $_1{}^1$P, $_0{}^1$n etc.) and/or the excess heat (excluding the heat caused by the chemical reactions) in the pressure range as low as 1 [atm] during the period of time as short as several days.

The authors [3] have ever pointed out the importance of "micro-defects" to the mechanism of cold fusion. Looking from the bulk material, surfaces are considered to be a kind of the defect. Therefore, it is expected to increase the effects of the surface micro defects with increasing surface area or "relative surface" S^* (= surface area / volume). One extreme state to realize this idea would be powders, which can be considered to be a key factor for the practical development of the cold fusion in future.

Forty years ago when one of the authors hit upon an idea of "Solid-state plasma fusion", he did not believe that the fusion reactions were obtainable only with electrolysis as are presented later by Fleischmann and others.[4] As in the "hot plasma fusion", one of the absolute conditions for the solid-state plasma fusion was believed to be the high-energy state of the deuterium ions confined in the Pd lattice with external shock-energy supply. This idea has raised questions on the Fleischmann's results, however, the recognition of these facts has lead to the "powder vessel" as one of the best vessels based on the above considerations of the characteristics of powders.

The authors immediately started the examination of the Fleischmanns' experiments using the following two ways with Pd powders. One was the way to use powders as a cathode and the other was performed with Pd cathodes spray-coated with Pd powders onto the surface.[3] The former method (not published yet) resulted in a number of troubles, where we examined the characteristics of the powders. As a result, the principal condition for the cold fusion was concluded to be that "surface effect" inherent to the powders enables 'the homogeneous and highly concentrated deuterization and the feasibility of large cathode without any

limitation on size.

Thereafter, significant effects are not expected in the ordinary surfaces on the plate- and/or the rod-configurations with small S^* due to the less chemical reactivity. With powders, on the other hand, S^* considerably and thus the reactivity abruptly increases with decreasing powders size and causes "spill over effect".[5] This causes the powders to function the "Pumping-up action" as shown in Fig. 1 and the powders continuously absorb deuterium up to $[D^*]\approx 1$. Especialy, it is well know that $[D^*]=1$ should instantaneously be achieved in the "cluster" (< 100 Å in diameter).[9] Consequently, characteristics of the deuterium absorption and its variation with pressure are greatly dependent on S^* as shown in **Fig. 3**.

Fig. 4 shows the recent experimental data on the excess-heat generation. These results show that the new "model" for the cold fusion is requested to describe the possibility of the continuous energy generation over 10 [watt/cm^3].

3. Proposal of the New "Latticequake Model" for Cold Fusion

One of the fundamentally important problems involved in the cold fusion is that the deuterium is in the ionic state in the Pd lattice and their motions are strongly limited by the intense constraint force by the Pd lattice, which is completely different from the physical situations in the "Hot" plasma fusion. This means that the position, the direction and the conditions for the fusion reactions are considerably limited, and thus the reaction process is considered to undergo different mechanism from that expected in the hot fusion. Therefore the theoretical approach for the cold fusion is required first to consider the wave function of the O-site (Octahedron), which is the stable site for deuterium, by assuming that the all of deuterium are confined in this site, and second to obtain the probable distribution to find the deuterium from the O-site to the T-site (Tetrahedron) surrounded by the several O-site. Here when we assume that the achievement of the fusion reactions by putting plural deuterium ions to interatomic distances of about 0.1 Å is explicitly driven by only thermal energy, the Pd lattice may explode out. This consideration has lead to a conclusion that the cold fusion is impossible.

However, as indicated in Fig 4 or similar data repeatedly, excess energy of 10 [W/cm^3] is continuously generated and obtained large energy around 100 [MJ] by the use of DS-cathode developed by the authors. The energy is extremely larger when compared to chemical reaction, therefore, no reaction except cold fusion exists. The authors proposed a new model that enables the generation of "CP-CF"(Continuous Powerful Cold Fusion).

Now, as well known, when the motion of atom in lattice exceeds Wigner energy, ε_w, the violent vibration is induced in the lattice as schematically shown in **Fig. 5**. The authors named the phenomena as "Latticequake". Suppose that the reaction occurred one time, as indicated in Appendix, the reaction products with high energy is certainly produced from the well-known two-body collision of deuterium (Rutherford type: [A-type]) to unknown two-body or multi-body collision [B-type]. Therefore, for the sake of simplicity, the reaction products is represented as $_2{}^4$He, and supposing its energy $\varepsilon_{He}=1\sim 20$ [MeV].

The necessary energy to generate "CP-CF", ie., Latticequake is obtained by the collision of $_2{}^4He$ against the atom on Pd lattice that transfers higher-energy to the atom. Then, the energy transfer from high energy $_2{}^4He$ to "cold-Pd atom" is described.

When the A_0 atom in Fig.5(A) moves toward $A_0(O_1)$ or O_3 (Center of O-site) along X_1-X_2 (<100>) axis, the neighboring atoms shift to $B_0 \rightarrow B_1$, $D_0 \rightarrow D_1$, $E_0 \rightarrow E_1$ or $C_0 \rightarrow C_1$, $F_0 \rightarrow F_1$, $G_0 \rightarrow G_1$. If the energy of A_0 atom is larger than Wigner energy, ε_w, A_0 atom jumps over A_1 or C_1 and moves following direction; $A_0 \rightarrow A_1 \rightarrow B_0 \rightarrow \cdots$, or $C_0 \rightarrow C_1 \rightarrow \cdots$, and the neighboring atoms quickly return to the original position. Such behavior of A_0 atom induces the collision of neighboring many atoms, and generate the multi collision phenomena, therefore, the outline could be grasped by "molecular-dynamics". For example, as described above, the following energy for $_2{}^4He$ is supposed.

$$\varepsilon_{He} \approx 1 \sim 20 \text{ [MeV]} \qquad [1]$$

The following energy is assumed as a mean value.

$$<\varepsilon_{He}> \approx 3 \text{ [MeV]} \approx 5 \times 10^{-13} \text{ [J]} \qquad [2]$$

As well known, when a particle with mass of m having energy of $<\varepsilon_m>$ collides head-on against a static particle with mass of M, energy $<\varepsilon_M>$ of particle M is expressed as the following.

$$<\varepsilon_M> = <\varepsilon_m> [4mM/(m+M)^2]$$
$$[\fallingdotseq 4(m/M)<\varepsilon_m>]; (M \gg m) \qquad [3]$$

Supposing that m=He, M=Pd, one collision gives about 15% of energy to Pd and He itself is rebounded with 85% of energy, the reaction occurs at O_3-site, if He with $<\varepsilon_{He}>$ collides head-on against A_o atom of Pd along $X_1 \rightarrow X_2$ axis, He atom is rebounded and then goes back and forth several times giving almost $<\varepsilon_{He}>$ to A_0 and c_0 atom, and the atoms are emitted toward $A_0 \rightarrow A_1 \rightarrow B_0$ or $C_0 \rightarrow C_1 \rightarrow$ respectively with $<\varepsilon_{He}>/2$ along X_1-X_2 axis direction. These A_0, and C_0 atoms give violent vibration on lattice as seismic atom ("S-atom") thus generate "Latticequake". This Latticequake severely crushes the O-site(include deuterium) along X_1-X_2 axis, simultaneously expands the O-site along Y and Z axis, the maximum expansion is as follows; $a_0a_0 \rightarrow a_1a_1$ and $b_0b_0 \rightarrow b_1b_1$. By this expansion both O-site and T-site simultaneously expand and integrates each other forming a cavern more than ten times larger than normal O-site, this a cavern is called "Lattice Hall". If the lattice contains 100% deuterium (D^*=1), "Lattice Hall" accommodate around 10 deuterons. Such "Lattice Hall" can shrinks rapidly to normal O-site size around 10^{-12} s, and severely compress the deuterium clusters with the density of deuterium over 10 times high than its solid one that makes possible

for the achievement of cold fusion. The phenomena is similar to "Laser implosion". Therefore the phenomena could be called as "Lattice implosion". The necessary condition for the achievement of "CP-CF" by this Lattice implosion is $D^* \geqq 1$.

Then, Latticequake moves with "S-atom". The energy of $<\varepsilon> \approx 20 \sim 30$[eV] (Wigner energy in metals) should be consumed by every movement of S-atom from A_0 to B_0. Generally, the movement distance a^*, movement frequency n^*, traveling length l^* and $<\varepsilon_w>$ are different according to the movement direction of "S-atom". However, In the case of ideal "Latticequake" due to the "S-atom" with the energy $<\varepsilon_{"s"}>$:

$$n^* = <\varepsilon_{"s"}> / <\varepsilon_w>, \quad l^* = (n^*+1)a^* \qquad [4]$$

When the historically evaluated result obtained by Vineyard, et al.[6] as shown in Fig. 5(B) is used, $n^* = 2$ and $l^* \approx 12$ [Å] are determined by giving $<\varepsilon_{"s"}> = 40$ [eV], $<\varepsilon_w> 20$ [eV] in the {100} plane and <100> direction. This is an example when the zone of ideal "Latticequake" is almost equivalent to the distance of Frenkel pair.

On the other hand, in the case of Pd in the {100} and <100>, when the ideal "Latticequake" due to the "S-atom" with the high energy $<\varepsilon_{"s"}>$ ($= <\varepsilon_{He}>/2$) is considered according to the [2]. [3] and [4] equations,

$$n^* \approx 5 \times 10^{4}, \quad l^* \approx 2 \times 10^{-3} \text{ [cm]} \ (=20 \text{ [}\mu\text{m]}) \qquad [5]$$

In the case, $<\varepsilon_w> = 30$ [eV] was used. In reality, however, a number of cases require 60~ 80 [eV].

The above description is an example concerning the behavior of an ideal 'Latticequake" due to "S-atom" generated under the ideal conditions. It should be quite important in understanding the "limitation" of practical phenomenon, knowing the events under such ideal enviroments.

As shown in Fig. 5(B), in general, a motion of "S-atom", A_0, is off from an ideal direction as the <100> direction. This indicates the movement of atoms in the (100) plane obtained on the basis of "molecular dynamics" by Vineyard.[6] when a "S-atom" is shot out at an angle of 15^o off Y axis (<100>). As understood from this figure, the "S-atom" with the energy more than the Wigner energy produces a "Frenkel pair" and "focusson" etc. in Pd Lattice. That is to say, the <100> and <110> direction are "focusson channels" for the Pd lattice and are regarded as "reaction roads" for deuteriums. Such reaction roads appear at certain points in any collision in the case of "S-atoms" of ultra-high energy. A "S-atom" of high energy should generally induce an intense cascade phenomenon which produces 100~1000 Frenkel pairs instantaneously by chain avalanche collision.[7),8)]

Now let's consider neutron energies generated by the D-D reaction due to hot plasma fusion by way of example. The neutron energies generated by the primary

reaction, ${}_1{}^2D(d,n)_2{}^3He$ and the secondary reaction, ${}_1{}^2D(t,n)_2{}^4H$ are defined as $<\varepsilon_{N1}>$ and $<\varepsilon_{N2}>$, respectively, and they are:

$$<\varepsilon_{N1}> = 2.45\ [MeV],\quad <\varepsilon_{N2}> = 14\ [MeV] \qquad [6]$$

In both cases, "S-atoms" with high energy can be produced. In the case of $<\varepsilon_{N2}>$, the energy $<\varepsilon_{"s"}>$ of "S-atoms"is reported to reach 2 [MeV] at maximum (and 0.3 [MeV] on the average). [7] Therefore, such S-atom can supply an energy$<\varepsilon_{"D"}>$ of approximately 40 [keV] (6 [keV] : average) to deuteriums. Moreover, such high energy "S-atom" would generally induce 10 to 20 sub-cascades. which consists of "vacanay clusters" with a concentration of vacascies 20~30%.[7),8)] In the case of Frenkel pair even when only one vacancy is produced, "Latticequake" is induced at the surrounding atoms clustered between a vacancy and internal atom in a Frenkel pair. Consequently, high conncentration of deuterons ara included in the intense cascade and much high energy levels are achieved there, leading to more opportunities of the D-D reaction. t is taken for granted that more defects should cause an intense shake more frequently and the D-D chain reaction would take place more easily.

The above descripitions are summarized in **Fig. 6.** In short, at the condition of the deuterium concentration $[D^*]\gtrsim 1$, only if one 'S-atom" is generated, the energy induces the "Latticequake", which acts as two functions. One is that it crushes "O-site". Thereby "Latticequake" hits the deuterium out of the O-site and supplies the deuterium with the high energy $<\varepsilon_{"D"}>$ as a "Lattice-accelerator". "S-atom" with an energy of 1 [MeV] produces deuterium with an energy of 20 [keV]. The other function of the "Latticequake" is that it makes a cavern, "Lattice-Hall", over 10 times wider than normal O-site by combining with many O-sites and T-sites. Instantly the "Lattice-Hall" accommodates deuterons, it shrinks for an extreme short time of about 10^{-12} [s] and thereby the "Latticequake" accelerates the deuterons toward the center of the "Lattice-Hall" as a "lattice accelerator". This enables the deuterons to be concentrated to the degree of 10 times more than its solid state and achieved nuclear fusion reaction. It seems that this phenomenon in cold fusion is similar to the "Laser implosion" in hot fusion, and we name it "Lattice implosion".

The basic differences between the cold fusion and hot fusion, are summariged in **Fig. 7**. In cold fusion, deuterons are strongly confined by latice field and, by "Latticequake", can attain the kinetic temperature of several million in spite of low lattice temperature. On the other hand, in hot fusion, the deuterium plasma confined by strong magnetic field is heated by high energy electrons in general. Thus, the lattice atoms play the crucial role in cold fusion,while the electrons in hot fusion. Therefore, in order to maintain the chain avalanche reaction stably for each nuclear fusion, the fundamental conditions are $[D^*]\gtrsim 1$ for cold fusion and "stability" for hot fusion. Both fusions require a similar "High Energitic Deuterons" in order to induce nuclear fusion reaction.

Appendix I : [*A-type*]. *Rutherford fusion reaction.*

$$ {}_1{}^2D + {}_1{}^2D \begin{cases} {}_2{}^3He + {}_0{}^1n\ (3.27\ [MeV]) & (a) \\ {}_1{}^3T + {}_1{}^1P\ (4.03\ [MeV]) & (b) \end{cases} \quad (1) $$

When this reaction is continued, ${}_1{}^2D\ ({}_1{}^3T,\ {}_0{}^1n)_2{}^4He$ and ${}_1{}^2D\ ({}_2{}^3He, {}_1{}^1P\ )_2{}^4He$ are set as a second reaction.

$$ \therefore 6_1{}^2D \rightarrow {}_2{}^4He\ (7.1) + 2\ {}_1{}^1P\ (17.7) + 2\ {}_0{}^1n\ (16.55) + (1.8) $$

Assuming that the energy of only charged particles transforms to the lattice, where the energy ε_D for the extinction of one deuterium is produced in lattice

$$ \varepsilon_D \approx 4\ [MeV]\ (=6.6\times10^{-13}\ [J]) \quad (2) $$

total energy ε_{cc} in Pd lattice of 1[cm^3] volum with [D^*] =1,

n_{Pd}= 7×10^{22} [atoms/cm3]

$$ \varepsilon_{cc} = n_{Pd} \quad \varepsilon_D \approx 4.6\times10^{4}\ [MJ/cm^3] \quad (3) $$

Appendix II : [*B-type*]. *Unknow fusion reaction.*

Assuming that the simplest reaction of unknown fusion is

$$ {}_1{}^2D + {}_1{}^2D = {}_2{}^4He + 23.4\ [MeJ] $$

$$ \therefore \varepsilon_D \approx 12\ [MeV]\ (\approx 1.9\times10^{-18}\ [MJ]) \quad (4) $$

$$ \varepsilon_{cc} \approx 1.4 \approx 1.4\times10^{5}\ [MJ/cm^3] \quad (5) $$

Note:

Since totalenergy in authors experimental data was $\varepsilon_{cc}^* > 100\ [MJ/cm^3]$, it is compared with (3) and (5) equations

$$ \varepsilon_{cc} / \varepsilon_{cc}^* \begin{cases} \approx 500 \text{ for [A type]} & (a) \\ \approx 1500 \text{ for [B type]} & (b) \end{cases} \quad (6) $$

This means that authors datas correspond to extinguish one deuterium among 1000 (~100) ones.

Acknowledgments. This research has been supported by a research grant from The Japan Acadamy the authors would like to express their appreciaton for the helpful discussion of Prof. H. Fujita of KinKi University, Prof. M. Kiritani of Nagoya University.

References

1. Y. Arata. and Y.C.Zhang (1993) Kakuyugo kenkyu 69, 963; (1993) ICCF4; (1994) Proc. Japan Acad. 70B, 106-101.
2. Proceedings of the Third and Fourth International Conf. on Cold fusion, ICCF3 and 4.
3. Y. Arata. and Y.C.Zhang (1992)Kakuyugo kenkyu 67; (1992) Fusion Technology 22, 287; (1992) ICCF3.
4. M.Fleischmann and S.Pons. (1989) J.Electronal, Chem.261, 301-308.
5. Proc. Third Inter. Conf. on Spillover (1993).
6. J.T. Gibson. A.N.Goland, M. Milgram,and G.H.Vineyard (1960) Phys. Rev. 120, 1229.
7. M. Kiritani, (1994) J. Nuclear Materials 216, 220-264.
8. Y. Shimomula. (1991) J. Nuclear Materials 905, 179-181.
9. H. Fujita. (1994) Material Trans., JIM. 35, 563-575.

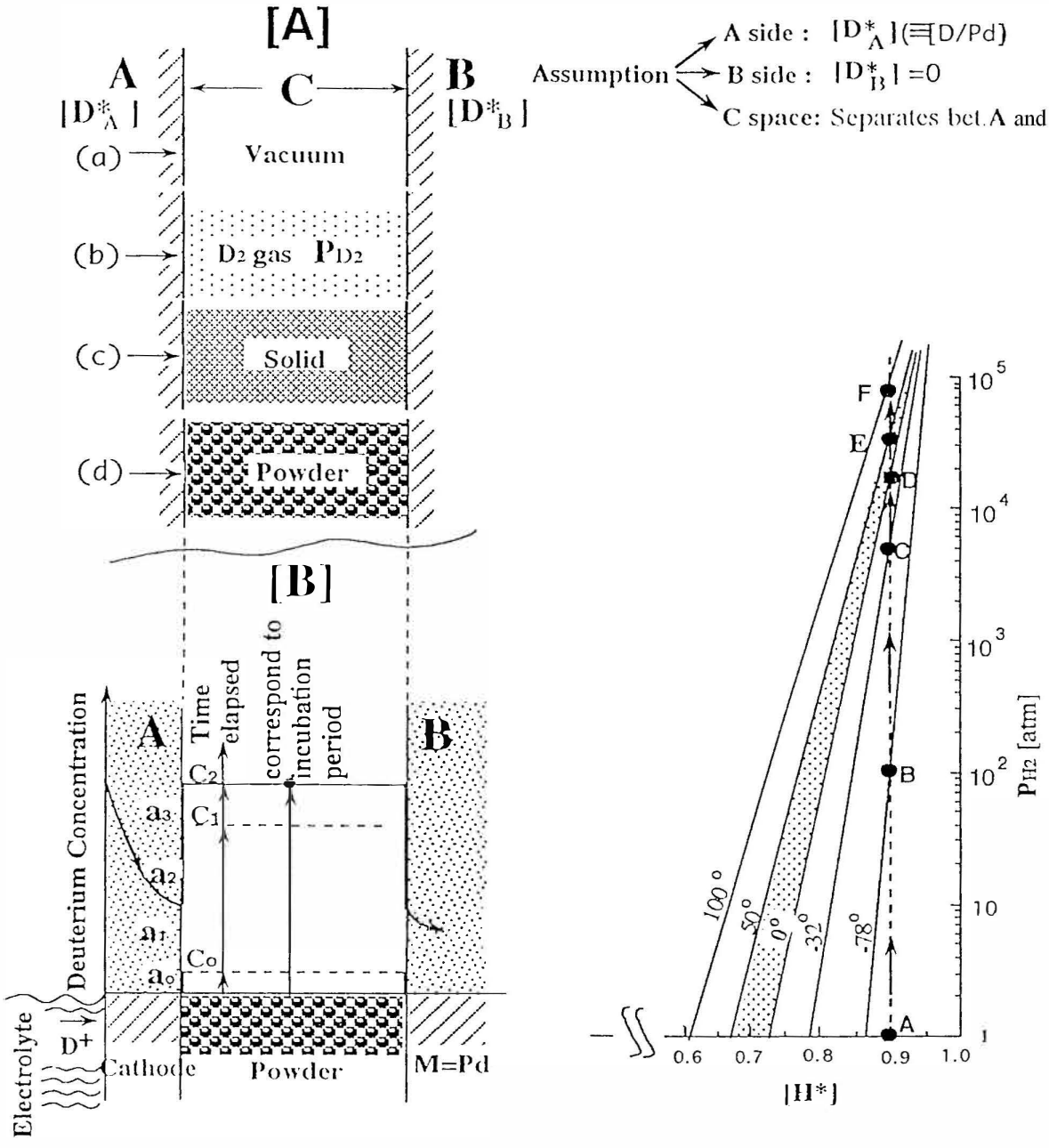

Fig. 1 Schematic diagram for deuterium movement from A to B, which is separated by C-space

Note[A]: Difference between Vacuum, Gas, Solid and Powder for deuterium movement

Note[B]: Illustration of "pumping -up action"(Spillover-effect) of fine powder, where a_o(C_o), a_1(C_1) and a_2, a_3...(C_2) are Deuterium Concentration Curve in outer (and inner) Cathode respectively.

Fig.2 Plot of "P-C-T" relationship at high concentration and pressure after many researchers:[H*](≡ H/Pd)=a+blogPH2, and [D*] requires the pressure around 30 times higher than [H*].

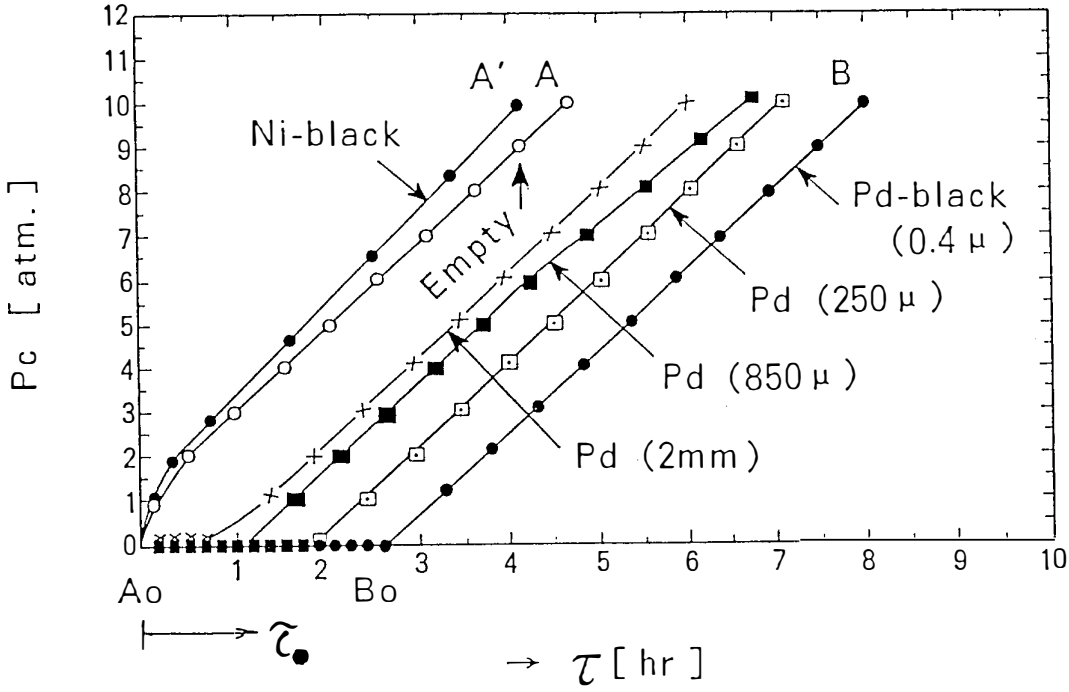

Fig.3 Relatioship between Pc — τ
($\tau_{●}$: incubation period) for a long period.

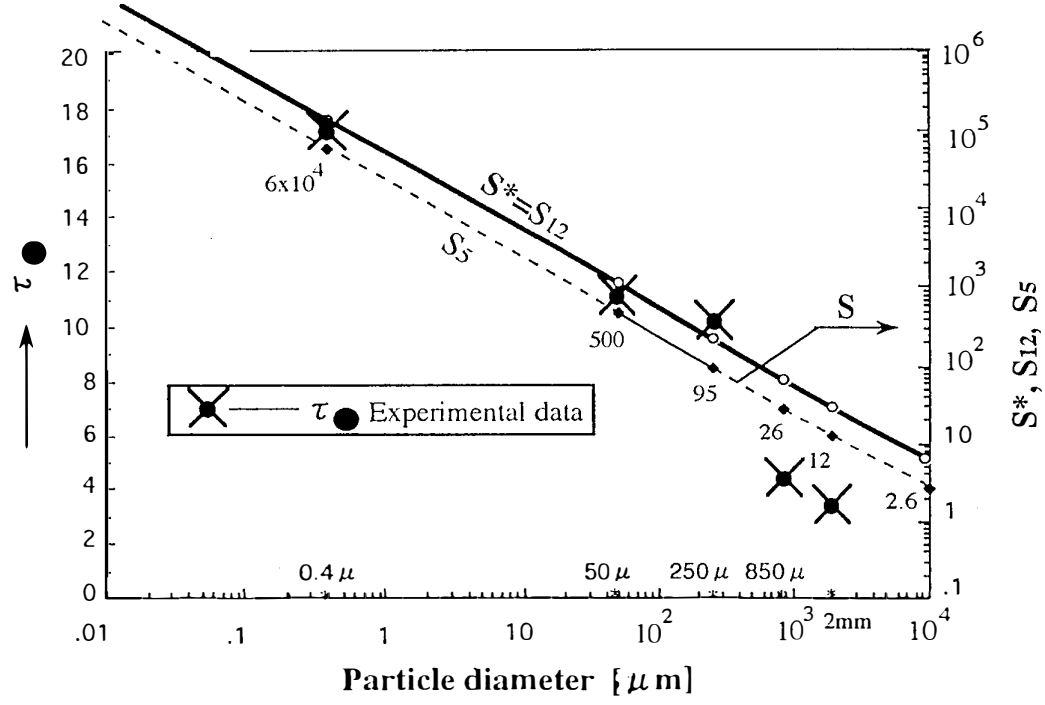

Fig. 3 Relationship between powder and incubation period $\tau_{●}$ relative surface S* and surface area (S_5 and S_{12}). S_5 and S_{12} are Pd 5 [g] and 12 [g] ($\fallingdotseq \rho$: Pd density), respectively. In general,

$$S^* = \frac{\rho}{Mn} Sn \quad (n=1, 2, 3, 4, \cdots; 12 \cdots) \quad \therefore S^* = S_{12}, \ (\rho = M_{12} \fallingdotseq 12 \text{ [gr]})$$

where, surface, Sn [cm²] and mass. Mn [gr]. n (=1, 2,- - - -).

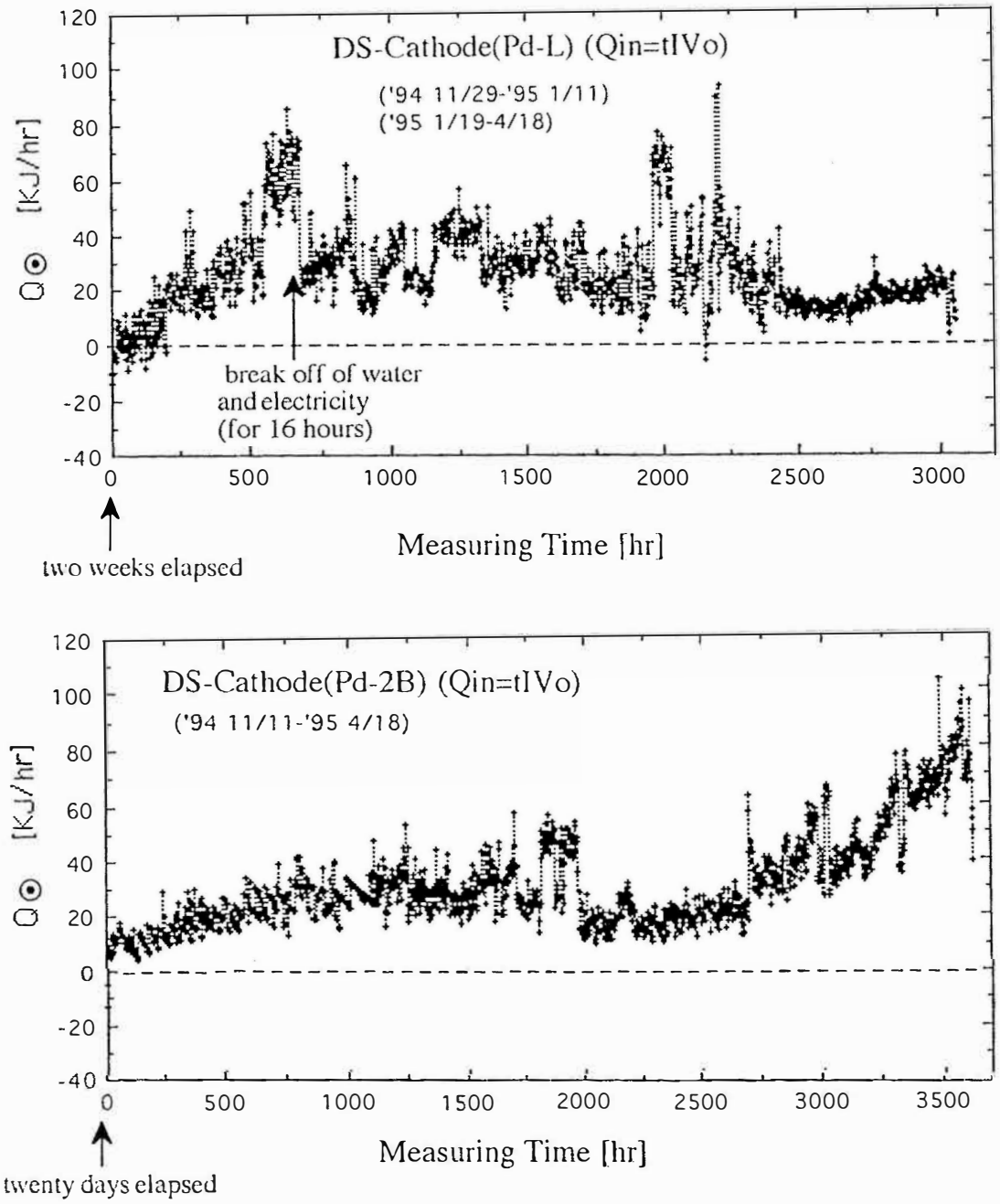

Fig. 4 Excess heat characteristics of two examples for long period. (upper side: Pd 5 [gr], low side: Pd 3 [gr] and excess heat $Q_{\odot}$ = output- input, [KJ/hr]; 10 [watt] = 36 [KJ/hr]

Fig5 [A]

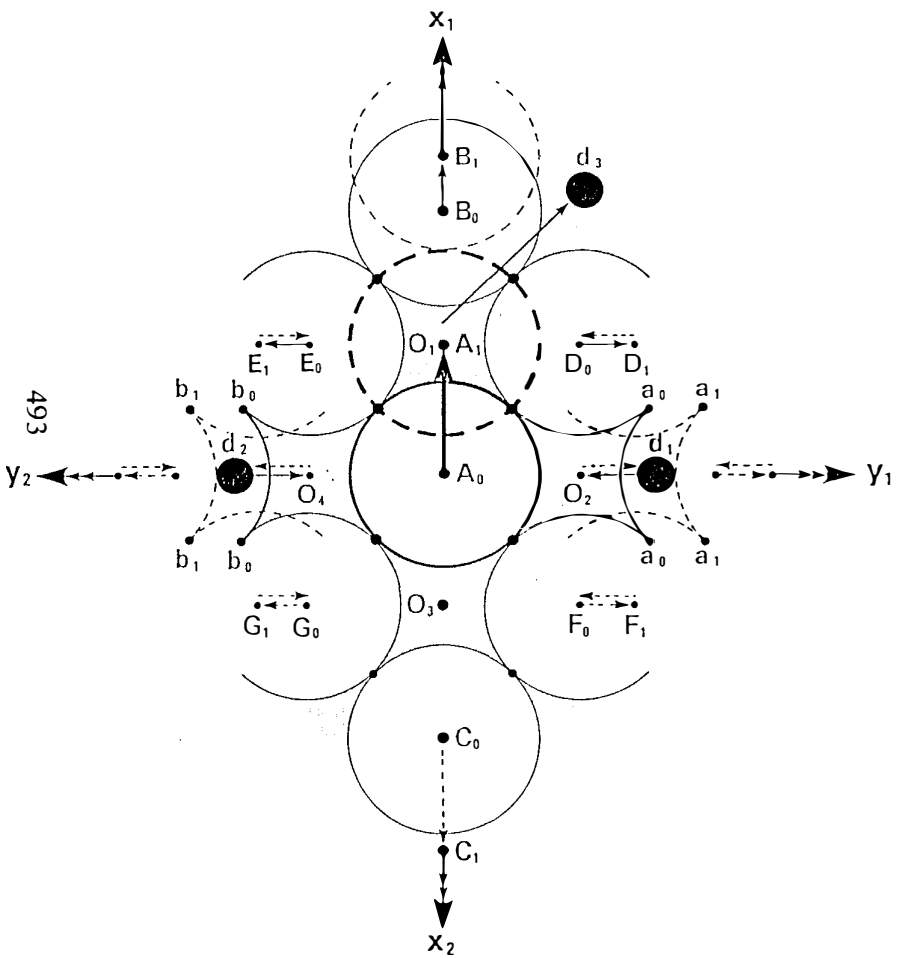

Fig5 [B]

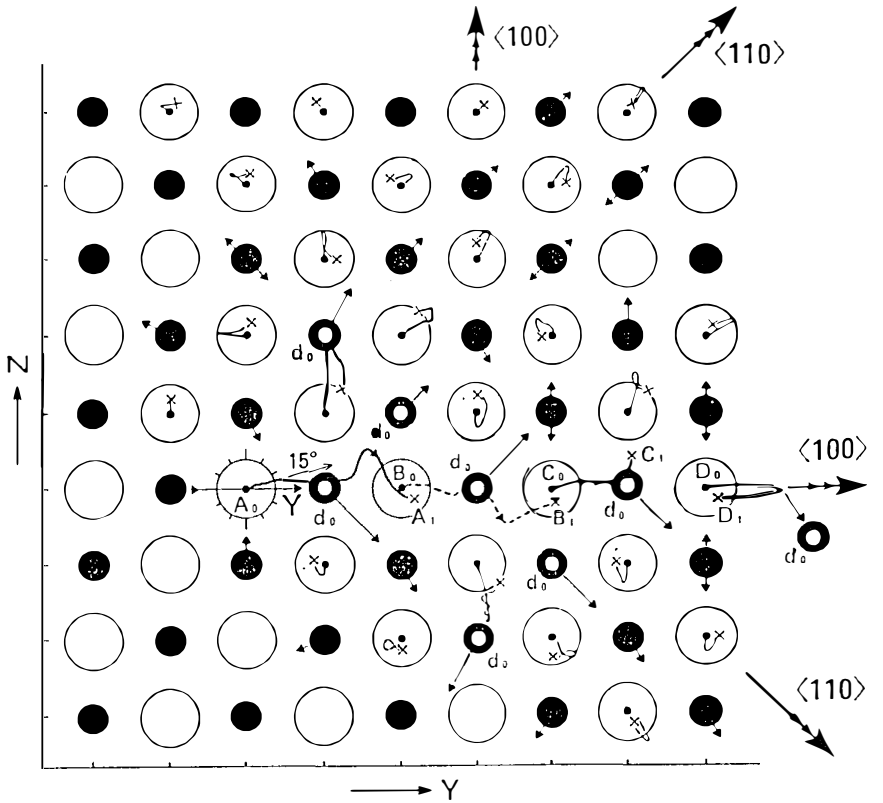

Fig 5 (B) Demonstration of high energy deuterons which were accelerated by "Latticequake" in {100} of Pd-lattice

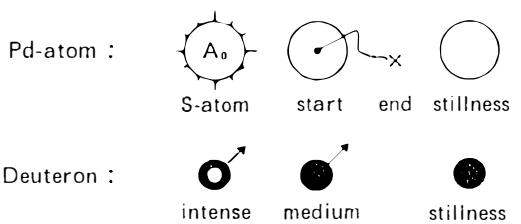

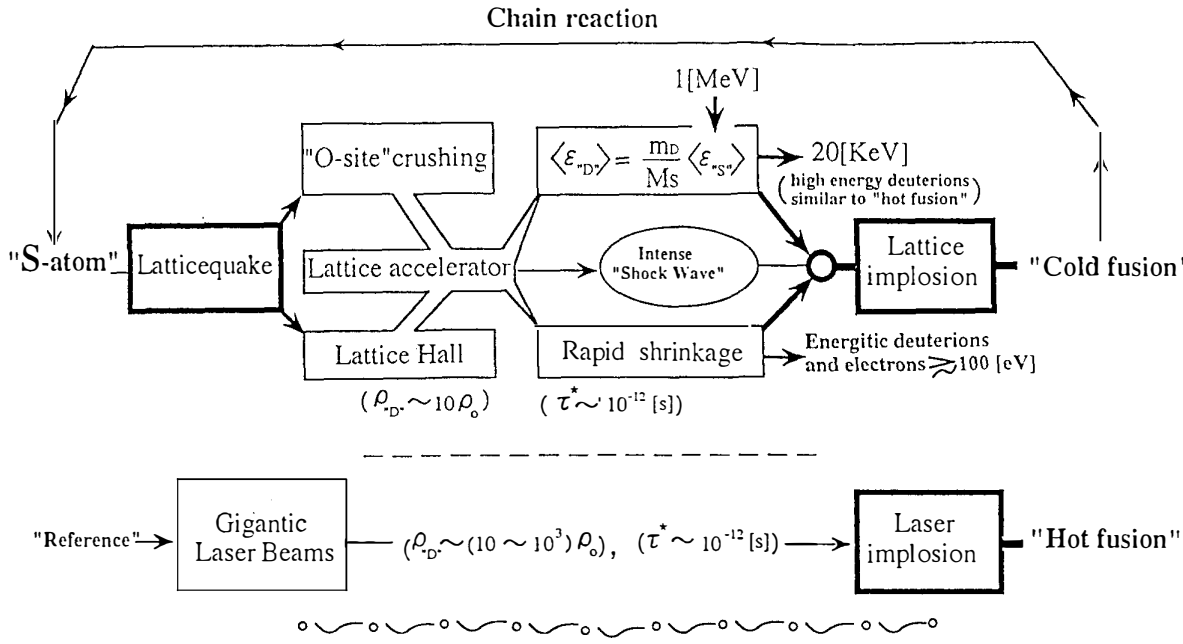

Fig. 6 Schematic digram of "Latticequake Model" for Cold fusion reaction

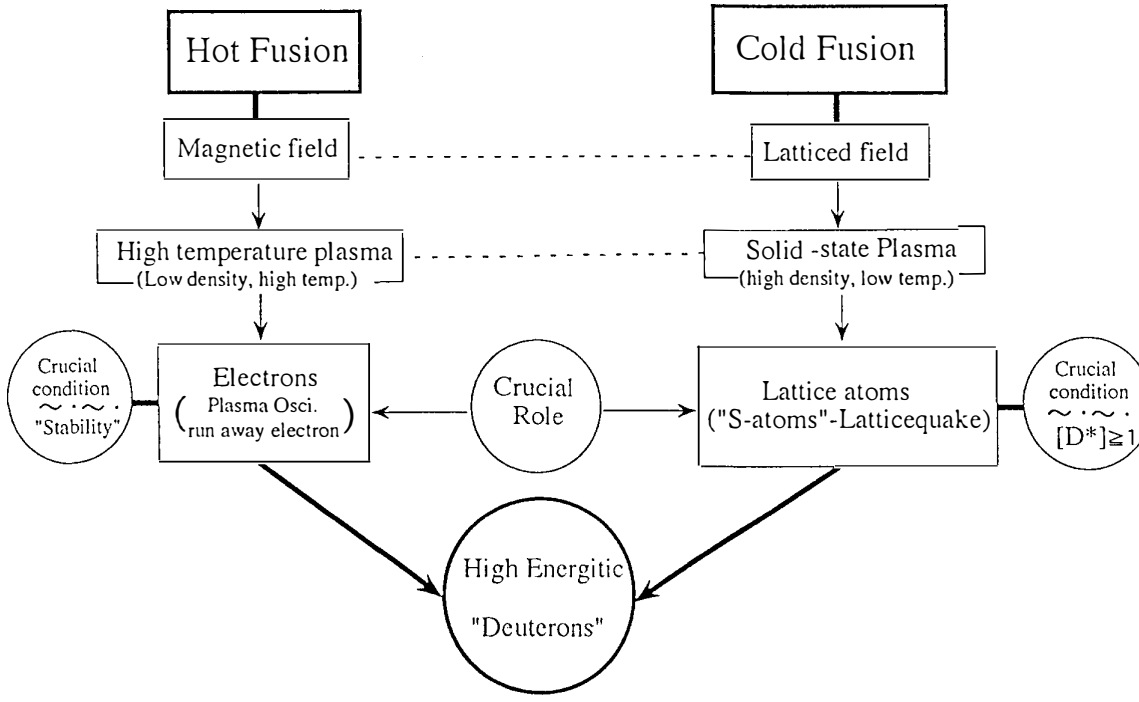

Fig. 7 Relation between Cold fusion and Hot fusion

Fifth International Conference on Cold Fusion
9-13 April, 1995 - Monte Carlo, Monaco
ICCF5 ©1995

Excess energy in the system Palladium/Hydrogen isotopes Measurement of the excess energy per atom hydrogen

J. DUFOUR, J. FOOS, J. P. MILLOT
Shell Research/ CNAM Laboratoire des Sciences nucléaires 2 rue Conté 75 003 Paris

Abstract

A search for the products of fusion reactions that could be triggered by sparking in hydrogen isotopes, was carried out. No signatures above background were found.
On the contrary, the excess energy production was confirmed, in the simple system hydrogen/palladium. The formation of a tightly bound state of the hydrogen (deuterium) atom is hypothesized to explain these results.

1. Introduction

Excess energy production up to several watts have been constantly observed when a metallic hydride forming metal (palladium, stainless steel) is contacted with a discharge struck in an hydrogen isotope ($^{1}_{1}H$ or $^{2}_{1}H$) at atmospheric pressure [1,2]. Such excess energy production is also observed when electrolysing water ($^{1}_{1}H_2O$ or $^{2}_{1}H_2O$) with metallic hydride forming metals (nickel,palladium) [3,4] . One possible explanation of this phenomenum, being the occurence of hydrogen isotopes fusion reactions in the metal, we have carried out a search for the products expected from these reactions. No signature above background have been found, that can explain the amount of excess energy produced.

We have thus concentrated our efforts on the way this excess energy is produced in the most simple system (pure palladium and pure hydrogen). We have measured the excess energy production per atom of hydrogen. We find that for a given set of experimental conditions, the excess energy production per atom hydrogen involved is constant. Values up to 6000 eV have been measured.

To explain our results, we hypothesize the formation of the Hydrex (Deutex) state of the hydrogen atom, occuring when a high current flows through metallic hydride forming metals containing large amounts of hydrogen isotopes. The properties of these hypothetical atomic species could account for secondary nuclear reactions explaining a number of the weak nuclear signatures observed in similar experiments.

2. Methods

Search for the products of the fusion reactions

This search was carried out using the reactors previously described [1,2]. The metallic hydride forming metal was palladium. Both hydrogen and deuterium were tested. $^{3}_{2}He$, $^{4}_{2}He$, $^{3}_{1}H$, neutrons, X and γ rays were monitored with following methods :

- $^{3}_{2}He$ and $^{4}_{2}He$ both in the gas phase and in the electrodes were monitored by a high resolution mass spectrometer, equiped with various getters and filters eliminating all gases, except rare gases and thus increasing the resolution. The gas phase was sampled in stainless steel bottles and tranferred to the mass spectrometer. The electrodes were melted in a furnace (heated by an ion beam) inside the mass spectrometer thus eliminating air contamination. $^{22}_{10}Ne$ was also measured in all samples.

- $^{3}_{1}H$ in the gas phase and in the electrodes was first oxidised and the resulting tritiated water was analysed by liquid scintillography.

- Neutrons were monitored by two $^{3}_{2}He$ counters with energy spectroscopy to identify the characteristic peak at 764 keV. Various moderators (water, paraffin) were used.

- X and γ rays were monitored by an ionisation chamber and by solid scintillography with energy spectrometry (CsI and NaI cristals).

Measurement of the excess energy production per atom H

For this, we have measured with precision the excess energy production and the hydrogen consumption in the system hydrogen/palladium (Pure hydrogen -Alphagaz N55- and pure palladium -Johnsonn Matthey Puratronic grade- were used).

- The excess energy production was measured in a system different from the one previously used [1]. The reactors are of the ozoniser type, cylindrical (typically 2 cm diameter, 60 cm long) with pyrex dielectric barriers. We have used either single dielectric barrier type reactors (the electrode in contact with the gas being a 0.25 mm palladium wire) or double dielectric barriers type reactors (the palladium in that case being a 0.1 mm thick foil,at a floating potential between the two barriers).Fig. 1 is a drawing of the double barriers type of reactor and Fig.2 of the single barrier one.

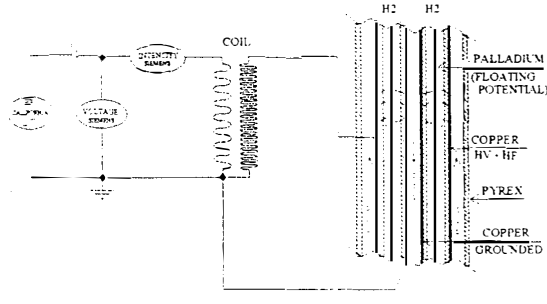

FIG 1 DOUBLE DIELECTRIC BARRIERS

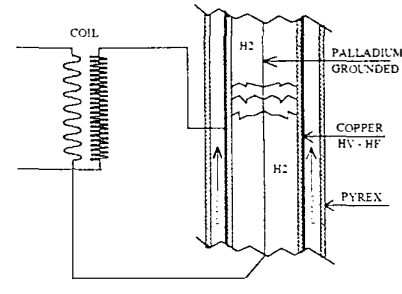

FIG 2 SINGLE DIELECTRIC BARRIER

The double barriers reactor type allows very representative blanks to be made, by withdrawing the palladium foil. The discharge in that case, still occurs between the two dielectric barriers, with no contact with any metal.

A single calorimeter contains the high voltage coil and the reactor. The high voltage coil is powered by a high frequency (50 to 5000 Hz), low voltage (0 to 220V)

generator (Invertron from California instruments) that delivers a quasi sinusoidal signal. The electrical power input is measured at the outlet of the Invertron by a high sampling frequency, numerical wattmeter (Siemens Functionmeter B 1082). The reactor and the coil are housed in a PVC cylinder (10 cm diameter, 110 cm high), that also contains the tubing for circulating silicon oil (Rodhorsil 47V20 Rhone Poulenc) through the reactor (and the coil) and the wires connecting the system to the Invertron. The PVC cylinder is wrapped in a 1 cm thick layer of insulating material (Polyethylen sponge, closed cells, 0.019 kcal/m°C) surrounded by a copper coil (110 cm high) made of joined whorls of copper tube (1 cm diameter) through which the silicon oil circulates. This coil is wrapped in a 5 cm thick layer of insulating material and the resulting cylinder (24 cm diameter is housed in a PVC cylinder (25 cm diameter, 140 cm high), closed at the bottom and the top by two insulating caps, 15 cm thick, with holes for passing the tubings and wires. The outer PVC cylinder is surrounded by a double coil made of joined whorls of PVC tubing (1.8 cm diameter), through which water flows, at a temperature maintained at 20°C (± 0.1 °C) by a cryothermostat (Huber HS 40). The double coil is itself wrapped in a 2 cm thick layer of insulating material. Fig. 3 gives an overall view of the calorimetric system.

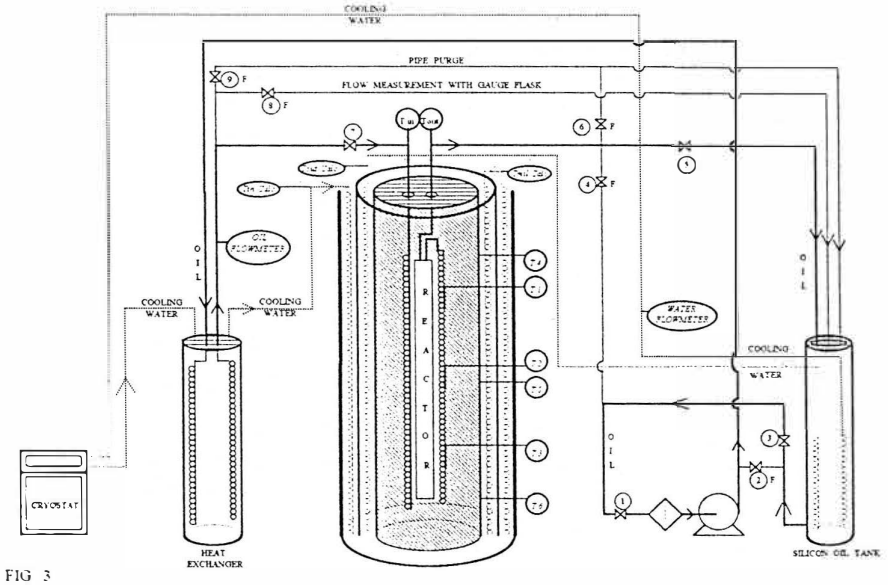

FIG 3

In spite of the use of high voltage/high frequency currents, this calorimetric system is electrically tight, that is no discharge occurs between the high voltage parts and the low voltage ones (except of course in the gaseous gap of the reactor).It is quasi adiabatic, 95 to 99 % of the heat being recovered in the flow of silicon oil circulating (volumetric FMI pump Model RP-D, 1/4" ceramic head) round (copper coil) and through the high voltage coil and the reactor. This heat flux is calculated from the measure of the silicon oil flow (111 Flo-Meter McMillan Co, checked 4 to 6 times per day with gauge flask and chronometer), and the measures of the inlet and outlet oil temperatures (PT 100 Platinum gauge AOIP). The variations of the specific gravity and

specific heat of the oil with temperature are taken into account. The oil stability during the runs is checked by periodic control of its specific gravity and by calibrations as will be described below. The heat flux wich is exchanged with the air of the laboratory (5 to 1 %) is determined by calibration (correlation between the heat lost and the difference of temperature between the reactor and the laboratory - see calibration).

- The hydrogen consumption is measured by a simple pressure balance of the reactor and its feeding reservoir (300 cm3 initial pressure 5 bars). The reservoir, the pressure regulating valve and the tubing of the hydrogen system are shown on Fig. 4. They are made from stainless steel. A 40 cm long, (1.6 mm ID, 3.2 mm OD) FET Teflon tube connects the stainless steel tubing to the pyrex reactor. The whole system is tight up to 1500 mb of reactor hydrogen pressure and no leakage is detectable on several days tests.

- All data required for the excess power and the hydrogen consumption measurement are collected every 15' by a data logging system (Centrale d'acquisition AOIP SA 70)

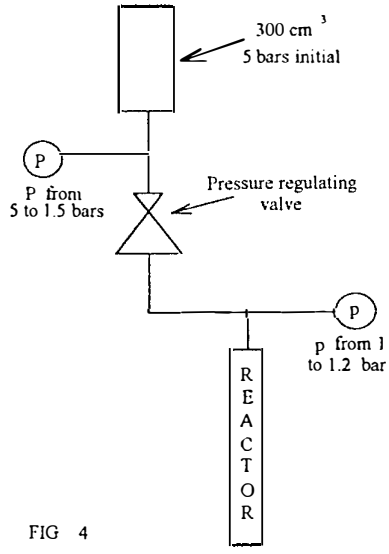

FIG 4

3. Results

Search for the products of fusion reactions

The results of that search can be summarized as follows :

- ${}_2^4He$ found in the gas phase come from air leaking through the pyrex or the joints of the reactor. This is clearly evidenced by the ratio ${}_2^4He/{}_{10}^{22}Ne$ calculated for the "apparent production" of these two isotopes (resulting from a mass balance between the gas input in the reactor and the gas after the experiment, taking into account the hydrogen absorbed by the palladium).Typical values are the following:

air : 3.13 ${}_1^1H$ experiment : 5.0 ${}_1^2H$ experiment : 6.0

showing a preferential leakage of ${}_2^4He$ from air, whatever is the hydrogen isotope used.

- No peak at mass 3 (${}_2^3He$) was detected in the gas phase.

- ${}_2^4He$ "apparent production" was also found in the electrodes. In all experiments, this can be explained by ionic implantation from the gas phase. This is evidenced by considering the evolution of the ratio ${}_2^4He/{}_{10}^{22}Ne$ from the zone of impact of the sparks, to the edge of the electrodes. Given the higher temperature of the impact zone and the evolution with temperature of the diffusion coefficents of ${}_2^4He$ and ${}_{10}^{22}Ne$, the former should be higher than the latter, when ${}_2^4He$ and ${}_{10}^{22}Ne$ are implanted by the discharge. This was found to be the case for all experiments both for ${}_1^1H$ and ${}_1^2H$. However, in all experiments, the impact ratio was higher than the one in the gas phase,

with a mean value of 30 (a value of 120 was found in one experiment with ${}_1^1H$). If we attribute to true generation the totality of ${}_2^4He$ found in the electrodes, we arrive at an upper limit of 10^5 atom/s (for the ${}_1^1H$ experiment above mentionned).

- A peak at mass 3 was detected in the gas from the electrode of one experiment with ${}_1^1H$, and one with ${}_1^2H$. This peak is very likely a HD peak, due to a memory effect of the spectrometer system. It gives an upper value for the true ${}_2^3He$ generation : $5x10^3$ atom/s.

- No ${}_1^3H$ was detected above detection limits for ${}_1^1H$ experiments or beyond what is contained in the feeding gas for ${}_1^2H$ ones. This gives the upper limit of production : $2x10^3$ atom/s.

- Neutron detection was also negative: the background flux has been shown to fluctuate from $0.5x10^{-3}$ to $1x10^{-3}$ n/cm^{2}xs (on a period of 4 months), with no correlation with the excess energy production.

- No X and γ rays were detected with the ionisation chamber. Copious signals have been detected with the solid scintillation counters, in the low energy region (< 100 keV). These signals are currently under study.

Measurement of the excess energy production per atom H

- The excess energy production is measured during "active runs" that last 3 to 6 weeks (in order to eliminate transient situations that can occur at the begining of a run). "Active runs" are runs were a discharge is struck through an hydrogen isotope, in contact with an hydride forming metal. Before each "active run", the temperature gauges are calibrated. Each "active run" begins with a calibration (2 to 3 days), where the reactor is under Ar or air and the system heated by resistors, powered by the California generator. This calibration ensures that the properties of the silicone oil are stable. The results of these "active run" calibrations are checked to fit the calibration curve , that was established in a way that will now be described.

- *The calibration curve* was established during "calibration runs", where the system was heated in different ways : resistors, discharges in Ar with the two types of reactor (with metal in contact with the discharge) and discharges in hydrogen in the double barriers type reactor, with no metal between the dielectric barriers. In the runs with resistors, the power was delivered either by a DC generator, or by the California generator (with cos φ varying from 0.35 to 1). The power lost to the air is :

Power lost = Power recovered in oil - Power in

and is correlated with the difference of temperature between the reactor and the air of the lab :

$$\text{Power lost} = K (T_{reac} - T_{air})$$

Fig. 5 shows that all calibration points fall on the same correlation, whatever the way the system is heated. Moreover the "calibration runs" with a discharge, show that the system is electrically tight, that is no discharge occurs, that could interact with the various components of the calorimetric system (insulation, PVC ...). Electrical charges

transport only occurs in the gas gap of the reactor.

The calibration runs were performed over a period of 4 months, including 3 complete dismantling of the reactor and calorimetric system. Over this period, the standard deviation of the excess power measurement (zero for calibration runs) is 0.7 W, demonstrating the stability of the system (this figure is reduced to 0.3 W, when only a single run is considered).

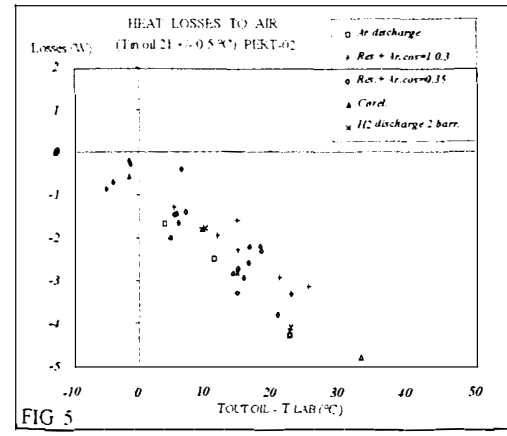

FIG 5

- *The results of the active runs* are very dependant on the type of palladium used :

- runs with foils gave results ranging from 0 to 3 W excess power (for 100 W power input). This erratic performance was shown to be related to the mechanical resistance of the palladium : the palladium that gave negative results was found after the experiment with scales on the surface. The loading ration for these negative experiments was of the order of 0.75. On the contrary, the surface of the palladium that gave positive results was found not altered after the experiment. In that case,a strange behaviour of the loading ratio was observed (figures up to 2.5 were measured). This will be discussed later.

- runs with wires gave positive results, the wires being never found altered after an experiment. The strange behaviour of the loading ratio was also observed. Excess power up o 5.5 W were observed (for 150 W power injected). Given the measured standard deviation (0.7 W) these results are very significant.

- *A comparison of two "active runs"*, one with negative results and one with positive ones is shown on Fig. 6 and 7. The negative run was with a palladium foil and a double dielectric barrier. During 1.5 million second, the excess power was 0 ± 1.4 w (99 % confidence level). The positive run was with a palladium wire and a single dielectric barrier. The excess energy increased on a period of 3.5 million second, to reach 5.5 ± 1.4 w (99 % confidence level). The increase observed at 2.8 million second is due to change in operating conditions (see below).

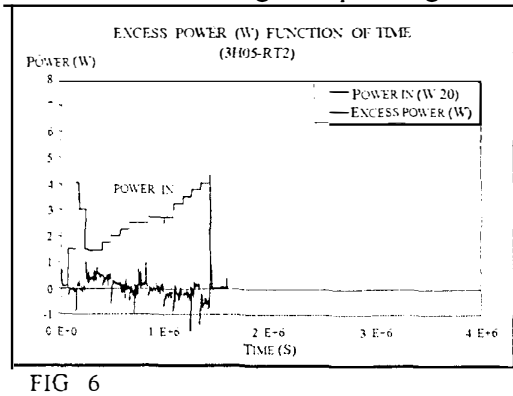

FIG 6

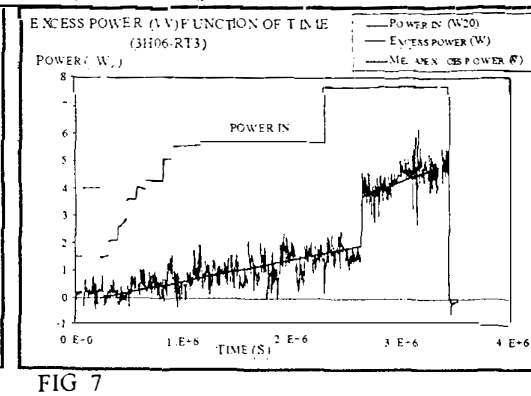

FIG 7

- The hydrogen consumption together with the weight of palladium used in an experiment, allows the calculation of the loading ratio. For experiments that gave negative results, the behaviour of this loading ratio is normal : values are limited to 0.7/0.75 and once this value is reached, it remains constant for the rest of the experiment. On the contrary, for experiments giving an excess energy, this ratio always increases. Values up to 5 have been measured in experiments with wires.
One obvious cause that could explain this, is leakage, which we exclude, because when the discharge is cut off, the consumption of hydrogen ceases. Another cause would be combination of hydrogen with material inside the reactor. This seems impossible, because the only material in contact with the discharge is pyrex (and of course palladium). Small amounts of copper and steel are also present in the reactor, but not in contact with the discharge. The quantities of hydrogen they could absorb, were calculated and found several order of magnitude lower than the missing hydrogen.Their presence cannot explain the phenomenum. Finally, by weighing the palladium before and after the experiment, we saw that, in all cases, the final loading ratio thus measured, did not exceed 0.8. No hydrogen is thus stored in cavities of the palladium after experiment.

The excess energy production per atom hydrogen can then be calculated from the above measurements. Fig. 8 is a plot of the cumulated excess energy versus the cumulated hydrogen consumption as measured in the experiment with a wire described previously. It can be seen that 3 straight lines can be drawn, corresponding to 3 different sets of operating conditions (see below). This means that under stable conditions, the excess energy per hydrogen atom is constant. These results are summarized in the following table.

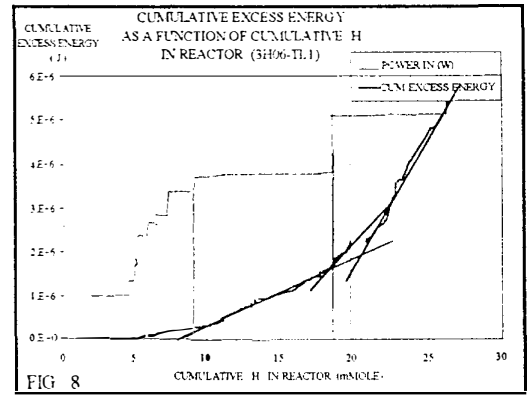

FIG 8

Period	Duration second	H consu--med mMole H	Excess energy on period J	Mean excess Power W	Exc. Ene. eV per atom H	Power input W	Temper . Reactor °C
CAL	230 000	0	0			Calibration	
INC	695 000	9.88	244 000			Increasing	
I	1 390 000	9.63	1 420 000	1.0	1500	115	56
II	342 000	1.41	571 000	1.7	4200	150	69
III	767 000	5.44	3 155 000	4.1	6100	150	50
Total	3 424 000	26.36	5 390 000				

At the beginning of period III, the decrease of the reactor temperature was achieved by increasing the oil flow. This decrease of temperaure was immediatly followed by a very fast increase in the hydrogen consumption (few minutes), followed

by a slightly slower increase in excess power generation (few hours).

After cuting off the discharge, the hydrogen consumption ceased. Weighing the palladium after experiment showed that it contained 4 mMole of hydrogen (corresponding to a loading ratio round 0.75, the quantity of palladium in the reactor being 5.35 mMole). During the experiment, a total of 22.36 mMole of hydrogen (16.48 during steady state situations) have been lost from the reactor in an unexplainable way .

We conclude from the measurement of the excess energy per atom hydrogen

- that this quantity is a constant for a set of physico-chemical parameters but changes when this set is changed. Values up to 6 000 eV per atom H have been measured.

- and that hydrogen is lost in an unexplained way, during the production of excess energy.

4. Discussion

The following experimental evidences have been gathered :

- the upper values found for the ashes expected from the known fusion reactions of ${}_1^2H$ are much too low (many orders of magnitude) to explain 2 W of excess energy (for 1 W these values should be 10^{12} per second for protons, tritons, neutron and ${}_2^3He$, 10^7 for ${}_2^4He$ and gamma rays of 24 MeV or $3x10^{11}$ for ${}_2^4He$ if this is the only ash). In the case of ${}_1^1H$, no gamma rays of 511 keV were observed, that could have resulted from the anihilation of positrons formed by the known ${}_1^1H$ fusion reaction.

- excess power generation have been measured with high confidence level (99 %). Taking into account the total excess energy generated (5 000 000 J), the following explanations have been eliminated (their effect would be several orders of magnitude lower than what is observed) : combustion of the hydrogen, combustion of silicon oil, reaction of hydrogen with materials in the reactor, exothermal modification of the pyrex under the influence of the electrical charges deposited by the discharge .

- this excess power is generated in a very specific way, the excess energy per atom of hydrogen being a constant for a given set of reactor conditions. The value of this energy is in the order of thousands eV. Moreover, this excess power generation occurs simultaneously with an unexplained loss of hydrogen from the reactor.

The Hydrex (Deutex) hypothesis : the hypothesis of the formation of a tightly bound state of hydrogen (deuterium) in "cold fusion" experiments, have been put forward [5,6]. In such bound states, the electron is much closer to the proton than in normal hydrogen. This could explain both an energy of formation and a capacity to diffuse through any material much higher than normal hydrogen. Hence, energies of formation of several thousands eV and loss of hydrogen through the walls of the reactor, could be explained.

We hypothesize that the formation of a one dimension (oscillator) bound state could occur, if the following conditions are met, for one proton and one electron inside the lattice of the palladium:

- their spins are parallel
- they get sufficiently close (100 to 500 fm ?)
- they have the same velocity

These conditions might be met at the occasion of the jump of an hydrogen (proton) from one octahedral site of the palladium to another, when a high electrical current flows through the palladium lattice. The first two conditions could be fulfilled when the current is sufficiently high and create a high magnetic field. Due to collisions, the last condition could be fulfilled for individual protons and electrons of the conduction band of the palladium, although their collective motions are opposite. Due to the action of the strong electromagnetic field created by the electron during its motion to and from the proton, this bound state, once formed, could remain stable, even after the external magnetic field has disappeared. This state being the result of the action of two potentials (electrostatic and magnetic) a continuum could be formed and this could explain that we measure energies of formation varying with operating conditions.

Expected properties of the Hydrex (Deutex) state of hydrogen :

Apart from its high energy of formation and its capacity to diffuse $H.$ (Hydrex), should be a permanent electric dipole of small dimensions (hundreds of fm). When getting sufficiently close to a nucleus present in the metal lattice, it could be confined against it. The probability of electron capture by the nucleus could thus be increased as with $^{40}_{19}K$ for example :

$$^{40}_{19}K + \underline{H}. = {}^{40}_{18}Ar + {}^{1}_{1}H^{+} + e^{-} + \nu$$

Similar reactions should be expected with $^{138}_{57}La$ and $^{50}_{23}V$, that give exothermal electron capture reactions.

If $\underline{H}.$ is confined for a sufficient long time, close to the nucleus, double electron capture could then occur, which could be the case for the following nuclei : $^{102}_{46}Pd$, $^{56}_{28}Ni$, $^{54}_{26}Fe$ and $^{40}_{20}Ca$.

These reactions could account for a number of weak nuclear signatures observed in the experiments

5. Conclusion

From these results, we conclude that a very promising reaction occurs in metallic hydride forming metals, when loaded with hydrogen isotopes and submitted to high transient electric currents. We think that explaining the phenomenum by a rearrangment of the binding between the proton and the electron, due to the confinement in the metal lattice, is more plausible (although not known) than invoking highly improbable fusion reactions. We intend to put more efforts in the understanding of this reaction.

References

1. J. Dufour « Cold fusion by sparking in hydrogen isotopes », *Fusion technology*, **24**, 205 (1993)

2. J. Dufour, J. Foos and J.P. Millot « Cold fusion by sparking in hydrogen isotopes. Energy balances an search for fusion by-products », *Transactions of Fusion technology*, **26** , 375 (1994)

3. R. Bush « A light water excess heat reaction suggest that cold fusion may be 0alkali hydrogen fusion », *Fusion technology*, **22**, 301 (1992)

4. M. Fleischmann and S. Pons « Electrochemically induced nuclear fusion of deuterium » , *J. Electroanal. Chem.* **261**, 301 (1989)

5. J. P. Vigier « New hydrogen (deuterium) Borh orbits » *Proceedings ICCF4*, **4**, 7-1 (1994).

6. J. A. Maly and J. Vavra « Electron transitions on deep Dirac levels » *Fusion Technology*, **24**, 307 (1993)

Fifth International Conference on Cold Fusion
9-13 April, 1995 - Monte Carlo, Monaco
ICCF5 ©1995

"COLD FUSION" IN TERMS OF NEW QUANTUM CHEMISTRY: THE ROLE OF MAGNETIC INTERACTIONS IN DENSE PHYSICA MEDIA

Neutron and X-ray detection in plasma focus and "capillary fusion" experiments

R.D. Antanasijevic, Dj. Konjevic, Z. Marie, D.M. Sevic, J.P. Vigier & A.J. Zaric

Abstract

Various recently reported "break even" in different types of "cold fusion" experiments have a common physical origin if one assumes that one should add, in dense states, the action of magnetic interactions of oriented nuclear spins to the usual Coulomb forces. In that case one is led to predict a) the existence of new "tight" quantum molecular states (associated to new "tight" Bohr orbits) which correspond to the emission of X-ray lines and excess energy b) the associated apparition of a certain amount of nuclear fusion reactions due to those magnetic interactions and enhanced tunneling by strong electron concentrations. They appear in the form of neutron (or γ) bursts and various types of "ashes" of particular nuclear fusion reactions in electrolysis, glow discharge, capillary devices, resonance sonoluminescence and plasma discharge experiments. They both contribute to observable energy excess in amounts which vary which chosen set-ups.

To explore this assumption two experiments are presented here i.e. 1) discharge experiments in plasma focus and "capillary fusion" devices (i.e. nuclear fusion) of 10^8 neutrons/burst 2) X-ray measurements in deuterium plasma focus which confirm the existence of new Bohr orbits.

New possible experiments to check it are also briefly discussed.

Introduction

The question of the physical interpretation of the growing set of experiments showing (apparent) energy-momentum violations (mostly in the form of the heat creation first observed by Pons and Fleischmann [1] is evidently still open. Publicly known under the label "cold fusion" the experiments now covers a wide range of different physical processes going from electrolysis (with water and heavy water) with Pd or Ni cathodes) to glow discharge; plasma focus, capillary fusion, sonoluminescence. The original idea that they had a common physical origin in nuclear fusion process realized in dense media i.e., different from the usual line of research based on Tokamak-type devices, has not been supported by subsequent experiments. The problem is that the fusion "ashes" which have been observed are nearly always a few orders of magnitude too low to explain this excess energy [8] and that it is not even clear that these experiments should be explained within a single theoretical frame.

In this paper we shall assume however that this is indeed the case and that "cold fusion" processes, or more precisely "break-even" energy production, are just the manifestation of the intervention of polarized nuclear magnetic moments in dense matter: a type of force which is negligible (w.r.t. the Coulomb force) in ordinary conditions.

To summarize this model assumes

a) That in certain particular physical conditions (in dense matter, under certain external or internal magnetic fields, the nuclear and intervenir electron spins, are oriented and one should add short range magnetic interactions to the usual Coulomb forces

b) This implies the existence of new "tight" Bohr orbits and the formation of new "tight" molecular states, which yield new quantum transitions within the frame of the usual quantum mechanical formalism.

c) If one imbeds such molecular states within electronic concentrations generated in metal lattices or convection currents their screening allows "tunneling" effects and thus allow fusion between nuclei which does not depend on high temperatures.

d) This implies the apparition of a new quantum chemistry in certain conditions which appears at our level, in the form of exothermic reactions accompanied by observable fusion reactions.
In other terms the new phenomena correspond to the usual quantum mechanical formalism acting in special physical circumstances.

POSSIBLE EXPERIMENTAL TESTS OF THE MAGNETIC INTERACTION MODEL

At the present stage of the experimental situation on "cold fusion" it appears possible to confront the preceding model/interpretation with the results of different experiments.

A) In order to test the assumption of the existence of new Bohr orbits one can

1) test directly the existence of new "tight" molecular states on hydrogen and deuterium in metal loading experiments.

Indeed their existence in metals (due to nuclear spin polarisation) implies that their internal density is high enough to correspond to a new phase in metals (their behave somewhat like a liquid or solid state at low temperature) so that one would expect

– to observe the creation of Cooper pairs in H or D in the metal i.e. the apparition of superconducting phenomena within loaded Palladium-Nicket etc.

– to observe a contraction of the loaded metal since internal thermal metal agitation would be reduced by the pressure of "tight" $\overline{H}_2^+$ or $\overline{D}_2^+$ molecules.

2) try to detect directly the existence of these "tight" $\overline{H}_2^+$ or $\overline{D}_2^+$ molecules in mass spectroscopy performed on gaz derived from such experiments and also try to measure their lifetimes in corresponding experiments.

3) examine (as already done by Reifenschweiler [9] the β decay of new "tight" radioactive molecules. Indeed the formation of "tight" states implies a new type of recoil in β or γ emissions which can explain apparent "anomalous" nuclear decay rates.

B) In order to test directly the existence of new electronic levels one can try to detect the corresponding soft X-ray lines. This has already been done in various cases (one will be discussed in this paper) with positive results. (See S. Szpak and P.A. Mosier-Bodd "On the behaviour of the cathodically polarized Pd/D system: Search for emanating radiation". PLA (in press) [10].

C) In order to test directly the possibility that the existence of such "tight" states can, when associated with strong electron concentrations (which favor "screening" processes) favor real nuclear fusion reactions (which, in their turn, decay into various types of isotopes, not present in the initial sets ups) one should follow the path opened by Prof. Takahashi and his group.

D) In order to test the possibility of a magnetic interaction as basic origin of the new energy producing mechanism one can develop non-electrolytic experimental devices such as

1) - the Lochte-Holtgreven capillary experiments [11]

2) - the Graneau-type water-plasma explosion devices in ceramic and metal cavities [12]

3) Direct energy producing devices from magnetic materials (some of which will be discussed after this talk) which rest on the idea that the apparition (by resonance excitation) of increased magnetic fields (resulting from the contribution of "tight" molecules in the ferrites of the stators of Gram-type machines) will result in stronger output currents.

This implies the validity of Ramsey's initial suggestion [13] (N. Ramsey Phys. Rev. 103 July 1 (1956) 20) that one can utilize nuclear spins as a separate (negative temperature) thermal bath to create a heat engine operating in a closed cycle that will produce no other effects than the extraction of heat from a negative temperature reservoir with the performance of the equivalent amount of work.

In this work we want to present the results of some experiments which seem to support:

- the existence of new Bohr orbits associated with X-ray emission i.e. resulting from magnetic interactions.
- the existence of neutron emission in plasma focus and « capillary fusion » experiments, which support the idea that fusion process are related with the existence of such interactions.

The experiments concern the measurement of the total neutron yield, achieved by using the large volume liquid scintillator neutron detector (NE343). The capacitor bank b.;-s charged up to 20kV giving current up to 400kV. Maximum neutron yield is about 10^{11}/pulse. The detection and analysis of the X-ray is done using roentgenographic method with aluminium foils of varying thickness. Soft X-ray ($\lambda > 20nm$) were detected.

The experiments we have performed (plasma focus and "capillary fusion.") require high detection efficiency of the neutron detector. [14] Among many possible types we have chosen a. detector based on a large loaded liquid scintillation medium. The main features of this type of counter is slowing down of neutrons in a large volume of a hydrogenous liquid and absorption by the loaded element (Gd) (15). In section 2 the construction and calibration of the detector will be explained, and in section 3 preliminary,- results concerning detection of the total neutron yield in the plasma focus and "capillary fusion" experiments will be presented. Section 4 is devoted to the study of X-ray emitted in the deuterium plasma focus devices.

2. Description of the experimental set-up

2a.Plasma focus and "capillary fusion" chambers

The plasma focus chamber is the Mather type (16) and consists of two brass coaxial electrodes (outer electrode consists of 18 cylindrically positioned brass roads, separated by the glass insulator sleeve at one end, where the breakdown of a gas discharge at an initial density of about 10^{17} cm^{-3} takes place. This chamber has been designed for the currents up to 1 MA and 10^{10} *neutrons/pulse.* (14) Development and acceleration of the plasma focus current sheath have been measured by means of the fiber optic cables that are "looking" at the certain spots inside the chamber. Corresponding windows are intended for the laser scattering measurements. Electric circuit parameters (charging voltage, capacitance and external inductance), electrode geometrical. dimensions and gas filling are chosen in such a. way that the radial compression. starts near the current maximum. A low inductance capacitor. bank (45 μF with triggered spark gap as a switching device) is used as an energy source with power transmission line between the power supply and two coaxial electrodes.

The main part of the data acquisition system is digital storage oscilloscope Tektronix 2440 (500 MSamples/s). It enables all voltage and current measurements. This is also most convenient and accurate way of caking data from neutron detector. Data transfer from Ibis oscilloscope to the personal computer is completed, so all data are available for numeric analysis.

Voltage measurements are taken with high voltage probes. A Rowgowski coil between the power transmission, plates monitors variations with the time of the electrode current.

2b. Construction and calibration of the large liquid scintillator neutron, detector

The efficiency of a large volume liquid scintillator neutron detector strongly depends on the shape and dimension of a scintillator tank. In order to check detector properties before construction, a simulation of detector performance, especially of the detection efficiency, was done using the Monte Carlo DENIS computer program. (18)

The neutrons are moderated by the hydrogenous material (toluene). After thermalization and diffusion, they are captured by the loaded element (0.2 per cent of gadolinium σ_{abs} = 3.6 x 10^1 barn). Gadolinium deexication by emission of three gamma rays (9 MeV total energy) and their interaction with scintillator are the second step in the neutron detection. Finally, light collection and detection are considered. Consequently, the total neutron efficiency of the detector is a product of the captured neutron efficiency, gamma rays detection efficiency and light detection efficiency. The input variables in the program are the diameter of the sphere, the initial neutron energy and the discrimination threshold of the photomultiplier signal. The capture time distribution and neutron detection efficiency as a function of discrimination threshold for gamma ray energy are the output results.

The calculated efficiency of neutron detection for a sphere of 1 meter in diameter, as a function of the initial neutron energy, is shown in Fig 1. We conclude that such a detector satisfies our demands on the total neutron yield measurement in plasma focus and "capillary fusion" experiments since the expected detection efficiency for neutrons from the D-D reaction (E=2.45MeV) and those from spontaneous fission ($\overline{E} \approx 2\text{-}2.5$ MeV) is about 90% for a source of neutrons placed in the center of the sphere. The results of simulation for fission neutron energy spectra are compared with the results of calibration made by a californium spontaneous fission source (Fig. 2 and Fig. 3).

The main body of our detection system is a spherical tank of 1 meter in diameter, made of stainless steel, filled with the scintillating solution (Fig.4). Twelve photomultipliers (Hamamatsu R1512, 5 inches in diameter) are mounted on quartz glass viewing windows. For the improvement of light collection (reflection), the inner walls of the sphere are electrochemically polished. The scintillating solution was kept oxygen free with argon gas.

The photomultiplier pulses are summed in two branches (six photomultipliers in each) and via a preamplifier, amplifier and discriminator transmitted to the coincidence unit. When coincident pulses are observed from bath branches, signals are accepted as neutron events and counted. Since at least two photomultipliers must give a signal, the effects of ran-

dom noise from photomultipliers are minimized. A block diagram of the electronic circuit used for calibration of the detector is given in Fig. 5.

The capture time distributions of simultaneously emitted neutrons is broad and has a peak at about 10 μs after their production (Fig. 2). In this way, about 83% of all emitted neutrons (for neutron energy fission spectra) are captured within a 35 μs time interval. The detection system was calibrated by a californium-252 spontaneous fission neutron source placed at the center of the spherical detector. A surface barrier detector was placed very near to the californium source and pulses from fission fragments were used as triggers for a neutron counting start. The fission rate of The source was about one per second and neutron counting was initiated after 1 μs delay with respect to the last fission, 1 μs so as to eliminate all prompt gamma signals from the source. The gate duration was set to 35 μs. Since the detector is very sensitive to cosmic and laboratory background, measurements without any source were also made. The detection efficiency is then obtained by using the equation:

$$\in = n_m - n_b / n_e \tag{1}$$

where: n_m is the mean value of measured neutrons, n_b is the background activity and n_e(=3.72) is the average number of neutrons emitted per fission.

Corresponding measurements were performed for different discrimination thresholds (Fig.3).

For the threshold corresponding to 2 MeV of gamma ray energy, the detection efficiency for ^{252}Cf neutrons is about 83% (Fig. 6). The neutron capture time distribution was also measured and compared with calculated values (Fig. 2). The agreement between measured and calculated values is satisfactory. We conclude that the detection system is able to detect simultaneously emitted neutrons within a broad time interval (about 40 μs). This is important for the case of the "capillary fusion" and plasma focus experiments since electro-magnetic interferences due to discharges can be avoided by a few μs delay of a neutron counting start.

2c. Data acquisition and analysis system

Since in detection experiments of spontaneous fission events of superheavy elements and of neutron yield from plasma focus and "capillary fusion" the frequency of the events is much lower than in the case of calibration with the californium source, the data acquisition and analysis system has been adapted in order to optimize the detection process, (dead time reduction, process automation).

The data acquisition system consists of nuclear detectors and electronic equipment, probes for high voltage and current measurements, and various diagnostics for plasma characteristics. The data analysis system is composed of a PC computer and software support. The main interface between the data analysis system and tho data acquisition system are the digital storage oscilloscopes Tektronix 2440 (500 MSamples/s) and 2430A (150 MSamples/s). This is a convenient and accurate way of taking data from neutron detectors. The oscilloscopes also transmit all voltage and current measurements. Data are transferred from the oscilloscopes to the computer and thus arc available for numerical analysis.

Although the whole setup of the experiment is properly grounded and well shielded, our nuclear electronic equipment is very sensitive to electromagnetic: interferences (EMI) generated by the discharges of the capacitor bank in the plasma focus chamber. Because of that, the signals from the photomultiplier tubes are mixed and recorded on the aforementioned digital oscilloscopes, which arc excellently protected from EMI. EMI arc also avoided by a few microsecond delay of a neutron counting start. The shape of signals are easy to analyze on the computer, thus reducing possible errors from EMI.

3. Preliminary results concerning neutron yield measurements in plasma focus and "capillary fusion" experiments

In the case of plasma focus experiments the position of the source of neutrons (plasma focus chamber) must be at a distance of several meters

from detector (shock hazard, EMI) and the overall detection efficiency decreases by several orders of magnitude. For example, the solid angle of the detector for a distance of 10m is only 0.066 per cent. The neutrons are detected with a few microseconds delay in a broad time interval of about 40 μs. This fact is very important for plasma focus experiments because of high EM radiation emission due to the discharge of the capacitor bank which occurs simultaneously with the neutrons.

The neutron yield experiments were performed with the detector 8 meters away from the plasma focus and "capillary fusion" chambers. The threshold neutron count rate was one event per pulse, meaning 10^3 emitted neutrons into a solid angle of 4π. Typical results obtained for a plasma focus experiment at constant pressure of 1.3 mbar is shown in Table I.

At higher pressures the neutron yield increases to reach 10^{10} neutrons per pulse at 4.5 mbar (Fig. 7).

Neutrons from the "capillary fusion" experiments could not yet be detected with this unfavorable geometry. Work is in progress to permit decreasing the distance between the source and the detector.

TABLE I

Neutron yield as a function of the involved energy at constant pressure for plasma focus experiments

Energy [kJ]	2.0	2.2	3.2	4.4	5.8	9.0
Voltage [kV]	9.2	10	12	14	16	20
J_{max}	200	210	240	290	350	450
Yield [n/pulse]	$<10^3$	8×10^5	1×10^5	2×10^5	2×10^5	$<10^3$

4. Studies of the emitted X-ray

The analysis of the X-ray emitted from the Mather type plasma focus device is carried out by the roentgenographic method. Two kinds of experiments were conducted. The discharge trough the pure deuterium gas and trough the mixture of 94% deuterium and 6% argon gases. The motivation for a use of the above mixture comes from the study of Japanese group. [10]

Spatial resolution of emitted X-ray was achieved using collimator disk made of stainless steel. The diameter of the collimator holes was 1mm,

the length 10mm and distance from central electrode 130mm. In the case of the soft X-ray detection the aluminum foil of 20μm in thickness was used to protect roentgenographic film from the visible light also emitted in the plasma focus (figure 8.). For the analysis of hard X-rays different thickness of an aluminum absorber, up to 400μm was used (figure 9.). When the working gas was pure deuterium only soft X-rays ($\lambda \geq 10nm$) are detected. The geometry of the experiment shows this emission might appear at times before the plasma takes its final form. Although it is known that the existence of the hot spots is in the plasma focus are connected with the neutron pulses emission. The coincidences between them and X-rays emission can not be affirmed as the established phenomena.

In the case of the deuterium-argon mixture beside the soft X-rays of the energy up to 8keV (which might belong to the argon K-lines) the hard X-rays are detected. The origin of these hard X-rays emission is uncertain, although the geometrical consideration made by the pinhole images suggests that it comes from a zone near the central electrode in the final stage of the plasma formation in the focus device.

CONCLUSION

In the experimental runs we have detected the neutron pulses of 10^8 in the plasma focus device. For the "capillary fusion" experiments, one concludes our experiment depends on the geometry which can be arranged in the way to detect the "threshold" of about 1062 neutron/pulse.

The detected soft X-ray in the discharges when the focus is filled by deuterium have energies of about 5keV. The hard X-rays ($E \approx 8keV$) appear in the deuterium-argon mixture. This suggests the strong dependence of the “fusion” reactions on electronic surroundings.

References

(1) M. Fleischmann and S. Pons, P. L. A. 176(1993)118 and Proceedings of ICCF4 in Hawaï (1994) E.P.R.I. Ed.

(2) A. Barut, Prediction of new tightly bound states in H_2+CD_2+) and « cold fusion experiments » (1992). Private communication.
J.P. Vigier, Proc. of the ICCF3 Nagoya. Japan (1992) Universal Acad. Press. H. Ikegami Ed.

(3) See discussion in J.P. Vigier « New Hydrogen (Denterium) Bohr orbits in Quantum Chemistry and « Cold Fusion Processes » ICCF4 Proceeding. Edited by E.P.R.I. (1994)

(4) See the publications of Professor Takahashi et al

(5) See Y.R. Kucherov et al, P. L. A. 170(1992)265 and J. Dufour, Fusion Technology 24 (1993) 205

(6) See the Lochte-Holgreven experiments

(7) See R. Stringham and Russ George's experiments

(8) See discussion in ref. (3) and (4)

(9) Reifenschweiler (see his contribution to this conference)

(10) S. Szpak and P. A. Mosier-Bogg, P. L. A. (in press)

(11) See ref. (7)

(12) P and N Graneau, P. LA (in press)

(13) N. Ramsey, Phys-Rev 103(1956)20

(14) R. Antanazijević, I. Lakićević, Z. Marić, D. Sević, A. Zarić, J.P. Vigier, Physics Letters A Volume 180, number 1,2 p. 25-32, August 1993

(15) B.C. Diven, J. Terrell and A. Hemmendinger, Phys. Rev. 120 (1960), 556

(16) J.W. Mather, The Physics of Fluids, vol. 8, no 2, feb. 1965

(17) J. J. Poitou and C. Signarbiex, Nucl. Instr. Meth. 114(1974), 113

(18) Y. Takaharna, M. Han, T. Yanagidaira and K. Hirano, Research report NIFS-PROC-18, 72 June 1994, Nagoya, 217.

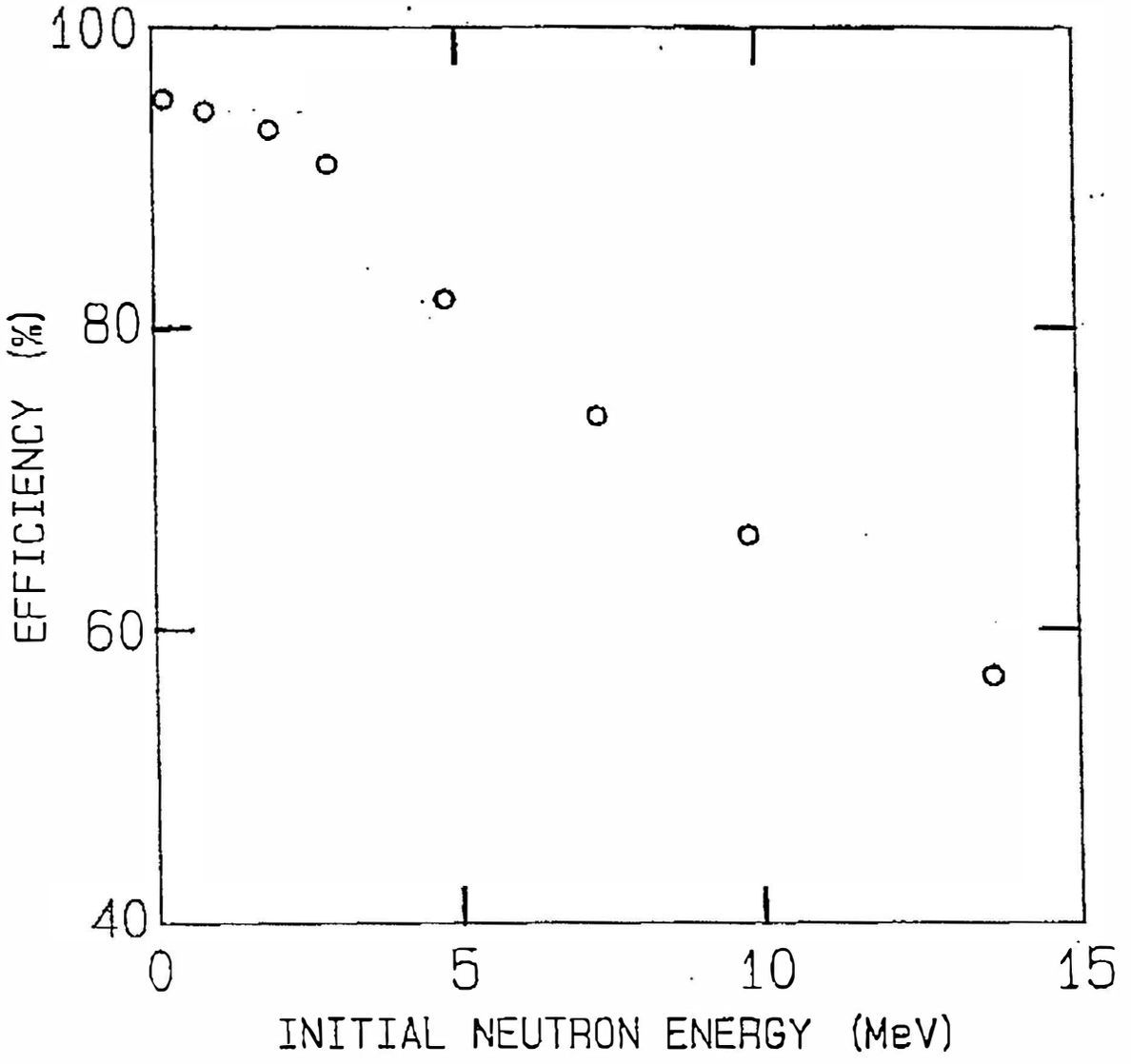

Figure 1: Efficiency of the large volume gadolinium loaded liquid scintillator detector calculated using the Monte Carlo method as a function of the initial neutron energy

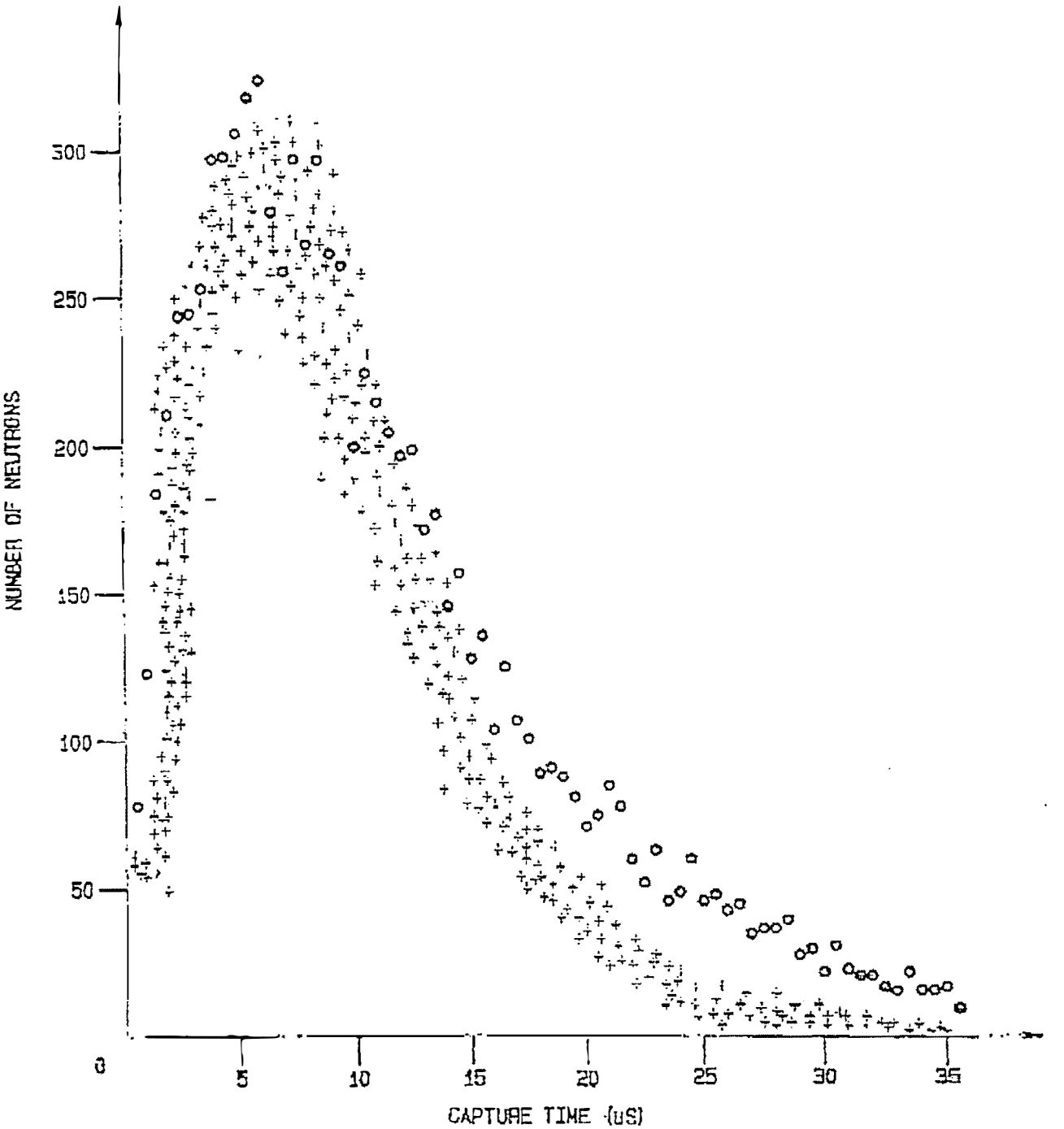

Figure 2: Neutron capture time distribution: o - calculated values and + - measured values

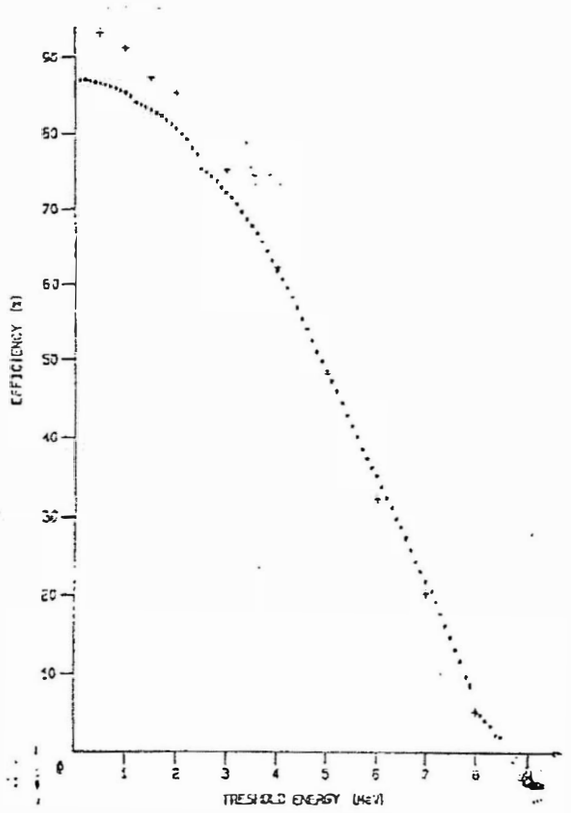

Figure 3: Neutron detection efficiency as a function of the threshold gamma ray energy: o - calculated values and + - measured values

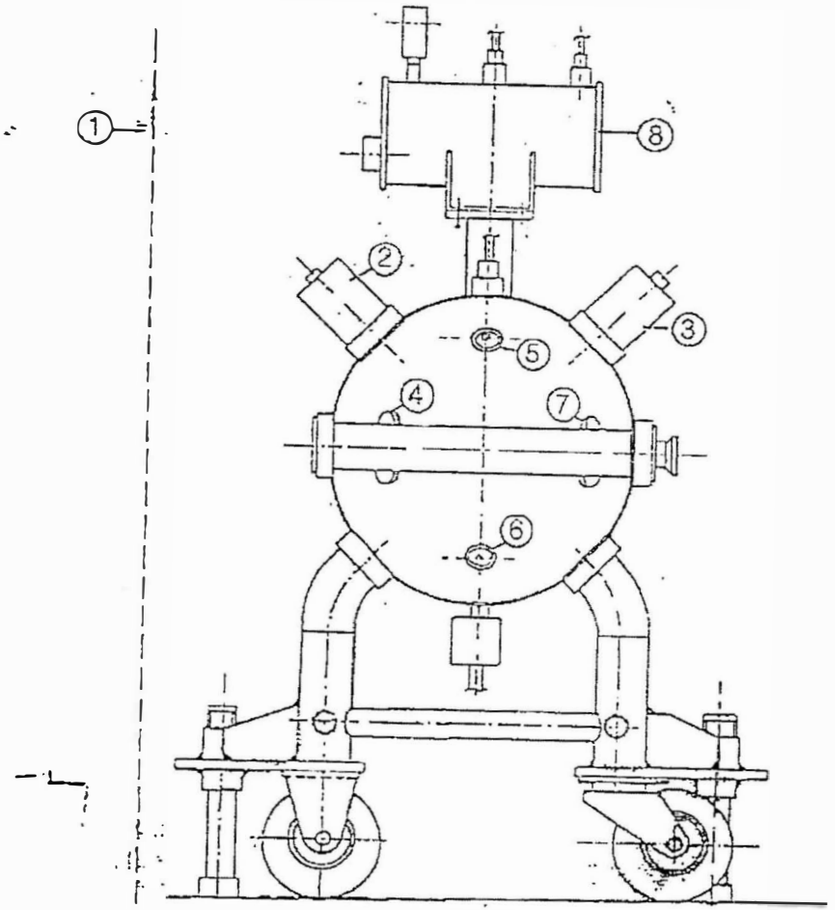

Figure 4: The large volume gadolinium loaded liquid scintillator detector: 1 - electromagnetic shield, (2 - 7) - photomultipliers and 8 - expansion tank

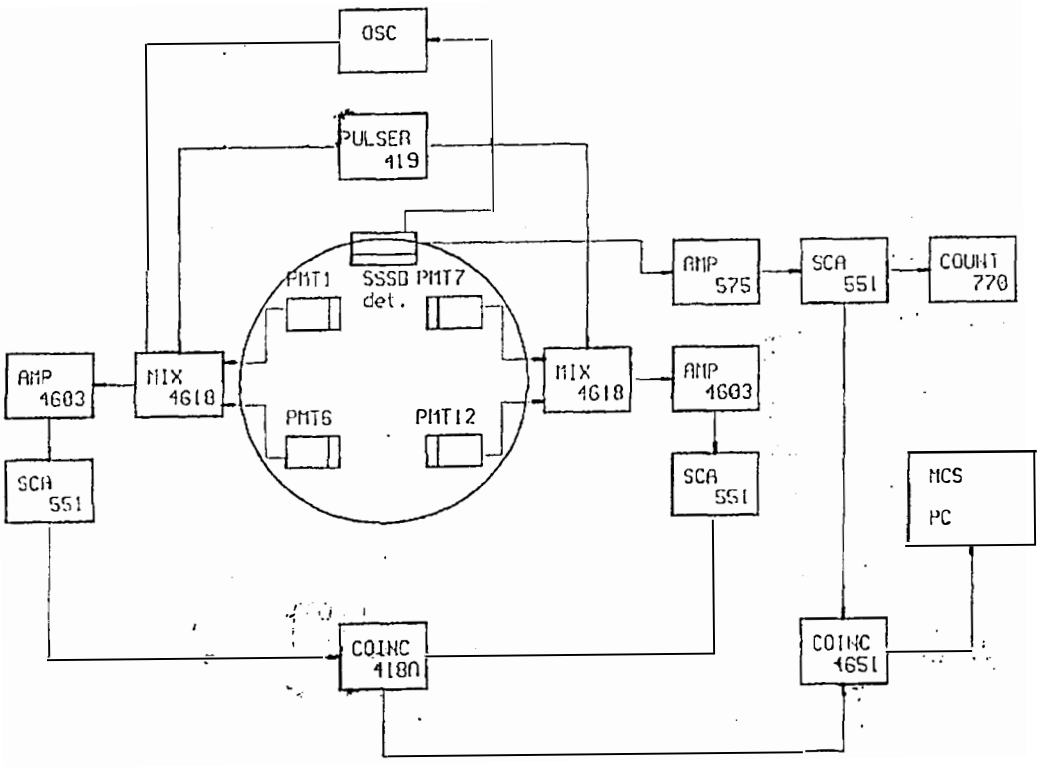

Figure 5: Block diagram of the electronic circuit for the large volume liquid scintillator detection system.

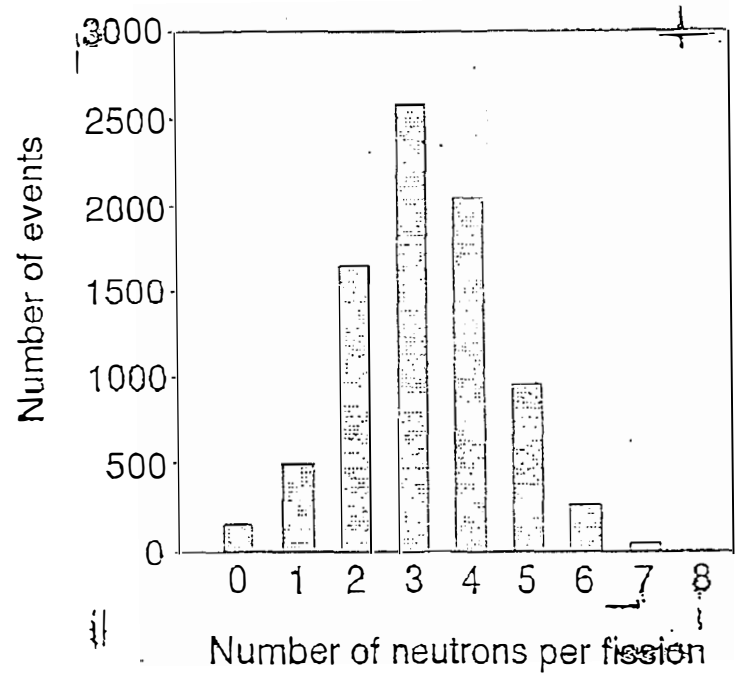

Figure 6: Neutron multiplicity distribution for the ^{252}Cf source. The average value is 3.48 and the corresponding efficiency is 83%

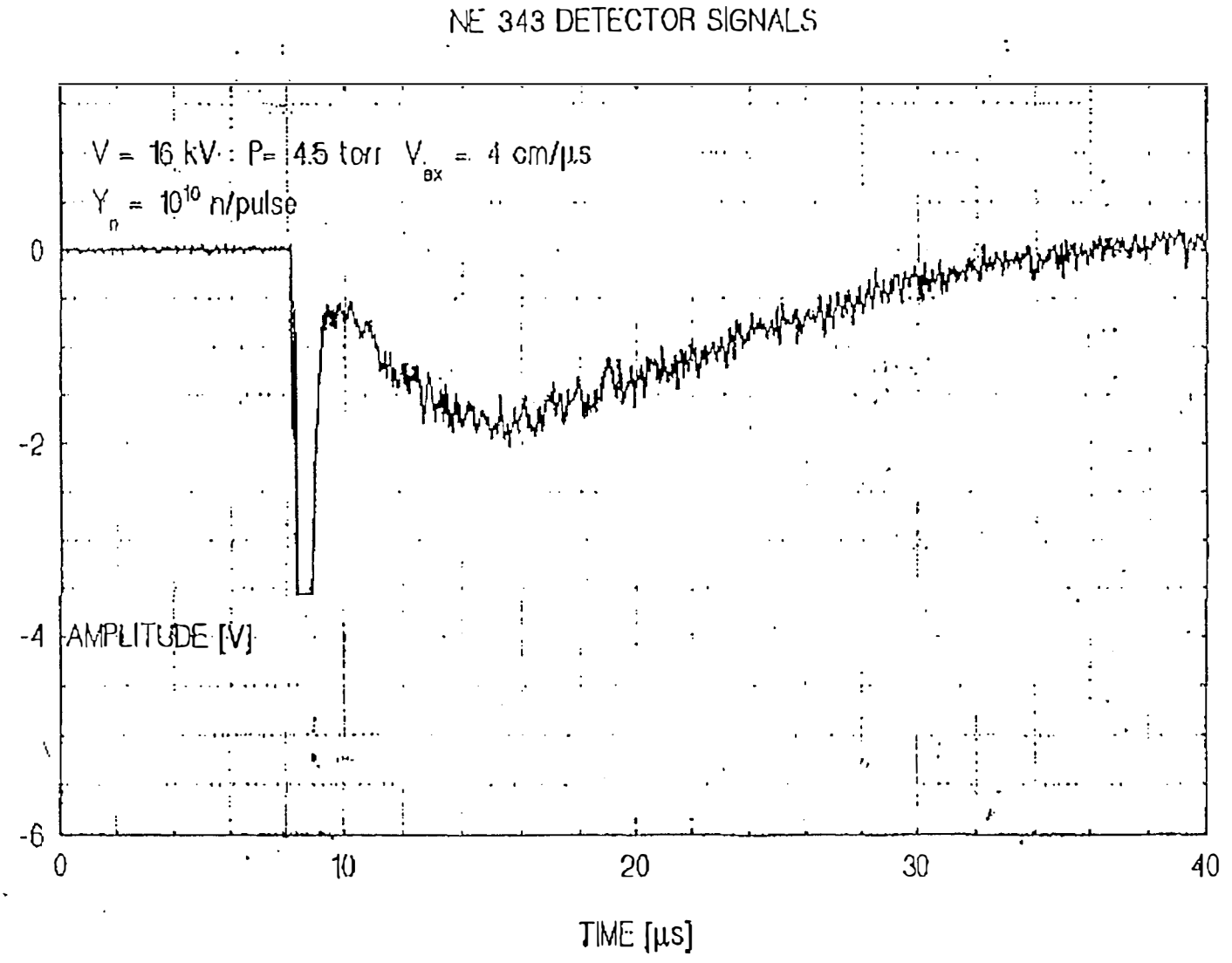

Figure 7: Signal from NE343 based neutron detector for plasma focus.

1. Central electrode
2. Outer electrodes
3. Soft X-ray emission area

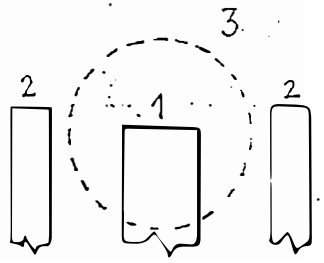

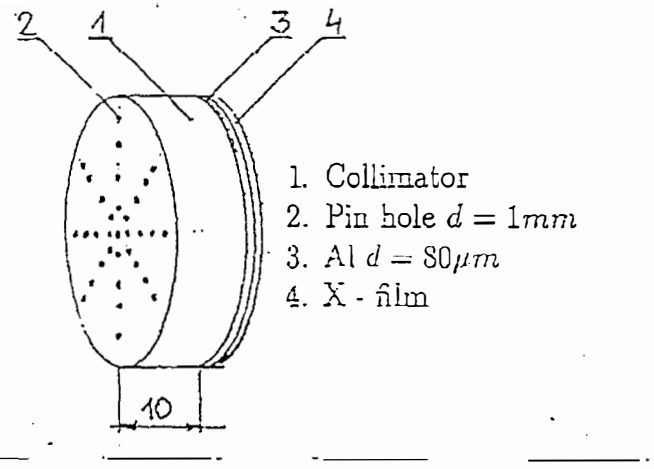

Figure 8: Zone of emission of soft X-rays from deuterium plasma focus

1. Central electrode
2. Outer electrodes
3. Hard X-ray emission area

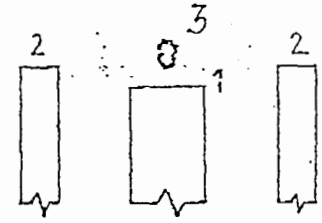

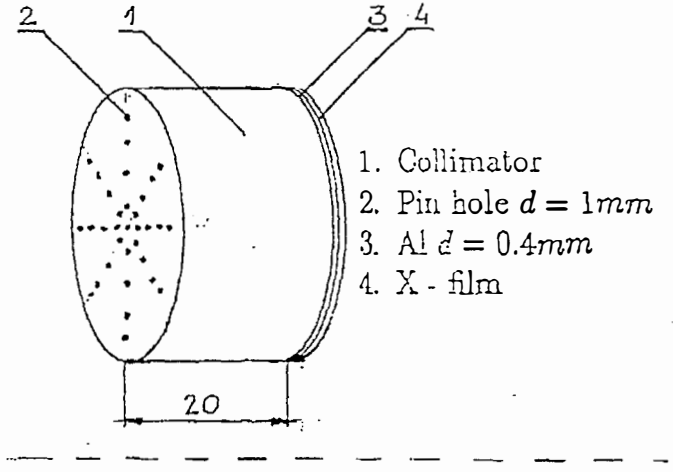

Figure 9: Zone of emission of hard X-rays from deuterium-argon plasma focus

Fifth International Conference on Cold Fusion
9-13 April, 1995 - Monte Carlo, Monaco
ICCF5 ©1995

Sonofusion
Compressibility of Liquid and Stability of Spherical Cavity

Kenji FUKUSHIMA
Physics Department, Joetsu University of Education
Yamayashiki, Joetsu, Niigata 943, Japan

Abstract

We proposed the sonofusion at ICCF3 and theoretically predicted by use of a simplified model that the temperature of gas whithin a supersonic cavity reaches more than $10^8 K$ if the initial radius of the cavity is less than $10 \mu m$, that is, temperatures high enough for the occurrence of hot fusion.

In the present paper we consider a more realistic model by taking into account the compressibility of liquid and search for the optimum values of supersonic parameters for getting high gas-temperature. In addition the stability of a spherical cavity is examined.

1. Maximum Temperature of Hot Spot

As well known, a supersonic pressure field applied to a liquid induces the forced oscillation of cavities. In the contraction phase of the oscillation the gas content is greatly, adiabatically compressed and as a result a small region of high temperature and density is transiently created in the liquid. The direct evidence for the hot spot is provided through the sonoluminescence phenomenon.

Many experimentalists[1,2] succeeded in directly measuring the hot-spot temperature and nowadays it is widely believed that the temperature may reach one hundred thousand Kelvin. On the other hand, we had been interested in the possibility of other catalyzers of nuclear fusion than muon particles. After so-called cold fusion, we have focused on the question of what exreme states could be realized under ambient conditions and have engaged in the determination of the upper bound of hot-spot temperatures.[3-5]

1.1 Zeroth Order Approxoimation

At first we assumed a gas-filled, spherical bubble and incompressible liquid. Moreover, the gas content was assumed to adiabatically respond to the motion of bubble wall. The time-evolution of the bubble radius R is, therefore,

subjected to the Rayleigh-Plesset equation[6-8]

$$R\ddot{R} + \frac{3}{2}\dot{R}^2 = \frac{1}{\rho}(P_L - P_\infty),$$

where

$$P_L = P_G - 2\sigma/R, \qquad P_\infty = P_0 - P_A \sin(2\pi f_A t).$$

The ρ and σ are the density of liquid and surface tension. The P_0 is the ambient pressure of liquid, P_L, P_G and P_∞ being pressures of liquid and gas at the bubble wall and pressure of liquid at a remote point from the bubble center, respectively. The gas is assumed to obey van der Waals' equation of states. The second term on the right hand side of the second equation stands for an applied supersonic field with amplitude P_A and frequency f_A.

The initial condition is

$$R(0) = R_0, \quad \dot{R}(0) = 0.$$

That is, at $t = 0$, the bubble with radius R_0 is assumed to be in a dynamical equilibrium with the ambient pressure P_0.

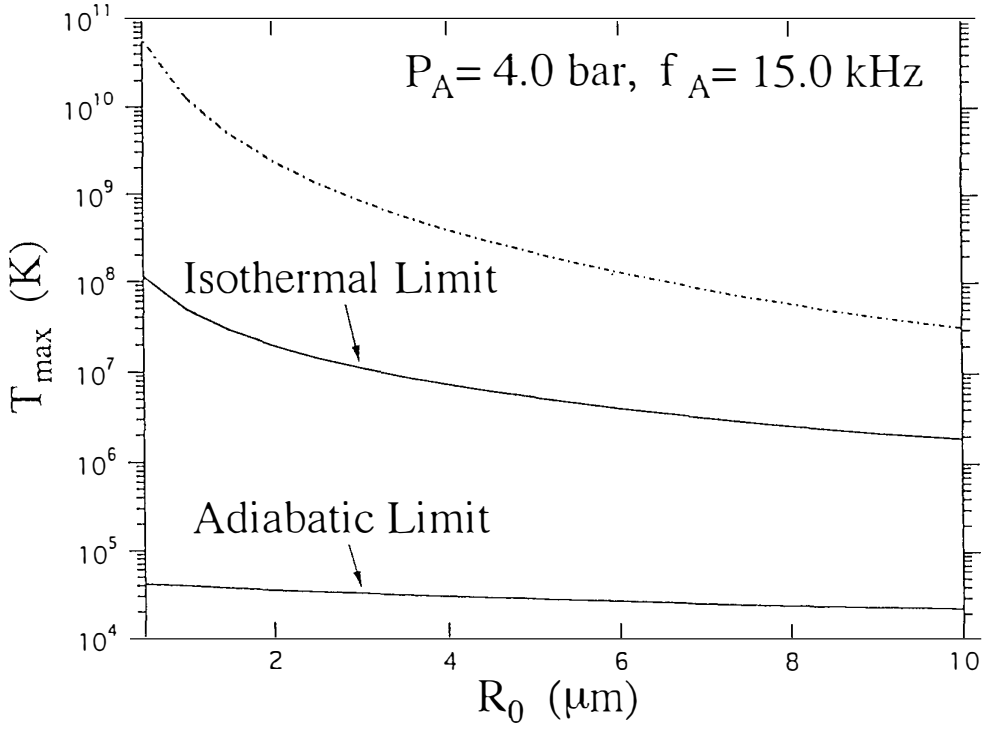

Fig. 1

We numerically solved the Rayleigh-Plesset equation and obtained the result depicted in Fig. 1 by a broken line. The values of supersonic parameters employed are also indicated. It was surprising that the maximum temperature T_{max} of hot spot exceeded 10^8 Kelvin when R_0 was less than 10 microns. This fact suggested the occurrence of hot fusion within a supersonic cavity if the gas content is D_2. The preliminary calculation was so successful that we turned to a more realistic model.

1.2 Compressible Liquid

In the present paper we treat the compressible liquid, whose equation of states is assumed to take the form of

$$\frac{P+B}{P_0+B} = \left(\frac{\rho}{\rho_0}\right)^n,$$

where

$$B = 3,000\ atm, \quad n \sim 7.0.$$

Namely, the liquid behaves like an incompressible one when $P \ll B$. The index n is chosen so as to reproduce the sound velocity of water, 1.45 km/s.

By use of the equations of continuity and of motion, and assuming the Kirkwood-Bethe hypothesis

$$\left(\frac{\partial}{\partial t} + (c+u)\frac{\partial}{\partial r}\right)\left(\frac{u^2}{2} + h\right) = 0,$$

where c and u are velocities of sound and liquid particle, respectively, and h is the enthalpy defined as

$$h = \int^P dP/\rho,$$

we can derive the Gilmore equation[6-8]

$$R\left(1-\frac{U}{C}\right)\dot{U} + \frac{3}{2}\left(1-\frac{U}{3C}\right)U^2 = \left(1+\frac{U}{C}+\frac{R}{C}\left(1-\frac{U}{C}\right)\frac{d}{dt}\right)\left(H-H_\infty\right).$$

The C, U and H are, respectively, values at the bubble wall of corresponding quantities c, u and h. The H_∞ is

$$H_\infty = \int^{P_\infty} dP/\rho.$$

By numerically solving the above equation, we obtained two solid curves as shown in Fig. 1. In the contraction phase of bubble oscillation, the gas-content

may surely be subjected to adiabatic compression because of the swift contraction of the bubble. The expansion, on the other hand, may occur isothermally or adiabatically, depending on the rapidness of the process. The upper solid curve corresponds to the isothermal expansion, the lower one to the adiabatic process. The reality may lie between two curves.

One of the most striking features of Fig. 1 is that at the transition from incompressible liquid to compressible one T_{max} decreases by a few orders of magnitude. This fact unveils that our zeroth order calculation is meaningless. Secondly, there is a great discrepancy between the isothermal limit and adiabatic one, that is, the diffenence of two to three orders of magnitude over the indicated span of R_0. It is noteworthy here that the isothermal curve still lies around 10^7 K when R_0 is a few microns. After all, the isothermal expansion is found to be indeed the one of neccessary conditions for getting high enough T_{max} to provoke the hot fusion.

1.3 Optimization of Parameters

Remind that there exist three adjustable parameters in the present problem, that is, the initial radius of bubble, R_0, and the amplitude and frequency of applied supersonic field, P_A and f_A. It is noteworthy here that the smaller the frequency f_A is, the more probable the occurrence of isothermal expansion is.

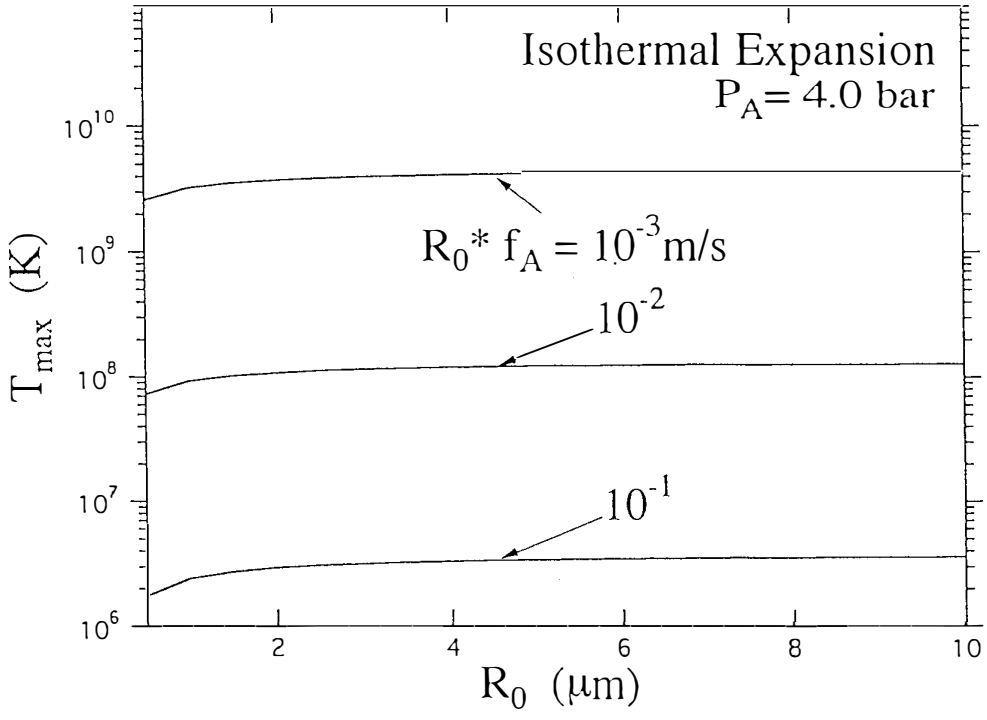

Fig. 2

Fig. 2 depicts T_{max} against R_0 for three fixed values of the product $f_A \times R_0$, where the isothermal expansion is postulated. Remarkable points of Fig. 2 are as follows: Three curves are almost parallel to the R_0-axis, which means that T_{max} depends on f_A and R_0 only through the product $f_A \times R_0$. The second point is that, with decreasing product $f_A \times R_0$, T_{max} increases without the tendency of saturation. In short, the smaller frequency f_A which assures, on the one hand, the isothermal expansion of bubble supports the higher T_{max} simultaneously. That is unexpectedly fortunate situations for us.

The T_{max} also depends on the amplitude P_A. Fig. 3 depicts T_{max} versus R_0 for various values of P_A. With increasing P_A, T_{max} increases, but there can be seen the apparent tendency of saturation.

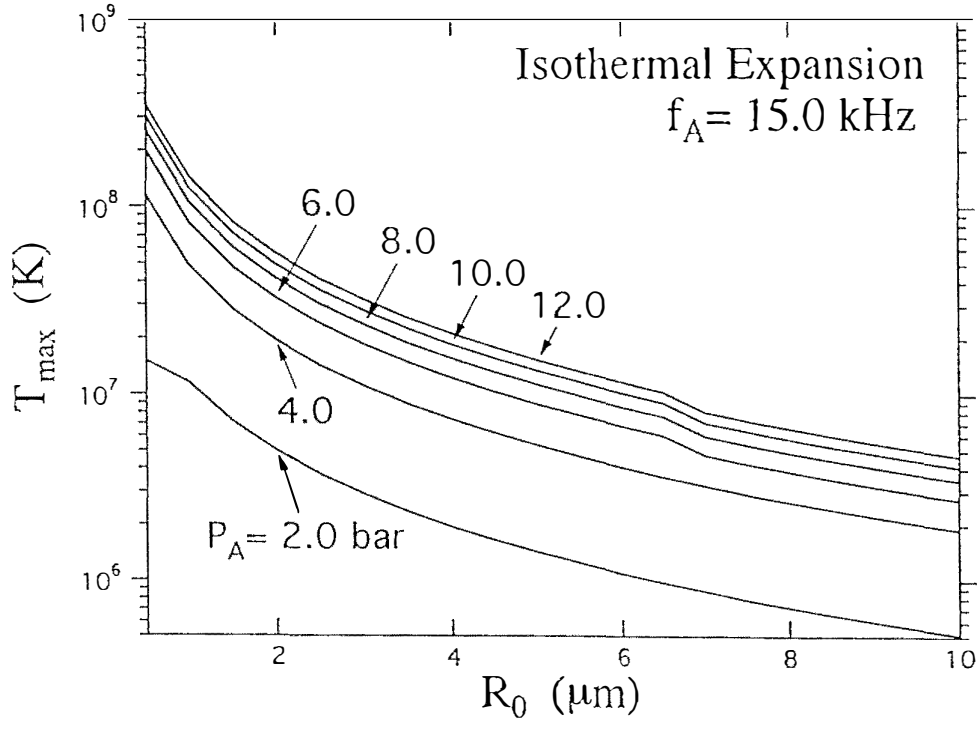

Fig. 3

2. Stability of Spherical Cavity

In this section we examine the time-evolution of a small deviation from the spherical symmetry of the bubble wall. This problem was investigated in detail by Plesset[8]. Let the distance between the bubble center and the bubble wall be $R_s(\theta, \phi, t)$, which can be written as

$$R_s = R + \sum_{l>1} a_{lm} Y_{lm},$$

where R is the radius of a spherical bubble and the last term on the right hand side describes a small deviation from the spherical symmetry. The Y_{lm} is the spherical harmonics. Up to the first order of the deviation parameter a_{lm}, we can get the Gilmore equation for R and so-called Plesset equation

$$\ddot{a} + 3\frac{\dot{R}}{R}\dot{a} = \frac{l-1}{R}\left(\ddot{R} - (l+1)(l+2)\frac{\sigma}{\rho R^2}\right)a$$

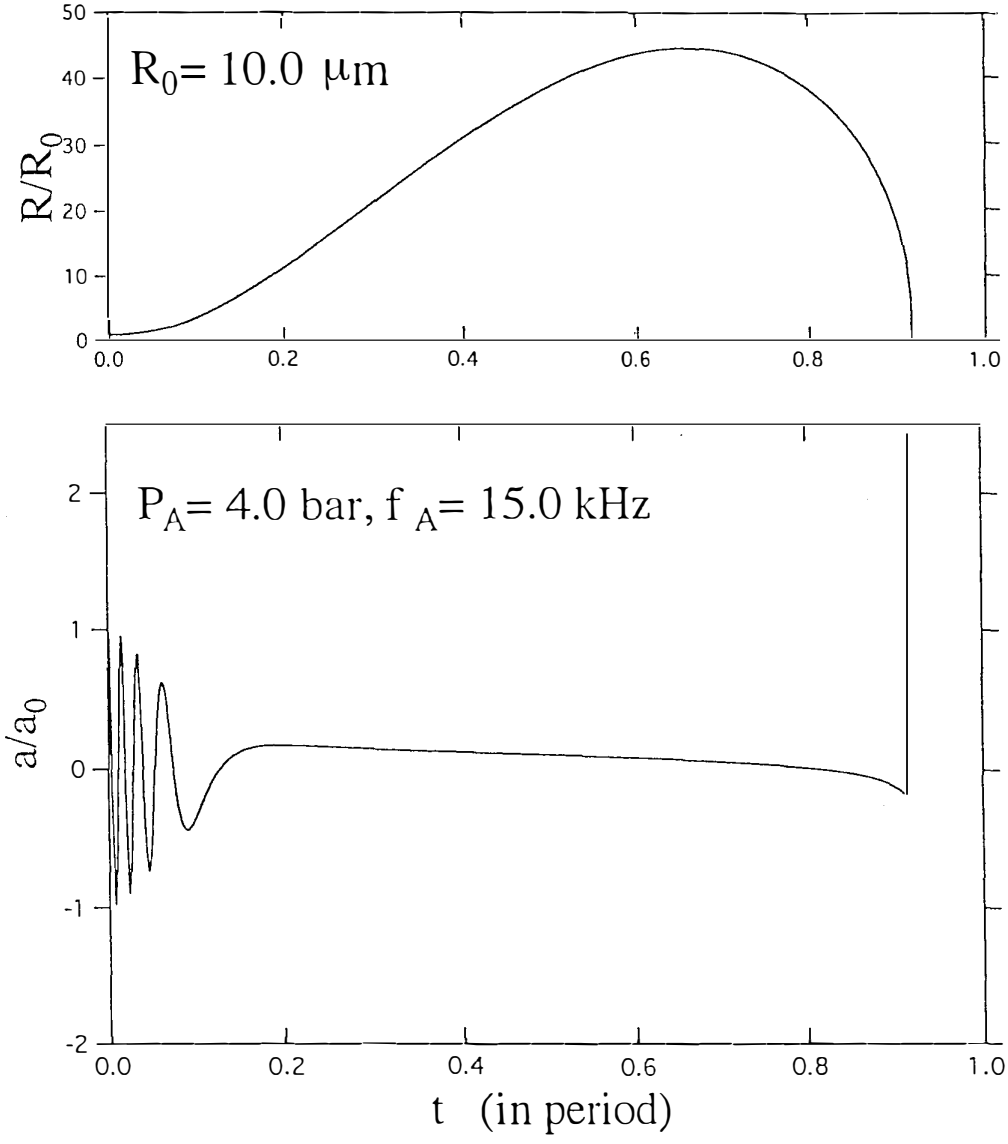

Fig. 4

Fig. 4 illustrates the time-evolution of R and a_{lm} over a period of supersonic field. That is, R starts from R_0 and goes up to the maximum value of about 40 times R_0. It then rapidly goes down to the minimum of about 0.1 times R_0. On the other hand, the deviation starts with its initial value a_0, oscillates for a while and then reduces to very small values. At the final stage of the contraction, it suddenly increases up to about 2.4 times a_0. In any way, the deviation remains finite and therefore the bubble is proven to be stable against a small deviation from the spherical symmetry.

In Fig. 4, only the $l = 2$ case is depicted. General case will be given in another place. In addition the spacial uniformity of the pressure field is assumed in our calculation. On the other hand, it is well-known experimentally that the cavity is unstable near solid surface, that is, in the presence of spatial nonuniformity of pressure field. It is interesting, therefore, to examine the stability of cavities against a small spatial variation of the pressure field.

3. Conclusion and Discussions

We calculated the maximum temperature T_{max} of a hot spot which is induced by an applied supersonic field. It is proven that the smaller the frequency f_A of the supersonic field is, the higher T_{max} can be obtained, which is indeed high enough for the occurrence of hot fusion. Especially without apparent tendency of saturation. Furthermore, with increasing amplitude P_A of the supersonic field the T_{max} increases with apparent saturation tendency. Finally, the stability of spherical cavity is verified.

In our calculation, however, a lot of simplifications are made and thereby our conclusion is still tentative and should not be laterally accepted. The following is the list of simplifying assumptions we have made: We considered a gas-filled cavity but completely neglected (1) the evaporation and condensation of vapor. Next in spite of the formation of a hot spot of high temperature and density, (2) the thermal irradiation, (3) heat conduction and (4) mass diffusion from the hot spot to surrounding liquid are not taken into account. Furthermore, the gas-content of a supersonic cavity should undergo (5) the phase transition and execute (6) the nonadiabatic response such as the formation of shock wave.

In order for getting quantitatively acceptable results, we should engage ourself in the calculation of T_{max} by taking account of the above effects and then we should identify the optimum experimental conditions for realizing the upper bound of T_{max}.

Acknowledgements

We deeply appreciate for the cooporation provided by Prof. Tsuguo Takahasi and Mr. Yasunobu Tomiyama of Tokyo Metropolitan University. We utilized the facilities of the Imformation Processing Center of Joetsu University of Education.

List of Symbols

a_{lm}, a = Deviation from Sphere
B = 3,000 atm
c = Sound Velocity of Liquid
C = Value of c at Bubble Wall(B.W.)
f_A = Frequency of ultrasound
h = Enthalpy of Liquid
H = Value of h at B.W.
H_∞ = Value of h at Remote Point(R.P.)
n = Index in EOS of Liquid
P = Pressure of Liquid
P_A = Amplitude of ultrasound
P_0 = Ambient Pressure of Liquid
P_∞ = Pressure at R.P.
P_G = Pressure of Gas at B.W.
P_L = Pressure of Liquid at B.W.
r = Distance from Origin
R = Radius of Bubble
R_0 = intial value of R
ρ = Density of Liquid
ρ_0 = Value of ρ at R.P.
σ = Surface Tension
t = Time
T = Temperature
T_{max} = Max. Temp. of Hot Spot
u = Velocity of Liquid Particle
U = Value of u at B.W.

References

1) E. B. Flint and K. S. Suslick, Science, **253**, 1397 (1991).
2) R. Hiller, S. J. Putterman and B. P. Barber, Phys. Rev. Letts., **69**, 1182 (1992).
3) K. Fukushima, Frontiers of Cold Fusion, edited by H. Ikegami, p609, Universal Academy press, Tokyo, (1992).
4) K. Fukushima and T. Yamamoto, Cold Fusion Source Book, edited by Hal Fox, Fusion Information Center, Salt Lake City, (1994).
5) K. Fukushima and T. Yamamoto, Proceedings of International Symposium on Cold Fusion and Advanced Energy Sources, p197, Belarusian State University, Minsk, Belarus, (1994).
6) E. A. Neppiras, Physics Reports, **61**, 159 (1980).
7) A. J. Walton and G. T. Reynolds, Advances in Physics, **33**, 595 (1984).
8) Robert T. Knapp, James W. Daily and Frederick G. Hammitt, "Cavitation", p140, McGraw-Hill, New York, (1970).

Fifth International Conference on Cold Fusion
9-13 April, 1995 - Monte Carlo, Monaco
ICCF5 ©1995

Nuclear Products of Cold Fusion Caused by Electrolysis in Alkali Metallic Ions Solutions

Reiko NOTOYA
Catalysis Research Center, Hokkaido University
Kita-11 Nishi-10, Kita-ku,
Sapporo, 060, Japan

Abstract

It was confirmed experimentally that some nuclei products of cold fusion were generated during electrolysis by use of cathodes of porous nickel and platinized platinum,in light(usual) water solutions of all alkali metallic ions investigated. The author reported in the previous work that 4ppm of calcium was detected in the electrolyte of potassium carbonate light water solution by flame photospectroscopy. The gamma-ray measurement revealed the formation of ^{24}Na during electrolysis in sodium carbonate solution. ICP-mass spectra of an electrolyte of cesium sulfate solution showed several peaks of the various nuclear products in the region from 132 to 140 amu. In all electrolytes investigated, the distinct increments of tritium were measured by liquid scintillation spectroanalyzer. Simultaneously, the excess heat was measured in the thermally open cell during electrolysis in these solutions of light or heavy water, which amounted to $\geqq$ 200% for the input power in potassium and cesium ions'solutions. From these results we can conclude that alkali-intermetallic compounds formed as the intermediate of hydrogen evolution reaction cause many types of cold fusion with neutron, proton, deuteron, triton and α - particle.

1. Introduction

Since the cold fusion due to electrolysis in heavy water was proposed by Fleischmann and Pons[1],just 6 years have been over. In the meanwhile,new types of cold fusion during electrolysis in light water solutions have been proposed by several groups which are summarized

in review articles[2,3] recently. The cold fusion takes place in the electrolytic cell of hydrogen evolution reaction(HER) in alkali metallic ions solutions, on the so-called low overvoltage metals.

The mechanism of HER in alkaline solution on the low overvoltage metals has been determined by works of A.Matsuda and his students using the galvanostatic transient method(GSTM). According to the mechanism, HER occurs through the following scheme, on platinum group metals, nickel, silver, titanium and so forth, in the solution of alkali and alkaline earth metallic ions[4]:

$$M^{x+} + xe^- \rightarrow M(I), \quad (1)$$

$$M(I) + xH_2O \rightarrow M^{x+} + xH(a) + xOH^-, \quad (2)$$

$$2H(a) \overset{A}{\rightarrow} H_2, \quad (3)$$

where M^{x+}, M(I) and H(a) denote the metallic cation with the valence x+, the intermediate of alkali-intermetallic compound formed with the cathode material, and an adsorbed or absorbed hydrogen species on or in the electrode, and A, rate determining, respectively.

It has been proposed that the d+d or/and d+d+d cold fusion was occurring in the solid phase of the cathode including D(a),because of using a palladium cathode and heavy water[1,5]. Recently,it was evident from some new results that the nuclei of the intermediates of HER ${}^{A}_{Z}m$ and ${}^{1}_{1}p$ of M(I) and H(a) were undergoing the following nuclear reaction in the surface layer of the cathode, though this possibility had been suggested on the basis of the mechanism of HER[6]:

$${}^{A}_{Z}m + {}^{1}_{1}p \rightarrow {}^{A+1}_{Z+1}m'. \quad (4)$$

In general, reaction(4) seems to produce not only ${}^{A+1}_{Z+1}m'$ but also some small nuclear particles and then m and a new nuclei m' also must undergo the following reaction with small particles in the vicinity:

$$m + m' + n, p, d, t, \text{ or } \alpha \rightarrow m' + m'' + n, p, d, t \text{ or } \alpha. \quad (5)$$

It was observed simultaneously that a certain amount of tritium was produced in parallel with reaction(5). Consequently, the mechanism of the cold fusion may be expressed as the chain reaction which is initiated by the formation of the intermetallic compound M(I) between electrode materials and alkali or alkaline earth metals species.

For the last four years,we have studied to find evidence of the cold fusion mainly caused by electrolysis of light water solutions and obtained the following results:

i. the excess heat measurement in K_2CO_3, Na_2CO_3 and Cs_2SO_4 light water solutions[7-9],

ii. Ca detection by flame photospectroscopic analysis in K_2CO_3 solution[7],

iii. tritium measurement by liquid scintillation spectroanalyzer in K_2CO_3 and Cs_2SO_4 light or heavy water solutions [7,9],

iv. ^{24}Na detection by gamma-ray spectrometer in Na_2CO_3 solution[9],

v. the products analysis by use of ICP-MS in Cs_2SO_4 solution[10].

The present paper concerns mainly v,comparing with the results from i to iv.

2. Intermetallic Compounds

As reported previously[10],the measurement of the pseudo differential capacity on the decay process of overvoltage after switching off of the polarizing current provided the behavior of the intermetallic compound M(I). On the basis of that,it was found that M(I) was formed by cathodic polarization and increased steeply at the potential $\phi = -0.7 \pm 0.1$volt(vs NHE) in a solution of every kinds of alkali metals ions on both cathodes Pt and Ni. The excess surface concentration of the alkali metallic species attained about 10^{16} atoms per true unit area in the region more cathodic than -0.8volt. Taking into account of the composition of M(I), it was obvious that M(I) could penetrate more than 1000 monoatomic layers of any electrode material.

It was possible to determine the time constant τ_1 of the electron transfer step(1) by applying GSTM to the analysis of the initial region of the potential-time curve. The kinetic behavior of τ_1 showed clearly that the discharge of M^{x+} was occurring as the electron transfer step of HER in an alkaline solution. Fig.1 shows the $\log\tau_1$ plotted against pH or $\log C_M{}^{x+}$[4]. As seen from this figure, in pure hydroxides $\log\tau_1$ varies linearly with pH with a gradient -1/2 but no regularity can be seen in pH-dependence of $\log\tau_1$ in sulfate solutions. However, when $\log\tau_1$ is plotted against $\log C_M{}^{x+}$, a definite linear relation is observed with gradient -1/2 in any case of pure hydroxides and sulfate solutions. τ_1 is defined by the product of the differential capacity C_D of the double layer and the reaction resistance r_1 of the most rapid electron transfer step at the equilibrium potential of HER, and further more from r_1 we can deduce the exchange rate of the electron transfer step i_{10}, as follows:

$$\tau_1 = C_D \cdot r_1, \tag{6}$$

$$r_1 = RT/F \cdot i_{10}, \tag{7}$$

where R,T and F denote respectively the gas constant, the Faraday and the absolute temperature. The above results mean that the exchange rate i_{10} is proportional to the square root of the alkali metal ion concentration, since C_D remains constant in these solutions,

$$i_{10} = k(C_{M^{x+}})^{1/2}. \qquad (8)$$

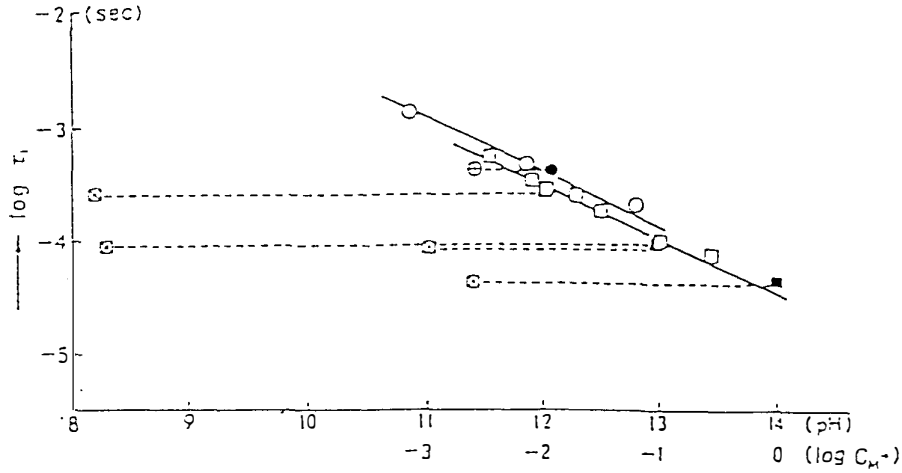

Fig.1 $\log\tau_1$ at the equilibrium potential of HER plotted against pH or $\log C_{M^+}$:
(□)-$NaOH_{aq}$;(⊠)-$Na_2SO_{4,aq}$ plotted against pH;
(■)-$Na_2SO_{4,aq}$ plotted against $\log C_{M^+}$;
(○)-$CsOH_{aq}$;(⊕)-$Cs_2SO_{4,aq}$ against pH;
(●)-$Cs_2SO_{4,aq}$ plotted against $\log C_{M^+}$.

It means that this behavior consists with the kinetics for electron transfer reaction of M^{1+} with the Tafel constant 1/2. It can be concluded from this fact that the electron transfer step of HER in alkaline solution consists in the discharge of alkali metallic ion, but not water molecule which has been widely shown in the literature.

3. Transmutation of Cesium

Cesium ion is one of the most appropriate reactant among alkali metallic ions to measure the amounts of the products of the nuclear reactions,owing to 100% of the natural abundance of $^{133}_{55}Cs$, as well as $^{23}_{11}Na$. Platinized platinum(Pt/Pt) and porous nickel cathodes were used for simultaneous experiments, namely, the measurement of excess heat and the determination of fusion products. Pt/Pt cathode was made of platinum mesh(1.0×0.5cm size) which was covered with ca.50mg Pt-black by electrodeposition. The density of porous nickel(1.0× 0.5cm

size, 0.1cm thickness) was 5.9± 0.1. The anode was made of platinum wire(ca.10cm length,0.5mm diameter). Electrolyte used for a series of these experiments was 0.1mol/l Cs_2SO_4(Merck, Suprapur) solution of light water, which meant twice distilled subterranean water prepared in the same ways as described in the previous works[8]. 20 ml of the electrolyte was used for each electrolysis.As described in the previous works[8,9], each test cell equipped with Pt/Pt or porous Ni cathode (hereafter it will be $cell_{Pt}$ or $cell_{Ni}$, respectively) was polarized galvanostatically. When the electrode potential and the cell temperature attained to these steady values, the current value was changed without intermission of polarization. Thus polarization was repeated several times. The electrolyte in the control cell was used as "the control electrolyte" in which the same electrodes of porous nickel and the platinum wire were immersed in the same way as the test cell, except for polarization,during the test cell's electrolysis. After a series of electrolysis, the electrolyte in $cell_{Pt}$ and $cell_{Ni}$ as well as the control electrolyte were analyzed by means of ICP-MS(SPQ-6500, Seiko Instruments). The ion counts(cps) were calibrated using the standard solutions of $^{138}_{56}Ba^{2+}$ which concentration were from 10 to 200 ppb. As the sample for ICP-MS measurement, the test electrolyte were diluted quantitatively with pure water 4000 or 10000-fold. On the other hand,the control one was diluted merely 100-fold. Therefore strong contamination with the control electrolyte remained at 133 amu and some others' on mass spectra. But it was not changing for measurements of the test samples.

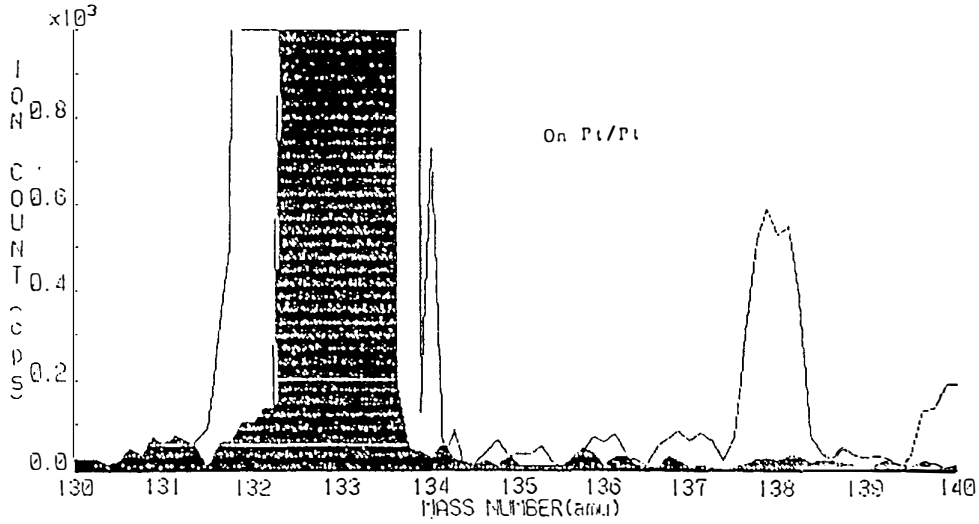

Fig.2 Mass spectrum of a test electrolyte in a cell with Pt/Pt cathode after 18.2 hours electrolysis; the spent electricity=18000± 200 coulomb.

Fig.2 shows the typical mass spectrum concerning the test electrolyte in $cell_{Pt}$, in the range of mass number from 130 to 140. The total quantity of electricity spent during 18.2 hours electrolysis in $cell_{Pt}$ was equal to 18000± 200 coulomb. In the control electrolyte, only 138amu species in the mass spectrum was found to be 0.4ppm except for 133amu, which consisted well with the total Ba determined to be 0.6ppm by a flame photospectrometer.

Comparing the mass spectra in the test electrolyte in $cell_{Pt}$ and the control electrolyte, the increment of the species at each amu is

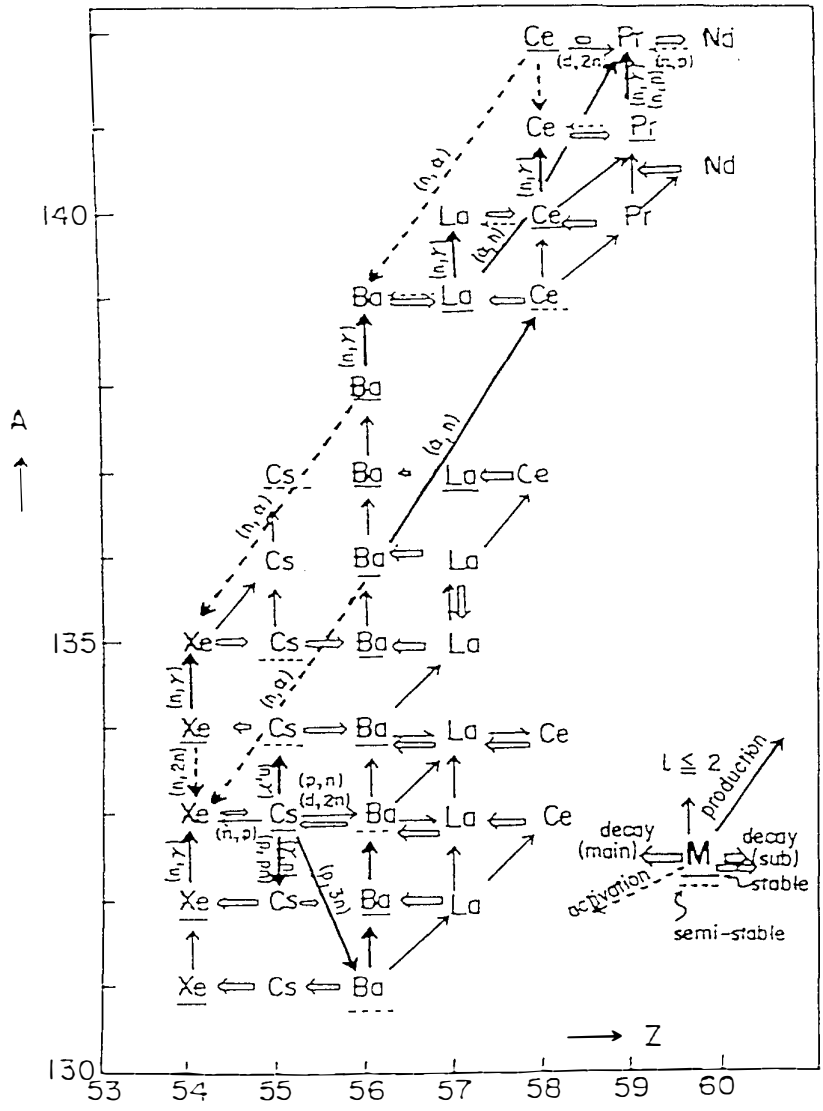

Fig.3 Diagram composed of known reactions occurring in a nuclear reactor and possible reactions of $l \leqq 2$.

Table I Amounts of cold fusion products of electrolysis of 0.1mol/l Cs_2SO_4 light water solution on Pt/Pt cathode, investigated by ICP-MS.

Mass No(amu) :	132	134	135	136	137	138	139	140
Δ amount(ppm):	+	+	0.4	0.3	0.5	4.7	0.2	1.8

summarized in Table I. The increments denoted by + in Table I at 132 and 134 amu couldn't be determined quantitatively because the resolution was insufficient, that was caused by too large ion counts for 133 amu species, but they seemed to be almost the same amount as 138amu.

In relation to the mass numbers in Table I, a diagram can be composed of known[11] reactions for nuclear production and activation in a nuclear reactor, and possible reactions whose spin changes 1 are found to be $\leqq 2$. Fig.3 shows it. It is possible to suppose that some nuclear species in the diagram are produced in $cell_{Pt}$.

On the other hand, in $cell_{Ni}$ violent dispersion of porous Ni was caused by cathodic polarization in Cs_2SO_4 solution. After a few hours' polarization the nickel cathode began to spurt a lot of very fine nickel powder. Such a violent dispersion of porous Ni occurred often in Cs_2SO_4 solution. There was nothing of the fusion products in $cell_{Ni}$, except for 132 and 138 amu which were found to be + and 1.0ppm by ICP-MS, respectively. The total electricity spent during 160 mins' electrolysis in $cell_{Ni}$ was equal to 180 coulomb. In spite of the little electricity, it was very surprising that the product of 138amu amounted to 0.6ppm in $cell_{Ni}$.

Before starting the dispersion, the heat evolution in $cell_{Ni}$ was far greater than that in $cell_{Pt}$, at the same current. For example, at 10m ampere, temperature increased 0.3℃ in $cell_{Pt}$, but 7.0℃ in $cell_{Ni}$. The excess heat in $cell_{Pt}$ was found to be 260%, but the input power in $cell_{Ni}$ wasn't determined because the potential fluctuated strongly.

4. Discussion and Conclusions

It is quite evident from Table I that cesium atomic species in the surface layer of these electrodes is undergoing the same types of nuclear reactions as that in a nuclear reactor. In both cases of the electrolysis in cesium and potassium solutions, the nuclear products amounted to ca.5ppm, simultaneously with the considerable excess heat evolution. During electrolysis of $^{23}Na_2CO_3$ solution, ^{24}Na was detected by gamma-ray spectroanalyzer, but it was far less than those. In this case, the excess heat was not observed practically. From these results we can conclude that the transmutation of the intermetallic compound

M(I) like as reaction(5) is occurring in all alkaline solutions on platinum or nickel cathode as well as the low overvoltage metals and it is predominant for heat evolution. However, it is sure that d+d or d+d+d is occurring in parallel with the cold fusion of M(I), because the increase of tritium was observed in all electrolytes.

References

1. Fleischmann and Pons,"Electrochemically Induced Nuclear Fusion of Deuterium,"J.Electroanal.Chem.,**261**,301(1989).

2. Fox,"Cold Nuclear Fusion,Space Energy Devices&Commercialization," Cold Fusion Source Book,Minsk,Belarus,May 24-26,1994,p.12.Fusion Information Center,Salt Lake City,Utah,(1994).

3. Storms,"A Critical Review of the Cold Fusion Effect,"Proc.ICCF-5 Monte-Carlo,Monaco,April 9-13,to be published(1995).

4. Matsuda,Notoya,Ohmori,Kunimatsu,Kushimoto,"Effect of Surface Potential on the Rate of Electron Transfer Step of HER,"J.Res. Inst.Catal.Hokkaido Univ.,**24**,187(1977).

5. Takahashi et al.,"Excess Heat and Nuclear Products by D_2O/Pd Electrolysis and Multibody Fusion,"Int.J.Appl.Electromagnet.Mat., **3**,221(1992).

6. Notoya,"Alkali Metallic Intermediate of Hydrogen Electrode Reaction,"Abs.18th Mtg.Hokkaido Electrochem.Soc.,Sapporo,Jan.18(1990).

7. Notoya,"Cold Fusion by Electrolysis in a Light Water-Potassium Carbonate Solution with Nickel Elec.,"Fusion Tech.,**24**,202(1993).

8. Notoya et al.,"^3t Generation and Large Excess Heat Evolution by Electrolysis in H_2O- and D_2O-K_2CO_3 on Ni,"ibid.,**26**,179(1994).

9. Notoya,"Cold Fusion in HER of Active Metals in Solution of Alkali Metallic Ions,"Proc.EEWWCE2,Sintra,Portugal,March,12-15,(1995).

10. Notoya,"Alkali-Hydrogen Cold Fusion Accompanied by Tritium Productionon Ni,"Transactions of Fusion Tech.,**26**,205(1994).

11. Japanese Isotope Association,Isotope Handbook,"Chapter 4,5,7,10, Maruzen,Tokyo(1992).

Fifth International Conference on Cold Fusion
9-13 April, 1995 - Monte Carlo, Monaco
ICCF5 ©1995

Biological Effects of Ultrasonic Cavitation

T. V. Prevenslik
2 E Greenery Court , Discovery Bay, Hong Kong

Abstract

Cavitation energy in a nearly evacuated bubble is shown to *not likely* reside in the thermal state of the water molecule. In a spherical bubble compression and until the bubble assumes a pancake collapse shape, a temperature increase does not occur in the bubble gas because the mean free path likely exceeds the bubble diameter. The subsequent collapse of the pancake shape to liquid density occurs with only a negligible volume change so that the temperature increase for compression heating of bubble gases is insignificant. Even near liquid density, a temperature increase does not occur as the energy transfer by molecular collisions is in the adiabatic limit for both vibrational and rotational modes. Instead, the IR radiation energy density present within the bubble is increased as required to satisfy standing wave boundary conditions with the bubble walls in the direction of collapse. For biological tissue in an opaque environment, bubble collapse is found to increase the 5-10 μm IR thermal radiation at ambient temperature to about 3-5 eV that is capable of dissociating the water molecule and forming the chemically reactive hydroxyl radical. Hence, the biological effects of ultrasonic cavitation are proposed to be caused by the chemical reaction of the organisms with the excited electronic states of dissolved oxygen and water molecules.

1. Introduction

Currently, the biological effects of ultrasonic cavitation[1-2] observed in water based systems are thought to be caused by high bubble gas temperatures postulated during cavitation that form reactive hydrogen and hydroxyl radicals. Subsequent disintegration of biological molecules occurs by chemical reaction or simply by the mechanical stresses of cavitation.

In this paper, the biological effect of ultrasonic cavitation is proposed to be of a quantum mechanical origin and is quite different from the current interpretation in that the bubble collapse occurs without a significant change in bubble gas temperature.

2. Theoretical Background

The biological effects of ultrasonic cavitation are presented for the nearly evacuated bubble prior to collapse that is filled solely with the vapor pressure of the water surroundings at ambient temperature, but may include trace amounts of dissolved gases. The cavitation of bubbles filled with external gases at atmospheric pressure bubbled through water in excess of saturation is similar in that bubble expansion tends to evacuate the bubble by cryogenic condensation prior to collapse.

Pancake Collapse Geometry

Bubble collapse is an unstable process following a minimum energy path. Since the collapse of a spherical bubble follows a path of maximum energy, a spherical collapse shape is an unlikely event during ultrasonic cavitation. Instead, a pancake-like shape of characteristic dimension δ following a minimum energy path is likely as illustrated in Figure 1.

If the initial bubble pressure is near atmospheric pressure, say by bubbling gases through the water, bubble expansion cools the gas molecules to cryogenic temperatures and tends to evacuate the bubble by condensation before collapse. The bubble *may be* initially spherical , but eventually is required to assume a pancake shape. Since the change in volume of a pancake collapse is negligible, a temperature increase by compression heating of the bubble gases is insignificant. A temperature increase, if any, may only occur over the time the volume changes and the bubble remains in an almost *exactly* spherical unstable state. In contrast, if the bubble initially is nearly evacuated before expansion, say filled with water vapor and only trace amounts of external gases, the bubble shape is unstable and likely pancake-like even prior to collapse so a temperature change during collapse is very unlikely.

Collision Induced Energy Change in a Nearly Evacuated Bubble

A bubble nucleated in water based biological tissue at temperature may be considered nearly evacuated as the vapor pressure is much less than atmospheric pressure. During bubble compression, changes in the thermal energy state of the water molecule depend on intermolecular collisions and may be quantified by the mean free path mfp in relation to the bubble radius $D_o / 2$ prior to collapse ,

$$mfp = \frac{\sqrt{2} K_b T_{vapor}}{2 P_{vapor} d^2} \qquad (1)$$

where, P_{vapor} , T_{vapor} are the water vapor pressure and temperature and K_b is Boltzmann's constant.

The condition for a change in the thermal state is the likelihood of intermolecular collisions within the bubble where $mfp < D_o / 2$. Conversely, if $mfp > D_o / 2$, a change in the thermal state of gas molecules within the bubble is unlikely as the molecules are likely to be found in the walls of the bubble. Since photon emission is

only known to occur from excited electronic states of the water molecule, photon emission is favored if a thermal state does not change, $mfp > D_o / 2$. Based on the vapor properties of water[3], the *mfp* of the water molecule from 0 to 40 C for $d = 0.3$ nm is shown in relation to bubble radius in Figure 2. At 20 C, the $mfp = 13.5$ μm. The *mfp* is observed to decrease and increase above and below 20 C. This means photon emission is favored at low temperatures.

In sonoluminescence, the observed[4] increase in photons at low ambient temperatures is also consistent with the dependence of photon emission on the *mfp* and the bubble radius $D_o / 2$. Schwinger commented[5] that the temperature independent Casimer model found difficulty in explaining the remarkable increase in photons as the temperature of liquid water nears the freezing point. However, an abrupt increase in photon emission is expected as the temperature is lowered. From Figure 2, in a nearly evacuated bubble the *mfp* ~ 50 and 13.5 μm at 0 and 20 C. Since the bubble radius cited in Schwinger's comment was 40 μm, and since *mfp* > 40 μm, photon emission is favored at 0 C. In contrast, *mfp* < 40 μm and a temperature change is favored at 20 C.

Collision Induced Energy Change Near liquid Density

As the liquid water walls of the bubble collide, the water molecule temperatures may increase by molecular collisions. The likelihood of temperature changes in the water molecule may be estimated[6] from the vibrational and rotational adiabaticity parameters ξ_v , ξ_r that provides a measure of the efficiency of the kinetic energy transfer in the collision,

$$\xi_v = \frac{t_c}{t_v} \quad \text{and} \quad \xi_r = \frac{t_c}{t_r} \tag{2}$$

where, t_c is the duration of the collision and t_v, t_r is the vibrational and rotational period of the water molecule. The collision time $t_c \sim a / V_{rel}$ where a is the range of intermolecular forces and V_{rel} is the relative velocity in the collision. At liquid water density, the range of intermolecular forces is of the order of the molecular spacing, $a \sim 0.3$ nm . For a pancake collapse at sonic velocity from both sides, $V_{rel} = 2\, V_{sonic}$, $t_c \sim a / 2\, V_{sonic}$. For water, V_{sonic} ~ 1460 m/s and $t_c \sim 0.1$ ps.

The vibrational period may be estimated from Planck's relation, $t_v \sim h / \Delta E_v$ where ΔE_v is energy level spacing and h is Planck's constant. For the observed[4] VIS energetics of the water molecule, $\Delta E_v >$ ~ 1 eV and $t_v \sim 0.004$ ps. Hence, ξ_v ~ 250 >> 1 and the molecular collision for the vibrational mode is in the adiabatic limit with very inefficient energy transfer. Usually, rotational energy transfer is efficient at ambient temperature because the energy level spacings ΔE_r are about 3 orders of magnitude smaller than ΔE_v for vibration, so $t_r \sim 1000\, t_v$ and $\xi_r \sim 0.25$ <1. However, at liquid density in the close packed spacing of neighbor molecules, the water molecule is restrained from rotation, so that t_c is large and $\xi_r >> 1$, or the rotational mode is also in the adiabatic limit. Hence, temperature changes are not expected as the bubble walls collide at liquid density .

Electronic Excitation Mechanism

The Doppler effect that increases the radiation energy density within the bubble from the IR to the UV as the bubble dimension δ vanishes during collapse is proposed as the mechanism to excite the electronic state of the water molecule to explain the biological effects in ultrasonic cavitation. Wien in formulating the displacement law[7] derived the relation between radiation wavelength and cavity size based on the Doppler shift from the collapse of a perfectly reflecting sphere. In the limit $\delta \rightarrow 0$, bubble collapse may increase IR radiation to soft X-rays.

The IR energy of the liquid surrounding the bubble of dimension δ_o is given by $E_o = hc/2\delta_o$, where $\delta_o = \lambda_o/2$ as required to satisfy the half wave boundary conditions with the bubble walls. At any instant of bubble collapse, the dimension $\delta < \delta_o$ requires an increase in the Planck energy $E > E_o$. Hence, bubble collapse serves as means of increasing the IR energy density. The unavailability of the thermal state is important. If the thermal state is available, energy is converted to a temperature increase instead of Planck energy.

A continuum of Doppler excitation frequencies from the IR to the X-ray limit may are generated as the bubble collapses. The dissociation of the water molecule to hydroxyl radicals requires the breaking of chemical bonds at about 5 eV and the oxygen singlet state may be excited from water molecule or dissolved oxygen at about 10 eV. The photon emission for noble gases is greater than for diatomic oxygen and triatomic water molecules because bonds are not present to quench the increase in the electronic state of the photo electrons. If the Doppler frequency does not match one of the excited states of the water molecule, the radiation is Rayleigh scattered elastically back throughout the bubble cavity. The energy required to excite the entrained bubble gas molecules follows Planck's law, $E = h\upsilon$, where, υ = excitation frequency of the respective electronic state.

Doppler Effect on Radiation Wavelength and Pulse Measurement

The Doppler effect for the relation of the bubble dimension δ to the wavelength λ of the radiation within the bubble cavity follows the Richtmyer[8] analogy for the adiabatic expansion and compression of blackbody radiation trapped between a piston and cylinder. For a pancake bubble of dimension δ collapsing at a velocity V, the average of the rate of change of the wavelength in the bubble cavity,

$$\left\langle \frac{d\lambda}{dt} \right\rangle = \frac{\lambda}{3\delta} \frac{d\delta}{dt} \tag{3}$$

Integrating from the nucleated bubble dimension δ_o and wavelength λ_o, the Doppler shifted wavelength λ is,

$$\lambda = \lambda_o \sqrt[3]{\frac{\delta}{\delta_o}} \tag{4}$$

Generally, the radiation may fill the bubble cavity with m modes of half wavelength $\lambda_o / 2$ where $m \geq 1$. Now, a wavelength change is negligible for large m where $\delta_o >> \lambda_o$. Only for $m = 1$ and specifically for $\delta_o > \delta > \delta_c$ is the wavelength change significant. Hence, the bubble gas molecules are excited by a blue shifted wavelength λ relative the IR bubble wavelength λ_o as the dimension $\delta \rightarrow \delta_c$.

The pancake collapse time $t_{collapse}$ provides an estimate of the pulse duration over which the Planck energy is concentrated and depends on how rapidly the wavelength changes as the bubble walls collapse, $t_{collapse} > \delta / 2 V_{sonic}$. For a photon detector with a range between 230 and 600 nm, the dimension δ ~ 370/2 ~ 185 nm gives $t_{collapse}$ ~ 60 ps and is consistent with the 50 ps observed[4].

Planck Energy and Work in Compressing Radiation Pressure

During cavitation, the radiation energy density ψ in the bubble during collapse is increased from the energy density ψ_o in the bubble before collapse. The Planck energies before and during collapse, E_o, E are,

$$E_o = A_o \delta_o \psi_o \text{ and } E = A \delta \psi \tag{5}$$

where, A_o, A are the areas orthogonal to the collapse direction and δ_o, δ are the bubble dimensions. Since the radiation pressure $p = \psi / 3$, the work done by the liquid walls to compress the radiation wavelength is $pdV_{vol} = - 1/3 A\psi \, d\delta$. For a pancake collapse, $A \sim A_o$ and $A \, d(\delta \psi) = A (\psi \, d\delta + \delta \, d\psi)$. Hence, $d\psi / \psi = - 4/3 \, d\delta / \delta$ and $\psi / \psi_o = (\delta_o / \delta)^{4/3}$. Substituting in (5) gives $E = A\psi_o (\delta_o / \delta)^{4/3} = E_o A/A_o (\delta_o / \delta)^{1/3}$. For $A \sim A_o$, $E = E_o (\delta_o / \delta)^{1/3}$ and since $E_o = hc / \lambda_o$,

$$E = \frac{hc}{\lambda_o \sqrt[3]{\frac{\delta}{\delta_o}}} = \frac{hc}{\sqrt[3]{2\delta\lambda_o^2}} \tag{6}$$

The Planck energy E as a function of the collapse dimension δ_c for various wavelengths λ_o of energy in the bubble cavity are shown in Figure 3.

Biological Surroundings Opaque to UV-VIS

For biological tissue in an environment opaque to UV-VIS, the bubble energy available for collapse depends solely on the IR thermal radiation of the water surroundings. At a blackbody temperature of 293 K, the maximum IR energy occurs at $\lambda_o \cong 9.86$ μm with a half wavelength corresponding to a nucleated bubble dimension $\delta_o \cong 5$ μm. For a liquid density collapse δ_c ~ 0.31 nm, the Planck energy is about 3.15 eV corresponding to a blue photon at about 390 nm. Although the IR energy at 5 μm is only 20% of that at 9.86 μm, the Planck energy is higher at about 5 eV corresponding to bactericidal UV at 250 nm.

Biological Surroundings Transparent to UV-VIS

If the organisms are isolated and placed in liquid water transparent to UV-VIS radiation, the Planck energy may be enhanced if the bubbles in the water are filled with UV-VIS photons. The bubbles are assumed to be filled with UV-VIS radiation at wavelength $\lambda_{\mu} = 2\delta_{\mu}$, say from external light sources. For UV irradiation at 200 nm, the Planck energy for a liquid density collapse is about 42 eV corresponding to XUV at about 30 nm.

3. Summary and Conclusions

The bubble collapse during the ultrasonic cavitation of water based systems most likely takes the shape of a pancake without a temperature change. A spherical bubble collapse produces high gas temperatures, but is an unlikely event.

The IR thermal energy at ambient temperature is increased to UV-VIS levels because the energy density trapped within the bubble is increased as the dimension in the pancake direction vanishes. The VIS blue light at about 390 nm observed in sonoluminescence is explained by the liquid density collapse of IR energy at 9.86 μm. However, 20 % of the IR energy is converted to bactericidal UV at about 250 nm. The VIS-UV energy pulse duration for a photon detector sensitive to from 600 nm VIS to 230 nm UV is on the order of 60 ps and may be longer if the IR above 600 nm is detected as well .

It is possible, at least in principle, to envision ultrasonic cavitation as a means of converting externally supplied UV radiation energy at 200 nm to XUV.

The energy amplification in ultrasonic cavitation from the IR at 9.86 μm to a blue photon in the VIS at 390 nm is about 25:1.

A dramatic increase in photons is predicted as the ambient temperature approaches the freezing point of water if the mean free path of the bubble gases exceeds the bubble radius after bubble expansion and prior to collapse.

There is no need to postulate high temperatures during bubble collapse to explain the biological effects of ultrasonic cavitation. For water in opaque biological tissue, near UV radiation is predicted at about 3-5 eV and is sufficient to form hydroxyl radicals. If the biological organisms are placed in a water solution irradiated with 200 nm UV, XUV capable of significant biological effects state are predicted.

An experimental program is underway to test the effects of UV enhanced ultrasound on E-coli and cholera. The latter are of significance for cleansing of water tanks holding live fish for human consumption in Hong Kong restaurants.

References

1. *Biological Effects, Ultrasound Mechanisms, and Clinical Applications*, NCRP Report No. 74, Bethesda, Md. 1983.
2. A. R. Williams, *Ultrasound Biological Effects and Potential Hazards*, Academic Press, London, 1983.
3. D. R. Lide, *CRC Handbook of Chemistry and Physics*, CRC Press, 1992.
4. R. Hiller, S. Putterman, and B. Barber, "Spectrum of Picosecond Sonoluminescence", Phys. Rev. Lett., 69, 8, 1182 (1992)
5. J. Schwinger, "Casimer Light: The Source", Proc. Natl. Acad. Scie., USA, 90, 2105, (1992)
6. R. D. Levine and R. B. Bernstein, *Molecular Reaction Dynamics and Chemical Reactivity* , Oxford University Press, 1987.
7. S. Gasiorowicz, *Quantum Physics*. Wiley and Sons., New York, 1974.
8. A. Richtmyer, *Introduction to Modern Physics,* Mc Graw-Hill, New York, 1969.

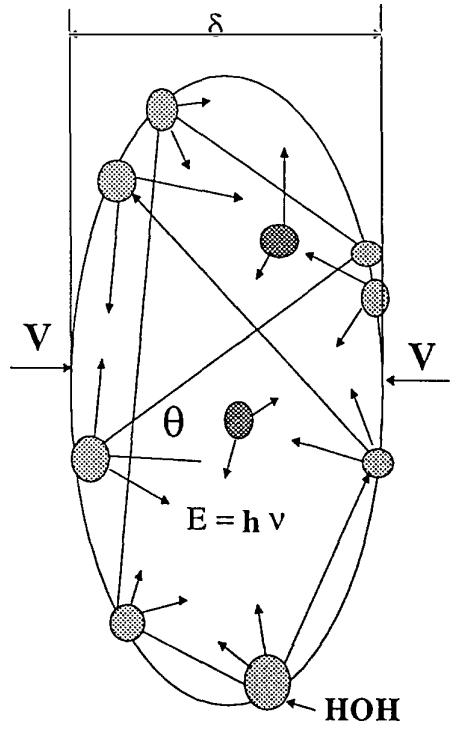

FIGURE 1 BUBBLE COLLAPSE IN ULTRASONIC CAVITATION

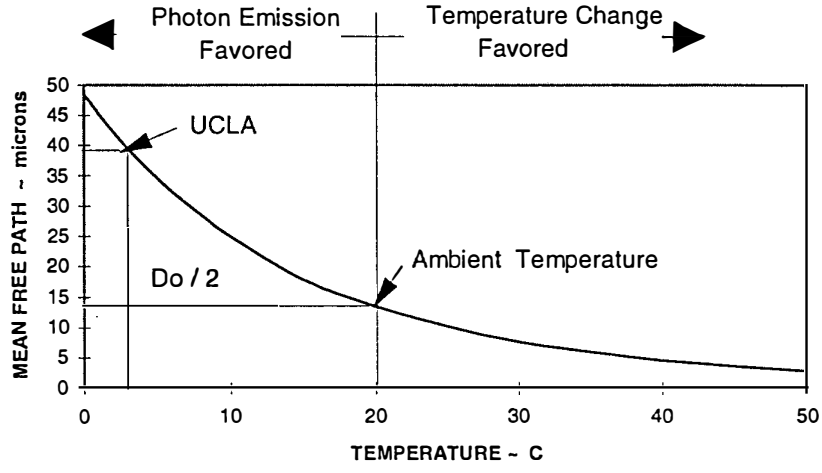

FIGURE 2 WATER MOLECULE ~ MEAN FREE PATH

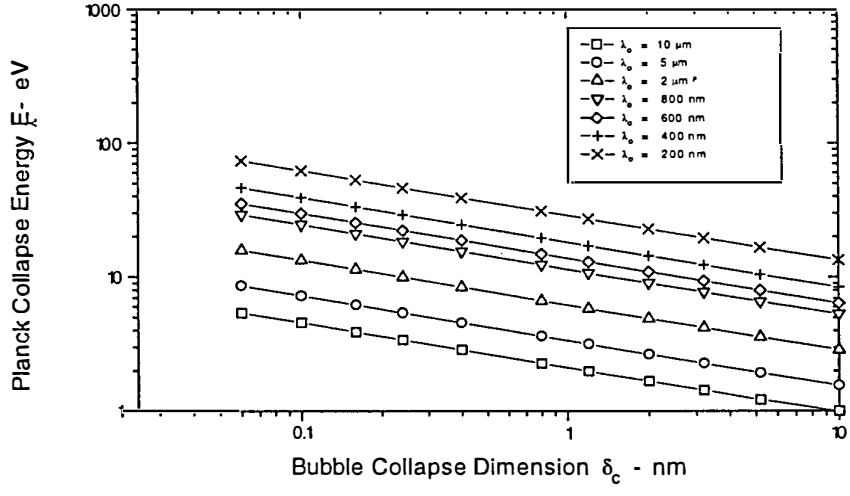

FIGURE 3 PLANCK ENERGY AND WAVELENGTH

Fifth International Conference on Cold Fusion
9-13 April, 1995 - Monte Carlo, Monaco
ICCF5 ©1995

Anomalous Heat Effects and Cold Fusion in KD_2PO_4 Crystals on the Ferroelectric Phase Transition

V.A.Kuznetsov, A.G.Lipson, E.I.Saunin, T.S.Ivanova

Institute of Physical Chemestry
of the Russian Academy of Sciences,
31 Leninsky prospect, Moscow, 117915, Russia

1.Abstract

The kinetic peculiar features of the phase transition heat (ΔH) have been investigated by the differential scanning calorimetry method in KH_2PO_4 and KD_2PO_4crystal on transition through the Curie point at preset rates of cooling and heating samples. It has been shown that on reaching a large number of thermal cycles the ΔH values of a KD_2PO_4 crystal are undergo inversion, so that the value of ΔH_{exo} begins to exceed that of ΔH_{endo}. Such an anomaly of the ΔH behavior is absent in the hydrogen-containing analogue of KD_2PO_4, a KH_2PO_4 crystal, for which $\Delta H_{exo} > \Delta H_{endo}$ for any number of thermal cycles. A phenomenological model of an anomalous thermal effect in KD_2PO_4 crystals on a ferroelectric phase transition has been suggested, the transition being effected under explicitly nonequilibrium conditions. Using that model as a basis, the contribution of the domain walls elastic energy to the total transition heat has been calculated, the contribution being due to exoenergetic nuclear reactions taking place in the KD_2PO_4 crystal lattice on the splitting up of deuterons interacting with giant fluctuations of the domain walls elastic energy density

.

1.Introduction

The heat of a ferroelectric phase transition in the KDP and DKDP crystals, determinable through a corresponding integration of the temperature dependences of heat capacities under a constant pressure, was measured in works [1,2]. It is worthwhile to emphasize that the heat capacity values (i.e. transition heats) in the KDP and DKDP crystals were measured in the above-cited works under explicitly equilibrium conditions. Therefore, the total transition heat ΔH, associated only with the rebuilding of the crystalline structure on a phase transition, proves to be the same with regard to modulus, both on the heating and the cooling of samples. Now, it is to be expected that when measuring the transition heat under definitely (a fortiori) nonequilibrium conditions

(on the linear regime of cooling and heating of samples at different rates) the values of ΔH in the exophase (cooling) and the endophase (heating) may substantially differ in magnitude and exhibit a distinctly pronounced dependence on the heating rate. In such a case, because of the presence of a temperature gradient in a sample, some portion of the surface energy of domain walls, whose value attains $W'=40$ erg/cm^2 [2], can transform into heat, thus giving rise to the anomalies of the phase transition heat during the thermocyclation of samples through the Curie point. In other words, this process must be equivalent to the appearance of an additional heat source ("cooler") in the crystal lattice, making a positive or negative contribution to the true transition heat.

In view of the aforesaid, the purpose of the present work consists in the investigation of a possibility of an additional yeld of heat on a ferroelectric phase transition in the KDP and DKDP crystals, and of quantitative changes in the transition heat in the process of multiple thermocyclation (cooling an heating) of samples in the vicinity of T_C by the differential scanning calorimetry method (DSCM).

2. Methods

The ferroelectric phase transition heat was measured by the DSCM using a METTLER TA 3000 SYSTEM microcalorimeter allowing for cooling and heating samples according to the linear mode at a preset rate ($v_1=4.8$ K/min and $v_2=0.5$ K/min) within a temperature range of 100-250 K, as well as for the integration of peaks, determination of the basis line and the temperature positions of peaks in an automatic regime. The KDP single crystals having the weight $m_H=6.5\cdot10^{-2}$ g and the DKDP single crystals (containing 97.0% deuterium) with the weight $m_D=5\cdot10^{-2}$ g were used as sample; the DKDP samples containing about 70% deuterium and having the weight $m_{HD}=5.0\cdot10^{-2}$ g were utilized for control.

3. Results

The experimental values of the thermal effect parameters in the KDP and DKDP crystals are presented in the Table. In the KDP crystals with any number of thermal cycles (n=1-82) the transition heat in exoeffect (ΔH_{exo}) substantially (more than twofold) exceeds is value in the endoeffect (ΔH_{endo}).

An increase in the number of thermal cycles up to n=80 leads only to an insignificant (about 5%) narrowing of thermal peaks and to some decrease in the value of

ΔH_{exo} (Fig.1). During thermocyclation microcracks develop in crystals, which eventually leads even to a failure of the samples (the process of generation of defects).

In the DKDP crystals containing about 97% deuterium, the endoeffect magnitude exceeds that of the exoeffect until a certaqin amount of defects has been stored up in a sample–that is, during 10 to 20 initial thermal cycles (see Table, Fig.2, curve 1). Moreover, in distinction from the KDP crystals, with a large number of thermal cycles for a DKDP sample, the inversion of the absolute value of the thermal effect does occur in it, so that the transition heat in the exoeffect begins to exceed its value in the endoeffect (see Fig.2, curve 2). The DKDP crystals containing about 70% deuterium demonstrate the behavior of the transition heat, which is in many respects similar to that of the DKDP crystal with a maximum deuteration degree (see the Table; Fig.2, curves 3); yet, owing to the isotopic substitution effect, they exhibit different temperature positions of thermal peaks and somewhat lower (by about 10–20%) transition heats.

Let us note that during the thermocyclation of the KDP and DKDP (containing 97%) deuterium samples under the conditions near to the equilibrium ones – that is, at cooling and heating rates of the samples, which are lower by one order of magnitude (v_2=0.5 K/min), – there occurs a substantial decrease in the transition heat values, both in the exoeffect and in the endoeffect (Fig.3). These approach to their equilibrium values [1,2]. The temperature positions of the thermal peaks of the exoeffects and endoeffects simultaneously approach to each other, and their half widths drastical narrow. It is essential that no inversion of the absolute value of the peaks does occur in relation to the thermal peaks obtained at high heating–cooling rates.

Thus, the experimental data show that ferroelectrics with the KDP structure, whether containing deuterium or not, demonstrate completely different behaviors of the phase transition heat on the thermocyclation in the vicinity of the T_C.

In our experiments with a large number of thermal cycles we have observed a noticeable difference between the values of ΔH_{exo} and ΔH_{endo}, which in a general case is explaine by the appearance of additional "sources" of energy in the crystalline lattice of samples used (owing to the generation of defects). We assume that in the case of cooling and heating the DKDP samples with a small number of thermal cycles ($n \leq 5–10$), the corresponding transition heat values (ΔH_{exo} and ΔH_{endo}) may be presented as follows:

$$\begin{cases} -\Delta H_{exo} = -\Delta H_t + \Delta H_{pl} + \Delta H_{el} \\ +\Delta H_{endo} = +\Delta H_t + \Delta H_{pl} + \Delta H_{el} \end{cases} \quad (1)$$

where ΔH_t is the truel transition heat associated exclusively with the rebuilding of the structure of a DKDP ideal crystal; ΔH_{pl} is the plastic deformation heat released on the friction of domain walls against each other owing to an extremely low mobility of the domains in the DKDP crystal [2]; and ΔH_{el} is the heat, into which the "elastic energy" of the domain walls might transform (i.e., the energy released on the elastic interaction of the domain walls). Since the heats ΔH_{pl} and ΔH_{el} are evolved both on cooling and on heating the samples, then a positive sign is given to then in both equations of the system (1). The system of equations (1) describes qualitatively correct the behavior of the transition heat in the DKDP crystal both in the endoeffect and in the exoeffect with a small number of thermal cycles.

As the number of thermal cycles increases up to n~80, the sample is overloaded by nonequilibrium point defects and dislocations, localized on the domain boundaries [3]. As a result, the mobility of domains becomes virtually equal to zero.

Under these conditions, the plastic deformation energy ΔH_{pl}, which has earlier been released owing to the friction of domains, now must dissipate on the formation of cracks in a sample. Therefore, the sign of the value of ΔH_{pl} is reversed to minus (which means the absorption of energy). As regards the "elastic energy" of domain walls, ΔH_{el}, so its value, with a large number of thermal cycles, becomes negligibly small as compared with ΔH_{pl}, because of a strong decrease in the effective thickness of domain walls.

Taking into account the remarks thus made, with a large number of thermal cycles (n>80), the system of equations (1) transforms as follows:

$$\begin{cases} -\Delta H_{exo} = -\Delta H_t - \Delta H_{pl} \\ +\Delta H_{endo} = +\Delta H_t - \Delta H_{pl} \end{cases} \quad (2)$$

Hence, it is easy to evaluate the mean value of ΔH_{pl}, energy of plastic deformations (dielectric losses) in the DKDP crystal, which, while taking into account the tabular data, amounts to $\langle \Delta H_{pl} \rangle \simeq 0.33$ J/g. Assuming the contribution of ΔH_{pl} to the total transition heat with the

initial thermal cycles to be the same as at n>80, we obtain a solution of the system of equations (1) in relation to the value of ΔH_{el}=0.16 J/g at n=2,3. Already at n=4, the value of ΔH_{el} decreases substantially and amounts to about ΔH_{el}=0.04 J/g. At n>5, the contribution of ΔH_{el} to the transition heat becomes virtually equal to zero.

Let us note that in the first thermal cycle (n=1) the contribution of ΔH_{pl} may be neglected as compared with that of ΔH_{el}, since the crystals are virtually without defects. There, assuming at n=1 that $\Delta H_{pl} << \Delta H_{el}$, we obtained ΔH_{el}=0.17 J/g.

The values of ΔH_{pl} and ΔH_{el}, calculated from the experimental data, allow for estimating the energy of the domain wall (W') in the DKDP crystal.Since the mean size (radius) of domains in the DKDP crystal r=1000 A [1], then energy of the domain wall, which is the surface energy, amounts to $W'=\Delta H_D/S \simeq 40$ erg/cm^2 at n=2;3, where $\Delta H_D=\Delta H_{pl}+\Delta H_{el}$, while S is the total surface of all the domains in 1 g DKDP. When the number of the thermal cycles increases n>5, the value of W' somewhat decreases, and amounts to $W' \simeq 25$ erg/cm^2. The estimations of the energy of the domain walls in the DKDP crystal are quite consistent with the literature data [1,2].]

For the KDP crystals (see Table, Fig.1) the system of equations of the energy balance with any number of thermal cycles, describing the experimental results,will have the following form:

$$\begin{cases} -\Delta H_{exo} = -\Delta H_t - \Delta H_D \\ +\Delta H_{endo} = +\Delta H_t - \Delta H_D \end{cases} \qquad (3),$$

where $\Delta H_D=\Delta H_{pl}+\Delta H_{el}$ represents the energy of the domain wall, which is equal to the sum of the energies of plastic and elastic deformations. The sign "minus" before the values of ΔH_{pl} and ΔH_{el} in the system of equations (3) means that there is no evolution of the energy of plastic and elastic deformations, since the energy is consumed obviously for the rotation of domains, whose mobility in the KDP crystal is approximately by 6 orders of magnitude higher than that in the DKDP crystal [2]. This is just the cause why during 82 thermal cycles the value of ΔH_D varies but slightly - from 0.95 J/g (at n=1) to 0.73 J/g (at n=82).

In distinction from the DKDP crystal, the KDP crystal exhibits a distinctly pronounced hysteresis loop at low frequencies, owing to which the magnitude of dielectric losses, i.e. that of the electric energy of domains, transforming into heat, should be in the case of KDP substantially higher than that in the case of DKDP, which is just observed in the experiment.

Thus, the experimental data obtained with the control KDP samples indicate that on the thermocyclation of these crystals in the vicinity of T_C there is no mechanism of the evolution of the energy of elastic and plastic deformations available, whose presence has been established for the DKDP crystals. It is obvious that such a distinction in the behavior of isomorphic ferroelectric crystals is associated only with the substitution of hydrogen in the KDP crystal for deuterium in the DKDP crystal,inasmuch as other structural characteristics of these crystals are very close to each other. Yet the absence of the channel for the release of the elastic energy of domain walls in the KDP crystal cannot be explained by a purely isotopic effect, because the presence of that effect leads only to a change in the Curie point and the transition heat, and does virtually not affect the elastic characteristics of domains (with the exception of their mobility, which is not an elastic characteristic in a general sense). Therefore, it is possible to suppose that the nature of the difference in heat evolution in the DKDP and KDP crystals is associated with the special properties of deuterium nuclei in the DKDP, which are not possessed by the protons in the KDP crystal.

4.Discussion

In the earlier studies [4,5], we had detected in the DKDP crystals the generation of the products of the nuclear dd-fusion (neutrons and tritium) on the phase transition through the Curie point. In the DKDP crystalline lattice, in addition to the processes leading to the generation of neutrons and tritium, there exists a possibility of the coherent transmission of a virtual neutron from the deuterium nuclei interacting with the giant fluctuations of the density of elastic energy, to neighboring acceptor nuclei (^{39}K, ^{31}P, etc.) [6]. If such be the case, then, on the phase transition through the T_C, the total transition heat would undergo changes due to the appearance of an additional heat source in the DKDP lattice. In this case, the following exoenergetic reactions might be one of the possible heat evolution channels:

$$\Sigma Ph + d \longrightarrow p + n + {}^{39}K \longrightarrow p + {}^{40}K + q\ (7{,}80\ MeV)$$

$$\Sigma Ph + d \longrightarrow p + n + {}^{31}P \longrightarrow p + {}^{32}P + q\ (7{,}94\ MeV) \qquad (4),$$

where q=7.80 MeV and q=7.94 MeV correspond to the energy of the neutron binding in the nuclei ^{40}K and ^{32}P, respectively [7]. Now, the "splitting up" condition of a deuteron in the ΣPh+d reaction will be $E_{\Sigma Ph} > 2.22$ MeV – that is, the multiphonon excitation energy must be greater than the deuteron binding energy. The process diagram is presented in Fig.4. In our opinion, the presence of the mechanism of the evolution of the elastic energy by the domain walls in the DKDP crystals and its absence in the KDP crystals is associated just with a possibility of the nuclear reactions of the type (4) in the DKDP crystalline lattice on the splitting up of deuterons interacting with the giant fluctuations of the density of the elastic energy of domain walls, – i.e. with the coherent multiphonon excitations arising on the concentration of elastic energy in separate domains.

Now let us consider in a general form the process of interaction of the elastic energy flux with a high-disperse crystalline medium, in particular, with the system of DKDP domains. We will assume that when crystalline particles have attained a sufficiently small size (r_{crit}) and a certain energy supply rate with the pulse mechanical loading, the absorption of elastic energy becomes of a quantum character. This means that the whole portion of elastic energy to be supplied to a particle will be absorbed by each of its atoms not uniformly, but will rather be concentrated in separate microregions of particles, which we have earlier called as "supercondensates" (SC) [8,9].

For the description of elastic processes occurring inside particles, we introduce a coefficient β, which represents the portion of elastic energy, absorbed by a particle, from the whole amount of energy $E_e = \beta E_t$ to be supplied to that particle (where E_t is the total power of mechanical effect, supplied to a unit mass of crystals, or specific power applied). From the physical standpoint the coefficient β represents a probability of the excitation of a phonon subsystem in the particle subjected to the mechanical effect. For the description of the processes of concentration of elastic energy we introduce a coefficient α of the transformation of elastic energy into that of the optical phonons of the crystal lattice with a Debye frequency ω_D, the coefficient representing a probability of the excitation of phonon modes at the frequency ω_D in a particle. In the first approximation that coefficient may

also be considered as a probability of concentration of optical phonons in the SC in a particle with the size $r<r_{crit}$ ($r_{crit}\simeq 10^{-5}$ 10^{-4} cm) under the conditions of its spherically-symmetric compression. When the particles attain the size $r\leq r_{crit}$ (when the conditions are provided for the spherically-symmetric compression of particle), the elastic energy to be transmitted to the particle is transformed into the energy of phonons. The latter are concentrated toward the symmetry center of the particle in the form of a converging elastic wave [8]. This process is carried into effect when the particle ceases to be transparent for optical phonons at a frequency of ω_D - i.e., when its size diminishes to $r_{min}\leq r_{crit}$, corresponding to the condition of the parametric resonance of the system at its natural frequency of $\omega=\omega_D$ [10]:

$$r_{crit}\simeq \frac{\pi\,(v_s\cdot c)^{1/2}}{\alpha\ \omega_D} \qquad (5)$$

where v_s is the average sound velocity in a crystal, c is the light velocity, and ω_D is the Debye frequency of the given crystal. Since the motion of the converging elastic wave is known to be coherent, the concentration of the energy of optical phonons may provide supercondensate in the particle only in the case when its size $r\leq r_{crit}$.

On the basis of suggested approach the conditions for the concentration of elastic energy in the crystalline particles with the size $r<r_{crit}$, in particular, for the case of "rigid" concentration (i.e. at $E'_e\leq E_{Ph}(\omega)$, where E'_e is the giant fluctuation of the density of elastic energy, and $E_{Ph}(\omega)$ is the density of the energy of optical phonons with a frequency ω), when the value of α is close to 1, may be written as follows:

$$\left.\begin{aligned} E'_e &= \alpha^2\, E_{Ph}(\omega) \\ \alpha\, E_{Ph}(\omega)\, V &= W_s \end{aligned}\right\} \qquad (6)$$

whence $\alpha=W_s/E_{Ph}(\omega)\cdot V$, where V is the volume of a particle having radius r_{min}, and W_s is the SC energy. The energy balance of the phonons concentration process may be expressed in terms of the parameters of an elastic wave in the particle with the radius r_{min}, using the relationship (6), i.e. $E'_e=\alpha^2 E_{Ph}(\omega)$. In this case, we take

into consideration that the energy increment per unit surface of the particle with the radius r_{min} for the time $\Delta\tau$ is determined as follows [11]:

$$d W_f = 16\pi \cdot \rho \cdot V_s \cdot \omega \, d\omega \cdot a_r \, da_r \cdot r \, dr \cdot \Delta\tau \qquad (7),$$

where ρ is the crystal density; a_r is the amplitude of an elastic wave at a distance r from the surface of the particle; and ω is the frequency of the elastic wave. The increment in the total energy of phonons in the same particle of the crystal with the lattice of the NaCl type may be written in the form [12]:

$$d W_{Ph}(\omega) = \frac{3(K-1) \cdot \hbar \cdot d\omega}{(2r_o)^3} \cdot 4\pi r^2 dr \qquad (8)$$

where $\hbar$ is the Plank constant, $(2r_o)^3$ is the volume of an elementary cell, and K is the number of particles in the elementary cell (K=27). Equating the expressions (7) and (8), while taking into account the conditions (6), we obtain the following equation for the energy balance of the phonons concentration process in the particle with the radius r_{min}:

$$16\pi \rho V_s \cdot \Delta\tau \int_0^{\omega_D} \int_0^{r_o} \int_0^{r_{min}} \omega \cdot a_r \cdot r \, d\omega \, da_r \, dr = \alpha^2 \frac{3\pi \cdot (K-1)\hbar}{2r_o^3} \cdot \int_0^{r_{min}} \int_0^{\omega_D} r^2 dr \, d\omega \qquad (9)$$

where the integration over the elastic wave amplitude is carried out in the range from 0 to r_o, i.e., to the maximum possible value of the amplitude of the elastic wave in a crystal, which is equal to the lattice constant r_o. Now, the integration over the elastic wave frequency (that is, over the frequency of phonons) is carried out in the range from 0 to the maximum possible frequency of phonons in the crystal, which is equal to the Debye frequency ω_D. It is easy to show that the time interval $\Delta\tau$ in the relationships (7) and (9) amount to $\Delta\tau = \frac{16\pi^2 r_o}{\alpha \cdot V_s}$ [12], and is, in the physical sense, the time of the maximum atomic shift, i.e., the time which is required for the elastic wave to attain the particle symmetry center

(i.e., to shake loose all the atoms of the particle), at which the oscillations amplitude is maximum and, as has been indicated above, is equal to the parameter of an elementary cell, r_o.

From the energy balance condition (9), an expression is derived for a possible particle size:

$$r_{min} = \frac{\omega_D^2 \cdot (2r_o)^3 \cdot \rho \cdot r_o^3}{2\alpha \cdot (K-1)\hbar\omega_D} \qquad (10).$$

Let us note that the value of $2(K-1)\ h\ \omega_D/r_o^3$ is the equilibrium modulus of dilatation, B_o, of a crystal, which can be expressd by the terms of the energy of optical phonons in an elementary cell having the volume $V=r_o^3$ [12]:

$$B_o = \frac{2(K-1)\hbar\omega_D}{r_o^3} \qquad (11).$$

Then the expressin (10) for r_{min} may be represented in the form:

$$r_{min} = \omega_D^2 / \alpha L \quad , \quad (12)$$

where the introduced value of L is determined as:

$$L = B_o / \rho (2r_o)^3 \qquad (13).$$

Representing a combination of fundamental parameters of the crystal, the value of L (the L factor) has the sense of a limit possible specific elastic energy density concentrated in the particle under the conditions of its spherically-symmetric compression. In other words, this is the density of the energy that is required for overcoming all the Coulomb (electomagnetic) bonds in 1 g of the crystal under conditions of its spherically-symmetric compression. The consequence of that is the transition of the crystal into the state of neutron matter (e.i. degenerated neutron Fermi gas [13]) having the density of $\rho \simeq 10^{14}$ g/cm^3.

A rough estimation of the SC energy for a particle having the radius r_{min} leads to a value of $W_s \simeq 10^7$ eV. This enables us to consider the SC as a virtual electromagnetic excitation of some nucleus which is found at the center of the symmetry of a crystalline particle having the radius r_{min}. In this case, the SC energy per nucleon (W_s') may be found from the equation of state of degenerated neutron gas [13], taking into account that the pressure in the SC is determined by the L factor:

$$W_s' = \frac{3}{5}(3\pi^2)^{2/5}\frac{\hbar^{6/5}}{m_n^{3/5}}(\alpha L)^{2/5} \quad ,(14)$$

where m_n is the neutron mass.

At $r \leq r_{crit}$, it is supposed that on the SC annihilation its energy in the form of virtual γ-quanta is transmitted to the ions of a surrounding lattice. In this case, the effective process of the rupturing of bonds in a particle becomes possible only on the surface of a sphere with the radius r_{min}, surrounding the SC [8]:

$$r_{min} = c\hbar / \alpha U_o \quad , (15)$$

where U_o is the cohesive energy of the crystal. Since $0 < \alpha \leq 1$, then the expressions (12) and (15) at $\alpha \lesssim 1$ represent a quantum comminution limit of crystals exclusively under the effect of elastic forces.

From the second condition of "rigid" concentration (6), it is possible to derive an expression for the probability of the concentration of elastic energy in a particle having the size $r \leq r_{crit}$ [9]:

$$\alpha \simeq \frac{1}{\pi^{5/2}} \frac{m_n c^2}{(\hbar \omega_D)^2} (\hbar m_n)^{1/2} E_e^{1/2} \quad , (16)$$

In this case, the coefficient β, representing a portion of the elastic energy from the whole amount of the energy applied ($E_e = \beta E_t$), is expressed as follows:

$$\beta \simeq E_f \cdot V_e / E_f \cdot V = 4\pi r_{min}^2 \cdot H / 4/3\, \pi r_{min}^3 = 3H/r_{min} \quad ,(17)$$

where E_f is the average density of energy in a particle having the size r_{min}; V_e is the volume of the elastic layer in the particle; H is the layer thickness; and V is the volume of the particle.

The above relationships allow one to give a sufficiently strict description of the processes of the interaction of the elastic energy flux with a high-disperse crystalline medium. In particular, the suggested approach permits one to calculate the contribution of the elastic energy of domain walls to the total heat of the phase transition in the DKDP crystal. We assume that on the splitting up of the DKDP crystal into domains with the size of $r \simeq 1000$ Å at the ferroelectric phase transition point (really, in the vicinity of the T_C with the width $\Delta T \simeq 3K$), the elastic energy of domain walls may concentrate inside separate domains.

The process results in the creation of high-energy

fluctuations (supercondensates) inside the domains. The system of domains in the vicinity of the T_C may be considered as a system of particles subjected to the effect of the external elastic energy for short periods of time (about $10^{-9}-10^{-6}$ s), which is analogous to the dispersion of an initial crystal into particles with the size r≃1000 Å. The supplied specific power (E_t) of the process of the concentration of energy in domains with the size r≃1000 Å will be determined as $E_t=W'S'/\rho V'$, where $W'=40$ erg/cm^2 is the energy of the domain wall in the DKDP crystals; S' is the domain surface energy with the radius r; V' is the domain volume, and ρ is the density of the DKDP crystal. From the relationship (17) we determine the coefficient $\beta=3H/r=9\cdot10^{-2}$. where H≃30 Å is the thickness of the domain wall, and r=1000 Å is the average size of the domain in the DKDP crystal. The magnitude of the elastic energy of the domain walls $E_e=\beta E_t$ is determined from the relationship $E_e=9H\ W'/\rho r^2$.

From the above relationships (16) and (14) we determine the coefficient $\alpha=0.23$ and the energy of SC, $W_s'=1.8\cdot10^{-5}$ erg – that is, approximately 11 MeV/nucleon.

The quantity of SC, i.e., the number of coherent multiphonon excitions (ΣPh) arising in the DKDP domains during the phase transition, while taking into account the condition (6), – amounts to $N_s=E_e/\alpha\ W_s'=1.2\cdot10^{11}$ SC/g. transition. Assuming that the formation of one SC leads to the carrying into effect of one reaction of the type (4), we obtain the value of $\Delta Q=N_s q$ for the contribution of the elastic energy of domain walls to the total transition heat, or, taking into account the relations (14), (16) and the expression for E_e, in the general form:

$$\Delta Q = 5\pi^{3/2}\left[\frac{\hbar^9\ \omega_D^{28}}{m_n^{15}\ c^{28}\ L^4}\right]^{1/10}\cdot q\cdot\left[\frac{9\ H\ W'}{\pi\ r^2}\right]^{3/10} \qquad (18)$$

where $\omega_D=6\cdot10^{13}$Hz is the Debye frequency of the DKDP crystal; $L=2\cdot10^{33}$ erg/cm^{3}g is the value of the L factor of the DKDP crystal; q is the reaction heat (4); $\rho=2.35$ g/cm^3 is the density of the DKDP. The calculation of ΔQ with the formula (18) gives the value of ΔQ=0.15 J/g, which is fairly well consistent with the experimentally determined contribution of the elastic energy of the domain walls,

ΔH_e, to the total heat of the phase transition in the DKDP crystals.

5.Conclusions

In conclusion, we point out that the energy ΔQ is by no means none"excessive", since it does not exceed the value of the total surface energy of the domain walls in the DKDP crystal. The choice of the value of $r \simeq 1000$ Å as the domain size in the DKDP crystal, which has been used in the calculations, should be recognized as reasonable, since its estimations from the relationship (12) lead to the same value of $r_{min} \simeq 1000$ Å. It will also be essential to emphasize that in the KDP crystals the reactions of the type (4) are impossible, since no nuclei of the elements with a low neutrons bonding energy are present in them. As a result, in the case of the KDP crystals the elastic energy of the domain walls cannot be evaluted in the form of heat.

Refefences

1. Iona F., Shirane G., Ferroelectric Crystals, Pergamon Press, Oxford-London-New-York-Paris (1962).
2. Lince M., Glass A. Ferroelectrics and Analogical Materials. (in Russian), Moscow: "Mir", (1981).
3. Atreshenko L.V., Borodich M.P., Salo V.I. et al. // Inorganic Materials (in Russian), v.30, No 5, p. 661 (1994).
4. Lipson A.G., Sakov D.M., Lalinin V.B., Derjaguin B.V. // J.Tech.Phys.Lett. (in Russian), v.18, No 16, p. 90 (1992).
5. Lipson A.G., Sakov D.M., Saunin E.I. et al. // JETP, 76 (6), 1070 (1993).
6. Hagelstein P.L. // Anomalous nuclear effects in deuterium/solid systems, Ed.by S.E.Jones et al., AIP Conf.Proc., No 228, N.Y., p.734 (1991).
7. Vlasov N.A. Neutrons (in Russian), Moscow "Nauka", (1971).
8. Kuznetsov V.A., Lipson A.G., Sakov D.M., J.Phys.Chem. (in Russian), v.67, No 4, p. 782 (1993).
9. Lipson A.G., Kuznetsov V.A. // Sov.Phys.Dokl.RAN, v.332, No 2, p.172 (1993).
10. Kuznetsov V.A., Lipson A.G, Saunin E.I., Ivanova T.S. // J.Tech.Phys., (1995) (in press).
11. Landau L.D., Lifshits E.M. // Theory of Elasticity (in Russian) Moscow :Nauka" (1965).
12. Ashcroft N., Mermin N. // Solid State Physics (in Russian), Moscow "Mir" (1979).
13. Landau L.D., Lifshits E.M. // Statististical Physics (in Russian), Moscow; "Nauka" (1964).

Table.

Heat effect parameters in DKDSP and KDP crystals at V_1=4,8 K/min*)

Crystal type	Cycle number	Exoeffect (cooling)			Endoeffect (heating)		
	n	ΔH, J/g	T_m, K	$\Delta T_{1/2}$, K	ΔH, J/g	T_m, K	$\Delta T_{1/2}$, K
KDP	1	3,52±0,11	118,8	6,1	1,63±0,05	124,4	2,4
	2	4,10±0,12	119,3	6,0	1,80±0,06	124,4	2,8
	.						
	.						
	81	3,10±0,10	119,0	5,0	1,88±0,06	124,0	2,5
	82	3,24±0,10	119,5	6,0	1,61±0,05	124,1	2,4
DKDP	1	5,90±0,10	216,3	3,1	6,25±0,12	218,1	2,5
(97%)	2	5,43±0,16	216,3	3,2	6,41±0,19	218,1	2,5
	3	5,62±0,17	215,8	3,3	6,60±0,23	218,7	2,6
	4	5,69±0,12	215,8	3,2	6,43±0,15	218,5	2,5
	.						
	.						
	81	6,27±0,19	214,8	3,9	5,56±0,17	219,3	3,0
	82	6,10±0,18	214,9	4,0	5,49±0,18	219,3	2,8
DKDP	1	4,68±0,11	200,1	6,5	4,95±0,12	206,9	4,3
(70%)	2	4,30±0,13	200,4	6,3	5,11±0,15	206,9	4,2

*) ΔH – experimental value of the phase transition heat;
T_m – temperature position of the peak's maximum
$\Delta T_{1/2}$ – halfwidth of the peak

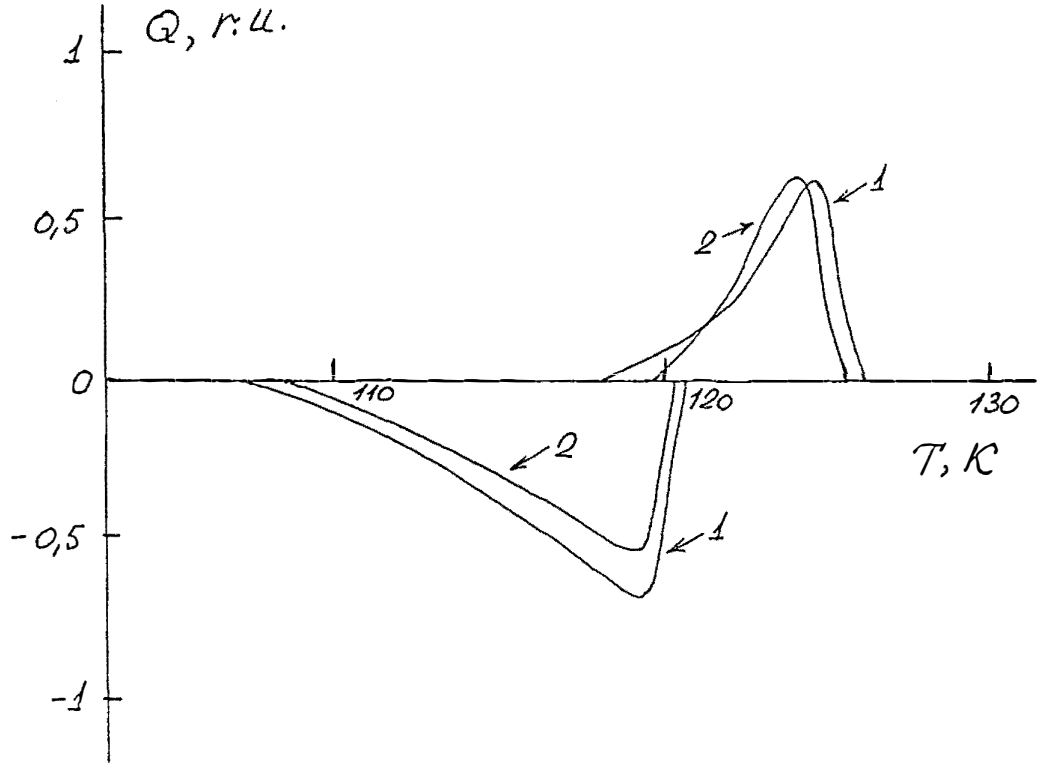

Fig.1. Heat effect kinetics on the phase transition in KDP crystals: 1 – cycle 2; 2 – cycle 82; v_1 4,8 K/min.

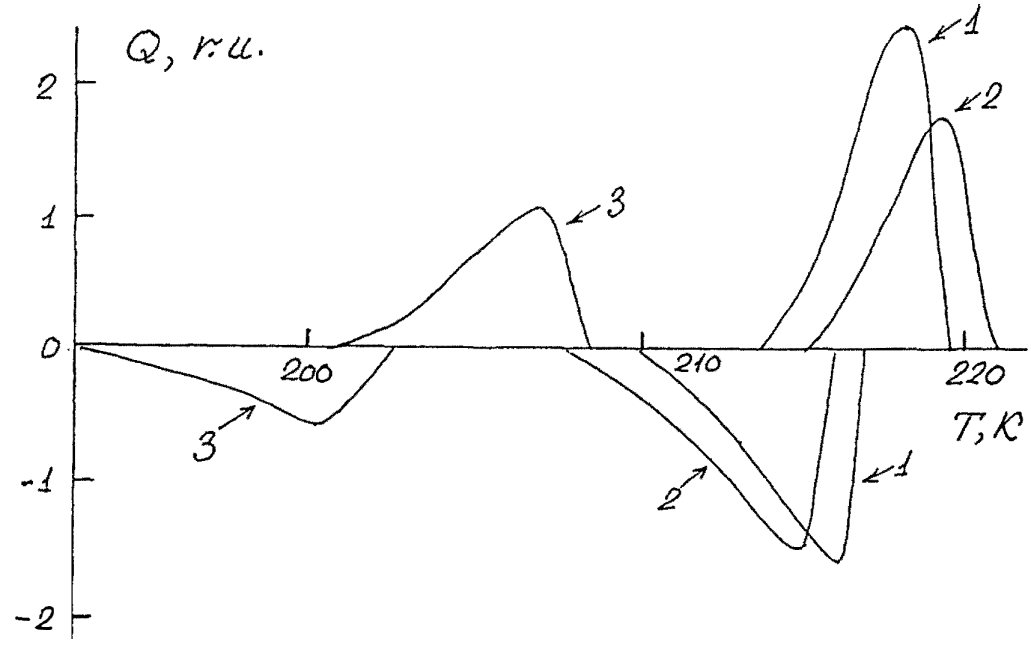

Fig.2. Heat effect kinetics on the phase transition in DKDP crystals:
1 – (97 % deuterium), cycle 2;
2 – (97 % deuterium), cycle 82;
3 – (70 % deuterium), cycle 2; v_1=4,8 K/min.

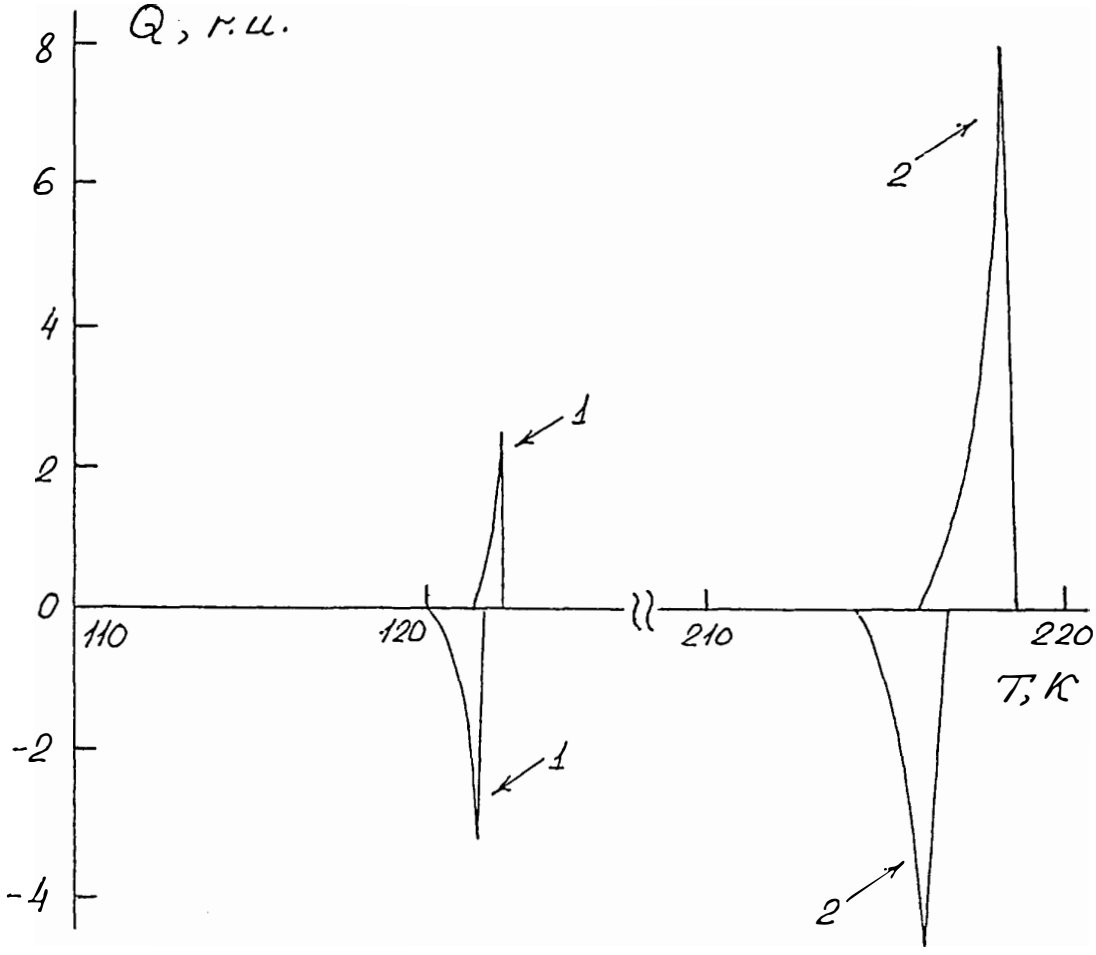

Fig.3. Heat effect kinetiks on the phase transition in KDP crystals at n=3 (curve 1) and in DKDP crystals at n=3 (curve 2); v_2=0,5 K/min.

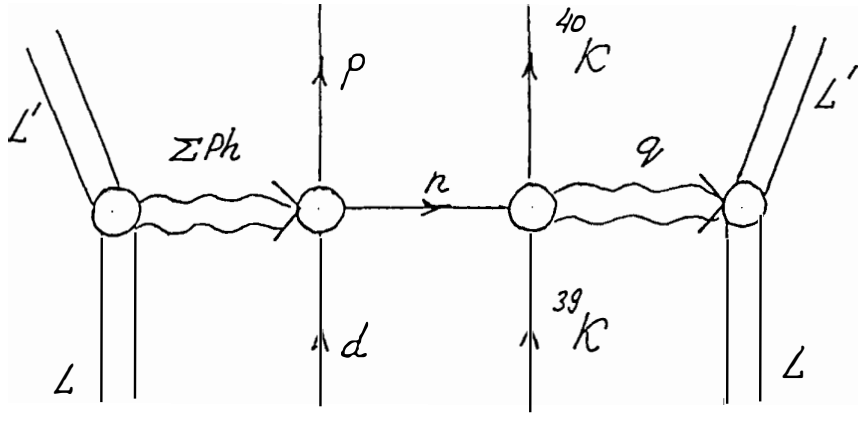

Fig.4. Feynman – like diagram for the proposed coherent production (the evolution of domain walls elastic energy) in DKDP crystal, which is responsible for reaction (4): L and L' – DKDP domain in non-excited and excited state respectively.

Fifth International Conference on Cold Fusion
9-13 April, 1995 - Monte Carlo, Monaco
ICCF5 ©1995

Possible Observation of the First Excited State of He^4 NucleusAccording to the γ-Emission Data in KD_2PO_4 Crystals upon Transition through Curie Point

A.G.Lipson, I.I.Bardyshev, D.M.Sakov

Institute of Physical Chemistry Russian Academy of Sciences,
31 Leninsky prospect 117915 Moscow, Russia

Abstract

The spectrum of γ-radiation (in the range of 3.0-8.5 MeV), generated by KD_2PO_4 crystals on the phase transition through Curie point, was studied by the use of a semiconductor, low-background detector. The maximum γ-radiation with the energy of 4.1±0.3 MeV and the width Γ=0.6±0.4 was detected. The maximum has been recorded in the course of the ferroelectric phase transition on KD_2PO_4 single crystals, and proves the decay of the first excited state of He^4 nucleus.

1. Introduction

Recently, in studies [1-4] an approach has been developed, permitting interpretation of the observable reaction of nuclear fusion in deuterated solids from the standpoint of the transfer of the energy of optical phonons of crystalline lattice (multiphonon excitations) directly to deuterium nuclei.

In particular, J.Schwinger et.al. [1,4] have examined a hypothetical possibility of the formation of the first excited state of He^4 as a result of the transfer of a multiphonon excitation with total energy E≥4 MeV to a compound He^4 nucleus which has been formed on the collision of accelerated deuterons in a nonequilibrium crystalline lattice. It has also been noted that the reactions of such a type are impossible on collisions of free deuterons, taking place in hot plasma or in a vacuum (on accelerants), since in such processes there does not exist a mechanism that could be able to provide excess energy of about 4 MeV for transferring the compound He^4 nucleus from the ground to first excited state ($j_p=0^+$, T=0), localized by 20.1 MeV higher than the ground state. The first excited state of He^4 is stable in relation to the decay along the He^3+n channel (situated below the threshold of that channel, which is equal to 20.578 MeV), but is unstable with regard to the decay along the T^3+p channel (19.875 MeV). Hence, that supposition could explain the asymmetry of the channels of solid-state dd-fusion which is predominantly of neutron-free character, simultaneously generating considerable amounts

of T^3. If this hypothesis were true, then rigid γ-quantums with energy E≃4 MeV, forming during the decay of the first excited state of He^4 along T^3+p channel, should be observed in nonequilibrium deuterated solids, in particular, on the controllable phase transitions that is, on the removal of excitation according to the scheme:

$$Ph + [d+d] \dashrightarrow {}^4He^* \dashrightarrow {}^3T + p + \gamma(4.0\ MeV)$$

In the present work, for the purpose of verification of the above hypothesis strict spectral measurements of γ-emission in KD_2PO_4 (DKDP) single crystal have been performed, upon a ferroelectric phase transition in the range of the energy of γ-quanta of 3.0–8.5 MeV.

2. Methods

To this aim KD_2PO_4 single crystals were used, grown from a solution of D_2O (contained 97.0%±1.0% deuterium), in which we had earlier observed the generation of neutrons and tritium on transition through T_C≃221 [5,6]. In total, 7 crystalline plates cut out from one single block in the (001) direction were used. In connection with a fairly rapid degradation of DKDP single crystals during thermocyclization, the average number of thermal cycles per crystal proved to be up to 15 [6]. The crystal were placed into a brass cryostat having walls 20 mm thick (h≃20 mm) [6]. They were cooled (or heated) in the linear regime at a rate of 0.1 K/s in the temperature range of 212–222 K, in which the maximums of the heat of ferroelectric transition had been localized according to the data of differential-scanning calorimetry. A semiconductor, coaxial, low-background HP Ge-detector GEM-20180-P (EG & G ORTEC), made on the basis of a high-purity germanium crystal with dimansions 50.7[64.4 mm having the energy resolution FWHM=1.73 KeV and the proper efficiency of 25% at the energy of γ-quata equal to 1.33 MeV (Co^{60}), was applied to record γ-quanta. The schematic diagram of the experimental setup for registration of γ-quanta is presented in Fig.1. The γ-background of the setup, to be measured before the beginning of the experiments, between these, and after their completion, reveals numerous γ-lines of radionuclides as contained in the surrounding medium, whose energy is within the range of 0.1–2.6 MeV. In the working range E≥3.0 MeV, the detector background is uniform on the scale of energies, and does not contain γ-lines. The detector was calibrated using a standard Na^{22} (γ-lines of 0.511 MeV and 1.27 MeV). While accounting for the energies, γ-quanta to be recorded, and the geometry of the setup employed, the total efficiency of the detector in the range of 3.0–8.5 MeV amounted to $3.1 \cdot 10^{-3}$–$1.9 \cdot 10^{-3}$.

3. Results

The recording of γ-quanta during thermocyclization of crystals in the temperature ranges localized outside the ΔT range corresponding to the phase transition ($T<<T_C$ and $T>>T_C$), was resorted to as control experiments. In total 100 temperature cycles (transitions through T_C) were performed on 7 crystals cut out from a single monoblock. The energy distribution of γ-quanta in the control experiments is well described (Fig.2, curve 1) by the distribution of the cosmic background of the detector, to be recorded in large time intervals (Fig.2, curve 2). Now, using the DKDP samples in the range of ΔT=212-222 K the values were obtained exceeding the background of the control experiments. The exesses in intensity are especially distinctly expressed in the range of 3.5-4.5 MeV and less distinctly in the range of 6.0-7.0 MeV (Fig.2, curve 3). In Fig. 3, the results are presented of subtraction of the data on curve 1 from these on curve 3. The parameters of the excess estimations over the background (so-called peaks) are given in Table 1. Note that excess estimations over the background of control measurements within the range of 3.5-4.5 MeV were observed for all 7 DKDP crystals used, which is especially well discernible during the first 10 cycles. Then the emission of γ-quanta would cease, which is associated with the degradation of crystals (cracking). (Similar degradation effects were also noted in [6] when measuring the emission of neutrons). On the basis of the statistics thus obtained the position of peak I (about 3.5-4.5 MeV and its width are determined as E_1=4.1±0.3 MeV and Γ_I=0.6±0.3 MeV, respectively. For peak II (6.0-7.0 MeV) these values are E_{II}=6.7±0.3 MeV and Γ_{II}0.5±0.4 MeV, respectivelly. The data on the position of peak E_I and width Γ_I to a sufficientl degree correspond to a possible position of γ-peak, which is likely to be observed on the decay of the first excited state of He^4 (E=4.1 MeV, Γ=0.6 MeV).

The appearance of wide intensity maxima in the rigid part of γ-spectrum (E>3 MeV) cannot be explained by the presence of radionuclides in the medium in the course of measurements, since, as has alredy been pointed out above, the range of γ-radiation of the given radionuclides corresponds to energy E<2.6 MeV. Moreover, the presence of radionuclides in the medium is not at all associated with the ferroelectric phase transition in the DKDP crystals, and, therfore, the γ-emission as caused by the radionuclides, should be revealed in the control experiments, too.

Another possible source of rigid γ-radiation could be

a nonelastic scattering of rapid background neutrons in the lead protection and a DKDP crystal during the ferroelectric phase transition [7]. For the purpose of verifying this supposition, we have exposed a cryostat-detector system (Fig.1) to irradiation by Cf^{252} source of neutrons (at an intensity $I=3\cdot10^{2}$ n/s in 4π), and repeated the control experiments with the thermocyclization of DKDP crystals in the vicinity of T_C.

The measurements have shown that in the range of 3.0–7.0 MeV already in the control experiments there is recorded a considerable increase in background counts (by a factor of 3–5) as compared to the background data obtained without the use of a neutrons source (Table 1). Now, in the energy range $\Delta E\simeq3.5\div4.5$ MeV during thermocyclization in the vicinity of T_C the excess value above the background of control experiments is retained, and its absolute value approximately coincides ($n_\gamma=2.10\pm0,51$ γ/s) with that of intensity, which has been obtained in the experiments carried out without a neutrons source. At the same time, the intensity of peak II, localised in the range of 6.0–7.0 MeV, becomes comparable to the background level of control experiment.

4.Discussions

The eperiments with the exposition of DKDP crystals to the irradiation from a Cf^{252} neutrons source, having a wide energy spectrum from kT to 10 MeV ($E_m=2.3$ MeV), enable one to reach conclusion that the appearance of the maximum of intensity of γ-counts within the range of 3.5 to 4.5 MeV on the phase transition through T_C is not at all conected with γ-radiation of inelastic scattering and capturing of background neutrons, whereas the maximum II in the range of 6.0–7.0 MeV should possibilly be attributed to that process [8]. From the aforesaid and the supposition on the collective transfer of the energy of phonons to the compound nucleus of He^4 ($E_\gamma=4.1$ MeV), it is possible to come to a conclusion that the decay of the first excited state of the nucleus of He^4 ($E_\gamma=4.1$ MeV) does actually correspond to the maximum in the range of 3.5–4.5 MeV. In this case, the excitation, can be provided due to the concentration of the energy of optical phonons generated in the course of the ferroelectric phase transition. Elementary estimations show that with an average domain size in the DKDP crystal equal to about $2\cdot10^{-5}$ cm [9] and at the Debye frequency $\omega_D\simeq8\cdot10^{13}$ Hz [10], the total energy of optical phonons in one domain during a phase transition amounts to $E_{ph}\sim5$–10 MeV, which

is sufficient for creation of the first exited state of He^4. If the energy of the domain wall in the DKDP crystal $W_d \simeq 40$ erg/cm^2 and its thickness $h \simeq 10$ Å corresponding to the depth of an elastic layer [9] were taken into account, then the energy of one domain at the moment of the ferroelectric transition would amount to $\Delta E = 5 \cdot 10^{-8}$ erg. Since the total number of domains $N = 1.1 \cdot 10^{14}$ g^{-1}, then the total energy of the domain wall per unit mass of DKDP will be equal to $\Sigma(\Delta E_I)_{i=1}^{N} = 5.4 \cdot 10^6$ erg/g. The elastic portion of the energy of the domain wall is determined as the ratio of the volume of the elastic layer to the volume of the whole domain $\beta \simeq 6 \cdot 10^{-2}$, whence $\Delta E_d = 3.3 \cdot 10^5$ erg.g. Therefore, the number of gigantic phonon fluctuations (N_s) with energy $W_s \simeq 10$ MeV, which are possible during the ferroelectric transition, will amount in the first approximation to $N_s = \Delta E_{el}/E_{ph} = 1.5 \cdot 10^{10}$ g^{-1} with an yield of γ (4.1 MeV)- quanta $n_\gamma = 2 \cdot 10^2$ /transition

To ensure the process of the formution of the compound nucleus of He^4 requires the approaching of two deuterons to each other, for the purpose of the overcoming the Coulomb barrier, which can be guarunted through acceleration of deuterons in the DKDP crystalline lattice on its repolarization (on transition through T_C) up to the energy of about 200 eV [11].

5.Conclusions

Thus, this study enabled us to substantiate the hypothesis on a possibility of the population of the first excited state of He^4 in nonequilibrium, deuterated solids. Note, however, that the decay of He^4 according to the T+p scheme cannot, probably, serve as the main tritium generation channel in the DKDP on the ferroelectric phase transition, since the really produced tritium concentrations are by 5 to 6 orders of magnitude higher (10^7-10^8/transition) [6].

References

1. Schwinger J. // Zeitschrift Fur Naturforschung v.45, N 5, p.756 (1990).
2. Schwinger J. // Proc.Natl. Acad.Sci. v.87, p.8370-8372 (1990).
3. Schwinger J. // Progr.Theor.Phys., v.85, N 4, p.711-712 (1991).
4. Takahashi H. // Anamalous nuclear effects in deuterium/solid systems. Ed. by S.E.Jones et.al. AIP Conf.Proc N 228, New York p.884-893.

5. Lipson A.G., Sakov D.M., Kalinin V.B., Derjaguin B.V. // J. Tech.Phys.Lett. (in Russian), v.18, No 16, p.90-95 (1992).
6. Lipson A.G., Sakov D.M., Saunin E.I. et.al. // JETP , v.76 (6), p.1070-1076 (1993).
7. Vlasov N.A. Neutrons (in Russian) Moscow, Nauka. (1971).
8. Alexandrov D.V. Nicolsky E.U., Novatsky et.al. // J. Exp.& Theor.Phys.Lett. (in Russian) v.59, N 5, p.301-304 (1994).
9. Iona F., Shirane D. Ferroelectric Crystals (in Russian) Moscow, Mir, (1965).
10. Lince M., Glass A. Ferroelectrics and Analogical Materials (in Russian) Moscow, Mir, (1981).
11. Derjaguin B.V., Andriankin e.I., Lipson A.G. et.al // Doclady Academii Nauk (in Russian) v.334, N 3, p.291-295 (1994).

Table1.
The parameters of the ranges featuring excess above the background level and shown in Fig.3.

ΔE (MeV)	$N_b \cdot 10^{-2}$ (count/s)	$N_b \cdot 10^{-2}$ (count/s) with Cf^{252} source	n_γ (γ/s)	n_γ (γ/s) with Cf^{252} source
3.5-4.5	1.51±0.12	5.62±0.65	2.43±0.40	2.10±0.51
6.0-7.0	1.20±0.09	2.58±0.90	1.25±0.32	0.20±0.32

where N_b is the number of background counts in the control experiments and n_γ is the intensity of the γ-radiation on subtracting the background of the control experiments, taking into account the efficiency of the detector.

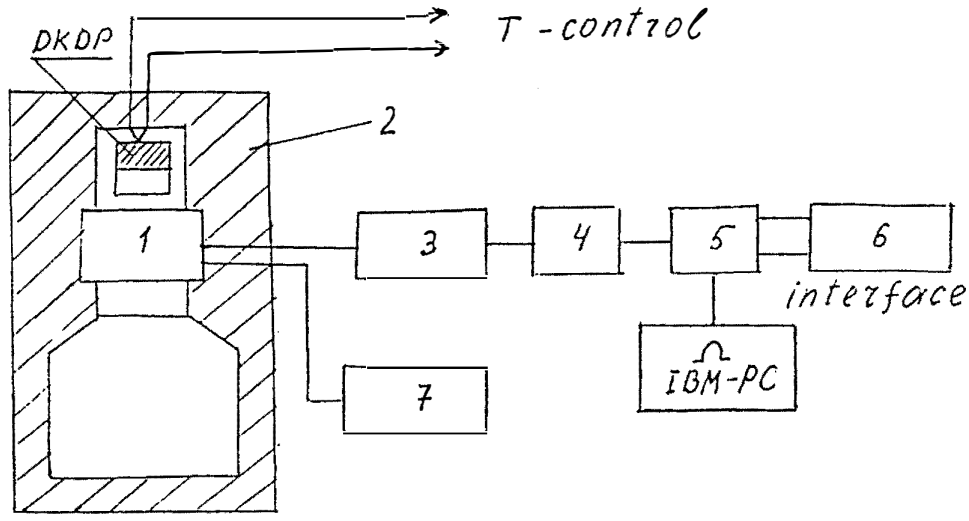

Fig.1. Shcematic diagram of the experimental setup for monitoring the emission of γ-quanta.

Key: (1) Ge-detector; (2) lead protection; (3) preamplifier; (4) amplifier together with a discriminator; (5) multichannel analyzer; (6) stabilizator; (7) high-voltage supply; (8) IBM computer.

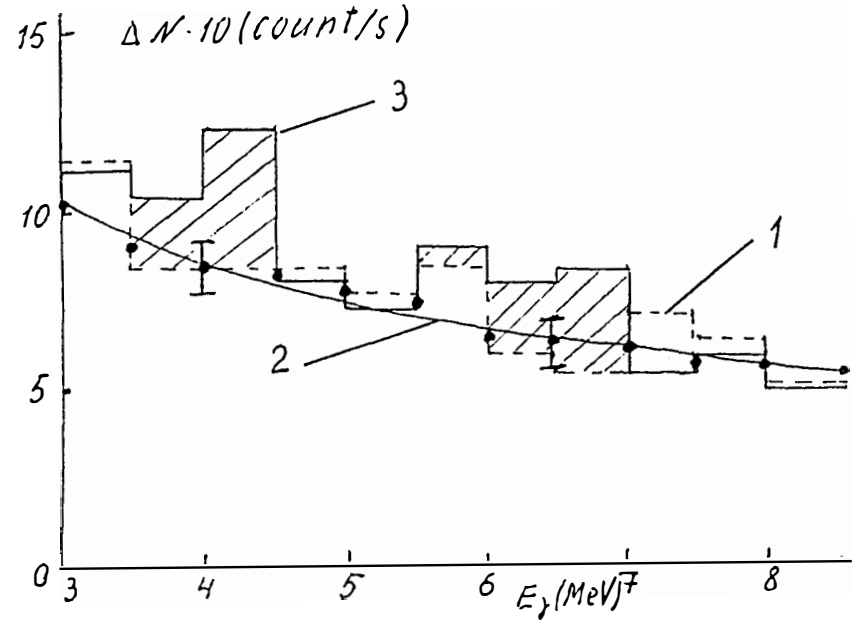

Fig.2. Energy distribution of γ-quanta as recorded: (1) in the control experiments (curve 2) during thermocyclization of DKDP crystals in the ranges $T<<T_C$ and $T>>T_C$. The exposure time E_τ=9461 s; (2) at T=300 K (the total exposure time $\tau=10^5$s); (3) during thermocyclization of the DKDP in the vicinity of T_C (in the range ΔT=212-222 K) $\Sigma\tau$=9461 s (100 transitions through Curie point (T_C)).

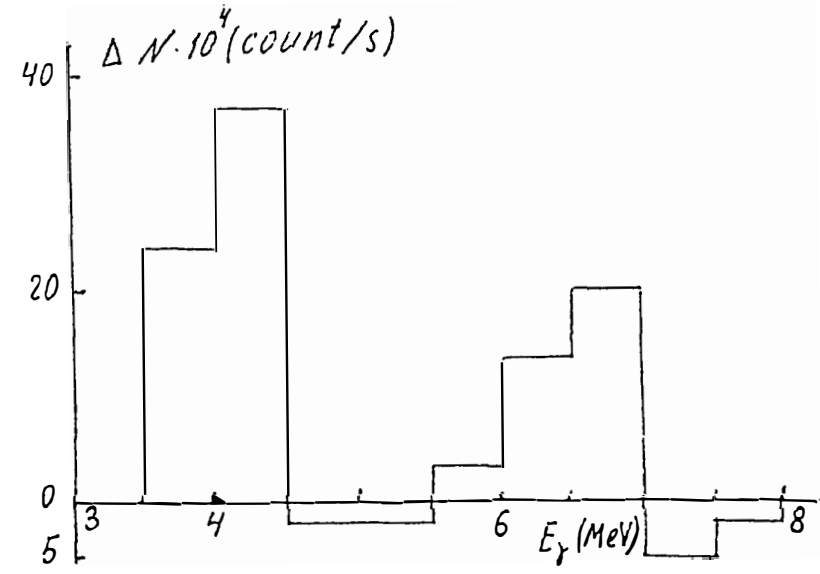

Fig.3. Result of subtracting curve 3 and 1, represented in Fig.2.

Fifth International Conference on Cold Fusion
9-13 April, 1995 - Monte Carlo, Monaco
ICCF5 ©1995

Amplification of the neutron flux transmitted through KD_2PO_4 single crystal at the ferroelectric phase transition state

A.G.Lipson and D.M.Sakov

Institute of Physical Chemistry
of the Russian Academy of Sciences,
31 Leninsky prospect, Moscow 117915 Russia

Abstract

The phenomenon of external neutron flux amplification (about 10% from total value) emitted from Cf^{252} neutron source ($I=3\cdot10^2$ n/s in 4π), than partialy moderated by use of polyethylene (Co) and transmitted through the KD_2PO_4 (DKDP) single crystal being at the ferroelectric phase transition state has been obtained. If DKDP crystal was out of the phase transition temperature interval upon the transmission of neutron flux through it, then amplification effect was not observed. The variation of excess neutron emission intensity ejected by DKDP crystal at the different detector's background level has been studied. The intensity of neutron emission (after subtraction of the background) is increased from 0.01 count/s at cosmic background level (0.01 count/s) to 0.20 count/s at 1.1 count/s background level of detector (with Cf^{252}). The dependence of count's rate of neutron events on the efficiency in DKDP crystal-detector system has been investigated too. It was determined the correlation between the value of external neutron flux transmitted through the DKDP crystal and intensity of excess neutron emission from this crystal. The non-isotropic distribution of excess neutron emission from DKDP crystals has been established. The data obtained for DKDP crystals irradiated by external neutron flux upon the ferroelectric phase transition could be the confirmation for next hypothesis: "cold fusion" neutron emission is induced by external irradiation of cold fusion objects by the cosmic background neutrons.

I. Introduction

Earlier in our works, it has been detected that on the phase transformations of the ferroelectric-paraelectric type, occurring on the transition of KD_2PO_4 single crystals through the Curie point, the generation of neutrons is observed at an intensity exceeding by 2-3 times the natural neutron background of the setup [1,2]. In these experiments, however, the reproducibility of the results even with controllable, (without defects) crystals did not exceed

90%. In most other works involving the observation of the nuclear dd-fusion reactions in nonequilibrium, deuterated solids, the reproducibility of the results was much worse [3-6]. In this connection, the question on the reality of the dd-fusion reactions in the crystalline lattice, and in particular, on the emission of neutrons, whose occurrence is considered as a direct confirmation of the $d(d,He^3)n$ reaction, remains so far open. In fact, the neutron effects in deuterated solids, in distinction from the effect of the generation of neutrons in an usual dd-reaction (in hot plasma, on accelerators, during the fission of heavy elements, etc.), exhibit a number of peculiar features that do not permit to a full extent consider them as the manifestation of the usual emission of neutrons [7,8]:

(a) the emission of neutrons is unsteady; it has the form of fluctuations, involving increases in the neutron activity of a sample for short periods of time [3-6];

(b) in most long-time experiments the signal-to-background ration did not exceed 2-3 [3-8];

(c) there is no distinctly pronounced dependence of the intensity of the emission of neutrons on the mass of the sample [2-5];

(d) and finally, what is the main feature, the absolute intensity of the "effect" (the count of neutrons with the subtraction of the background), depends on the background level and the efficiency of the neutrons detector: the lower background level leads to the lower absolute intensity of the "effect"; and the higher detector efficiency leads to the lower "effect" value [3].

The most important is the feature (d), since logically, with the hypothetically zero level of the cosmic neutron background, the intensity of neutron emission should tend to zero. In this connection, a question arises as to whether the emission of neutrons in the aforisaid experiments is a property inherent to deuterated solids that are in an essentially nonequilibrium state (the dd-fusion proper), or whether the secondary neutrons are registrated, generated by "seed" neutrons of the cosmic background, interacting with deuterium in the crystalline lattice? In such a case, the non-reproducibility of the results on the emission of neutrons (in addition to purely material-science aspects) will be connected with the non-reproducibility of the cosmic background-that is, with the probability of the appearance of a cosmic neutron in the same space region, in which the sample is found during the experiment.

For the purpose of veryfying that hypothesis, we have carried out experiments on the irradiation by an external source of the neutrons of deuterated KD_2PO_4 sample, being emitted own neutrons throughout the entire temperature

range ΔT=212–222 K, corresponding to the ferroelectric transition [1,2].

2. Methods

We have utilized the DKDP single-crystal samples that had been well studied in our foregoing works. The samples in the form of plates were cut out from a single monoblock oriented in the (001) direction, having a weight of 15 g, in such a way that their cross-section be equal to 1 cm^2 with a thickness h=2 mm. The samples were placed into a brass cryostat cooled down to a temperature of 100 K, and then heated up in the linear regime at a rate of 0.1 K/s. Neutrons were detected in temperature ranges outside T_C: $T<<T_C$ and $T>>T_C$ (control experiments), as well as in the temperature range of 212–222 K, corresponding to the ferroelectric phase transition, in accordance with the measurements of the transition heat by the DSK-method.

The effect for DKDP samples within the temperature range of 212–222 K for 20 passes through T_C was found to amount (with the subtraction of the cosmic background) to $\Delta N=(6.0\pm1.3)\cdot10^{-3}$ count/sec, or to $\Delta I=0.56\pm0.14$ n/s; while taking into account the detector efficiency with the cosmic background $N_b=0.12\pm0.004$ count/s. The count rate of neutrons in the ranges of $T<<T_C$ and $T>>T_C$ during the thermocycling of the samples would also correspond to that background level. In the experiments on the external irradiation of a DKDP crystal, Cf^{252}-source of neutrons (E_{max}=2.3 MeV) [9] with an intensity of 300 n/s in 4π angle was used. The neutrons source was placed at the center of a lead capsule 4 cm in diameter (Fig.1). The changes in the background level and the detector efficiency were varied by changing the distance in the source-detector system. For the purpose of varying the detection efficiency in the crystal-detector system, the crystal-detector and the source-crystal distance were also varied. In some cases, the source (detector) was shielded by means of standard polyethylene "neutrostop" (Co) blocks, in order to diminish the background (Fig.1). In connection with a rather rapid degradation of DKDP, only 20 transitions through the T_C were made for the purpose of determining the intensity of neutron events at one detector background value, N_b, (or at one fixed source-crystal distance). Then the DKDP crystal was replaced by a new one.

3. Results

The experiments have shown that on the transmission of the neutron flux (from the Cf^{252}-source of neutrons)

through the cryocell with a DKDP crystal, in the process of the ferroelectric phase transition there is observed a real enhancement of the neutron flux (depending on the efficiency of the crystal-detector system). At $N_b/N_{b.c.}=100$, that amplification of the neutron flux may amount to about 10% of the intensity of the source proper ($\Delta I_{max}=29.5\pm2.7$ n/s in 4π). In such a case, the maximum value of the absolute effect increases by about 50 times as compared with the effect magnitude observable under the conditions of the cosmic background (Fig.2, curve 2), whereas the value ΔN (without taking into account E) increases only by a factor of 20 (Fig.2, curve 1). Now, no changes of the source count rate have been recorded in the same geometry in the temperature ranges lying outside the T_C. It has also been found that the intensity of counting neutron events in the given systems strongly depends on the source-crystal distance (with one and the same value of E in the crystal-detector system). In this case, a sharp increase in ΔN is observed for the neutrons cross the DKDP crystal with the range of 0 to 10 n/transition. Then the value of ΔN is stabilized in the range of $10<n_c<80$ (Fig.3). The dependence of the ΔN on the source-crystal distance indicates on the correlation between the external flux of neutrons crossed the crystal and the intensity of the excess emission of neutrons (ΔI) from the crystal. Moreover, the form of the function ΔI (E) indicates on the nonisotropic distribution of the neutron flux, as generated by the DKDP crystal exposed to the external flux of neutrons (Fig.4). In fact, at $E=1.0\cdot10^{-3}$, the value of the excess emission of neutrons, ΔI, is rather small, since the crystal is remote at a considerable distance from the detector; and therefore, the flux of neutrons as generated by the crystal cannot make a considerable contribution to the change in the count rate of the Cf^{252}-source. Now, the values of ΔN_b at the points $E=3.3\cdot10^{-3}$ and $E=1.1\cdot10^{-2}$, prove to be approximately equal, in spite of different crystal-detector distances, what cannot be attained with the isotropic distribution of neutrons (the Cf^{252}-source itself may serve as an example). The obtained dependence of ΔI (E) can be naturally explained only in the case, where we suppose that the main flux of neutrons from the crystal is directed according to a taper perpendicular to the detector surface, but not distributed in spherical symmetry 4π-angle.

4. Discussions

The dependences of the count rates of neutron events for DKDP crystals exposed to the external neutron flux

during the phase transition through the T_C confirm a hypothesis on the generation of neutrons in deuterated solids as secondary neutrons initiated by the cosmic neutron background. In fact, the absolute value of the "effect" proves to be strongly connected with the background level of the detector (Fig.2). The magnitude of the effect increases with the background level (within the range of 1 to 100), and depends in the nonlinear way on the detector efficiency (in the detector–crystal system), because of the nonisotropy of the distribution of secondary neutrons. In principle, another variant could have been suggested to explain the observed effects, which is not connected with the multiplying of background neutrons. It may be determined by the transformation of the spectrum of neutrons from the Cf^{252}–source, as a result of their moderation to energies of about kT in polyethylene walls of a measuring chamber (Fig.1). In such a case, part of neutrons emitted by the source and moderated to an energy of kT do not get into the detector, becouse it is coated by a Cd–foil. If we suppose that during the pass through the T_C the phonons of the DKDP lattice do scatter thermal neutrons as the energy of the latter increases above 0.1 eV, then such neutrons would be able to overcome the cadmium protection. However, no dependence of ΔN on the source–detector distance should be observed in the measurement geometry, since the density of the flux of thermal neutrons is constant throughout the whole volume of the measurement chamber. Therfore, that variant is not suitable for explaining the effect.

The obtained results prove that a decrease in the cosmic background would also lead to a decrease in the magnitude of the effect. They also permit one to suppose that the main portion of the emitted neutrons in the experiments on the initiation of nuclear reactions in deuterated solids is associated with the registration of the secondary neutrons generated by "seed" (background) neutrons in crystal [10].

At present, the mechanism of the generation of secondary neutrons is still far from being elucidated. In our opinion, however, one of the possible models may be related to an injection into the DKDP crystal (in the state of a phase transition), of thermal neutrons that will stay therein for a considerable length of time, $\Delta\tau \sim 10^{-4} - 10^{-5}$ sec. During the time $\Delta\tau$, a thermal neutron diffusing into the crystal can obtain many times a portion of excess kinetic energy (from 5 to 10 MeV) from the multiphonon excitations [11] induced, when the elastic energy is released by the domain wall during the ferroelectric phase transition. In such a case, one neutron during the time $\Delta\tau$ can many times interact with several deuterons ($n+d \int p+2n$), thus generating a cascade

of secondary neutrons possessing energy of several MeV. The birth of secondary neutrons will cease after the thermal neutron will have left the crystal. Let us note that short-time bursts of the emission of the neutrons of short duration will be observed in the process described, the duration being comparable to the time $\Delta\tau$ [3-6].

The nonisotropy of the distribution of neutrons emitted on the ferroelectric transition, is, in our view, associated with the crosswise polarization of the crystal-target (oriented DKDP), that leads to an azimuthal asymmetry of the differential cross-section of deuterons in the reaction of generation of secondary neutrons [9].

5. Conclusion

To understand the mechanism of the "secondary emission" of neutrons requires making further investigations, including the application of the time-distribution of neutron pulses and the monochromatic sources of neutrons with different energy values.

References

1. A.G.Lipson, D.M.Sakov, V.B.Kalinin et.al // Sov.Tech. Phys.Lett. v.18(16), p.90-95 (1992).
2. A.G.Lipson, D.M.Sakov, E.I.Saunin et.al // JETP 76 (6) p.1070-1076 (1993).
3& S.E.Jones, E.P.Palmer, J.B.Czirr et.al. // Nature v.338,p.737-740 (1989); S.E.Jones Proc of ICCF-4 6-9 December 1993, Maui, Hawaii, USA.
4& B.V.Derjaguin, A.G.Lipson, V.A.Kluev et. al. // Nature v.341, p.492 (1989).
5& A. De Ninno, A.Frattolillo, G.Lollobatista et.al. // Europhys Lett. v.9, p. 229-232 (1989).
6& H.O.Menlove, M.M.Fowler, E.Garcia et.al. // J.Fusion Energy v.9(4), p.495-506 (1990).
7. D.R.O.Morrison // Uspeckhi fisitcheskih nauk, 161(12) p.127-140 (1991).
8. V.A.Tsarev // Uspeckhi fisitcheskih nauk, 162 (10) p.63-92 (1992).
9. N.A.Vlasov. Neutrons. Moscow, "Nauka", p 552, (1971).
10. H.Kozima // Nuovo Cimento 27A, p. 1781 (1994).
11& P.L.Hagelstein In: Anamalous nuclear effects in deuterium/solid systems, Ed. by S.E.Jones et.al., AIP Conf. Proc. N 228, N.Y., p.734-778 (1991).

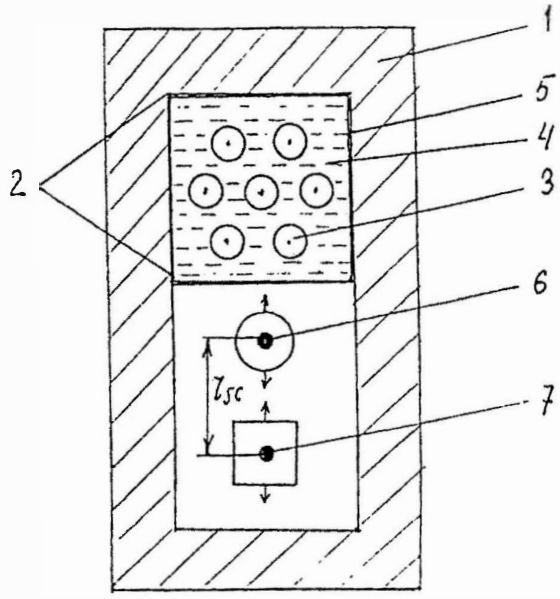

Fig.1. Schematic diagram of the experimental setup.

Key: 1. Polyethylene (Co); 2. detector; 3. counters; 4. silicone oil; 5. Cd-foil; 6. cryostat with a DKDP crystal; 7. Cf^{252}-source of neutrons.

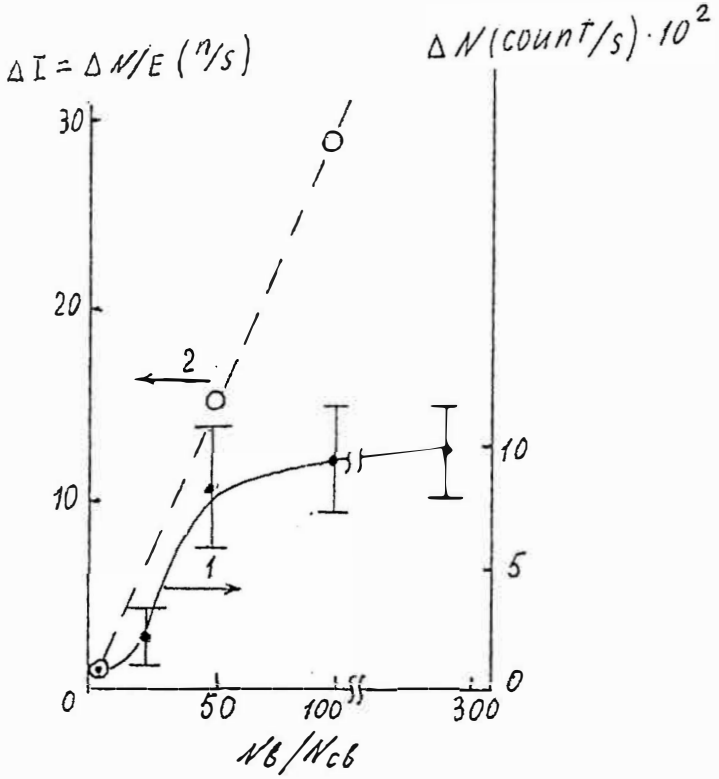

Fig.2. Dependence of the intensity of the emission of neutrons (with the subtraction of the source background) emitted by the DKDP crystal on the ferroelectric transition, on the relative value of the detector background, $N_b/N_{b.c.}$ (the source-crystal distance has been fixed, and is equal to r=6 cm) without taking into account the efficiency E in the crystal-detector system (curve 1); while taking into account E in the assumption on the 4π-distribution of neutrons (curve 2)

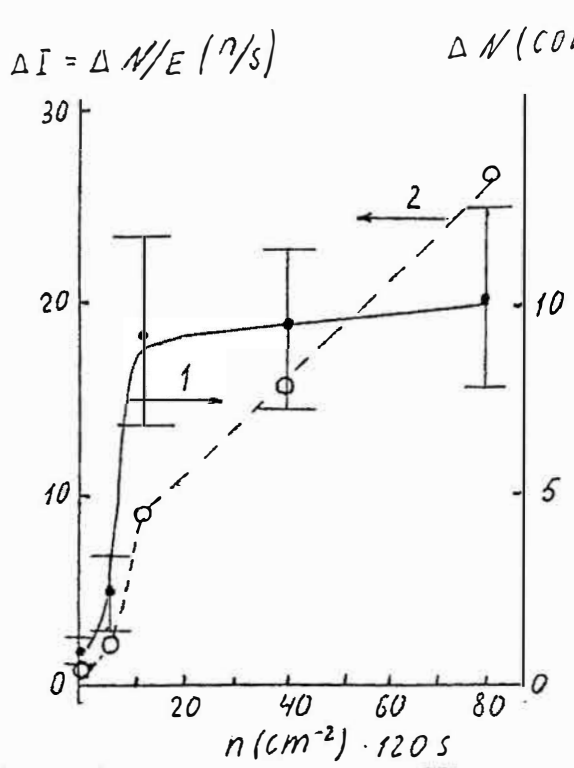

Fig.3. Dependence of intensity of neutron emission generated by DKDP-crystal (with the subtraction of the source background) on the valuem of neutron flux (n_f), that passed the crystal during the ferroelectric transition without taking into account the efficiency E in the crystal-detector system (curve 1); while taking into account E in the assumption on the 4π-distribution of neutrons (curve 2)

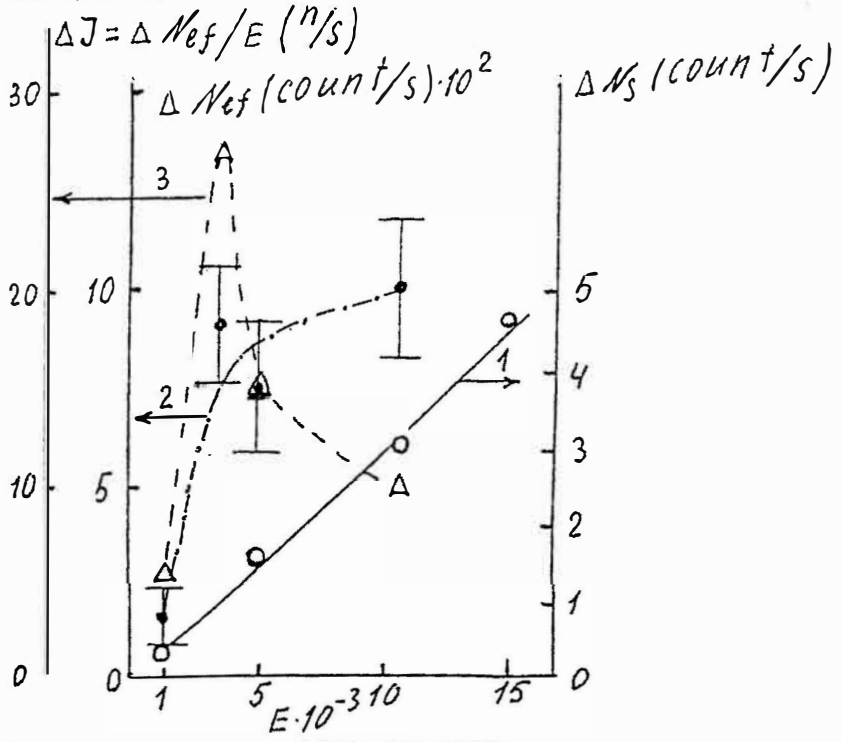

Fig.4. Dependence of the rate of counting of neutrons from the Cf^{252}-source on the efficiency in the source-detector system (curve 1); the intensity of the emission of neutrons emitted by the DKDP crystal (with the subtraction of the source background) as the function of the efficiency of detecting E in the crystal-detector system (curves 2,3).

Fifth International Conference on Cold Fusion
9-13 April, 1995 - Monte Carlo, Monaco
ICCF5 ©1995

In-situ ERD Analysis of Hydrogen Isotopes during Deuterium Implantation of Pd

Akira KITAMURA, Takakazu SAITOH and Hiroshi ITOH
Department of Nuclear Engineering
Kobe University of Mercantile Marine
5-1-1 Fukaeminami-machi, Higashinada-ku, Kobe 658, Japan

Abstract

The elastic recoil detection (ERD) analysis is successfully applied to *in-situ* measurements of hydrogen isotope distributions formed in Pd during deuterium ion implantation aiming at observation of peculiar phenomena in connection with the so-called cold fusion. The beam-target D(d,p)t reaction yield during the implantation is found dependent on the beam current or the deuterium flux. This is interpreted in terms of a temperature dependence of the deuterium concentration that is measured *in situ* with the ERD method. When both surfaces of the Pd sample are coated with 7.5-μm thick films of aluminum oxide, the reaction yield is observed to increase by a factor of about 5, and the ERD spectra show distributions of D more localized near the surface.

1. Introduction

A trial is made to find anomalous phenomena in both charged particle spectra and yield under bombardment of deuterated Pd targets with keV/MeV ion beams. One of the key factors for the appearance of the excess heat in the electrolysis experiments has been found to be the concentration n_D of D atoms in Pd[1]. An abnormality has also been induced by a mechanical stress in the lattice of a deuterated Pd with a surface coating[2].

In view of the somewhat transient nature of these anomalous phenomena, it is very important to know the space- and time-dependent $n_D(x,t)$ in relation to the appearance of the reaction products. Moreover, since hydrogen isotopes are easily movable in metals, it is desirable to make the analysis of $n_D(x,t)$ *in situ*.

A keV-D ion implantation/irradiation system equipped with an *in-situ* elastic recoil detection (ERD) analysis system has been constructed, and the effectiveness of the *in-situ* measurements has been demonstrated[3]. In this paper we discuss a correlation between the d-D reaction yield and $n_D(x,t)$, and an effect of a surface coating with aluminum oxide both on the d-D reaction yield and $n_D(x,t)$.

2. *In-situ* Analysis System

A schematic of the system is shown in Fig.1. The system is the same as that described in detail in ref.3, except for the target. The target located at the center of the chamber is a 5 μm thick Pd film or a similar Pd film coated with Al. The Al layer was established using a vacuum evaporation, and exposed to atmosphere for oxidization.

The layer was later analyzed with RBS to find the thickness of 7.5 μm and the composition of Al_2O_x, where x≅3.5.

D_2^+ ions produced in a duoplasmatron ion source with an maximum voltage of 30 kV are used exclusively in the present work. They are injected into the target chamber through a transport chamber having a Wien filter for the mass selection. It has an exit aperture of 4 mm in diameter. The beam enters the target at an incident angle of 15° with a current density ranging from 1 to 10^2 μA/cm^2.

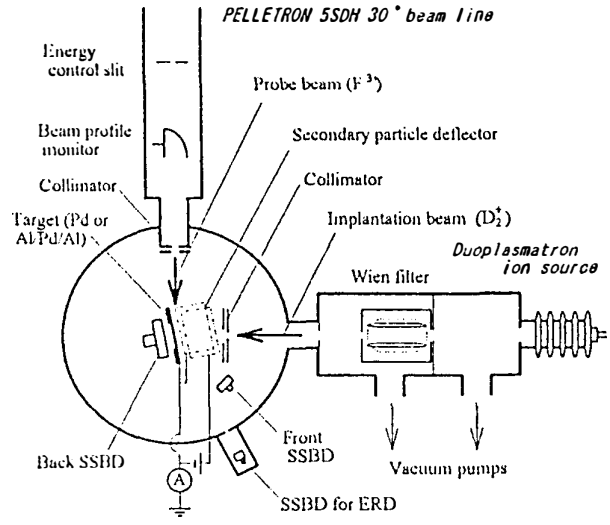

Fig 1. Schematic of experimental apparatus

The spatial distribution of the implanted D together with that of adsorbed hydrogen is measured with the ERD method occasionally; after interrupting the implantation or during the implantation. The accelerator beam for the ERD analysis is incident on the target with an incident angle of 75° through a collimating aperture of 0.5 mm in diameter. 6-MeV F^{3+} ions are used for the analyzing beam with a current of the order of 1 nA.

Three charged particle detectors, Si surface barrier detectors (SSBDs), are prepared around the target. The largest one with an effective area of 300 mm^2 is located just behind the target to detect nuclear reaction products with a large solid angle of 3.4 sr, and covered with a 15-μm Al foil to stop delta electrons and recoil particles. Another SSBD located at an angle of 30° with respect to the analyzing beam serves as an ERD detector. A 3-mm diameter aperture in front of it defines the solid angle to 8.2 ×10^{-4} sr. To stop scattered (or recoil, if any) particles heavier than ^{4}He a 6.2-μm thick Mylar film covers the aperture. The third detector having an effective area of 25 mm^2 and a similar Mylar film is placed at an angle of 60° and used for measurement of scattered particles during the ERD analyses.

3. d-D Reaction Yield during Implantation

During the implantation of the targets with D ions the usual beam-target reactions D(d,p)t and D(d,n)^{3}He produce 3.02-MeV p, 1.01-MeV t and 0.82-MeV ^{3}He. For comparison with measurements, the reaction probability is calculated for a uniformly saturated composition of $PdD_{0.85}$ using a TRIM code with a modification to include the nuclear reaction[3].

An example of the evolution of the D(d,p)t reaction yield during the implantation is shown in Fig.2, where the measured yield of p, Y_m, normalized to the calculated one, Y_c, is plotted against the fluence of deuterons injected in the form of 18-keV D_2^+ molecular ions. During the run an intentional change in the beam current is cyclically

made in expectation of the Takahashi effect[4].

We note almost the same dependence of Y_n on the current density as that found in our previous work[3]; the normalized reaction yield $Y_n = Y_m/Y_c$ changes following the cyclic change in the beam current. The lower is the current density, the larger is the reaction yield.

This phenomena was interpreted[3] in terms of the temperature dependence of the saturated amount of D atoms in Pd. The current density was varied in a range from 14 μA/cm^2 to 110 μA/cm^2, when Y_n changed from 1 to 0.1. In the case of the largest current density the target temperature becomes higher than the phase change temperature of Pd around 100°C, where the atomic fraction of D in Pd decreases down to 0.03. This explained the behavior of Y_n observed experimentally.

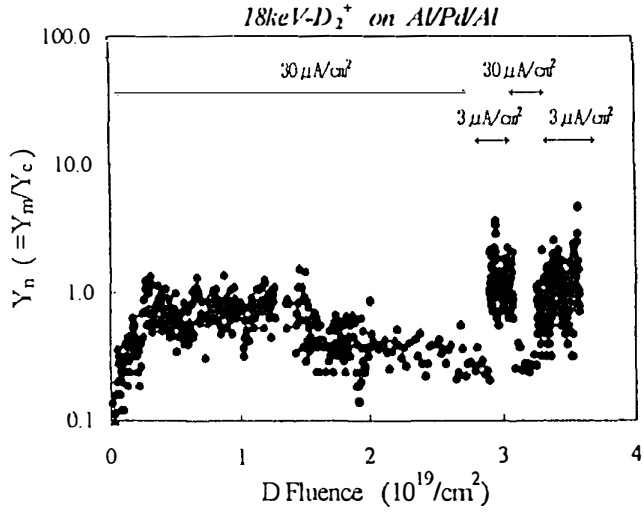

Fig.2. Evolution of normalized reaction yield Y_n during implantation of the 5 μm-thick Al/Pd/Al target.

Below about 20 μA/cm^2, however, the temperature remains almost at the room temperature, and therefore n_D should remain constant at the highest composition of 0.85. Nevertheless Y_n increases above 1 as shown in Fig.2. This may be due to an effect of surface plugging by the Al_2O_x coating.

4. Deuterium Distribution in Pd and Al/Pd/Al Samples

The changes in n_D have been observed with ERD measurements made at several phases of the implantation history. In the case of Pd without Al_2O_x the D distribution has its maximum at a depth 10-20 nm into the bulk[3], which is much shallower than 55 nm, the stopping range of 8-keV deuterons in Pd. This could be interpreted qualitatively as follows. Deuteriums prefer a region having more damage as their permanent abode. On the other hand, they escape from the bulk out of the surface due to recombination into D_2 molecules. The former effect moves the distribution peak toward the surface, while the latter into the bulk. The peak is therefore determined by a compromise between the two effects.

An example of the D distributions in the Al_2O_x-covered Pd is shown in Fig.3. The distribution peak is even at a shallower depth than that in the bare Pd; near the surface or near the boundary of the Al_2O_x layer and Pd bulk. The FWHM of the peak is approximately 20 nm, which should be compared with 34 nm of that in the bare Pd. This seems to contradict the above interpretation for the shallow location of the distribution peak in Pd, since we expect a suppressed loss of D for the Al_2O_x layer.

The reaction yield Y_m should be reduced a little by the reduction of D concentration near the surface compared with the case of the fully saturated distribution,

since the reaction cross section decreases rapidly with decreasing energy. As shown in Fig.2, however, the maximum value of Y_n exceeds 1.

The implantation was done up to a fluence such that the whole Pd film could become over-saturated. The target structure seems therefore to have been completely amorphised near the surface region. The value of Y_n exceeding 1 might suggest that the amorphization could cause an increase in the saturation concentration of D in Pd.

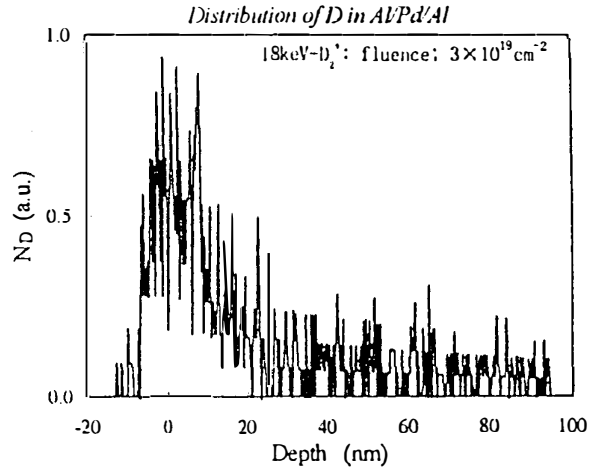

Fig.3. Typical distribution of D atoms in the Al/Pd/Al target.

5. Conclusion

The evolution of the D(d,p)t reaction yield during the D implantation of Pd with cyclically changing fluxes has been observed both on the bare Pd and on the Al_2O_x-coated Pd, and discussed in terms of the temperature dependence of the saturated concentration of D in Pd. The Al_2O_x coating is found to have an effect to localize the D distribution near the boundary.

Thanks are due to Dr. Y. Furuyama and G. Sakata for their assistance.

This work has been partly supported by a grant-in-aid for Basic Research on New Hydrogen Energy from MITI, Japan.

References

1. e.g., Kunimatsu et al., "Deuterium Loading Ratio and Excess Heat Generation during Electrolysis of Heavy water by a Palladium Cathode in a Closed Cell Using a Partially Immersed Fuel Cell Anode", Proc. 3rd Int. Conf. on Cold Fusion, Universal Academy Press, p.31(1993).
2. Yamaguchi et al., "Direct Evidence for Nuclear Fusion Reactions in Deuterated Palladium", Proc. 3rd Int. Conf. on Cold Fusion, Universal Academy Press, p.179(1993).
3. Kitamura et al., "In-situ ERD Analysis of Hydrogen Isotopes during Deuterium Implantation into Metals of Interest for Cold Fusion", to be published in Fusion Technology
4. Takahashi et al., "Anomalous Excess Heat by D_2O/Pd Cell under L-H Mode Electrolysis", Proc. 3rd Int. Conf. on Cold Fusion, Universal Academy Press, p.79(1993).

Fifth International Conference on Cold Fusion
9-13 April, 1995 - Monte Carlo, Monaco
ICCF5 ©1995

Cold Fusion Experiments Using Sparking Discharges In Water

Takaaki MATSUMOTO
Department of Nuclear Engineering
Hokkaido University
North 13, West 8
Sapporo 060, JAPAN

Abstract

Experiments on the DC discharge associated with microsparks were performed in ordinary water. Thin metal wires of Pd, Ni, Ti, Fe, Cd, Mo, Pt and W were used as the electrodes. Numerous sparks appeared on the surface of the electrodes, in high voltage over 40 V, and simultaneously extraordinary phenomena were observed, such as ball-lightning like phenomena.

1. Introduction

The author has been proposing the Nattoh Model, in which cold fusion reactions can be easily induced by an electrical discharge, especially with high voltage or current density (1) and showed that many extraordinary phenomena appeared in the experiments of the pulsed electrical discharge in water (2). This paper describes experiments on DC discharges with thin metal wire electrodes in ordinary water, in which microsparks caused extraordinary phenomena such as ball-lightning.

2. Experiment

Cold fusion experiments on the discharges were performed using thin wire electrodes. Pure metals of Pd, Ni, Ti, Fe, Cd, Mo, Pt and W (0.5 - 2.0 mmϕ) were used. The electrodes were vertically immersed in ordinary water mixed with about 1.5 Mol/l potassium carbonate in a 50 ml beaker. The effective lengths of the objective and reference electrodes were about 3 mm and 15 mm, respectively. With the shorter electrode, the pinch effect of the current worked effectively to compress hydrogen or oxygen gas (1). The DC was continously employed between the electrodes, in which the voltage was varied up to about 150 V under the constant voltage mode.

3. Results and Discussion

a. Nonlinear I/V curve

Figure 1 shows the I/V curve with the Ni wire cathode and the Pt reference anode. Those features were common with the other materials except Ti. The figure shows strong nonlinearity, divided into three regions. Linearity was still maintained in the lower voltage region, but the current strongly fluctuated between

about 40 and 60 V, in which the hydrogen gas seemed to explosively evolve from the surface of the cathode. Tiny sparks began to appear on the bottom tip of the cathode, and, as the voltage increased, the number of tiny sparks increased to eventually cover the whole cathode. In this case, the current was significantly suppressed to a stable level of about 0.1 A. With Ti, however, the sparks appeared on the anode and the current increased with the sparks.

When the polarity was reversed, a similar I/V curve was obtained, but the sparks began to appear over 80 V.

b. VTR Observation of Microsparks

The tiny sparks were observed in situ with a VTR system. Figure 2 shows that the tiny spark consisted of a large number of microsparks, repeatedly created or broken on the surface of the Ni cathode. The microsparks could sometimes form ring clusters with a diameter of about 20 μm, and could decay into a black cloud. Furthermore, there were strong bright spots among the microsparks. A corona-like discharge was observed from the bright spot (Sec. 3.e). On the cathode, on the other hand, the pinch effect worked strongly to induce the cold fusionreactions and to make a bank of clouds evolve with luminescence, as shown in Fig. 3.It appeared to be like the sparks.

c. Emission of Radiations

Radiations were monitored by a CsI(Tl) scintillation spectroscopy, which was placed over the water surface. When the sparks appeared, the counting rate was significantly higher than the background. The energy spectra of the radiations were continuous and declined monotonously as the energy increased. The high energy tail expanded more widely as the voltage increased. The intensity of the radiations dropped sharply as the distance between the detector and the electrodes increased. The radiations were neither gamma rays nor X-rays. The signals were generated by electromagnetic waves picked up with the circuit.

d. Nuclear Transmutation

Several elements were found by EPMA among deposited materials on the Pd wire anode: Ni, Ca, Ti, Na, Al, Cl, Cd and I. They were not observed in a reference region of the Pd wire. Furthermore, a significant amount of Ni was detected by the X-ray spectroscopy. These elements could not be asigned to impurities, but rather suggested a nuclear transmutation during the electrical discharges associated with the microsparks. For example, Cl, Ca and Ni could be transmuted by the capture of electrons, a proton and hydroxide with a K nucleus, respectively. On the other hand, Cd and I could be transmuted by the capture of a proton and oxygen with a Pd nucleus, respectively. Such captures could occur in the highly compressed state of the hydrogen cluster (Sec. 3.e).

e. Decay of Microsparks

Many ring clusters were successfully caught on the surface of the Fe cathode, as shown in Fig. 4. They decayed to a regularly hexagonal plate within a few days, as shown in Fig. 5. The intermediate stage of the decay was also observed, in which an outer zone was expanded but an inner circular zone still remained.

The ring and the hexagonal products were examined with EPMA, which obtained a two dimensional distribution of elements around the products. Besides Fe of the host metal and K of the electrolyte, some elements of Ca, Na, Cl and Cd were observed both in the ring and the hexagonal products. In particular, two circular zones that were seen for Cd were clearly separated from each other in the ring products, as shown in Fig. 6. Those observation suggested that the ring product could consist of the hydrogen cluster, and that the process of the nuclear transmutation took place in the clusters or during the formation of the clusters.

f. Nuclear Emulsions

The nuclear emulsions were placed to monitor particles that were emitted during the electrical discharge. Extraordinary rail-like traces were observed on the surface of the first nuclear emulsion. The traces suggested one-touch printing that was caused by some particles walking around on the surface. The extraordinary traces were generated by the ring products that escaped from the cell. The diameter of the ring was about 10 μm, approximately the same as that of the ring clusters observed on the Fe electrode (Sec. 3.c). This observation suggested an extraordinary result, that the ring product could penetrate the glass wall of the cell and the water region. Those curious behaviors of the ring product were previously reported (3) and were very similar to the ball-lightning phenomena in the natureal environment (4). The mechanisms of the extraordinary penetration could be caused by the itonic state of the cluster, but the details are not clear now.

Other types of exptraordinary traces were observed on the nuclear emulsions, such as a bacteria like trace, as shown in Fig. 7. It was very similar to that observed in the previous experiment of the pulsed discharge in water (3).

g. Miscellaneous

Other extraordinary phenomena were observed during or after the discharge experiments. The first was the formation of string products, which was observed with SEM on the surface of the Pd cathode after the discharges. The analysis with EDX indicated that there were only K elements in the string products. Similar string products were observed by the VTR system during the discharges. The second was the formation of film products, which were observed with the VTR system. The film product was formed at the bottom portion of the cathode, where the microsparks were frequently generated. The third was the magnetization of the Pt wires (0.5 mmϕ), which were used as leading wires. The magnetization effect was noticed at the tip of the Pt wires in which the electrodes were connected. The magnetization could be related to the formation of the ring cluster, in which the closed current flows to induce the magnetic field.

References

(1) T. Matsumoto, "Mechanisms of Cold Fusion: Comprephensive Explanations by the Nattoh Model", Fusion Technology, Submitted in March (1993).

(2) T. Matsumoto, "Extraordinary Traces Produced during Pulsed Discharges in Water," Fusion Technology, Submitted in January (1993).

(3) G. Elgey, "The Mysterious Ball-Lightning", Japanese Edition by Maruzen Co., Ltd., (1990).

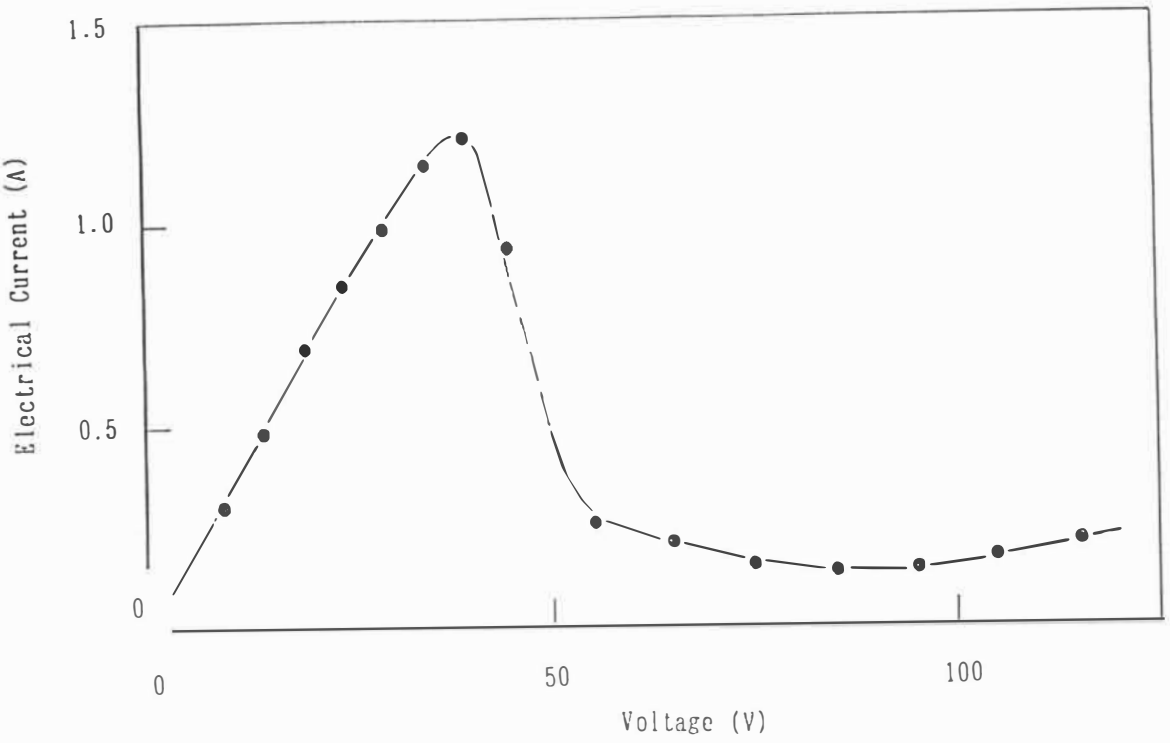

Fig. 1: Nonlinear I/V Curve

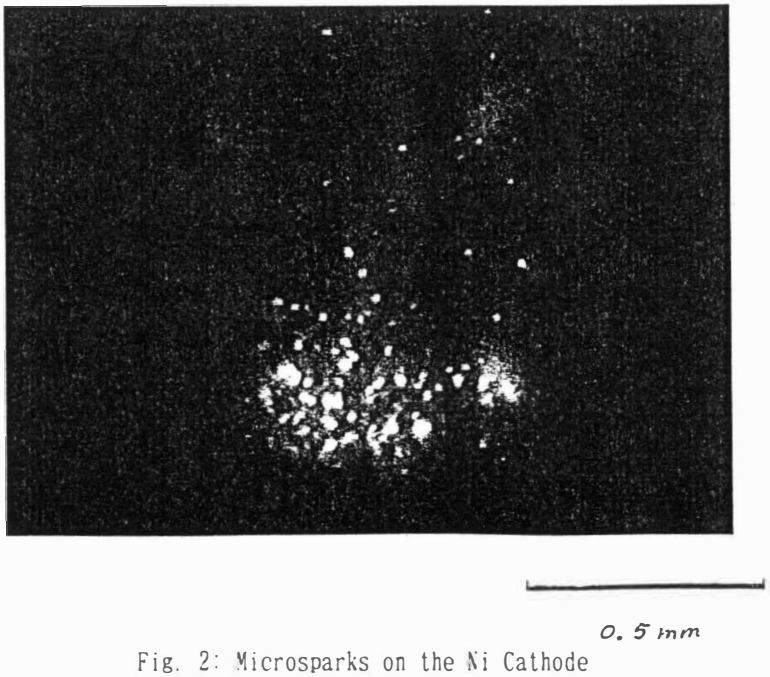

Fig. 2: Microsparks on the Ni Cathode

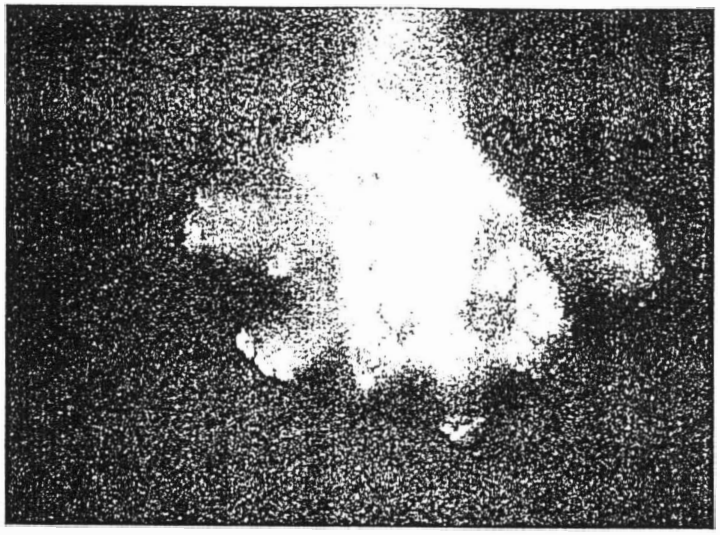

0.5 mm

Fig. 3: Cluster Evolution on the Ni Anode

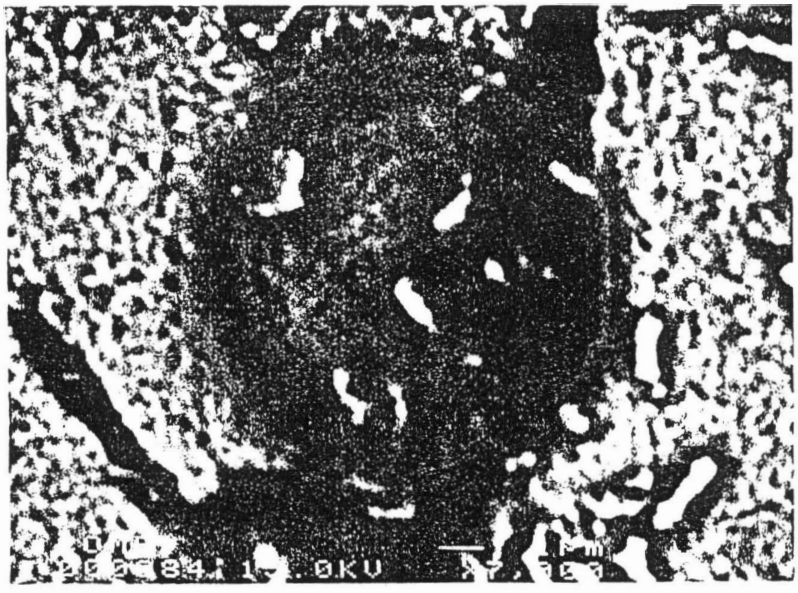

1 μm

Fig. 4: Ring Cluster on Fe Electrode

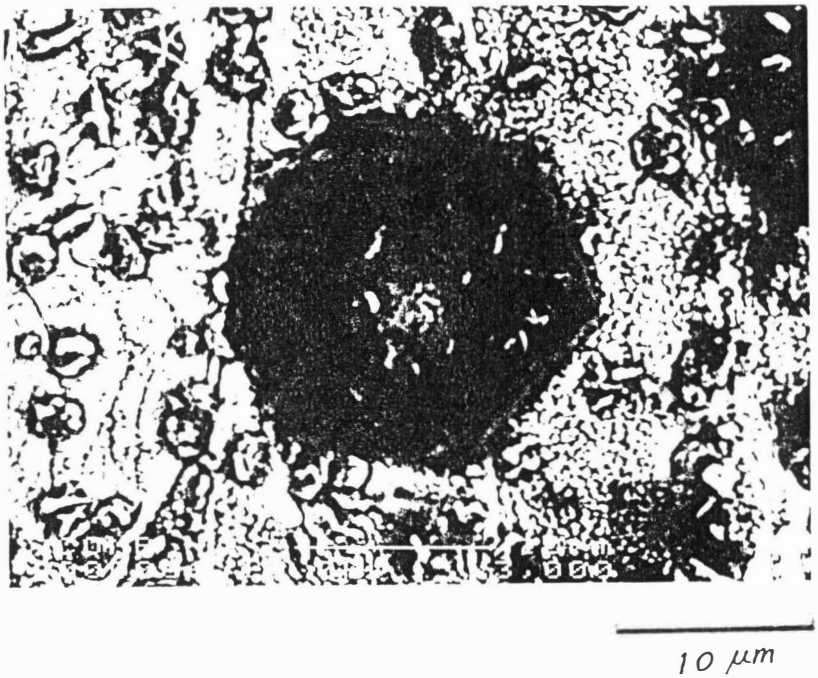

Fig. 5: Decay Product of the Ring Cluster

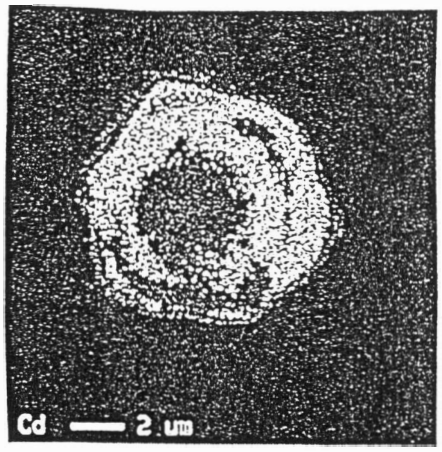

Fig. 6: Cd Distribution in the Ring Cluster

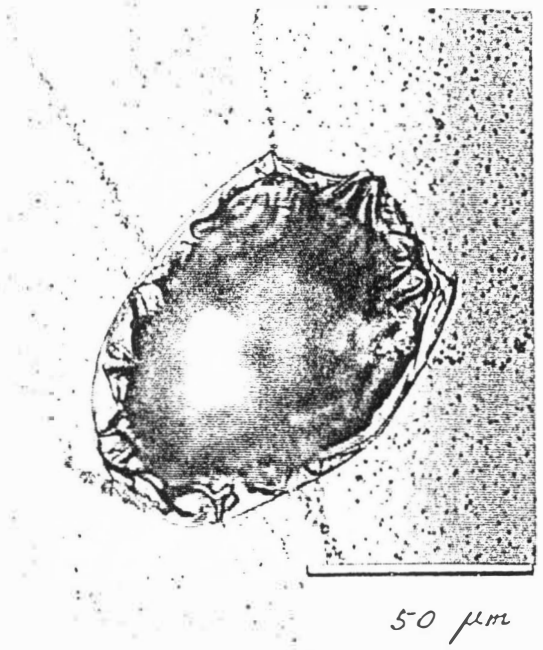

Fig. 7: Extraordianry Trace Suggesting a Prototype of Microbacteria

Fifth International Conference on Cold Fusion
9-13 April, 1995 - Monte Carlo, Monaco
ICCF5 ©1995

A Development Approach for Cold Fusion

Bruce KLEIN
5681 Columbia Road, #102
Columbia, MD 21044 USA

Abstract

A plan is presented for investigation and development of the cold fusion effect, ultimately leading to implementation of commercial devices. The plan represents a methodical approach for identifying and addressing theoretical, scientific, engineering and economic concerns.

The plan is presented from the perspective of a large architect/engineering corporation which performs work in established energy industries and which is not currently involved in cold fusion. The plan consists of a number of phases designed to establish the corporation's level and method of involvement in the field.

The phased plan provides a number of decision points; at each decision point a commitment to a higher level of funding is made on the basis of additional information which has been generated by the plan to that point. In this way the corporation can control its financial outlay, yet funding is appropriate so that pursuit of the plan is not hampered.

1. Introduction and Premise

Successful development of commercial cold fusion devices has the potential to substantially impact a corporation which is presently involved in traditional energy markets. This impact could be negative, if the corporation ignores cold fusion developments and finds itself reacting to fundamental changes in its market. Energy companies have already been buffeted in the United States by deregulation of the electric utility industry, a declining market for new energy production facilities, and falling prices for new construction due to intense competition. The impact of cold fusion could be much greater.

The impact could also be very positive, if the energy company were to position itself properly for future developments. This requires involvement early (i.e. now) to assist in the development of the technology, to establish what a profitable future corporate position is, and to prepare accordingly. This paper presents a plan for an energy company to do these things.

There are two premises upon which this paper is based. The first is that the cold fusion effect in its various forms is real. There exists sufficient experimental evidence at this time that this issue no longer needs to be addressed. It is not justified to devote additional resources to demonstrate the existence of the effect.

The second premise is that it is not in the company's interest to try to develop cold fusion by itself, without cooperation from others who are already working in the

field. Commercial cold fusion will come to fruition more quickly if cooperative arrangements can be made with those who are knowledgeable in the field, and if joint ventures are established with individuals and companies which have the requisite expertise.

2. Background

It is well known that the involvement by large corporations in cold fusion research and development is very limited. Nevertheless, there are a variety of strong reasons for an established energy company to become involved with cold fusion at this time. These reasons are all economical, and deal both with current market conditions as well as those which may come to pass in the future. The discussion which follows is presented from the viewpoint of an architect/engineering (A/E) corporation.

In general, an A/E does not build hardware, such as boilers, pumps, or electronic control systems. An A/E specifies the requirements for these components and designs their interconnection (civil foundations, piping, cabling and electrical distribution, etc.). In short, an A/E does all the design and engineering work required to assemble the many thousands of different components which make up a power plant or other large industrial facility. In general the A/E will purchase all the equipment and will oversee the manufacture of this equipment by its vendors. Finally, the A/E will construct the facility or will provide construction management.

From the perspective of the energy-related A/E, energy use can be broadly classified into four categories. The type of work the A/E performs in each area, and the changes which could occur to the respective markets are discussed below.

a. Electricity generation and consumption

In support of electricity generation and consumption, a typical A/E designs power plants, mining and fuel processing facilities, waste disposal facilities, and environmental remediation projects. The economics of cold fusion electric power generation devices may dictate that they are large-scale facilities like the central generating stations which exist today. This would support a traditional A/E role of system integration and construction.

On the other hand, economics may indicate that the preferable method of implementation is smaller-scale devices either located in neighborhoods or individual homes and businesses. This would disrupt the traditional A/E involvement in this market and would suggest that a different, non-traditional approach is necessary.

In either case, if cold fusion power generating devices are developed and they are economically attractive in comparison with other methods of electricity generation, an energy-related company would want to be involved in a positive manner. This industry is ferociously competitive around the world. There is an oversupply of engineering and production capacity for producing power plants, and establishing a competitive advantage is essential for a company's survival.

b. **Propulsion (internal combustion engines, gas turbines, etc.)**

An energy-related A/E is typically involved in projects required to produce and process fuel for propulsion. For almost all propulsion the fuel is petroleum, and example projects would consist of oil production facilities, refineries, and pipelines.

If cold fusion devices can be developed that are sufficiently compact and powerful that they can economically replace the internal combustion engine, petroleum use will drop precipitously. Existing industrial capacity will be sufficient to supply chemical, lubrication and plastics use of petroleum for the foreseeable future. The market for large facilities in this energy sector may virtually disappear. This suggests that a substantially different approach would be required by an A/E interested in staying involved in this market.

c. **Industrial uses**

Industrial energy use typically consists of electricity and heat. Often these are supplied by fossil-fueled power plants which produce steam; some of the steam is used for heating purposes and some of the steam is used to generate electricity. A typical A/E role is to design and construct the steam and electric generation plants. The same changes which cold fusion devices will make to electric power production will occur to industrial energy facilities.

d. **Home use (heating, air conditioning, and electrical loads)**

A/E's are typically not involved directly in this area. Instead the involvement is with the industrial base required to supply energy to the home. Again this consists of electricity, petroleum and natural gas. If self-contained home heating and/or generating units are developed, the need for external energy supply to the home will decrease. The impact on the industrial energy supply structure is obvious.

An A/E would have to adopt a very non-traditional posture to continue to generate revenue from this energy market sector.

So, the impetus to become involved in the cold fusion field, should it ultimately prove successful, is obvious.

3. The Important Questions

As has been mentioned previously, the important question is not, "Does cold fusion occur?" Instead, for a company interested in becoming profitably involved in the cold fusion field, the important questions which require answers are:

- Can cold fusion be used as the basis for useful, practical energy producing machinery?
- Will that machinery achieve widespread use?
- Can the machinery be made available in the foreseeable future?
- If the first three questions can be answered in the affirmative, how can and

should the company become involved?

To answer these questions, a phased approach to investigation and development is recommended. The phases, their purpose, and the methods used to accomplish them are described in the following.

4. Phase 1 -- Survey the Field

This purpose of this phase of the investigation is to develop a solid corporate understanding of the state of the cold fusion field. This phase of the plan is intended to generate the following information:

a. A detailed understanding of the different techniques known to produce the cold fusion effect.

b. The state of development of each of the cold fusion techniques, including:

- Method and apparatus
- Level of excess heat or energy production
- Known parameters and unknown factors requiring additional investigation
- Materials involved

c. An understanding of the theoretical explanations for the effect, along with supporting evidence for each theory.

d. An acquaintance with the researchers in the field; an understanding of their capabilities, funding, and plans; and an understanding of their willingness to participate with a large corporation.

To the maximum extent possible this phase of the investigation will be performed on a first-hand basis. Researchers will be visited at their laboratories, and their experimental apparatus will be observed. Theoreticians will be contacted, and their theories will be discussed in depth. A corporate cold fusion library will be established, and a systematic review of key publications will be performed.

5. Phase 2 -- Establish the Broad Parameters of Practical Machinery, Economic Attractiveness, and Timetable

The purpose of this phase of the investigation is to make educated guesses concerning the form commercial cold fusion devices may take. The cost of commercial devices will be estimated based on these guesses. Approximate timetables for the development of each technique will be generated, based upon the state of development the technique. This will involve performing the following steps for each of the techniques known to produce the cold fusion effect:

a. Select a device configuration. A reasonable approach would seem to be to choose an existing experimental cold fusion device which has demonstrated high levels of excess heat in a repeatable manner.

b. Estimate the size of the device needed to produce power at usable levels. A prudent approach would be to examine three sizes which will cover the range of possible devices: Electric power plant size (hundreds of megawatts), home heater/generator size (tens of kilowatts), and an intermediate size.

c. Estimate the cost of the devices if they were to be commercially produced. There is the possibility of large errors in this step, but one approach would be to identify existing industrial machinery for which a production cost is known and which is similar in form to the cold fusion device under study. The production cost could then be adjusted to account for differences in the materials of construction, difficulty of manufacture, and expectations of production volume.

d. Estimate the life-cycle cost of the device. This would include replacement of materials, operating costs, fuel costs, etc. Again, the most promising approach would be to make comparisons with similar machinery in use today.

e. Perform economic sensitivity analyses. These would examine the impact on device costs of changes in the parameters which are presently uncertain. This would include:

- **Performance of the device:** For example, how would the cost of the machine vary if a higher level of excess power were achievable? Is there a minimum level of excess power which makes the machine economically viable?

- **Cost of materials:** For example, if increased demand for palladium were to substantially increase its cost, what impact would this have on the cost of the total machine?

- **Size of the Device:** The machine may be most economical in a particular size range. This will impact the way the device is ultimately implemented in the marketplace.

f. Based on the above estimates, compare the cold fusion device with energy sources available today. Determine the implications for the ultimate economic attractiveness of the device.

g. Make a realistic estimate of the size of the market.

h. Establish an approximate timetable for development of the device. This timetable would be based upon the current state of development and the amount of additional work and research required to bring the device to a state of commercial viability.

6. Phase 3 -- Examine the Legal Implications

The purpose of this phase of the plan is to attempt to define the legal arena in which the company will be operating.

The sorry state of the cold fusion patent situation is well known. Almost no patents have been granted, and most researchers are operating without patent protection. This has probably had the effect of limiting communication among researchers to some extent. But this is not likely to be a corporation's major concern.

To a corporation interested in becoming involved in this field, securing patent rights will be an important aspect of that involvement. Several hundred patent applications have been prepared for cold fusion devices, and they undoubtedly have many overlapping claims. Detailed legal research will be necessary to attempt to understand the legal necessities of operating in this field.

7. Phase 4 -- Identify the Work Remaining

There are many issues which must be addressed before practical cold fusion devices are developed. The purpose of this phase of the plan is to identify the issues, determine what work remains to be accomplished to address them, and determine what talents must be assembled to perform that work. Some of the more critical issues are discussed below.

a. Theoretical Basis

A sound theoretical basis for the cold fusion effect will ultimately be required. Without it, improving the performance of devices will be a trial-and-error affair. A theory with predictive capabilities would be extremely helpful. A series of experiments is required to test the more promising theories.

b. Configuration

Configurations which produce higher rates of excess heat generation need to be examined. Examples include electrode surface area and volume, and the role of grain boundaries. A systematic examination of configuration effects will need to be devised.

c. Temperature

Most experimentation to date has been at low temperatures. Producing practical devices at these temperatures will most likely be difficult. The extent to which more thermodynamically useful temperatures can be achieved requires investigation.

d. Repeatability

In terms of much cold fusion research to date, repeatability means the ability to reliably produce the cold fusion effect. This in itself will not ultimately be sufficient. A practical device will need to reliably produce the cold fusion effect at a power level which is known and repeatable.

e. Throttling

To be truly useful as a practical machine, it will be necessary to have a mechanism to throttle a cold fusion device. This means the ability to turn it on and off at will, and to vary its output. Mechanisms to accomplish this will need to be explored.

f. Radiation

The general attitude in the cold fusion community is that radiation generated during experiments is good, because it demonstrates that a nuclear process is at work. The business perspective is exactly the opposite. Concerns about radiation (whether those concerns are rational or not) have severely affected the development of fission power in the United States and other parts of the world. Even if the radiation emitted from cold fusion devices is very low, irrational fears could be very damaging. The levels of radiation which can be expected from practical devices needs to be well examined.

g. Long-term Performance

Many cold fusion experiments have been short-term. Longer term testing is required to determine what periodic maintenance and replacement will be necessary with a commercial device. In other words, will the electrodes or some other parts of the devices "wear out" with time? How often will these parts need replacement or replenishment? How will this be done and how much will it cost?

A series of long-term experiments will be necessary to examine this issue.

h. Power Conversion

Methods must be developed for converting the excess heat generated by cold fusion devices into electricity. Reasonably high conversion efficiencies are likely to be required. It is not sufficient to say that the source of energy is cheap and plentiful and therefore conversion efficiency is not an issue. Solar energy is cheap and plentiful, yet low conversion efficiencies have so far made widespread implementation of solar power uneconomical.

So, potential power conversion technologies will have to be identified. Modifications required to match them to the output characteristics of cold fusion devices will have to be explored.

8. Phase 5 -- Establish Working Relationships

Phase 4 described above will identify the areas requiring work. Based on this, the talents and resources required to perform the work will be established. The purpose of Phase 5 will be to establish relationships with other organizations. In its traditional role as systems integrator for large, complex projects involving many different organizations, the A/E may be particularly suited to establishing consortium and joint venture arrangements.

Participants would include researchers in the field, companies and laboratories with the necessary expertise to perform the work, and companies with an interest in sharing costs and risks.

9. Phase 6 -- Perform Directed Experimentation

The purpose of this phase is to perform experimentation and research in a logical manner to address the issues raised in Phase 4. The work would be performed by the organizations assembled in Phase 5.

10. Phase 7 -- Develop Prototypes

Once a sufficient number of the outstanding technical and economic questions have been addressed, it will be possible to build and test prototype devices. By this time in the process, the information which has been generated will probably have narrowed the candidate configurations to a small number. The most promising will be constructed.

11. Phase 8 -- Initiate Commercial Implementation

If all the earlier phases of this plan achieve success, and the economic outlook is positive, the ultimate goal of all the cold fusion efforts will be possible: commercial implementation. It is not possible at this time to describe the form this implementation will take; generating that information is the goal of the first seven phases of the plan.

12. Summary

The potential impact of cold fusion on a company currently involved in the energy industry is too great to ignore. If a phased approach is used, in which each phase represents an increment of financial and technical involvement, the company can minimize its financial exposure while still establishing a favorable competitive position. The benefits of such a plan are further enhanced if the company pursues this work in cooperation with others already involved in the field.

Fifth International Conference on Cold Fusion
9-13 April, 1995 - Monte Carlo, Monaco
ICCF5 ©1995

A MODEL FOR COMMERCIALIZATION UTILIZING PATENTS

PRESENTED BY FREDERICK G. JAEGER
PRESIDENT OF **ENECO**
UNIVERSITY OF UTAH RESEARCH PARK
391-B CHIPETA WAY * SALT LAKE CITY, UTAH 84108 USA
PH (801) 583-2000 FX (801) 583-6245

The biggest impediment to commercial development today is lack of widespread demonstration devices and firm scientific understanding of the mechanism or mechanisms responsible for variously reported cold fusion and enhanced energy effects. With scientific understanding, the possibility of commercial amplification and replication could rapidly occur, which would quickly spawn a wide variety of initial commercial products.

The commercial development of cold fusion and enhanced energy devices will probably follow a normal cycle of science > technology > commercial products. First generation products will probably take advantage of 50 - 100 degrees C heat output, and move to higher temperatures with increased product sophistication.

The first tier of entrepreneurial companies are already active in the field. With market maturation, inevitable second stage consolidations and joint ventures will occur. In the third stage, the technology ultimately will best lend itself to optimum development by large multi-national companies who already have a well-established business infrastructure in place. Speed of technology dissemination will be crucial.

Our model examines the role that patents, as a basic building block, play in the commercialization process. Patents are generally granted to citizens of a country to promote overall technological advancement. The basic concept is that in exchange for an inventor laying open their ideas to the public to stimulate innovation, their government will grant an individual monopoly use of the invention for a period of time, typically 17 -20 years. In the U.S., patent rights were granted to citizens in the original constitution.

Patents essentially are the property of the inventor, just like real estate or personal property. The patent holder can exclusively determine, via license or assignment agreements, who shall be allowed to make, use, or sell products that embody their patented property. Internationally, there presently exist a well established patent infrastructure, known as the Patent Cooperative Treaty (PCT) that protects and facilitates the filing of patent applications in over 70 countries. International patent rules are also influenced by General Agreement on Trade & Tariffs (GATT), another well established system to facilitate commercial transactions.

Timing and priority dates for patents are important. There is an early need to file for cold fusion patents now, even under conditions of some scientific uncertainty in order to protect the commercial rights of inventors later. The first step, of course, is to make a

discovery or conceive an invention. The next step is to verify an innovative concept and reduce it to practice by an experimental device. You can obtain a patent on a device even though you may not understand why or how it works. For example, you can patent a new fishing lure even though you have no idea why fish like it! "Theory patents", without experimental data and devices, won't be successful in areas of new technology.

Once you have reduced an invention to a device that can be uniquely described in a specification, you should obtain enough operating data to substantiate your claims, and then file a patent to protect your rights (Figure 1). Generally, once you file in your home country, you have a year to determine in which foreign countries you intend to seek protection under a PCT application. Finally, you can reap the financial benefit from the fruits of your labor by presenting your invention to public markets via licenses and products.

Consolidation of individual patent building-blocks into a coherent, well balanced portfolio minimizes scientific and commercial risks while providing maximum market opportunities and commercial applications (Figure 2). The portfolio concept also removes certain intra-mural barriers between contributors and allows direct dialogue and exchange of ideas between inventors to further scientific understanding. During this early stage, co-operation often achieves goals quicker than competition.

ENECO was formed by scientists who wished to take advantage of the economies-of-scale afforded by a portfolio in order to commercialize their inventions, pool resources in a multi-disciplinary field, and share knowledge/network without early competitive barriers. Many of the founding scientists are current shareholders and members of our external **Science Advisory Board** (SAB). We are a privately held corporation, financed by accredited individuals and commercial entities with the goal of providing a basic commercial structure, utilizing a patent portfolio, to concurrently track and facilitate scientific advancements in order to expeditiously reach a viable commercial stage.

Our basic intent is to non-exclusively license cold fusion and enhanced energy inventions that will serve as basic "competitive tools" or "templates" for our clients. Our "open architecture" licensing format will encourage others to file their own add-on patent improvement in their respective fields. We anticipate that our manufacturing licensees, in order to more effectively compete in their respective markets, will create their own improvements on top of our basic patents. For example, auto manufacturers will develop one set of improvements, while aerospace companies will naturally pursue a different direction. The common thread, however, will be basic cold fusion technologies that energize products in each market.

To build a sustainable competitive advantage, the portfolio must maintain cutting edge scientific leadership and file its own improvements as continuations on the early priority dates of pioneering patents in each sub-category. Judicious mixing and matching of patent

assets within the portfolio enables individual properties to achieve their fullest, value-added leverage for commercial development.

To be accepted into the portfolio, individual invention candidates are routinely screened regarding their scientific merit, strategic fit, economic parameters, priority date and legal position. Philosophically, common goals and good personal "chemistry" must exist between inventor-contributors and portfolio managers to help ensure a mutually productive, long-term relationship.

ENECO's current portfolio has over 40 intellectual properties, including several issued patents. We also have the exclusive worldwide commercial and patent rights to the original Pons-Fleischmann inventions. ENECO has to pursue a balanced portfolio now even though much of the basic science is not yet understood and leading commercial products have yet to be identified. Once a major scientific break-through occurs in any area, it will be too late to go back and try to assemble the right patent package after-the-fact. Now that the initial collection is in place, it could influence the birth and direction of a whole new industry of clean energy.

Potential portfolio assets provide a type of "futures market" of value for current investors. The technological "gill net" provided by the portfolio minimizes risks while we are forced to operate in the presently uncertain scientific environment. Our chances of catching at least a couple major commercial opportunities are enhanced through diversification. The economic parameters in cold fusion development are such that a few winners in this field provide a large enough reward to easily pay for others that don't develop into major commercial applications. Actually, the scientific uncertainty over the past six years has provided a unique opportunity to assemble a comprehensive energy portfolio under one-roof in order to keep resources focused on research and understanding rather than towards unproductive litigation involving fragmented patent claims.

The portfolio provides one-stop shopping convenience and saves valuable time for industrial users who wish to select coherent, al-la-carte license packages to suit their individual needs. Some of the pioneer patents we have already acquired include the original 1989 Pons-Fleischmann inventions. Light water applications include early Bush-Eagleton work at California Polytechnical Institute. Molten salt electrolytes were contributed by Drs. Liebert and Liaw at University of Hawaii. Glow discharge inventions involve early Russian work at LUCH Institute from Drs. Kucherov, Karabut, and Savatimvoma. Solid electrolytes also came from Russia at the Institute of High Temperature Electrochemistry under Dr. Samgin's direction. Cavitation technology includes filings for rotor and rotor-less systems. Transmutation includes early electrolytic Rb to Sr isotope work performed by Drs. Bush and Eagleton. The portfolio also includes trigger/control, RF, magnetic pulsing, efficient thermo-electric converters and related enhanced energy devices.

The common scientific thread that connects various elements in the portfolio enhances understanding from a unique perspective. For example, behavior of current density effects or loading ratios are remarkably similar between electrochemical devices and glow discharge experiments.

From an overall schematic viewpoint, the portfolio is a useful mechanism to perform several requisite value-added services for inventions (Figure 3). For inventors, ENECO's value added processes convert their initial patent applications (raw material) into marketable products that have the highest possible chance for widespread commercial success. The economies-of-scale are provided by a full-time, professional patent staff that performs all the "business partner" needs of inventors while portfolio managers provide scientist-contributors with targeted research and development support and royalty income.

For investors, the portfolio concept provides a rational balance between risk and reward through diversification, to obtain a critical mass of assets to attract investment capital in a "futures market" format.

For customers, the logical convenience of one-stop, worldwide shopping for a comprehensive ready-to-go product line suits their individual needs without having to cross cultural boundaries or seek out several different inventors in order to stitch together the patents and deals that they need in order to incorporate cold fusion inventions into their various lines of business.

Providing the market with a comprehensive product line is essential (Figure 4). Customer oriented convenience, time savings, variety, and price are all crucial elements of a successful marketing mix needed for commercial users. A comprehensive product line that contains all these elements will encourage customers to quickly buy and incorporate technologically superior tools into their own lines of business, rather than pursue a slower, less productive route of "invent around" and "steal and litigate".

Our portfolio concept has a successful, and well-established precedent in the field of music and copyright-licensing. The majority of copy-righted music is already distributed through centralized organizations that facilitate widespread dissemination from many different artists through a unified, convenient marketing organization.

ICCFPRO

ENECO

A MODEL FOR COMMERCIALIZATION UTILIZING PATENTS

INVENTOR/SCIENTIST
(Idea)

↓

DEVICE/PRODUCT
(Prototype)

↓

APPLY FOR PATENT
(Method and Apparatus)

↓

MARKET DEVICES/LICENSES
(Financial Reward)

University of Utah Research Park
391-B Chipeta Way • Salt Lake City, Utah • 84108 • Ph (801) 583-2000 • Fx (801) 583-6245

FIG 1

PATENT PORTFOLIO CONCEPT

ENECO

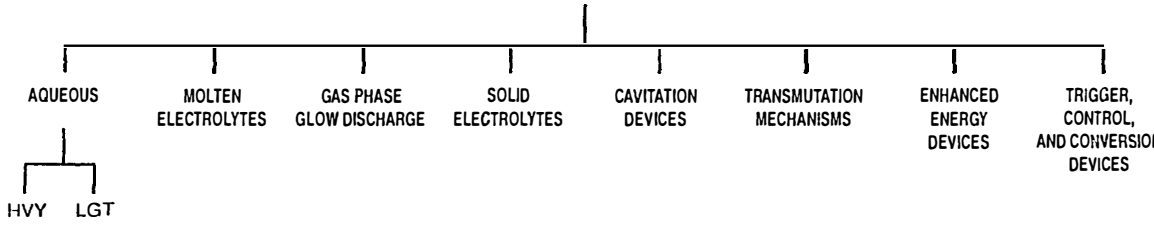

University of Utah Research Park
391-B Chipeta Way • Salt Lake City, Utah • 84108 • Ph (801) 583-2000 • Fx (801) 583-6245

FIG 2

ENECO

SCHEMATIC OVERVIEW

INDIVIDUALS, INVENTORS, SCIENTISTS, AND TECHNOLOGY COMPANIES

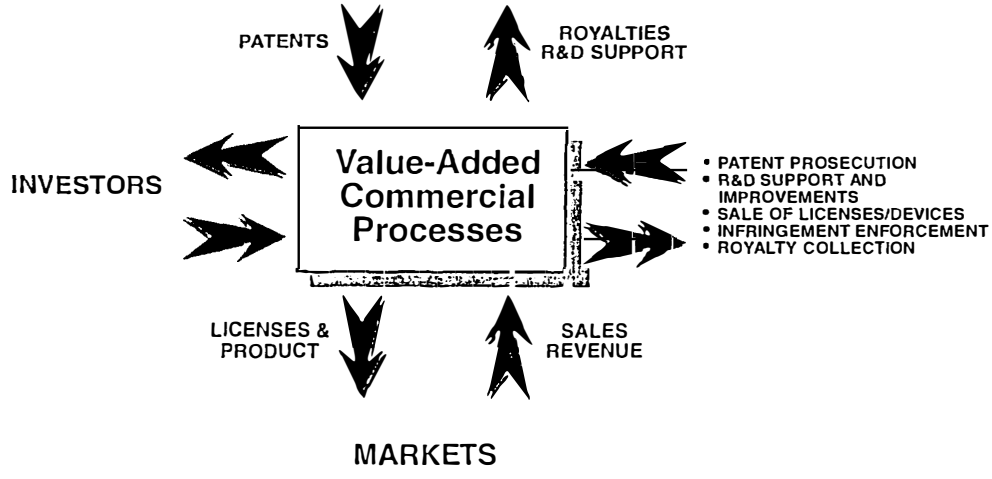

MARKETS

University of Utah Research Park
391-B Chipeta Way • Salt Lake City, Utah • 84108 • Ph (801) 583-2000 • Fx (801) 583-6245

FIG 3

ENECO

DETAILED PRODUCT LINE

1) **License:** Legal right to make, use, and sell products.

2) **Demonstration Device:** R&D proof-of-concept with operating instructions.

3) **Proprietary Materials:** Pre-tested/formulated to yield reproducible results.

4) **Information:** R&D updates and technology upgrades to all licensees.

5) **Consulting:** To suit specific customer requirements or unique applications.

University of Utah Research Park
391-B Chipeta Way • Salt Lake City, Utah • 84108 • Ph (801) 583-2000 • Fx (801) 583-6245

FIG 4

Fifth International Conference on Cold Fusion
9-13 April, 1995 - Monte Carlo, Monaco
ICCF5 ©1995

CHARTING THE WAY FORWARD IN THE EPRI RESEARCH PROGRAM ON DEUTERATED METALS

Thomas O. PASSELL

Nuclear Power Group
Electric Power Research Institute
P.O. Box 10412
Palo Alto, California 94303

ABSTRACT

Over six years have elapsed since the first announcement by Fleischmann, Pons and Hawkins (1) of the observation of excess heat from palladium heavily loaded with deuterium. The EPRI program began in April, 1989, and has continued to the present time attempting to replicate the claimed excess heat and determine its source. Under conditions difficult to achieve, some 16 separate experiments have successfully reached that goal out of some 35 major attempts. The conditions found necessary for an observation of excess heat were found to be at least three in number: 1) atomic loading ratio (D/Pd) > ~0.9; 2) Initiation time of 8 to 23 days; 3) current density >0.1 amperes per cm2 of cathode area. A fourth condition suggested by the results of a recent experiment is that the FLUX of deuterium across the palladium metal surface must be above some threshold value. No definitive source for the excess heat has been yet robustly determined, but measurable helium-4 has been observed in the cell vapor space in a few cases. The major evidence that the heat may be from nuclear reactions is its magnitude - some 10 to 100 times larger than any known chemical reaction. The objective of the continuing effort is focussed upon identifying the source of the excess heat. Sonic cavitation at a Pd-D2O interface has apparently produced both He-4 in the vapor phase as well as apparent excess heat. This research has identified a huge matrix of possible experiments to confirm or refute various hypotheses on the source of the heat. To acquire sufficient resources to explore this matrix requires, in my opinion, a definitive signature of a nuclear reaction connected with the production of heat. Then and only then, with the promise of a potential energy source of almost unlimited size, will the necessary research funds be forthcoming.

1. INTRODUCTION

The subject of cold fusion has aroused considerable controversy since its announcement some six years ago. This controversy was predictable in any proposed

new potential energy source that would threaten the position of research on existing and other potential energy sources in a period of shrinking budgets. This atmosphere of controversy plus the natural tendency of inventors to protect their intellectual property via secrecy has slowed the resolution of the scientific issues. The EPRI program had two major objectives at the outset: 1) to obtain the largest possible amount of excess heat; and 2) to observe the neutrons and tritium everyone expected from the D + D fusion reaction. Since that time the focus has not shifted on the excess heat issue but the search for neutrons and tritium has shifted to a search for helium-4 and possible isotopic abundance shifts among stable nuclei within the cathode. Several credible episodes of neutrons and tritium were seen in the EPRI-sponsored work and by others but at levels far too low to be the primary heat-producing reactions, and in most instances, from experiments not designed to measure excess heat.(2)

2. THE SEARCH FOR EXCESS HEAT IN PALLADIUM

Almost 80% of the effort by EPRI has been directed to understanding the process that produces excess heat. This work has been reported by McKubre and coworkers (3,4). The initial strategy was to get so much heat as to be unequivocal and to exploit its use even before its source was known. This seemed logical because the excess heat already appeared to be at least one or two orders of magnitude greater than any known chemical process within so small a mass of palladium. Therefore the heat source was presumed to be a nuclear reaction. The low levels of neutrons and tritium made it clear almost from the beginning that the heat must be coming from an entirely different nuclear reaction or different D+D reaction pathway. The small but definite levels of neutrons and tritium credibly observed by a few investigators indicate that some unexplained phenomena are occurring in the palladium metal lattice - at levels some 40 or more orders of magnitude larger than existing theory predicts - even though 6 to 12 orders of magnitude too small to explain the excess heat observed (5-8)! Furthermore, the ratio of neutrons to tritium is 6 or more orders of magnitude lower than the 1:1 ratio observed for the D+D reaction in plasma physics experiments. This evidence is an indication that nuclear processes are indeed possible in highly deuterated palladium and that they differ from the ones widely studied heretofore in "hot" fusion research.

If enough excess heat per unit mass of Pd can be generated (>1 gigajoule per mole of Pd) the more subtle evidences of nuclear transformations such as isotopic abundance shifts of stable nuclides and/or helium-4 production will eventually reach levels large enough to measure unequivocally. This assumes that the palladium lattice loaded with deuterium cannot distort the normal reaction pathways of the D+D reaction so completely as to conform to the observations so far reported , i.e., less than one neutron per million tritum atoms and helium-4 production without emission of the normally observed 23.8 Mev gamma ray.

Reproducibility is the issue continually faced by active researchers in the search for excess heat. Clearly the conditions thus far found necessary for achieving a positive result are not easily attained. Most deuterium charging of palladium by electrochemical means reaches a D/Pd ratio of 0.7 but not higher without careful manipulation of electrochemical and cathode metallurgical conditions. It is thus understandable that not everyone who has attempted the experiment, especially those operating within a limited time horizon, has observed the phenomenon. Since hydrogen charging of, and diffusion within palladium has been intensively studied for over 100 years without discovery of the anomalaous heat effect, the conditions for it must be very rarely achieved. This is indeed the experience of the few research groups who have claimed success - that is, a large fraction of the experiments are not successful. One significant reason for such a situation is the issue of achieving the apparently required D/Pd loading ratio. Pons has remarked that a batch to batch variability has been observed among palladium used for cathodes (9). In one batch, a significant fraction of cathodes give the heat effect, whereas in another batch, none of the cathodes show it. This effect is reminiscent of the batch to batch variability in heats of stainless steels in their susceptibility to stress corrosion cracking, due to variations in the previous heat treatment and impurity content.

Figure 1 gives the excess heat results as a function of the electrical resistance ratio (relative to the resistance of pure, unloaded Pd) of the palladium cathode, the means by which the D/Pd ratio is continuously monitored (3). Note that above a maximum achieved loading of 0.95 every cell gave excess heat whereas below a D/Pd ratio of 0.9 no cell gave the effect. In the gap between these peak loading ratios about half the cells showed the anomalous heat effect. It should be noted that the value plotted in Fig. 1. is the peak loading achieved during a very long run (many hundreds of hours). Invariably, this peak loading was maintained during only a small part of the total run length, the average loading usually being smaller than the peak value by about 0.05 units.

Table 1 gives a summary of results of some 26 major attempts by McKubre and coworkers to replicate the excess heat phenomenon in deuterated palladium (10). As an illustrative example of one of the cells in Table 1, Figure 2 gives the fraction of excess power in cell P-15 over a ~100 hour period. The fraction is calculated two ways - 1) relative to the total input power which includes a compensating joule heater to maintain isothermal conditions during changing electrochemical conditions and 2) relative to the electrochemically generated power alone. Relative to the latter the excess maintains about a 10%level with a peak at ~25%. Figure 3 is a corresponding curve of the cathode resistance ratio for P-15 during the same period as Figure 2 relative to pure, unloaded palladium. A resistance ratio of 1.58, the lower plateau on the curve corresponds to a D/Pd ratio of 0.97. Similar data for cell P-16 is also shown in Figure 3. Note that P-16 achieved a higher peak resistance ratio of 1.6 corresponding to a D/Pd ratio of 0.94. Table 1 indicates P-16 also showed a lower excess heat effect than P-15.

Another issue being addressed is the comparison of results from ordinary light versus heavy water electrolytes. Figure 4 gives a side by side comparison between cells P-13 (light water) and P-14 (heavy water) over a 200 hour period (3). The two cells operated in series electrically in the same water bath and were monitored by the same instruments on a time shared basis. While the loading ratios for H and D of the two cathodes were not precisely the same, there was a clear difference in excess heat favoring the heavy water cell. Within the limits of error, cell P-13 registered near zero excess heat. It is an apparently valid criticism that an inadequate number of so-called "blanks" with light water have been run. The investigators' response has been that an even better "blank " is a heavy water cell that produces no effect. There is some evidence from work elsewhere that light water is also effective in producing excess heat in different cell configurations, namely with nickel cathodes and alkali carbonate electrolytes.

Figure 5 shows the effect upon excess heat production from the addition of 1 cc of light water to the ~20 cc of the electrolyte of an operating heavy water cell (P-22 in Table 1). In about 100 hours the excess heat died away to near zero. It is known that light hydrogen will preferentially displace deuterium in the palladium lattice so that a 5% concentration in the electrolyte may bring about a much higher H/D ratio in the solid. This replacement of heavy with light hydrogen is expected to be more rapid than the 100 hour decay time observed. It is possible that this addition of fresh electrolyte is perturbing the electrolyte/cathode interface in some adverse manner similar to that observed by a number of investigators when makeup heavy water is added to open cells to replace that which has been electrolytically deomposed to a gas (e.g. see Ref. 8).

3. THE SEARCH FOR NUCLEAR REACTIONS IN PALLADIUM

About 20% of the total EPRI effort has been focussed upon the search for the nuclear products, neutrons and tritium. No tritium above the background level present in the heavy water electrolyte was seen in any of the excess heat experiments shown in Table 1. A low level neutron capability was not in place for those experiments.

Low level neutron episodes in deuterium loaded palladium have been reported (5). However, in no case has the level been more than three times the background level from cosmic rays. Nonetheless, this is still over 40 or more orders of magnitude greater than expected from calculations for the presumed normal deuteron spacings in the palladium lattice. The conditions for neutron emission appear to be only very rarely achieved in electrolysis of Pd in heavy water based electrolytes.

More recently some nuclear reactions of a more definitive nature have been observed in deuterated palladium but their full, open publication awaits a replication of the results (11). Figures 6-10 give the spectrum of gamma rays observed for one of three cathodes that exhibited the effect. Figure 11 gives the isotopes believed produced consistent with the gamma ray spectrum. From this work there is some indication that

consistent with the gamma ray spectrum. From this work there is some indication that BOTH the deuteron and the proton can enter even a nucleus with as high an atomic number as that of palladium (Z=46). Assuming only reactions with a positive Q are possible, Rh-99 can only be produced by a (p,alpha) reaction on Pd-102. If confirmed, this result implies that many possible nuclear reactions at lower atomic number than palladium but well above that of deuterium, are possible in this system and should be explored as the possible source of the excess heat.

Ultrasonic cavitation at a palladium-heavy water interface has resulted in a few observations of added helium-4 in the argon cover gas (12). EPRI has funded confirmation of the earlier helium measurements at a laboratory highly experienced in such measurements. While the excess heat is more difficult to measure quantitatively in this system , the investigators claim there is a general indication of excess heat in the 10% range correlated with the finding of excess helium-4 in the cover gas. The amount found is approximately commensurate with expectations based upon production of several Mev per helium-4 atom.

4. CURRENT STATUS

Current batches of palladium appear to be difficult to load to the previously determined required level for an excess heat episode. Therefore, the current effort searching for increased excess heat is focussed upon finding what uncontrolled variable is preventing achievement of high loading. Impurity content of the most successful palladium batch appears to be slightly higher than the less successful batches. Most of this impurity content is the remnant of materials added during the final pouring of the ingot to remove oxygen, calcium boride being the primary constituent with a significant silicon level as well. One hypothesis is that oxygen content remaining in the palladium after production is a significant factor preventing full loading. The mechanism suggested is analagous to the one operative in copper used in high-temperature reducing environments. In that case porosity is created when hydrogen reacts with impurity oxygen to produce water. Porosity would offer a means for deuterium deloading into such pores, ultimately raising the pore gas pressure to levels capable of cracking the metal. Cracks reaching the metal surface have been observed to prevent high loading in palladium. Usually oxygen is not measured among the impurities so there is as yet no definitive evidence supporting this hypothesis.

Efforts are continuing to attempt replication of the nuclear reactions previously seen apparently connected with low level neutron emission (13). If and when successful, this effort would provide unmistakable and unambiguous evidence of nuclear reactions in palladium in electrochemical cells at high deuterium loadings, whether or not directly connected with heat production. By inference, the presence of such reactions make more plausible the postulation of heat-producing nuclear reactions of deuterium (and light hydrogen) with elements of intermediate atomic numbers between 1 and 46.

5. FUTURE PROSPECTS

If we take at face value the numerous experimental results giving excess heat and/or nuclear products, then the following inferences can be made: 1) The alleged nuclear reaction must be taking place at the cathode surface or at grain boundaries within the metal that communicate with the external vapor phase - otherwise the helium-4 observed would be trapped within the metal and not observed in the gas phase; 2) A nuclear reaction producing alpha particles with no neutrons must be the primary source of the excess heat, i.e., a (d,alpha) or (p, alpha) reaction; 3) Since (d, alpha) reactions have been tentatively observed in Pd at atomic number 46 at a million times too small an amount to explain the excess heat, then a (d,alpha) reaction with an element of lower atomic number may be the heat source (this assumes that the d,alpha reaction will be at higher rates for lower Z elements having lower coulomb barriers); 4) Since FLUXES of deuterons across surfaces of metallic grain boundaries appear to be involved in the heat production process, research attempting to control interfaces between the metal and its surroundings and grain boundary compositions should be fruitful; 5) The elemental content at the interface may be the crucial variable - the long initiation time of 8 to 23 days implies the need for diffusion transport within the metal of some key species; 6) The classic (d+d) reaction apparently occurs in this system on rare occasions as a "side show" but is obviously not the primary heat producer; 7) The observation of tritium, since it is over one million times greater than the neutron emission rate may be from yet another reaction of deuterons on impurities of low atomic number, such as beryllium, for which the (d,t) reaction has a positive Q of 4.6 Mev (beryllium has been observed at the 1.5 ppm level in one batch of palladium); 8) Since in general, diffusion along grain boundaries is well known to be much faster than intragranular diffusion, species entering the lattice from the electrolyte such as lithium or boron are most likely to be found in those locations, just where we have surmised the nuclear reaction producing helium-4 must be if the helium is to appear in the vapor phase of the cells; 9) Because one of the rhodium isotopes observed by Wolf (Rh-99) can only be produced (assuming the reaction must be one with a positive Q) by a (p,alpha) reaction on Pd-102, the implication is clear that light hydrogen may also be a credible player in this phenomena and that the several reports of heat with light water may be credible. 10) Only a tiny fraction of the total matrix of possible significant experiments have been performed on the palladium/hydrogen system so it is premature to claim any general understanding of these phenomena; 11) It is likely that MANY different nuclear reactions are possible in this system of metal and hydrogen and that therefore, this is a very large experimental matrix to explore!

The investment required to bring about any practical use of the excess heat phenomena will probably not occur until a wide spectrum of scientists and engineers are convinced that a nuclear reaction is the source of the excess heat, whether from light or heavy hydrogen. The investment in research and development could thus occur with the assurance of an almost infinite supply of fuel for this potential energy source. The

above assumption is the basis for EPRI's program emphasis upon proving or refuting the (presumed) nuclear reaction providing the heat.

6. CONCLUSIONS

Evidence for low level nuclear reactions in heavily deuterated palladium is accumulating from many different laboratories but only in the observation of He-4 is the amount commensurate with the few watts of excess heat observed. Either some other nuclear reaction is the heat producer or the D + D reaction has been entirely changed from its known characteristics so that the reaction pathway favors He-4 and does so without the 23.8 Mev gamma ray being emitted.

Because the batch to batch variation in both the production of excess heat and tritium from palladium is so prominent, it is not unlikely that some of the major impurities are the source of the heat, tritium, neutrons, radioactivity, and helium-4 observed. The most likely suspect in this category is boron since the (d, alpha) reaction on B-10 produces three He-4 atoms with a positive energy release of 17.8 Mev. The most likely impurity for tritium production is beryllium which exhibits a (d,t) reaction with a positive energy release of 4.6 Mev. Boron is almost universally present in otherwise pure Pd at concentrations of 50-200 PPM.

The search for the source of the excess heat will continue to dominate EPRI's interest because the power industry's major business is the conversion of heat to electricity. If it turns out that a nuclear reaction is proved to be the source of the excess heat, then it would remain to find the laws for scale up to practical levels. However, that scaleup effort could occur with the assurance of a very large supply of fuel far beyond any existing ones in current use.

7. ACKNOWLEDGEMENTS

The support and encouragement of numerous EPRI colleagues have made the progress reported here possible. Particular thanks are due Richard Balzhiser, John Bateman, Jason Chao, Bindi Chexal, Paul Grant, Robin Jones, Fritz Kalhammer, Milt Klein, John Maulbetsch, Mario Rabinowitz, Don Rubio, Joe Santucci, Bob Shaw, Tom Schneider, Chauncey Starr, John Taylor, Fritz Will, David Worledge, and Kurt Yeager.

8. REFERENCES

1. Fleischmann, Pons, and Hawkins, "Electrochemically Induced Nuclear Fusion of Deuterium," J. Electroanalytical Chem., 261, 301 (1989).

2. Storms, "Review of Experimental Observations about the Cold Fusion Effect", Fusion Technology, 20, 433 (1991)

3. McKubre, Crouch-Baker, Rocha-Filho, Smedley, Tanzella, Passell, and Santucci, "Isothermal Flow Calorimetric Investigations of the D/Pd and H/Pd Systems", J. Electroanalytical Chem., 368, 55 (1994)

4. McKubre, Crouch-Baker, Riley, Smedley, and Tanzella, "Excess Power Observation in Electrochemical Studies of the D/Pd System; the Influence of Loading", Frontiers of Cold Fusion, p. 5, Universal Academy Press, Tokyo.(1993)

5. Wolf, K.L., Shoemaker, J., Coe, D.E. and Whitesell, L., "Neutron Emission from Deuterium-Loaded Metals", AIP Conference Proceedings 228, 341(1991)

6. Will, Cedzynska, and Linton, "Reproducible Tritium Generation in Electrochemical Cells Employing Palladium Cathodes with High Deuterium Loading", J. Electroanalytical Chem., 360, 161(1993).

7. Tuggle, Claytor, and Taylor, "Tritium Evolution from Various Morphologies of Palladium", Proceedings of the Fourth International Conference on Cold Fusion , Vol. 1, 7-1 Electric Power Research Institute Report TR-104188, (1994)

8. Takahashi, Iida, Takeuchi, and Mega, "Excess Heat and Nuclear Products by D20/Pd Electrolysis and Multibody Fusion", International Journal of Applied Electromagnetics in Materials 3, 221(1992)

9. Pons, S., Presentation at Third International Conference on Cold Fusion, Nagoya,, Japan. (1992)

10. McKubre, Crouch-Baker, Tanzella, Smedley, Williams, Wing, Maly-Schreiber, Rocha-Filho, Searson, Pronko, and Koehler, "Nuclear Processes in Deuterated Metals", EPRI Report TR-104195, (1994).

11. Wolf, K.L. , Private Communcation (1992)

12. George, R., Private Communication, (1995)

13. Wolf, K.L., Private Communication (1993)

9. LIST OF FIGURES AND TABLES

Table 1. OVERVIEW OF CALORIMETRIC RESULTS FROM 26 ELECTROCHEMICAL CELLS

#	Electrode A (cm)	B (cm)	C metal	D	E	F (M)	G	H °C	I (psi)	J	Maximum Loading R/R°	D/Pd	H/Pd	Calor-imeter type	Duration Expt. (h)	Init. (h)	Maximum Power Input (W)	Excess (W)	%	Total Energy Input (MJ)	Excess (MJ)	%	K #
Differential:																							
P1a	5	0.7	AECL		LiOD	1.0		7	650	682	1.20	1.06		Bulk	696	369	3.35	1.75	52.2%	3.4	0.07	2.1%	5
P1b	5	0.7	EP		LiOD	1.0		7	650	682	?	?		Plate	696	299	3	0.2	51.0%	3.0	0.02	0.7%	2
Mass flow:																							
P2	4.5	0.4	JM	AR	LiOD	1.0		4	1000	495	1.65	0.94		Si-oil	1393	504	3.8	2	52.6%	50.2	1.07	2.1%	4
P3	4.5	0.4	JM	AR	LiOD	1.0		25	1000	265	1.70	0.92		Si-oil	1250					18.0			0
P7	4.5	0.3	E#1	AR	LiOD	1.0		8	1000	259	?	?		Si-oil	145					2.1			0
P4	5	0.3	E#1	AR	LiOD	0.1		30	100	509	1.80	0.88		Si-oil	1165					16.8			0
P5	5	0.3	E#1	AR	SO4	0.5		16	100	849	1.70	0.92		Si-oil	287					4.1			0
P6	5	0.3	E#1	AR	SO4	0.5	As	4	100	573	1.70	0.92		Si-oil	649					9.3			0
P8	3	0.3	E#1	AR	LiOD	0.1		35	100	637	1.65	0.94		Si-oil	186					2.7			0
P9	3	0.3	E#1	AR	LiOD	1.0		35	52	531	1.65	0.94		Si-oil	597					21.5			0
P10	4.5	0.4	JM	AR	LiOD	1.0		35	900	47	?	?		Si-oil	18					0.3			0
P11	4.5	0.4	JM	AR	LiOD	1.0		35	1025	1179	1.65	0.94		Si-oil	85					1.2			0
P12	3	0.3	E#1	4He	LiOD	1.0	Al	30	50	884	1.55	0.97		Si-oil	1631	316	10	0.97	9.7%	58.7	0.80	1.4%	4
P13	3	0.3	E#1	AR	LiOH	1.0	Al	30	50	884	1.10	0.97		Si-oil	815		15	0	0.0%	11.7	0.00	0.0%	0
P14	3	0.3	E#1	3He	LiOD	1.0	Al	30	50	884	1.60	0.95		Si-oil	692	184	10.5	0.5	4.8%	10.0	0.20	2.0%	2
P15	3	0.3	E#1	AR	LiOD	1.0	Al	30	40	884	1.58	0.96		***	1104	684	10	2.4	24.0%	39.7	0.55	1.4%	3
P16	3	0.3	E#1	3He	LiOD	1.0	Al	30	40	884	1.70	0.92		***	1104	948	10	0.4	4.0%	39.7	0.10	0.2%	4
P17	3	0.3	E#1	AR	LiOD	1.0	Si	30	40	389	1.29	1.04		water	1202	1040	10	0.2	2.0%	13.0	0.10	0.7%	2
P20	3	0.3	E#1	AR	LiOD	1.0	Al	35	40	707	1.55	0.97		water	954	650	12	0.28	2.3%	17.2	0.16	1.0%	3
P19	3	0.3	E#1	AR	LiOD	1.0	B	35	40	672	1.45	0.99		water	1287	261	0.25	0.85	340%	42.0	0.79	1.9%	5
P21	3	0.3	E#1		LiOD	1.0	B	30	40	707	1.60	0.95		water	764	390	10.5	0.6	5.7%	13.8	0.04	0.3%	2
P22	3	0.3	E#1		LiOD	1.0	B	30	40	707	1.30	1.03		water	1480	378	0.27	0.08	30%	21.3	0.27	1.3%	3
C1	30	0.1	E	AR	LiOD	1.0	Al	30	50	764	1.65	0.94		water	866	390	45	1.35	3.0%	49.1	1.12	2.3%	1
C2	100 um		JM	AR	LiOD	1.0	Al	30	50	120	1.60	0.95		water	356	190	35	3	8.6%	14.4	0.56	3.9%	1
L1	3	0.3	E#3	AR	LiOD	1.0	Al	30	20	1088	1.99	0.76		water	1600		50			95.0			0
L2	3	0.3	E#3	AR	LiOD	1.0	Al	30	20	1088	1.99	0.76		water	900		30			50.0			0

Electrode characteristics:

A. Length. B. Diameter. C. Metal Source. AECL = Atomic Energy of Canada Limited;
EP = electroplate. JM = Johnson Matthey; E#1 = Engelhard lot #1. E = Engelhard; E#3 = Engelhard lot #3
D = surface preparation: AR = aqua regia rinse; 4He = ^{4}He implantation; 3He = ^{3}He implantation

Electrolyte characteristics:

E. Electrolyte type (SO4 = Li_2SO_4). F. Electrolyte concentration. G. Additives (at 200 ppm)

Physical characteristics:

H. Bath Temperature. I. Gas pressure (D_2 or H_2). J. Maximum current density
Maximum loading determined from resistance ratio (R/R°)
Calorimetry fluid Si-oil = silicone oil. Water = H_2O

Excess power observations:

K. Number of instances of excess power observed in that experiment

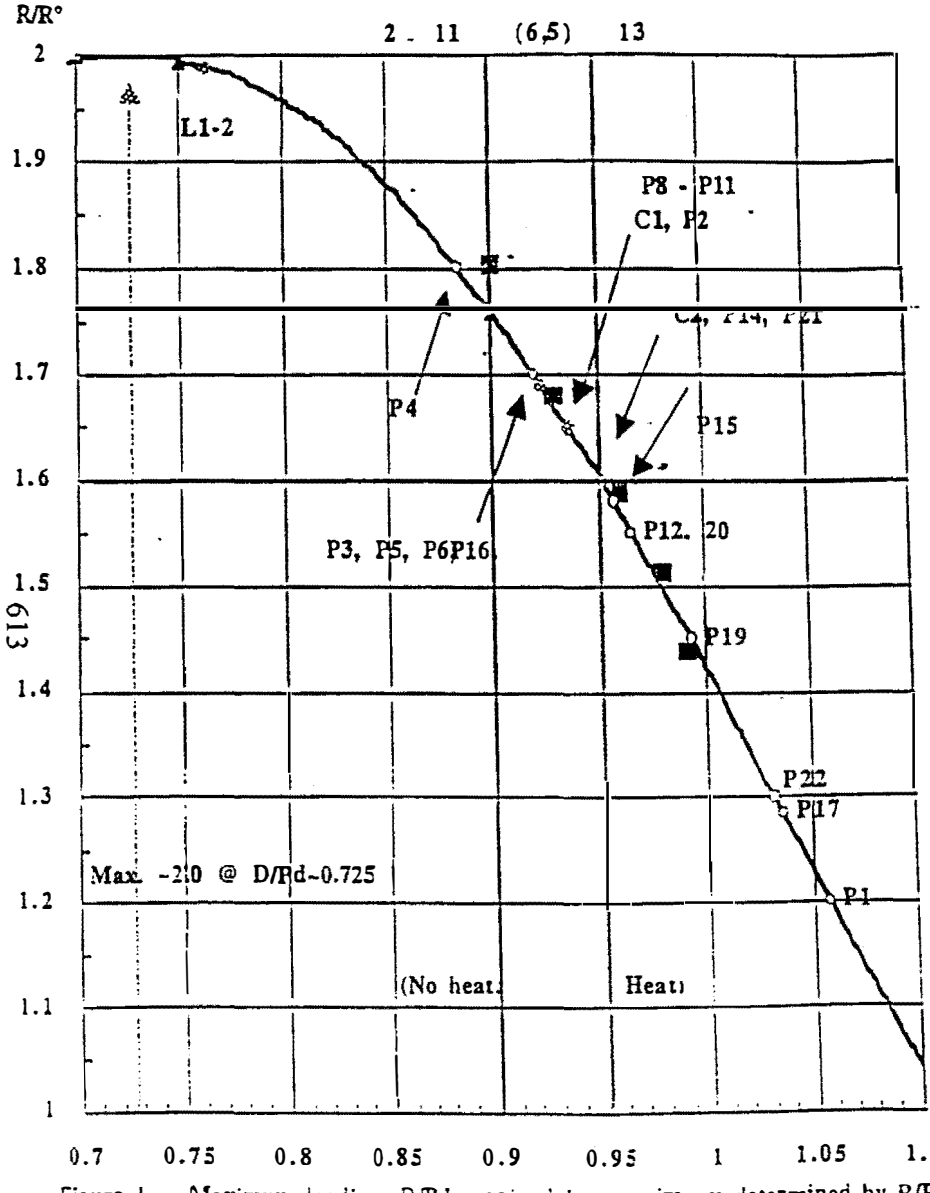

Figure 1 Maximum loading, D/Pd, attained in experiment: determined by R/R°.

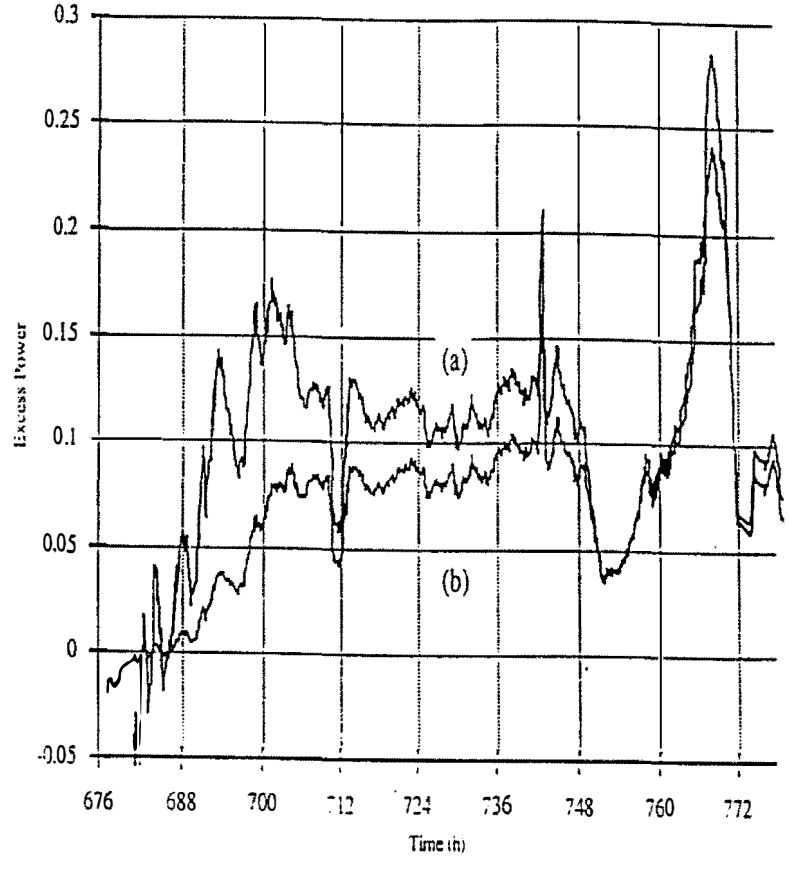

Figure 2
Variation of excess power for P15 with time (since start of experiment), expressed (a) as a fraction of the electrochemical power, and (b) as a fraction of the total input power

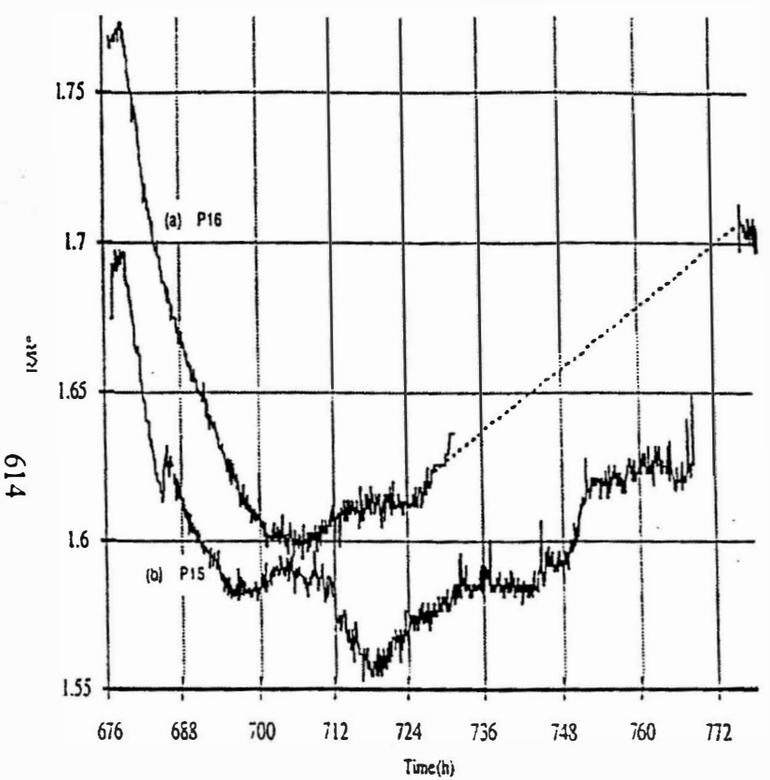

Figure 3
Resistance ratio variations for (a) P16 and (b) P15 with time (since start of experiment)

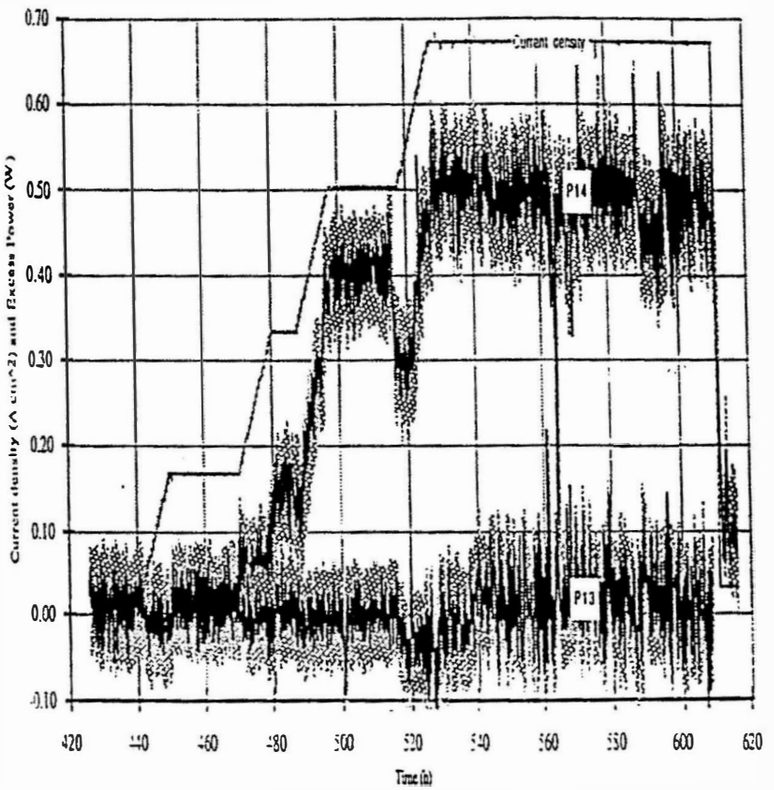

Figure 4
Variation of current density (A cm^{-2}) for P13 and P14, excess power (W) for P14, and excess power (W) for P13 with time (since start of P13). For each excess power curve (heavy line), the associated uncertainty span (hatched line) is superimposed

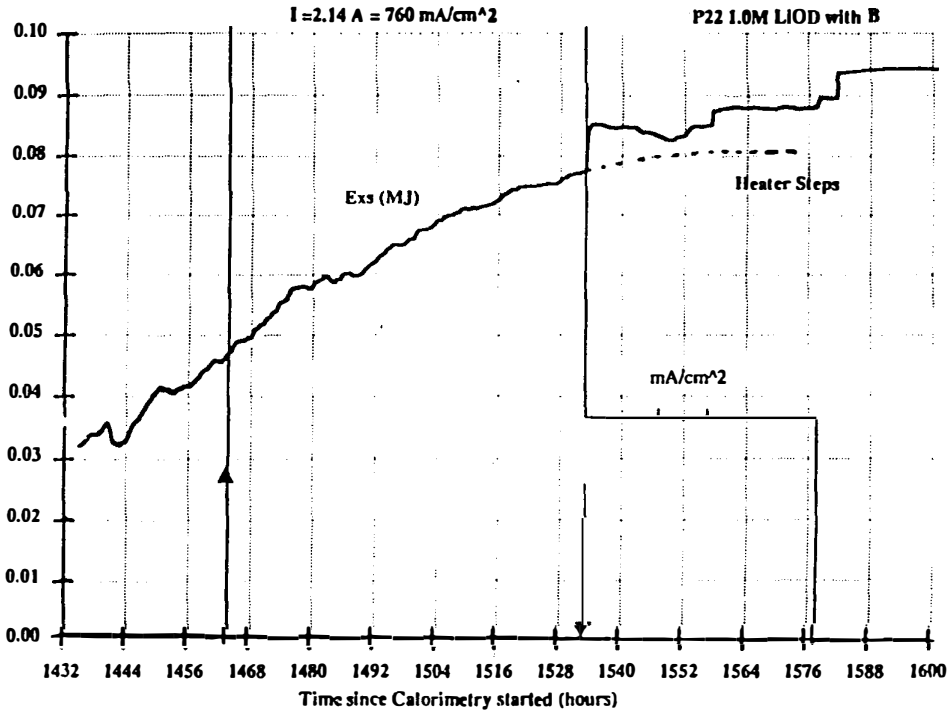

Fig. 5. Decay of Excess Heat upon Addition of Light Water to Achieve a 5 % Fraction of Light in Heavy Water Electrolyte (Cell P-22).

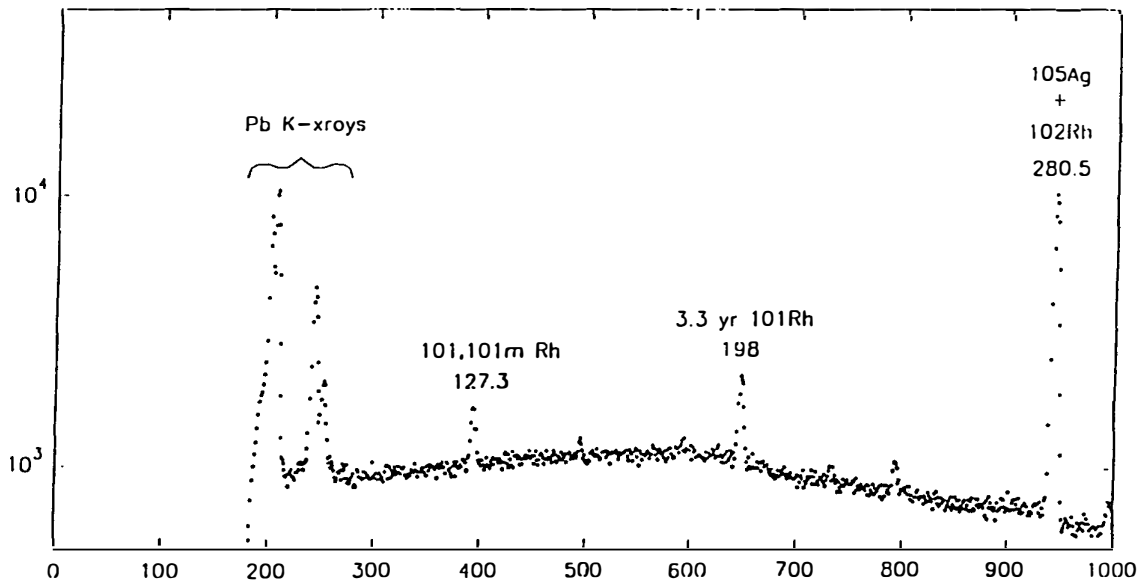

Fig. 6. Gamma Spectrum over the Energy Range 0-295 keV from a Palladium Cathode of dimensions 0.6 cm diameter by 6 cm length loaded with Deuterium in a cell having a Nickel mesh anode and using an electrolyte containing 0.1 M LiOD and ~100 PPM of Boron and Aluminum.

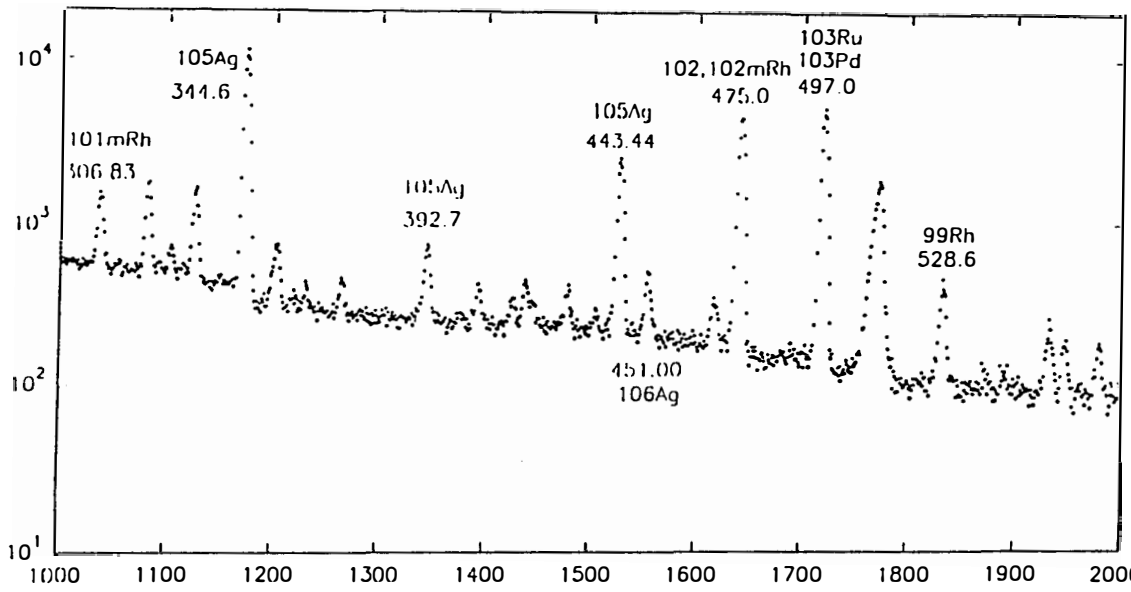

Fig. 7. Gamma Spectrum from 295 keV to 574 keV for the same cathode as in Fig. 6.

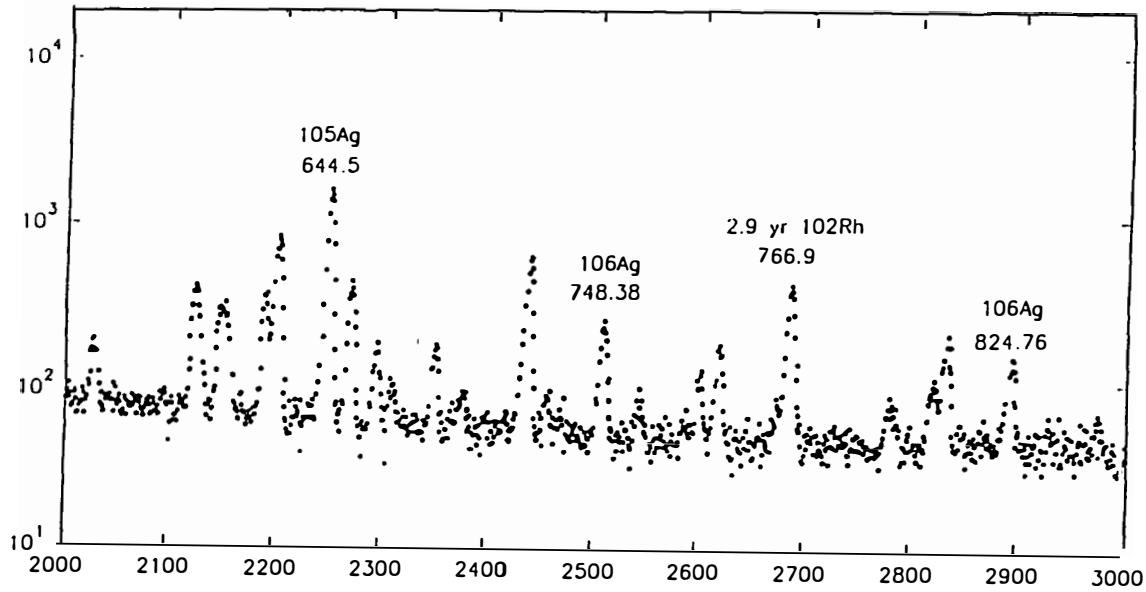

Fig. 8 Gamma Spectrum from 574 keV to 855 keV for the same cathode as in Fig 6.

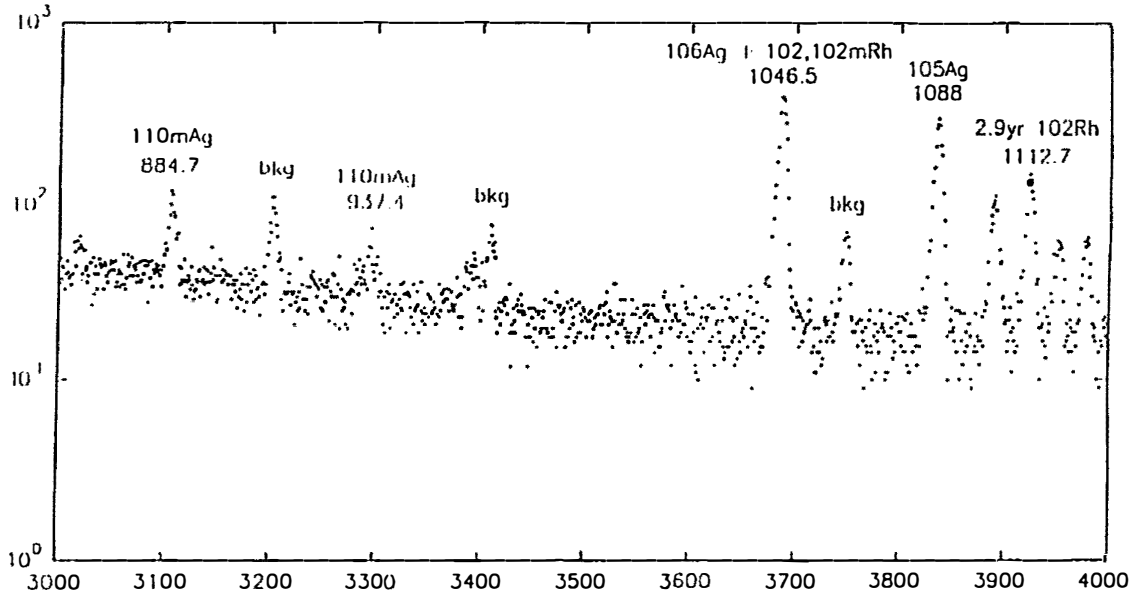

Fig. 9. Gamma Spectrum from 855 keV to 1133 keV for the same cathode as in Fig. 6.

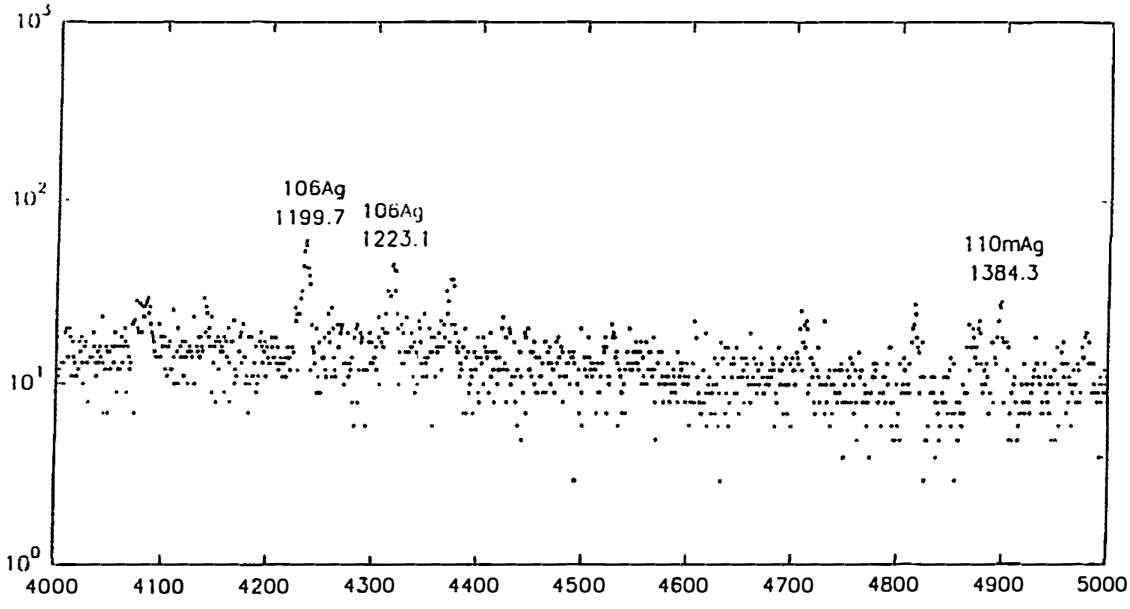

Fig 10. Gamma Spectrum from 1133 keV to 1412 keV for the same cathode as in Fig. 6

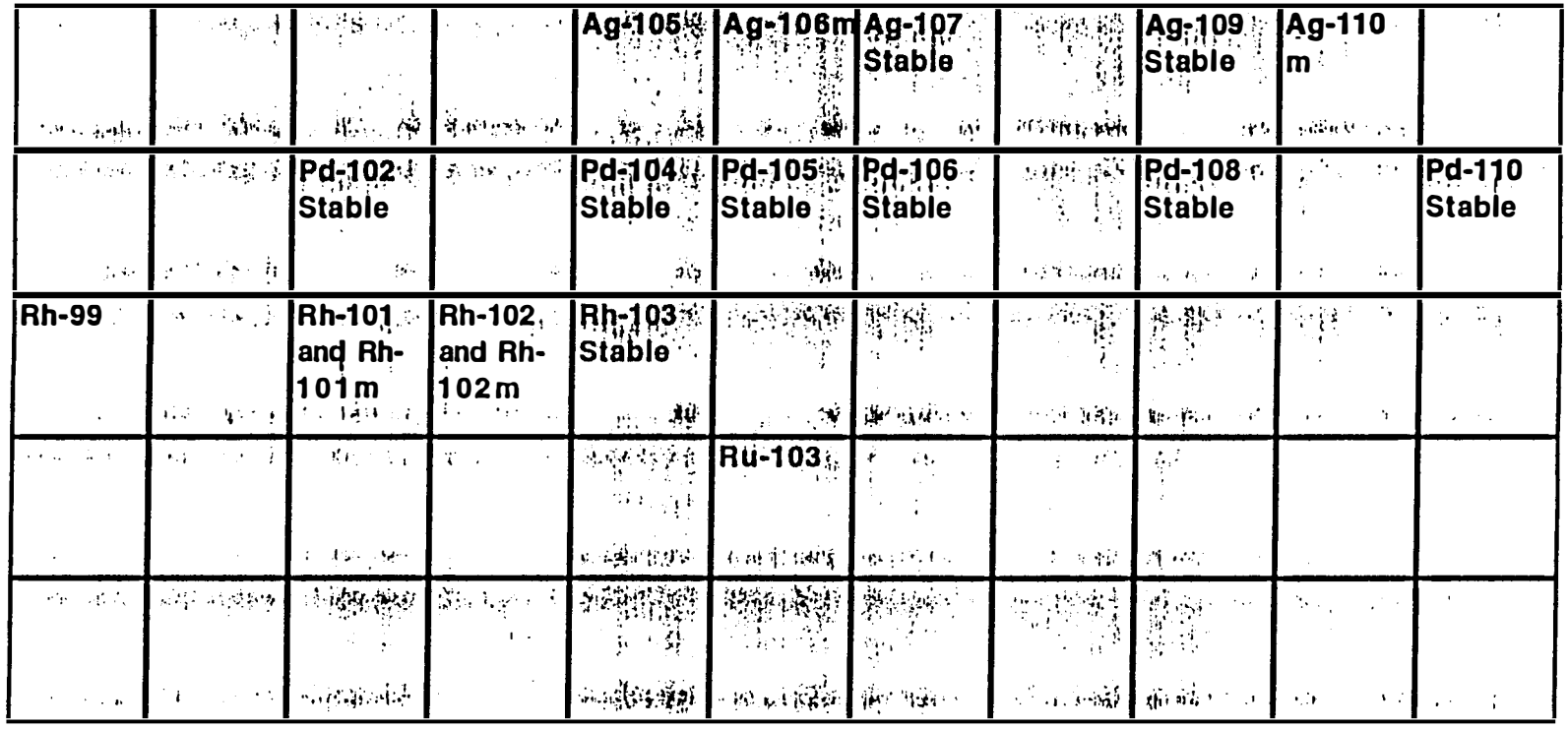

Fig. 11 Portion of the Isotopes Table for Palladium, Silver, Rhodium, and Ruthenium showing Isotopes Consistent with the Gamma Spectra in Figures 6-10

Fifth International Conference on Cold Fusion
9-13 April, 1995 - Monte Carlo, Monaco
ICCF5 ©1995

Synthesis of Substance and Generation of Heat in Charcoal Cathode in electrolysis of H2O and D2O Using Various Alkalihydrooxides

Ryoji TAKAHASHI
University of Tokyo
Setagaya-ku Seta 2-26-21,Tokyo,Japan 158

Abstract

Charcoal was used for the cathode with interest in the fabricated micro-channels which may produce the microdrops responsible for the synthesis of material and C.F.in the electrolysis as reported in the previous proceeding.

The synthesis of material was detected with the change in color of the electrolite,from colorless to dark brown. The excess heat was not detected for H2O. However,for a mixture of 25%H2O and 75%D2O with 0.25NLiOH,the excess heat reached as high as about 30% of the input power.

1.Introduction

It is well known that charcoal has micro-channels built in biologically,and that it has high electrical conductivity when prepared at high temperatures. So it is of interest whether the cathodic use of charcoal may perform the working of the microdrop,the synthesis of material and the evolution of heat,as shown previously(1).

2.Charcoal Cathode

The specimen was sampled from the twig charcoal by sawing cross sectionally for various lots,forms and sizes.The ash elements were removed by immersing the specimen into HCl for about three days and the acid was removed by washing in hot water.The electrode applied was a piece of solder wire, Pb-Sn alloy,pushed into a drilled hole.The side surface of the specimen was coated with Araldite resin to maintain the mechanical strength and to diminish the waste current which does not take part in the electrolysis in the micro-channel.

3.Synthesis of Substance in Charcoal Cathode

The specimen was dipped partially into an electrolyte

containing 0.25N of an Alkalihydrooxide,i.e.LiOH,NaOH,KOH, RbOH and CsOH respectively.The electrolysis was done in a cell containing 50-80cc of the electrolyte under the input power less than about 4 watt.

From the early stage of the experiment for NaOH,it was found that the electrolyte used was often colored with dark brown in about half an hour.As there was no substance responsible for the colorization other than charcoal,Araldite was not yet used at that time,it was supposed that some materials are created in the cathode.To assure this idea a heating experiment was done for the sliced and powdered charcoal respectively in 0.25N NaOH-water solution at about 90 °C for 4 hours. As a result the former produced slight colorization of dark brown,but the latter did not at all. This shows that the colorization is due to the structure-dependent synthesis action in the charcoal and not due to the extraction of substance from the charcoal. In this way the synthesis action of the microdrop was assured and the colorization became a compass needle for the xperiment.

4.Generation of Heat in Cathode

The working microdrop evolves heat as a parallel phenomenon to the synthesis.The temperature rise in the cathode was measured by using two sets of thermistor thermometers as shown in Fig.1.The temperature rise ΔT is given by,

$$\Delta T = Tc - Tw, \tag{1}$$

where Tc and Tw show the temperatures in the cathode and the electrolyte respectively.By applying a constant DC voltage

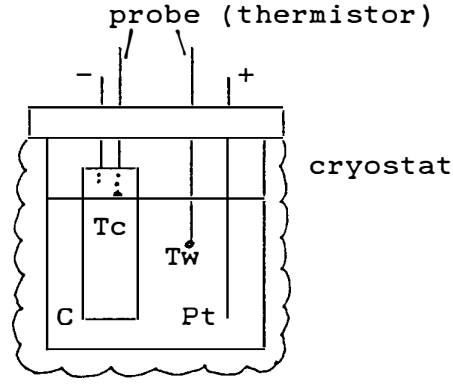

Fig.1 Arrangement for measuring temperature rise in cathode by electrolysis.

Tc and Tw were measured as functions of time,and it was found that the colorization is strongly correlated with ΔT,

and ΔT is almost constant during a run of the electrolysis.

5.Measurement of Excess Heat

The measurement of the excess heat evolved in this system was carried out by detecting the temperature rise in Tw for an input power for 20 minuits using the apparatus shown in Fig.1.The volume of the electrolyte used was 50cc and the mass of the cathode was 3g. First the temperature rise by the Joule heating was measured by using a simple resistor for various input power,and the result is shown by a solid line in Fig.2. The temperature rise measured for

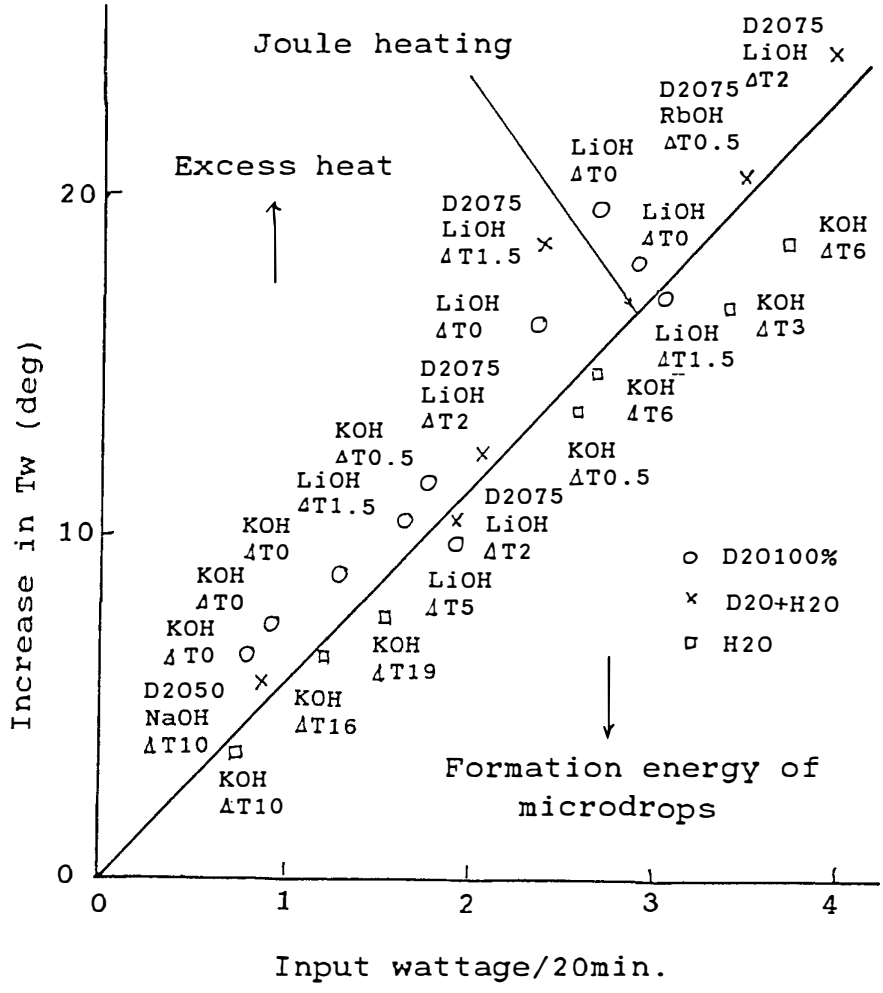

Fig.2 Excess heat generation in the electrolysis using charcoal cathode for D2O,D2O and H2O mixture and H2O.

various charcoal cathodes,for D2O,the mixture of D2O and H2O and H2O were plotted in Fig.2 by circles,crosses and squares respectively. The squares distribute under the line of Joule heating independent of the value ofΔT. The reason is attributed to the necessary formation energy of microdrops to corrode the cathode.The distribution of the circles and the crosses are mostly above the line of Joule heating,showing that excess heat larger than the formation energy is evolved in these experiments. Excess heat as much as about 30% of the input power was detected for a D2O75% electrolyte with 0.25NLiOH.

6.Conclusion

1)The synthesis action expected for the microdrops which arise in the charcoal cathode was very noticeable. The electrolysis changed the color of the electrolyte from colorless into dark brown.

2)Heat evolution was detected in the cathode as a parallel phenomenon to the synthesis action.

3)Excess heat was detected in the electrolysis for D2O and for the mixture of D2O and H2O but it was not detected for H2O.

4)Charcoal tends to form chemical compounds in the electrolysis and from this reason the fusion between deuterons, the cause of the excess heat,is poor.

5)It is doubtless that the microdrop plays the key role in the cold fusion.It is important to improve the fusion efficiency for the fundamental research and also for the practical application.

Referece

1.Takahashi,"Cold Fusion Explained by Negentropy Theory of Microdrop of Heavy Water,"Proc.4th Int.Conf.on Cold Fusion, Volume 4,29-1.

Fifth International Conference on Cold Fusion
9-13 April, 1995 - Monte Carlo, Monaco
ICCF5 ©1995

Experimental Evidences for the Harmonic Oscillator Resonance and Electron Accumulation Model of Cold Fusion.

Michel RAMBAUT
57H rue De La Hacquinière
91440, Bures-sur-Yvette, France.

Abstract

Cold Fusion outside any substratum is again considered from the Harmonic oscillator resonance and electron accumulation (HOREA) model point of view. If one adds Fractal theory, one gets a more straigthforward agreement with the experimental growth of fusion burst after the apex I of a fast current, and varying approximately like the tenth power I^{10}. Then it is shown that the model could account for the solar neutrino discrepancy. The paper ends up by a short reminder of two experimental data, in agreement with the HOREA point of view: experimentally noticed Electron accumulations, and Top-Table soft X-ray Laser operation.

1. Introduction

The fusion process in a deuterated medium, outside any substratum has been told previously as being a particular one, among the various process, famed as being Cold Fusion processes [1]. The process described by the HOREA model is probably the most general process underlying the experimental observations, even in the case where the phenomenon occurs in a substratum like Palladium, Nickel, or in any other substrat which can absorb Hydrogen [2]. Inspite experimental data are still scarce and sometimes questionable,in the case of the process without substratum, if coupled with the HOREA model, they are leading to a quantitative description. This Cold Fusion approach has links with some frontier problems, like the fractality of a medium, the operation of a star like the Sun, and also with the validity of the Heaviside Fitzgerald and Lodge interpretation the Maxwellian Electrodynamics, which came out in 1888 [3].

2. The Fractal Point of view: A new insight into the fusion experiments by fast transitory currents.

The fractal point of view gives a more striking picture of the agreement between the Kiel and NRL experiments [2] and the HOREA model. During the leading edge of the current pattern, the medium was ionized; and as soon as the peak was reached, the neutron burst occured, which is conjectured to be only a testimony-like of the $D+D \rightarrow {}^4He$ reactions. According this model, the phenomenon is marked by a Poisson distribution of two colliding deuteron places and it is possible to take into account, as a good representative parameter, the De Broglie wavelength of the Deuteron. This distribution is the mark of the fractal character [4] of the fusible medium. Using the Schrödinger equation, it has been obtained, a linear relationship in logarithmic scale, of the fusion production term T, in function of the Deuteron energy, which has the same slope, than the one in function of the De Broglie wavelength [1]. The box counting dimension, practical approximation of the Hausdorff dimension [4], is obtained by dividing the fusible medium into a three-dimensional mesh, composed of boxes or practically of cubes, whose side length is δ; it is the limit of the logarithm of the number N_δ of boxes containing an element of the medium, in function of the logarithm of the cube size inverse $1/\delta$. Practically, one uses only an approximation of D, with a finite size δ, determined by Physics. In the specific case of the electron accumulation fusion medium, one can convert the D expression into one depending on the mean rate μ of Deuteron in a cubic box of side δ, given by the Poisson law. The probability P_1 for a boxe containing one Deuteron is thus, n being the number of Deuteron per volume unit.

$$P_1 = e^{-\mu}\,\mu = \delta^3\, n \qquad (1)$$

And the probability P_2 for a boxe containing two Deuterons:

$$P_2 = \frac{1}{2} e^{-\mu} \mu^2 = \frac{1}{2} \delta^6 n^3 \qquad (2)$$

The number of boxes with two Deuterons being $\frac{1}{2} \delta^6 n^2$, and as δ is typically in the range of 10^{-9} cm, for colliding Deuterons, and n of the order of $10^{23}/cm^3$, μ is low, and $e^{-\mu}$ can be replaced by one. So the practical expression of the fractal dimension D is:

$$D = \lim \frac{\frac{1}{2} \delta^6 n^3}{\text{Log } 1/\delta} \qquad (3)$$

The mean ratio between the number of boxes, and containing two Deuterons, and the number of boxes containing one Deuteron is very close to $\mu/2$. Given that all boxes containing one unique Deuteron are supposed to give up their electron to the boxe containing two Deuterons, one can express the fractal dimension D in function of the ν number of the electrons accumulated around the two colliding Deuterons [1] ($\nu = 2/\mu$),n and taking into account the relationship,

$$\delta = (\mu/n)^{1/3} \qquad (4)$$

the fractal dimension is thus:

$$D = \frac{\text{Log } 2n/\nu^2}{1/3 \text{ Log } n\nu/2} \qquad (5)$$

This D expression, makes a link with the quantum calculation, which was fulfilled for some specific values of ν [1]. The NRL I^{10} power law, surprising at first sight, is directly linked with the fractality of the fusible medium. A medium which would be submitted to thermonuclear conditions, would not give such a power law, given that the fratal dimension would be evidently equal to 3. The figure 1 gives the fractal dimension D variations in function of the logarithm of the density n, for 3 values of the electron number accumulated around two colliding Deuterons. It is interesting to emphazize on the agreement of those values with the ones resulting from Schrödinger calculations. For example, for $n=10^{22}/cm^3$, the fractal dimension deduced from Schrödinger calculations is 1.92, the electron number being equal to $\nu = 1.3 \times 10^3$, whereas the direct calculation gives 1.94 for the fractal dimension. The agreement between the two ways to get the fractal dimension has a deep physical significance, which needs to be still digged deeper.

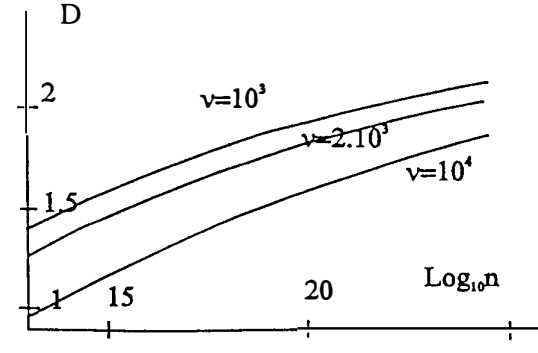

Figure 1: Plot of the fractal dimension D vs the number n of particle/cm^3, and for 3 values of the electron number ν.

3. Account for the solar neutrino discrepancy.

The solar neutrino counting reveals a discrepancy of approximately 30 percents, confirmed recently [5] between the 123 SNU, predicted by the standard model, and the 83 SNU, effectively detected with a uncertainty of 21 SNU (One Solar Neutrino Unit (SNU) corresponds to 10^{-36} neutrino interaction per atom of the detector and per second). The solar

standard model describes the sun as being roughly constituted of three parts: the core, the radiative zone, and the convection zone [6]. It is characterized by some physical parameters: the solar luminosity: $L_\odot = 3.826\ 10^{33}$ erg s^{-1} , the solar radius: $R_\odot = 6.9598\ 10^{10}$ cm, the inner convection zone radius: 0.73 $R_\odot$, corresponding to a temperature of 1.3×10^6 K, to a density of 0.15 g cm^{-3} [7], and to a pressure of 6×10^{12} dynes/cm^3.

In the convection zone there is no possiblity of thermonuclear reaction, but there should be some possibilities of fusion reactions, by the HOREA process. This hypothesis is in agreement with the effect of electron accumulation bringing about the fusion process, which can only occur in an ionized medium, submitted to turbulence, for example during the trailing edge of a fast current pattern[2].

The cold fusion process in solar convection zone is supposed essentially due to nuclear reactions between Deuterons. With the above parameters, the number of nuclei per cm^3 is in the range of some units of 10^{22}, and given the relative great rate of Hydrogen [7], the Hydrogen particle number n is close to this value. Taking into account the mass fraction of Hydrogen and Helium, one has approximately n(H) =0.92 n, so one can take in first approximation $n = 1.0 \times 10^{22}/cm^3$, for the mean hydrogen nuclei number in the convection zone, and as the Deuterium/Hydrogen ratio is $D/H < 4 \times 10^{-5}$, the Deuterium density is approximately determined by $n(D) < 4.0 \times 10^{17}/cm^3$.

The expression of the Fusion energy production of the HOREA model is rather different from the one deduced from the Lawson criterium [8].

$$E = n^2/4\ T\ e\ \Delta t \qquad (6)$$

E is the energy produced during the Δt lapse of time, n is a particle number, able to participate to the fusion nuclear reaction, T called "the production term", describes the crossing of the "screened" Coulomb barrier, e is the energy, given off by one nuclear reaction.

The T value is obtained from the relationship, depending on the fractal dimension D, between the "production term" T and the Deuteron energy ε ($T/T_0 = (\varepsilon/\varepsilon_0)^D$). Supposing a Deuteron energy given by the Boltzmann equality ($\varepsilon = 3/2\ k\ \theta$), one gets $\varepsilon = 129$ eV. But the interesting parameters of the laboratory experiment T_0 and ε_0 are in fact poorly known. The ion energy mean value ε_0 is largeley superior to the thermal one (less than 1 eV in Kiel conditions), at the time of the fast current decrease, by resonance effect [2]. With D around 1.5, T_0 should be estimated in the range 10^{-27} -10^{-26} cm3/sec, and T in the solar convection zone ,should be in the maximum range 10^{-25} -10^{-24} cm3/sec.

But the behaviour of the medium cannot be described completely by the above expression of the energy E, whereas the number of fusible Deuterons is very low in comparison with the number of the other ions. One has in fact to multiply the "production term" T, by the probability for fusible ions, to be in touch. This probability can be evaluated considering a volume V of the medium containing two Deuterons and 2xH/D non fusible ions. If V is cubic, for the simplicity of calculation, and containing ζ cells, one can show that this probability p_f of collision for a possible fusion process in the elementary box is:

$$p_f = 2x26(\ \zeta - 6\zeta^{2/3}\ )\ (\ \zeta - 2\ )!/\ (\zeta)! \qquad (7)$$

The E fusion rate of formula (6) has thus to be multiplied by p_f. With the above numerical values, one gets $p_f < 8.6\ 10^{-4}$, and for the total energy production per second W, in the convection zone:

$$1.0\ 10^{33}\ \text{erg/sec} < W < 1.0\ 10^{34}\ \text{erg/sec}$$

This range includes the third of solar luminosity. One ought get a value close to $L_\odot/3 = 1.2753 \times 10^{33}$ erg s^{-1}. New well instrumented experiments, a little similar to the Kiel ones, and new complete computer calculations, could let us to conclude, but the rough estimate, utilizing the mean values, does not gives a great discrepancy. In fact the solar central inner core could a little cooler than is usually estimated.

3. Non Fusion Experiments in agreement with the HOREA model

Electron clusters, as great as 2×10^{10} are told to be produced by a variety of sources. In the ref.[9], is given the description of a specific one. Nevertheless the possible existence of those cluster is linked with the question of physical validity of the so called Maxwell equations,

which are in fact the result of an interpretation of Maxwell theory by Heaviside and Al [3]. Assigning a physical value to the vector potential, like in Schrödinger calculations for HOREA, a possible explanation could based on a possible energy oscillation with the De Broglie wavelength, of the Faraday field, like has been claiming P.Beckmann [9].

Another experiment is a lasing one at 46.5 nm: it has been achieved recently by J.J.Rocca et Al [10]. The basic idea was to perform a direct excitation of the plasma medium by a pulsed discharge, instead of exciting it by an exterior flux: it has consisted of running a pulsed current through the lasing medium. The current pulse had an amplitude of 40 kA and a half period of 60 ns. Diagnostics using a 5 ns detector gate indicate that lasing occurs near the moment of maximum compression, shortly after the peak of the current pulse. This observation has to be brought nearer wit a similar observation made in the Kiel and NRL experiments, showing that neutron production occurs shortly after the peak of the current pulse [1] [2]. Apart the fact that nuclear reactions cannot occur, it seems that the process leading to lasing phenomenon could be described by the HOREA model.

5.Conclusion

Even if the experimental data are still too scarce and imprecise, there is an growing agreement with HOREA model. Firstly, the tentative fusion pulsed experiments, considered from the fractal point of view, reveal the existence of a dispersed process in a cold medium. In another terms it is an indirect proof of the Cold Fusion existence. As for the application of the model to the solar case, reveals that it could account for the thirty percent deficiency of solar neutrinos, inspite the approximative knowledge of the Deuteron density and of the production termT, the inner solar core being cooler than usually estimated.

All those experimental facts, linked with the HOREA model, constitute a network of non contradictory elements revealing the effectiveness of Cold Fusion outside any specific substratum. Those elements are moreover non contradictory with non fusion experiments, like electron accumulation experiments, and Table-Top X-ray laser experiments.

References

[1]. M.Rambaut, Physics Letters A 163 (1992) 335-342, 30 march 1992, & Physics Letters A 164 (1992), 155-163, 13 April 1992.

[2] M.Rambaut, Transactions of Fusion Technology, volume 26, Number 4T, Part 2, 486-492, December 1994 & Proceedings: Fourth International Conference on Cold Fusion,Volume 4, 24-1, EPRI publication 1994.

[3] T.W.Barret, Electromagnetic Phenomena not explained by Maxwell's equations, in Essays on the Formal Aspects of Electromagnetic Theory, Editor Akhlesh Lakhtakia, World Scientific, 1993.

[4] B.Mandelbrot, "Les objets fractals",Flammarion, Paris, (1975); "Fractals: Form, Chance and Dimension, Freeman, San Francisco, (1977); "The Fractal Geometry of Nature", Freeman, San Francisco (1983).

[5] P.Anselman et al., Physics Letters B, 285, 376, 1992 & 285, 390, 1992.

[6] John N.Bahcall, Walter F.Huebner, Stephen H.Lubow, Peter D.Parker, Roger K.Ulrich, Review of Modern Physics, Vol. 54, N 3, July 1982.

[7] Kenneth R.Lang, Astrophysical Formulae, Springer-Verlag, 1986.

[8]. M.Rambaut, Frontiers of Cold Fusion, ICCF3, Nagoya, October 21-25, 1993, Universal Academic Press,Inc, pages 601-604.

[9] Petr Beckmann, "Electron clusters", Galilean Electrodynamics, vol.1, N 3, pp.55-58, Sept/Oct 1990.

[10] J.J Rocca, V.Shlyaptsev, F.G.Tomasel, O.D.Cort zar, D.Hartshorn, and J.L.A.Chilla, Physical Review Letters, Volume 73, Number 16, 17 October 1994 & G.P.Collins, Physics Today, October 1994, 19-22.

Fifth International Conference on Cold Fusion
9-13 April, 1995 - Monte Carlo, Monaco
ICCF5 ©1995

Nuclear Reactions of Cold Fusion - A systematic Study

W. J. M. F. COLLIS
Strada Sottopiazzo, 18
14056 Boglietto (AT), ITALY

Abstract

A computer is used make an exhaustive search for simple nuclear reactions between naturally occurring isotopes with a view to identifying possible primary cold fusion reactions and materials which might support theoretical models. We discuss the difficulties in producing neutrons and tritium in light water experiments.

1. Introduction

Despite substantial progress made in demonstrating Cold Fusion phenomena, it is still not clear what nuclear reactions, if any, are taking place. Many workers have reported small quantities of possible products including neutrons, tritium, helium isotopes and other unidentified short lived radioactive isotopes. No systematic pattern has emerged, but it has been suggested independently by various workers[8,10] that the usual nuclear parameters reaction energy, spin and parity conservation are important criteria.

We have created a simple database of some 2400 atomic weights and nuclear spins and parities[7] on a personal computer. Many sources of atomic data contain significant errors, so we first checked the atomic weights for consistency by performing a least squares fit to a model independent equation of the form:

$$A.W. = g_1(Z)+g_2(N)+g_3(N+Z)+g_4(N-Z)$$

where g_n are four arrays for a total of 570 coefficients. The average error was 10^{-4} amu, about an order of magnitude more accurate than the semi-empirical liquid drop formulae. A simpler version of this formula was first proposed by Garvey et al in 1969[13] when it was not possible to solve the 570 simultaneous equations on available computers!

The program searches for generic reactions limited to 1 or two reactants and / or products:-

$$R + S \rightarrow P + Q \quad (1)$$

where R and S are one of the 278 naturally occurring nuclides and P and Q are nuclear products such as tritium, neutron, helium isotopes. We assume that any weak interactions will be insignificant (excepting possible decay of P and Q) and therefore the number of neutrons and protons in the system are conserved.

2. Selection Criteria

Only exothermic reactions are considered involving naturally occurring nuclides. In order to reduce the number of possibilities further we may need to suppose that[8] the products are stable to beta decay, and nuclear spin and parity are conserved.

Apart from the laws of physics, we can impose criteria on the basis of possible reactants, such as the materials constituting the cold fusion system. Alternatively we can examine those reactions which produce a specific product such as He, tritium or neutrons.

3.0 Product Oriented Approach

The approach of searching for reactions which generate specific products does not give many positive results. For example ^{4}He can be formed in hundreds of different reactions between natural nuclides and hydrogen isotopes. Consequently the detection of helium alone, even quantities commensurate with heat production is not definitive evidence of simple deuterium fusion, nor indeed of any other specific reaction. Identical arguments apply to neutron production in deuterium systems. In contrast ^{3}He and tritium production from deuterium are limited to a dozen or so simple reactions, and results are published elsewhere[16]. However such products cannot be part of any major reaction not being commensurate with heat production.

3.1 Light Hydrogen Systems

The product oriented approach can usefully concentrate on neutron and tritium production from protium with interesting negative results. The computer finds **no** simple exothermic reactions of the form:

$$^{1}H + {}^{A}R \rightarrow {}^{3}H + {}^{A-2}P \quad (2)$$

At least two independent groups have detected tritium production in light water electrolysis[4,5]!

We find only one exothermic neutron producing reaction:

$$^{1}H + {}^{40}K \rightarrow {}^{1}n + {}^{40}Ca \quad +0.530 \text{ Mev}$$

We should not be surprised that such reactions are rare, as they must be endothermic for all beta stable nuclei. There are few naturally occurring beta unstable isotopes, and ^{40}K with a half life of about 10^9 years is one of them. However there may be some difficulty with ^{40}K as a source of neutron production in light hydrogen experiments[6,17]. Firstly the above reaction does not conserve nuclear spin nor parity so the neutron production channel will be strongly suppressed. ^{40}K constitutes only one part in ten thousand of natural potassium. Finally, there is no reason to suppose that any potassium was present in the experiments.

Bush[14] has reported the detection of both the above strontium isotopes in same isotopic proportions as natural rubidium. The different spin changes suggest that the rate of fusion will be different for the two rubidium isotopes, and one presumes that any cold fusion is occurring in a very limited zone where essentially all the rubidium is being transmuted! An alternative explanation is that the two rubidium isotopes are transmuted by neutron transfer (as discussed subsequently in this paper) which then beta decay to strontium. In this case there are no unfavourable spin changes, and one would expect tiny quantities of ^{86}Kr also as an minor decay product of ^{86}Rb.

Bush has also extended the Cold Alkali Fusion, CAF hypothesis to hydrogen fusion with other nuclides and suggests that the reaction energy is an important criterion. The author has discussed this idea elsewhere[15].

4. Palladium Fission

In 1992 Karabut et al.[8] reported unexpected quantities of Na, Mg, Al, Si, S, Ca, Ti, Cr, Fe, Ni, Zn, Ge, Br, Sr, Mo after glow discharge of deuterium gas between palladium electrodes and tentatively suggested fission as an explanation. They excluded simple reactions of type (1) for R=deuterium on the grounds of conservation laws cited previously. However the following reactions do conserve spin and parity and produce stable products:

$^{1}H + {}^{102}Pd \rightarrow {}^{19}F + {}^{84}Sr$	+1.49 MeV
$^{1}H + {}^{104}Pd \rightarrow {}^{19}F + {}^{86}Sr$	+3.90 MeV
$^{1}H + {}^{106}Pd \rightarrow {}^{19}F + {}^{88}Sr$	+6.78 MeV
$^{2}H + {}^{106}Pd \rightarrow {}^{14}N + {}^{94}Zr$	+7.63 MeV
$^{1}H + {}^{105}Pd \rightarrow {}^{23}Na + {}^{83}Kr$	+8.38 MeV
$^{2}H + {}^{104}Pd \rightarrow {}^{14}N + {}^{92}Zr$	+9.33 MeV
$^{2}H + {}^{102}Pd \rightarrow {}^{14}N + {}^{90}Zr$	+11.11 MeV
$^{1}H + {}^{106}Pd \rightarrow {}^{31}P + {}^{76}Ge$	+15.03 MeV
$^{1}H + {}^{104}Pd \rightarrow {}^{31}P + {}^{74}Ge$	+15.76 MeV
$^{1}H + {}^{102}Pd \rightarrow {}^{31}P + {}^{72}Ge$	+16.39 MeV
$^{2}H + {}^{105}Pd \rightarrow {}^{23}Na + {}^{84}Kr$	+16.68 MeV
$^{2}H + {}^{105}Pd \rightarrow {}^{37}Cl + {}^{70}Zn$	+26.04 MeV
$^{2}H + {}^{102}Pd \rightarrow {}^{49}Ti + {}^{55}Mn$	+31 47 MeV

Absent from this list are Mg, Al, Si, S, Ca, Cr, Fe, Ni, Mo. Perhaps the selection criteria may be excessively restrictive. Relaxing spin conservation we could expect Ni, Cr, Mo, Al, Se, B as additional stable products. In 1993 Karabut et al.[9] reported more refined detection of palladium "impurities" after glow discharge including isotope shifts in He, Li, C, K, Zr.

A difficulty with the fusion / fission approach is that even if the hydrogen nuclide can penetrate the Coulomb barrier, an intermediate silver nucleus is unlikely to be sufficiently excited to break up into fission fragments. On the other hand results of other workers at this conference do lend experimental support for transmutations (ie Dash J, Wolf K., George R.).

5.0 Polyneutrons

Fisher has proposed the involvement of neutral hypothetical poly-neutrons agents in an attempt to overcome the usual objections of Coulomb and other energy barriers to Cold Fusion[3]. The hypothesis explains the sporadicity of heat production and the substantial absence of gamma rays. Poly-neutrons are speculated to be generated from super heavy hydrogen isotopes present in water and concentrated with deuterium. In

contrast to other the neutron transfer theories, the role of hydrogen isotopes is explained.

Excess heat is speculated to be produced by poly-neutron growth by the exchange of neutron pairs. The computer compiles the following table of isotopes which can accept neutron pairs yielding some 11 MeV or less (these isotopes should not allow ^{6}n shrinkage).

	Accept MeV	Donate MeV	Neutron X Section barns	Abund. %
^{1}H	8.4	-	.332	100
^{4}He	0.9	-28.3	0	100
^{6}Li	9.2	-31.8	941*	7.5
^{7}Li	6.0	-12.9	.0395	92.5*
^{9}Be	7.3	-20.5	.0081	100
^{11}B	8.2	-19.8	.00053	80.1*
^{13}C	9.3	-23.6	.00141	1.1*
^{15}N	8.3	-21.3	.000041	0.372*
^{136}Xe	9.8	-14.4	.262	8.9*
^{208}Pb	9.1	-14.1	.00493	52.4*
^{209}Bi	9.7	-14.3	.011	100
^{232}Th	10.9	-11.5	7.347	100
^{238}U	10.7	-11.2	2.71	99.3

However the lighter nuclides, with the exception of ^{7}Li cannot assist in ^{6}n growth because they cannot donate a pair of neutrons for 15 MeV or less. ^{6}Li has a high neutron absorption cross-section and would be expected to poison polyneutron creation. In the table an asterisk (*) indicates an unsuitable parameter.

The best materials appear to be Bi, Th and U. However the fact that deuterides of these metals have been successfully prepared in the laboratory without noticeable effects[12] suggests that any successfully poly-neutron theory may require modification. Both thorium and uranium hydrides (deuterides) are pyrophoric - they catch fire spontaneously in air. It is quite possible that any anomalous heat production may have been discounted as being due to atmospheric contamination. Similarly, any radioactivity could be discounted as being natural.

The polyneutron theory can explain both the creation of neutrons and tritium in light water experiments. Neutrons are predicted to be created in bursts as a result of ^{4}n decay. Tritium may be created when an excited poly-neutron donates a pair of neutrons to protium. The theory predicts neutron amplification now verified experimentally[11].

6.0 Neutron Transfer

According to Hagelstein[2], neutrons may be able to hop from one nucleus to another in the lattice. Such a possibility is conjectured to be favoured if spin and parity are conserved for the production and absorption of the free virtual s-wave neutron and if the overall reaction energy is small (near resonance). The computer finds these reactions:

$^{37}Cl + ^{195}Pt \rightarrow {}^{38}Cl + {}^{194}Pt + 3$ keV
$^{85}Rb + ^{184}Os \rightarrow {}^{86}Rb + {}^{183}Os + 3$ keV
$^{70}Ge + ^{184}W \rightarrow {}^{71}Ge + {}^{183}W + 4$ keV
$^{204}Hg + {}^{6}Li \rightarrow {}^{205}Hg + {}^{5}Li + 4$ keV
$^{76}Se + ^{184}W \rightarrow {}^{77}Se + {}^{183}W + 7$ keV
$^{125}Te + ^{120}Sn \rightarrow {}^{126}Te + {}^{119}Sn + 7$ keV
$^{117}Sn + ^{103}Rh \rightarrow {}^{118}Sn + {}^{102}Rh + 8$ keV
$^{199}Hg + ^{172}Yb \rightarrow {}^{200}Hg + {}^{171}Yb + 9$ keV
$^{69}Ga + {}^{57}Fe \rightarrow {}^{70}Ga + {}^{56}Fe + 9$ keV

Given that atomic weights are generally not known much more accurately than 10 keV, the actual reaction energies are approximate. The reaction rate is enhanced if the energy is low due to possible resonance. Reaction energy of say 1 keV requires some 10^{15} atomic products per Joule which have never been detected. Consequently some other reaction is required for power production and in the above table the decay of ^{5}Li would seem a good candidate. This decay is extremely fast and produces no gamma rays and could explain ^{4}He production. However such decays, may produce at least X-rays, and these are lacking.

In the latest version of the neutron transfer theory, possible donor elements ^{A}X should have a naturally occurring sister isotope ^{A-1}X which can accept the neutron with perfect energy matching, (resonance). This and the s-wave requirement cast some doubt on the above table and the only permitted donor isotopes will be: ^{2}H, ^{4}He, ^{29}Si, ^{30}Si, ^{111}Cd, ^{112}Cd, ^{112}Cd, ^{115}Sn, ^{116}Sn, ^{117}Sn, ^{118}Sn, ^{119}Sn, ^{120}Sn, ^{125}Te, ^{126}Te, ^{129}Xe, ^{130}Xe. In addition to the above donor elements, acceptors can be Mg, Al, P, Cl, As, Rb, Mo, Cs, Ba, Yb, Th. Note the absence of Pd and Ni from this list.

Conclusions

A computer is ideally suited to scanning through many reactions to select possibilities for more detailed study. By eliminating all simple reactions of type (2) for the production of neutrons and tritium, we can focus attention on other possibilities including error which otherwise might have seemed improbable. Reactions with more than two products have been excluded from this study. But the fission of any sufficiently heavy nucleus can yield multiple products including neutrons and tritium. The identification of potential materials to demonstrate specific theories may stimulate further experimental and theoretical research.

Acknowledgements

We thank the Brookhaven National Laboratory for atomic data[7] provided in computer readable format by the OECD Nuclear Energy Agency (Paris). The author acknowledges the encouragement of Dr Macerata, Fiat Research Centre, Orbassano.

References

2. Hagelstein P L, Kaushik S.; "Neutron Transfer Reactions", *Proc. ICCF4*, Vol 1, 10-1.

3. Fisher J C, "Polyneutrons as agents for Cold Fusion reactions", *Fusion Technology* Vol 22, p 511, Dec 1992.

4. Notoya R., "Alkali-Hydrogen Cold Fusion Accompanied with Tritium Production on Nickel", *Proc. ICCF4*, Vol 3, 1-1.

5. Sankaranarayanam T, Srinivasan M, Bajpai M, Gupta D; "Investigation of Low Level Tritium Generation in Ni-H_2O Electrolytic Cells", *Proc. ICCF4*, Vol 3, 3-1.

6. Manduchi et al; "Anomalous Effects During the Interaction of Subatmospheric D_2 (H_2) with Pd from 900°C to Room Temperature", *Il Nuovo Cimento*, vol 107 A, no 2, pp 171-183. Feb. 1994.

7. Tuli J K, "Nuclear Wallet Cards", July 1990 Brookhaven National Laboratory.

8. Karabut A B, Kucherov Y R, Savvatimova I B, "Possible Nuclear Reaction Mechanisms at Glow Discharge in Deuterium", p 165 in *Frontiers of Cold Fusion* Edited by H. Ikegami, (1992), Frontiers Science Series n.4, Univ. Acad. Press, Tokyo (Japan).

9. Karabut A B, Kucherov Y R, Savvatimova I B, "Cathode Material Change after Deuterium Glow Discharge Experiments", p 389 in *Trans. Fusion Technology*, vol 26, No 4T, part 2, December 1994, 1-540. (ICCF4).

10. Robert T. Bush, "An Interpretation of the Piantelli effect based upon the LANT hypothesis and ECFM model for Cold Fusion", in *Cold Fusion Source Book*, International Symposium on Cold Fusion and Advanced Energy Sources 1994, Minsk, Belarus, Hal Fox Editor.

11. B. Stella, M. Corradi, F, Ferrarotto. V, Milone, F Celani, A. Spallone, "Evidence for Stimulated Emission of Neutrons in Deuterated Palladium," *Frontiers of Cold Fusion",* Proceedings of the Third International Conference on Cold Fusion, ed. H. Ikegami pages 437-440, Universal Academy Press, Tokyo (1993).

12. M.S. Costantino, J.F. Lakaer and R. Bastasz, "Synthesis of Monolithic Uranium Hydride and Uranium Deuteride," *Journal of the Less-Common Metals*, vol. 159, 1990, pp 97-108, 14 refs.

13. Garvey G. T. et al,, "Set of nuclear mass relations and a resultant mass table", *Rev. Mod. Phys.* 41 (1969) S1.

14. Robert T. Bush, R Eagleton, "Evidence for Electrolytically induced Transmutation and Radioactivity Correlated with Excess Heat in Electrolytic Cells with Light Water and Rubidium Salt Electrolytes", *Proc. ICCF4*, Vol 3, 2-1.

15. Collis W J M F, "LANT and the Piantelli Effect.", to be published in 2nd edition *Cold Fusion Source Book*, International Symposium on Cold Fusion and Advanced Energy Sources 1994, Minsk, Belarus, Hal Fox Editor.

16. Collis W J M F, "Le reazioni nucleari della fusione fredda. Un'analisi sistematica", in *21mo Secolo Scienza e Tecnologia*, Anno V, n. 3, 1994 (in Italian).

17. Piantelli F, "Evidence for the production of heat and nuclear effects in the Siena experiment", presented at Siena, 24-25 March 1995. Bruno Stella Editor.

Fifth International Conference on Cold Fusion
9-13 April, 1995 - Monte Carlo, Monaco
ICCF5 ©1995

Transformation from Heat of Low Temperature Sources into Work Fundamentals for a Maximum of Efficiency

Maurizio VIGNATI
ISPESL
Via Urbana 167, 00184 Roma
Italy

Abstract

The problem of converting the heat produced by cold fusion into work, meets with a classical limit consisting in the second principle of thermodynamics, because the heat produced within electrolytic cells is released to the heavy water, and remains at a low thermal degree. However, this paper draws attention to the existence of ideal thermodynamic cycles the efficiency of which is considerably higher than the efficiency attained by the corresponding Carnot cycle between the same temperatures. In addition to this, it can be shown that combinations of these cycles can attain even higher efficiencies. Owing to the characteristics of these cycles and combinations of cycles, and being also possible to put them into practice, they could be taken into consideration for projects aiming at the transformation into work of the heat produced by cold fusion or other heat sources at low temperature.

1. Introduction

Making use of data on real fluids, it is possible to calculate the efficiency of ideal cycles with various fluids. A milestone in this field is a publication (ref.1) of the National Bureau of Standards (now National Institute of Standards and Technology), concerning the thermodynamic properties of Argon (1969). A more recent work is the publication of the thermodynamic properties of water (ref.2), (1988). And many other thermodynamic properties of different fluids have been published in books and reviews (ref. 3 - 8). Most of these papers propose a mathematical model of the fluid under study. It is possible, therefore, to make part these mathematical models of interactive programmes which allow to calculate the efficiency of ideal cycles and combinations of ideal cycles with the same fluid.

2. Ideal Conditions

Our aim is to demonstrate the existence of cycles the efficiency of which is greater than the efficiency of the Carnot cycle. In order to do this, we will assume the same assumptions generally accepted to deal with ideal cycles, that is, that every kind of energy or heat loss can be avoided by the use of ideal devices and conditions. Except the Carnot cycle, other cycles need to be conceived with a heat recuperator, so that we also assume that this device may be perfectly insulated and sized in such a way as to render the internal viscous losses negligible. Isothermic and isochoric transformations will be assumed ideal as well.

3. Theorems on Ideal Transformations and Cycles

On the basis of the assumptions made in the previuos point, it is possible to demonstrate ten theorems concerning the thermodynamic behaviour of the ideal

heat recuperator when applied to cycles with real fluids in gaseous phase. It is not possible to give extensive information, here, about this very important subject. Interested readers are adressed to the references (ref. 9-10). What can be said here is that the perfect heat recuperator allows perfect compensation of the isothermic quantities of heat of an Ericsson cycle, if the quanties of heat are the same. In addition, it allows perfect compensation of the isochoric transformations of a Stirling cycle, if the quantities of heat are the same. If the quanties of heat are not the same, the entire difference of heat is absorbed by (or imparted to) one heat source only.

4. Programmes to Calculate Efficiency

Once the theorems are stated and demonstrated, it is possible to use them in numerical (computerized) calculations of the performances of ideal thermodynamic cycles. These programmes have been made for argon, making use of data available in ref.1. To facilitate more people to undestand these programmes, they have been written in BASIC programming language (ref.15-16). Five programmes have been set up, named CARNOT, STIRLING, STIRREV, ERICSSON, ERIXREV. They are interactive programmes, which require the user to type in a few numbers at the beginning. The user have to type in the thermodynamic characteristics of the main points of the cycle chosen. In addition to the said theorems, these programmes merely apply the rules to calcultate energy and heat exchanges of the various sections of the cycles, in particular, they make use of the first principle of thermodynamics.

5. Result: The Ideal Carnot Cycle with Gaseous Argon

To check the validity of this kind of calculation, we first applied CARNOT to the Carnot cycle. The result of this verifications is fully satisfactory, because it is always verified the identity between theoretical efficiency and numerically calculated efficiency.

6. Result: The Ideal Stirling Cycle with Gaseous Argon

Once the validity of the calculation method has been assured, we can extend our research to other kind of cycles. The ideal Stirling cycle can be provided with a perfect heat recuperator, or it can be missing. Making the calculations with STIRLING, we find that if the perfect heat recuperator is applied, efficiency is practically equal to the efficiency of the Carnot cycle, but a small irreversibility occurs. If the heat recuperator is missing, efficiency is lower.

7. Result: Combinations of Stirling Cycles

We can imagine to pair two adjoining and opposed Stirling cycles and provide them with a common heat recuperator. Using STIRREV, we *always* find couples of opposed Stirling cycles with overall efficiency exactly equal to the one due to the Carnot cycle. These couples are reversible as a whole.

8. Result: The Ericsson Cycle with Gaseous Argon

The same procedure can be applied to the Ericsson cycle. It can be imagined with or without a perfect heat recuperator. However, running ERICSSON we have a big surprise, because the efficiency pattern of the Ericsson cycle is very unusual: it shows peaks over and below the efficiency value of the Carnot cycle. What more counts is

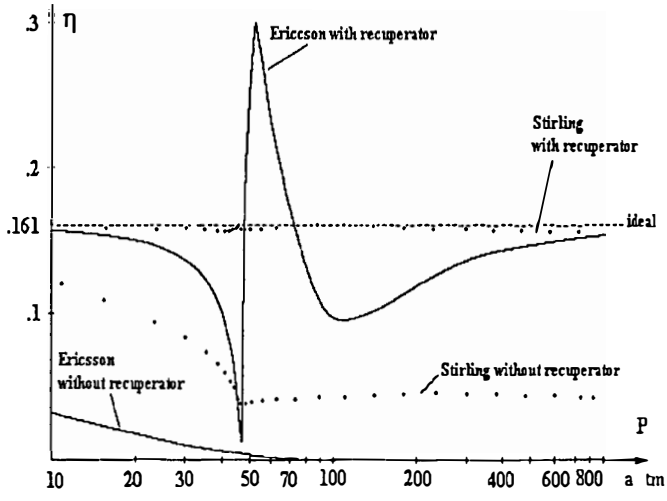

Fig.1 Efficiency of various cycles with gaseous argon

Recapitulary diagram with the efficiency patterns of the indicated cycles, versus the highest pressure encountered along the cycles. The "hot" source is at the temperature of 180 K, while the cold source is at 151 K.

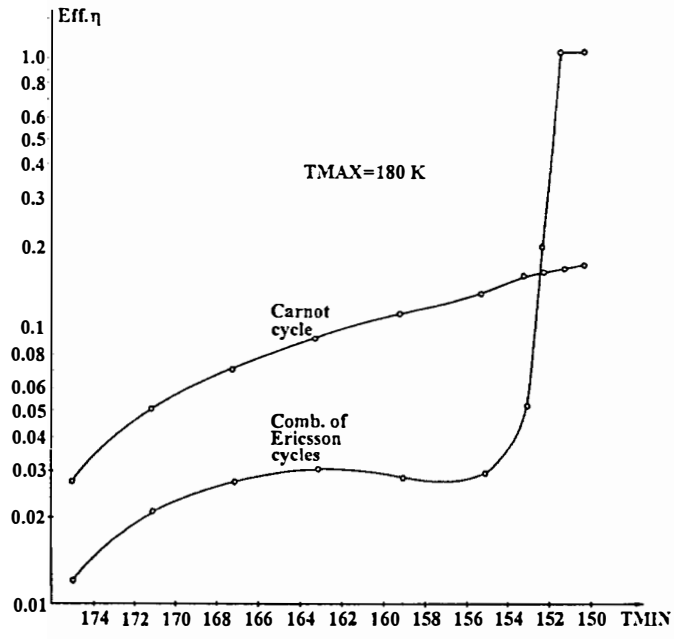

Fig.2 Efficiency of a combination of Ericsson cycles

By pairing two adjoining and opposed Ericsson cycles, it is possible to obtain conditions in which the overall efficiency η is greater than the efficiency of the equivalent Carnot cycle. This depends, mainly, on the vicinity of the temperature of the cold source to the critical temperature Tc of the gas used. The case shown is relative to argon (Tc = 150.86 K) with PE = 60 and PK = 40 atm. TMAX is fixed to 180 K, while TMIN is variable (in abscissa).

the fact that the maximum efficiency depends heavily on the proximity of the cold temperature to the critical temperature, and it depends also on the position chosen on the P-V plane. In addition, it is possible to show that the Ericsson cycle attaining maximum efficiency is reversible. Fig.1 shows the patterns of efficiency of the various cycles examined.

To prove that these results are not due to ill-conditioning of the programme ERICSSON, we can make the calculation by hand, and verify the exactness of the calculations made by ERICSSON, since we obtain the same results. It is also possible to find the same conditions of increased efficiency with many other fluids in gaseous phase employed in the Ericsson cycle, namely: He-4, N_2, Kr, Xe, NH_3, CH_4, Ethane, Propane, Isobuthane, Normal Buthane,Ethylene and Water. With all these elements and substances it is possible to determine Ericsson cycles with an efficiency value about twice the efficiency of the equivalent Carnot cycle.

9. Result: Combinations of Ericsson Cycles with Gaseous Argon

We can imagine to pair two adjoining and opposed Ericsson cycles and provide them with a common heat recuperator. When this is done, we *always* find couples of opposed Ericsson cycles reversible as a whole. As regards the efficiency, the overall efficiency depends,

once more, on the position chosen on the P-V plane, but it also depends on the proximity of the temperature of the cold source to the critical temperature of argon (Fig.2).

10. Conclusions

Since our reasonings concern ideal conditions, it is difficult to establish at the moment to what extent these high efficiency cycles can be put into practice. However, this study shows that it is possible to go far beyond the limit of efficiency which derives from the thermodynamic theory - theory which, we remember, obtains this limit from Kelvin and Clausius' postulates by means of demonstrations based on *reductio ad absurdum*. The numerical calculations give quite another limit of efficiency. What I showed is nothing but a possible track that could be followed by those who are interested in exploiting heat sources at low temperature. About the aspects of the matter which seem to be in contrast with the principle of the increase of entropy, there is not enough space to master the subject here. Interested readers could consult ref. 9-10. I will only say that if we stick to the operative modalities with which one states, case by case, that entropy is increased after the occurence of an irreversible transformation, then we can say that the principle holds, notwithstanding we have discovered cycles which attain an efficiency greater than the efficiency of the corresponding Carnot cycle.

References

1. Gosman L.A., McCarty R.D., Hust J.G., *Thermodynamic Properties of Argon From The Triple Point to 300 K at Pressures to 1000 Atmospheres*, p.150, NBS-27 National Bureau of Standards, (1969).
2. Sato H., Uematsu M., Watanabe K., Saul A., Wagner W., "New International Skeleton Tables for the Thermodynamic Properties of Ordinary Water Substance" *J. Phys. Chem Ref. Data*, 17, N.4, 1439-1539 (1988).
3. Rabinovich V.A., Vasserman A.A., Nedostup V.I., Veksler L.S., *Thermophysical Properties of Neon, Argon, Krypton and Xenon*, p. 622, National Standard Reference Data Service of the USSR. Theodore B. Selover, Jr. English-Language Editor, Hemisphere Publication Co. (1988).
4. McCarty R.D., *Thermophysical Properties of Helium-4 for Temperatures from 2 to 1500 K with Pressures to 100 Mn/m²*, p. 155, NBS report 9762, (1970).
5. Jacobsen R., "Thermodynamic Properties of Nitrogen from the Freezing Line to 2000K at Pressures to 1000 MPa", *J. Phys. Chem. Ref. Data* 15, N.2, 736-909 (1986).
6. Haar L., "Thermodynamic Properties of Ammonia" *J. Phys. Chem. Ref. Data* 7,N.3 635-972 (1978).
7. Younglove B.A. "Thermophysical Properties of Fluids Methane, Ethane, Propane, Isobuthane and Normal Buthane" *J. Phys. Chem. Ref. Data* 16, N.4 577-798 (1987).
8. McCarty R.D., "Thermophysical Properties of Ethylene from the Freezing Line to 450 K at Pressures to 260 MPa", *J. Phys. Chem. Ref. Data* 15, N.2 593-734 (1986).
9. Vignati M. *Riflessioni sulla Potenza Motrice del Calore Ambientale*, p288, 1 floppy disk, Astrolabium Ed., Viale Garibaldi 4, Civitavecchia, Italy (1993).
10. Vignati M., *Crisis of a Dogma - Clausius' Theorem at the settling of accounts* p.160, 1 floppy disk, Astrolabium Ed., Viale Garibaldi 4, Civitavecchia, Italy, telefax 766 - 501648, (1995).

Fifth International Conference on Cold Fusion
9-13 April, 1995 - Monte Carlo, Monaco
ICCF5 ©1995

Cold Fusion and Quantum Mechanics

Alexandre LAFORGUE
3 Rue des Carmes. 02570 Chézy-sur-Marne. France.

Abstract

One explain the cold fusion by a permanent state of collision between the deutons of the double layer. Each one collides with the total mass of the network with an energy surpassing the potential barrier. This state is determined by the dimension of the quantum mechanical path of deutons under the Bohr-Heisenberg limit. The discussion of the quantum path itself could be bessered by a new model of quantum mechanical wave corpuscle.

1. Introduction.

Cold fusion has been discovered in 1989 under the form of Fleischmann-Pons effect [1] and has remained until now a controversial subject because lack of reproducivity and excess of interpretations.

This paper concerns only the fusion of deutons. We examine in Part 2 the quantum mechanical problem without any hypothesis. We do not succeed of course to calculate the effect. But we show that, if it exists, it satisfies a necessary condition which explains the reported stranges characters such as initial latence, bursts, quasi explosive character, non harmonic oscillations etc...

In part 3, with the alone hypothesis that it can exist quantum paths of non integer fractal dimension (this dimension corresponding to its delocalisation), we show that the effect can be predict.

In part 4, we suggest a new model.

2. Necessary condition of the cold fusion.

The occurence of fusion between two deutons depends

1°) on the collision probability, P_{coll},

2°) on the probability that collision is inelastic , P_{inel} .

Refering to an usual approximation in the theories of chemical reactions [2], we write

$$P_{fus} = P_{coll} \times P_{inel} \qquad (1)$$

P_{inel} cancels except at very high temperature (hot fusion). Hence, for many people, fusion should not occur.

But such derivation is not true because, mathematically as well physically, a finite quantity can be expressed on the form $o \times \infty$.

The consequence of the condition

$$P_{inel} = O \qquad (2)$$

is then, if cold fusion exists,

$$P_{coll} = \infty \qquad (3)$$

2A Chemical structure should be labile.

To take into account the condition (3), we have first to consider in what case the collisions are avoided: a) Chemical structures which can be involved in

the electrochemical process, such as D_2, D_2O, ..., possess defined bond length D_2. b) If two deutons are situated in two different molecules it exists between them a minimal distance of approach That excluds the collision. Consequently the chemical structures containing deutons have to be labile. In other words, the concerned molecular orbitals should be unoccupied (i.e. lower than H.O.M.O.)

2B. Necessity of fractal dimension of the quantum paths d>1.

From the theory of the hydrogen atom,the quantum path of the peripheral electron is:

1°) a hyperbola if the atomic level is $W > W_0$, W_0 electronic detachment level (they have the dimension d= 1)

2°) a quantum path associated to the quantum number n = 1, 2, ...$^\infty$, discussed long time before the concept of fractal arises, (L.de Broglie [3], Feynman [4]), assessed to the dimension d= 2 by Abbot and Wise [5], discussed by Nottale [6]. Now the nucleus of the hydrogenoïd atom is homothetic of electron with respect to the center of mass. At the end the deutons moving on the energy level W follow a path of dimension d = 1, if $W > W_D$, of dimension d>1 if $W \leq W_D$ (W_D energy of the deuterium atom, at the electronic detachment level)

2C. Comparison between quantum consequence and chemical consequence of the necessary condition.

We observe that the conditions 1°) and 2°) are expressed by the same inequation

$$W \geq W_D \qquad (4)$$

We have not yet demonstrated that the condition is sufficient. But we will first point out important characters resulting only of the necessary condition (3).

2D. Permanent state of collision between deutons

In the above reported mechanism, for a given mass, deutons undergo an infinite number of collisions but a finite number of fusions. The condition (3), $P_{inel} \simeq 0$, is not immediately understandable..Infinite number of collisions means a permanent state of collision. This concept was introduced in Physics by J. Perrin [7] to derive thermodynamical properties of solids from the kinetic theory of gas. Here it should be extended from the atom to the nucleus. Taking into account the electroneutrality, the permanent state of collision does not concern a volume but only a bidimensional (or monodimensional) variety. Cold fusion is a non volume process The confined deutons are the positive part of the double layer.

This permanent state of collision determines a finite number of fusions but not as a result from a lottery. In the solids, one can observe thermal waves and, especially in the explosives, detonation waves, resulting from elastical or non elastical collisions in the network. In the twodimensional deutons network,we can imagine elastical waves and non elastical waves propagating following wave lines or detonation lines,possessing in each case a welldefined velocity. We are interested here in the detonation lines. In this case (of inelastic collisions), a deuton collides with the total mass of the network. The collision energy is hence multiplied by the number of involved deutons. In other words the height of the potential barrier should be divided by the number of deutons to obtain the effective potential barrier governing the rate of the cold fusion.

The experimental verification of this prediction were possible if an area can be defined for different double layers. Indirectly it were perhaps possible by manufacturing the electrodes to guide the wavelines and compare different

situations (e.g. convergency and divergency)

2E. Explosive character of the cold fusion.

The propagation of a detonation line following the twodimensional network of deutons suggests:

1°)the process of cold fusion is a set of events,each starting with a threshold in loading,

2°)the successives are non identical. One can speak about a reproducible diversity.

2F Anharmonic oscillations of cold fusion.

On th other hand,if cold fusion occurs (i.e. a set of events above described) the produced enthalpy contributes to increase the temperature of the medium, so that the energy level of the deuterium atom, when included in any chemical structure, increases until the detachment potential.

As demonstrated above, the two phenomena: 1°) liberation of deutons by thermal effect, 2°)fusion of deutons by crossing their quantum path, increase together. The difference of rates between the two processes is favourable to the generation of anharmonic oscillations. The rate of destabilisation of chemical structures cannot follow the rate of atomic excitation which is self accelerated.

The reported kinetics of the Fleischmann-Pons effect shows such oscillations [8].

We can explain : after many fusion events, the number of liberated deutons is no more sufficient to determine new events. The fusion stops. It can only restart if new deutons are liberated, but not immediately.

The two successions limited respectively by abundance of deutons and by temperature should not be confused The thermal cycle contains many events of propagation of a non elastical wave.

3. Prediction of the cold fusion.

The part 2 considers the consequences of the condition $\{3\}, P_{coll} = \infty$ which leds immediately to the condition that quantum paths possess a fractal dimension d>1. We have not calculated the value of d. For fractal dimension of a quantum path the alone noticeable value d=2 was calculated by Abott and Wise [5] on the basis of the Brownian model of Nelson . .

3A. Physical interpretation of the fractal dimension of a quantum path.

We propose that d corresponds to the amount of delocalisation in the quantum path.. The increasing d from d=1 corresponds to excursions from a line. The final value 2 corresponds to a complete delocalisation.

It is clear that localisation favours individual processes delocalisation favours collective processes. Cold fusion is a typical collective process.

3B. Calculation of dimension of a set of collisions.

The space dimension is normally N=3. It has be restricted (N=2) above;but the electroneutrality is a statistical condition which changes nothing to the possible motions.. The domain of collision between two particles is the set of the intersection of their paths.

If we consider two varieties of dimensions D_1 and D_2 in a space of dimension E, the dimension of the intersection is d

$$d = D_1 + D_2 - E \quad | \; D_1 + D_2 - E > 0$$

$$d = 0 \quad | \; D_1 + D_2 - E \leq 0$$

we suppose first that the letters correspond to integer; then we admit the same relation for non integer value.

3C. Postulat.

Let us assume that d is the dimension of the set of collisions between particles. If d increases, the collective character of the process increases.

If two nuclei are identical bosons

$$D_1 = D_2 = D, \quad E = 3$$

$$\begin{array}{l|l} d = 2D - 3 & D > 3/2 \\ d = 0 & D \leq 3/2 \end{array}$$

From this expression, it results that if the dimension of the quantum path varies between the limits 1 and 2

$$D = 1 \nearrow 1{,}5 \nearrow 2 ,$$

one observes

$$d = 0 \rightarrow 0 \nearrow 1$$

We point out a threshold effect following the variation of D. From $d \geq 0$, the collective effect start, cold fusion can take place.

It is the same effect as this one analysed in §§2D,2E, but otherwise explained.

4 .New assumptions..

We try to elaborate a new model where the quantum path can be postulated of any dimension. As a physical meaning corpuscle is no more a little body, but propagates as a crack in a solid. Quantum mechanics can be modelized by propagation of a strain tensor which guides a crack [9]..The conditions, stated above, concerning the fractal dimension can be represented as fissuration conditions in the vacuum. That explains in general terms the few reproducivity of cold fusion.

Références

1 .M.FLEISCHMANN and S.PONS. *J.Electroanal.Chem.***261** 301 (1989)

2. K.J. LAIDLER. *Theories of chemical reaction rates* Mc Graw Hill. New York (1969)

3. L. de BROGLIE. '*Une tentative d'interprétation causale et non linéaire de la mécanique ondulatoire* Gauthier-Villars, Paris, (1956)

4. R.P. FEYNMAN. *Rev.Mod.Phys.***20** 367 (1948)

5. L.E. ABOTT and M.B. WISE. *Am.J.Phys.* **49** (1) 37 (1981)

6. L. NOTTALE. *Fractal space time and microphysics.* chap 4, World Scient. Singapore (1993)

7 J. PERRIN. *Les atomes.* Alcan . Paris (1913)

8. M. FLEISCHMANN and S. PONS. *Phys.Letter* A **176** 113 (1993)

9. A. LAFORGUE. *Acta Biotheor.* **40** 221 (1992); La réaction nucléaire est-elle impossible a priori en milieu biologique, *13°Sémin.S.F.B.T.;(1993)ibid* sous presse.

AUTHOR INDEX